Synthetic Molecular Walkers

by

Max von Delius

Degree of Doctor of Philosophy

School of Chemistry

The University of Edinburgh

August 2010

Für meine Eltern

Success is never certain – failure is never final.

(Anonymous – Fortuitously quoted by Gaussian ’03 on an afternoon in May 2008)

Table of Contents

Abstract and Layout of Thesis

The work presented in this thesis was inspired by one of the most fascinating classes of naturally occurring molecules: bipedal motor proteins from the kinesin, dynein and myosin superfamilies walk along cellular tracks (see Figure 1), carrying out essential tasks, such as vesicle transport, muscle contraction or force generation. Although a few synthetic mimicks based on DNA have been described, small-molecule analogues that exhibit the most important characteristics of the biological walkers were still missing until recently. In this thesis, the design, synthesis and operation of several small-molecule walker-track systems is described. All presented systems share a similar molecular architecture, featuring disulfide and hydrazone walker-track linkages, yet deviate fundamentally in the mechanism and energy input that is required for directional walker transport.

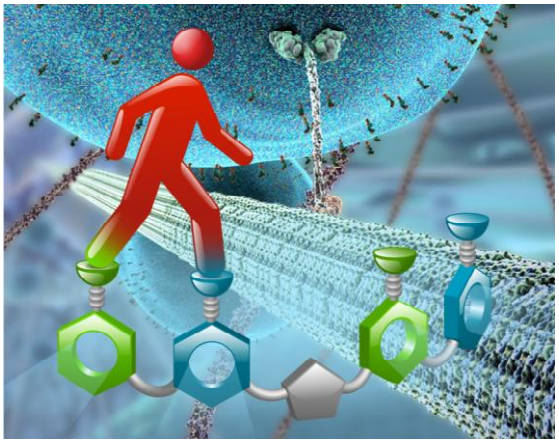

Figure 1. *Schematic representation of one molecular walker-track conjugate (front) described in this thesis and a representation of the inspiration: motor protein kinesin (background).*

Chapter I includes an overview of the biological walker proteins, as well as a comprehensive review of the DNA-based mimicks published to date. A set of fundamental walker characteristics is identified and special emphasis is given to the underlying physical mechanisms.

Chapter II describes a series of experiments, which lay the groundwork for all small-molecule walker systems presented in the following Chapters of this thesis. The mutually exclusive nature of disulfide and hydrazone exchange under basic and acidic reaction conditions, was demonstrated using an unprecedented type of macrocycle.

The first small-molecule walker-track system (see Figure 1) is described in Chapter III. Due to the passive nature of both the track and the walker unit, an oscillation of acidic

and basic reaction conditions led to a directionally un-biased, intramolecular 'diffusion' of the walker unit along the track. Using an irreversible redox-reaction for one of the foot-track exchange reactions conferred a certain degree of directionality to the walking sequence, with the oxidant iodine providing the chemical fuel for the underlying Brownian information ratchet mechanism.

Chapter IV contains a comprehensive investigation of the dynamic properties of a series of walker-track conjugates derived from the walker-track conjugate presented in Chapter III. The most significant observation was that ring strain appears to be a requirement for the emergence of directional bias, a phenomenon that has also been found in biological walkers.

In Chapter V a different type of walker-track conjugate is described, in which the track plays an active role and light is used as the fuel required for directional walker transport. The key for achieving directionality was the presence of a stilbene unit as part of the molecular track, through which ring strain could be induced in the isomer where the walker unit bridges the *E*-stilbene linkage. Significantly, the underlying Brownian energy ratchet mechanism allowed walker transport in either direction of the molecular track.

Chapters II to V are presented in the form of articles that have recently been published or will be published in due course in peer-reviewed journals. No attempt has been made to re-write this work out of context, other than to avoid repetition, insert cross-references to other Chapters (where appropriate) and to ensure consistency of presentation throughout this thesis. Chapters II, III, IV and V are reproduced in the Appendix, in their published formats. The Outlook contains closing remarks about the scope and significance of the presented work as well as ideas for the design and operation of a next generation of small-molecule walkers, some of which are well under way in the laboratory.

Declaration

The scientific work described in the present thesis was carried out in the School of Chemistry at the University of Edinburgh between September 2007 and July 2010. Unless otherwise stated, it is the work of the author and has not been submitted in whole or in part in support of an application for another degree or qualification at this or any other University or institute of learning.

Signed:

Date:

Meetings Attended and Presentations Given

1. **Organic Research Seminars**, School of Chemistry, University of Edinburgh, UK, 2007-2010.
   a) *Towards a Dynamic Covalent Molecular Shuttle*, October 2007.
   b) *A Dynamic Covalent Molecular Walker*, February 2009.
   c) *Organic Molecules that can Walk along Tracks*, April 2010.

2. **School of Chemistry Visiting Speaker Colloquia**, School of Chemistry, University of Edinburgh, UK, 2007-2010.

3. **RSC Perkin Division 35th Scottish Regional Meeting**, University of Glasgow, UK, December 2007.

4. **Bruker Avance and TopSpin™ course**, five-day onsite training at the Bruker UK headquarters, Coventry, UK, February 2008.

5. **EPSRC Molecular Nanoscience Symposium**, University of Reading, UK, June 2008.

6. **Special Symposium in Honour of David Reinhoudt**, University of Edinburgh, UK, November 2008.
   Oral presentation: *A Non-Interlocked Molecular Shuttle.*

7. **Supra-Nano Meeting**, University of Birmingham, UK, December 2008.
   Poster presentation: *A Non-Interlocked Molecular Shuttle.*

8. **10th Tetrahedron Symposium: "Challenges in Organic and Bioorganic Chemistry"**, Paris, France, June 2009.
   Poster presentation: *A Synthetic Molecule that Walks down a Track.*

9. **59th Nobel Laureate Meeting: "The Role and Future of Chemistry for Renewable Energy"**, Paris, France, June 2009.

10. **42nd IUPAC Meeting**, Glasgow, UK, August 2009.
    Poster presentation: *A Synthetic Small Molecule that Walks down a Track.*

11. **RSC Supramolecular and Macrocyclic Meeting**, University of Cambridge, UK, December 2009.
    Poster presentation: *Synthetic Small-Molecule Walkers.*

12. **ACS Spring Meeting**, San Francisco, USA, March 2010.
    Oral presentation: *Synthetic Small Molecules that can Walk along Tracks.*

13. **21st SCI Postgraduate Symposium**, University of Aberdeen, UK, March 2010.
    Oral presentation: *Organic Molecules that can Walk.* Awarded 1st Prize.

14. **School of Chemistry, Organic Section Firbush Symposium**, Firbush Point Centre, University of Edinburgh, UK, April 2010.

    Oral presentation: *Organic Molecules that can Walk along Tracks.* Awarded 1st Prize.

15. **School of Chemistry, Postgraduate Seminar Afternoon**, University of Edinburgh, UK, May 2010.

    Oral presentation: *Organic Molecules that can Walk along Tracks.* Awarded 1st Prize (Eleanor Greene Memorial Prize).

16. **3rd EuCheMS Congress**, Nuremberg, Germany, August 2010.

    Oral presentation: *Synthetic Small Molecules that can Walk along Tracks.*

Acknowledgments

First of all, I would like to thank my supervisor Prof. David Leigh for his enthusiastic support throughout my stay in his laboratory. It has been a privilege to learn from him (paper writing!), to discuss various fascinating scientific matters with him and to be able to conduct top-notch research without having to watch every penny.

Secondly, I would like to express my deep gratitude to Dr. Edzard Geertsema. I consider myself very fortunate to have worked with him on several projects in the first two years of my doctorate. I sincerely admire his level and friendly approach and his ability to keep a good spirit and make the right decisions when a project is at the brink of failure.

Many thanks to all past and present members of the Leigh group for creating a stimulating and friendly working environment. In the obligatory alphabetical order ☺: Adam (aka Gustavo), Amaya, Angel, Anne, Anthony, Araceli, Armando, Augustinas, Aurélien, Barry, Bartek, Bea, Bryan, Christian, Christiane, Christoph, Costanza, Craig, Daniel Dan-Tam, Daniel D'Souza, David, Diego, Dominik, Edzard (aka the Dutch Dragon), Erika, Euan, Francesca, Francesco, James, Jean-Francois, Jhenyi, John, Jon, Jordi, Katherine, Kathleen, Kevin, Luca, Luciana, Marcus, Maria, Marius, Mark, Michael, Miguel, Mike, Miriam, Monica, Mustafa, Nathalie, Nick, Patrick, Pau, Paul, Philipp, Raul, Romen, Roy, Satoshi, Steffen, Steve, Tao, Takeshi, Ula, Uma, Vicky and Victor.

Special thanks within the group go to everybody with who I had the pleasure to work with on various projects: Angel, Ara, Armando, Bea, Daniel Dan-Tam, Edzard, Kathleen, Kevin, Mike and Ula. I would also like to thank Marius Kroll and Aurélien Viterisi who not only set up the first (old-school) HPLC facility in our group, but also taught me all about this technique, which proved to be crucial for the research described in this thesis. Mark Symes, Paul McGonigal, Adam Wilson and Bartosz Lewandowski are acknowledged for their heroic effort with maintaining the Leigh group NMR spectrometer (which I know is a very tough task). Further thanks go to Steve Goldup and Daniel D'Souza who were always eager to help out with their tremendous knowledge of synthetic organic chemistry. Kevin Hänni is thanked for supplying (sometimes surreal) music in the office and for conducting with me the most fascinating "green chemistry" experiment I have ever done. Aurélien Viterisi is thanked

for sharing my passion for home-cooking projects and for having a truly idealistic approach towards science. Marius Kroll is thanked for hosting some legendary parties and for allowing me to practice my frankonian accent on a regular basis. Finally, I would like to thank everybody who spent quality time with Sarah and me outside of the lab - it is fantastic to have colleagues that are also friends.

I would further like to thank several members of the School of Chemistry staff without who none of this work would have been possible: Annette and Amanda for their help with administrative queries, Martin Reid and Manolo for making sure the occasional expense claim is processed, all the guys in the Chemical Stores for doing a terrific job (Derek, Tim, Raymond, John, Kenny), Stewart, David and Donald from the mechanical and electrical workshops, Stuart the glassblower, David, Jim and Michael from the IT support, Alan Taylor and Paul Angus for running the mass spectrometry facilities and last, but certainly not least, Juraj (clearly the department's Superman), Marijka and John for the mammoth task of ensuring all NMR spectrometers are in working order. I would also like to thank Louise and Stewart for keeping our lab in good shape and helping out with the synthesis of precursors.

Then I would like to thank everybody who makes sure every single trip back home to Franconia is a great experience: First, I have to thank Easyjet for firstly not being Ryanair and for secondly maintaining a direct connection between Edinburgh and Munich. Much more importantly, I would like to thank all my close friends for staying in touch and for reminding me that there is a world outside science. The members of the legendary LK Bier deserve special mention: Fump, Schoko, Schosch, Strassi, Tasso, Ted and Triebi, I hope we will go on brewery hikes, summer holidays and city trips for many years to come.

Thank you, Sarah, for all your love and understanding during these, sometimes tough, three years in Edinburgh. This thesis is also yours.

Finally, I would like to thank my parents, Andreas and Inge, for their counsel and support (emotionally and financially) during these past 22 years (!) of education. This thesis is dedicated to you.

List of Abbreviations

ADP	adenosine-5'-diphosphate
AFM	atomic force microscopy
aq.	aqueous
APCI	atmospheric pressure chemical ionisation
ATP	adenosine-5'-triphosphate
calcd.	calculated
CuAAC	copper(I)-catalysed azide alkyne cycloaddition
Da	Dalton
DBU	1,8-diazabicyclo[5,4,0]undec-7-ene
DCM	dichloromethane
dec.	decomposition
DNA	desoxyribonucleic acid
DTT	DL-dithiothreitol
δ	chemical shift
ESI	electrospray ionisation
Et_2O	diethylether
Et_3N	triethylamine
equiv.	equivalent
EtOAc	ethyl acetate
EtOH	ethanol
DIPEA	diisopropylethylamine
DMF	*N,N'*-dimethylformamide
DMSO	dimethylsulfoxide
FAB	fast atom bombardment
HPLC	high performance liquid chromatography
HRMS	high resolution mass spectrometry
Hz, MHz	Hertz, megahertz
IPA	isopropyl alcohol (2-propanol)

LCMS	liquid chromatography mass spectrometry
LRMS	low resolution mass spectrometry
m.p.	melting point
MeCN	acetonitrile
MeOH	methanol
min	minutes
mRNA	messenger RNA
MS	mass spectrometry
NMR	nuclear magnetic resonance
3-NOBA	3-nitrobenzyl alcohol
PAGE	polyacrylamide gel electrohphoresis
PCC	pyridinium chlorochromate
PDA	photo diode array
P_i	inorganic phosphate
ppm	part per million
RNA	ribonucleic acid
RT	room temperature
satd.	saturated
SEM	scanning electron microscopy
TBTA	tris[(1-benzyl-1*H*-1,2,3-triazol-4-yl)methyl]amine
TFA	trifluoroacetic acid
THF	tetrahydrofuran
TLC	thin layer chromatography
UV	ultraviolet (light)

Note: conventional abbreviations for units and physical quantities are not included.

General Remarks on Experimental Data

Unless otherwise stated, all reagents were purchased from commercial sources and used without further purification. Dry CH_2Cl_2, $CHCl_3$ and THF were obtained by passing the solvent (HPLC grade) through an activated alumina column on a PureSolv™ solvent purification system (InnovativeTechnologies, Inc., MA). Dry DMF and MeOH were purchased from Sigma-Aldrich. Flash column chromatography was carried out using Kieselgel C60 (Merck, Germany) as the stationary phase. Analytical TLC was performed on precoated silica gel plates (0.25 mm thick, 60F254, Merck, Germany) and observed under UV light. All ^{1}H and ^{13}C NMR spectra were recorded on Bruker AVA 400, AVA 500 (cryoprobe), AVA 600 or AVA 800 (cryoprobe) instruments, at a constant temperature of 298 K. Chemical shifts are reported in parts per million and referenced to residual solvent. Coupling constants (*J*) are reported in Hertz (Hz). Standard abbreviations indicating multiplicity were used as follows: m = multiplet, quint. = quintet, q = quartet, t = triplet, d = doublet, s = singlet, b = broad. Assignment of the ^{1}H NMR signals was accomplished by two-dimensional NMR spectroscopy (COSY, NOESY, HSQC, HMBC). All melting points were determined using a Sanyo Gallenkamp apparatus and are uncorrected. Mass spectrometric analysis was carried out by the mass spectrometry services at the University of Edinburgh and by the EPSRC National Centre at the University of Wales, Swansea.

Chapter I

Walking Molecules

"Many of the cells are very tiny, but they are very active; they manufacture various substances; they walk around; they wiggle; and they do all kinds of marvelous things---all on a very small scale. Also, they store information. Consider the possibility that we too can make a thing very small which does what we want---that we can manufacture an object that maneuvers at that level!"

(Richard P. Feynman, 1959)

Acknowledgments

Dr. Kathleen Mullen is gratefully acknowledged for proof-reading this Chapter and for giving valuable feedback. Sarah von Delius is gratefully acknowledged for proof-reading the entire manuscript. Dr. Armando Carlone is gratefully acknowledged for inspecting the entire manuscript for formal mistakes

1.1 Synopsis

Movement is essential to life. Over the last 25 years cell biologists have established that most forms of movement are powered by tiny molecular motors from the dynein, myosin and kinesin superfamilies. Using a simple model these protein motors can be described as 'molecular walkers' that travel along a network of cellular 'motorways'. In complex organisms evolution has generated a vast variety of these fascinating motors: some walk only towards the periphery of the cell, whereas others walk towards the centre; some walk several hundred steps along their track, whereas others fall off after only one step; some operate individually, while others function in cooperation with thousands of their fellow-motors; some have only one 'foot', where others have two 'feet'. Their cellular functions are as diverse as their molecular designs and operating mechanisms, ranging from organelle, vesicle and mRNA transport to muscle contraction and sensory transduction.

The naturally occurring molecular walkers have inspired the development of artificial analogues. Several DNA-based molecular walkers have been shown to walk in either direction of their track upon sequential addition of appropriate chemical fuels. In other studies, autonomous operation, i.e. walker migration without external intervention, has been demonstrated. In the most recent example a non-autonomous DNA walker has been programmed to grab molecular cargo when passing by on a two-dimensional track.

In this thesis the first examples of entirely synthetic molecular walkers are described. While the overall size of DNA walkers is similar to the biological motor proteins, the minimalistic small-molecule walkers reported herein are ca. ten times smaller in length and ca. 1000 times smaller in molecular weight.

1.2 Introductory Remarks

In 1959 Richard Feynman gave his famous speech "*There is plenty of room at the bottom*"[1] at the California Institute of Technology. Now, 50 years later, many of the challenges Feynman proposed in his speech have been met and many ideas and visions he expressed have been realized, possibly beyond his expectations. Just as Feynman predicted, scientists are now able to manipulate single atoms on surfaces[2] and modern microscopes have reached a resolution that allows the elucidation of the three-dimensional structure of molecules.[3]

Over the last 25 years, biophysicists have established that many of the "*marvellous*" cellular processes that have fascinated and inspired Richard Feynman are generated by a diverse group of chemical compounds designated molecular motor proteins.[4] These motor proteins will be introduced in section 1.3 and the particular case of motor proteins that walk along cellular tracks will be discussed in more detail in sections 1.3.1 and 1.3.2.

One of Feynman's toughest proposed challenges is what he called the "*manufactur[ing]*" and "*maneuver[ing]*" of nanoscopic objects in the same manner that nature does. The development of synthetic molecular motors[5] that consume energy and do mechanical work at the molecular level is addressing this challenge. Although synthetic molecular 'machines' capable of molecular motion are increasingly prevalent in the literature, very few are able to drive a system away from equilibrium, so can be classified as motors. While great progress has been made with the development of synthetic *rotary*[6] molecular motors, there are still only relatively few examples of synthetic *linear* molecular motors, i.e. motor systems which can walk along a track. Until recently, all artificial molecular walkers were based on DNA building blocks.[7] These DNA-based systems will be reviewed in section 1.5, after some general principles for the design of synthetic molecular walkers are outlined (section 1.4).

1.3 Molecular Motor Proteins

Nature has evolved a vast range of protein-based molecular motors[8] (see Figure 1.1), including: ion pumps[9] that are able to transport charged particles against considerable potential gradients (Figure 1.1a); translocation pores[10] which move proteins selectively against a concentration gradient across membranes (Figure 1.1b); DNA helicases[11] that perform the energetically costly task of 'unzipping' complementary

DNA strands (Figure 1.1c); DNA or RNA polymerases[12] which can assemble monomeric nucleotides to polymeric material with astonishing sequence-specifity (Figure 1.1d); the rotating motor[13] F_0F_1 ATPase[14] that uses energy from a proton gradient to produce the cellular currency unit ATP (Figure 1.1e,f); the flagellar motor[15] which propels bacteria at a speed of several hundred micrometers per second (Figure 1.1g) and a whole army of molecular walkers from the dynein, myosin and kinesin families that walk either short or long distances along the cell's motorways to perform tasks such as organelle transport, muscle contraction, mitosis and sensory transduction (Figure 1.1h,i,j).[16]

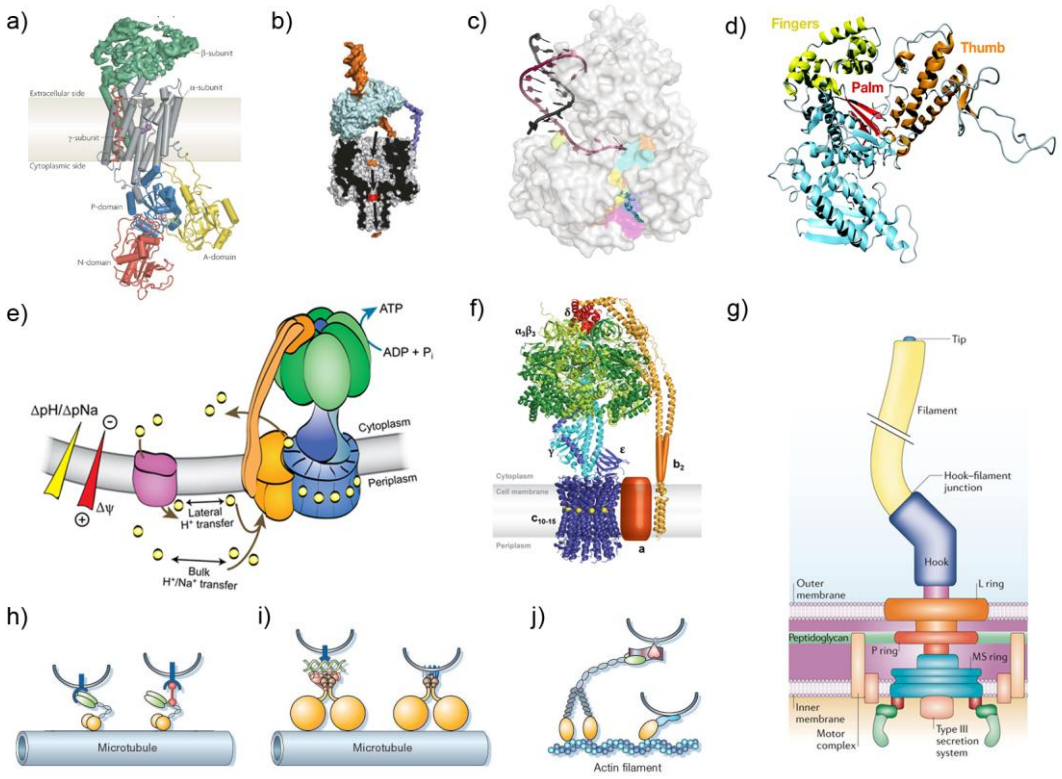

Figure 1.1. *Cellular motor proteins. a) Na/Ka ion pump;[9] b) nuclear translocation pore;[10b] c) DNA helicase;[11a] d) DNA polymerase;[12b] e) F_0F_1 ATP synthase (schematic);[14b] f) F_0F_1 ATP synthase (protein structure);[14b] g) bacterial flagellar motor (schematic);[15a] h) kinesin walker on microtubule track (schematic);[16c] i) dynein walker on microtubule track (schematic);[16c] j) myosin walker on actin filament (schematic).[16c] Graphics reproduced with permission (Nature Publishing Group (a, b, g-j); Annual Reviews (c-f)).*

Although the molecular architectures and cellular roles of biological motor proteins are very diverse, all motor proteins do have some important characteristics in common. Firstly, they convert an energy input (supplied by either nucleotide hydrolysis or ionic gradients) into mechanical and/or chemical work. Secondly, their design restricts the degrees of freedom of the motor and/or the substrate. This is a key element for the

underlying Brownian ratchet mechanisms (*vide infra*). For example, DNA and RNA polymerases 'pull' the blueprint DNA strand in only one direction through a narrow, rigid clamp and molecular walkers, such as conventional kinesin, walk along rigid, essentially one-dimensional tracks. Thirdly, all molecular motor proteins operate under the challenging conditions present in the cytoplasm, in other words they have to "*swim in molasses and walk in a hurricane.*"[17] The omnipresent thermal Brownian motion does, however, not constitute a problem, but provides a randomizing element that is necessary for most motor mechanisms (*vide infra*).[18]

One particular class of motor proteins, which in the cell biological literature is commonly referred to as cytoskeletal motor proteins,[16] is of special importance in the context of this thesis, since it provided the inspiration for the experimental work presented in Chapters II to V. An overview of these motors, sometimes also called molecular walkers or bipeds, will be given in section 1.3.1, but first some terminology needs to be introduced that is commonly used to describe their dynamic behaviour:

(i) *Processivity*: the ability of a molecular motor, particularly a molecular walker to remain attached to its track, i.e. to migrate along, or pull through, a molecular scaffold for more than a single motor cycle. Mechanistically this is not trivial to achieve, since molecular walkers, unlike their macroscopic counterparts, cannot rely on gravity in order to remain attached to their track. Not all molecular motors operate in a processive manner, most non-processive motors can, however, only perform work when operating in large ensembles.

(ii) *Directionality*: implies that, as long as an energy input is present, the molecular motor migrates in only one direction of a molecular track, pumps ions in only one distinct direction or rotates either clockwise or counter-clockwise.

(iii) *Autonomous operation*: the ability of the molecular motor to continually function as long as an energy input is present, i.e. without external intervention such as the application of a sequence of stimuli. Autonomous operation is a necessity in the biochemical environment of the cell, where fuel is always available.

(iv) *Repetitive operation*: the motor's property to repeatedly perform similar mechanical cycles.

(v) *Progressive operation*: the ability of the molecular motor to be reset at the end of each mechanical cycle without undoing the physical task that was originally performed.

1.3.1 Nature's Pack Horses: Myosins, Dyneins and Kinesins

Motor proteins from the myosin,[19] dynein[20] and kinesin[21] superfamilies move along cytoskeletal polymers to transport various cellular cargos, including membranous organelles, protein complexes and mRNAs. The cytoskeletal is formed by two types of polymers: microtubules and actin filaments. Microtubules[22] are linear, rigid structures, consisting of 13 linear polymeric protofilaments, which when wrapped together constitute a cylindrical tube. Each protofilament is formed by polymerisation of α and β tubuline units, a process that is reversible and highly dynamic. Actin filaments are formed by dynamic polymerisation of actin units, which leads to a scaffold with helical geometry. Transport along microtubule filaments is mediated by kinesins (mostly moving towards the 'plus' ends, i.e. the cell periphery) and dyneins (which move towards the 'minus' ends, i.e. the cell nucleus), whereas myosins transport cargo along actin filaments.[23]

Myosin, dynein and kinesin motors are ATPases, i.e. they convert chemical energy derived from ATP hydrolysis into mechanical work. Precise spatial and temporal regulation of motor-based transport is essential to ensure efficient cargo delivery. In light of their diverse cellular roles, it is not surprising that defects in motor-dependent transport are associated with a large range of diseases, including neurodegeneration, tumorigenesis and developmental defects.[16b] Not all members of the myosin, kinesin or dynein families, however, exhibit the same motor characteristics. In mammals, for example, 40 distinguishable kinesins, 40 myosins and more than 12 dyneins can be found.[16c]

In the context of this thesis, which is concerned with the design and operation of synthetic molecular walkers, there are two important questions relating to the molecular mechanisms behind the complex operation of cytoskeletal protein motors:

(i) How do (almost all) cytoskeletal protein motors achieve near perfect directionality?

(ii) How do (most) cytoskeletal protein motors achieve high processivity?

Conventional myosin (also: myosin-II), for example, is a directional, but non-processive motor. The motor mechanism features attachment to the actin track, exerting a force of several pN on the filament,[16c] and rapid detachment from the track after only one cycle of ATP hydrolysis. Thus to achieve motor operation, it must work in large groups, constituting the so called sarcomeric ensemble[16c]. If myosin remained attached to its

track for more than one cycle, the whole process would be slowed, thus it is in this case the lack of processivity that makes this motor protein effective.

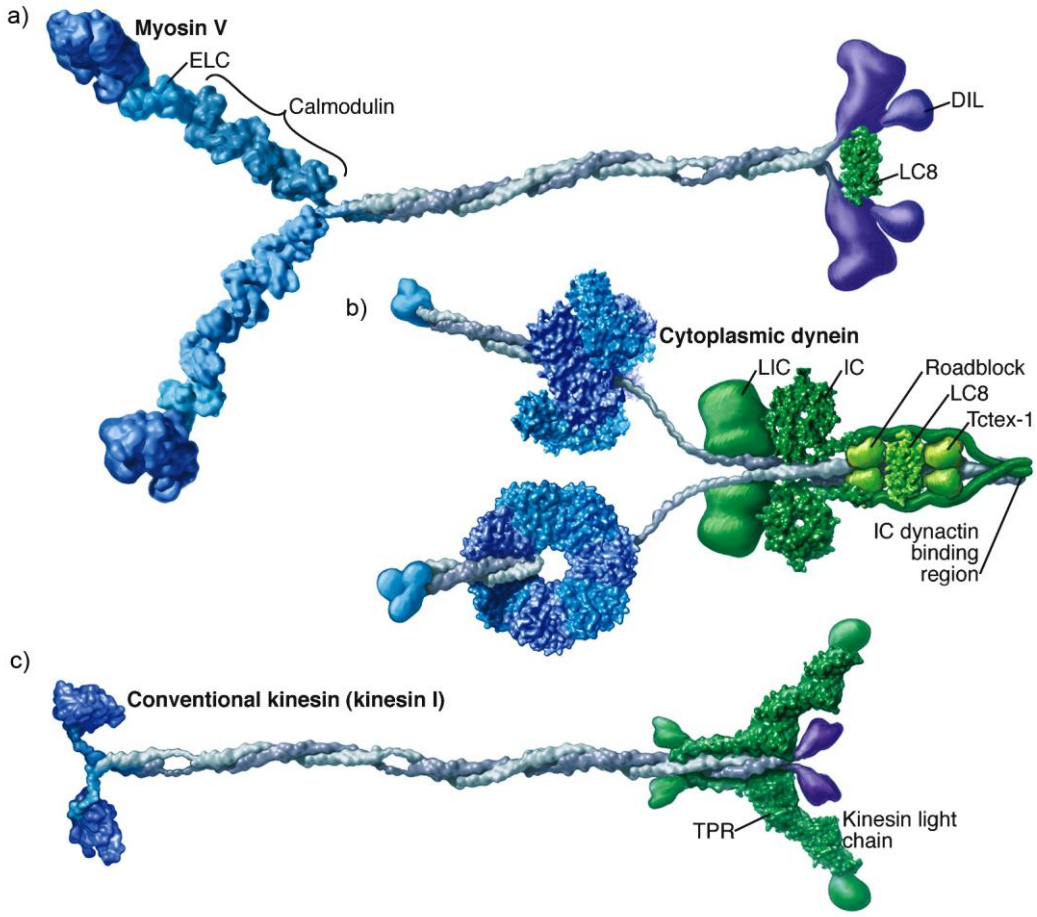

Figure 1.2. *Three processive motor proteins, representing the three major superfamilies: a) Myosin-V; b) Cytoplasmic dynein; c) Conventional kinesin. Structures based on atomic resolution structures[16b]. Colour coding: blue: motor domains; light blue: mechanical amplifiers; purple: cargo attachment site; green: associated motor units. Reproduced with permission (Cell Press).*

Myosin-V (Figure 1.2a) on the other hand is a processive member of the myosin family, which remains attached to its actin track for many consecutive steps.[24] This behaviour reflects the cellular function of the motor, as myosin-V is responsible for long-range organelle transport towards the minus-end of the actin filaments. The main mechanistic difference between the two processive and non-processive myosins is that in myosin-V both motor heads (or 'feet') are involved in track binding, while in myosin-II only one head binds to the track.

The involvement of two track-binding elements is, however, neither a necessary, nor a sufficient requirement for the emergence of processivity. KIF1A, for example, is a monomeric (single-foot) kinesin motor protein that walks processively along

microtubules.[21e] In the case of KIF1A, processivity is maintained through secondary interactions between its only foot and the track. The translocation of KIF1A thus resembles more of a sliding than a walking movement. Alternatively, dimeric motor proteins like kinesin-I (Figure 1.2c) and myosin-V (Figure 1.2a) maintain processivity by coordinating the actions of their two feet, so that at any time during the catalytic cycle at least one of the two feet is bound strongly to the track. This is particularly impressive for kinesin, which achieves this remarkable behaviour despite both feet being chemically identical (see section 1.3.2).

Whereas the mechanism to preserve processivity is quite different between the different motor protein families, the mechanism that confers directional bias to the walking mechanism is very similar in myosins, dyneins and kinesins. In each case, a small conformational change that occurs at the motor domain during a specific stage of the ATP hydrolysis cycle is transduced into a large-amplitude motion in the forward direction. Figure 1.3 shows this process schematically for myosin, kinesin and dynein, while highlighting the subtle differences in the respective mechanisms. In myosin (Figure 1.3a) the release of inorganic phosphate (P_i) triggers a conformational change in the motor domain that is conveyed to a long and rigid lever arm (light blue region in Figure 1.2). As a result, this lever arm is immediately propelled 25 nm forward towards the next binding site. Thermal diffusion of the detached foot is believed to play only a minor role in this 'power-stroke' mechanism.[16d] The mechanism found in kinesins is very similar (Figure 1.3b) and the motor domains in kinesins and myosins have been shown to be essentially identical,[25] with only two notable differences. (i) For kinesin, the crucial conformational change occurs during ATP binding, not phosphate release; and (ii) in kinesin the element that acts as a mechanical amplifier is flexible, which indicates that a power-stroke mechanism can only marginally be involved. The exact details of the mechanochemical processes that occur in dynein are still not understood in detail (Figure 1.3c).

As kinesin is the inspiration for the projects described in this thesis, the next section will describe its walking mechanism in detail.

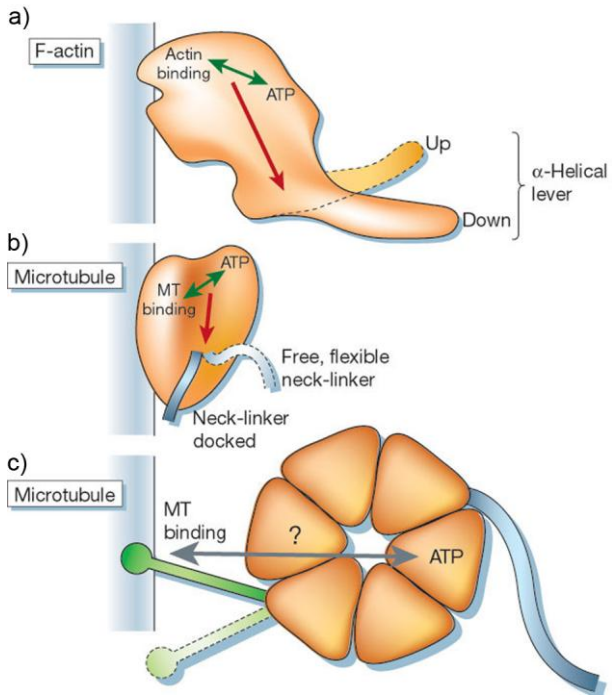

Figure 1.3. *Generation of unidirectional movement during the ATP hydrolysis cycle of cytoskeletal motor proteins.[16c] a) Myosin: a conformational change in the motor domain triggers the large-amplitude swing of a long rigid lever arm (Power-stroke mechanism); b) kinesin: a conformational change triggers forward-directed docking of the flexible neck-linker to the motor domain; c) dynein: details are still unclear, but the mechanism most likely resembles the one for myosin or kinesin. Reproduced with permission (Nature Publishing Group).[16c]*

1.3.2 Kinesin-I

Kinesin-I (also known as conventional kinesin and in the following also referred to as kinesin) was first isolated in 1985 by Ronald Vale,[26] whose laboratory has significantly contributed to the vast body of knowledge that is available now.[27,28] Conventional kinesin can be extracted in relatively large quantities from the brain.[27b] For this practical reason it is the most studied member of the superfamily, which is why it serves as a gold standard to which the properties of other family members are compared. Kinesin is a homodimeric protein consisting of two chains of 120 to 130 kDa each. The dimer comprises three distinct regions (see Figure 1.4): (i) a tail that is responsible for cargo binding and most likely plays a part in the regulation of the motor activity;[27a] (ii) an intertwined stalk, which is mostly responsible for the dimeric nature of kinesin, but may also play a subtle role in the motor mechanism; (iii) two identical heads (350 amino acids each) which are responsible for ATP hydrolysis and binding to the microtubular track. From a mechanistic point of view, the ATP hydrolysis domain and the neck and hinge region (see Figure 1.4) are particularly important.

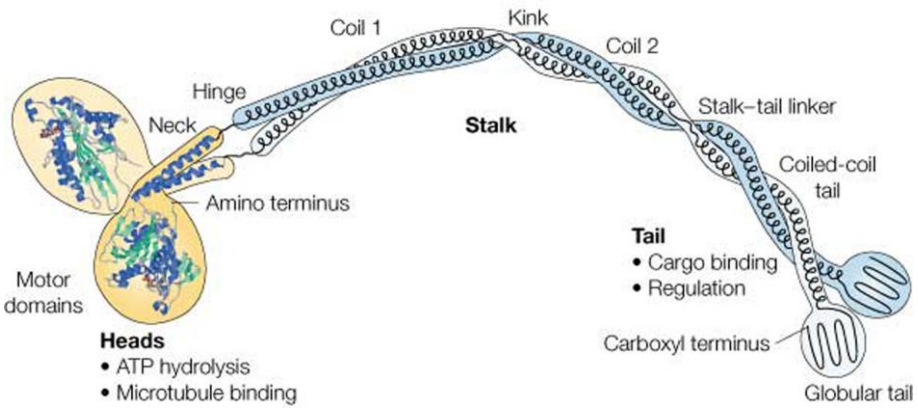

Figure 1.4. *Conventional kinesin has three distinct domains: heads stalk and tail. Based on solid state structural data.[29] Reproduced with permission (Nature Publishing Group).[27a]*

It has been established soon after its discovery that kinesin migrates along the microtubular tracks with high processivity. For example, an average run length of ~1 mm, which corresponds to ~100 steps, has been found in optical trapping experiments.[28a,b,f,30] Similar experiments have shown that the length of individual steps is 8 nm,[28h] which corresponds exactly to the smallest distance between two binding sites (α/β-tubuline dimers) on the polymeric track. The mechanism of kinesin's gait has, however, remained controversial until recently, due to initially conflicting experimental results. Theoretically, a molecular biped with two identical feet can walk along a track in three different ways: (i) symmetric hand-over-hand (where the two feet exchange leading and trailing positions, but alternate steps are identical); (ii) asymmetric hand-over-hand (where the two feet exchange leading and trailing positions, but alternate steps differ mechanistically); and (iii) inchworm (where one head is always leading). On one hand it was found that kinesin does not rotate its stalk while walking along the microtubule, a result that was interpreted in favour of the inchworm mechanism.[28h] Fluorophore foot labelling experiments, however, have shown that each motor domain moves in steps of 16 nm,[28p] an observation that strongly points towards a hand-over-hand mechanism (kinesin's centroid would still move 8 nm per step, as earlier experiments have shown). The asymmetric hand-over-hand mechanism supports both observations and evidence has been found for a 'limping' that occurs during every second step.[28o] One reason why kinesin might have adapted an asymmetric rather than a symmetric hand-over-hand mechanism might be that a constant rotation of the stalk with the cargo attached would be energetically disfavoured (kinesin has been shown to operate with >50% efficiency[31]). It is still unclear, however, how asymmetric stepping (i.e. alternate 'limping') is achieved, but

torsional effects in the head or coiled-coil region have been named as possible explanations.[21b]

Two questions remain, however, that biophysicists are currently trying to answer: What is the molecular basis for kinesin's behaviour and in particular, how does kinesin, with two identical feet, achieve processivity and directionality?

While many details are still under debate, Block has recently proposed a "consensus model",[21b] which will be explained below (see Figure 1.5):

1. **Resting state** (Figure 1.5, I and II). For the situation where one motor domain is bound to ADP and the other motor domain is vacant, an equilibrium between two conformers has been found (I and II in Figure 1.5). In both conformers, the foot including the vacant motor domain (yellow in Figure 1.5, lhs) binds strongly with the track. In conformer I, the ADP bound foot interacts with the track, which results in a certain amount of ring strain in the neck-linker region. In conformer II, which represents the only unstrained intermediate in the catalytic cycle, the ADP bound foot is detached from the microtubule. Toprak et al.[28u] have determined an equilibrium constant between I and II of ~1.4 (k_1/k_{-1}).

2. **ATP binding** (Figure 1.5, II→III)**.** There is evidence to suggest that ATP binding in the leading foot is only possible in the absence of strain (only in conformer II in Figure 1.5). This strain gate coordinates the actions of the two feet, which is responsible for kinesin's high processivity.

3. **Neck linker docking** (Figure 1.5, II→III). The binding of ATP releases significant energy, which drives a conformational change that results in docking of the neck linker to the motor domain. This leads to a small (~1-2 nm) movement of the rear foot towards the plus-end of the microtubule (power-stroke).

4. **Diffusional search** (Figure 1.5, II→III). The unbound foot can now undertake a diffusional search for the next forward binding site, in order to complete the ~16 nm step. At this stage, there is a finite probability of the foot to attach to the rearward binding site again, but the neck-linker docking[28j] makes the forward stepping energetically more favourable. Such a mechanism, which makes use of a combination of an asymmetric energy potential (here: through neck-linker docking) and the omnipresent thermal motion (here: foot diffusion) is called a Brownian ratchet mechanism.[5] The feet have now swapped the relative position and the centroid of kinesin has moved by 8.2 nm, which corresponds to the

microtubulin dimer repeat distance. The transition from state II to state III (Figure 1.5) proceeds much faster than the other steps (indicated by reaction arrow width in Figure 1.5), which is an important factor for the high processivity of kinesin.

5. **ADP release** (Figure 1.5, III→IV). After the purple foot has reached the forward binding site (state III in Fig), ADP is released, which leads to tight binding with the microtubule and ring strain (communicated through the neck linker or the microtubule). The strain suppresses premature binding of ATP to the leading foot before the rear foot had a chance to hydrolyse its own ATP.

6. **P_i release** (Figure 1.5, IV→I). The release of inorganic phosphate completes the catalytic cycle.

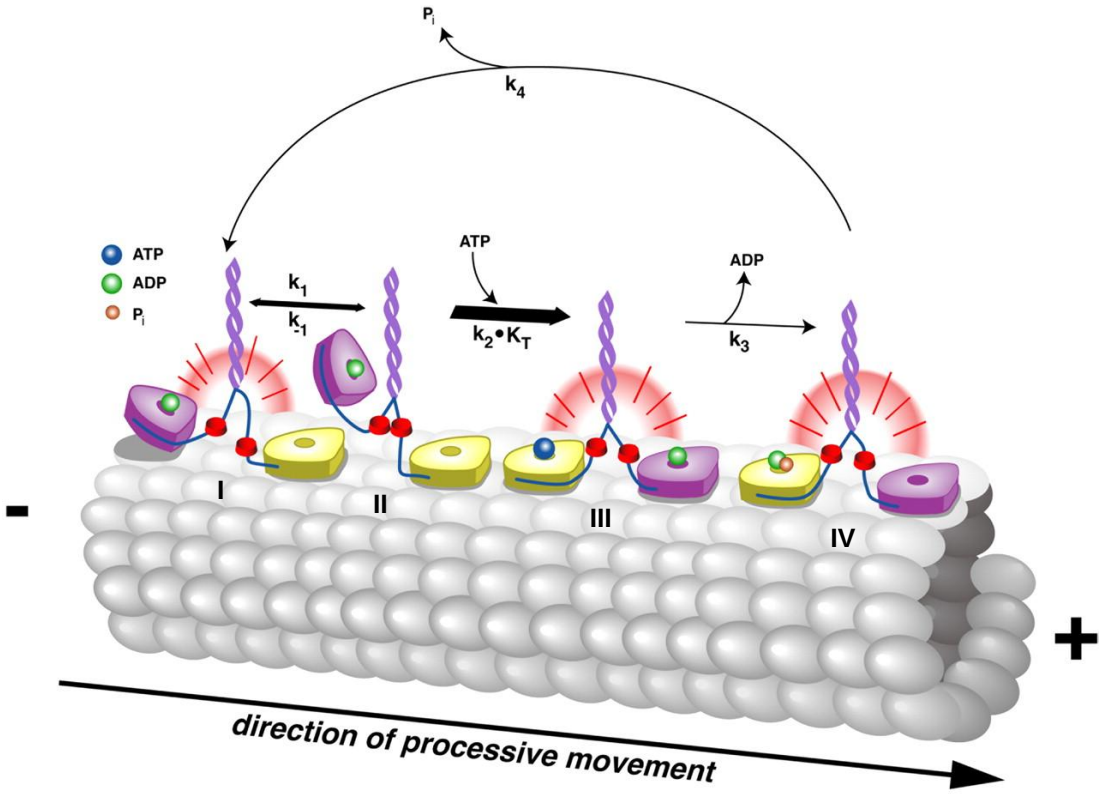

Figure 1.5. *Schematic illustration of the kinesin mechanochemical cycle. Reproduced with permission (National Academy of Sciences of the United States of America).*[28u]

In summary, kinesin's high processivity is a result of a strain-related gating mechanism that keeps the biochemical cycles of its two feet strictly out of phase. The directional bias mainly stems from a Brownian ratchet mechanism that is powered by the ATP-induced docking of the neck-linker to the leading head. Since both feet are identical, it is the interaction between the feet and the track that is crucial for both the achievement of processivity (the important strain gate is only possible since both feet do not 'fit'

perfectly on two neighbouring α/β-tubuline dimers) and directionality (neck-linker docking creates bias towards plus end of the polymer).

1.4 Design Principles for Synthetic Molecular Walkers

The complex biological molecular walkers presented in section 1.3 have emerged over the course of millions of years through a process of random molecular mutations and natural (molecular) selection. Experimental scientists intending to create and study synthetic molecular walkers must, however, carefully design their systems, particularly in light of the motor characteristics processivity, directionality and autonomous operation (for definitions see page 6).

1.4.1 Processivity–Interaction between Feet, Fuel and Track

Nature has produced both processive and non-processive translational motor proteins. The latter can, however, only perform useful work when operating in large ensembles. Such a sophisticated cooperation between several synthetic motor molecules appears difficult to realise, and, in fact, there is no literature precedence for an artificial rotary or linear molecular motor that is non-processive, but can still perform work. Thus in the design of a synthetic molecular walker processivity is highly desirable.

To preserve processivity, complete detachment of the walker moiety must be prevented by having one foot connected to the molecular track at all times. This can be realised by having two chemically different feet and two strictly mutually exclusive reaction conditions (fuels) for foot labilisation (Figure 1.6a). The two feet could, however, be chemically equivalent (as in kinesin-I), provided the interaction of the feet with the track renders the feet chemically inequivalent (Figure 1.6b). Another requirement for processivity is that a walker should never be able to form a 'bridge' between several tracks (i.e. swap tracks). In biological systems this is guaranteed by the polymeric nature of microtubules or actin filaments. In artificial systems this could also be realised by applying very dilute reaction conditions or by tethering the track or the walker to a surface. For molecular walkers with only one foot (biological example: KIF1A), secondary interactions between the foot and the track are essential for processivity (Figure 1.6c). The mode of action is thus rather a sliding than a walking along a track. Aside from this semantic issue, it has to be doubted if a mechanism for good directional bias is viable for a one-legged molecular walker/slider (even nature (KIF1A) has not found a solution to achieve this). Finally, processivity could also be realised in a device with more than two legs. A 'spider-walker' with several

simultaneously dynamic feet could migrate with relatively high processivity along a track with the probability for detachment being a statistical function of the number of legs.

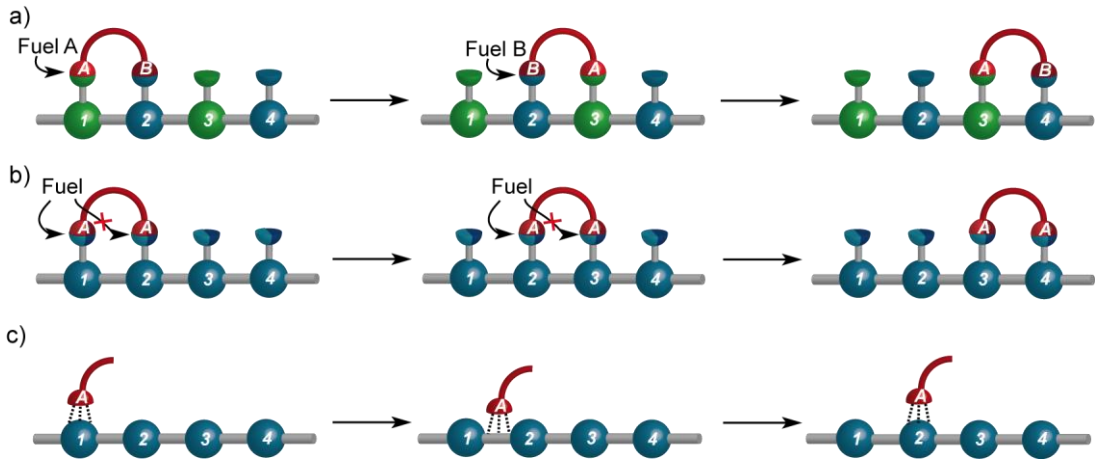

Figure 1.6. *Three possible strategies to confer processivity on the walker migration: a) two different feet and two different reaction conditions/fuels; b) two identical feet, but an interaction with the track that renders the breaks the symmetry between the feet and makes one foot significantly more susceptible to the fuel; c) one-legged walker that relies on secondary (tether) interactions (indicated by dashed lines) with the track.*

1.4.2 Directionality – Brownian Ratchet Mechanisms

The fact that all biological molecular walkers operate with directional bias towards one end of the respective track indicates that directionality is the most important characteristic of a translational molecular motor. In fact, a molecule that migrates in both directions of a track with equal probability, could not be considered a motor (it does not create net-mechanical work) and, more importantly, it could not perform any useful task (such as transporting cargo to the periphery of the cell).

While biological molecular walkers, such as kinesin-I, myosin-V or KIF1A can provide some valuable ideas for how to realise processivity in artificial analogues (see section 1.4.1), it is doubtful if nature can also teach synthetic chemists how to realise significant directional bias. The reason for this is that the molecular design and the (allosteric) operating mechanisms in nature's protein motors are so complex that, at present, they are hardly understood in detail. The most valuable information for devising synthetic molecular motors thus comes from theoretical physics and in particular from the field of non-equilibrium statistical mechanics.

The Principle of Detailed Balance[32] states that, at equilibrium, transitions between any two states take place in either direction at the same rate. For molecular walkers, this

implies that at equilibrium no directional walker migration can occur and that for the emergence of directionality detailed balance must be broken (i.e. the equilibrium state must be disturbed), for which an energy input will be necessary. At first sight, one might think that this energy input could be provided by the abundant Brownian motion. This would, however, correspond to a molecular version of a perfect heat engine, which is impossible according to the second law of thermodynamics[33] that precludes the spontaneous emergence of heat gradients. So, how can directed movement at the molecular scale be achieved? During the past decade, theoretical physicists have developed a theory (usually referred to as Brownian ratchet theory[34]), which successfully explains the motor behaviour of both biological and synthetic molecular motors.[17,18,35] According to Brownian ratchet theory, there are three fundamental requirements for the emergence of directed transport of a Brownian particle.[5]

(i) **A randomizing element**: this is provided by Brownian motion in all molecular-scale motors, biological or synthetic).

(ii) **An energy input**: in biological systems this is often supplied by ATP hydrolysis; however in synthetic systems many other forms of energy input are conceivable.

(iii) **An asymmetric potential** of energy or information in the direction in which the motion occurs.

Many different theoretical variations based on these three requirements have been discussed in the physics literature, with a particularly extensive account provided by Reimann in 2002.[34g] For the design of synthetic molecular motors, it is beneficial to distinguish between two general classes of ratchet mechanisms: energy ratchets and information ratchets.

In an energy ratchet mechanism, the potential energy surface is perturbed periodically in a way that involves both the thermodynamic minima and kinetic barriers experienced by the Brownian particle. In the example shown in Figure 1.7, a Brownian particle (shown in red) experiences an asymmetric potential energy surface, consisting of a periodic series of two different minima and two different maxima. By simultaneously (or sequentially) reversing the relative position of the two pairs of thermodynamic minima and the kinetic barriers, the particle is transported predominantly from left to right (occasional transport over a barrier in the wrong

direction can occur). Importantly, the direction of particle migration depends on the relationship between the thermodynamic minima and the kinetic barriers. In Figure 1.7, for example, the purple and blue relative minima always have the taller kinetic barrier to their left. It is theoretically possible that in a single molecular system this relationship of thermodynamic minima and kinetic barriers can be inverted, resulting in particle transport in the opposite direction. A molecular walker which operates by such a mechanism is discussed in Chapter V. In addition to this, several synthetic catenane- and rotaxane-based molecular motors have been reported, which operate through Brownian energy ratchet mechanisms.[36]

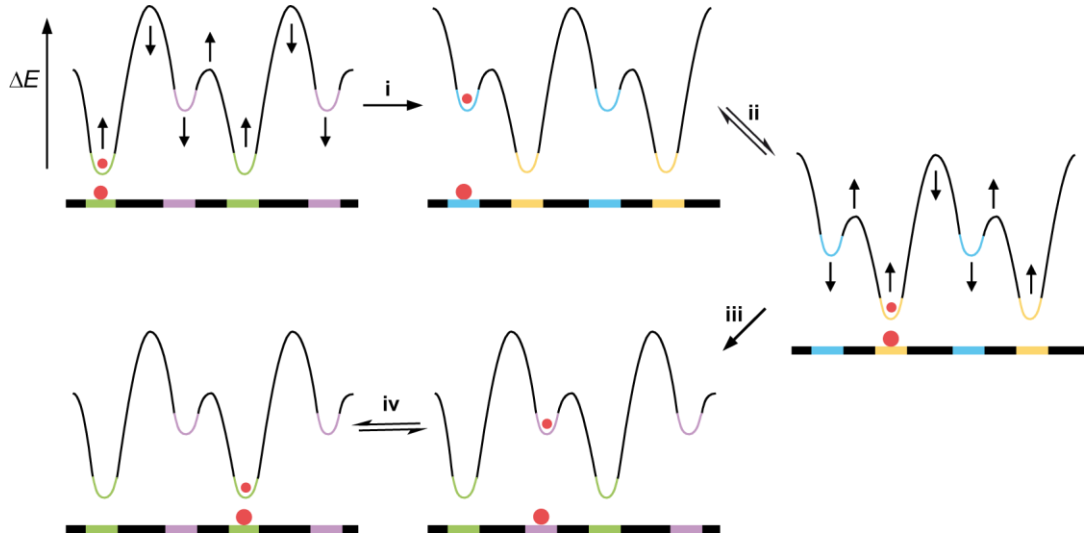

Figure 1.7. *A flashing type of Brownian energy ratchet mechanism. Sequential manipulation of the thermodynamic minima and kinetic barriers experienced by a Brownian particle (indicated by red dot). Inversion of the relationship between steps i+ii and iii+iv would result in transport in the opposite direction.*

The difference between an energy ratchet mechanism and an information ratchet mechanism is that in the latter the thermodynamic minima along the trajectory of the Brownian particle remain unaltered. The key for achieving directional transport must therefore lie in the kinetic barriers between the thermodynamic minima (or in an interaction of the particle with the barriers). In Figure 1.8 an example is illustrated in which information on the position of the particle is communicated to the kinetic barrier. The particle starts in one of the identical energy wells and can communicate its presence only to the kinetic barrier to its right. As a result, the barrier is lowered and Brownian motion allows the particle to sample both wells, resulting in a 50:50 distribution between the two states. After the barriers are raised, the process is repeated. Although one unbiased reversible step is involved (ii), this mechanism leads

to directed movement, because a backward step is impossible (probability for steps forward = ½; probability for steps backward = 0). To date, only two examples for rotaxane-based information ratchet motors have been reported.[37] In one example, a macrocycle can only from one side of a stilbene gate effectively communicate with the gate (and open it), which leads to a disproportionately high amount of macrocycles on the station that is spatially remote from the gate.[37a] In another example, a kinetically controlled gating reaction at the centre of the track leads to an uneven distribution of isoenergetic enantiomers when a chiral catalyst was employed.[37b] Two molecular walker systems which operate through a Brownian information ratchet mechanism are described in Chapters III and IV.

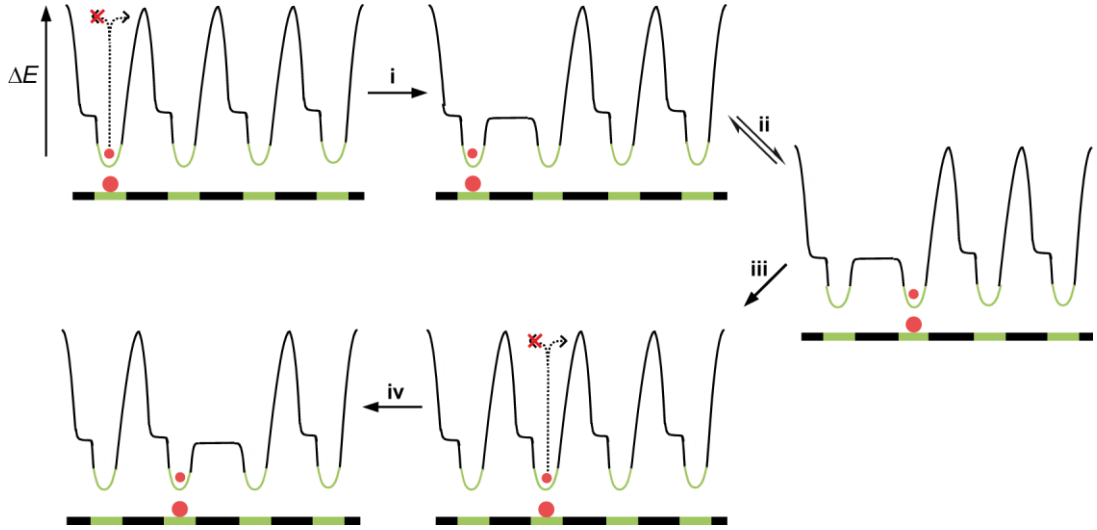

Figure 1.8. *An information ratchet mechanism leading to linear transport of a Brownian particle (in bright red) along an asymmetric potential energy surface. Asymmetry in the relative height of the kinetic barriers results from an information transfer between the particle and the barrier (indicated by dotted arrows).*

Having established the theoretical aspect of the mechanisms that can lead to directional walker migration, the question arises how the two major ratchet mechanisms can be realised in practice.

In Figure 1.9 four possibilities are illustrated for the achievement of directional bias in bipedal walker-track systems.

The first possibility (Figure 1.9a) features fully reversible foot detachment and rebinding processes and corresponds to the mechanism adopted by biological walkers such as kinesin. Key for achieving directional bias is the conversion of a high-energy fuel X to low-energy fuel waste product Y, which must be coupled to a stride of the walker moiety in the forward direction. The driving force behind directional bias is the

corresponding gain in free energy. This mode of action, where the walker unit acts as a catalyst for the reaction of X to Y is viable for bipeds with two different (Figure 1.9a; A≠B; i≠ii; X≠X'; Y≠Y'; operation autonomous or by sequential fuel addition) or two identical feet (Figure 1.9a; A=B; i=ii; X=X'; Y=Y'; operation necessarily autonomous). Since this process does not involve a manipulation of the ground state energies of the walker-track conjugates (the depicted resting states are isoenergetic), this would correspond to an information ratchet mechanism.[38]

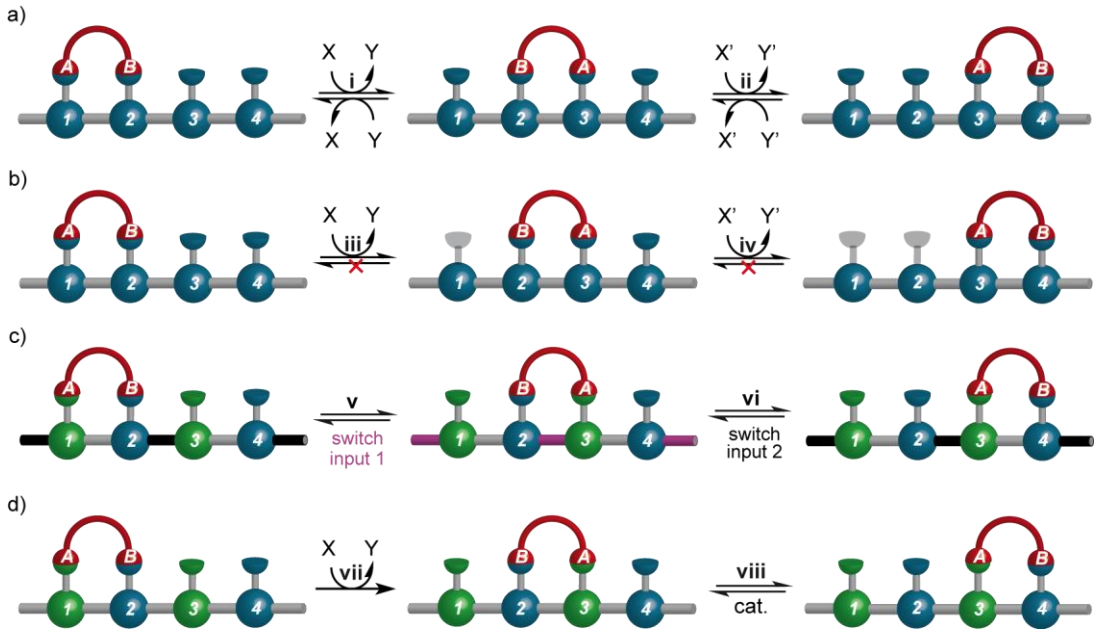

Figure 1.9. *Four possible strategies to confer directionality on the walker migration: a) Reversible foot exchange coupled to consumption of stoichiometric, complex fuel X (an information ratchet mechanism). Feet can be identical (coordination required) or different; b) A burnt-bridges walker catalyses the decomposition of the footholds, thus rendering any step in the forward direction essentially irreversible (an information ratchet mechanism); feet can be identical (coordination required)) or different; b) Reversible migration processes that can be induced by catalytic reagents, but require energy input through switching stimulus (an energy ratchet mechanism). Feet have to be different; d) One (or more) irreversible, kinetically controlled, migration process under condition vii (an information ratchet mechanism). Feet have to be different.*

Directional bias (Figure 1.9b) can also be realised in a so called 'burnt-bridges' walker. If the walker unit starts from one end of the track and destroys the footholds it was attached to upon forward movement, this makes any stride forward irreversible, which will eventually result in the walker unit being transported to the end of the track. Since a burnt-bridge walker reduces the entropy of the system, an energy input is also required. The energy input acts as a fuel for the foothold destruction reaction, for which the walker unit only acts as catalyst. A walker-track system whose directional bias is entirely based on a burnt-bridges mode of action (formally an information ratchet

mechanism) does however come with two important disadvantages. Firstly, the track cannot be reused (or needs a reset operation) and, secondly, if the walker unit starts from a position somewhere in the middle of the track, it will migrate in a random (not necessarily the desired) direction.

In a walker with two different feet, directional bias is also viable when the two migration processes (v, vi) are fully reversible (Figure 1.9c), as long as there is a switchable element in either the track or the walker unit. The switch could be used to raise the ground state energy of states where one particular foot is leading (e.g. the state where foot A is leading and the walker resides on the purple track linkage could be energetically less favoured; middle of Figure 1.9c), which, together with a control of the kinetic barriers, leads to movement in only one direction. This corresponds to a classic energy ratchet mechanism (see Figure 1.7).

Finally, directionality can also be achieved if one or more of the feet migration processes are irreversible (Figure 1.9d). Thus the stepping outcome is kinetically controlled and not a function of the ground state energies of the two walking states, but a function of the different activation barriers. For example, if during the irreversible step (vii) a high-energy macrocycle could be formed, which in the subsequent reversible step (viii) is mostly converted to the low-energy macrocycle, a net-directional bias towards the right end of the track would result. Such a behaviour corresponds to an information ratchet mechanism (see Figure 1.8). This mode of action could, however, only be realised in a walker system where the two feet can be addressed separately (sequential mode of operation).

1.4.3 Autonomous Operation – Coordination between Feet

The activity of cytoskeletal motor proteins is regulated through allosteric mechanisms and not through alternating the presence or absence of fuel. As the fuel for biological motors (ATP) is present at all times, this means that they operate in an autonomous manner. If autonomous operation is to be achieved in an artificial molecular walker, that is intended to be processive, the action of the two feet must be coordinated (otherwise both feet could coordinate fuel and detach). This means that a structural gate (e.g. in the track) must guarantee that, when one foot is detached, the other cannot dissociate from the track at the same time.

However, sequential operation can also offer important benefits (as opposed to autonomous operation): (i) the walker migration can proceed in both directions of the

molecular track (no natural or artificial autonomous walking devices achieve this); (ii) the rate of oscillation of the reaction conditions and thus the speed of walker migration can be controlled; (iii) the walker migration can be stopped at any time which allows the travel distance of the walker to be controlled.

1.5 DNA-Based Molecular Walkers

Since 2004, a number of molecular walker-track systems, which are either in part or entirely assembled from DNA building blocks, have been reported. These DNA-walkers[7] are genuine mimicks of kinesin-I, since they exhibit all four of the fundamental characteristics of translational molecular motors; namely progressive, repetititve, processive and directionally biased transport of a molecular fragment (walker unit) along a track (see section 1.3).

There are, however, also reports of small-molecule systems[39] whose behaviour has been interpreted as 'molecular walking'. Nevertheless, none of these systems satisfy all four of the above criteria. Their dynamic behaviour either lacks processivity, or, more commonly, directional bias, which is why they are not included in the following overview.

1.5.1 Non-Autonomous DNA Walkers

The first example of a non-autonomous DNA walker, i.e. one that relies on the sequential addition of suitable chemical fuels, was described in 2004 by Sherman and Seeman.[7a] With the exception of psoralen and biotin tags, which both serve practical purposes, the entire walker-track system is constructed of DNA oligonucleotides. A double-stranded 'triple crossover'[40] DNA structure (in solid black; Figure 1.10a) serves as the rigid backbone of the track, from which three single stranded footholds of differing nucleotide sequence protrude (dark blue, green and light blue; Figure 1.10a). The biped is constructed of two double-stranded 'legs' (black; Figure 1.10a), two different single-stranded 'feet' (red and orange; psoralene tags in bright red; Figure 1.10a) and three flexible linker strands (black curved lines), which connect the two legs and remain single-stranded throughout all experiments. The starting position of the walker on the track is established in buffered aqueous solution at 16 °C[41] by the addition of anchor strands, which are partially complementary to the two strands in one foot/foothold pair. Anchor strand 1A (Figure 1.10a) for example is designed to be complementary to the single-stranded regions of foothold 1 and foot A, while anchor strand 2B matches foothold 2 and foot B. In contrast to biological walkers, such as

kinesin-I, Seeman's device does not rely on direct interactions between the walker and the track. Instead, the anchor strands, act as molecular Velcro, holding the walker and the track together through the effect of 20 cooperative base pair interactions.

After the first self-assembly step, the biped, anchor strands 1A and 2B and the track form an aggregate that is only metastable, because the anchor strands have been designed so that an overhang ('toehold' in Figure 1.10b) of eight bases remains unpaired. The overlapping toehold regions allow the removal of an anchor strand through a process called competitive hybridisation, which can be compared to the closing of one zipper at the cost of opening another. Fuel strand 2B, for example, can bind to the toehold region of the anchor strand and completely displace it from the foot, leaving a free foot behind. This process is powered by the free energy gained through the formation of eight new base pairs in the stable duplex waste[42] (average free energy gain per base pair ca. 1 kcal/mol[43]).

Once foot B is detached from the track (Figure 1.10c), it is free to diffuse within the restrictions imposed by the three single-stranded spacer strands (length ca. 2 nm). Addition of an anchor strand 3B can lead to reattachment of the leading foot to foothold 3 on the track (Figure 1.10d). Repetition of analogous detachment and anchoring procedures leads to a walker-track conjugate in which both feet have moved one foothold in the forward direction (Figure 1.10f). Seeman and co-workers have also demonstrated that their device can be induced to walk backwards.

The composition of the mixtures has been analysed by means of polyacrylamide gel electrophoresis (PAGE). Non-denaturing gels confirmed that monomeric walker-track conjugates were stable and represented the major component of the mixture throughout the experiments. Psoralene cross-linking led to the formation of characteristic fragments at each stage of the experiment, as observed by denaturing PAGE.

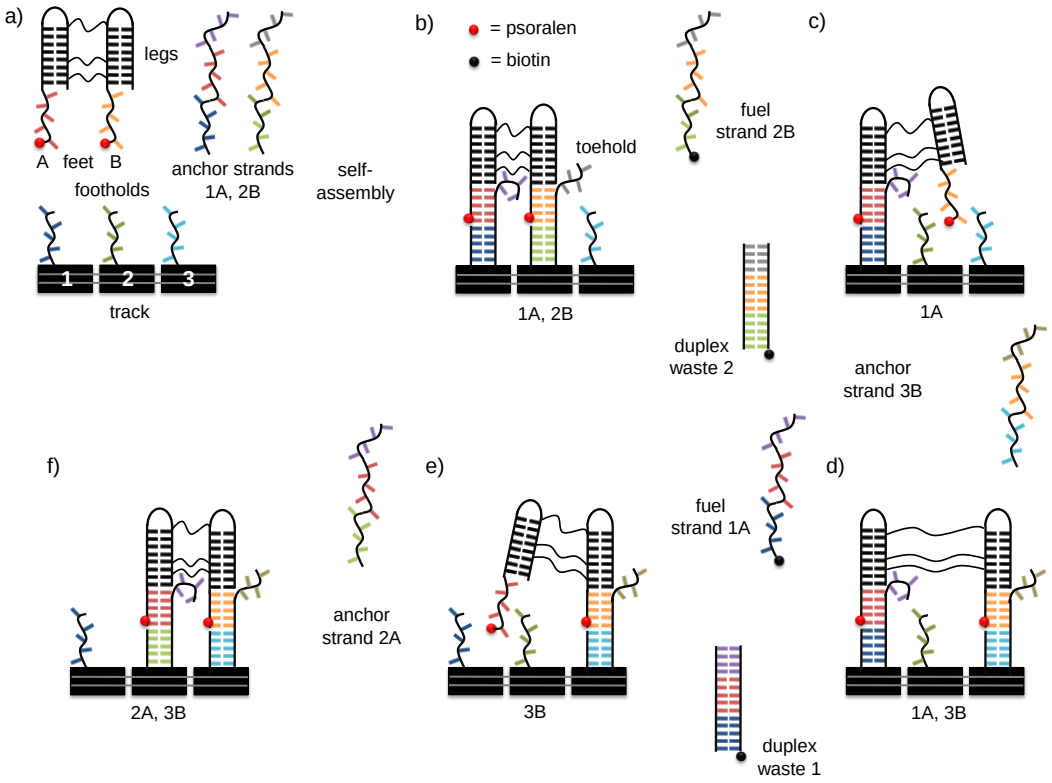

Figure 1.10. *Non-autonomous inchworm walker described by Sherman and Seeman.[7a] a) Self-assembly of the system from three components: rigid triple-crossover track featuring three protruding single-stranded footholds; walker including two single-stranded feet (featuring psoralene tags), separated by three single-stranded spacers; two anchor strands which act as molecular Velcro to attach the feet to the footholds; b) initial position of the walker on the track established by self-assembly; c) foot B released from track after detachment procedure (competitive hybridization); d) foot B attached to foothold 3 after addition of anchor strand 3B; e) foot A released from foothold 1; f) foot A anchored to foothold 2. Matching colours indicate complementary sequences between strands; lines indicating base pairing are purely schematic and do not represent a particular number of bases.*

From a mechanistic perspective, the walker migration depicted in Figure 1.10 is different from kinesin-I or myosin-V, since it corresponds to an inchworm (foot A is always leading), not a hand-over-hand gait.[5] The walker is, however, processive, because complete walker detachment is impossible at 16 °C and a scrambling of the walker moiety between different tracks is unlikely at the low concentrations applied (0.26 to 0.5 µM). The driving force for directional bias is supplied by the free energy gain resulting from the pairing of eight bases in the toehold region of an anchor strand with the complementary bases in a fuel strand (corresponding to a gain in free energy of ca. 8 kcal/mol[43]).

Shin and Pierce have reported on a conceptually very similar DNA-walker that, like kinesin, walks in a hand-over-hand gait.[7b] The design of the walker-track system is

more minimalistic, with the backbone of the track consisting of one linear double helix and the walker comprising two partially complementary oligonucleotides (see Figure 1.11a). The walker-track conjugate was assembled by the sequential addition of anchor strand 1A and anchor strand 2B to the walker and the track (Figure 1.11b). Foot A can be detached from the track through competitive hybridisation upon addition of a fuel strand, which allows foot A to bind to the third foothold of the track. Using four different anchor and fuel strands, Shin and Pierce were able to control their device and induce it to walk either direction down the track (Figure 1.11f).

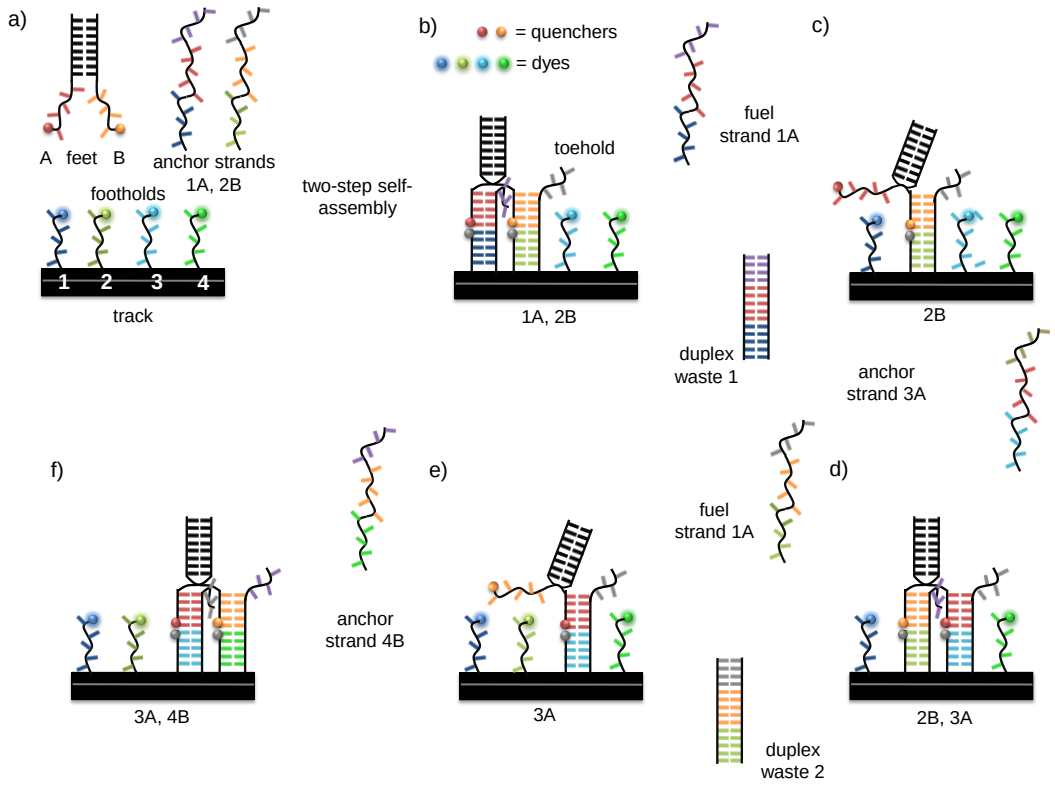

Figure 1.11. *Hand-over-hand DNA-walker described by Shin and Pierce.[7b] a) Self-assembly of the system from three components: rigid, double-stranded track featuring four protruding single-stranded footholds functionalised with fluorescence dyes; walker including two single-stranded feet (functionalised with quenchers), held together by duplex domain; two anchor strands which act as molecular Velcro to attach the feet to the footholds; b) initial position of the walker on the track established by stepwise self-assembly; c) foot A released from track after detachment procedure (competitive hybridization); d) foot A attached to foothold 3 after addition of anchor strand 3A; e) foot B released from foothold 2; f) foot B anchored to foothold 4. Matching colours indicate complementary sequences between strands; lines indicating base pairing are purely schematic and do not represent a particular number of bases.*

The progress of the walking experiments was analysed by non-denaturing PAGE and fluorescence spectroscopy. The terminus of each foothold was functionalised with a fluorescent dye of a characteristic emission wavelength, while each foot of the walker

unit was functionalised with an appropriate quencher (Figure 1.11b). Visualizing the gels with different fluorescent scans allowed deducing the position of the walker on the track. After foot A is attached to foothold 1, for example, the fluorescence of the dye on foothold 1 is almost entirely quenched, while the fluorescence of the dye on foothold 2 remains unaltered. Using multiplexed real-time fluorescent monitoring, Shin and Pierce were able to follow the process of the walking.

More recently, Seeman and coworkers[7h] have impressively demonstrated that both extending the DNA-based tracks and performing sophisticated tasks is possible with a DNA walker.[44] As a track, Seeman and co-workers assembled a large (ca. 300 nm wide) two-dimensional DNA origami[45] tile from a total of 202 DNA oligonucleotides. The origami tile was designed to exhibit 18 protruding single-stranded footholds and three large slots (Figure 1.12a). The footholds were positioned in a precise pattern on the DNA origami tile in order to allow a four-legged triangular DNA walker to perform an essentially one-dimensional locomotion of its centroid, while the walker's extremities rotate 120° during each step. The structure of the walker moiety, a tensegrity triangle organisation constructed from seven oligonucleotides, is shown in Figure 1.12b. The walker has four feet and three hands, all consisting of single-stranded DNA segments. As in the previously discussed systems, the walker is attached to the track through complementary anchor strands, featuring a toehold region. Figure 1.12c illustrates the transition of the walker from a three-foot-bound state to a two-foot-bound state, while the whole triangular shape rotates by an angle of 120°.

At three positions on its linear trajectory, the walker comes into proximity of the three cassettes, which carry different DNA-bound gold nanoparticles. The DNA machines on these cassettes are positional ON-OFF switches, which by the addition of fuel strands can be induced to either offer the gold cargo to a bypassing walker, or not. The mechanism of the cargo handover, a competitive hybridisation event, is illustrated in Figure 1.12d. The role of the fourth foot (F4) is to keep the walker in a conformation where one hand of the walker is in proximity to the cargo (F4 would not be needed for the translation/rotation of the walker). Depending on the state of the DNA cargo delivery machines (ON or OFF), the walker can thus assemble eight (2^3) different cargo combinations during the course of its journey.

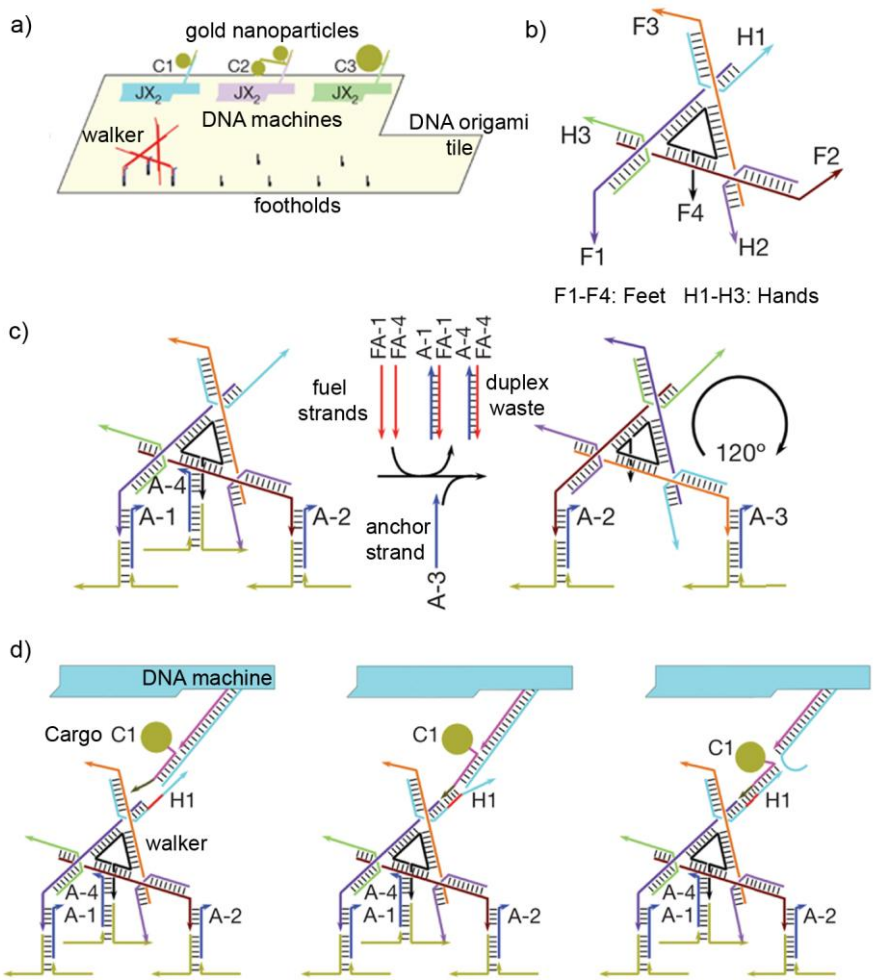

Figure 1.12. *Nanoscale assembly line published by Seeman and co-workers.[7h] a) Schematic illustration of the entire assembly, consisting of a large DNA origami tile (track), three cassettes each including a DNA ON-OFF switch which carry three different DNA-bound gold nanoparticles; triangular walker moiety; b) structure of the walker moiety, featuring seven single-stranded domains: four feet (F1 to F4) and three hands (H1 to H3); c) one 'stride' of the walker moiety, requiring the sequential addition of two fuel strands and one anchor strand (walker rotated by 120°), d) handover of DNA-bound cargo (C1) from the DNA machine to the walker. Adapted with permission (Nature Publishing Group).[7h]*

Seeman and co-workers have studied the dynamic processes of their device by polyacrylamide gel electrophoresis (PAGE), atomic force microscopy (AFM) and scanning electron microscopy (SEM). While AFM could not resolve several gold nanoparticles attached to one walker, but could be performed during the course of the experiments, SEM delivered higher resolution, but required isolation of the cargo-bound walkers after the experiments were completed. Through a statistical analysis of the SEM data, Seeman and co-workers were able to show that in each of the eight experiments the expected walker-cargo products were formed in yields of 75% to >90%.

1.5.2 Autonomous DNA Walkers

In 2004 and 2005 three reports of autonomous DNA walkers were published by the groups of Turberfield, Reif, Yan and Mao (Figure 1.13).[7c-e] In all three cases, the directional bias relied on the enzymatic cleavage of DNA or RNA strands the walker locomotion resembles more "a bucket being passed along a fire brigade"[46] rather than a hand-over-hand or inchworm gait of a biped.

The operation of the first autonomous walker, published by Turberfield, Reif and Yan,[7c] is illustrated in Figure 1.13a. The track consists of a DNA duplex to which three mainly double-stranded footholds are connected through a short single-stranded hinge (see Figure 1.13a). The walker (shown in red) consists of only six DNA nucleotides and is initially ligated to foothold 1 (Figure 1.13, state 1-W). In addition to the walker-track adduct, three enzymes were added to the buffer solution: a ligase (T4 ligase) and two restriction enzymes (PfIM I and BstAP I).

Owing to the flexible nature of the hinges, footholds 1 and 2 can hybridise their toehold regions (Figure 1.13a, 1-W 2), which allows T4 ligase to ligate the walker to foothold 2 (Figure 1.13a, 1-W-2). The ligation step creates a recognition site for one of the restriction enzymes (PfIM I), which selectively cuts the walker from foothold 1 (Figure 1.13a, 1 W-2). The energy required for this step, which represents the crucial process for the emergence of net-directionality, is supplied by ATP hydrolysis of the restriction enzyme. Repetition of the ligation and cleavage processes (with only restriction enzyme BstAP I recognising a cleavage site), leads to the partial formation of walker state W-3 (Figure 1.13a). The walker migration occurs with overall net-directionality, as there is no mechanism for the walker to take steps backward. Turberfield and colleagues have provided evidence for the processive and directional behaviour of their system using denaturing PAGE and a radioactively (γ-P^{32}) labelled walker unit.

In 2005, Turberfield and co-workers reported the design and operation of an autonomous 'burnt-bridges walker' that achieves directionality by destroying the track, as the walker moves forward.[7d] The system consists of a track with three almost identical footholds, a single-stranded DNA walker (shown in red in Figure 1.13b) and a single enzyme that cuts off the terminal part of a foothold only when the walker is attached to it. The employed enzyme, restriction nuclease N.BbvC IB, accomplishes this task by first recognising a particular sequence in a walker-foothold duplex, and then catalysing the hydrolysis of the foothold strand.

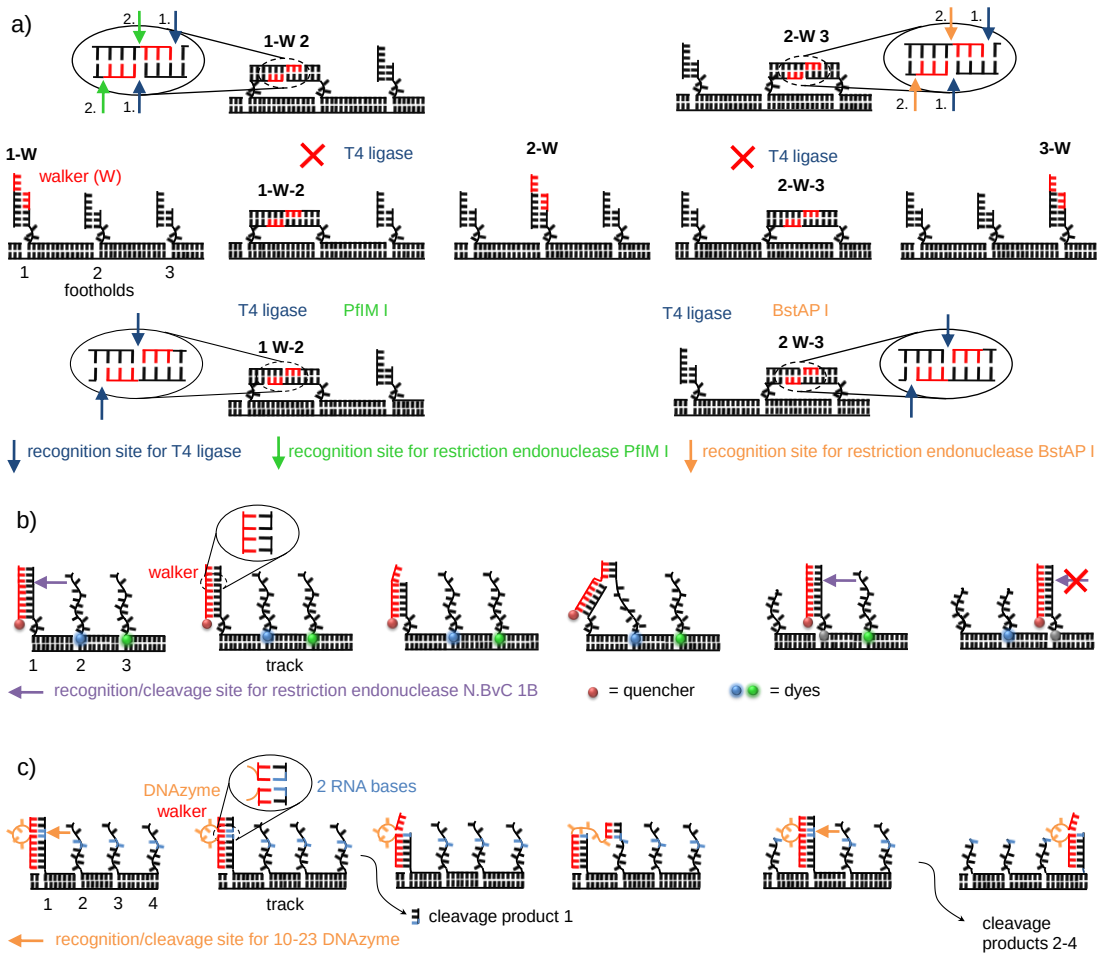

Figure 1.13. *Three different enzyme-dependent autonomous DNA walkers.[7c-e] a) Autonomous walker locomotion mediated by three enzymes, described by Turberfield and co-workers.[7c] The walker consists of six DNA bases (displayed in red). In the descriptions of the states, covalent attachment of the walker (W) to a foothold is indicated by a hyphen; lines indicating base pairing are purely schematic and do not represent a particular number of bases; b) Turberfield's autonomous 'burnt-bridges' walker, mediated by restriction endonuclease N.BvC 1B.[7d]; A walker unit consisting of 26 DNA bases (in red) indirectly destroys the track (provides recognition site for enzyme) while it is moving forward; lines indicating base paring are purely schematic and do not represent a particular number of bases; c) Mao's autonomous 'burnt-bridges' walker, mediated by a DNAzyme in the walker unit.[7e] The DNAzyme walker directly destroys the track while it is moving forward; lines indicating base pairing are purely schematic and do not represent a particular number of bases.*

When the walker is located on the left hand side of the track[47] (Figure 1.13b), the action of the restriction enzyme leads to the cleavage of a short (eight base) duplex at the terminus of the foothold, which is released into solution due to its melting temperature being considerably lower than the operating temperature of the motor. As the walker unit now possesses a toehold region that can reach the second foothold, competitive hybridisation results in the attachment of the walker to foothold two. A backward step is extremely unlikely, because attachment to the longer footholds is

connected with a ~10 kcal gain of free energy. The process is then repeated so that the walker will eventually be located on foothold 3, which, due to a sequence mismatch, is not cleaved by the applied enzyme (Figure 1.13c, right hand side). The partial hydrolysis of the first two footholds of the track provides the energy source for unidirectional walker transport. Turberfield and co-workers functionalised footholds 2 and 3 with two different fluororescence dyes and the walker with a quencher, which allowed the verification of the unidirectional behaviour of their system and the extraction of kinetic data.[48]

Mao and co-workers published a conceptually very similar burnt-bridges walker (Figure 1.13c),[7e] however in their case no external enzyme needs to be added, as the walker itself acts as the enzyme. The track is constructed of duplex DNA (shown in blue in Figure 1.13c) with four evenly spaced slightly different footholds, consisting of 21 DNA (shown in black) and 2 RNA (shown in blue) residues. The walker is a DNAzyme[49] capable of cleaving RNA strands with sequence specifity (catalytic core shown in orange in Figure 1.13c). Once the system is assembled in a convergent self-assembly step (Foothold 1/walker + footholds 2,3,4/Track), a reaction cascade occurs that is essentially identical to the previously described system (Figure 1.13b and c). One notable difference is that in Mao's system all footholds are susceptible to recognition by the DNAzyme, so that the final foothold is also hydrolysed. Mao and co-workers verified the unidirectional behaviour of their system by monitoring the time order in which the short single-stranded cleavage products appear (denaturing PAGE).

In 2007, Winfree, Rothemund and Pierce reported an autonomous polymerisation motor[50] reminiscent of the Rickettsia bacteria;[51] an intracellular pathogen, which achieves locomotion by polymerising actin moieties at their surface. The active motor component is a single-stranded DNA oligonucleotide that continuously catalyses the polymerisation of two hair pin fuels.[52] Although the movement of the motor domain is processive, the direction in which it occurs is random.

An enzyme-free, autonomous locomotion of a DNA fragment along a DNA track was described by Pierce in 2008.[53] Walker locomotion was achieved through the use of DNA hairpin[54] strands, but, due to the lack of coordination between the two feet, the process occurred with random directionality and low processivity.

The first enzyme-free, autonomous, processive and directional DNA walker was reported by the group of Turberfield in 2009 (Figure 1.14).[7f] This system is

reminiscent of kinesin-I, as it uses a strain gate between two identical feet to guarantee processivity. Directionality is achieved (see Figure 1.14), as it is impossible for both feet to hybridise completely to the track, which in turn results in the two feet consuming the fuel at different rates. The track consists of one single DNA oligonucleotide that features three partial binding sites for the walker feet (dark colour tones in Figure 1.14a). This minimalistic design of the track makes it impossible to extend Turberfield's system without obtaining folding products. The walker consists of two identical oligonucleotides that assemble to a joint double- (black and grey) and two single-stranded regions (feet A and A'; light colour tones).

When the two single-stranded feet of the walker are hybridised to the left hand side of the track (Figure 1.14a), the feet have to compete for binding to the track (highlighted by a black arrow in Figure 1.14a). Starting from this equilibrium, part of the left foot can be lifted from the track (Figure 1.14b), which reveals a toehold region that is complementary to the toehold region of one of the hairpin fuels (H1, Figure 1.14b). In a branch migration process, hairpin H1 displaces the left foot from the track, which in turn reveals a binding site for hairpin fuel H2 (Figure 1.14c). In the next step, hairpin H2 displaces hairpin H1 from the left foot (Figure 1.14d).

During this reaction sequence (Figure 1.14, i to iv), the left foot of the walker has catalysed the formation of duplex waste H1-H2[55]. The energy released by this process has allowed the left foot to detach from the track[56] (Figure 1.14d), so that it can either bind on the first or the third site of the track. Although this reattachment occurs without bias (50% attachment on either side), the overall process is directional, because the mechanism that has been discussed above (steps i to iv in Figure 1.14) is not possible when starting from state *2,3*, where the feet are attached to the right hand side of the track (Figure 1.14e). This kinetic effect is due to steric reasons (the toehold region that was exposed in the left foot in step 'ii' is sterically shielded in the case of the right foot) and results in the process *2,3→2* being 100 times slower than the process *1,2→2*. Turberfield and co-workers studied the dynamic behaviour of the full three-site system with PAGE and the kinetic behaviour of a smaller two-site model system with fluorescence spectroscopy.

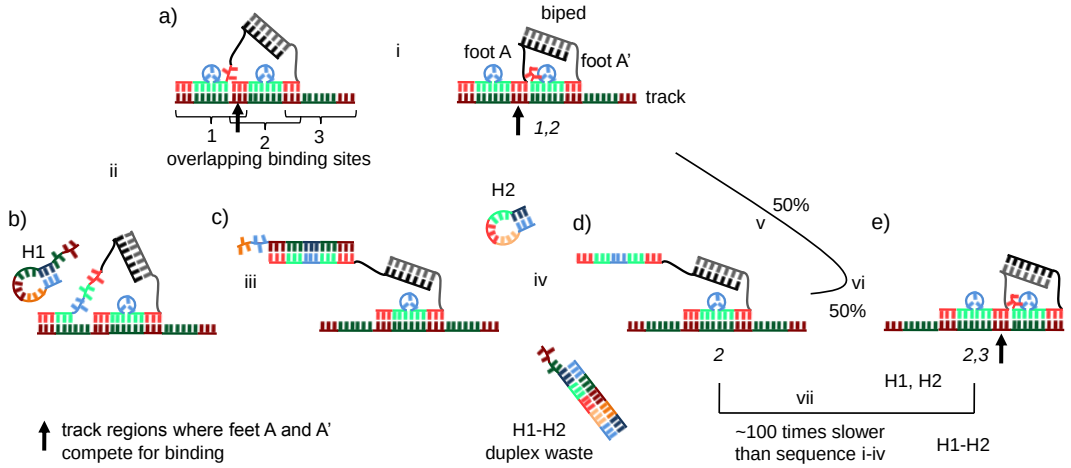

Figure 1.14. *Turberfield's autonomous, bipedal DNA walker, powered by two DNA hairpin fuels (H1 and H2).*[7f] *a) Equilbrium between two starting states that results from competition of the two walker feet over the binding site highlighted with an arrow; b) the left foot can partially lift from the track and expose a toehold, which is complementary to the toehold in fuel H1; c) branch migration leads to detachment of the left foot; d) fuel H2 can displace H1 from the left foot; intermediate 2 (shown for reasons of clarity) or an intermediate of the previous branch migration process can either rebind at site 1 or site 3, which occurs with statistical product distribution (50:50); e) starting from the 2,3 state, steric reasons preclude the mechanism shown in steps i to iv; the 2,3⟶2 process is therefore 100 times slower than 1,2⟶2; complementary nucleotide sequences are indicated by the use of light and dark colour tones (e.g. a dark red region is complementary to a light red region); lines indicating base pairing are purely schematic and do not represent a particular number of bases.*

An impressive[57] example of an autonomous DNA biped with coordinated feet was published by the group of Seeman in 2009.[7g] Their system (Figure 1.15a) consists of a rigid track and biped with two different single-stranded feet (A and B). The track is a ~49 nm long double-crossover DNA structure that is decorated in a directionally polar manner with different metastable DNA stem-loop motives (T1 to T4; consisting of one 'signalling' and one 'foothold' strand each). The walker comprises two different single-stranded feet that, unlike in the previously discussed bipeds, are not joined by a duplex region, but by a covalent 5',5' linkage. Overall, processivity is guaranteed by signalling strands, which mediate the interaction between feet and fuel strands in a way that only one foot can detach from the track. Directionality is achieved through the hybridisation of metastable hair pin fuel strands to the track, and thus this system can be considered a 'brunt-bridges' walker.

In the starting position (Figure 1.15a), where the walker is located on the left end of the track, foot B is hybridised to the foothold strand of stem-loop T2. The free signalling strand T2 hybridises with one half of hairpin fuel F1 (Figure 1.15b), whereupon the other half of the fuel displaces foot A from foothold strand T1. Fuel strand F1 now

forms a stable aggregate with the track (Figure 1.15c) and foot A is free to diffuse to a forward binding site (Figure 1.15d). After foot A has hybridised with foothold strand T3, a second resting state is formed (Figure 1.15e), in which the order of the feet has reversed (hand-over-hand gait). The interaction of signalling strand T3 with fuel strand F2 initiates a second motor cycle that will lead to a third resting state where the walker is attached to T3 and T4 (not shown in Figure 1.15). In the third motor cycle, signalling strand T4 will activate fuel F1, which leads to displacement of the trailing foot from foothold strand T3. The walker thus takes two and a half steps and in the final resting state only foot A is attached to foothold strand T4.

Seeman and co-workers have demonstrated that their device can complete a full walking cycle by covalently cross-linking [58] a radioactively labelled walker (^{32}P) to its track in successive walking states and observing fragments with characteristic mobilities during autoradiogram analysis of denaturing PAGE.

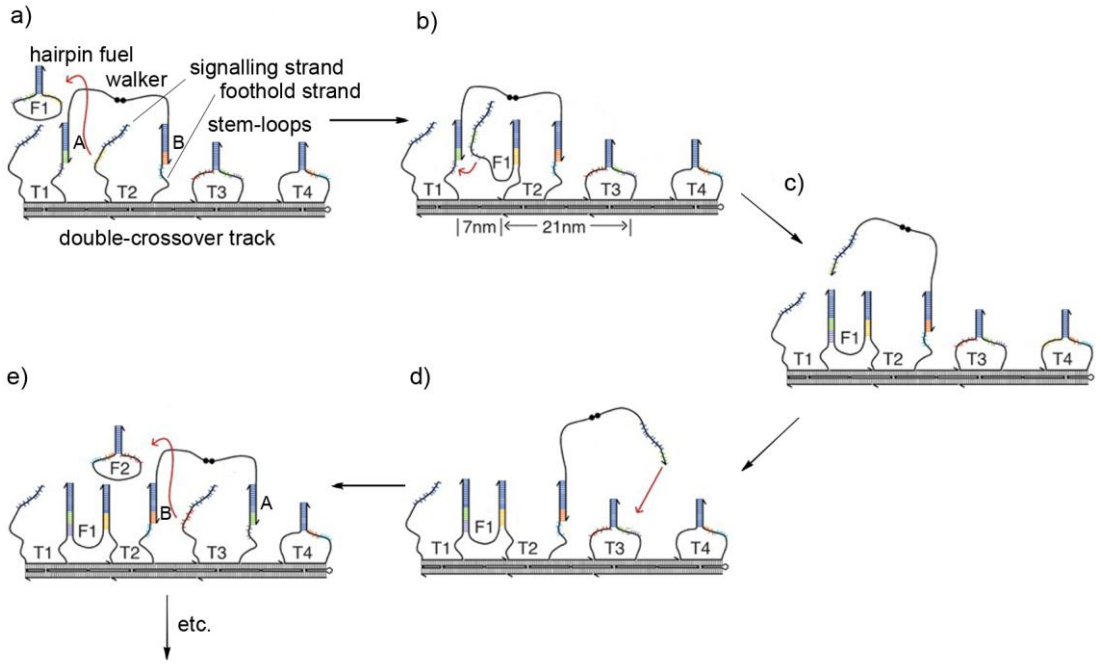

Figure 1.15. *Seeman's autonomous DNA biped, in which coordination between the feet is achieved through signal strands on the track.[7g] a) Resting state 1; walker in starting position (foot B leads); signal strand T2 hybridises with hairpin fuel F1; b) activated fuel strand F1 hybridises with toehold on T1 foothold strand and displaces foot A from foothold T1; c) foot A is free; d) foot A diffuses to stem-loop T3, hybridises with its toehold and frees signal strand T3; e) resting state 2 (foot A leads); signal strand T3 hybridises with hairpin fuel F; repetition of these steps leads to a final resting state where foot B is bound to foothold T4 and foot A is free. Adapted with permission (American Association for the Advancement of Science).[7g]*

DNA-based walkers comprising more than two feet have also been reported. A study published in 2006 by Stojanovic described autonomous, processive multipedal walkers

with 2-6 DNAzyme feet.[59] The movement of some of these 'spider' walkers occurred with relatively high processivity, but the direction of the movement occurred in random directions of the nucleotide matrix that served as track (the authors later used the term random walkers[7h]).

In 2010, a more sophisticated use of the previously described molecular spiders was reported by the groups of Stojanovic, Winfree, Walter and Yan.[7h] Through their interaction with appropriately designed two-dimensional DNA origami[45] tiles, the multipedal walkers could carry out robotic actions, such as 'start', 'follow', 'turn' or 'stop'. The molecular spider used in the study is illustrated in Figure 1.16a. Four single-stranded DNA oligonucleotides are attached to an inert streptavidin core. Three of the single strands, the spider's legs, are DNAzymes, which can recognise and cleave oligonucleotide substrates containing one RNA base. The fourth single-strand functions as a capture leg, which is used to position the molecular spider with precise control on the track.

The interaction between the DNAzyme legs and the DNA/RNA-chimeric footholds that decorate the track, is shown in Figure 1.16b. Similar to Mao's autonomous walker, the employed 8-17 DNAzyme first hybridises with the foothold (substrate) strand and then cuts of an eight base section that is released into solution. The DNAzyme binds significantly weaker to the shorter resulting product strand, which results in its dissociation and quick reattachment to a nearby product or substrate strand. The device operates processively (average step number ~200), because the DNAzyme legs spend a relatively long time on substrate strands, but only a short time on product strands and even less time in an unbound state. As a consequence, at any time the probability is very high that one or two legs are attached to the track.

Three pseudo-one-dimensional pathways for the directionally-biased migration of a molecular spider are illustrated in Figure 1.16c. If placed on a pathway decorated with substrate strands, the spider will move unidirectionally towards the substrate region and will even follow turns. Foothold strands that lack the RNA base (shown in red in Figure 1.16c), act as a thermodynamic trap for the spider, because the DNAzyme leg is not able to hydrolyse these footholds. The effect of these thermodynamic traps is so powerful that they can even impose net-directionality to a spider that performs a fully random walk along a pathway constructed exclusively of product strands. The behaviour of the spiders on 48 and 90 nm pathways on the origami landscape (Figure 1.16d) was analysed by atomic force microscopy (AFM) and real-time total internal

reflection fluorescence microscopy. Statistical analysis of the AFM data showed that on the 90 nm track, 70% of the spiders reached the 'Stop' site within 60 minutes. Almost no spiders were found on a control site (red, top of Figure 1.16d) on the origami tile, which confirmed the high processivity of the walker locomotion.

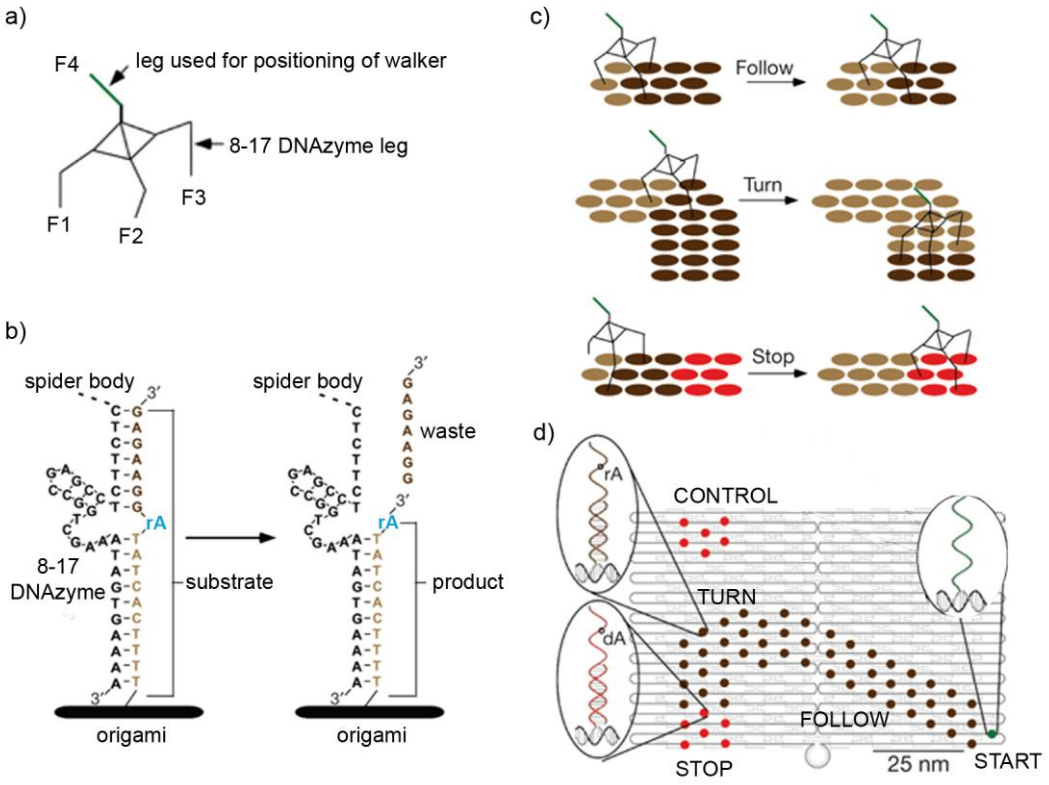

Figure 1.16. *A molecular spider with three DNAzyme legs that can carry out autonomous, robotic behaviour on a DNA origami landscape.[7h] a) Components of the employed molecular spider: inert streptavidin body; three 18-17 DNAzyme feet that can cleave RNA substrates; one capture leg, which is used to position the spider on the origami tile; b) illustration of the interaction between the spider legs and the footholds on the origami tile (DNAzyme leg shown in black, foothold shown in brown, RNA base, at which cleavage by the DNAzyme occurs, highlighted in blue); c) robotic behaviour of the spider as determined by the foothold sequence (substrate footholds shown in brown; hydrolysed product footholds shown in beige; 'Stop'-footholds lacking the RNA base are shown in red); d) representative origami landscape including 'Start', 'Follow', 'Turn', 'Stop' and 'Control' sites. Adapted with permission (Nature Publishing Group).[7h]*

1.6 Conclusions and Aim of this Project

A marvellous collection of motor proteins walks up and down tracks in the cells of complex organisms. In light of the diverse designs and functions of biological molecular walkers, two conclusions can be drawn for the development of artificial analogues and the technological potential of such devices: first, nature has shown that there are many roads to success. Important motor characteristics such as processivity and directionality seem to be attainable in many different ways and any particular motor mechanism appears to be adapted to the specific desired function carried out. Second, the biological motor systems play such an important role in all complex living forms that it is hard to conceive that mankind couldn't one day profit from a similar man-made technology.

The DNA-based linear motors discussed in the second half of this Chapter represent a first step towards such a technology. Although the DNA-based systems operate with remarkable efficiency and can be prepared through automated synthesis, small-molecule systems can be expected to provide valuable new insights, particularly when coupled with powerful analytical techniques, such as NMR or HPLC (these techniques are of limited use in DNA systems).

The aim of this project is to create the first small-molecule system, in which a processive and directional migration of a walker unit along a molecular track is achieved. For the crucial connections between the walker unit and the track, dynamic covalent hydrazone and disulfide linkages were identified as the most promising candidates. This proposal has led to experimental work that has evolved from a simple hydrazone-disulfide model study (Chapter II) to the first small-molecule walker system (Chapter III), from there to comprehensive mechanistic studies (Chapter IV) and finally to a light-driven walker system (Chapter V).

1.7 Notes and References

[1] a) Richard P. Feynman, *California Institute of Technology Journal of Engineering and Science* **1960**, *4*, 23–36; b) http://www.its.caltech.edu/~feynman/plenty.html (retrieved: 03/08/2010); c) for an interesting article on the historical background and the impact of Feynman's speech see: A. Junk, F. Riess, *Am. J. Phys.* **2006**, *74*, 825-830.

[2] D. M. Eigler, E. K. Schweizer, *Nature* **1990**, *344*, 524.

[3] a) L. Gross, F. Mohn, N. Moll, P. Liljeroth, G. Meyer, *Science* **2009**, *325*, 1110; b) H. Tanaka, T. Kawai, *Nature Nanotech.* **2009**, *4*, 518; c) L. Gross, F. Mohn, N. Moll, G. Meyer, R. Ebel, W. M. Abdel-Mageed, M. Jaspars, *Nature Chem.* **2010**, DOI: 10.1038/nchem.765.

[4] M. Schliwa (ed.), *Molecular Motors*, Wiley-VCH, Weinheim, **2003**.

[5] E. R. Kay, D. A. Leigh, F. Zerbetto, *Angew. Chem. Int. Ed.* **2007**, *46*, 72.

[6] T. R. Kelly, H. De Silva, R. A. Silva, *Nature* **1999**, *401*, 150; b) N. Koumura, R. W. J. Zijlstra, R. A. van Delden, N. Harada, B. L. Feringa, *Nature* **1999**, *401*, 152; c) D. A. Leigh, J. K. Y. Wong, F. Dehez, F. Zerbetto, *Nature* **2003**, *424*, 174; J. V. Hernandez, E. R. Kay, D. A. Leigh, *Science* **2004**, *306*, 1532; d) R. A. van Delden, M. K. J. ter Wiel, M. M. Pollard, J. Vicario, N. Koumura, B. L. Feringa, *Nature* **2005**, *437*, 1337; e) S. P. Fletcher, F. Dumur, M. M. Pollard, B. L. Feringa, *Science* **2005**, *310*, 80; f) R. Eelkema, M. M. Pollard, J. Vicario, N. Katsonis, B. S. Ramon, C. W. M. Bastiaansen, D. J. Broer, B. L. Feringa, *Nature* **2006**, *440*, 163.

[7] a) W. B. Sherman, N. C. Seeman, *Nano Lett.* **2004**, *4*, 1203; b) J.-S. Shin, N. A. Pierce, *J. Am. Chem. Soc.* **2004**, *126*, 10834; c) P. Yin, H. Yan, X. G. Daniell, A. J. Turberfield, J. H. Reif, *Angew. Chem. Int. Ed*. **2004**, *43*, 4906; d) J. Bath, S. J. Green, a. J. Turberfield, *Angew. Chem. Int. Ed.* **2005**, *44*, 4358; e) Y. Tian, Y. He, Y. Chen, P. Yin, C. Mao, *Angew. Chem. Int. Ed*. **2005**, *44*, 4355; f) S. J. Green, J. Bath, A. J. Turberfield, *Phys. Rev. Lett.* **2008**, *101*, 238101; g) T. Omabegho, R. Sha, N. C. Seeman, *Science* **2009**, *324*, 67; h) H. Gu, J. Chao, S.-J. Xiao, N. C. Seeman, *Nature* **2010**, *465*, 202; i) K. Lund, A. J. Manzo, N. Dabby, N. Michelotti, A. Johnson-Buck, J. Nangreave, S. Taylor, R. Pei, M. N. Stojanovic, N. G. Walter, E. Winfree, H. Yan, *Nature* **2010**, *465*, 206.

[8] Note that the term molecular motor is not consistently used in the biochemical literature. Here it is used for any biological system that converts energy derived from fuel into mechanical. In many reports, the term protein motor is only used, however, for the cytoskeletal walker proteins dynein, kinesin and myosin. The term protein machine is then used for ion pumps, helicases etc, although it is somewhat ambiguous. Ion channels, for example, which are mere ON-OFF switches, could also be included, although they consume no fuel and perform no mechanical or chemical work.

[9] For a recent review article on the Na/K ion pump see: D. C. Gadsby, *Nat. Rev. Mol. Cell Biol.* **2009**, *10*, 344.

[10] For recent review articles on translocation pores see: a) Y. Yoneda, *J. Biochem.* **1997**, *121*, 811; b) D. Branton, D. W. Deamer, A. Marziali, H. Bayley, S. A. Benner, T. Butler, M. Di Ventra, S. Garaj, A. Hibbs, X. H. Huang, S. B. Jovanovich, P. S. Krstic, S. Lindsay, X. S. S. Ling, C. H. Mastrangelo, A. Meller, J. S. Oliver, Y. V. Pershin, J. M. Ramsey, R. Riehn, G. V. Soni, V. Tabard-Cossa, M. Wanunu, M. Wiggin, J. A. Schloss,

Nature Biotechnol. **2008**, *26*, 1146 ; c) D. E. Makarov, *Acc. Chem. Res.* **2009**, *42*, 281.

[11] For recent review articles on helicases see: a) M. R. Singleton, M. S. Dillingham, D. B. Wigley, *Annu. Rev. Biochem.* **2007**, *76*, 23; b) E. J. Enemark, L. Joshua-Tor, *Curr. Opin. Struct. Biol.* **2008**, *18*, 243; c) A. M. Pyle, *Annual Review of Biophysics* **2008**, *37*, 317.

[12] For recent review articles on DNA and RNA polymerases see: a) K. S. Murakami, S. A. Darst, *Curr. Opin. Struct. Biol.* **2003**, *13*, 31; b) S. Prakash, R. E. Johnson, L. Prakash, *Annu. Rev. Biochem.* **2005**, *74*, 317; c) A. J. Berdis, *Chem. Rev.* **2009**, *109*, 2862.

[13] For a review article on rotary protein motors see: G. Oster, H. Wang, *Trends Cell Biol.* **2003**, *13*, 114.

[14] For recent review articles on the F_0F_1 ATP synthase motor see: a) R. K. Nakamoto, J. A. B. Scanlon, M. K. Al-Shawi, *Arch. Biochem. Biophys.* **2008**, *476*, 43; b) C. von Ballmoos, G. M. Cook, P. Dimroth, *Annu. Rev. Biophys.* **2008**, *37*, 43.

[15] For recent review articles on the flagellar motor a) H. C. Berg, *Annu. Rev. Biochem.* **2003**, *72*, 19; b) M. J. Pallen, N. J. Matzke, *Nature Rev. Microbiol.* **2006**, *4*, 784; c) Y. Sowa, R. M. Berry, *Quart. Rev. Biophys*. **2008**, *41*, 103.

[16] For review articles covering myosins, dyneins and kinesins see : a) R. D. Vale, R. A. Milligan, *Science* **2000**, *288*, 89; b) R. D. Vale, *Cell*, **2003**, *112*, 467 ; c) M. Schliwa, G. Woehlke, *Nature* **2003**, *422*, 759 ; d) L. A. Amos, *Cell Mol. Life Sci.* **2008**, *65*, 509.

[17] R. D. Astumian, *Phys. Chem. Chem. Phys*. **2007**, *9*, 5067.

[18] R. D. Astumian, *Biophys. J.* **2010**, *98*, 2401.

[19] For recent reviews on members of the myosin superfamily see: a) J. R. Sellers, C. Veigel, *Curr. Opin. Cell Biol.* **2006**, *18*, 68; b) M. Vicente-Manzanares, X. Ma, R. S. Adelstein, A R. Horwitz, *Nature Rev. Mol. Cell Biol.* **2009**, *10*, 778.

[20] For recent reviews on members of the dynein superfamily see: a) M. P. Koonce, M. Samsó, *Trends Cell Biol.* **2004**, *14*, 612; b) K. Oiwa, H. Sakakibara, *Curr. Opin. Cell Biol.* **2005**, *17*, 98; c) J. R. Kardon, R. D. Vale, *Nature Rev. Mol. Cell Biol.* **2009**, *10*, 854.

[21] For recent reviews on members of the kinesin superfamily see: a) N. J. Carter, R. A. Cross, *Curr. Opin. Cell Biol.* **2006**, *18*, 61; b) S. M. Block, *Biophys. J.* **2007**, *92*, 2986; c) N. Hirokawa, Y. Noda, Y. Tanaka, S. Niwa, *Nature Rev. Mol. Cell Biol.* **2009**, *10*, 682; d) K. J. Verhey, J. W. Hammond, *Nature Rev. Mol. Cell Biol.* **2009**, *10*, 765; e) N. Hirokawa, R. Nitta, Y. Okada, *Nature Rev. Mol. Cell Biol.* **2009**, *10*, 877; h) J. A Spudich, S. Sivaramakrishnan, *Nature Rev. Mol. Cell Biol.* **2010**, *11*, 128.

[22] a) T. Mitchison, M. Kirschner, *Nature* **1984**, *312*, 237; b) K. Hirose, J. Löwe, M. Alonso, R. A. Cross, L. A. Amos, *Cell Struct. Funct.* **1999**, *24*, 277; c) F. Kozielski, I. Arnal, R. H. Wade, *Curr. Biol.* **1998**, *8*, 191; d) A. Marx, J. Müller, E.-M. Mandelkow, A. Hoenger, E. Mandelkow, *J. Muscle Res. Cell. Motil.* **2006**, *27*, 125.

[23] K. C. Holmes, D. Popp, W. Gebhard, W. Kabsch, *Nature* **1990**, *347*, 21.

[24] K. Shiroguchi, K. Kinosita, *Science* **2007**, *316*, 1208.

[25] F. J. Kull, E. P. Sablin, R. Lau, R. J. Fletterick, R. D. Vale, *Nature* **1996**, *380*, 550.

[26] R. D. Vale, T. S. Reese, M. P. Sheetz, *Cell* **1985**, *42*, 39.

[27] For review articles on kinesin-I see: a) G. Woehlke, M. Schliwa, *Nature Rev. Mol. Cell. Biol.* **2000**, *1*, 50; b) N. J. Carter, R. A. Cross, *Curr. Opin. Cell Biol.* **2006**, *18*, 61; c) S. M. Block, *Biophys. J.* **2007**, *92*, 2986.

[28] Selected articles on aspects of the motor mechanism of kinesin-I: a) J. Howard, A. J. Hudspeth, R. D. Vale, *Nature* **1989**, *342*, 154; b) S. M. Block, L. S. Goldstein, B. J. Schnapp, *Nature* **1990**, *348*, 348; c) K. Svoboda, C. F. Schmidt, B. J. Schnapp, S. M. Block *Nature* **1993**, *365*, 721; d) S. M. Block, *Trends Cell Biol.* **1995**, *5*, 169; e) E. Berliner, E. C. Young, K. Anderson, H. K. Mahtani, J. Gelles, *Nature* **1995**, *373*, 718; f) R. D. Vale, T. Funatsu, D. W. Pierce, L. Romberg, Y. Harada, T. Yanagida, *Nature* **1996**, *380*, 451; g) W. Hua, E. C. Young, M. L. Fleming, J. Gelles, *Nature* **1997**, *388*, 390; h) M. J. Schnitzer, S. M. Block, *Nature* **1997**, *388*, 386; i) S. M. Block, *Cell* **1998**, *93*, 5; j) S. Rice, A. W. Lin, D. Safer, C. L. Hart, N. Naber, B. O. Carragher,S. M. Cain, E. Pechatnikova, E. M. Wilson-Kubalek, M. Whittaker, E. Pate, R. Cooke, E. W. Taylor, R. A. Milligan, R. D. Vale, *Nature* **1999**, *402*, 778; k) K. Kawaguchi, S. Ishiwata, *Science* **2001**, *291*, 667; l) W. R. Schief, J. Howard, *Curr. Opin. Cell Biol.* **2001**, *13*, 19; m) W. Hua, J. Chung, J. Gelles, *Science* **2002**, *295*, 844; n) S. Rice, Y. Cui, C. Sindelar, N. Naber, M. Matuska, R. Vale, R.Cooke, *Biophys. J.* **2003**, *84*, 1844; o) C. L. Asbury, A. N. Fehr, S. M. Block, *Science* **2003**, *302*, 2130; p) A. Yildiz, M. Tomishige, R. D. Vale, P. R. Selvin, *Science* **2004**, *303*, 676; q) T. Mori, R. D. Vale, M. Tomishige, *Nature* **2007**, *450*, 750; r) R. Dixit, J. L. Ross, Y. E. Goldman, E. L. F. Holzbaur, *Science* **2008**, *319*, 1086; s) V. Bormuth, V. Varga, J. Howard, E. Schaffer, *Science* **2009**, *325*, 870; t) N. R. Guydosh, S. M. Block, *Nature* **2009**, *461*, 125; u) E. Toprak, A. Yildiz, M. T. Hoffman, S. S. Rosenfeld, P. R. Selvin, *Proc. Natl. Acad. Sci. USA* **2009**, *106*, 12717.

[29] F. Kozielski, S. Sack, A. Marx, M. Thormählen, E. Schönbrunn, V. Biou, A. Thompson, E.-M. Mandelkow, E. Mandelkow, *Cell* **1997**, *91*, 985.

[30] a) D. D. Hackney, *Nature* **1995**, *377*, 448; b) R. D. Vale, T. Funatsu, D. W. Pierce, L. Romberg, Y. Harada, T. Yanagida, *Nature* **1996**, *380*, 451; c) R. B. Case, D. W. Pierce, N. Hom-Booher, C. L. Hart, R. D. Vale, *Cell* **1997**, *90*, 959; d) L. Romberg, D. W. Pierce, R. D. Vale, *J. Cell Biol.* **1998**, *140*, 1407; e) K. S. Thorn, J. A. Ubersax, R. D. Vale, *J. Cell Biol.* **2000**, *151*, 1093; f) J. Yajima, M. C. Alonso, R. A. Cross, Y. Y. Toyoshima, *Curr. Biol.* **2002**, *12*, 301.

[31] S. M. Block, *Trends Cell Biol.* **1995**, *5*, 169.

[32] L. Onsager, *Phys. Rev.* **1931**, *37*, 405.

[33] *The Second Law of Thermodynamics. Memoirs by Carnot, Clausius and Thomson: Harper's Scientific Memoirs* (Ed.: W. F. Magie), Harper & Brothers, New York, **1899**.

[34] Brownian ratchet theory. a) R. D. Astumian, M. Bier, *Biophys. J.* **1996**, *70*, 637; b) M. Bier, *Contemp. Phys.* **1997**, *38*, 371; c) R. D. Astumian, I. Derényi, *Eur. Biophys. J.* **1998**, *27*, 474; d) L. Mahadevan, P. Matsudaira, *Science* **2000**, *288*, 95; e) C. Bustamante, D. Keller, G. Oster, *Acc. Chem. Res.* **2001**, *34*, 412; f) R. D. Astumian, *Appl. Phys. A* **2002**, *75*, 193; g) P. Reimann, *Phys. Rep.* **2002**, *361*, 57; h) B. J. Gabryś, K. Pesz, S. J. Bartkiewicz, *Physica A* **2004**, *336*, 112; i) M. Kurzynski, P. Chełminiak, *Physica A* **2004**, *336*, 123.

[35] a) F. Jülicher, A. Ajdari, J. Prost, *Rev. Mod. Phys.* **1997**, *69*, 1269; b) R. D. Astumian, *Science* **1997**, *276*, 917; c) A. Mogilner, G. Oster, *Curr. Biol.* **2003**, *13*, R721; d) G. Oster, H. Y. Wang, *Trends Cell Biol.* **2003**, *13*, 114.

[36] a) D. A. Leigh, J. K. Y. Wong, F. Dehez, F. Zerbetto, *Nature* **2003**, *424*, 174; b) J. V. Hernandez, E. R. Kay, D. A. Leigh, *Science* **2004**, *306*, 1532; c) M. N. Chatterjee, E. R. Kay, D. A. Leigh, *J. Am. Chem. Soc.* **2006**, *128*, 4058.

[37] a) V. Serreli, C.-F. Lee, E. R. Kay, D. A. Leigh, *Nature* **2007**, *445*, 523; b) M. Alvarez-Pérez, S. M. Goldup, D. A. Leigh, A. M. Z. Slawin, *J. Am. Chem. Soc.* **2008**, *130*, 1836.

[38] It could be argued that kinesin, for example, operates through an energy ratchet mechanism, because at one crucial stage of the mechanism the neck-linker docking breaks the symmetry of the thermodynamic minima corresponding to forward and backward stepping, respectively. This shows that sometimes a clear distinction between energy ratchet, information ratchet and even power-stroke mechanisms is not possible.

[39] Selected examples of small-molecule 'walkers', which are either not directional or not processive: a) S. Mitra, R. G. Lawton, *J. Am. Chem. Soc*. **1979**, *101*, 3097; b) M. Möhring, G. Fink, *Angew. Chem., Int. Ed*. **1985**, *24*, 1001; c) L. K. Johnson, C. M. Killian, M. Brookhart, *J. Am. Chem. Soc*. **1995**, *117*, 6414; d) K.-Y. Kwon, K. L. Wong, G. Pawin, L. Bartels, S. Stolbov, T. S. Rahman, *Phys. Rev. Lett.* **2005**, *95*, 166101; e) H. D. F. Winkler, D. P. Weimann, A. Springer, C. A. Schalley, *Angew. Chem. Int. Ed.* **2009**, *48*, 7246; f) D. P. Weimann, H. D. F. Winkler, J. A. Falenski, B. Koksch, C. A. Schalley, *Nature Chem.* **2009**, *1*, 573; g) R. Tkachov, V. Senkovskyy, H. Komber, J.-U. Sommer, A. Kiriy, *J. Am. Chem. Soc*. **2010**, *132*, 7803.

[40] T. LaBean, H. Yan, J. Kopatsch, F. Liu, E. Winfree, J. H. Reif, N. C. Seeman, *J. Am. Chem. Soc.* **2000**, *122*, 1848.

[41] The biped and the track are prepared in an annealing step at 95°C from the corresponding oligonucleotides. At this temperature all base pairs interactions are essentially dynamic, which facilitates the self-assembly of the large structures. All further experiments require the backbones of the biped and the track to remain stable which is why a temperature of 16 °C was used (where competitive hybridisation can still occur).

[42] The biotin-tag on the unset strand interacts strongly with streptavidin-coated magnetic beads that can be removed with a permanent magnet.

[43] J. SantaLucia, *Proc. Natl. Acad. Sci. USA* **1998***, 95,*1460*.*

[44] L. M. Smith, *Nature* **2010**, *465*, 167.

[45] P. W. K. Rothemund, *Nature* **2006**, *440*, 297.

[46] T. R. Kelly, *Angew. Chem. Int. Ed.* **2005**, *44*, 4124.

[47] The starting state was established by self-assembly between the track and the walker (footholds 2 and 3 were designed to bind the walker considerably less strong).

[48] A stepping rate of ~0.01 s^{-1} was calculated from the kinetic data.

[49] R. R. Breaker, G. F. Joyce, *Chem. Biol.* **1994**, *1*, 223.

[50] S. Venkataraman, R. M. Dirks, P. W. K. Rothemund, E. Winfree, N. A. Pierce, *Nature Nanotech.* **2007**, *2*, .490.

[51] E. Gouin, M. D. Welch, P. Cossart, *Curr. Opin. Microbiol.* **1999**, *8*, 35.

[52] a) A. J. Turberfield, J. C. Mitchell, B. Yurke, A. P. Mills, Jr., M. I. Blakey, F. C. Simmel, *Phys. Rev. Lett.* **2003**, *90*, 118102; b) S. J. Green, D. Lubrich, A. J. Turberfield, *Biophys. J.* **2006**, *91*, 2966.

[53] P. Yin, H. M. T. Choi, C. R. Calvert, N. A. Pierce, *Nature* **2008**, *451*, 318.

[54] a) A. J. Turberfield, J. C. Mitchell, B. Yurke, A. P. Mills, Jr., M. I. Blakey, F. C. Simmel, *Phys. Rev. Lett.* **2003**, *90*, 118102; b) S. J. Green, D. Lubrich, A. J. Turberfield, *Biophys. J.* **2006**, *91*, 2966.

[55] In the absence of the walker-track-conjugate, H1 and H2 form H1-H2 only very slowly (slow background reaction).

[56] Note that the left foot does not necessarily need to be fully detached from fuel strand H1 (as shown for clarity in Figure 1.14d) in order to be able to reattach on track binding sites 1 or 3.

[57] W. Sherman, *Science* **2009**, *324*, 46.

[58] As in Seeman's non-autonomous walker (reference 7a), psoralene tags were used for UV-light-initiated cross-linking.

[59] R. Pei, S. K. Taylor, D. Stefanovic, S. Rudchenko, T. E. Mitchell, M. N. Stojanovic, *J. Am. Chem. Soc.* **2006**, *128*, 12693.

Chapter II

A Hydrazone-Disulfide Macrocycle and its Ring-Opening under Acidic and Basic Conditions

Published as *Synthesis and solid state structure of a hydrazone-disulfide macrocycle and its dynamic covalent ring-opening under acidic and basic conditions*, M. von Delius, E. M. Geertsema, D. A. Leigh, A. M. Z. Slawin, *Org. Biomol. Chem.* **2010**, *8*, 4617.

Selected as an OBC "Hot Paper" 2010.

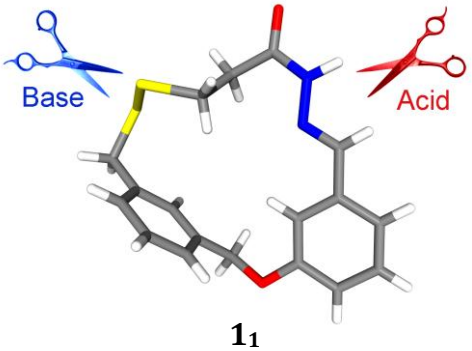

1_1

"A model should be as simple as possible, but no simpler."
(Albert Einstein, attributed)

Acknowledgements

Dr. Edzard M. Geertsema is gratefully acknowledged for his contribution to this chapter: E. M. G. had performed the synthesis of macrocycle **1_1** prior to the author's arrival in Edinburgh. The rest of the presented work was a joint effort between the author and E. M. G.. Prof. Alexandra M. Z. Slawin is acknowledged for solving the crystal structure of macrocycle **1_1**.

Synopsis

*The synthesis and characterisation, including solid state structure, of an unprecedented macrocycle (**1**$_1$) containing both a hydrazone and a disulfide linkage is described. In the context of this thesis, **1**$_1$ represents a model for a molecular walker featuring one hydrazide and one thiol foot, which is attached to a two-foothold section of a molecular track. The solid state structure of **1**$_1$ afforded valuable structural insights, most importantly that a certain amount of strain is caused by having several rigid elements within the framework of the 17-membered ring.*

*To probe the dynamic chemistry of **1**$_1$, and thus the potential application of hydrazone and disulfide chemistry for a molecular walking device, three types of experiments were conducted, each involving ring-opening and each carried out under thermodynamic control. The results of these experiments indicated that the disulfide bond in macrocycle **1**$_1$ exchanges only under basic conditions, whereas the hydrazone bond exchanges only under acidic conditions and that each dynamic exchange reaction is not affected by building blocks that could theoretically lead to the opening of both bonds at the same time (a process that has to be strictly avoided in all molecular walking devices).*

2.1 *Introduction*

2.1.1 Dynamic Covalent Chemistry

Synthetic organic chemistry has been dominated by kinetically controlled reactions that lead to the irreversible formation of stable covalent bonds. The outcome of such reactions is governed by the relative magnitude of the activation barriers, and by careful choice of reagents and/or catalysts even compounds with high ground state energies can be obtained.[1] In contrast, reversible reactions are subject to thermodynamic control and the product distribution is determined by the relative free energy of all possible products.

Over the last ten years the interest in reversible covalent reaction processes has dramatically increased, while Lehn[2], Sanders[3] and others[4] have shaped the concepts of a new discipline: dynamic covalent chemistry (DCC).[3a] Dynamic covalent chemistry combines the dynamic characteristics of supramolecular chemistry[5] with the robust characteristics of traditional covalent synthesis. One of the key advantages of operating under thermodynamic control is that the components of a system are subject to an 'error-correction' process and quickly respond to external stimuli. Factors such as temperature, concentration, pressure, the presence of catalysts or binding partners can dramatically influence the product distribution in a system. This has been used to advantage in the successful amplification of desired products.

Dynamic covalent chemistry has found applications in a broad range of areas, including dynamic polymers (so called dynamers),[6] sensors,[7] the synthesis and manipulation of mechanically interlocked architectures[8] and systems chemistry.[9] Its most significant application, however, is expected to be in the area of drug discovery, where in a so called virtual dynamic combinatorial library a targeted receptor would amplify the formation of the strongest binding library member at the cost of the others.[10] In nature, the dynamic chemistry of disulfide bonds plays an important role in the establishment of the secondary structure of most proteins.[11]

Scheme 2.1 shows a selection of reversible reactions, which form the 'toolbox' of dynamic covalent chemistry.[3b] Recent studies by Furlan and Otto describe substrates containing both hydrazone and disulfide linkages, which could be selectively addressed under mutually exclusive conditions.[12] In the context of this project it was thought that this could potentially form the basis of a bipedal molecular walking system and thus

only hydrazone and disulfide exchange will be discussed further (sections 2.1.1.1 and 2.1.1.2).

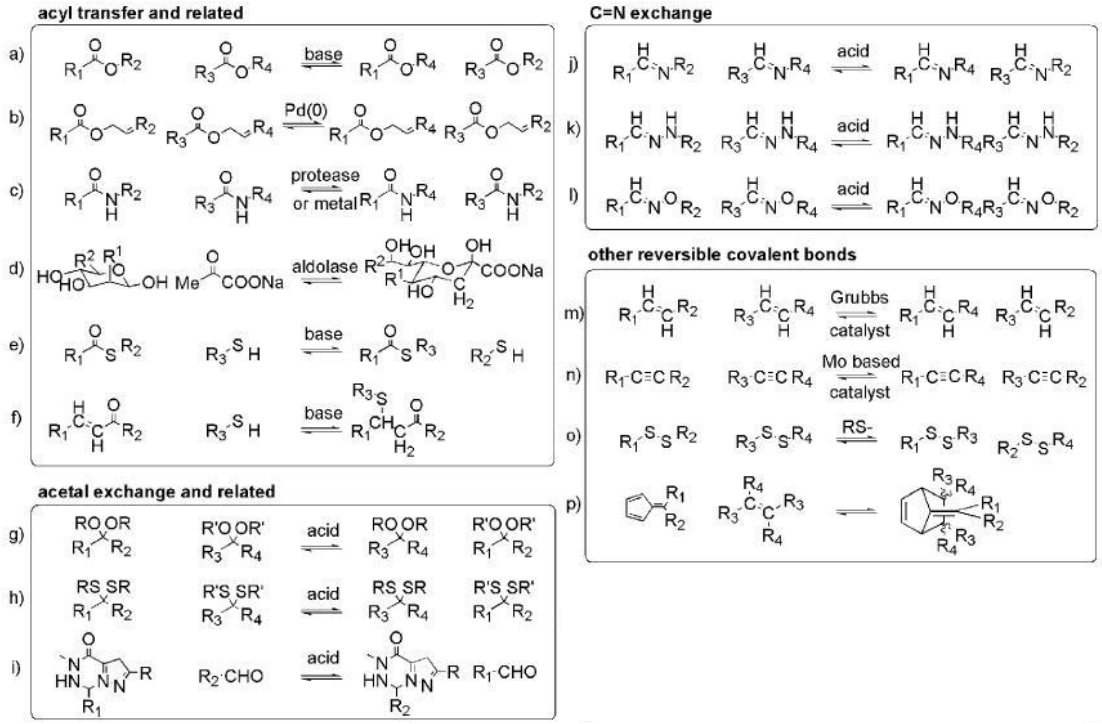

Scheme 2.1. *Incomprehensive list of reversible covalent reactions representing the 'toolbox' of dynamic covalent chemistry. Adapted with permission (American Chemical Society).*[3b]

2.1.1.1 Hydrazone Exchange

Although the dynamic covalent chemistry of imines is well-studied,[13] the use of hydrazones can offer important advantages. This is due to the fact that in hydrazone exchange, the equilibrium lies far on the side of the hydrazone product, while the concentration of hydrolysed monomers is still sufficient to allow for exchange reactions. Secondly, unlike imine exchange, hydrazone exchange generally only occurs when catalysed by acid,[14] or as recently discovered by nucleophilic base.[15] Thus it can be effectively frozen under neutral or basic conditions, a feature which can be useful in multi-level systems (see section 2.1.2).

The mechanism of hydrazone exchange, i.e. the reversible exchange reaction between two or more different hydrazones, involves the initial hydrolysis of the hydrazones followed by a subsequent condensation reaction to give new 'scrambled' products. The two elemental steps of the hydrolysis reaction are shown in Scheme 2.2. The acid-catalysed addition of water to the sp^2 carbon atom, which is rate limiting at pH close to neutral, is followed by the dissociation of the hemiaminal.[3b]

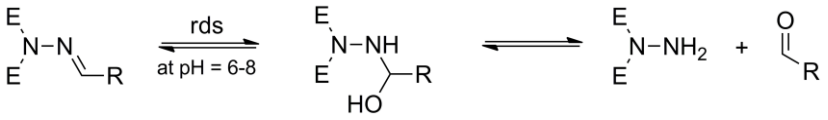

Scheme 2.2. *Mechanism of the reversible hydrolysis of a hydrazone. rds = rate determining step. E = electron-withdrawing substituents (commonly: E = acyl).*

Hydrazone exchange is effective in both aqueous[16] and organic media.[17] In the latter case, TFA is often employed as acid catalyst, which allows the use of acetals as starting materials (TFA mediates both cleavage of the acetal and subsequent hydrazone exchange). Sanders and co-workers have used such a strategy to identify an artificial acetylcholine receptor[8j]. A breakthrough towards the application of DCC in drug discovery was recently reported by the group of Greaney, who demonstrated that aniline catalysed acylhydrazone exchange is compatible with the use of enzyme templates.[18]

2.1.1.2 *Disulfide Exchange*

Scheme 2.3 shows the mechanism of disulfide exchange (or perhaps more accurately termed: thiol-disulfide exchange). Initially, a thiolate anion attacks the weak disulfide bond, which through an S_N2-type process leads to the formation of a new disulfide and a new thiolate anion. If the disulfide is unsymmetric, the free thiolate can also attack the other sulfur atom, which implies that, at equilibrium, a mixture of three different disulfides can be expected.[3b]

Scheme 2.3. *S_N2-type mechanism of reversible thiol-disulfide exchange.*

The mechanism shown in Scheme 2.3 has two important implications. Firstly, even if a disulfide is brought together with a free thiol, the reaction can only occur when there is a sufficient concentration of deprotonated thiolate anions. As a consequence thiol-disulfide exchange cannot be observed under acidic conditions. Secondly, if two disulfides are brought together, even addition of base is not sufficient to initiate equilibration. A catalytic amount of thiolate needs to be present, which can conveniently be generated by addition of a suitable reducing agent. Again, the possibility to halt disulfide exchange could be useful in the development of bipedal molecular walking systems (*vide infra*).

The application of disulfide exchange in synthetic dynamic covalent chemistry was pioneered by Otto and Sanders.[19] In the laboratory, dithiothreitol (DTT) is commonly employed for the generation of free thiolates (see Scheme 2.4), since it is particularly stable in its oxidized state and will not interfere with the desired exchange products.

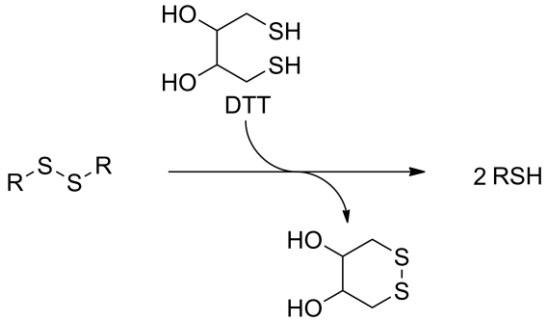

Scheme 2.4. *Reduction of a symmetric disulfide (RSSR) by DL-dithiothreitol (DTT).*

Similar to hydrazone exchange, the majority of studies on dynamic covalent disulfide exchange are carried out in aqueous solution, where the free thiolate concentration can be adjusted by buffer systems.[20] Yet, disulfide exchange can also take place in organic solvents.[21] Here, typically triethylamine or DBU are used as bases, while the initiation step is mediated by DTT. An interesting self-replicating system, based on disulfide exchange was recently reported by Otto and co-workers.[22]

2.1.2 Multi-Level Dynamic Systems

When the components of a dynamic chemical system are interconnected by several types of reversible exchange reactions—rather than just one—complex behaviour of the molecular network can emerge, a phenomenon that lies at the core of systems chemistry.[9] To date, several such multi-level constitutionally dynamic[23] systems have been described.[24] In these systems the various exchange processes can relate to each other in one of two ways: (i) orthogonal,[24a] where the exchange reactions do not interfere with each other; and (ii) communicating,[24b] where the products of the exchange reactions cross over and influence the outcome of the other. Adding a further level of control by having the reactions no longer occur concurrently could prove useful for ratcheting the distribution away from the thermodynamic minimum,[25] a feature useful for—amongst other things—the development of new molecular motor systems.[26] To achieve this, the conditions under which the different exchange reactions occur need to be mutually exclusive. In a double-level[27] system this requires that under one set of conditions only one of the two bond types is dynamic and the

other is kinetically locked, and that under a second set of conditions the relative rates of bond forming/breaking are reversed.

In recent independent studies, the groups of Furlan[12a] and Otto[12b] described simple (acyclic) substrates containing a disulfide and hydrazone moiety that undergo reversible exchange reactions under different sets of reaction conditions. We were interested in the implications of applying reactions that occur under mutually exclusive conditions to a cyclic substrate featuring such linkages.[12] Aside from establishing a viable synthetic route to such systems, our aim was to investigate the dynamic covalent ring-opening of such a macrocycle in a situation where fully reversible intra- and intermolecular exchange processes compete. Here we report on the synthesis (Scheme **2.5**) and dynamic chemistry (Figure 2.3 and Scheme 2.6) of macrocycle $\mathbf{1_1}$[28], which contains both a hydrazone and a disulfide unit within the bonds that make up the ring. We demonstrate selective ring-opening of $\mathbf{1_1}$ at either the disulfide or the hydrazone moiety by reversible covalent bond formation under two sets of mutually exclusive reaction conditions (acidic and basic).

We probe the dynamic chemistry of $\mathbf{1_1}$ through three types of experiments, each carried out under thermodynamic control: First, we treated $\mathbf{1_1}$ with acid or base conditions to demonstrate that under either set of conditions reversible covalent bond formation gives rise to a mixture of cyclic oligomers of type $\mathbf{1_n}$[28] (Figure 2.2). Second, $\mathbf{1_1}$ was treated with an acyclic disulfide or hydrazone scavenger, in the presence of acid or base, to demonstrate that the disulfide bonds exchange only under basic conditions and the hydrazone bonds exchange only under acidic conditions (Scheme 2.6 and Figure 2.3). Finally, $\mathbf{1_1}$ was subjected to basic or acidic conditions in the presence of both a disulfide *and* a hydrazone scavenger (Figure 2.4) to demonstrate that each dynamic exchange reaction is not affected by the presence of the other building blocks (which are inactive under the others set of reaction conditions).

2.2 *Results and Discussion*

2.2.1 Synthesis of Macrocycle $\mathbf{1_1}$

Macrocycle $\mathbf{1_1}$ was prepared according to the route shown in Scheme 2.5. Bis-aromatic scaffold **3** was obtained from benzylic chloride **2** and 3-hydroxybenzaldehyde *via* Williamson ether synthesis (step a). Alcohol **3** was converted into bromide **4**, followed by nucleophilic substitution with potassium thioacetate. Condensation of hydrazide **6** with aldehyde **5** yielded hydrazone **7** (step d). The synthesis was completed by sodium

methoxide mediated deprotection of the thioacetate group and oxidative ring-closure using iodine, which provided macrocycle $\mathbf{1_1}$ in 56% yield.[29]

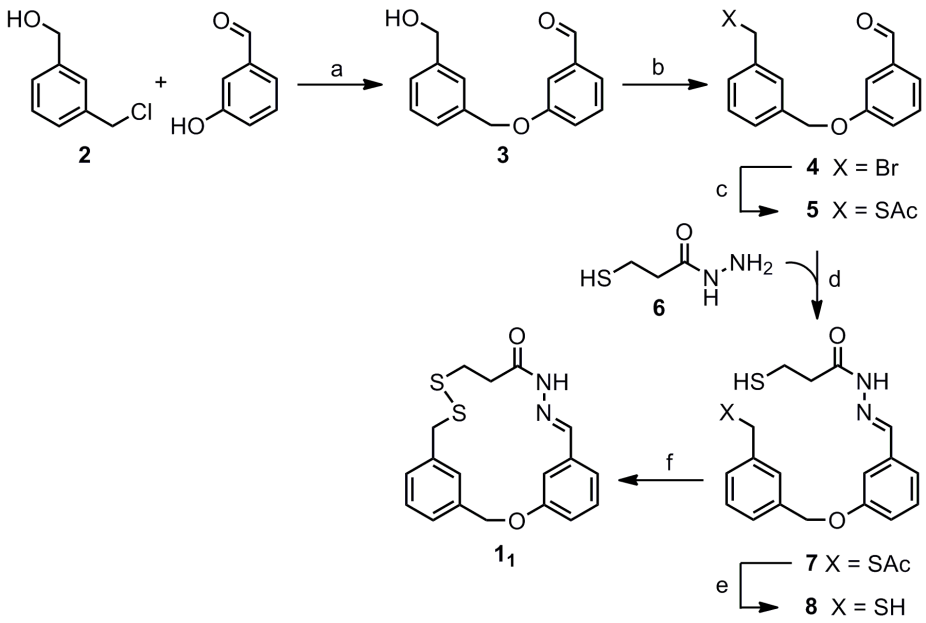

Scheme 2.5. *Synthesis of macrocycle* $\mathbf{1_1}$*. Reaction conditions: a) NaH, DMF, RT, 3 h, 83%; b)* $SOBr_2$*, benzene, RT, 36 h, 73%; c) KSAc, DMF, RT, 12 h, 95%; d) AcOH (cat.), MeOH, RT, 3h, 88%; e) NaOMe, MeOH, RT, 2 h, 78%; f)* I_2*,* $MeOH/CH_2Cl_2$*, 0 °C, 30 min, 56%.*

2.2.2 Solid State Structure of Macrocycle $\mathbf{1_1}$

Single crystals of $\mathbf{1_1}$ suitable for X-ray crystallography were obtained by slow cooling of a hot saturated solution of $\mathbf{1_1}$ in ethanol. The solid state structure revealed several interesting features of macrocycle $\mathbf{1_1}$ (Figure 2.1): the two aromatic rings are almost orthogonal (torsion angle 94°) and the hydrazone double bond is in the *E* configuration (also shown by ^{1}H NMR studies in $CDCl_3$) and planar (conjugated) with the adjacent aromatic ring. The C–S–S–C torsion angle (101°) deviates by 11° from the 90° angle typically found[30] for such functional groups and the two adjacent methylene groups between the disulfide and the hydrazone moiety are closer to an eclipsed than to a staggered conformation (dihedral angle 137°). These observations suggest that the presence of the three rigid elements (two aromatic rings and the acylhydrazone) in the macrocycle result in a significant amount of ring strain in $\mathbf{1_1}$.

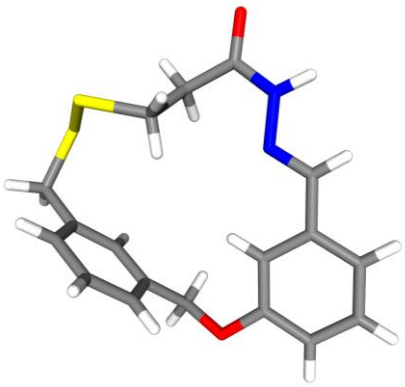

1_1

Figure 2.1. *Solid state structure of* ***1_1*** *determined by single crystal X-ray diffraction. C: grey, H: white, O: red, N: blue, S: yellow. Selected bond lengths [Å] and angles [°]: S-S 2.0335(11); N-N 1.376(3); C-S-S-C 100.92(13).*

2.2.3 Dynamic Chemistry I: Oligomerisation of Macrocycle 1_1 in the Absence of Scavengers

To investigate different aspects of the dynamic chemistry of macrocycle **1_1**, we carried out three types of experiments that involved macrocycle ring-opening under thermodynamic control. In the first experimental series we subjected **1_1** to different chemical reagents (trifluoroacetic acid-d_1 (TFA-d_1), triethylamine (Et_3N), diazabicyclo-[5,4,0]undec-7-ene (DBU), DL-dithiothreitol (DTT)),[31] solvents ($CDCl_3$, DMSO-d_6) and reaction temperatures (RT, 55 °C), in order to find effective conditions for cyclooligomerisation via reversible disulfide and hydrazone exchange (see Figure 2.2a). Deuterated solvents were employed to enable the progress of reactions to be followed by ^{1}H NMR spectroscopy.

Acid-mediated oligomerisation proved efficient at room temperature in $CDCl_3$ (one day equilibration time) using five equivalents of TFA-d_1 and millimolar initial concentrations of substrate (**1_1**). Base-induced oligomerisation was most efficient (two days equilibration time at room temperature) in $CDCl_3$ employing the strong base DBU (1.0 equiv.) and DTT (0.1 equiv.) as a catalytic reducing agent (Figure 2.2a). Hydrazone exchange did not occur using DMSO-d_6 and disulfide exchange was extremely slow (equilibration time more than 7 days at 55 °C) when the weaker base triethylamine was employed.

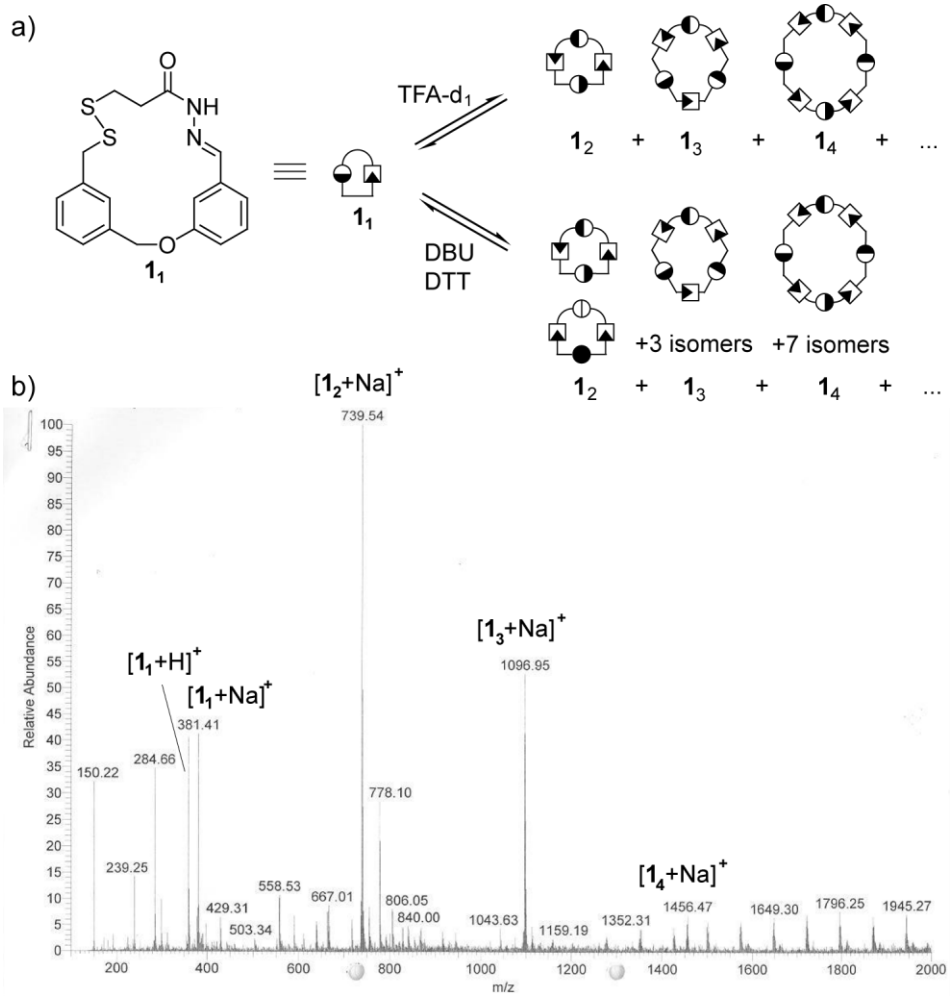

Figure 2.2. *a) Two sets of reaction conditions for the efficient conversion of macrocycle* $\mathbf{1_1}$ *into a distribution of cyclic oligomers* $\mathbf{1_n}$ *by dynamic covalent bond formation:[32] (acidic)* $\mathbf{1_1}$ *(7.0 μmol, 1 equiv.), 0.5 mL* $CDCl_3$*, TFA-*d_1 *(35 μmol, 5 equiv.) 1 day, RT; (basic)* $\mathbf{1_1}$ *(7.0 μmol, 1 equiv.), 0.5 mL* $CDCl_3$*, DBU (7 μmol, 1 equiv.) and DTT (0.7 μmol, 0.1 equiv.), 2 days, RT. b) ESI⁺ mass spectrum of an equilibrium mixture containing* $\mathbf{1_1}$ *and higher oligomers* $\mathbf{1_n}$ *after treatment of* $\mathbf{1_1}$ *in* $CDCl_3$ *under acidic conditions:* $\mathbf{1_1}$ *(7.0 μmol, 1 equiv.), 0.5 mL* $CDCl_3$*, TFA-*d_1 *(35 μmol, 5 equiv.) 1 day, RT. Note: The mass spectrum shows a disproportionately high amount of oligomers. See section 2.4.4 for the corresponding* ^{1}*H NMR spectrum (which shows that in fact only <5% oligomers are present in the mixture) and for further comments.*

Under the two most efficient sets of acidic and basic conditions (TFA-d_1 in $CDCl_3$ and DBU/DTT in $CDCl_3$), small, but detectable amounts (see section 2.4.4 for an ^{1}H NMR spectrum) of dimeric ($\mathbf{1_2}$), trimeric ($\mathbf{1_3}$) and tetrameric ($\mathbf{1_4}$) macrocyclic analogues[32] of $\mathbf{1_1}$ were found in the equilibrium mixtures after a typical equilibration time of 1-2 days at RT (after which time the composition of the reaction mixtures no longer changed) as confirmed by electrospray ionisation-mass spectrometry (ESI-MS) (Figure 2.2b). (Note: the two mixtures resulting from acidic or basic conditions should not be identical—experimental evidence for this was provided by slight differences in the ^{1}H NMR

spectra—because disulfide exchange can result in a higher number of constitutional isomers for each group of cyclic oligomers $\mathbf{1_n}$ with n>1; see Figure 2.2a[32]).

2.2.4 Dynamic Chemistry II: Ring-Opening of Macrocycle $\mathbf{1_1}$ in the Presence of a Single Disulfide or Hydrazone Scavenger

A second series of experiments was conducted with the objective of confirming which functional group was dynamic under which set of conditions, opening macrocycle $\mathbf{1_1}$ at either the disulfide or at the hydrazone linkage in the presence of acyclic 'scavenger' molecules (Scheme 2.6).

For disulfide exchange the symmetric benzylic disulfide **9** was used as the scavenger (Scheme 2.6a) and for hydrazone exchange the scavenger employed was acylhydrazone **10** (Scheme 2.6b). First, the optimised basic conditions determined from the dynamic experiments in the absence of scavengers (initial concentration of $\mathbf{1_1}$ 12 mM, $CDCl_3$, 1.0 equiv. DBU and 0.1 equiv. DTT, RT, 1-2 days) were applied to a mixture of $\mathbf{1_1}$ and an excess (5 equiv.) of **9** (Scheme 2.6a), resulting in formation of **11** in 28% isolated yield (along with $\mathbf{1_1}$ and small amounts of higher cyclic and open-chain oligomers). In a separate experiment $\mathbf{1_1}$ was subjected to the optimised acidic conditions (initial concentration of $\mathbf{1_1}$ 12 mM, $CDCl_3$, 5 equiv. of TFA-d_1, RT, 6-12 hours) in the presence of an excess (5 equiv.) of hydrazone scavenger **10** (Scheme 2.6b), which gave **12** in 26% isolated yield (along with small amounts of oligomeric species).

When only one equivalent of scavenger was used, **11** and **12** were each formed as roughly 5% of the product mixture (as determined by ^{1}H NMR) under the basic and acidic conditions, respectively (see Figure 2.3a). To prove that these mixtures were indeed at thermodynamic minimum, pristine ring-opened products **11** and **12** in the absence of scavenger were subjected to basic (**11**) or acidic (**12**) conditions in two 'reverse-equilibration' experiments (Figure 2.3).

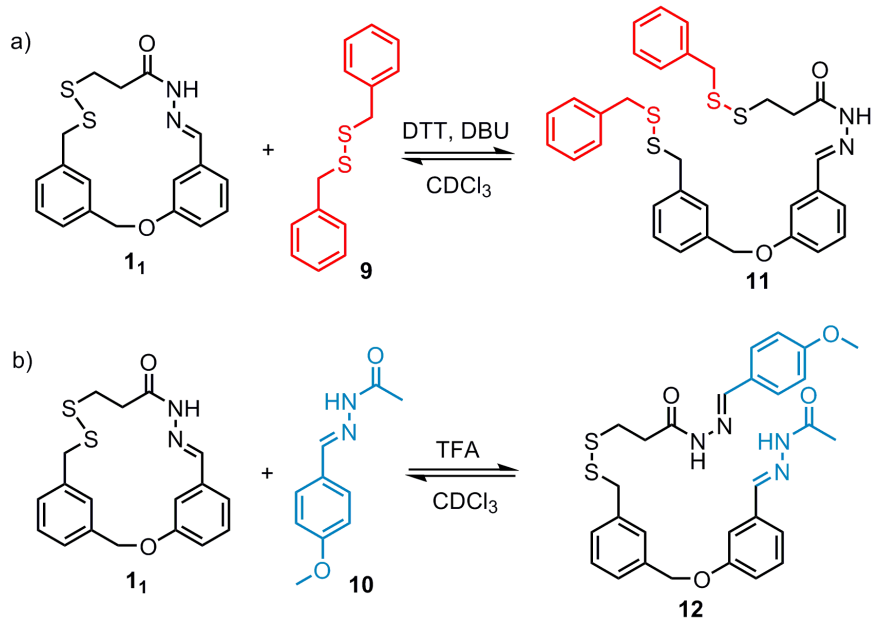

Scheme 2.6. *Dynamic covalent ring-opening of macrocycle* ***1₁*** *in the presence of an acyclic disulfide or hydrazone scavenger. a) Disulfide exchange of macrocycle* ***1₁*** *(59 μmol, 1 equiv.) with disulfide scavenger* ***9*** *(0.29 mmol, 5 equiv.) under basic conditions (DBU, 59 μmol, 1 equiv.; DTT, 5.9 μmol, 0.1 equiv.) in $CDCl_3$ (5 mL, initial concentration of* ***1₁*** *12 mM) after 24-48 hours at RT led to an equilibrium mixture of* ***1₁***, ***9*** *and ring-opened product* ***11*** *(molar ratios:* ***1₁:9:11*** *13:82:5). b) Acid-mediated (TFA-d_1, 0.29 mmol, 5 equiv.) hydrazone exchange of macrocycle* ***1₁*** *(59 μmol, 1 equiv.) with hydrazone scavenger* ***10*** *(0.29 mmol, 5 equiv.) in $CDCl_3$ (5 mL, initial concentration of* ***1₁*** *12 mM) after 6-12 hours at RT led to an equilibrium mixture of* ***1₁***, ***10*** *and ring-opened product* ***12*** *(molar ratios* ***1₁:10:12*** *13:82:5). Note: small amounts of oligomers (<5% as indicated by ^{1}H NMR) were also present in the equilibrium mixtures.*

Figure 2.3b shows the conversion of **11** back into $\mathbf{1_1}$ as monitored by ^{1}H NMR spectroscopy. Starting from pure **11**, a 95% conversion into macrocycle $\mathbf{1_1}$ was observed over 24 h under the standard basic conditions (Figure 2.3a). Similarly **12** was converted back into $\mathbf{1_1}$ in approximately 95% yield under acidic conditions. These results confirmed that under the basic and acidic reaction conditions an ~95:5 molar ratio of macrocycle to ring-opened product corresponds to the thermodynamic minimum of the system (at a substrate concentration of 12 mM in $CDCl_3$ at RT). The ^{1}H NMR spectrum displayed at the front of Fig. 2b also shows minor peaks that are indicative for cyclic oligomers $\mathbf{1_n}$ (with n>1). The total amount of these species did, however, not exceed ~5% of the mixture.

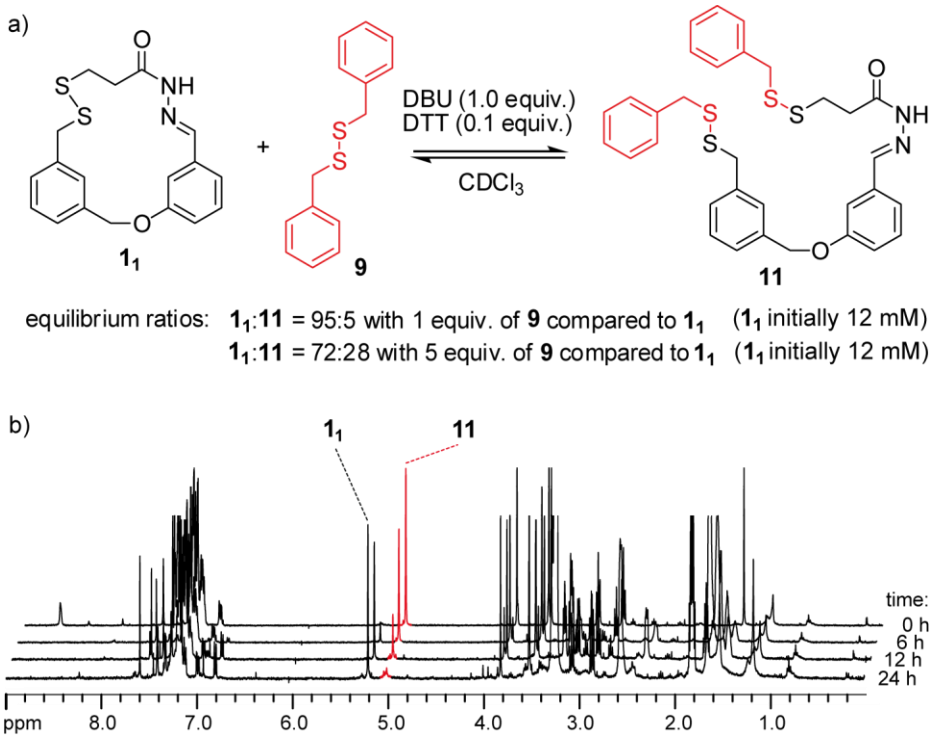

Figure 2.3. *a) Composition of equilibrium between* ***1₁****,* ***9*** *(1 or 5 equiv.) and* ***11****. Reaction conditions: Initial concentration of* ***1₁*** *or* ***11****: 12 mM, DBU (1 equiv.), DTT (0.1 equiv.), RT, 24-48 hours. b)* ^{1}*H NMR monitoring of reverse-equilibration experiment (initial concentration of* ***11*** *12 mM). Pristine ring-opened product* ***11*** *(rear spectrum) was converted back into a mixture containing predominantly macrocycle* ***1₁*** *(****1₁****:****11*** *~95:5) (front spectrum). The signals for the methylene groups in the ether linkages (in the region* δ *= 5.0-5.15 ppm), which differ significantly in chemical shift in* ***1₁*** *and* ***11****, are highlighted.*

2.2.5 Dynamic Chemistry III: Competition Experiments with Macrocycle 1_1 in the Presence of Both Disulfide and Hydrazone Scavengers 9 and 10

Figure 2.4a shows a third series of experiments on the dynamic ring-opening of macrocycle **1₁**. In a competition experiment, a mixture of macrocycle **1₁** and both scavenger compounds **9** (5 equiv.) and **10** (5 equiv.) was subjected to the optimised conditions for either, (i), disulfide or, (ii), hydrazone exchange (see section 2.4.2 for reaction conditions). HPLC analysis (Figure 2.4b) of the resulting mixtures revealed that under basic conditions only ring-opened compound **11** (resulting from disulfide exchange) was obtained (yellow peak in trace (i)), whereas **12** (which would arise from hydrazone exchange) was not observed. Under acidic conditions the opposite result occurred, hydrazone-exchanged ring-opened product **12** (purple peak in trace (ii)) was formed without any of **11**. As in all previous experiments, ^{1}H NMR indicated the presence of a low amount (<5%) of oligomeric species that were formed as byproducts under the applied reaction conditions. These results confirm that conditions (i) and (ii)

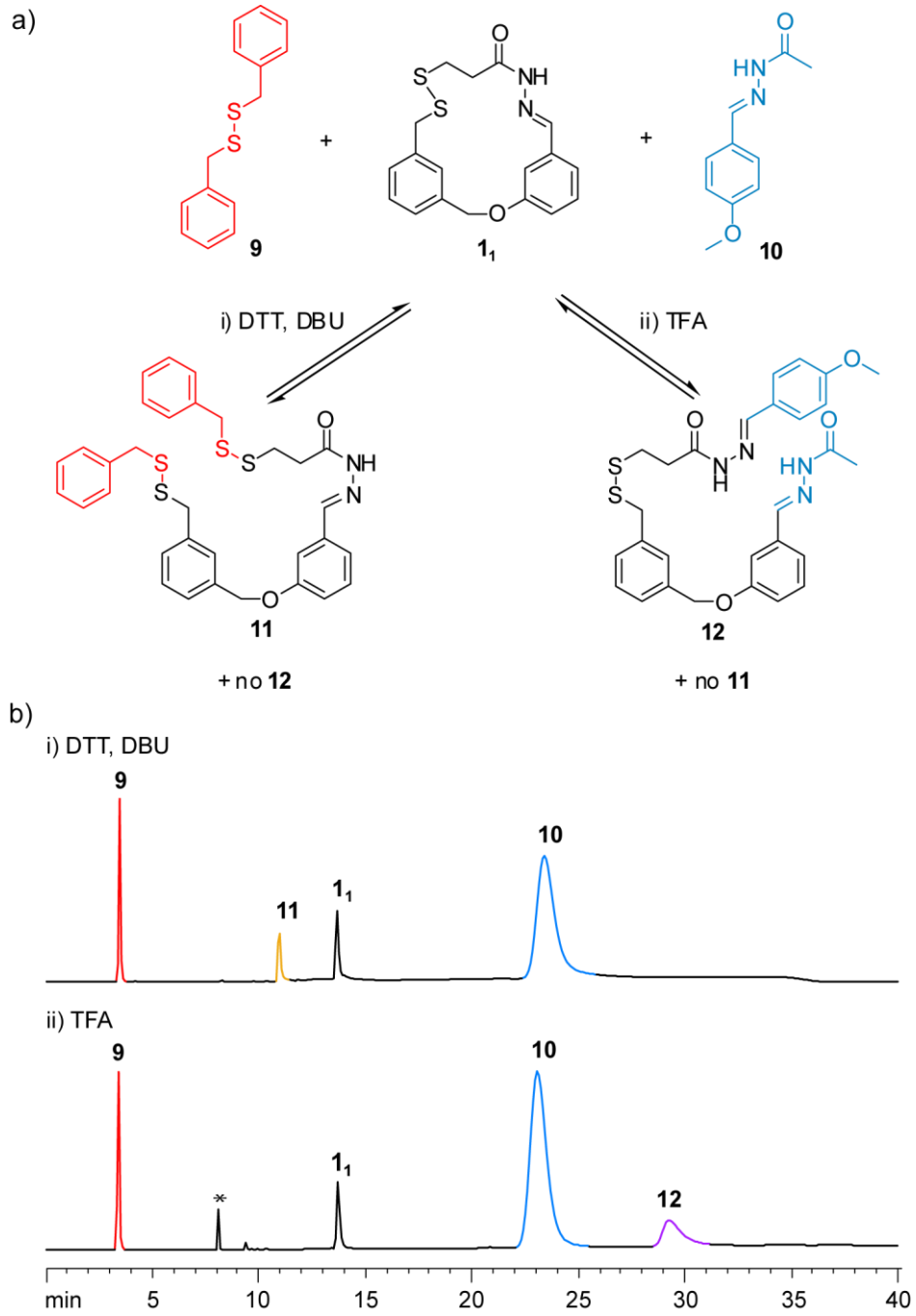

Figure 2.4. *Competition experiments in the presence of both scavengers* ***9*** *and* ***10*** *which demonstrated the mutually exclusive nature of conditions (i) and (ii) for disulfide and hydrazone exchange. a) A mixture of macrocycle* $\mathbf{1_1}$ *(1 equiv.), disulfide scavenger* ***9*** *(5 equiv.) and hydrazone scavenger* ***10*** *(5 equiv.) was subjected to two sets of conditions in independent experiments: (i) basic conditions; DTT (0.1 equiv.), DBU (1.0 equiv.) in* $CDCl_3$ *(5 mL); (ii) acidic conditions; TFA (5 equiv.) in* $CDCl_3$ *(5 mL), 6 h. Initial concentration of* $\mathbf{1_1}$ *12 M in both experiments (see experimental section for further details). b) HPLC traces showing the outcome of the two competition experiments. i) Equilibrium composition after treatment of a mixture of* $\mathbf{1_1}$, ***9*** *and* ***10*** *with DBU and DTT (see experimental section for details). ii) Equilibrium composition after treatment with TFA (mixture was quenched with* Et_3N *prior to dilution for HPLC analysis). * Hydrolysis product of* ***10****, p-methoxybenzaldehyde. Note: the chromatographic method (see experimental section) does not account for oligomeric species (significantly more polar).*

are, indeed, mutually exclusive with respect to the dynamic covalent exchange processes that they induce.

Basic conditions, (i), promote disulfide exchange and preclude hydrazone exchange and *vice versa*: acidic conditions, (ii), induce hydrazone exchange and preclude disulfide exchange. Equally importantly, neither set of conditions are affected by the presence of the scavenger that does not undergo dynamic exchange under those conditions.

The macrocyclic hydrazone-disulfide system is subject to different entropic considerations to the previously studied acyclic systems.[Fehler! Textmarke nicht definiert.] This is apparent in the remarkable dependence of the equilibrium composition on concentration. For example, we were only able to obtain HPLC trace (ii) shown in Figure 2.4b when hydrazone exchange was quenched in the concentrated reaction mixture (12 mM in $CDCl_3$) by addition of Et_3N prior to dilution for HPLC analysis (after dilution: ~0.5 mM in $CHCl_3/CDCl_3$). When the diluted, unquenched solution (still containing 5 equiv. TFA) was not immediately injected for analysis, the still-dynamic system quickly responded to the dilution by a dramatic change in composition so that product **12** was no longer

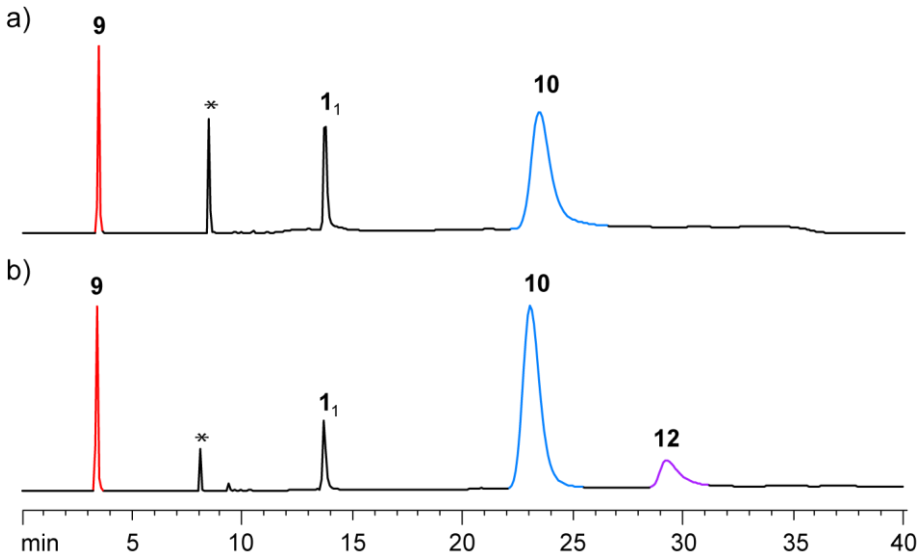

Figure 2.5. *Two HPLC traces obtained from <u>one</u> TFA-promoted hydrazone exchange competition experiment (see Figure 2.4a and conditions (ii) specified in the caption of Figure 2.4). a) Sample prepared by dilution (~20-fold) and left standing for an hour prior to HPLC analysis. Since this sample was still dynamic after dilution, virtually all of* ***12*** *that had been present had been converted back to* ***1₁*** *and* ***10****. b) Sample treated with excess Et_3N before dilution and left standing for an hour prior to HPLC analysis. Since addition of the base neutralised the acid, hydrazone exchange was switched off. Therefore this HPLC trace reflects the composition of the mixture before dilution. Note: the chromatographic method (see experimental section) does not account for oligomeric species (significantly more polar).*

detected (see Figure 2.5a). Figure 2.5 provides a direct comparison of the HPLC traces corresponding to the unquenched (Figure 2.5a) and quenched (Figure 2.5b) samples.

These observations are explained by the fact that formation of **12** by reaction of macrocycle $\mathbf{1_1}$ with scavenger **10** is a bimolecular process and is therefore slower at lower concentrations. The reverse process of **12** into $\mathbf{1_1}$ and **10** is unimolecular and therefore occurs independent of concentration. This may also explain why, despite the solid state structure of macrocycle $\mathbf{1_1}$ showing evidence of ring strain, equilibration in the presence of scavengers under the conditions investigated (the second and third series of dynamic experiments) only gave minor amounts of the ring-opened products. The dynamic chemistry of the hydrazone-disulfide macrocyclic system is thus governed by a delicate balance of enthalpic and entropic effects. This offers the opportunity to manipulate relatively strained monomeric macrocycles under thermodynamic control without obtaining significant amounts of less strained ring-opened or oligomeric side products. These features were recently exploited to provide a mechanism by which a small molecule can "walk" processively down a molecular track (see Chapter III).[25]

2.3 *Conclusions*

We have developed methodology for the synthesis of a novel macrocycle that contains both a disulfide and a hydrazone moiety and studied its dynamic chemistry. The solid state structure suggests that a certain amount of strain is caused by having several rigid elements within the framework of a 17-membered macrocycle. Sets of reaction conditions were established whereby the disulfide and hydrazone moieties can selectively undergo dynamic covalent exchange reactions in a mutually exclusive manner. Applications based on these systems are currently on-going in our laboratory.

2.4 *Experimental Section*

2.4.1 General Information

Compounds **2**,[33] **6**[34] and **10**[35] were prepared according to modified literature procedures. Compound **9** and 3-hydroxybenzaldehyde were purchased from Sigma Aldrich.

Analytical and preparative HPLC was performed on instruments of Gilson Inc., USA. For all shown chromatograms, a normal-phase column (Kromasil-Si, 250 × 4.6 mm) was used with gradient elution (1 mL/min, CH_2Cl_2/MeCN, 0 → 62.5% MeCN, UV detection @ 260 nm).

2.4.2 Procedures for Competition Experiments

(i) Dibenzyl disulfide **9** (72 mg, 0.29 mmol, 5.0 equiv.), benzoic acid [1-phenyl-meth-(*E*)-ylidene]-hydrazide **10** (56 mg, 0.29 mmol, 5.0 equiv.), DBU (8.8 mg, 58.6 μmol, 1.0 equiv.), DTT (1 mg, 6.5 μmol, 0.1 equiv.) and macrocycle $\mathbf{1_1}$ (21 mg, 58.6 μmol, 1.0 equiv.) were dissolved in $CDCl_3$ (5 mL, initial concentration of $\mathbf{1_1}$ 12 mM) and the mixture was stirred at room temperature until analytical HPLC indicated that the equilibrium composition was reached (24-48 h).

(ii) Dibenzyl disulfide **9** (72 mg, 0.29 mmol, 5.0 equiv.), benzoic acid [1-phenyl-meth-(*E*)-ylidene]-hydrazide **10** (56 mg, 0.29 mmol, 5.0 equiv.), TFA (33 mg, 22 μL, 0.29 mmol, 5.0 equiv.) and macrocycle $\mathbf{1_1}$ (21 mg, 58.6 μmol, 1.0 equiv.) were dissolved in $CDCl_3$ (5 mL, initial concentration of $\mathbf{1_1}$ 12 mM) and the mixture was stirred at room temperature until analytical HPLC indicated that the equilibrium composition was reached (6-12 h).

2.4.3 Syntheses

3-Chloromethylbenzyl alcohol

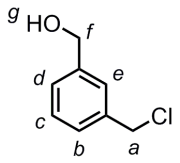

2

Synthesised according to a modified literature procedure.[33] At 5 °C, a solution of ethyl chloroformate (1.69 mL, 17.2 mmol, 1.0 equiv.) in THF (7 mL) was added dropwise to a solution of 3-(chloromethyl)-benzoic acid (3.02 g, 17.2 mmol, 1.0 equiv.) and Et_3N (2.39 mL, 17.2 mmol, 1.0 equiv.) in THF (30 mL). The reaction was allowed to proceed at 5 °C for 30 min before the Et_3NHCl precipitate was filtered off and washed with THF (40 mL). The combined THF phases were added over 30 min to a solution of $NaBH_4$ (1.66 g, 43 mmol, 2.5 equiv.) in H_2O (14 mL) at 10 °C. The mixture was stirred over night at room temperature and then acidified with 10% HCl (17 mL). The solution was extracted with Et_2O (3 × 50 mL), washed with a solution of 10% NaOH (50 mL) and brine (50 mL), dried ($MgSO_4$), and concentrated under reduced pressure. Flash column chromatography (SiO_2, hexane/EtOAc 8:2) of the residue gave **2** (2.50 g, 85%) as a colourless oil. ^{1}H NMR (400 MHz, $CDCl_3$): δ = 7.34 (m, 4H, H_b, H_c, H_d, H_e), 4.68 (s, 2H, H_f), 4.60 (s, 2H, H_a), 2.32 (bs, 1H, H_g); LRMS (EI): m/z = 156.1 $[M]^+$.

3-(3-(Hydroxymethyl)benzyloxy)benzaldehyde

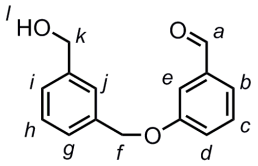

3

Under N_2, 3-hydroxybenzaldehyde (3.87 g, 31.69 mmol, 1.0 equiv.) was dissolved in DMF (25 mL) and cooled to 0°C. NaH (60% in mineral oil, 1.27 g, 31.75 mmol, 1.0 equiv.) was added and the mixture was stirred until all NaH was dissolved (temperature allowed to raise to room temperature). A solution of **2** (3.31 g, 21.14 mmol, 0.67 equiv.) in DMF (25 mL) was added dropwise. The reaction was stirred for 48 h at room temperature and monitored by TLC (silica gel, toluene/EtOAc 3:1). After TLC showed that no starting material remained, 1M HCl (50 mL) was added and the mixture was extracted with EtOAc (3 × 50 mL). The combined organic layers were washed with 1M HCl (50 mL) H_2O (50 mL) and brine (50 mL), and dried over $MgSO_4$. Concentration under reduced pressure yielded a residue, which was purified by flash column chromatography (SiO_2, toluene/EtOAc 15:2) to give **3** (4.27 g, 83%) as a colourless oil. ^{1}H NMR (400 MHz, $CDCl_3$): δ = 9.97 (s, 1H, H_a), 7.50 – 7.45 (m, 4H, H_{Ar}), 7.42 – 7.34 (m, 3H, H_{Ar}), 7.27 – 7.24 (m, 1H, H_{Ar}), 5.13 (s, 2H, H_f), 4.73 (s, 2H, H_k), 1.79 (bs, 1H, H_l); ^{13}C NMR (100 MHz, $CDCl_3$): δ = 192.13 (d), 159.27 (s), 141.46 (s), 137.81 (s), 136.65 (s), 130.15 (d), 128.91 (d), 127.60 (d), 127.60 (d), 126.03 (d), 123.79 (d), 122.20 (d), 113.21 (d), 70.12 (t), 65.07 (t); HRMS (ESI): m/z = 260.1279 $[M+NH_4]^+$ (calcd. 260.1281 for $C_{15}H_{18}NO_3$).

3-(3-(Bromomethyl)benzyloxy)benzaldehyde

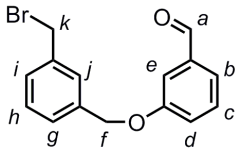

4

Under N_2, **3** (2.10 g, 8.67 mmol, 1.0 equiv.) was dissolved in benzene (25 mL). A solution of $SOBr_2$ (3.75 g, 1.40 mL, 18.05 mmol, 2.1 equiv.) in benzene (20 mL) was added dropwise at 0 °C. The reaction was monitored by TLC (SiO_2, toluene/EtOAc 3:1). Stirring was continued for 48 h at room temperature until TLC indicated that no

starting materials remained. H_2O (25 mL) was added and the mixture was extracted with EtOAc (2 × 25 mL). The combined organic layers were washed with H_2O (50 mL), dried with brine (50 mL) and over $MgSO_4$ and concentrated under reduced pressure to yield a brownish oil. The residue was purified by flash column chromatography (SiO_2, cyclohexane/CH_2Cl_2/ EtOAc 15:1:1) to yield **4** (1.92 g, 73%) as a colourless oil. ^{1}H NMR (400 MHz, $CDCl_3$): δ = 9.98 (s, 1H, H_a), 7.51 – 7.45 (m, 4H, H_{Ar}), 7.39 – 7.37 (m, 3H, H_{Ar}), 7.27 – 7.24 (m, 1H, H_{Ar}), 5.12 (s, 2H, H_f), 4.52 (s, 2H, H_k); ^{13}C NMR (100 MHz, $CDCl_3$): δ = 192.00 (d), 159.18 (s), 138.29 (s), 137.86 (s), 137.04 (s), 130.18 (d), 129.18 (d), 128.86 (d), 128.05 (d), 127.50 (d), 123.86 (d), 122.16 (d), 113.20 (d), 69.81 (t), 33.15 (t); HRMS (ESI): *m/z* = 322.0433 $[M+NH_4]^+$ (calcd. 322.0437 for $C_{15}H_{17}NO_2Br$).

Thioacetic acid S-[3-(3-formyl-phenoxymethyl)-benzyl] ester

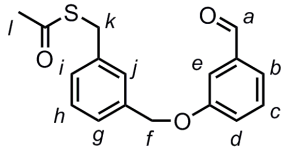

5

4 (1.81 g, 5.93 mmol, 1.0 equiv.) was dissolved in DMF (20 mL) and a solution of KSAc (1.36 g, 11.91 mmol, 2.0 equiv.) in DMF (20 mL) was added dropwise. The mixture was stirred over night at room temperature. The reaction was quenched by addition of a saturated aqueous solution of NH_4Cl (20 mL). The mixture was extracted with EtOAc (3 × 30 mL) and the combined organic layers were washed with 1M HCl (20 mL), H_2O (20 mL), and brine (20 mL) and dried ($MgSO_4$). Concentration under reduced pressure yielded **5** (1.70 g, 95%) as a brownish oil that did not require further purification. ^{1}H NMR (400 MHz, $CDCl_3$): δ = 9.98 (s, 1H, H_a), 7.50 – 7.44 (m, 3H, H_{Ar}), 7.37 (s, 1H, H_{Ar}), 7.34 – 7.31 (m, 2H, H_{Ar}), 7.29 – 7.24 (m, 2H, H_{Ar}), 5.09 (s, 2H, H_f), 4.14 (s, 2H, H_k), 2.36 (s, 3H, H_l); ^{13}C NMR (100 MHz, $CDCl_3$): δ = 195.02 (s), 192.09 (d), 159.22 (s), 138.22 (s), 137.81 (s), 136.75 (s), 130.16 (d), 129.01 (d), 128.70 (d), 127.97 (d), 126.50 (d), 123.73 (d), 122.15 (d), 113.27 (d), 69.95 (t), 33.27 (t), 30.36 (q); HRMS (ESI): *m/z* = 318.1157 $[M+NH_4]^+$ (calcd. 318.1158 for $C_{17}H_{20}NO_3S$).

3-Mercaptopropanehydrazide

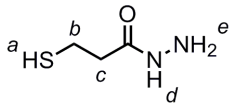

6

Synthesised according to a modified literature procedure.[34] Methyl 3-mercaptopropionate (10 g, 83 mmol, 1.0 equiv.) was added dropwise to a solution of hydrazine monohydrate (10 g, 200 mmol, 2.4 equiv.) in MeOH (30 mL). The reaction mixture was stirred over night at room temperature. Evaporation of the solvent, followed by flash column chromatography (SiO_2, Et_2O/MeOH 8:2) gave **6** (4.99 g, 50%) as a colourless oil. ^{1}H NMR (400 MHz, $CDCl_3$): δ = 6.81 (bs, 1H, H_d), 3.93 (bs, 2H, H_e), 2.84 (dt, *J* = 8.4 Hz, 6.4 Hz, 2H, H_b), 2.50 (t, *J* = 6.7 Hz, 2H, H_c), 1.61 (t, *J* = 8.4 Hz, 1H, H_a).

Thioacetic acid *S*-(3-{3-[(3-mercapto-propionyl)-hydrazonomethyl]-phenoxymethyl}-benzyl) ester

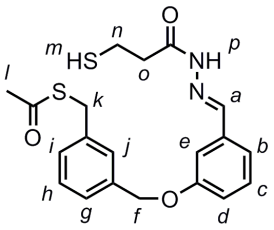

7

5 (1.325 mg, 4.38 mmol, 1.0 equiv.) was dissolved in MeOH (25 mL) and 5 drops of acetic acid were added. A solution of **6** (673 mg, 5.60 mmol, 1.3 equiv.) in MeOH (15 mL) was added dropwise after which the mixture was stirred for 3 h at room temperature. The reaction was monitored by TLC (SiO_2, cyclohexane/EtOAc 5:2). The solvent was removed *in vacuo* and the residue was purified by flash column chromatography (SiO_2, cyclohexane/EtOAc 5:2 → 3:2) to yield a mixture of thioester **7** and dithiol **8** in a ratio of 85:15 (1.52 g, 88%). *E*/Z ratio of the hydrazone was approximately 9:1. Major *E*-isomer: ^{1}H NMR (400 MHz, $CDCl_3$): δ = 9.13 (s, 1H, H_p), 7.72 (s, 1H, H_a), 7.34 (s, 1H, H_{Ar}), 7.34 – 7.27 (m, 5H, H_{Ar}), 7.21 (d, *J* = 7.6 Hz, 1H, H_{Ar}), 7.02 (ddd, *J* = 8.2, 2.7, 0.8 Hz, 1H, H_{Ar}), 5.07 (s, 2H, H_f), 4.14 (s, 2H, H_k), 3.12 (t, *J* = 6.9 Hz, 2H, H_o), 2.91 (dt, *J* = 8.3, 6.9 Hz, 2H, H_n), 2.36 (s, 3H, H_l), 1.74 (t, *J* = 8.3 Hz, 1H, H_m); some characteristic signals of the minor *Z*-isomer; 8.70 (s, 1H, H_p), 8.12 (s, 1H, H_a), 5.06 (s, 2H, H_f), 2.64 (t, *J* = 6.6 Hz, 2H, H_o); ^{13}C NMR (100 MHz, $CDCl_3$): δ = 195.04 (s), 173.83 (s),

159.02 (s), 143.85 (d), 138.14 (s), 137.10 (s), 135.04 (s), 129.88 (d), 128.99 (d), 128.61 (d), 127.95 (d), 126.50 (d), 120.58 (d), 117.01 (d), 112.66 (d), 69.96 (t), 36.95 (t), 33.32 (t), 30.35 (q), 19.47 (t); HRMS (ESI): m/z = 403.1144 $[M+H]^+$ (calcd. 403.1145 for $C_{20}H_{23}N_2O_3S_2$).

3-Mercapto-propionic acid [1-[3-(3-mercaptomethyl-benzyloxy)-phenyl]-meth-(E)-ylidene]-hydrazide

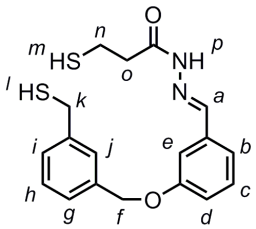

8

Under N_2, a mixture of starting material **7** and the product **8** (85:15, 1.50 g, 3.80 mmol, 1.0 equiv.) was dissolved in MeOH (25 mL). A solution of NaOMe (246 mg, 4.55 mmol, 1.2 equiv.) in MeOH (15 mL) was added. After 2 h NH_4Cl, (satd., 20 mL) was added and the mixture was stirred for another 15 min. The mixture was extracted with EtOAc (3 × 25 mL) and the combined organic layers were washed with H_2O (2 × 50 mL) and brine (25 mL) and dried ($MgSO_4$). The solvent was removed under reduced pressure to yield a 15:1 mixture of **8** and $\mathbf{1_1}$ (1.07 g, 78%) as a thick transparent oil. The dithiol **8** was found in an E/Z ratio of about 9:1. Major E-isomer. ^{1}H NMR (400 MHz, $CDCl_3$): δ = 9.23 (s, 1H, H_n), 7.72 (s, 1H, H_a), 7.43 (s, 1H, H_{Ar}), 7.38 – 7.30 (m, 5H, H_{Ar}), 7.22 (d, J = 7.7 Hz, 1H, H_{Ar}), 7.02 (ddd, J = 8.2, 2.6, 0.8 Hz, 1H, H_{Ar}), 5.10 (s, 2H, H_f), 3.77 (d, J = 7.6 Hz, 2H, H_k), 3.12 (t, J = 6.9 Hz, 2H, H_o), 2.91 (dt, J = 8.2, 6.9 Hz, 2H, H_n), 1.79 (t, J = 7.6 Hz, 1H, H_l), 1.74 (t, J = 8.2 Hz, 1H_m); characteristic signals of the minor Z-isomer: 8.71 (s, 1H, H_n), 8.12 (s, 1H, H_a), 5.08 (s, 2H, H_f), 2.64 (t, J = 6.5 Hz, 2H, H_m); ^{13}C NMR (100 MHz, $CDCl_3$): δ = 174.10 (s), 159.01 (s), 144.08 (d), 141.61 (s), 137.14 (s), 135.10 (s), 129.90 (d), 129.04 (d), 127.86 (d), 127.20 (d), 126.27 (d), 120.64 (d), 116.99 (d), 112.60 (d), 69.94 (t), 36.94 (t), 28.89 (t), 19.52 (t); HRMS (ESI): m/z = 378.1300 $[M+NH_4]^+$ (calcd. 378.1304 for $C_{18}H_{24}N_3O_2S_2$).

2-Oxa-10,11-dithia-15,16-diazatricyclo[16.3.1.1^{4,8}] tricosa-1(22),4,6,8(23),16,-18,20-heptaen-14-one

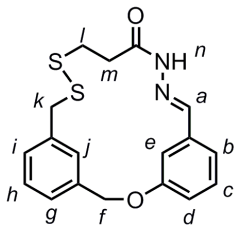

$\mathbf{1_1}$

Under N_2, a mixture of dithiol **8** and disulfide $\mathbf{1_1}$ (15:1, 360 mg, 1.00 mmol, 1.0 equiv.) was dissolved in MeOH (100 mL) and CH_2Cl_2 (100 mL). A solution of KI (51 mg, 0.303 mmol, 0.3 equiv.) in MeOH (~5 mL) was added and subsequently, at 0°C, a solution of I_2 (267 mg, 1.05 mmol, 1.05 equiv.) in MeOH (~ 25 mL) was added dropwise until the brown colour persisted. Na_2SO_3 was added and, when decolourisation was complete, stirring was continued for 15 min. H_2O (100 mL) and CH_2Cl_2 (100 mL) were added and the H_2O layer was extracted another time with CH_2Cl_2 (100 mL). The combined organic layers were washed with H_2O (100 mL) and with brine (100 mL) and dried ($MgSO_4$). Removal of the solvents under reduced pressure and purification by flash column chromatography (SiO_2, $CHCl_3$/EtOAc 3:1) yielded pure $\mathbf{1_1}$ (200 mg, 56%) as a colourless solid. M.p. 188 °C. ^{1}H NMR (400 MHz, $CDCl_3$): δ = 9.48 (s, 1H, H_n), 7.66 (s, 1H, H_a), 7.48 (s, 1H, H_j), 7.39 (dd, *J* = 2.6, 1.5 Hz, 1H, H_e), 7.30 – 7.28 (m, 3H, H_c, H_g, H_h), 7.19 (ddd, *J* = 6.7, 1.5, 0.9 Hz, 1H, H_i), 7.06 (ddd, *J* = 8.4, 2.6, 0.9 Hz, 1H, H_d), 6.89 (d, *J* = 7.4 Hz, 1H, H_b), 5.28 (s, 2H, H_f), 3.89 (s, 2H, H_k), 3.14 (dd, *J* = 7.7, 7.1 Hz, 2H, H_m), 2.92 (dd, *J* = 7.7, 7.1 Hz, 2H, H_l); ^{13}C NMR (100 MHz, DMSO-d_6): δ = 172.37 (s), 157.95 (s), 142.07 (d), 137.35 (s), 137.05 (s), 135.36 (s), 129.91 (d), 129.68 (d), 129.00 (d), 128.19 (d), 126.10 (d), 122.24 (d), 119.69 (d), 107.31 (d), 68.81 (t), 41.08 (t), 31.14 (t), 30.37 (t); ε (260 nm, CH_2Cl_2) = 7872.5 dm^3 mol^{-1} cm^{-1}; HRMS (ESI): *m/z* = 359.0882 $[M+H]^+$ (calcd. 359.0882 for $C_{18}H_{19}N_2O_2S_2$).

Benzoic acid [1-phenyl-meth-(E)-ylidene]-hydrazide

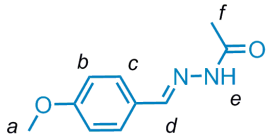

10

Synthesised according to a modified literature procedure.[35] A mixture of *p*-anisaldehyde (2.0 g, 14.7 mmol, 1.0 equiv.) and acethydrazide (1.21 g, 14.7 mmol, 1.0 equiv.) in EtOH (100 mL) was stirred at room temperature for 3 h. Filtration of the precipitate and recrystallisation from EtOH gave **10** (1.84 g, 65%) as a colourless, crystalline solid. ^{1}H NMR (400 MHz, $CDCl_3$): δ = 9.58 (bs, 1H, H_e), 7.75 (sb, 1H, H_d), 7.61 (d, *J* = 8.8 Hz, 2H, H_c), 6.92 (d, *J* = 8.8 Hz, 2H, H_b), 3.85 (s, 3H, H_a), 2.37 (s, 3H, H_f); ε (260 nm, CH_2Cl_2) = 6353.5 $dm^3\,mol^{-1}\,cm^{-1}$.

3-Benzyldisulfanyl-propionic acid [1-[3-(3-benzyl disulfanylmethyl-benzyloxy)-phenyl]-meth-(E)-ylidene]-hydrazide

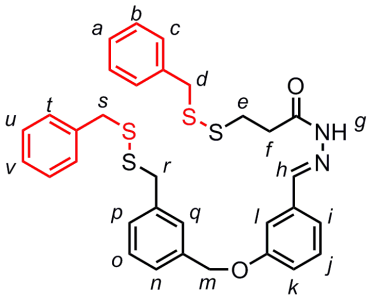

11

Dibenzyl disulfide **9** (72 mg, 0.29 mmol, 5.0 equiv.), DBU (45 mg, 0.30 mmol, 5.1 equiv.), DTT (1 mg, 6.48 µmol, 0.1 equiv.) and macrocycle $\mathbf{1_1}$ (21 mg, 58.6 µmol, 1.0 equiv.) were dissolved in $CDCl_3$ (5 mL, initial concentration of $\mathbf{1_1}$ 12 mM) and the mixture was stirred for 48 h. The reaction mixture was directly subjected to flash column chromatography (SiO_2, $CHCl_3$/EtOAc 5:1) to yield **11** (10 mg, 28%) as an oil. Signals for the minor *Z*-isomer were also observed (<10%). Major *E*-isomer: ^{1}H NMR (400 MHz, $CDCl_3$): δ = 9.13 (s, 1H, H_g), 7.66 (s, 1H, H_h), 7.36 – 7.16 (m, 17H, $H_{a\text{-}c}$, H_i, H_j, H_l, $H_{n\text{-}q}$, $H_{t\text{-}v}$), 7.03 (ddd, *J* = 8.2, 1.9, 0.7 Hz, 1H, H_k), 5.09 (s, 2H, H_m), 3.93 (s, 2H, H_r), 3.59 (s, 2H, H_s or H_d), 3.57 (s, 2H, H_s or H_d), 3.08 (t, *J* = 7.3 Hz, 2H, H_f), 2.82 (t, *J* = 7.3 Hz, 2H, H_e); characteristic signals of minor *Z*-isomer: 8.48 (s, 1H, H_g), 8.05 (s, 1H, H_h), 3.92 (s, 2H, H_r), 2.72 (t, *J* = 7.0 Hz, 2H, H_e), 2.50 (t, *J* = 7.0 Hz, 2H, H_f); ^{13}C NMR (100 MHz, $CDCl_3$):

δ = 173.48 (s), 158.99 (s), 143.39 (d), 137.88 (s), 137.31 (s), 137.22 (s), 136.98 (s), 134.95 (s), 129.91 (d), 129.43 (d), 129.32 (d), 129.19 (d), 128.80 (d), 128.57 (d), 128.51 (d), 128.48 (d), 127.50 (d), 127.47 (d), 126.56 (d), 120.58 (d), 117.81 (d), 112.55 (d), 69.87 (t), 43.57 (t), 43.28 (t), 43.03 (t), 32.98 (t), 32.79 (t); ε (260 nm, CH_2Cl_2) = 9677.9 dm^3 mol^{-1} cm^{-1}; HRMS (ESI): m/z = 626.11647 $[M+Na-H]^+$ (calcd. 626.11606 for $C_{32}H_{31}N_2O_2S_4Na$).

3-{3-[3-(Acetyl-hydrazonomethyl)-phenoxymethyl]-benzyl disulfanyl}-propionic acid [1-(4-methoxy-phenyl)-meth-(E)-ylidene]-hydrazide

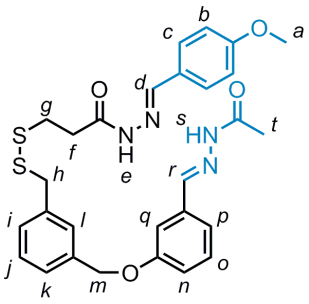

12

Hydrazide **10** (67 mg, 0.35 mmol, 5.0 equiv.) and macrocycle $\mathbf{1_1}$ (25 mg, 69.7 μmol, 1.0 equiv.) were dissolved/suspended in $CDCl_3$ (6 mL, initial concentration of $\mathbf{1_1}$ 12 mM). TFA-d_1 (40 mg, 26 μL, 0.35 mmol, 5.0 equiv.) was added and the mixture was stirred for 12 h. The reaction was monitored by ^{1}H NMR. During the reaction, the mixture slowly turned transparent yellowish. The reaction mixture was directly subjected to flash column chromatography (SiO_2, $CHCl_3$/EtOAc 1:1 → 1:3) to give **12** (10 mg, 26%) as an oil. Signals for the minor *Z*-isomers were also observed (<10%). Major *E*-isomer: ^{1}H NMR (400 MHz, $CDCl_3$): δ = 10.39 (s, 1H, H_e or H_s), 10.13 (s, 1H, H_e or H_s), 7.77 (s, 1H, H_d or H_r), 7.75 (s, 1H, H_d or H_r), 7.60 (d, J = 8.8 Hz, 2H, H_c), 7.41 (s, 1H, H_l), 7.32 – 7.26 (m, 5H, H_i, H_j, H_k, H_o, H_q), 7.12 (d, J = 1.7 Hz, 1H, H_p), 6.98 (ddd, J = 6.7, 2.7, 2.4 Hz, 1H, H_n), 6.90 (d, J = 8.8 Hz, 2H, H_b), 5.10 (s, 2H, H_m), 3.93 (s, 2H, H_h), 3.83 (s, 3H, H_a), 3.10 (dd, J = 7.1, 6.9 Hz, 2H, H_f), 2.89 (dd, J = 7.1, 6.9 Hz, 2H, H_g), 2.35 (s, 3H, H_t); ^{13}C NMR (100 MHz, $CDCl_3$): δ = 174.26 (s), 174.02 (s), 161.27 (s), 158.80 (s), 144.22 (d), 144.15 (d), 137.93 (s), 137.18 (s), 135.19 (s), 129.81 (d), 129.03 (d), 128.97 (d), 128.75 (d), 128.21 (d), 126.42 (s), 126.37 (d), 119.37 (d), 117.46 (d), 114.22 (d), 113.39 (d), 69.85 (t), 55.38 (q), 43.22 (t), 34.30 (t), 33.06 (t), 20.32 (q); ε (260 nm, CH_2Cl_2) = 14079.0 dm^3 mol^{-1} cm^{-1}; HRMS (ESI): m/z = 551.1777 $[M+H]^+$ (calcd. 551.1781 for $C_{28}H_{31}N_4O_4S_2$).

2.4.4 ^{1}H NMR Spectrum Corresponding to ESI Mass Spectrum in Figure 2.2

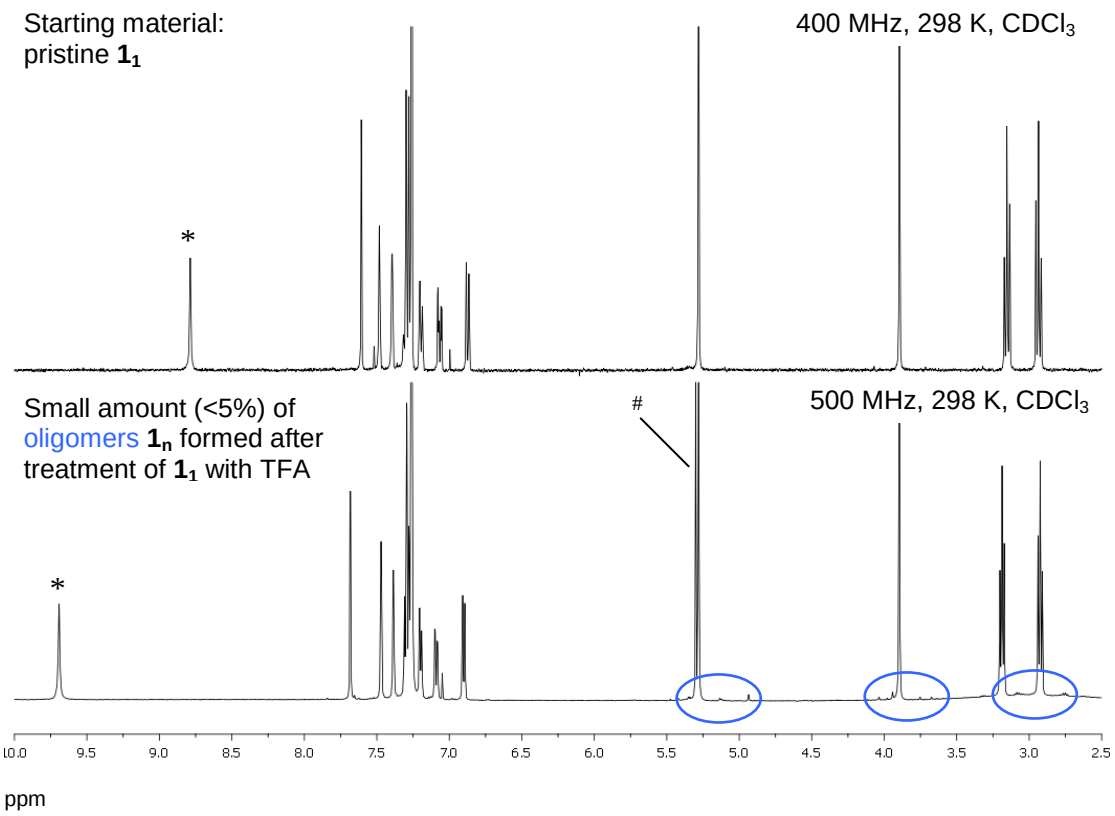

Figure 2.6. *^{1}H NMR spectrum corresponding to dynamic covalent exchange process and ESI mass spectrum shown in Figure 2.2. It is evident that only a small amount of oligomers was formed during this experiment (highlighted in blue circles). *: hydrazone N-H proton, exchanges with solvent. #: residual CH_2Cl_2 peak (from workup).*

Comments:

The ^{1}H NMR spectrum indicates that there is only a small amount of oligomers $\mathbf{1_n}$ (<5%) present and monomer $\mathbf{1_1}$ is by far the major compound in the mixture.

The relative peak heights in the ESI mass spectrum would, however, indicate that $\mathbf{1_2}$ is the major compound in the mixture.

Since low-resolution ESI mass spectrometry, unlike ^{1}H NMR spectroscopy, is not a quantitative analytical technique, we are certain that the mass spectrometric data is misleading. The most likely reason for this is the relatively low tendency of the monomer $\mathbf{1_1}$ to form a sodium-aggregate $[M+Na]^+$, whereas the oligomers under the ESI conditions seem to form rather stable sodium aggregates. Because only ionised particles will be able to reach the detector of the mass spectrometer, the different

tendency to form $[M+Na]^+$ species will have an impact on the observed relative peak heights. This hypothesis is supported by the fact that only for the monomer $\mathbf{1_1}$, but not for $\mathbf{1_2}$ or $\mathbf{1_3}$, a significant $[M+H]^+$ peak is observed (the $[M+H]^+$ peaks are therefore probably a better indicator for the composition of the mixture).

2.4.5 Crystallographic Data

Table 2.1. *Crystal data and structure refinement for* $\mathbf{1_1}$.

Empirical formula	$C_{18}H_{18}N_2O_2S_2$	
Formula weight	358.46	
Temperature	93(2) K	
Wavelength	0.71073 Å	
Crystal system	Monoclinic	
Space group	P2(1)/n	
Unit cell dimensions	a = 6.886(2) Å	α= 90°
	b = 9.252(3) Å	β= 96.481(5)°
	c = 26.755(8) Å	γ= 90°
Volume	1693.5(10) $Å^3$	
Z	4	
Density (calculated)	1.406 Mg/m^3	
Absorption coefficient	0.327 mm^{-1}	
F(000)	752	
Crystal size	0.0800 x 0.0800 x 0.0800 mm^3	
Theta range for data collection	2.33 to 25.33°.	
Index ranges	-8<=h<=8, -11<=k<=11, -32<=l<=29	
Reflections collected	14385	
Independent reflections	2984 [R(int) = 0.0813]	
Completeness to theta = 25.00°	96.6 %	
Absorption correction	Multiscan	
Max. and min. transmission	1.0000 and 0.9163	
Refinement method	Full-matrix least-squares on F^2	
Data / restraints / parameters	2984 / 1 / 223	
Goodness-of-fit on F^2	0.949	
Final R indices [I>2sigma(I)]	R1 = 0.0517, wR2 = 0.1273	
R indices (all data)	R1 = 0.0553, wR2 = 0.1344	
Extinction coefficient	0.050(9)	
Largest diff. peak and hole	0.311 and -0.283 $e.Å^{-3}$	

2.5 Notes and References

[1] For two articles that impressively demonstrate the utility of kinetically controlled reactions for the generation of thermodynamically unstable products, see: a) R. Hoffmann, H. Hopf, *Angew. Chem. Int. Ed*. **2008**, *47*, 4474; b) I. B. Seiple, S. Su, I. S. Young, C. A. Lewis, J. Yamaguchi, P. S. Baran, *Angew. Chem. Int. Ed*. **2010**, *49*, 1095.

[2] a) J.-M. Lehn, *Chem. Eur. J.* **1999**, *5*, 2455; b) J.-M. Lehn, A. V. Eliseev, *Science* **2002**, *291*, 2331; c) J.-M. Lehn, *Chem. Soc. Rev.* **2007**, *36*, 151.

[3] a) S. J. Rowan, S. J. Cantrill, G. R. L. Cousins, J. K. M. Sanders, J. F. Stoddart, *Angew. Chem. Int. Ed.* **2002**, *41*, 898; b) P. T. Corbett, J. Leclaire, L. Vial, K. R. West, J.-L. Wietor, J. K. M. Sanders, S. Otto, *Chem. Rev.* **2006**, *106*, 3652.

[4] a) S. Ladame, *Org. Biomol. Chem.* **2008**, *6*, 219; b) A. Herrmann, *Org. Biomol. Chem.* **2010**, *7*, 3195; c) M. Mastalerz, *Angew. Chem. Int. Ed*. **2010**, *49*, 5042.

[5] a) J.-M. Lehn, *Science* **1985**, *227*, 849; b) J.-M. Lehn, *Angew. Chem. Int. Ed.* **1988**, *27*, 89; c) J.-M. Lehn, *Science* **1993**, *260,* 1762; d) *Supramolecular Chemistry*, J.-M. Lehn, Wiley-VCH, Weinheim, **1995**.

[6] Selected references on dynamic polymers: a) *Principles of Polymerization*, G. Odian, Wiley-Interscience, New York, **1991**, 68; b) H. D. Maynard, R. H. Grubbs, *Macromol.* **1999**, *32*, 6917; c) T. Ono, T. Nobori, J.-M. Lehn, *Chem. Commun.* **2005**, 1522; d) H. Otsuka, K. Aotani, Y. Higaki, A. Takahara, *Chem. Commun.* **2002**, 2838; e) H. Otsuka, K. Aotani, Y. Higaki, A. Takahara, *J. Am. Chem. Soc.* **2003**, *125*, 4064; f) W. G. Skene; J.-M. Lehn, *Proc. Natl. Acad. Sci. USA* **2004**, *101*, 8270; g) E. Kolomiets, J.-M. Lehn, *Chem. Commun.* **2005**, 1519; h) Y. Ruff, J.-M. Lehn, *Angew. Chem. Int. Ed.* **2008**, *47*, 3556; i) S. Ulrich, J.-M. Lehn, *Angew. Chem. Int. Ed.* **2008**, *47*, 2240; j) C.-F. Chow, S. Fujii, J.-M. Lehn, *Angew. Chem. Int. Ed*. **2007**, *119*, 5095; k) P. Reutenauer, E. Buhler, P. J. Boul, S. J. Candau, J.-M. Lehn, *Chem. Eur. J.* **2009**, *15*, 1893; l) S. Fuji, J.-M. Lehn, *Angew. Chem. Int. Ed.* **2009**, *48*, 7635; m) T. Maeda, H. Otsuka, A. Takahara, *Prog. Polym. Sci.* **2009**, *34*, 581; n) Y. Ruff, E. Buhler, S. J. Candau, E. Kesselman, Y. Talmon, J.-M. Lehn, *J. Am. Chem. Soc.* **2010**, *132*, 2573; o) J.-M. Lehn, *Aust. J. Chem.* **2010**, *63*, 611.

[7] Selected references on DCC-based chemical sensors: a) S. Kubik, R. Kirchner, D. Nolting, J. Seidel, *J. Am. Chem. Soc.* **2002**, *124*, 12752; b) *Creative Chemical Sensor Systems*, S. Otto, K. Severin, Springer, Berlin, **2007**, 267; c) S. Hagihara, H. Tanaka, S. Matile, *J. Am. Chem. Soc.* **2008**, *130*, 5656.

[8] Selected references on the use of DCC in the synthesis and dynamic manipulation of mechanically interlocked architectures see: a) S. J. Cantrill, S. J. Rowan, J. F. Stoddart, *Org. Lett*. **1999**, *1*, 1363; b) S. J. Rowan, J. F. Stoddart, *Org. Lett*. **1999**, *1*, 1913; c) D. A. Leigh, P. J. Lusby, S. J. Teat, A. J. Wilson, J. K. Y. Wong, *Angew. Chem. Int. Ed.* **2001**, *40*, 1538; d) P. T. Glink, A. I. Oliva, J. F. Stoddart, A. J. P. White, D. J. Williams, *Angew. Chem. Int. Ed*. **2001**, *40*, 1870; e) Y. Furusho, T. Oku, T. Hasegawa, A. Tsuboi, N. Kihara, T. Takata, *Chem. Eur. J.* **2003**, *9*, 2895; f) J. D. Badjic, S. J. Cantrill, R. H. Grubbs, E. N. Guidry, R. Orenes, J. F. Stoddart, *Angew. Chem. Int. Ed.* **2004**, *43*, 3273; g) K. S. Chichak, S. J. Cantrill, A. R. Pease, S.-H. Chiu, G. W. V. Cave, J. L. Atwood, J. F. Stoddart, *Science* **2004**, *304*, 1308; h) Y. Furusho, T. Oku, G. A. Rajkumar, T. Takata, *Chem. Lett.* **2004**, *33*, 52; i) D. A. Leigh, E. M. Perez, *Chem Commun.* **2004**, 2262; j) R. T. S. Lam, A. Belenguer, S. L. Roberts, C. Naumann, T. Jarrosson, S. Otto, J. K. M. Sanders, *Science* **2005**, *308*, 667; k) T. Takata, *Polym. J.* **2006**, *38*, 1; l) B. H. Northrop, F. Arico, N. Tangchiavang, J. D.

Badjic, J. F. Stoddart, *Org. Lett.* **2006**, *8*, 3899; m) C. D. Meyer, C. S. Joiner, J. F. Stoddart, *Chem. Soc. Rev*. **2007**, *36*, 1705; n) T. Umehara, H. Kawai, K. Fujiwara, T. Suzuki, *J. Am. Chem. Soc*. **2008**, *130*, 13981; o) S.-Y. Hsueh, K.-W. Cheng, C.-C. Lai, S.-H. Chiu, *Angew. Chem. Int. Ed*. **2008**, *47*, 4436; p) K. Patel, O. S. Miljanic, J. F. Stoddart, *Chem. Commun*. **2008**, 1853; q) Y. Jiang, J. Wu, L. He, C. Tu, X. Zhu, Q. Chen, Y. Yao, D. Yan, *Chem. Commun.* **2008**, 6351; r) P. C. Haussman, J. F. Stoddart, *Chem. Rec.* **2009**, *9*, 136; s) L. M. Klivansky, G. Koshkakaryan, D. Cao, Y. Liu, *Angew. Chem. Int. Ed*. **2009**, *48*, 4185; t) H. Y. Au-Yeung, G. D. Pantos, J. K. M. Sanders, *Proc. Natl. Acad. Sci USA* **2009**, *106*, 10466; u) H. Y. Au-Yeung, G. D. Pantos, J. K. M. Sanders, *J. Am. Chem. Soc*. **2009**, *131*, 16030; v) M.-K. Chung, P. S. White, S. J. Lee, M. R. Gagné, *Angew. Chem. Int. Ed*. **2009**, *48*, 8683; w) H. Y. Au-Yeung, G. D. Pantos, J. K. M. Sanders, *Angew. Chem. Int. Ed*. **2010**, *49*, 5331.

[9] Selected references for the use of DCC in the context of systems chemistry: a) P. T. Corbett, J. K. M. Sanders, S. Otto, *Angew. Chem. Int. Ed*. **2007**, *46*, 8858; b) R. F. Ludlow, S. Otto, *Chem. Soc. Rev.* **2008**, *37*, 101; c) R. F. Ludlow, S. Otto, *J. Am. Chem. Soc.* **2008**, *130*, 12218; d) R. J. Sarma, J. R. Nitschke, *Angew. Chem. Int. Ed.* **2008**, *47,* 377; e) J. R. Nitschke, *Nature* **2009**, *462*, 736; f) N. Wagner, G. Ashkenasy, *Chem. Eur. J.* **2009**, *15*, 1765; g) R. Nguyen, L. Allouche, E. Buhler, N. Giuseppone, *Angew. Chem. Int. Ed.* **2009**, *48*, 1093; h) R. F. Ludlow, S. Otto, *J. Am. Chem. Soc.* **2010**, *132,* 5984; i) P. Mal, J. R. Nitschke, *Chem. Commun.* **2010**, *46*, 2417; j) V. E. Campbell, X. de Hatten, N. Delsuc, B. Kauffmann, I. Huc, J. R. Nitschke, *Nature Chem.* **2010**, *2*, 684.

[10] a) A. V. Eliseev, J.-M. Lehn, *Combin. Chem. Biol.* **1999**; *243*, 159; b) I. Huc, R. Nguyen, *Combin. Chem. High Throughput Screen.* **2001**, *4*, 53; c) S. Otto, R. L. E. Furlan, J. K. M. Sanders, *Drug Discovery Today* **2002**, *7*, 117; d) S. Otto, R. L. E. Furlan, J. K. M. Sanders, *Curr. Opin. Chem. Biol.* **2002**, *6*, 321; e) Y. Y. Chen, G. Liu, *Prog. Chem.* **2007**, *19*, 1903; f) M. F. Schmidt, J. Rademann, *Trends Biotechnol.* **2009**, *27*, 512.

[11] The investigation of the dynamic chemistry of cysteine-based disulfide bonds in proteins was pioneered by Anfinsen who was awarded the 1972 Nobel Prize in chemistry for the development of his 'thermodynamic hypothesis'. See: a) C. B. Anfinsen, *Science* **1973**, *181*, 723; b) M. Sela, F. H. White, C. B. Anfinsen, *Science* **1957**, *125*, 691; c) F. H. White, Jr., C. B. Anfinsen, *Ann. N. Y. Acad. Sci*. **1959**, *81*, 515; d) F. H. White, Jr., *J. Biol. Chem*. **1961**, *236*, 1353; e) C. B. Anfinsen, E. Haber, M. Sela, F. H. White, Jr., *Proc. Nat. Acad. Sci. USA* **1961**, *47*, 1309; f) E. Haber, C. B. Anfinsen, *J. Biol. Chem*. **1962**, *237*, 1839.

[12] a) A. G. Orrillo, A. M. Escalante, R. L. E. Furlan, *Chem. Commun.* **2008**, 5298; b) Z. Rodriguez-Docampo, S. Otto, *Chem. Commun.* **2008**, 5301.

[13] Selected references on the dynamic covalent chemistry of imines: a) K. Oh, K. S. Jeong, J. S. Moore, *Nature* **2001**, *414*, 889; b) M. Hochgurtel, H. Kroth, D. Piecha, M. W. Hofmann, C. Nicolaou, S. Krause, O. Schaaf, G. Sonnenmoser, A. V. Eliseev, *Proc. Natl. Acad. Sci. USA* **2002**, *99*, 3382; c) M. Hochgurtel, R. Biesinger, H. Kroth, D. Piecha, M. W. Hofmann, S. Krause, O. Schaaf, C. Nicolau, A. V. Eliseev, *J. Med. Chem.* **2003**, *46*, 356; d) J. R. Nitschke, J.-M. Lehn, *Proc. Natl. Acad. Sci. USA* **2003**, *100*, 11970; e) N. Giuseppone, J.-M. Lehn, *J. Am. Chem. Soc.* **2004**, *126*, 11448; f) J. R. Nitschke, *Angew. Chem. Int. Ed.* **2004**, *43*, 3073; g) N. Giuseppone, J. L. Schmitt, E. Schwartz, J.-M. Lehn, *J. Am. Chem. Soc.* **2005**, *127*, 5528; h) M. Hutin, R. Frantz, J. R. Nitschke, *Chem. Eur. J*. **2006**, *12*, 4077; i) M. Hutin, C. A. Schalley, G. Bernardinelli, J. R. Nitschke, *Chem. Eur. J*. **2006**, *12*, 4069; j) C. S. Hartley, J. S. Moore, *J. Am. Chem.*

Soc. **2007**, *129*, 11682; k) R. J. Sarma, J. R. Nitschke, *Angew. Chem. Int. Ed*. **2008**, 47, 377; l) S. Xu, N. Giuseppone, *J. Am. Chem. Soc.* **2008**, *130*, 1826; m) K. Ziach, J. Jurczak, *Org. Lett.* **2008**, *10*, 5159; n) P. Vongvilai, O. Ramström, J. *Am. Chem. Soc.* **2009**, *131*, 14419.

[14] R. Nguyen, I. Huc, *Chem. Commun*. **2003**, 942.

[15] A. Dirksen, S. Dirksen, T. M. Hackeng, P. E. Dawson, *J. Am. Chem. Soc*. **2006**, *128*, 15602.

[16] Selected references on hydrazone exchange in water: a) T. Bunyapaiboonsri, O. Ramström, S. Lohmann, J.-M. Lehn, L. Peng, M. Goeldner, *ChemBioChem* **2001**, *2*, 438; b) L. H. Eckardt, K. Naumann, W. M. Pankau, M. Rein, M. Schweitzer, N. Windhab, G. von Kiedrowski, *Nature* **2002**, *420*, 286; c) M. S. Congreve, D. J. Davis, L. Devine, C. Granata, M. O'Reilly, P. G. Wyatt, H. Jhoti, *Angew. Chem. Int. Ed.* **2003**, *42*, 4479; d) T. Bunyapaiboonsri, H. Ramström, O, Ramström, J. Haiech, J.-M. Lehn, *J. Med. Chem.* **2003**, *46*, 5803; e) L. F. Bornaghi, B. L. Wilkinson, M. J. Kiefel, S. A. Poulsen, *Tetrahedron Lett.* **2004**, *45*, 9281; f) O. Ramström, S. Lohmann, T. Bunyapaiboonsri, J.-M. Lehn, *Chem. Eur. J.* **2004**, *10*, 1711; g) B. Levrand, Y. Ruff, J.-M. Lehn, A. Herrmann, *Chem. Commun*. **2006**, 2965.

[17] Selected references on hydrazone exchange in organic solvent: a) G. R. L. Cousins, S. A. Poulsen, J. K. M. Sanders, *Chem. Commun.* **1999**, 1575; b) R. L. E. Furlan, G. R. L. Cousins, J. K. M. Sanders, *Chem. Commun.* **2000**, 1761; c) G. R. L. Cousins, R. L. E. Furlan, Y.-F. Ng, J. E. Redman, J. K. M. Sanders, *Angew. Chem. Int. Ed.* **2001**, *40*, 423; d) R. L. E. Furlan, Y.-F. Ng, S. Otto, J. K. M. Sanders, *J. Am. Chem. Soc.* **2001**, *123*, 8876; e) R. L. E. Furlan, Y.-F. Ng, G. R. L. Cousins, J. E. Redman, J. K. M. Sanders, *Tetrahedron* **2002**, *58*, 771; f) S. Choudhary, J. R. Morrow, *Angew. Chem. Int. Ed.* **2002**, *41*, 4096; g) L. A. Ingerman, M. L. Waters, *J. Org. Chem.* **2009**, *74*, 111; h) M.-K. Chung, C. M. Hebling, J. W. Jorgenson, K. Severin, S. J. Lee, M. R. Gagné, *J. Am. Chem. Soc.* **2008**, *130*, 11819; i) G. Gasparini, F. Bettin, P. Scrimin, L. J. Prins, *Angew. Chem. Int. Ed.* **2009**, *48*, 4546; j) M. G. Simpson, M. Pittelkow, S. P. Watson, J. K. M. Sanders, *Org. Biomol. Chem.* **2010**, *8*, 1173; k) M. G. Simpson, M. Pittelkow, S. P. Watson, J. K. M. Sanders, *Org. Biomol. Chem.* **2010**, *8*, 1181; l) L. L. Lao, J.-L. Schmitt, J.-M. Lehn, *Chem. Eur. J.* **2010**, *16*, 4903.

[18] a) V. T. Bhat, A. M. Caniard, T. Luksch, R. Brenk, D. J. Campopiano, M. F. Greaney, *Nature Chem.* **2010**, *2*, 490; b) B. L. Miller, *Nature Chem.*, **2010**, *2*, 433.

[19] S. Otto, R. L. E. Furlan and J. K. M. Sanders, *J. Am. Chem. Soc.* **2000**, *122*, 12063.

[20] Selected references on disulfide exchange in water: a) B. G. Bag, G. von Kiedrowski, *Angew. Chem. Int. Ed.* **1999**, *38*, 3713; b) K. C. Nicolaou, R. Hughes, S. Y. Cho, N. Winssinger, H. Labischinski, R. Endermann, *Chem. Eur. J.* **2001**, *7*, 3824; c) S. Otto, R. L. E. Furlan, J. K. M. Sanders, *Science* **2002**, *297*, 590; d) S. Otto, S. J. Kubik, *J. Am. Chem. Soc.* **2003**, *125*, 7804; e) B. Brisig, J. K. M. Sanders, S. Otto, *Angew. Chem. Int. Ed.* **2003**, *42*, 1270; f) J. Leclaire, L. Vial, S. Otto, J. K. M. Sanders, *Chem. Commun.* **2005**, 1959; g) P. T. Corbett, J. K. M. Sanders, S. Otto, *J. Am. Chem. Soc.* **2005**, *127*, 9390; h) P. T. Corbett, L. H. Tong, J. K. M. Sanders, *J. Am. Chem. Soc*. **2005**, *127*, 9390-9392; i) T. Hotchkiss, H. B. Kramer, K. J. Doores, D. P. Gamblin, N. J. Oldham, B. G. Davis, *Chem. Commun.* **2005**, 4264; j) K. R. West, K. D. Bake, S. Otto, *Org. Lett.* **2005**, *7*, 2615; k) L. Vial, J. K. M. Sanders, S. Otto, *New J. Chem.* **2005**, *29*, 1001; l) B. Danieli, A. Giardini, G. Lesma, D. Passarella, B. Peretto, A. Sacchetti, A. Silvani, G. Pratesi, F. Zunino, *J. Org. Chem.* **2006**, *71*, 2848; m) B. R. McNaughton, B. L. Miller, *Org. Lett.* **2006**, *8*, 1803; x) Lukáš Kumprecht, Miloš Buděšínsky, Jiří Vondrášek, Jiří Vymětal, Jiří Černy, Ivana Císařová, Jiří Brynda,

Vladimír Herzig, Petr Koutník, Jiří Závada, Tomáš Kraus, *J. Org. Chem.* **2009**, *74*, 1082; x) H. Y. Au-Yeung, P. Pengo, G. D. Pantos, S. Otto, J. K. M. Sanders, *Chem. Commun.* **2009**, 419; x) Kevin R. West, R. F. Ludlow, P. T. Corbett, P. Besenius, F. M. Mansfeld, P. A. G. Cormack, D. C. Sherrington, J. M. Goodman, M. C. A. Stuart, S. Otto, *J. Am. Chem. Soc.* **2008**, *130*, 10834.

[21] Selected references on disulfide exchange in organic solvent: a) H. Hioki, W. C. Still, *J. Org. Chem.* **1998**, *63*, 904; b) A. L. Kieran, A. D. Bond, A. M. Belenguer, J. K. M. Sanders, *Chem. Commun.* **2003**, 2674; c) A. T. ten Cate, P. Y. W. Dankers, R. P. Sijbesma, E. W. Meijer, *J. Org. Chem.* **2005**, *70*, 5799; d) A. L. Kieran, S. I. Pascu, T. Jarrosson, J. K. M. Sanders, *Chem. Commun*. **2005**, 1276; e) A. L. Kieran, S. I. Pascu, T. Jarrosson, M. J. Gunter, J. K. M. Sanders, *Chem. Commun*. **2005**, 1842-1844; f) T. Billig, T. Oku, Y. Furusho, Y. Koyama, S. Asai, T. Takata, *Macromol.* **2008**, *41*, 8496.

[22] J. M. A. Carnall, C. A. Waudby, A. M. Belenguer, M. C. A. Stuart, J. J.-P. Peyralans, S. Otto, *Science* **2010**, *327*, 1502.

[23] We use the term 'constitutionally dynamic' here to include both reversible metal coordination and dynamic covalent processes (see reference 1b).

[24] a) V. Goral, M. I. Nelen, A. V. Eliseev, J.-M. Lehn, *Proc. Natl. Acad. Sci. USA* **2001**, *98*, 1347; b) J. Leclaire, L. Vial, S. Otto, J. K. M. Sanders, *Chem. Commun*. **2005**, 1959; c) D. Schultz, J. R. Nitschke, *Angew. Chem. Int. Ed.* **2006**, *45*, 2453; d) R. J. Sarma, S. Otto, J. R. Nitschke, *Chem. Eur. J.* **2007**, *13*, 9542; e) N. Christinat, R. Scopelliti, K. Severin, *Angew. Chem. Int. Ed.* **2008**, *47*, 1848; f) M. Hutin, G. Bernardinelli, J. R. Nitschke, *Chem. Eur. J.* **2008**, *14*, 4585; g) R. J. Sarma, J. R. Nitschke, *Angew. Chem. Int. Ed.* **2008**, *47*, 377; h) V. E. Campbell, X. de Hatten, N. Delsuc, B. Kauffmann, I. Huc, J. R. Nitschke, *Chem. Eur. J.* **2009**, *15*, 6138; i) P. Mal, J. R. Nitschke, *Chem. Commun.* **2010**, *46*, 2417.

[25] M. von Delius, E. M. Geertsema, D. A. Leigh, *Nature Chem.* **2010**, *2*, 96.

[26] E. R. Kay, D. A. Leigh, F. Zerbetto, *Angew. Chem. Int. Ed.* **2007**, *46*, 72.

[27] The term double-level (dynamic covalent) system denotes a system whose building blocks are interconnected by two different types of exchange processes (see, for example, references 12a, 12b, 24a and 24b).

[28] $\mathbf{1_1}$ is the smallest cyclic oligomer of type $\mathbf{1_n}$, where **1** denotes the repeat structure and the subscript **n** denotes the numbers of repeat units in the molecule.

[29] An alternative strategy to introduce the disulfide linkage prior to ring-closure by hydrazone condensation failed, as various methodologies for the synthesis of unsymmetric disulfide bonds [a) R. Hunter, M. Caira, N. Stellenboom, *J. Org. Chem.* **2006**, *71*, 8268; b) S. Antoniow, D. Witt, *Synthesis* **2007**, 363; c) J. Kowalczyk, P. Barski, D. Witt, B. A. Grzybowski, *Langmuir* **2007**, *23*, 2318.] proved low-yielding or unsuccessful in our hands.

[30] T. J. Kucharski, Z. Huang, Q.-Z. Yang, Y. Tian, N. C. Rubin, C. D. Concepcion, R. Boulatov, *Angew. Chem. Int. Ed*. **2009**, *48*, 7040.

[31] a) G. R. L. Cousins, S.-A. Poulsen, J. K. M. Sanders, *Chem. Commun.* **1999**, 1575; b) A. T. ten Cate, P. Y. W. Dankers, R. P. Sijbesma, E. W. Meijer, *J. Org. Chem.* **2005**, *70*, 5799; c) A. L. Kieran, A. D. Bond, A. M. Belenguer, J. K. M. Sanders, *Chem. Commun.* **2003**, 2674.

[32] Cyclooligomerisation of $\mathbf{1_1}$ *via* disulfide exchange is possible either in a head-to-head (two benzylic disuflide fragments), tail-to-tail (two thioethyl hydrazone fragments) or head-to-tail (one of each) fashion, while hydrazone exchange alone can only give rise to head-to-tail oligomers.

[33] N. Iqbal, C.-A. McEwen, E. E. Knaus, *Drug Devel. Res.* **2000**, *51*, 177.
[34] M. D. Costioli, D. Berdat, R. Freitag, X. André, A. H. E. Müller, *Macromol.* **2005**, *38*, 3630.
[35] J. R. Dimmock, S. C. Vashishtha, J. P. Stables, *Eur. J. Med. Chem.* **2000**, *35*, 241.

Chapter III

The First Synthetic Small Molecule that can Walk down a Track

Published as *A synthetic small molecule that can walk down a track*, M. von Delius, E. M. Geertsema, D. A. Leigh, *Nature Chem.* **2010**, *2*, 96.

Selected Highlights: *Big Steps for Little Feet*, J. S. Yeston, *Science* **2010**, *327*, 127. *Tiny Steps*, S. Otto, *Nature Chem.* **2010**, *2*, 75. *Two-legged molecular walker takes a stroll*, S. Hadlington, *Chem. World* **2010**, *7*, 26. *Tiny molecular track walker*, B. Halford, *Chem. & Eng. News* **2009**, *87*, 34.

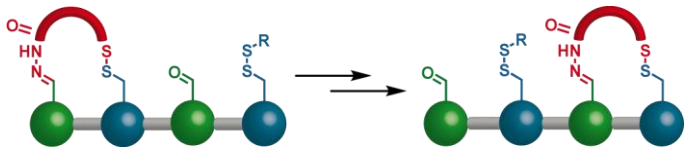

"The journey of one thousand miles starts with a single step."
(Lao-tzu, ~550 B.C.)

Acknowledgements

The work presented in this Chapter was a joint effort between the author and Dr. Edzard M. Geertsema. The multistep synthesis of compounds **E2** and **E14** was perfomed by E. M. G. Juraj Bella is acknowledged for assistance with high-field NMR spectroscopy.

3.1 Synopsis

Although chemists have previously made small molecule rotary motors, up to now there have been no reports of small molecule linear motors. In this Chapter the synthesis and operation of a 21-atom 'two-legged' molecular unit is described that is able to 'walk' up and down a four-'foothold' molecular track.

High processivity is conferred by designing the track-binding interactions of the two 'feet' to be labile under different sets of conditions such that each foot can act as a temporarily fixed pivot for the other. The walker randomly and processively takes zero or one 'steps' along the track using a 'passing-leg' gait each time the environment is switched between acid and base.

Replacing the basic step with a redox-mediated disulfide exchange reaction directionally transports the bipedal molecules away from the minimum energy distribution by a Brownian ratchet mechanism. The ultimate goal of such studies is to produce artificial linear molecular motors that move directionally along polymeric tracks, transporting cargoes and performing tasks in a manner reminiscent of biological motor proteins.

3.2 Introduction

Molecular motors are utilised throughout biology to drive chemical systems away from equilibrium, thereby enabling tasks to be performed, cargoes to be directionally transported, and work to be done.[1] Spectacular examples include the kinesin, myosin and dynein bipedal motor proteins which are directionally-driven along microtubule or actin filament tracks by ATP hydrolysis.[1] Despite fundamental advances in recent years,[2-10] most of the artificial molecular machines prepared to date fall well short of the degree of control over motion exhibited by such biomolecules.[11] To date the only synthetic structures that can, even in principle, take repetitive, processive (that is, without detaching or exchanging with other molecules in the bulk), 'steps' along a molecular track are systems constructed from DNA.[12-19] Here we report on the synthesis and operation of a synthetic small molecule that is able to 'walk' repetitively up and down a four-'foothold' molecular track in response to a changing chemical environment. High processivity is conferred by designing the track-binding interactions of the two 'feet' to be labile under different sets of conditions (acid and base): under acidic conditions the disulfide bond between one 'foot' of the walker and the track is kinetically locked while the hydrazone unit that joins the other foot to the track is labile allowing that foot to sample two different ('forward' and 'backward') footholds through hydrazone exchange; under basic conditions the relative kinetic stabilities of the foot-track interactions are reversed and the disulfide foot samples forward and backward binding sites on the track while the hydrazone foot is locked in place. The walker molecule thus randomly and processively takes zero or one steps along the track using a 'passing-leg' gait each time the environment is switched between acid and base. For an ensemble of walker-track conjugates a steady-state, minimum energy, distribution of walkers on the four-foothold tracks is reached after several acid-base oscillations, irrespective of which end of the track the walkers start from. Alternating between acidic conditions and a kinetically controlled redox reaction causes the two-legged molecule to walk down the track with inherent directionality through an information ratchet[10,11,20,21] type of Brownian ratchet mechanism.

3.3 *Results and Discussion*

3.3.1 Design of a Dynamically Processive Small Molecule Walker-Track System

Molecular level motors and machines operate by (and must be designed according to) chemical laws and statistical mechanisms, not the Newtonian laws for momentum and inertia that dictate the mechanisms of mechanical machines in the macroscopic world.[11,20] The design outline for the small molecule walker-track system intended to mimic some of the basic characteristics of linear motor protein dynamics, namely progressive, processive, repetitive motion of a walker unit up and down a molecular track without fully detaching or exchanging with others in the bulk, is shown in Figure 3.1. The walker unit (shown in red) traverses the track by a 'passing-leg' gait involving two chemically different 'feet' ('*A*' and '*B*') which reversibly bind to different regions of the track. Linear motor proteins and the synthetic DNA walkers use non-covalent interactions for track binding, but the understanding of how to sequentially kinetically lock and release different artificial hydrogen bond (for example) recognition sites in the desired manner is beyond the capabilities of present day synthetic supramolecular chemistry. We instead chose to utilise dynamic covalent chemistry[22-24] for this purpose, which combines some of the features of supramolecular chemistry (reversibility, dynamics) with those of covalent bond chemistry (bond strength, robustness). To prevent the walker from completely detaching from the track during the walking process, the different feet form covalent bonds that are labile or kinetically locked under different sets of conditions.[25-27] Under condition I (Figure 3.1a), foot *A* can dissociate from the track and then rebind, either to its original foothold or to another one within reach, while foot *B* remains in position on the track. Under condition II (Figure 3.1b) the situation is reversed and foot *B* can detach from the track and rebind while the bond between foot *A* and the track is kinetically locked. Switching repeatedly between conditions I and II should cause the walker to move randomly up and down the track, taking zero or one steps each time the conditions are changed. If the reactions employed are fully reversible then, without the consumption of an additional fuel, the oscillation in conditions will eventually lead to a steady-state, energy minimum, distribution of the walker on the track. It is interesting to note that although this distribution is arrived at through a process analogous to the attaining of a thermodynamic equilibrium (it is the average of a statistical sampling of exchanging chemical entities), each walker-track positional (constitutional) isomer is actually only

ever in chemical equilibrium with a limited number of the other isomers. For example, there is no single set of conditions whereby the *1*,*2*-isomer (Figure 3.1a) is able to exchange with the *3*,*4*-isomer (Figure 3.1b). Their interconversion only occurs *via* the *2*,*3*-isomer, which under condition I is in equilibrium with the *1*,*2*-isomer and under condition II is in equilibrium with the *3*,*4*-isomer. This unusual property of the system confers processivity on the walking process.

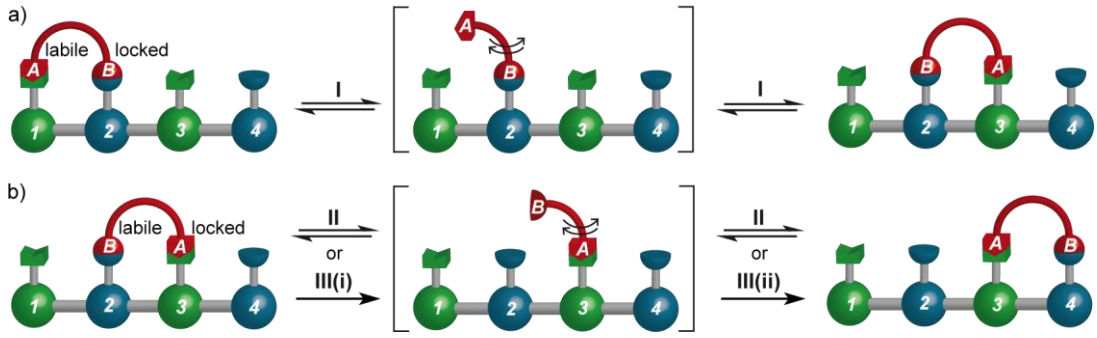

Figure 3.1. *Binding requirements for the processive migration of a two-legged 'walker' molecule (red) along a track featuring two possible binding sites (green and blue) for each 'foot'. For the walking action to be processive, the two feet of the walker (labelled 'A' and 'B') must never be disconnected from the track at the same time (note the two key intermediate states, shown in square brackets, in which one or other foot is disconnected from the track). A way to achieve this is to design the foot-track bond forming and breaking events to occur under different sets of conditions (I and either II or III) for each foot. If conditions are used in which the chemical reaction used to generate one of the two steps proceeds with a different forward/backwards ratio to the other step (pathway I + III), directional processive transport of the walker along the track will occur.*

3.3.2 Synthesis, Characterisation and Directionally-Unbiased Walking

A walker-track conjugate, *1*,*2*-**1**, in which the molecular walker is attached to a four-foothold track *via* hydrazone (labile in acid; locked in base) and disulfide (labile in base; locked in acid) linkages,[26,27] was constructed as shown in Scheme 3.1a (see section 3.5.11 for full experimental procedures and compound characterisation). The four-foothold track contains two potential sites of attachment for the hydrazide foot (shown in green: position *1* and the aldehyde at position *3*) and two potential sites of attachment for the sulfur foot (shown in blue: position *2* and the benzylic mercaptan at position *4*, masked with a 'placeholder' aliphatic unit as a disulfide in *1*,*2*-**1**).

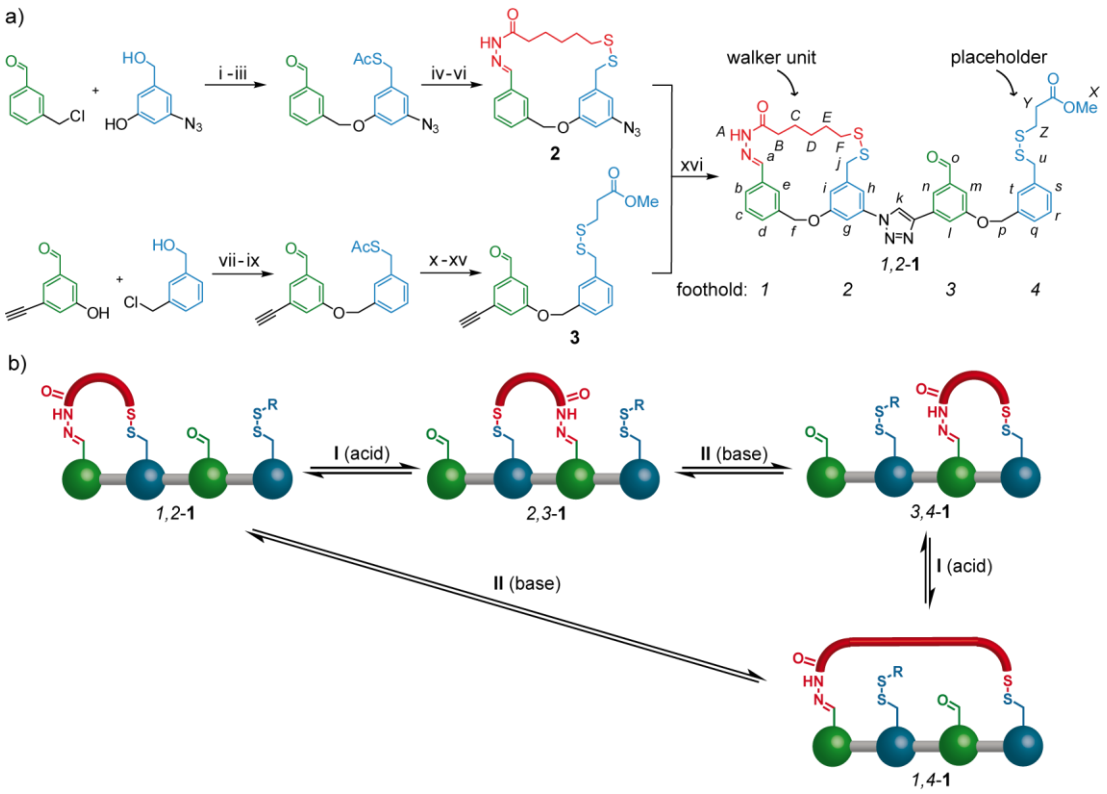

Scheme 3.1. *Synthesis and operation of molecular walker-track conjugate 1,2-1 under different sets of conditions (acid-base) for reversible covalent bonding of each foot with footholds on the track. a) Synthesis of 1,2-**1**: (i) NaH, dimethylformamide (DMF), room temperature (RT), 16 h, 88%; (ii) methanesulfonyl chloride (MsCl), Et_3N, CH_2Cl_2, 0 °C, 30 min; (iii) KSAc, DMF, RT, 3 h, 77% (over two steps); (iv) 6-mercaptohexanoic acid hydrazide, AcOH (cat.), MeOH, RT, 2 h, 78%; (v) NaOMe, MeOH, RT, 2 h; (vi) I_2, KI, CH_2Cl_2, RT, 5 min, 32% (over two steps); (vii) NaH, DMF, 0 °C to RT, 16 h, 65%; (viii) MsCl, Et_3N, CH_2Cl_2, RT, 16 h; (ix) KSAc, DMF, RT, 3 h, 66% (over two steps); (x) $HC(OMe)_3$, p-toluenesulfonic acid (p-TsOH), MeOH, RT, 30 min; (xi) NaOMe, MeOH, RT, 30 min; (xii) 3-mercaptopropionic acid, I_2, KI, CH_2Cl_2, RT, 5 min; (xiii) trifluoroacetic acid (TFA), CH_2Cl_2, RT, 30 min, 58% (over four steps); (xiv) H_2SO_4 (cat.), MeOH, RT, 16 h; (xv) TFA, CH_2Cl_2, RT, 30 min, 40% (over two steps); (xvi) $Cu(MeCN)_4PF_6$, tris[(1-benzyl-1H-1,2,3-triazol-4-yl)methyl]amine (TBTA), CH_2Cl_2/tetrahydrofuran (THF)/MeOH, RT, 16 h, 79%. b) Local equilibria that connect the four positional isomers 1,2-**1**, 2,3-**1**, 3,4-**1** and 1,4-**1** under various conditions. The upper pathway represents the major 'passing leg' mechanism from 1,2-**1** to 3,4-**1** (via 2,3-**1**), while the lower pathway (via 1,4-**1**) is a minor 'double step' mechanism. Oscillation between acid (I) and base (II) leads to a steady state distribution of 39:36:19:6 (±2) for 1,2-**1**:2,3-**1**:3,4-**1**:1,4-**1**, see Figure 3.3.*

The starting position of the walker at footholds *1* and *2* in the walker-track conjugate was established by synthesising macrocycle **2** and coupling this to the building block (**3**) containing footholds *3* and *4* (Scheme 3.1a, step p). We also prepared isomer *3,4*-**1** unambiguously through synthesis (see section 3.5.10.4) and isolated and characterised isomers *2,3*-**1** and *1,4*-**1** from reactions that could not produce unknown positional isomers. The partial ^{1}H nuclear magnetic resonance (NMR) spectra of the four walker-track positional isomers *1,2*-**1**, *2,3*-**1**, *3,4*-**1** and *1,4*-**1** confirmed their structures and, together with the parent track **4**, are shown in Figure 3.2. While the structural

similarity between the compounds is immediately evident from the spectra, differences in chemical shift occur for the protons of the methylene groups in the five-carbon spacer unit (shown in red; H_B-H_F) which reflect the difference in the shape and environment of the macrocycle formed between walker and track in each isomer. A useful probe for the position of the walker is shown in the expanded aldehyde region around 10.05 parts per million (ppm) chemical shift (Figure 3.2). In the four walker-track positional isomers the aldehyde proton (H_o in *1,2*-**1** and *1,4*-**1**; H_a in *2,3*-**1** and *3,4*-**1**) is diagnostic of the aldehyde foothold that is free. Similarly, the methylene protons (H_Z and H_Y) serve as distinctive markers for the position of the placeholder disulfide.

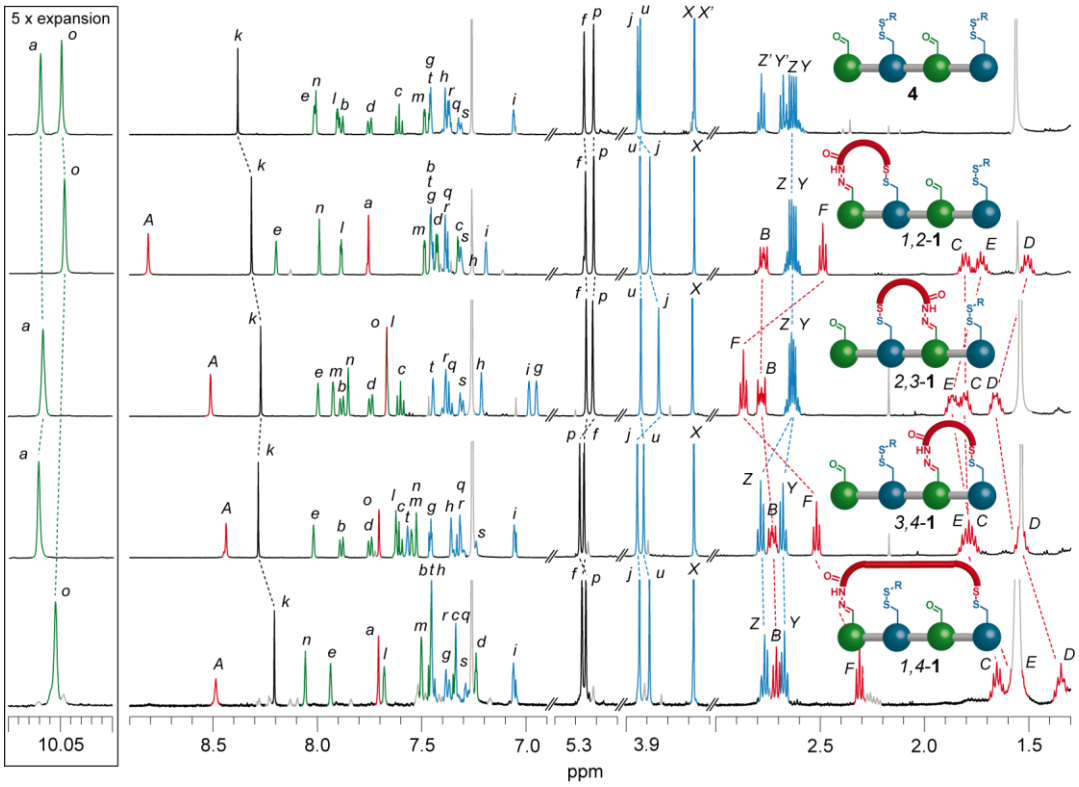

Figure 3.2. *Partial ^{1}H NMR (500 MHz, $CDCl_3$, 298 K) spectrum of molecular track* ***4*** *and the four walker-track positional isomers 1,2-***1***, 2,3-***1***, 3,4-***1*** and 1,4-***1***. Dotted lines connect signals that differ significantly in chemical shift as a result of the position of the red walker unit. For example, the expanded aldehyde region (framed) shows distinctive shifts for the two chemically different protons labeled 'o' and 'a' (see chemical structure in Scheme 3.1 for the labelling system).*

The dynamic behaviour of the walker-track conjugate system upon cycling between acid and base is shown in Figure 3.3. When a dilute solution of *1,2*-**1** in chloroform ($CHCl_3$) was treated with a catalytic amount of trifluoroacetic acid (TFA), intramolecular hydrazone exchange gave rise to a mixture of *1,2*-**1** and its positional

isomer *2*,*3*-**1** in a 51:49 ratio (Figure 3.3, cycle 1, condition I). Treatment of this mixture with a strong base, 1,8-diazabicyclo[5.4.0]undec-7-ene (DBU), DL-dithiothreitol (DTT) (which promotes disulfide exchange by acting as a source of a nucleophilic thiolate anion[28]), and dimethyl 3,3'-disulfanediyldipropanoate ($(MeO_2CCH_2CH_2S)_2$), the placeholder disulfide, generated a mixture of all four positional isomers, *1*,*2*-**1**, *2*,*3*-**1**, *3*,*4*-**1** and *1*,*4*-**1**, in a 45:36:11:8 ratio, as determined by HPLC (Figure 3.3b, cycle 1, condition II; see section 3.5.6 for details). Switching between conditions I and II over several cycles (Figure 3.3aA) led to convergence of the distribution of the positional isomers to a ratio of *1*,*2*-**1**:*2*,*3*-**1**:*3*,*4*-**1**:*1*,*4*-**1** 39:36:19:6 (±2) (Figure 3.3b). A very similar distribution of isomers was obtained by starting from pristine *3*,*4*-**1** and carrying out the operation sequence over two or three cycles (Figure 3.3aB and Figure 3.3b). Thus, irrespective of which end of the track the walker starts from, the effect of the passing-leg gait operations is to reach the same (global minimum energy) distribution of positional isomers of the walker on the track.

In addition to the major passing-leg gait mechanism route from *1*,*2*-**1** to *3*,*4*-**1**, the somewhat unexpected presence of *1*,*4*-**1** in the product distributions (albeit in small amounts, 4-10%)—we originally suspected it might be too strained to be present in observable quantities using reversible chemical reactions—provides a minor 'double step' route from *1*,*2*-**1** to *3*,*4*-**1** (Scheme 3.1b). It is interesting to note that occasional statistical 'errors' to the major pathway mechanisms also occur with some biological motor proteins.[1,29]

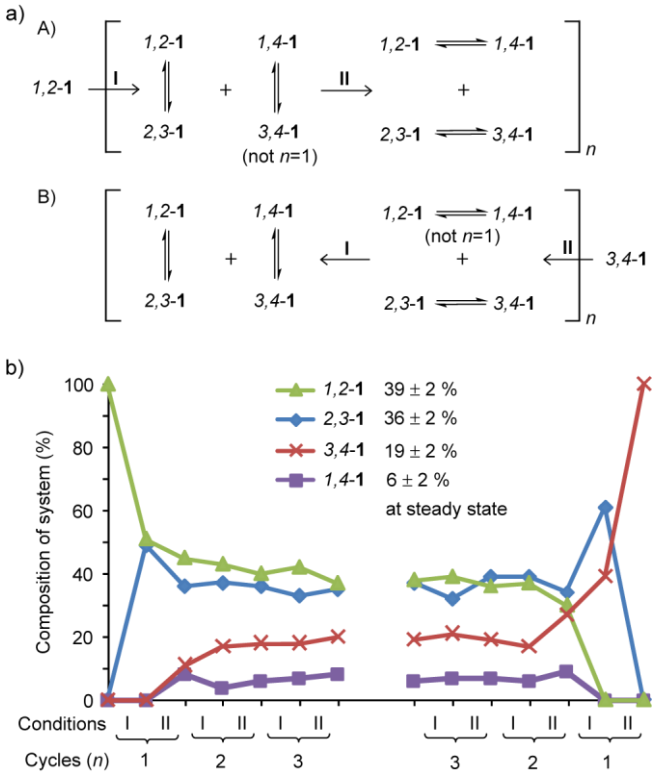

Figure 3.3. *Dynamic behaviour of molecular walker-track conjugates 1,2-**1** and 3,4-**1**, each under cycling of conditions (acid-base) for reversible covalent bonding of each foot with pairs of footholds on the track. a) Experimental sequence that, over a number of operational cycles (n), leads to a steady state, minimum energy, distribution of the walker on the track. Condition I (reversible hydrazone exchange): 0.1 mM, TFA, $CHCl_3$, RT, 6-96 h (allowed to continue until the distribution no longer changed, as monitored by HPLC). Condition II (reversible disulfide exchange): 0.1 mM, DTT (10 equiv.), DBU (40 equiv.), dimethyl 3,3'-disulfanediyldipropanoate (20 equiv.), $CHCl_3$, RT, 12-48 h (allowed to continue until the distribution no longer changed, as monitored by HPLC). b) Product distribution. Under each set of conditions (I and II) two different pairs of positional isomers are in equilibrium. Values are based on HPLC integration and are corrected for the absorbance coefficients at 290 nm (see section 3.5.8).*

3.3.3 Directionally-Biased Walking

Starting with the walker at one end of the track (i.e. pristine *1,2*-**1** or *3,4*-**1**) and cycling between conditions I and II results in some walkers moving from one end of the track to the other (Figure 3.3). However, this is a consequence of the initial distribution of walker-track conjugates being away from the minimum energy distribution and the system relaxing towards it, the walking sequence outlined in Figure 3.3a is not intrinsically directional (by this we mean that in the internal region of a polymeric track made of alternating benzaldehyde-benzylic disulfide footholds, the walker would move, over several acid-base oscillations, in each direction with equal probability). The lack of intrinsic directionality in the movement of the walker may appear counterintuitive given the stimuli-induced changes in its position reported in Figure 3.3, but ignoring substituents and the minor *1,4*-isomer there are only two

fundamentally different types of macrocycles formed between the walker and the track—one in which the track ether linkage is internal to the macrocycle (present in *1,2*-**1** and *3,4*-**1**) and one in which the track triazole unit is internal to the macrocycle (*2,3*-**1**). Each operation I or II thermodynamically equilibrates this pair of macrocycles about the pivot (kinetically locked) foot and, unless the macrocycles happen to have different relative thermodynamic stabilities in acid and base, the ratio produced should not depend upon which foot, disulfide or hydrazone, is the one fixed to the track. The difference in the amount of *1,2*-**1** and *3,4*-**1** present in the minimum energy distribution is therefore largely a consequence of the different substitution patterns on the macrocycles in these compounds. In the internal region of a polymeric track made of alternating benzaldehyde-benzylic disulfide footholds no net-directionality of walking would occur using a pair of operations that give the same ratio (e.g. both give the thermodynamic ratio) of the two different macrocycles.

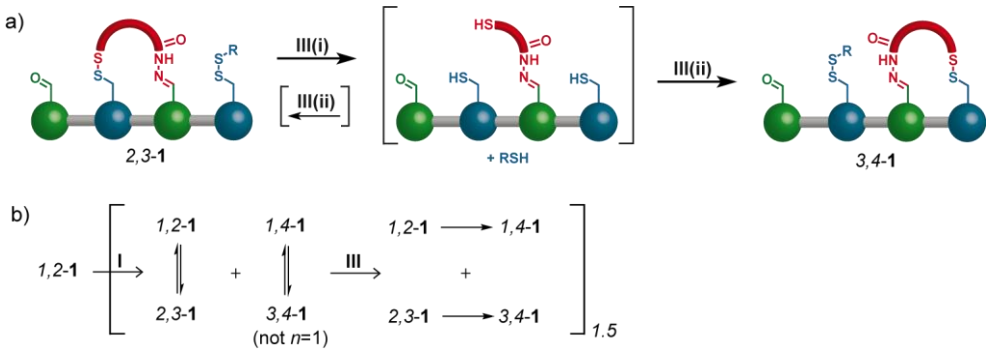

Figure 3.4. *Processive directionally-biased walking starting from 1,2-**1**, under cycling of conditions (acid-redox) for covalent bonding of each foot with pairs of footholds on the track. a, Redox-mediated reaction sequence illustrated for 2,3-**1**. III(i): Reductive ring opening quantitatively generates the trithiol. III(ii): Rapid oxidation recyclises to the disulfides. The redox sequence is carried out under kinetic control and gives a different product ratio to the base-promoted reversible disulfide exchange shown in Scheme 3.1 and Figure 3.3. This bias in the product distribution leads to inherently directional transport of the walker away from the minimum energy distribution. b, Reaction sequence. Condition I (reversible hydrazone exchange): 0.1 mM, TFA, $CHCl_3$. Condition III (kinetically-controlled disulfide exchange): (i) 1.0 mM, DTT (6 equiv.), DBU (3 equiv.), $CHCl_3$, reflux, 2-12 h (allowed to continue until the reduction of all disulfide bonds was complete, as monitored by ^1H NMR); (ii) $MeO_2CCH_2CH_2SH$ (8 equiv.), I_2, Et_3N, $CHCl_3$/MeOH 1:1, RT, 5 min.*

To create a system in which the walker can be transported with a directional bias even in the middle of a polymeric track, and therefore be able to transport cargo or generate a progressively increasing force, it is necessary to replace one of the walking operations with a step that proceeds with a different forward-backwards ratio to the other step. This was achieved for the four-foothold track by replacing the base-promoted disulfide exchange reaction with a two stage redox process (Figure 3.4a and Figure 3.1b) in

which the ring-opened intermediate shown in square brackets is generated in the absence of the placeholder disulfide (1 mM walker-track conjugate, DBU (3 equiv.), DTT (6 equiv.), $CHCl_3$, reflux), and then reoxidised rapidly with iodine (0.1 mM walker-track conjugate, I_2, $MeO_2CCH_2CH_2SH$ (8 equiv.), Et_3N, $CHCl_3$/MeOH 1:1) to regenerate the walker-track disulfide linkages. Because the reoxidation occurs virtually instantaneously and is irreversible under the reaction conditions, reattachment of the sulfur foot to the track occurs under kinetic control and gives a product ratio different to that achieved by the reversible disulfide exchange reaction. The effect of introducing this operation into the walking sequence is shown in Table 3.1. In just 1.5 cycles starting from 100% *1,2*-**1** the walker moves down the track to give 43% *3,4*-**1**, compared to the 19% of *3,4*-**1** present at the steady state using the two sets of reversible conditions. As long as the product ratio obtained from III is different to the ratio obtained from II on a polymeric—or cyclic—track then directionally-biased walking would occur at any point (although the bias on a polymer may not be as great as for the four-foothold track, where the disulfide foothold is unsubstituted at the end of the track). The biased walking mechanism reported in Figure 3.4 relies on the increased rate of accessibility of a foothold given the particular position of the walker on the track (i.e. which is the pivot foot). As such it corresponds to an information ratchet[10,11,20,21] type of Brownian ratchet mechanism.

Table 3.1. *Table showing the evolution of the mixture of positional isomers over three acid-redox operations compared to the acid-base sequence. In the right hand column, the composition of the mixture at its steady state using the acid-base conditions is shown (see Figure 3.3b). The remarkable difference in the amount of 3,4-**1** after only one biased step is highlighted in bold.*

Cycles	0	0.5	1	1.5	Steady state from
Conditions		I	III	I	Figure 3.3, *n*=3
1,2-**1**[a]	100%	52%	28%	24%	39%
2,3-**1**[a]	-	48%	20%	24%	36%
3,4-**1**[a]	-	-	28%	**43%**	**19%**
1,4-**1**[a]	-	-	24%	9%	6%

[a] *Percentages are based on HPLC integration and are corrected for the absorbance coefficients at 290 nm (see Experimental Section).*

3.3.4 Processivity

Both under directionally biased and un-biased operating conditions the walker migration appears to occur with perfect processivity, at least in respect to a possible dissociation of the walker moiety from the track. We can deduce that complete

detachment of the walker moiety from the track is negligible from the fact that we never observed (by HPLC) the formation of all four possible isomers during an exchange experiment starting from a pristine single isomer (i.e. under basic conditions *1,2*-**1** only gave *2,3*-**1** but never *3,4*-**1** or *1,4*-**1**; likewise, under basic conditions *1,2*-**1** only gave *1,4*-**1** but never *2,3*-**1** or *3,4*-**1**). A study with the objective to find out if, and to which extent, processivity is lost via other mechanisms will be presented in Chapter IV.

3.4 Conclusions

We have described a system in which a 21-atom molecular walker moves up and down a four-foothold track primarily through a passing-leg gait mechanism, each step induced by an acid-base oscillation. The feet-track interactions feature covalent bonds that are dynamic under mutually exclusive sets of conditions and ensure that walker moiety cannot fully disconnect from the molecular track. Replacing one of the reactions with a kinetically controlled redox operation biases the directionality of one of the steps. This is sufficient to directionally transport the walker away from its minimum energy distribution on the four-foothold track. The two passing-leg gait steps taken by the walker to go from one end of the four-foothold track to the other is the full repeat cycle necessary for the molecule to walk down a hypothetical polymeric track made of alternating benzaldehyde-benzylic disulfide footholds. Such extended tracks, and walkers that can carry cargoes along them, are currently under construction in our laboratory.

3.5 Experimental Section

3.5.1 General Information

Compounds **E1, E4, E5, E6, E7, E10, E11, E12** and **E23** were prepared according to literature procedures.[30-34]

Analytical and preparative HPLC was performed on instruments of Gilson Inc., USA and Agilent Technologies (1200 LC system with photodiode array detector). Normal-phase columns (Kromasil, analytical: 250 × 4.6 mm, preparative: 250 × 20 mm) were used with combined isocratic and gradient elution (analytical: 0.8 mL/min, CH_2Cl_2/^{i}PrOH, 3% → 3% → 15% → 15% → 3% ^{i}PrOH; preparative: 10 mL/min, CH_2Cl_2/MeOH, 1.0% → 1.0% → 20% → 20% → 1.0% MeOH, UV detection @ 290 nm). LCMS analysis was performed on an Agilent Technologies 1200 LC system with 6130 single quadrupole MS detector (APCI source; column and method as specified above).

3.5.2 General Procedure for Acid-Catalysed Hydrazone Exchange (I)

To a 0.1 mM solution of *1,2*-**1** (typically 1 mg in ca. 10 mL; 1.0 equiv.) in $CHCl_3$ (HPLC grade) were added 5 drops of a solution containing 20% v/v TFA (CF_3CO_2H) and 1% v/v H_2O in $CHCl_3$ (HPLC grade). The mixture was stirred at room temperature and the progress of the equilibration followed by analytical HPLC (see sections 3.5.1 and 3.5.6). When the relative ratios of the isomers were stable (6 to 96 hours), the mixture was washed with an aqueous solution of $NaHCO_3$. The layers were partitioned and the aqueous layer was extracted with $CHCl_3$. The combined organic layers were dried over $MgSO_4$. The solvents were removed under reduced pressure and the amount and constitution of the mixture determined by weight and, after dissolving in a defined amount of $CHCl_3$, analytical HPLC.

3.5.3 General Procedure for Base-Catalysed Disulfide Exchange (II)

To a 0.1 mM solution of *3,4*-**1** (typically 1 mg in 10 mL; 1.0 equiv.) in $CHCl_3$ (HPLC grade) was added DBU (40 equiv.), DTT (10 equiv.) and 3,3'-disulfanediyldipropanoate (20 equiv.) from stock solutions. The mixture was stirred at room temperature and the progress of the equilibration followed by analytical HPLC. When the relative ratios of the isomers were stable (12 to 48 hours), the excess of DTT was oxidised by dropwise addition of a solution of I_2 in $CHCl_3$ until a slight brown colour persisted. An aqueous solution of NH_4Cl and Na_2SO_3 was added and the mixture was stirred vigorously until decolourisation was complete. The layers were partitioned and the aqueous layer was extracted with $CHCl_3$. The combined organic layers were dried over $MgSO_4$. After work up the product distribution was no longer dynamic (free of DTT and DBU) and the solvent could be removed to allow analysis by weight and analytical HPLC (see sections 3.5.1 and 3.5.6).

3.5.4 General Procedure for Redox-Mediated Disulfide Exchange (III)

i) Reduction Step. DTT (6 equiv.) and DBU (3 equiv.) were added from stock solutions to a 1 mM solution of *2,3*-**1** (1 equiv.) in $CDCl_3$ or $CHCl_3$. The mixture was heated under reflux until ^1H NMR showed that all disulfide bonds had been reduced (2 to 12 hours). ii) Oxidation Step. The above solution was diluted to 0.1 mM with a 1:1 mixture of $CHCl_3$ and MeOH (both HPLC grade). Et_3N (5 drops) and methyl 3-mercaptopropionate (8 equiv.) were added. At room temperature, a solution of I_2 in $CHCl_3$ was added to the mixture until the brown colour persisted. An aqueous solution of NH_4Cl and Na_2SO_3 was added and the solution was stirred vigorously until decolourisation was complete. The layers were partitioned and the aqueous layer was extracted with $CHCl_3$. The combined

organic layers were dried over $MgSO_4$. At this stage a broad-window preparative HPLC was carried out (retaining the products in a window of 5-12 minutes retention time, see sections 3.5.1 and 3.5.6) to remove excess reagents, waste products, and other impurities (the two-step redox sequence produces more byproducts than the acid or base catalysed procedures). The samples were analysed by HPLC before and after to confirm that the walker-track isomer ratios remained unchanged by this procedure.

Note: The molar ratios of DBU and DTT used during the base-catalysed disulfide exchange experiments (40 and 10 equivalents, respectively) are higher than those used during the reduction step of the redox disulfide exchange experiments (3 and 6 equivalents, respectively) since there is a tenfold difference in concentration at which the experiments were carried out (0.1 mM and 1.0 mM, respectively). The DBU:DTT ratio is also reversed (from 4:1 to 1:2) in the two experiments. The rationale behind these changes reflect the different objectives of the two types of exchange experiments: during the base-catalysed exchange experiment, DTT is added to increase the rate of disulfide exchange for which thiolates are a necessary intermediate; during the redox operation the excess DTT results in quantitative reduction of the disulfide bonds. The resulting thiols are subsequently rapidly oxidised by iodine to affect a kinetically controlled reaction outcome.

3.5.5 LCMS Data

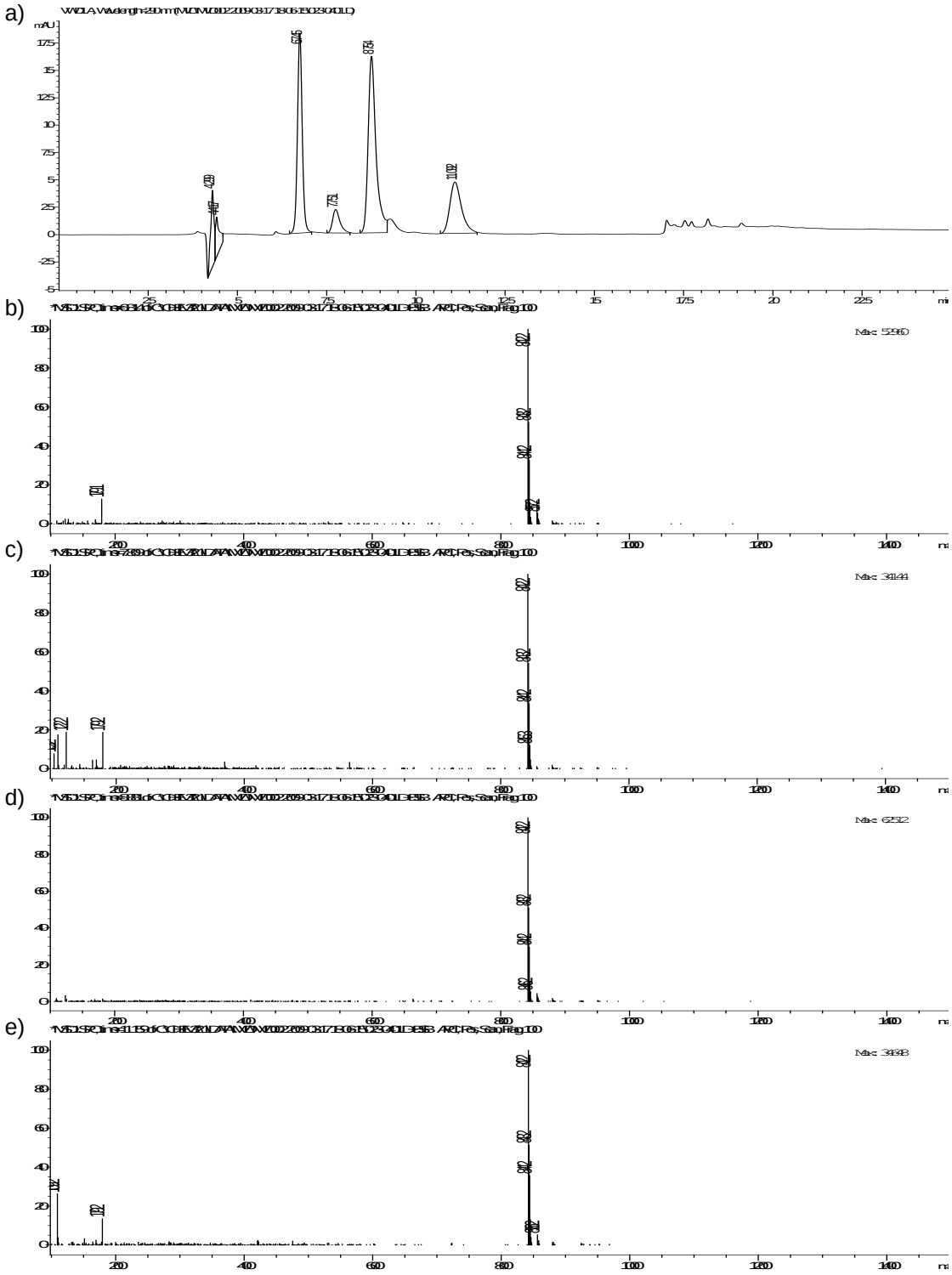

Figure 3.5. *LCMS data. a) HPLC trace of a mixture of isomers 1,2-**1**, 2,3-**1**, 3,4-**1** and 1,4-**1**. b)-e): mass spectra corresponding to the four peaks shown in the HPLC trace at the top (for instrumental details see Section 3.5.1). In all four spectra the largest peak is at m/z = 842.2 $[M+H]^+$ confirming that the four compounds are isomers.*

3.5.6 HPLC Data

In this section a collection of HPLC traces is shown that illustrate the evolution of the isomer mixtures during the three fundamental experimental sequences depicted in Figure 3.3 and Figure 3.4. The peaks of the four positional isomers are colour-coded, while the corresponding retention times are given in minutes on top of the peaks. The variations in retention times from different runs are typical of those found with normal phase HPLC on unbonded silica columns.

3.5.6.1 Acid-base cycles starting from 1,2-1

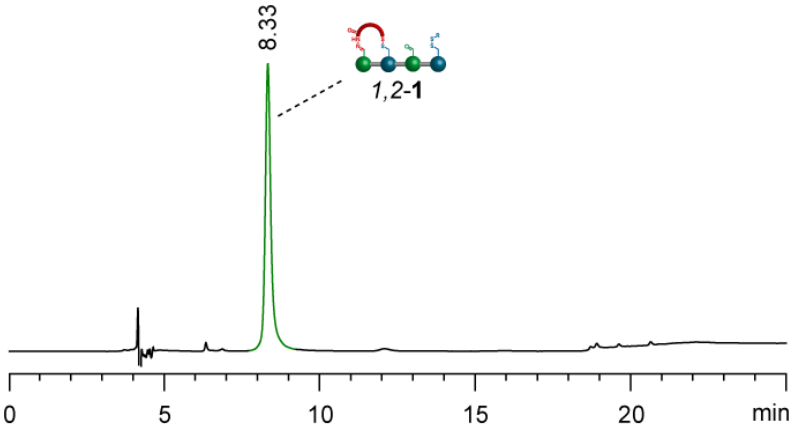

Figure 3.6. *Starting material: pristine 1,2-**1**.*

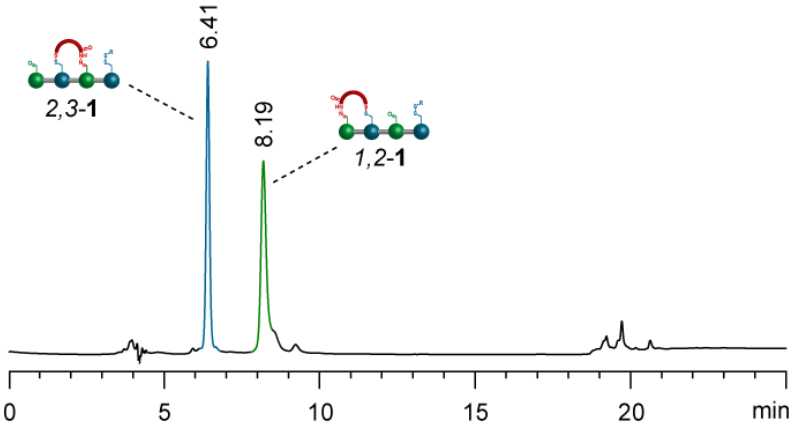

Figure 3.7. *Mixture after first operation (TFA): 1,2-**1** + 2,3-**1** [Left-hand side, Cycle 1, Condition I of Figure 3.3]*

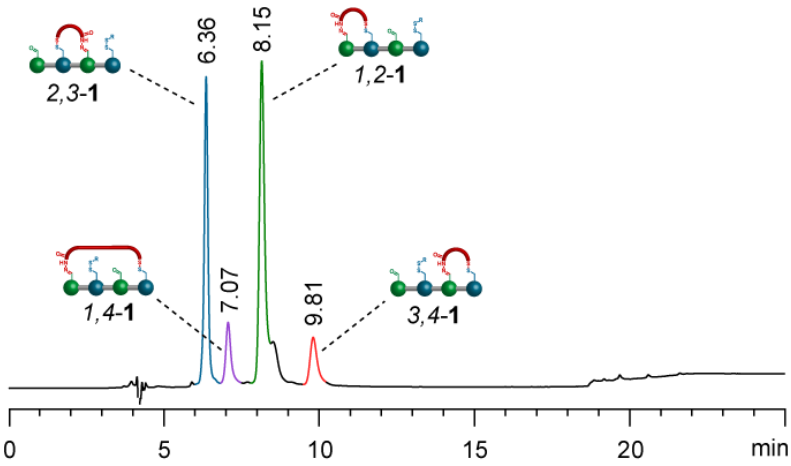

Figure 3.8. *Mixture after second operation (DBU, DTT): 1,2-**1** + 2,3-**1** +3,4-**1** + 1,4-**1**. [Left-hand side, Cycle 1, Condition II of Figure 3.3]*

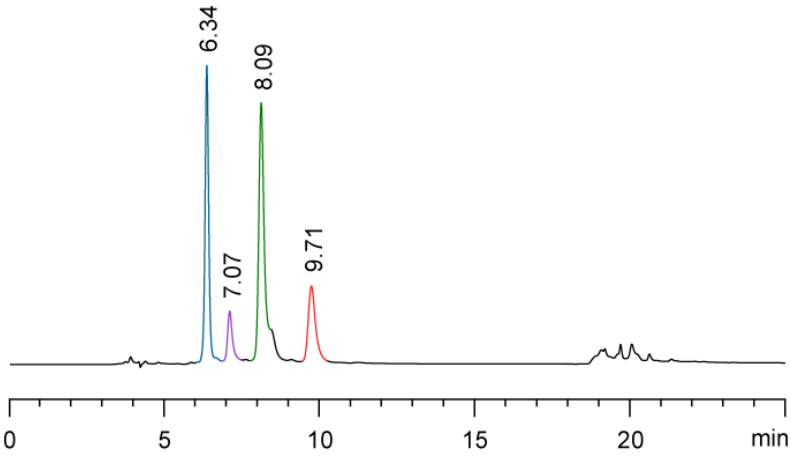

Figure 3.9. *Mixture after sixth operation: 1,2-**1** + 2,3-**1** +3,4-**1** + 1,4-**1** at the steady state, energy minimum, distribution. [Left-hand side, Cycle 3, Condition II of Figure 3.3]*

3.5.6.2 *Acid-Base Cycles Starting from 3,4-1*

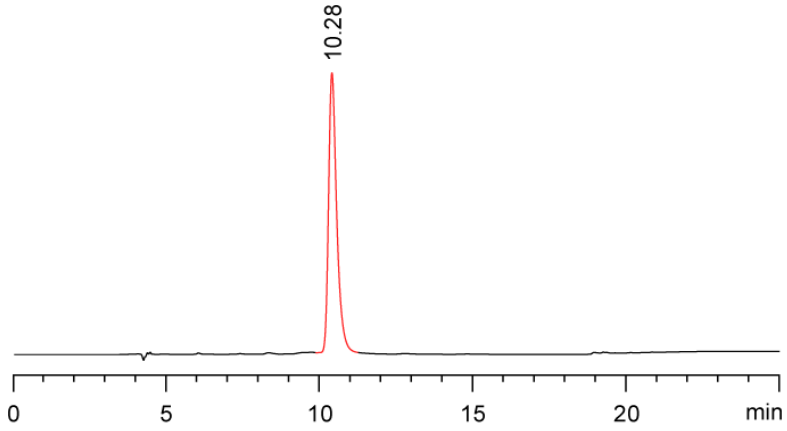

Figure 3.10. *Starting material: pristine 3,4-**1**.*

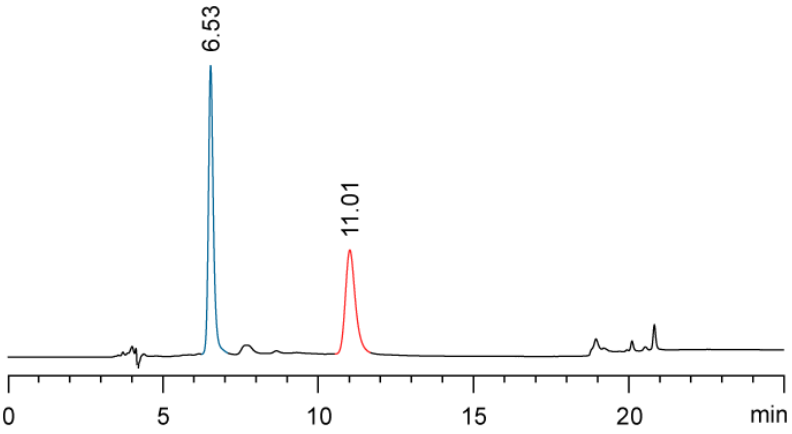

Figure 3.11. *Mixture after first operation (DBU, DTT): 2,3-**1** + 3,4-**1**.[Right-hand side, Cycle 1, Condition I of Figure 3.3]*

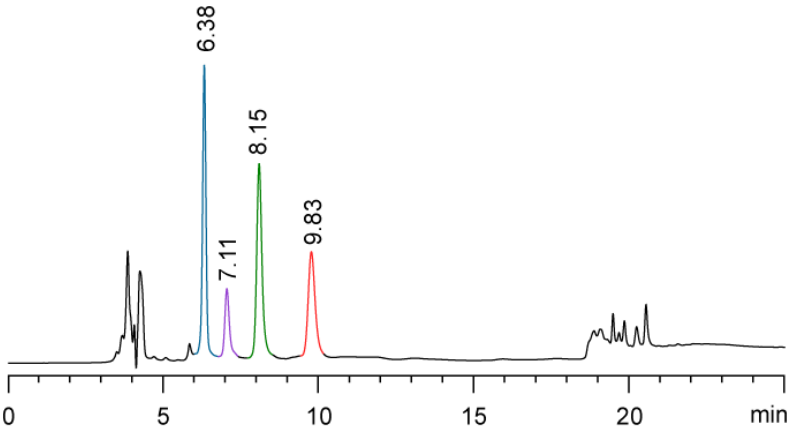

Figure 3.12. *Mixture after second operation (TFA): 1,2-**1** + 2,3-**1** +3,4-**1** +1,4-**1**. [Right-hand side, Cycle 1, Condition II of Figure 3.3]*

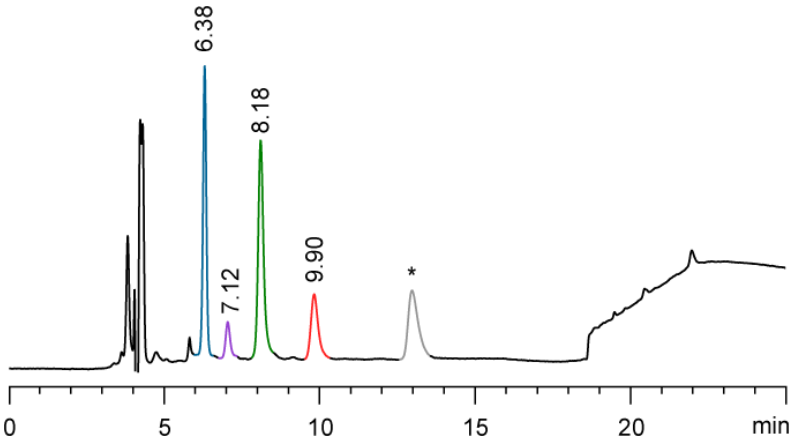

Figure 3.13. *Mixture after sixth operation: 1,2-**1** + 2,3-**1** +3,4-**1** + 1,4-**1** at the steady state, energy minimum, distribution. *: Unknown, but unrelated (PDA & MS detectors), impurity introduced into the sample at a late stage of the operation. [Right-hand side, Cycle 3, Condition II of Figure 3.3]*

3.5.6.3 Acid-Redox Cycles Starting from 1,2-1

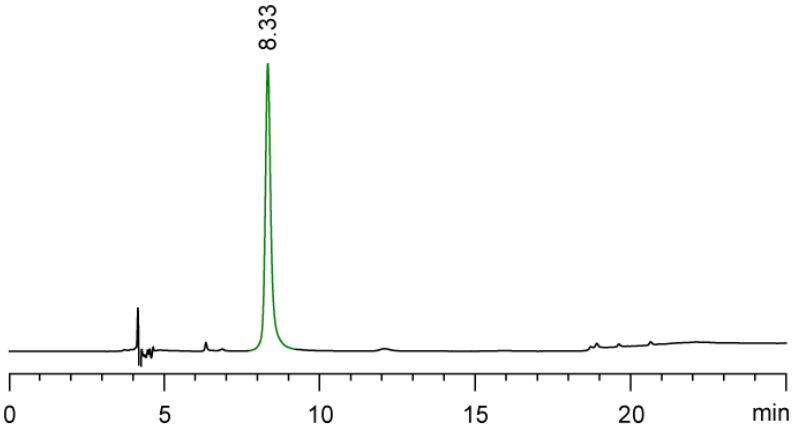

Figure 3.14. *Starting material: pristine 1,2-**1**.*

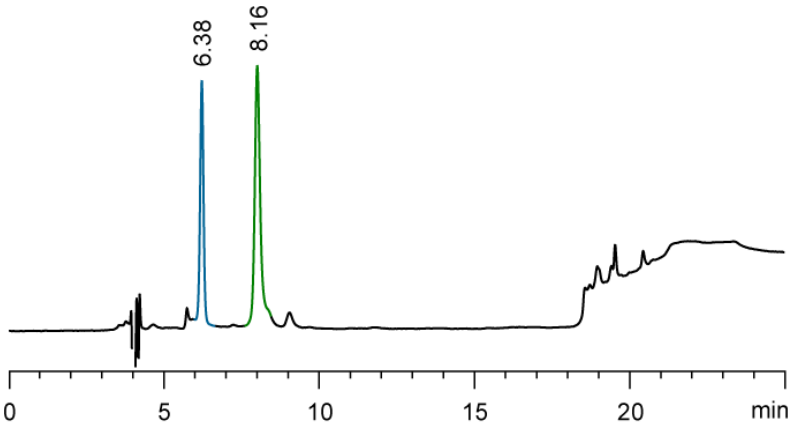

Figure 3.15. *Mixture after first operation (TFA): 1,2-**1** + 2,3-**1**. [Cycle 1, Condition I of Figure 3.4]*

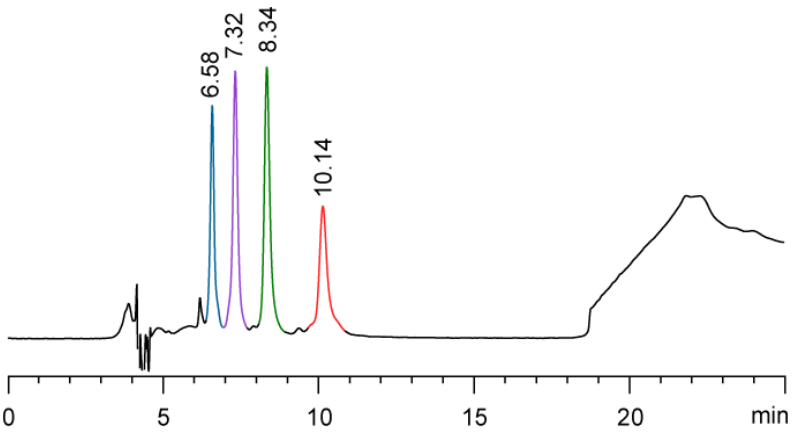

Figure 3.16. *Mixture after second operation (DBU, DTT reduction; I_2 oxidation): 1,2-**1** + 2,3-**1** +3,4-**1** + 1,4-**1**. [Cycle 1, Condition III of Figure 3.4]*

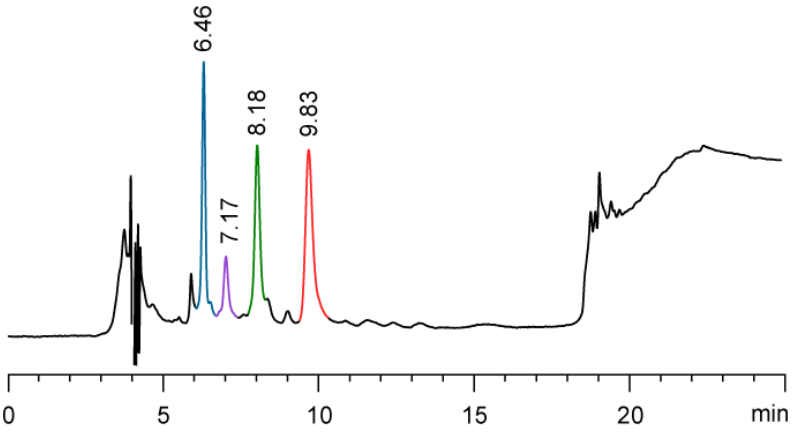

Figure 3.17. *Mixture after third operation (TFA): 1,2-**1** + 2,3-**1** +3,4-**1** + 1,4-**1**. [Cycle 2 (labelled '1.5'), Condition I of Figure 3.4]*

3.5.7 Table Showing the Isomer Ratios at Each Stage of Each Cycle in All Walking Experiments

Table 3.2. *Full details of the composition (in %) of the isomer mixtures during the three performed experimental sequences. (see Figure 3.3 and Figure 3.4). a) Acid-base non-biased walking experiment over 3 operational cycles starting from pure 1,2-**1**. b) Acid-base non-biased walking experiment over 3 operational cycles starting from pure 3,4-**1**. c) Acid-redox directionally biased walking experiment over 1.5 operational cycles starting from pure 1,2-**1**.*

	Start	Cycle 1		Cycle 2		Cycle 3	
a)		I[b]	II[c]	I[b]	II[c]	I[b]	II[c]
1,2-**1**[a]	100%	51%	45%	43%	40%	42%	37%
2,3-**1**[a]	-	49%	36%	37%	36%	33%	35%
3,4-**1**[a]	-	-	11%	17%	18%	18%	20%
1,4-**1**[a]	-	-	8%	4%	6%	7%	8%
b)		II[c]	I[b]	II[c]	I[b]	II[c]	I[b]
1,2-**1**[a]	-	-	30%	37%	36%	39%	38%
2,3-**1**[a]	-	61%	34%	39%	39%	32%	37%
3,4-**1**[a]	100%	39%	27%	17%	19%	21%	19%
1,4-**1**[a]	-	-	9%	6%	7%	7%	6%
c)		I[b]	III[d]	I[b]			
1,2-**1**[a]	100%	52%	28%	24%			
2,3-**1**[a]	-	48%	20%	24%			
3,4-**1**[a]	-	-	28%	43%			
1,4-**1**[a]	-	-	24%	9%			

[a] *Percentages are based on HPLC integration and are corrected for the absorbance coefficients at 290 nm (see section 3.5.8).* [b] *'I': 0.1 mM, TFA, $CHCl_3$; see section 3.5.2.* [c] *'II': 0.1 mM, DTT, DBU, dimethyl 3,3'-disulfanediyldipropanoate; see section 3.5.3.* [d] *'III': 1.0 mM, DTT, DBU, methyl 3-mercaptopropionate; see section 3.5.4.*

3.5.8 Absorbance Coefficients ε

In this section, a series of experiments is described which allows the conversion of ratios of isomers *1,2*-**1**, *2,3*-**1**, *3,4*-**1** and *1,4*-**1** based on UV detection, into molar ratios.

All HPLC traces (see section 3.5.6) were recorded at a constant wavelength of 290 nm, which roughly corresponds to the absorbance maximum of the respective hydrazone moieties. Since pure compounds *2,3*-**1** and *1,4*-**1** were only accessible in small amounts via dynamic covalent exchange processes after preparative HPLC (see section 3.5.11), a convenient way to obtain a set of absorbance coefficients ε for all four isomers was developed as follows:

i) Determination of the absolute ε for pure, synthesised isomer *3,4*-**1** using standard methods (spectrophotometric dilution series).

ii) Establishment of a relative set of absorbance coefficients by 800 MHz ^{1}H NMR and HPLC integration of the same mixed sample of all four isomers *1,2*-**1**, *2,3*-**1**, *3,4*-**1** and *1,4*-**1**.

3.5.8.1 Determination of the absolute ε value of 3,4-1

On a microbalance, 1.87 mg (2.22 μmol) of *3,4*-**1** was weighed and, in a standard flask, dissolved in 5.0 mL of HPLC grade CH_2Cl_2. From this stock solution (concentration: C_0) six more diluted solutions were prepared and the corresponding absorbance at 290 nm was measured in 1 cm quartz cuvettes with a UV spectrometer. Table 3.3 shows the obtained absorbance values and Figure 3.18 displays the absorbance versus concentration plot with the obtained gradient ε and the R^2 value.

Table 3.3. *Results of spectrophotometric dilution series for 3,4-**1**.*

	Concentration (μM)	Absorbance
C_0	444	
C_1	44.4	0.677
C_2	35.5	0.548
C_3	26.6	0.404
C_4	17.8	0.281
C_5	8.88	0.149
C_6	4.44	0.069

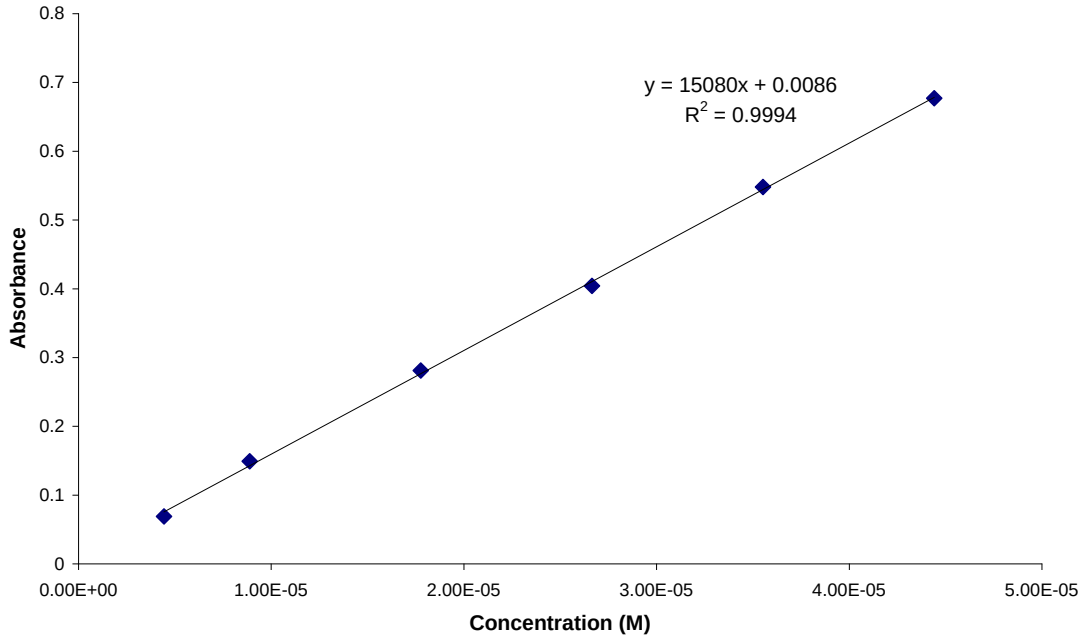

Figure 3.18. *Absorbance versus concentration plot for 3,4-**1** (including best fit line).*

3.5.8.2 *Determination of a relative set of absorbance coefficients*

Mixed samples of *3,4*-**1**/*1,4*-**1** and *1,2*-**1**/*2,3*-**1** were obtained by intramolecular dynamic covalent hydrazone exchange (as described section 3.5.2) followed by preparative HPLC. The two purified mixed samples were combined, the solvents evaporated and the sample dissolved in $CDCl_3$. Figure 3.19 shows the partial 800 MHz ^{1}H NMR spectrum (aldehyde region), which was used for integration.

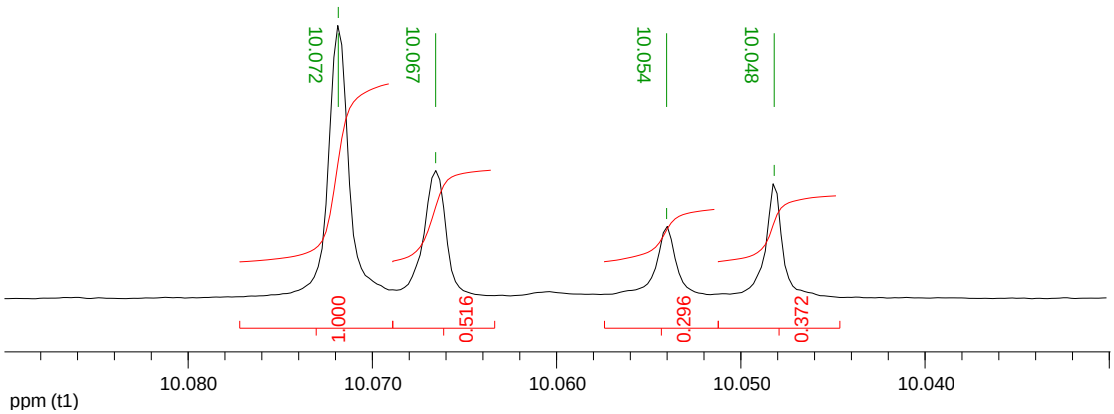

Figure 3.19. *Partial ^{1}H NMR spectrum (800 MHz, $CDCl_3$, 298 K) of a mixture of 3,4-**1**, 2,3-**1**, 1,4-**1** and 1,2-**1** including integration values.*

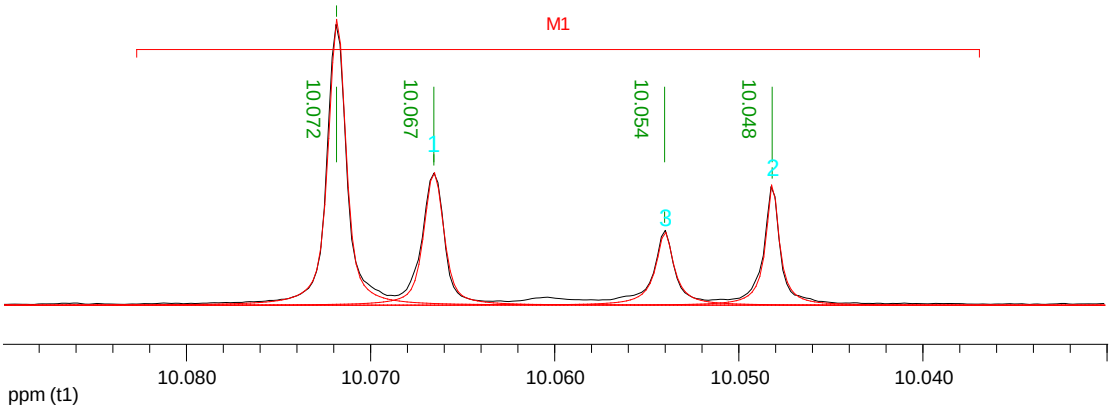

Figure 3.20. *Partial ^{1}H NMR spectrum (800 MHz, $CDCl_3$, 298 K) of a mixture of 3,4-**1**, 2,3-**1**, 1,4-**1** and 1,2-**1** and line fit performed with MestreC.[35]*

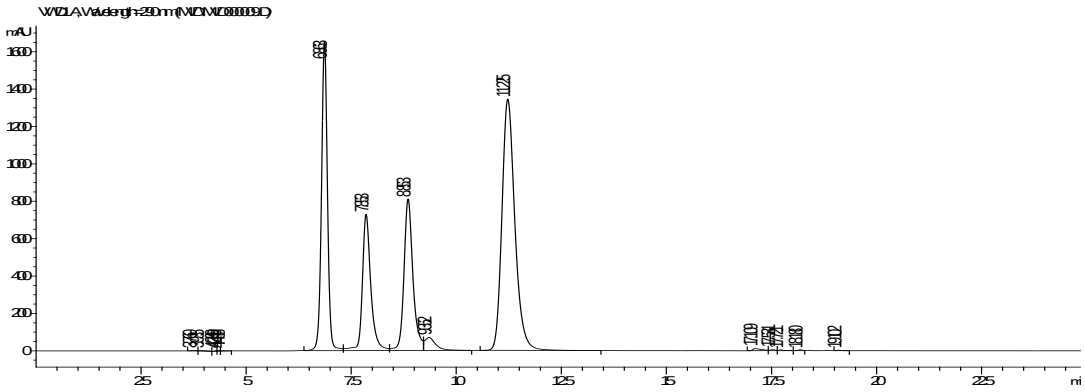

Figure 3.21. *HPLC trace of the same sample (see below for integration).*

Figure 3.21 shows the HPLC trace that was obtained from the same sample directly after recording the 800 MHz ^{1}H NMR spectrum. Table 3.4 shows how the relative and absolute absorbance coefficients were calculated according to the integration of the ^{1}H NMR spectrum (Figure 3.20) and HPLC chromatogram (Figure 3.21).

Table 3.4. *Comparison of integration values obtained by ^{1}H NMR and HPLC and resulting relative and absolute absorbance coefficients ε. Integration values of isomer 3,4-**1** were normalised to 1.00.*

	NMR Integration fit	HPLC Integration	Relative ε	Absolute ε (10^3 cm^2mol^{-1})
2,3-**1**	0.521	0.561	1.08	16300
1,4-**1**	0.274	0.353	1.29	19500
1,2-**1**	0.337	0.417	1.24	18700
3,4-**1**	1.000	1.000	1.00	15100

Because of the inherent inaccuracy of ^{1}H NMR integration (even based on line-fitting with well-separated resonances at 800 MHz resolution) and the presence of a minor side product, we estimate that this procedure involves an error of about 2-5% in the absolute ε values. For the context of the work described in this Chapter, only the relative ε values of the positional isomers are required, not the exact values.

3.5.9 Computational Chemistry

Semi-empirical (AM1) calculations on each possible positional isomer (with various lengths of chain in the walker unit and different track motifs) were performed at the design stage of the project in order to predict a suitable length of walker unit and distance between the various footholds for the target structures.[36] Too high ring strain in the *2,3*-isomer, for example, would dramatically increase (to >100 in some cases we studied) the number of cycles required to reach the steady state minimum energy distribution of walkers on the track. Later on we also performed more sophisticated molecular modeling at the B3LYP/cc-pVDZ level of density functional theory. [37] Figure 3.22 shows the structure optimisations[38] for the four positional isomers *1,2*-**1**, *2,3*-**1**, *3,4*-**1** and *1,4*-**1** in vacuum.

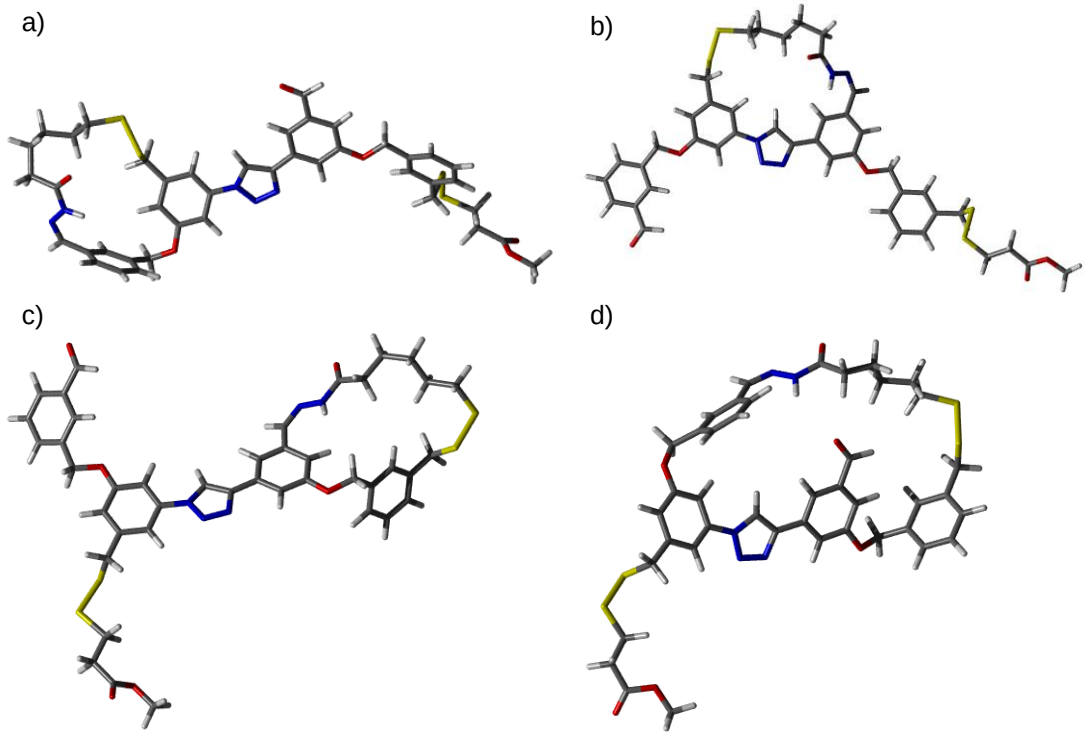

Figure 3.22. *Geometry optimisations obtained by DFT calculations (B3LYP/cc-pVDZ) in vacuum. a) 1,2-**1**; b) 2,3-**1**; c) 3,4-**1**; d) 1,4-**1**. C: grey, H: white, O: red, N: blue, S: yellow.*

Some general trends, such as the higher energies of isomers *3,4*-**1** and *1,4*-**1** are reproduced by the calculations (Table 3.5). However, this level of theory appears to be insufficient to reproduce the precise isomer ratios found experimentally.

Table 3.5. *Comparison of integration values obtained by ^{1}H NMR and HPLC and resulting relative and absolute absorbance coefficients ε. Integration values of isomer 3,4-**1** were normalised to 1.00.*

Isomer	Total Energy (Hartree)	Total Energy (kcal/mol)	Relative Energies (kcal/mol)
1,2-**1**	-3944.4009778	-2475149.085	2.21
2,3-**1**	-3944.4044999	-2475151.296	0
3,4-**1**	-3944.3948837	-2475145.261	6.03
1,,4-**1**	-3944.3977119	-2475147.036	4.26

3.5.10 Synthetic Schemes

3.5.10.1 Synthesis of Walker Moiety E3

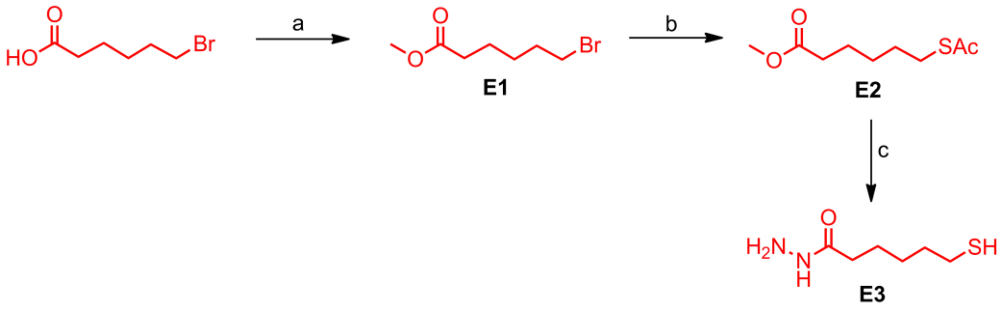

Scheme 3.2. *Reaction conditions: a) MeOH,* p-*TsOH, reflux, 16 h, 92%; b) KSAc, DMF, RT, 1 h, 85%; c)* $N_2H_4 \cdot H_2O$*, MeOH, reflux, 16 h, 44%.*

3.5.10.2 *Synthesis of Two-Foothold Precursors*

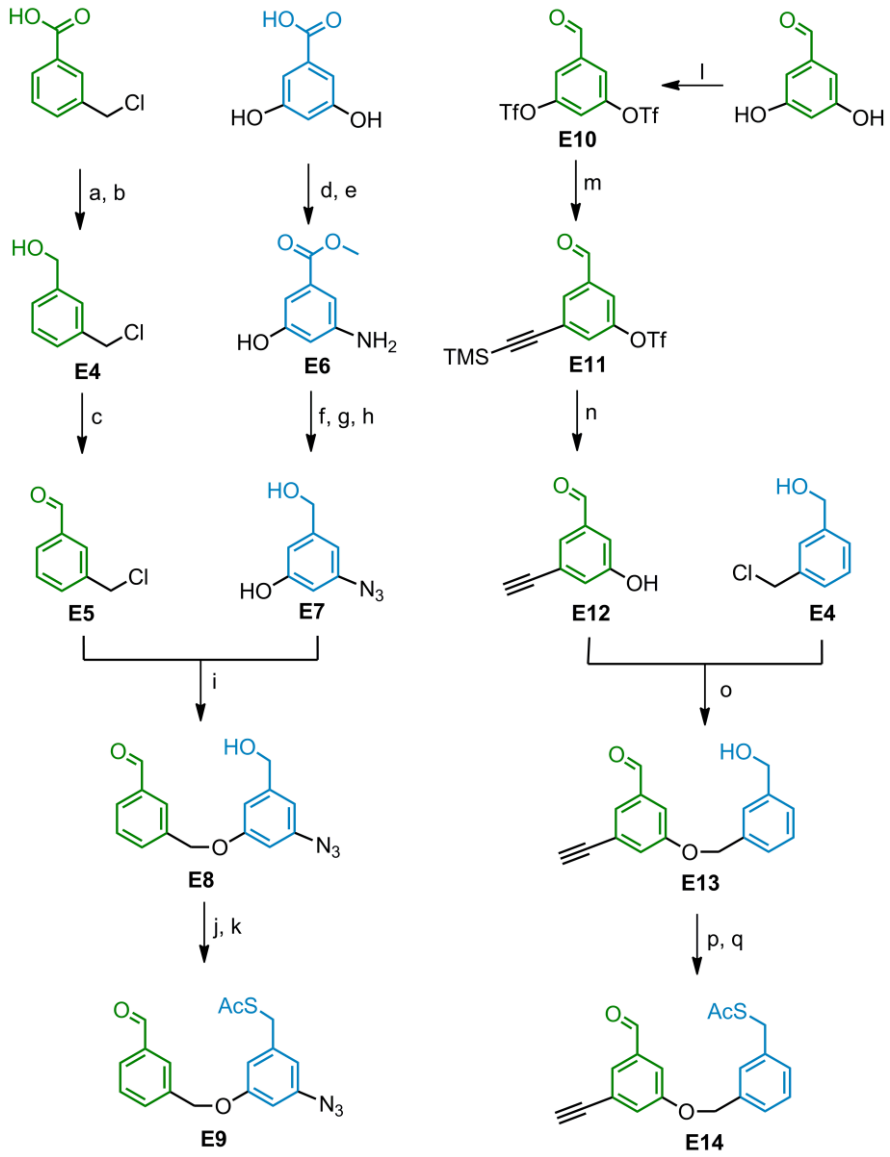

Scheme 3.3. *Reaction conditions: a) EtOCOCl, NEt_3, THF, 5 °C, 30 min; b) $NaBH_4$, H_2O, RT, 16 h, 85% (two-step); c) PCC, MS 4 Å, CH_2Cl_2, RT, 15 min, 78%; d) NH_4Cl, NH_4OH, steel bomb, 180 °C, 40 h; e) MeOH, H_2SO_4, reflux, 36 h, 70% (two-step); f) $LiAlH_4$, THF, reflux, 16 h; g) $NaNO_2$, H_2SO_4, H_2O; 0 °C, 5 min; h) NaN_3, H_2O, RT, 16 h, 72%; i) NaH, DMF, RT, 16 h, 88%; j) MsCl, NEt_3, CH_2Cl_2, 0 °C, 30 min; k) KSAc, DMF, RT, 3 h, 77% (two-step); l) Tf_2O, NEt_3, CH_2Cl_2, 0 °C → RT, 2 h, 58%; m) TMS-acetylene, $Pd(PPh_3)_2$, CuI, NEt_3, THF, 0 °C → RT, 2 h, 79%; n) LiOH, MeOH, 0 °C → RT, 16 h, 83%; o) NaH, DMF, 0 °C → RT, 16 h, 65%; p) MsCl, NEt_3, CH_2Cl_2, RT, 16 h; q) KSAc, DMF, RT, 3 h, 66% (two-step).*

3.5.10.3 *Synthesis of 1,2-1*

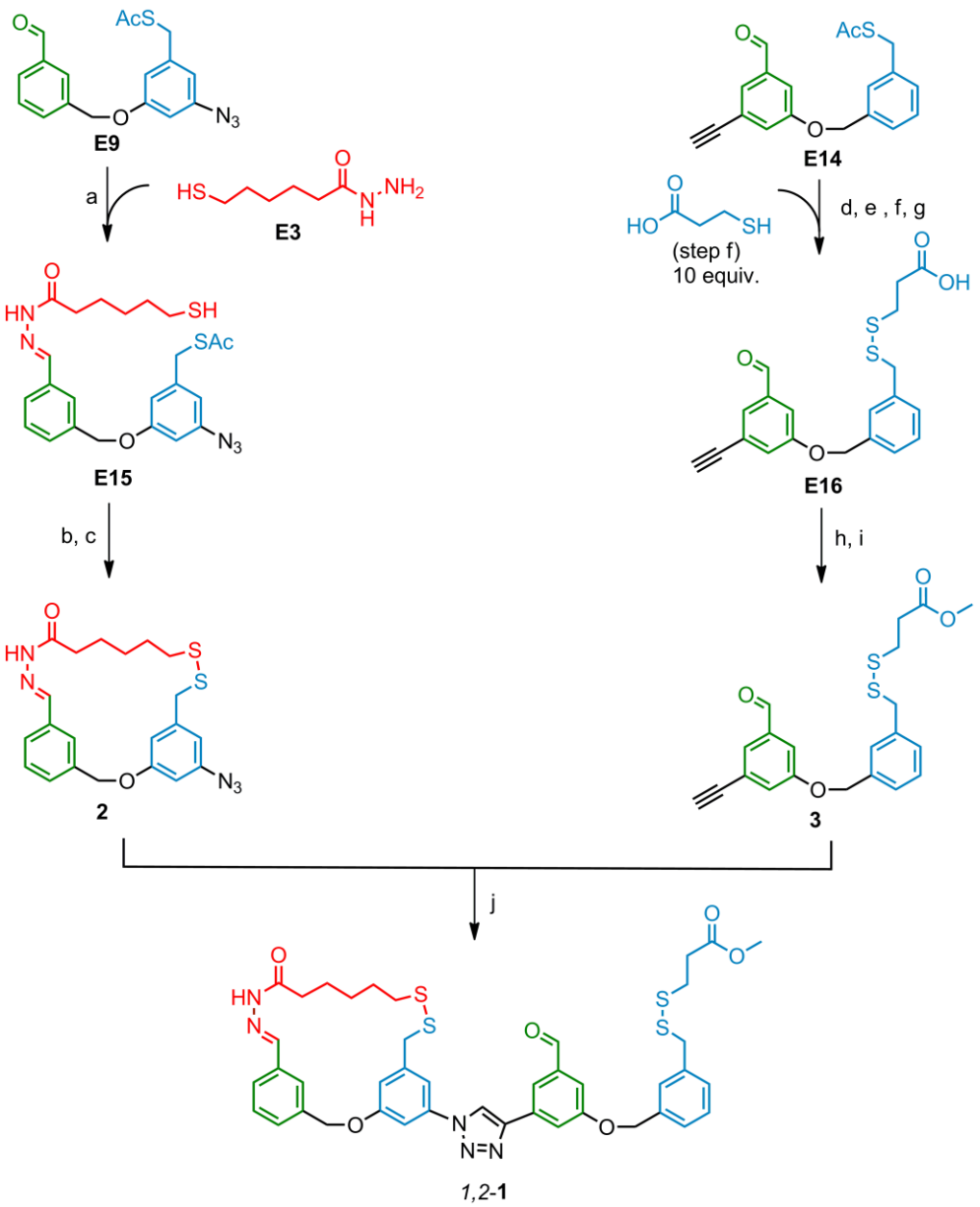

Scheme 3.4. *Reaction conditions: a) AcOH (cat.), MeOH, RT, 2h, 78%; b) NaOMe, MeOH, RT, 2 h; c) I_2, KI, CH_2Cl_2, RT, 5 min, 32% (two-step); d) $HC(OMe)_3$,* p-*TsOH, MeOH, RT, 30 min; e) NaOMe, MeOH, RT, 30 min; f) I_2, KI, CH_2Cl_2, RT, 5 min; g) TFA, CH_2Cl_2, RT, 30 min, 58% (4-step); h) H_2SO_4 (cat.), MeOH, RT, 16 h; i) TFA, CH_2Cl_2, RT, 30 min, 40% (2-step); j) $Cu(MeCN)_4PF_6$, TBTA (**E23**), CH_2Cl_2/THF/MeOH, RT, 16 h, 79%.*

3.5.10.4 *Synthesis of 3,4-1*

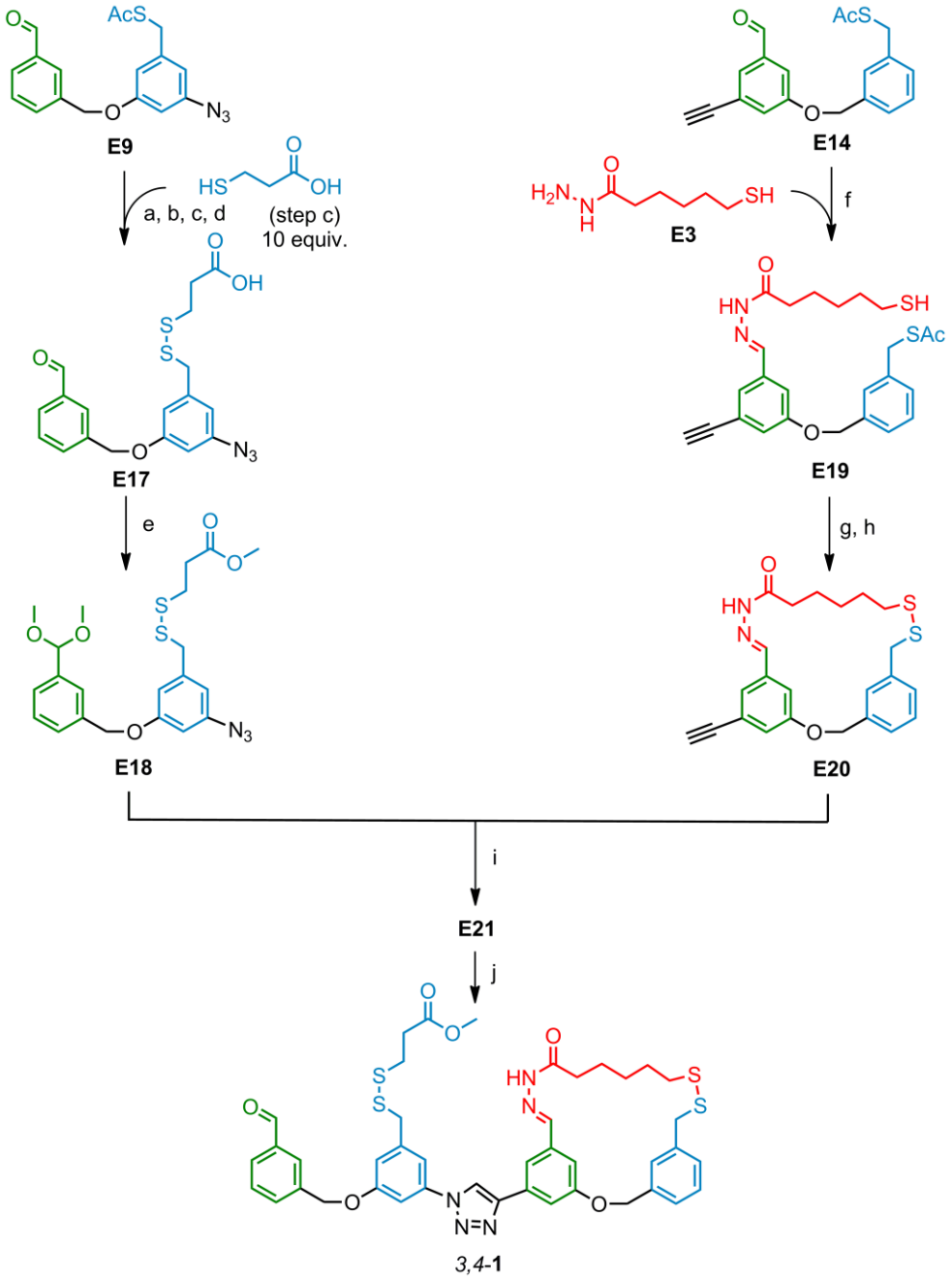

Scheme 3.5. *Reaction conditions: a) $HC(OMe)_3$,* p*-TsOH, MeOH, RT, 30 min; b) NaOMe, MeOH, RT, 30 min; c) I_2, KI, CH_2Cl_2, RT, 5 min; d) TFA, CH_2Cl_2, RT, 30 min, 84% (4-step); e) H_2SO_4 (cat.), MeOH, RT, 16 h, 70%; f) AcOH (cat.), MeOH, RT, 2 h, 86%; g) NaOMe, MeOH, RT, 2h; h) I_2, KI, CH_2Cl_2, RT, 5 min, 32% (two-step); i) $Cu(MeCN)_4PF_6$, TBTA (**E23**), CH_2Cl_2/THF/MeOH, RT, 16 h, 85%; j) TFA, DCM, RT (quant.) .*

3.5.10.5 *Synthesis of Track 4*

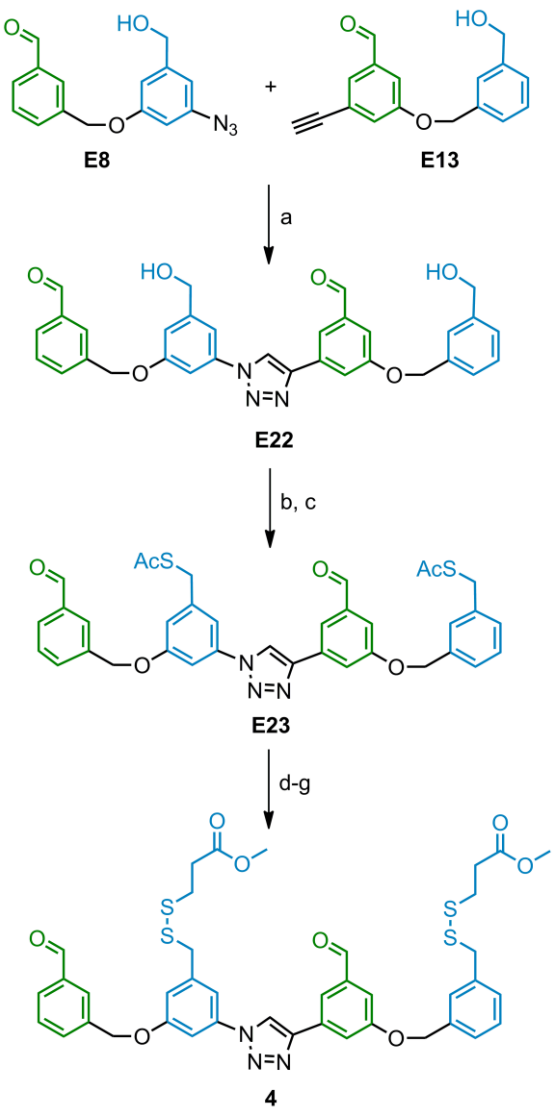

Scheme 3.6. *Reaction conditions: a) $Cu(MeCN)_4PF_6$, DIPEA, CH_2Cl_2/MeOH, RT, 20 h, 75%; b) MsCl, NEt_3, CH_2Cl_2, RT, 16 h; c) KSAc, DMF, RT, 30 min, 54% (two-step); d) $HC(OMe)_3$, p-TsOH, MeOH, RT, 30 min; e) NaOMe, MeOH, RT, 60 min; f) methyl 3-mercaptopropionate, I_2, KI, CH_2Cl_2, RT, 5 min; g) TFA, CH_2Cl_2, RT, 60 min, 3% (4-step).*

3.5.11 Synthetic Procedures and Characterisation Data

Methyl 6-bromohexanoate

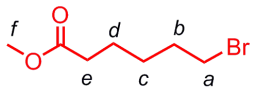

E1

Synthesised according to a literature procedure.[30] A solution of 6-bromohexanoic acid (20.0 g, 0.103 mmol, 1.0 equiv.) and *p*-TsOH (2.0 g, 11.6 mmol, 0.11 equiv.) in MeOH (200 mL) was refluxed over night. After evaporation of the solvent the residue was dissolved in benzene (100 mL), washed with H_2O and a $NaHCO_3$ solution and dried ($MgSO_4$). Removal of the solvent under reduced pressure gave **E1** (19.5 g, 92%) as a colourless oil. ^{1}H NMR (400 MHz, $CDCl_3$): δ = 3.67 (s, 3H, H_f), 3.41 (t, *J* = 6.8 Hz, 2H, H_a), 2.33 (t, *J* = 7.3 Hz, 2H, H_e), 1.88 (quint., *J* = 7.1 Hz, 2H, H_b), 1.66 (quint., *J* = 7.6 Hz, 2H, H_d), 1.51 – 1.44 (m, 2H, H_c).

Methyl 6-acetylsulfanyl-hexanoate

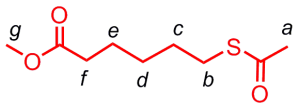

E2

Methyl 6-bromohexanoate **E1** (4.45 g, 21.28 mmol, 1.0 equiv.) was dissolved in DMF (30 mL). A solution of KSAc (3.65 g, 31.93 mmol, 1.5 equiv.) in DMF (20 mL) was added dropwise. The reaction was stirred at room temperature and monitored by TLC (SiO_2, Et_2O/hexane 1:2). After 1 h the reaction was complete and the solvent removed under reduced pressure. The residue was dissolved in Et_2O (30 mL) and NH_4Cl (satd., 30 mL). The layers were partitioned and the H_2O layer was extracted once more with Et_2O. The combined Et_2O layers were washed with HCl (1M), H_2O, and brine, dried over $MgSO_4$ and concentrated under reduced pressure to yield a brown residue. Purification by flash column chromatography (SiO_2, hexane/Et_2O 8:1) gave **E2** (3.71 g, 85%) as a yellowish oil. ^{1}H NMR (400 MHz, $CDCl_3$): δ = 3.66 (s, 3H, H_g), 2.86 (t, *J* = 7.3 Hz, 2H, H_b), 2.32 (s, 3H, H_a), 2.31 (d, *J* = 7.5 Hz, 2H, H_f), 1.64 (dt, *J* = 7.8, 7.5 Hz, 2H, H_c or H_e), 1.58 (dt, *J* = 7.6, 7.3 Hz, 2H, H_c or H_e), 1.37 (dt, *J* = 7.8, 7.6 Hz, 2H, H_d); ^{13}C NMR (100 MHz, $CDCl_3$): δ = 195.93, 173.98, 51.50, 33.82, 30.62, 29.17, 28.83, 28.20, 24.38; HRMS (ESI): *m*/*z* = 205.0895 $[M+H]^+$ (calcd. 205.0898 for $C_9H_{17}O_3S$).

6-Mercaptohexanehydrazide

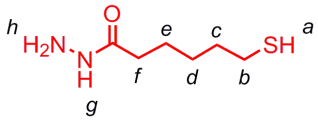

E3

Under N_2, hydrazine monohydrate (1.98 mL, 40.8 mmol, 5.0 equiv.) was added dropwise to a solution of **E2** (1.67 g, 8.2 mmol, 1.0 equiv.) in dry MeOH (30 mL) after which the solution was refluxed overnight. The bulk of the solvent was removed under reduced pressure, H_2O (50 mL) was added and the mixture was extracted with CH_2Cl_2 (3 × 100 mL). The combined organic phases were washed with brine, dried ($MgSO_4$) and the solvent removed under reduced pressure. Purification by flash column chromatography (SiO_2, Et_2O/MeOH 9:1) gave **E3** (587 mg, 44%) as a colourless solid. ^{1}H NMR (400 MHz, $CDCl_3$): δ = 6.67 (bs, 1H, H_g), 3.90 (bs, 2H, H_h), 2.53 (q, J = 7.4 Hz, 2H, H_b), 2.16 (t, J = 7.5 Hz, 2H, H_f), 1.64 (m, 4H, H_c, H_e), 1.43 (m, 2H, H_d), 1.34 (t, J = 7.8 Hz, 1H, H_a); ^{13}C NMR (100 MHz, $CDCl_3$): δ = 170.07, 33.81, 33.50, 27.73, 24.63, 24.35; HRMS (ESI): m/z = 163.0896 $[M+H]^+$ (calcd. 163.0900 for $C_6H_{15}ON_2S$).

3-Chloromethylbenzyl alcohol

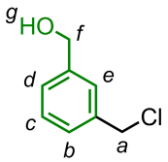

E4

Synthesised according to a modified literature procedure.[31] At 5 °C, a solution of ethyl chloroformate (1.69 mL, 17.2 mmol, 1.0 equiv.) in THF (7 mL) was added dropwise to a solution of 3-(chloromethyl)-benzoic acid (3.02 g, 17.2 mmol, 1.0 equiv.) and Et_3N (2.39 mL, 17.2 mmol, 1.0 equiv.) in THF (30 mL). The reaction was allowed to proceed for 30 min at 5 °C after which the Et_3NHCl precipitate was filtered off and washed with THF (40 mL). The combined THF phases were added over 30 min to a solution of $NaBH_4$ (1.66 g, 43 mmol, 2.5 equiv.) in H_2O (14 mL) at 10 °C. The mixture was stirred over night at room temperature and was acidified with 10% HCl (17 mL). The solution was extracted with Et_2O (3 × 50 mL). The combined organic layers were washed with a solution of 10% NaOH (50 mL) and brine (50 mL), dried ($MgSO_4$), and concentrated under reduced pressure. Flash chromatography (SiO_2, hexane/EtOAc 8:2) gave **E4**

(2.50 g, 85%) as a colourless oil. ^{1}H NMR (400 MHz, $CDCl_3$): δ = 7.34 (m, 4H, H_b, H_c, H_d, H_e), 4.68 (s, 2H, H_f), 4.60 (s, 2H, H_a), 2.32 (bs, 1H, H_g); LRMS (EI): m/z = 156.1 $[M]^+$.

3-Chloromethylbenzaldehyde

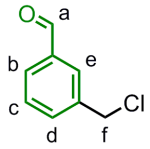

E5

Synthesised according to a literature procedure.[31] A solution of **E4** (6.48 g, 41.4 mmol, 1.0 equiv.) in CH_2Cl_2 (500 mL) was stirred with molecular sieves (40 g, 4 Å) for 30 min. Pyridinium chlorochromate (18.2 g, 82.8 mmol, 2.0 equiv.) was added and the mixture stirred at room temperature for 15 min. The mixture was poured into Et_2O (600 mL) and the resulting brown solid and molecular sieves were removed by suction filtration through a pad of celite. After evaporation of the solvents, the brown residue was purified by flash chromatography (SiO_2, hexane/EtOAc 8:2), which gave **E5** (5.13 g, 80%) as a light yellow oil. ^{1}H NMR (400 MHz, $CDCl_3$): δ = 10.00 (s, 1H, H_a), 7.88 (s, 1H, H_e), 7.82 (d, J = 7.6 Hz, 1H, H_b), 7.64 (d, J = 7.6 Hz, 1H, H_d), 7.52 (t, J = 7.6 Hz, 1H, H_c), 4.63 (s, 2H, H_f); LRMS (ESI): m/z = 154.0 $[M]^+$.

Methyl 3-amino-5-hydroxybenzoate

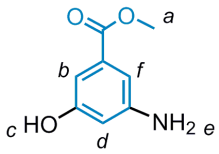

E6

Synthesised according to a literature procedure.[32] A mixture of 3,5-dihydroxybenzoic acid (14.0 g, 91 mmol), NH_4Cl (11.9 g, 224 mmol) and 28% aq. NH_3 (42 mL, 301 mmol) was heated in a steel bomb at 180°C for 40 h. After cooling, the solution was evaporated to dryness and the residue taken up in MeOH (500 mL). Concentrated H_2SO_4 (21 mL) was added dropwise and the solution kept at reflux for 36 h. The solvent was evaporated under reduced pressure, the residue taken up in ice-cold H_2O, and the aqueous solution extracted with Et_2O. The combined extracts were washed with cold 1N H_2SO_4 and subsequently with brine. The aqueous solution and H_2SO_4 washings were combined, adjusted to pH 7 with solid $NaHCO_3$ and extracted with EtOAc. The extracts

were washed with brine, dried ($MgSO_4$) and evaporated. Flash chromatography (SiO_2, CH_2Cl_2/EtOAc 7:3) gave **E6** (10.58 g, 70%) as a pale yellow solid. Mp 124 °C (lit. 125-127°C); ^{1}H NMR (400 MHz, acetone-d_6): δ = 8.26 (s, 1H, H_c), 6.85 (t, *J* = 2.2 Hz, 1H, H_f), 6.75 (t, *J* = 2.2 Hz, 1H, H_b), 6.41 (d, *J* = 2.2 Hz, 1H, H_d), 4.83 (bs, 2H, H_e), 3.79 (s, 3H, H_a); LRMS (EI): *m*/*z* = 167.1 $[M]^+$.

3-azido-5-hydroxybenzyl alcohol

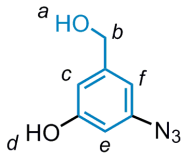

E7

Synthesised according to a modified literature procedure.[33] Under N_2, a solution of **E6** (2.5 g, 14.9 mmol, 1.0 equiv.) in dry THF (150 mL) was added to a suspension of $LiAlH_4$ (3.6 g, 89.7 mmol, 6.0 equiv.) in dry THF (500 mL), and the mixture was refluxed overnight under N_2. After cooling, the mixture was neutralised with saturated aqueous NH_4Cl, and after subsequent addition of H_2O (100 mL), the mixture was filtered through a pad of celite and concentrated under reduced pressure to give the crude 3-amino-5-hydroxybenzyl alcohol as a yellow-orange oil (2.07 g, 97%). Due to its instability in air, the crude amine was used directly for the next synthetic step.

The crude was dissolved in 6 M HCl (15 mL). At 0°C, a solution of $NaNO_2$ (2.34 g, 32.9 mmol, 1.1 equiv.) in H_2O (13 mL) was added dropwise. After 5 min a solution of NaN_3 (3.89 g, 59.8 mmol, 2.0 equiv) in H_2O (10 mL) was added and the solution was left to stir at room temperature over night. After addition of H_2O, the solution was extracted with Et_2O (3 × 200 mL), the combined organic phases were dried ($MgSO_4$) and concentrated under reduced pressure. Flash chromatography (SiO_2, CH_2Cl_2/EtOAc 8:2) gave **E7** (3.58 g, 72% over two steps) as a pale yellow solid. M.p. 112 °C; ^{1}H NMR (400 MHz, acetone-d_6): δ = 8.64 (s, 1H, H_d), 6.68 (s, 1H, H_c), 6.60 (s, 1H, H_f), 6.41 (s, 1H, H_e), 4.57 (d, *J* = 5.9 Hz, 2H, H_b), 4.30 (t, *J* = 5.9 Hz, 1H, H_a); ^{13}C NMR (100 MHz, acetone-d_6): δ = 159.55, 146.98, 141.65, 118.17, 111.15, 108.74, 105.21, 64.06; HRMS (EI): *m*/*z* = 165.0533 $[M]^+$ (calcd. 165.0533 for $C_7H_7N_3O_2$).

3-((3-Azido-5-(hydroxymethyl)phenoxy)methyl)benzaldehyde

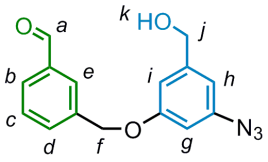

E8

Under N_2, **E7** (3.53 g, 21.3 mmol, 1.0 equiv.) was dissolved in dry DMF (100 mL). At 0 °C, NaH (60% in mineral oil, 0.9 g, 1.05 equiv.) was added and the solution was allowed to stir for 1 h, while warming to room temperature. At 0 °C, a solution of **E5** (3.30 g, 21.3 mmol, 1.0 equiv.) in dry DMF (20 mL) was added dropwise and the mixture was allowed to stir over night at room temperature. NH_4Cl (satd., 200 mL) was added and the mixture extracted with Et_2O (5 × 200 mL). The combined organic phases were washed with brine, dried ($MgSO_4$) and concentrated under reduced pressure. Flash column chromatography (SiO_2, CH_2Cl_2/EtOAc 95:5) gave **E8** (5.33 g, 88%) as a colourless oil. ^{1}H NMR (400 MHz, $CDCl_3$): δ = 10.03 (s, 1H, H_a), 7.94 (s, 1H, H_e), 7.85 (d, J = 7.6 Hz, 1H, H_b), 7.69 (d, J = 7.6 Hz, 1H, H_d), 7.57 (t, J = 7.6 Hz, 1H, H_c), 6.79 (s, 1H, H_i), 6.69 (s, 1H, H_h), 6.54 (s, 1H, H_g), 5.12 (s, 2H, H_f), 4.66 (s, 2H, H_j), 1.95 (bs, 1H, H_k); ^{13}C NMR (100 MHz, $CDCl_3$): δ = 192.13, 159.73, 144.24, 141.61, 137.72. 136.69, 133.24, 129.61, 129.41, 128.29, 110.01, 109.48, 104.94, 69.28, 64.66; HRMS (ESI): m/z = 301.1297 $[M+NH_4]^+$ (calcd. 301.1295 for $C_{15}H_{17}N_4O_3$).

***S*-3-Azido-5-(3-formylbenzyloxy)benzyl ethanethioate**

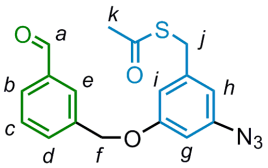

E9

a) At 0 °C, **E8** (4.67 g, 16.5 mmol, 1.0 equiv.) was dissolved in CH_2Cl_2 (300 mL) and NEt_3 (3.44 mL, 24.7 mmol, 1.5 equiv.) was added. After 5 min, MsCl (1.91 mL, 24.7 mmol, 1.5 equiv.) was added dropwise and the mixture was stirred at 0 °C for 30 min. H_2O (200 mL) was added and the layers were partitioned. The aqueous layer was extracted with CH_2Cl_2 (2 × 150 mL). The combined organic phases were washed with H_2O, dried ($MgSO_4$) and concentrated under reduced pressure.

b) At 0 °C, the crude mesylate was dissolved in dry DMF (150 mL) and a solution of KSAc (2.01 g, 17.24, 1.05 equiv.) in DMF (50 mL) was added dropwise. The mixture was stirred at room temperature for 3 h and the bulk of DMF was removed under reduced pressure. H_2O (200 mL) was added and the mixture extracted wit EtOAc (3 × 150 mL). The combined organic phases were washed with brine, dried ($MgSO_4$) and concentrated under reduced pressure. Flash chromatography (SiO_2, hexane/EtOAc 8:2) gave **E9** (4.22 g, 75% two-step) as a yellow solid. M.p. 48 °C. ^{1}H NMR (400 MHz, $CDCl_3$): δ = 10.04 (s, 1H, H_a), 7.94 (s, 1H, H_e), 7.86 (d J = 7.6 Hz, 1H, H_b), 7.69 (d, J = 7.6 Hz, 1H, H_d), 7.57 (t, J = 7.6 Hz, 1H, H_c), 6.71 (s, 1H, H_i), 6.59 (s, 1H, H_h), 6.51 (s, 1H, H_g), 5.10 (s, 2H, H_f), 4.05 (s, 2H, H_j), 2.35 (s, 3H, H_k); ^{13}C NMR (100 MHz, $CDCl_3$): δ = 194.79, 192.05, 159.63, 141.59, 140.99, 137.63, 136.71, 133.27, 129.53, 129.40, 128.42, 112.25, 111.85, 104.75, 69.29, 33.14, 30.34; HRMS (EI): m/z = 341.0834 $[M]^+$ (calcd. 341.0829 for $C_{17}H_{15}N_3O_3S$).

5-Formyl-1,3-phenylene bis(trifluoromethanesulfonate)

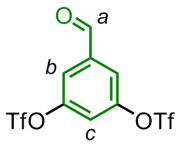

E10

Synthesised according to a modified literature procedure.[34] Under N_2, 3,5-dihydroxy-benzaldehyde (5.62 g, 40.68 mmol, 1.0 equiv.) was dissolved in CH_2Cl_2 (50 mL) and Et_3N (122.1 mmol, 17.0 mL, 12.35 g). The mixture was cooled to 0 °C and a solution of $(CF_3SO_2)_2O$ (25 g, 88.61 mmol, 2.2 equiv.) in CH_2Cl_2 (25 mL) was added dropwise. The reaction mixture was stirred for another 2 h and allowed to warm up to room temperature during this period. H_2O (75 mL) was added and the product was extracted with CH_2Cl_2 (2 × 50 mL). The combined organic layers were washed with 1M HCl (50 mL), H_2O (50 mL) and brine (25 mL), dried ($MgSO_4$) and concentrated under reduced pressure. The brown residue was purified by flash column chromatography (SiO_2, hexane/EtOAc 4:1) to yield **E10** (9.50 g, 58%) as a slightly yellowish powder. ^{1}H NMR (400 MHz, $CDCl_3$): δ = 10.04 (s, 1H), 7.86 (d, J = 2.3 Hz, 2H), 7.50 (t, J = 2.3 Hz, 1H).

3-Formyl-5-((trimethylsilyl)ethynyl)phenyl trifluoromethane sulfonate

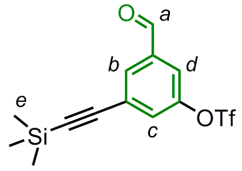

E11

Synthesised according to a modified literature procedure.[34] Under N_2, **E10** (9.13 g, 22.7 mmol, 1.0 equiv.) was dissolved in THF (100 mL) and NEt_3 (50 mL). $Pd(PPh_3)_2Cl_2$ (161 mg, 0.23 mmol, 0.01 equiv.) and CuI (88 mg, 0.46 mmol, 0.02 equiv.) were added and the mixture was degassed. The mixture was cooled to 0°C and a solution of TMS-acetylene (3.21 mL, 22.7 mmol, 1.0 equiv.) in THF (50 mL) was slowly added dropwise. The reaction was monitored by TLC (SiO_2, hexane/EtOAc 4:1 → 1:1). The mixture was stirred for another 2 h during which time the temperature was allowed to raise to room temperature. The solvents were removed under reduced pressure and NH_4Cl (satd., 60 mL) and EtOAc (100 mL) was added. The layers were partitioned and the H_2O layer was extracted with EtOAc (100 mL). The combined organic layers were washed with H_2O (100 mL) and brine (100 mL), dried ($MgSO_4$) and concentrated under reduced pressure. Purification by flash column chromatography (SiO_2, cyclohexane/EtOAc 30:1) gave **E11** (6.27 g, 17.88 mmol, 79%) as a colourless oil. ^{1}H NMR (400 MHz, $CDCl_3$): δ = 9.99 (s, 1H), 7.97 (dd, *J* = 1.4, 1.3 Hz, 1H), 7.71 (dd, *J* = 2.4, 1.3 Hz, 1H), 7.59 (dd, *J* = 2.4, 1.4 Hz, 1H), 0.28 (s, 9H).

3-Ethynyl-5-hydroxybenzaldehyde

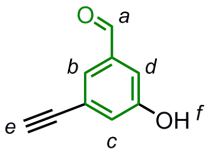

E12

Synthesised according to a modified literature procedure.[34] **E11** (6.27 g, 17.88 mmol, 1.0 equiv.) was dissolved in MeOH (40 mL). At 0°C, a solution of LiOH (3.0 g, 71.5 mmol, 4.0 equiv.) in MeOH (35 mL) was added and the temperature was allowed to rise to room temperature overnight. The mixture was extracted with Et_2O (3 × 40 mL) and the combined organic layers were washed with H_2O (30 mL) and brine (20 mL) and dried ($MgSO_4$). Concentration under reduced pressure and purification by flash column

chromatography (SiO_2, cyclohexane/Et_2O 2:1) gave **S15** (2.17 g, 83%) as a colourless powder. ^1H NMR (400 MHz, $CDCl_3$): δ = 9.92 (s, 1H), 7.57 (dd, *J* = 1.3, 1.3 Hz, 1H), 7.34 (dd, *J* = 2.6, 1.3 Hz, 1H), 7.23 (dd, *J* = 2.6, 1.3 Hz, 1H), 5.21 (s, 1H), 3.15 (s, 1H).

3-Ethynyl-5-(3-(hydroxymethyl)benzyloxy)benzaldehyde

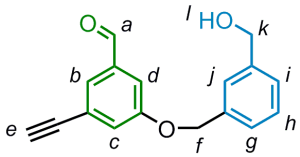

E13

Under N_2, **E12** (1.38 g, 9.44 mmol, 1.0 equiv.) was dissolved in DMF (30 mL). NaH (60% in mineral oil, 372 mg, 9.3 mmol, 0.95 equiv.) was added at 0°C and the mixture was stirred for 30 min, while the temperature was allowed to rise to room temperature. A solution of **E4** (1.97 g, 12.59 mmol, 1.33 equiv.) in DMF (15 mL) was added dropwise and the mixture was stirred over night at room temperature. The reaction was monitored by TLC (SiO_2, toluene/EtOAc 3:1). 1M HCl (30 mL) was added and the mixture was extracted with EtOAc (2 × 60 mL). The combined organic layers were washed with 1M HCl (30 mL), H_2O (30 mL), brine (30 mL) and dried ($MgSO_4$). Purification by flash column chromatography (SiO_2, toluene/EtOAc 10:1 → 4:1) gave **E13** (1.63 g, 65%) as an orange oil. ^1H NMR (400 MHz, $CDCl_3$): δ = 9.93 (s, 1H), 7.59 (dd, *J* = 1.3, 1.3 Hz, 1H), 7.47 – 7.44 (m, 2H), 7.43 – 7.39 (m, 1H), 7.37 – 7.35 (3H), 5.12 (s, 2H), 4.74 (d, *J* = 5.6 Hz, 2H), 3.15 (s, 1H), 1.73 (t, *J* = 5.6 Hz, 1H); ^{13}C NMR (100 MHz, $CDCl_3$): δ = 191.20, 158.92, 141.43, 137.66, 136.14, 128.87, 127.23, 126.80, 126.67, 125.93, 124.73, 124.21, 114.06, 81.89, 78.75, 70.20, 64.90; HRMS (ESI): *m/z* = 284.1281 $[M+NH_4]^+$ (calcd. 284.1281 for $C_{17}H_{18}NO_3$).

***S*-3-((3-Ethynyl-5-formylphenoxy)methyl)benzyl ethanethioate**

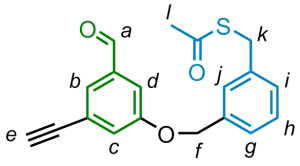

E14

a) At 0 °C, **S18** (1.25 g, 4.7 mmol, 1.0 equiv.) was dissolved in CH_2Cl_2 (10 mL) and NEt_3 (3.0 mL, 21.5 mmol, 4.6 equiv.) was added. After 5 min MsCl (3.0 mL, 38.8 mmol, 8.3 equiv.) was added dropwise and the mixture was stirred overnight at room

temperature. H_2O (50 mL) was added and the layers partitioned. The aqueous layer was extracted with CH_2Cl_2 (2 × 50 mL). The combined organic phases were washed with brine, dried ($MgSO_4$) and concentrated under reduced pressure. Purification by flash column chromatography (SiO_2, cyclohexane/CH_2Cl_2 2:1) gave 3-ethynyl-5-(3-(chloromethyl)benzyloxy)-benzaldehyde (1.16 g, 87%) as a colourless oil. ^{1}H NMR (400 MHz, $CDCl_3$): δ = 9.94 (s), 7.60 (dd, *J* = 1.2 Hz, 1H), 7.48 – 7.46 (m, 2H), 7.41 – 7.38 (m, 3H), 7.36 (dd, *J* = 1.3, 2.4 Hz, 1H), 5.12 (s, 2H), 3.68 (s, 2H), 3.15 (s, 1H); ^{13}C NMR (100 MHz, $CDCl_3$); δ = 191.07, 158.91, 137.99, 137.77, 136.52, 129.13, 128.49, 127.57, 127.44, 127.33, 124.74, 124.31, 114.06, 81.88, 78.76, 69.91, 45.92; HRMS (EI): *m*/*z* = 284.0596 $[M]^+$ (calcd. 284.0599 for $C_{17}H_{13}ClO_2$).

b) 3-Ethynyl-5-(3-(chloromethyl)benzyloxy)benzaldehyde (1.4 g, 4.93 mmol, 1.0 equiv.) was dissolved in dry DMF (50 mL) and a solution of KSAc (1.13 g, 9.86, 2.0 equiv.) in DMF (20 mL) was added dropwise. The mixture was stirred at room temperature for 3 h and the bulk of DMF was removed under reduced pressure. H_2O (100 mL) was added and the mixture extracted wit EtOAc (3 × 50 mL). The combined organic phases were washed with brine, dried ($MgSO_4$) and concentrated under reduced pressure. Flash chromatography (SiO_2, cyclohexane/EtOAc 8:1) gave **E14** (1.30 g, 81%) as a yellow oil. ^{1}H NMR (400 MHz, $CDCl_3$): δ = 9.93 (s, 1H), 7.59 (d, *J* = 1.2 Hz, 1H), 7.45 (dd, *J* = 2.5, 1.3 Hz, 1H), 7.36 – 7.27 (m, 5H), 5.08 (s, 2H), 4.14 (s, 2H), 3.11 (s, 1H), 2.36 (s, 3H); ^{13}C NMR (100 MHz, $CDCl_3$); δ = 194.98, 191.10, 158.96, 138.26, 137.75, 136.30, 129.01, 128.78, 127.89, 127.20, 126.42, 124.75, 124.26, 114.17, 81.92, 78.70, 70.12, 33.21, 30.32; HRMS (ESI): *m*/*z* = 342.1156 $[M+NH_4]^+$ (calcd. 342.1158 for $C_{19}H_{20}NO_3S$).

Thioacetic acid *S*-(3-azido-5-{3-[(6-mercapto-hexanoyl)-hydrazonomethyl]-benzyloxy}-benzyl) ester

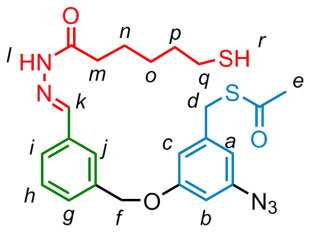

E15

Under N_2, **E9** (426 mg, 1.25 mmol, 1.0 equiv.) was dissolved in dry MeOH (10 mL). Two drops of acetic acid were added after which a solution of **E3** (243 mg, 1.50 mmol,

1.2 equiv.) in dry MeOH (5 mL) was added dropwise. The reaction was monitored by TLC (SiO_2, CH_2Cl_2/EtOAc 9:1). After 2 h the solvent was removed under reduced pressure and the residue was purified by flash column chromatography (SiO_2, CH_2Cl_2/EtOAc 9:1) to yield **E15** (464 mg, 76%) as a colourless solid. ^{1}H NMR (400 MHz, $CDCl_3$): δ = 9.72 (bs, 1H, H_l), 7.81 (s, 1H, H_k), 7.70 (s, 1H, H_j), 7.62 (m, 1H, H_k), 7.44 (m, 2H, H_i, H_g), 6.71 (s, 1H, H_c), 6.59 (s, 1H, H_a), 6.51 (s, 1H, H_b), 5.05 (s, 2H, H_f), 4.05 (s, 2H, H_d), 2.78 (t, J = 7.5 Hz, 2H, H_m), 2.55 (q, J = 7.6 Hz, H_q), 2.35 (s, 3H, H_e), 1.79-1.65 (m, 4H, H_n, H_p), 1.52 (m, 2H, H_o), 1.34 (t, J = 7.6 Hz, H_r); ^{13}C NMR (100 MHz, $CDCl_3$): δ = 194.75, 176.12, 159.78, 142.96, 141.51, 140.86, 137.04, 134.23, 129.10 (2C), 126.86, 126.03, 112.08, 111.85, 104.70, 69.73, 33.70, 33.13, 32.50, 30.30, 28.01, 24.44, 24.07; HRMS (ESI): m/z = 508.1448 $[M+Na]^+$ (calcd. 508.1448 for $C_{23}H_{27}N_5O_3NaS_2$).

(*E*)-23-Azido-2-oxa-18,19-dithia-10,11-diaza-tricyclo[19.3.1.1^{4,8}]hexacosa-1(25),4,6,8(26),9,21,23-heptaen-12-one

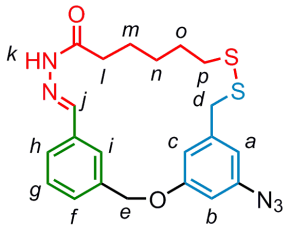

2

Under N_2, **E15** (434 mg, 0.89 mmol, 1.0 equiv.) was dissolved in MeOH (20 mL) and CH_2Cl_2 (5 mL). A solution of NaOMe (97 mg, 1.79 mmol, 2.0 equiv.) in MeOH (5 mL) was added. After 2 h of stirring at room temperature, CH_2Cl_2 (200 mL) and KI (30 mg, 0.18 mmol, 0.2 equiv.) were added. A solution of I_2 (227 mg, 0.89 mmol, 1.0 equiv.) in CH_2Cl_2 (30 mL) was added dropwise until the brown colour persisted. Na_2SO_3 was added to reduce the excess of I_2 and, when decolourisation was complete, stirring was continued for 15 min. H_2O (250 mL) was added and the phases separated. The H_2O layer was extracted another time with CH_2Cl_2 (100 mL). The combined organic layers were washed with brine (100 mL) and dried ($MgSO_4$). Removal of the solvents under reduced pressure and purification by flash column chromatography (SiO_2, CH_2Cl_2/EtOAc 9:1) yielded pure **2** (125 mg, 32%) as a colourless solid. M.p. 192 °C. ^{1}H NMR (400 MHz, $CDCl_3$): δ = 8.65 (s, 1H, H_k), 8.14 (s, 1H, H_j), 7.72 (s, 1H, H_i), 7.42 (m, 2H, H_g, H_f or H_h), 7.30 (d, J = 7.2 Hz, 1H, H_f or H_h), 6.88 (s, 1H, H_c), 6.59 (s, 1H, H_a), 6.49 (s, 1H, H_b), 5.12 (s, 2H, H_e), 3.77 (s, 2H, H_d), 2.77 (m, 2H, H_l), 2.41 (t, J = 7.3 Hz, 2H, H_p),

1.78 (m, 2H, H_m), 1.70 (m, 2H, H_o), 1.47 (m, 2H, H_n); ^{13}C NMR (100 MHz, $CDCl_3$): δ = 175.84, 159.56, 141.82, 141.48, 141.25, 137.53, 134.34, 129.07, 128.97, 128.58, 123.20, 114.08, 112.21, 103.51, 69.62, 43.31, 38.43, 33.18, 28.63, 28.35, 25.13; HRMS (ESI): m/z = 442.1371 $[M+H]^+$ (calcd. 442.1366 for $C_{21}H_{24}N_5O_2S_2$).

3-((3-(3-Ethynyl-5-formylphenoxy)methyl)benzyl)disulfanyl) propanoic acid

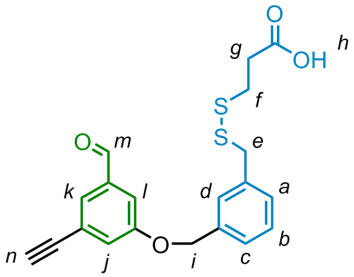

E16

Under N_2, **E14** (300 mg, 0.92 mmol, 1.0 equiv.), trimethyl orthoformate (103 mg, 106 µL, 0.97 mmol, 1.05 equiv.) and *p*-TsOH·H_2O (8.8 mg, 46 µmol, 0.05 equiv.) were dissolved/suspended in MeOH (20 mL). This mixture was stirred at room temperature for 1 h. NaOMe (100 mg, 1.85 mmol, 2.0 equiv.) was added and the mixture was stirred for 30 min at room temperature. KI (153 mg, 0.92 mmol, 1.0 equiv.) as well as a solution of 3-mercaptopropionic acid (0.98 g, 9.2 mmol, 10.0 equiv.) and NaOMe (497 mg, 9.2 mmol, 10.0 equiv.) in MeOH (15 mL) were added. The resulting mixture was titrated with a solution of I_2 (1.28 g, 5.06 mmol, 5.5 equiv.) in MeOH (10 mL) until the brown colour was persistent. Na_2SO_3 was added and the mixture was stirred until decolourisation was complete. 1M HCl (25 mL) and CH_2Cl_2 (25 mL) were added and the two layers were separated in a separating funnel. The water layer was extracted with CH_2Cl_2 (3 × 25 mL). The combined CH_2Cl_2 layers were dried over $MgSO_4$. TFA (524 mg, 0.34 mL, 4.60 mmol, 5.0 equiv.) was added and the mixture was stirred for 1 h at room temperature. The mixture was washed with H_2O and dried over $MgSO_4$. The solvents were removed under reduced pressure and the resulting residue was purified by flash column chromatography (SiO_2, $CHCl_3$/EtOAc 4:1) to yield **E16** (208 mg, 58%) as a yellowish oil. A minor impurity was observed, however, no further purification was undertaken at this step. ^{1}H NMR (400 MHz, $CDCl_3$): δ = 9.92 (s, 1H, H_m), 7.59 (dd, J = 1.3, 1.3 Hz, 1H, H_{Ar}); 7.46 (dd, J = 2.5, 1.3 Hz, 1H, H_{Ar}); 7.40 (s, 1H, H_{Ar}), 7.38 – 7.33 (m, 3H, H_{Ar}), 7.30 (ddd, J = 6.7, 2.1, 1.7 Hz, 1H, H_{Ar}), 5.11 (s, 2H, H_i), 3.91 (s, 2H, H_e), 3.15 (s, 1H, H_n), 2.64 (dd, J = 9.7, 4.7 Hz, 2H, H_f or H_g), 2.59 (dd, J = 9.7, 4.7 Hz, 2H, H_f or H_g); ^{13}C NMR

(100 MHz, $CDCl_3$): δ = 191.22, 177.53, 158.93, 137.83, 137.71, 136.33, 129.21, 128.96, 128.31, 127.26, 126.63, 124.75, 124.26, 114.23, 81.91, 78.78, 70.07, 43.15, 33.64, 32.31; HRMS (ESI): m/z = 404.0993 $[M+NH_4]^+$ (calcd. 404.0990 for $C_{20}H_{22}NO_4S_2$).

Methyl 3-((3-(3-ethynyl-5-formylphenoxy)methyl)benzyl)disulfanyl) propanoate

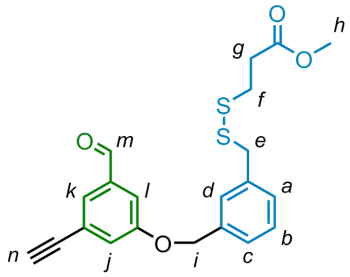

3

E16 (200 mg, 0.52 mmol, 1.0 equiv.) was dissolved in MeOH (15 mL) and 2 drops of conc. H_2SO_4 were added. This mixture was stirred at room temperature for 3 h. The reaction was monitored by TLC (SiO_2, $CHCl_3$/EtOAc 3:1; R_f acid ~0.3; R_f product ~0.95). H_2O (20 mL) and $CHCl_3$ (20 mL) were added to the reaction mixture and the layers were separated in a separatory funnel. The H_2O layer was once more extracted with $CHCl_3$ (20 mL). The combined organic layers were washed with water (2 × 20 mL) and dried ($MgSO_4$). The solvents were removed under reduced pressure and the residue was dissolved in $CHCl_3$ (10 mL). TFA (0.3 mL) was added and the mixture was stirred at room temperature over night. H_2O and $CHCl_3$ were added and the layers were separated in a separating funnel. The water layers were extracted with $CHCl_3$ (2 × 15 mL) and the combined organic layers were dried over $MgSO_4$. Removal of the solvents under reduced pressure yielded a residue that was purified by flash column chromatography (SiO_2, toluene) to give **3** (84 mg, 40%) as a yellowish oil. ^1H NMR (400 MHz, $CDCl_3$): δ = 9.94 (s, 1H, H_m), 7.59 (dd, J = 1.3, 1.3 Hz, 1H, H_{Ar}); 7.47 (dd, J = 2.5, 1.3 Hz, 1H, H_{Ar}); 7.40 (s, 1H, H_{Ar}), 7.39 – 7.32 (m, 3H, H_{Ar}), 7.31 (ddd, J = 6.7, 2.0, 1.7 Hz, 1H, H_{Ar}), 5.12 (s, 2H, H_i), 3.91 (s, 2H, H_e), 3.67 (s, 3H, H_h), 3.15 (s, 1H, H_n), 2.65 (dd, J = 10.8, 4.3 Hz, 2H, H_f or H_g), 2.60 (dd, J = 10.8, 4.3 Hz, 2H, H_f or H_g); ^{13}C NMR (100 MHz, $CDCl_3$): δ = 191.07, 172.10, 158.95, 137.85, 137.76, 136.30, 129.22, 128.94, 128.32, 127.22, 126.58, 124.73, 124.27, 114.18, 81.91, 78.73, 70.09, 51.81, 43.17, 33.73, 32.75; HRMS (ESI): m/z = 418.1147 $[M+NH_4]^+$ (calcd.418.1147 for $C_{21}H_{24}NO_4S_2$).

***1,2*-1**

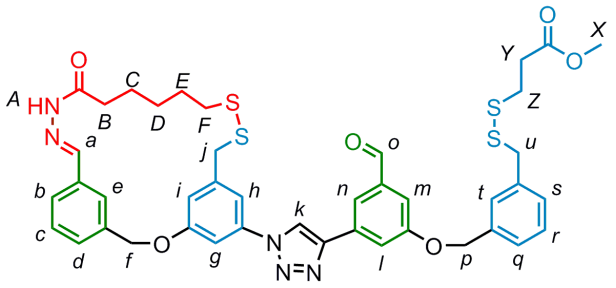

1,2-**1**

Under N_2, **3** (72 mg, 182 µmol, 1.0 equiv.) was dissolved in CH_2Cl_2 (10 mL) and a solution of **2** (80 mg, 182 µmol, 1.0 equiv.) in THF (10 mL) was added. A solution of **E23** (10.0 mg, 18 µmol, 0.1 equiv.) and $Cu(MeCN)_4PF_6$ (7 mg, 18 µmol, 0.1 equiv.) in MeOH (10 mL) was added to the reaction mixture, which was allowed to stir over night at room temperature. Evaporation of the solvents under reduced pressure and flash column chromatography (SiO_2, CH_2Cl_2/EtOAc 8:2 then 7:3) gave *1,2*-**1** (121 mg, 79%) as a colourless solid. M.p. 160-165 °C. ^{1}H NMR (500 MHz, $CDCl_3$): δ = 10.05 (s, 1H, H_o), 8.81 (s, 1H, H_A), 8.32 (s, 1H, H_k), 8.20 (s, 1H, H_e), 7.99 (s, 1H, H_n), 7.89 (m, 1H, H_l), 7.75 (s, 1H, H_a), 7.49 (m, 1H, H_m), 7.45 (m, 3H, H_g, H_t, H_b), 7.42 (d, *J* = 3.3 Hz, 1H, H_d), 7.38 (m, 2H, H_q, H_r), 7.31 (m, 2H, H_c, H_s), 7.26 (s, 1H, H_h), 7.19 (m, 1H, H_i), 5.25 (s, 2H, H_f), 5.21 (s, 2H, H_p), 3.92 (s, 2H, H_u), 3.88 (s, 2H, H_j), 3.67 (s, 3H, H_X), 2.76 (m, 2H, H_B), 2.65 (m, 4H, H_Z, H_Y), 2.49 (t, *J* = 7.3 Hz, 2H, H_F), 1.80 (m, 2H, H_C), 1.73 (m, 2H, H_E), 1.50 (m, 2H, H_D) Assignment of the signals was accomplished by means of 2-D NMR (COSY, ROESY, HMQC, HMBC); ^{13}C NMR (201 MHz, $CDCl_3$): δ = 191.73, 175.69, 172.15, 159.78, 159.47, 146.99, 141.72, 141.58, 138.37, 138.00, 137.87, 137.23, 136.59, 134.40, 132.50, 129.20, 129.17, 129.08, 128.96, 128.64, 128.41, 126.69, 123.17, 120.47, 118.55, 118.36, 118.01, 114.11, 113.20, 104.86, 70.20, 69.91, 51.84, 43.30, 43.06, 38.67, 33.81, 33.14, 32.85, 28.66, 28.43, 25.06; UV (CH_2Cl_2): λ_{max} = 278 nm; ε (CH_2Cl_2, 290 nm) = 15.7 × 10^3 $dm^3mol^{-1}cm^{-1}$; HRMS (ESI): *m/z* = 842.2174 $[M+H]^+$ (calcd. 842.2169 for $C_{42}H_{44}N_5O_6S_4$).

***2,3*-1**

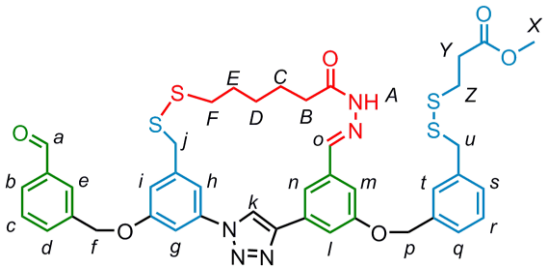

2,3-**1**

1,2-**1** (0.7 mg, 3.4 µmol) was dissolved in CH_2Cl_2 (5 mL) and 3 drops of TFA were added. The mixture was stirred over night at room temperature. Purification by preparative HPLC (see section 3.5.1 for details) gave *2,3*-**1** (0.33 mg, 47%) as a colourless solid. ^{1}H NMR (500 MHz, $CDCl_3$): δ = 10.07 (s, 1H, H_a), 8.51 (s, 1H, H_A), 8.27 (s, 1H, H_k), 8.00 (s, 1H, H_e), 7.93 (s, 1H, H_m), 7.89 (d, *J* = 7.7 Hz, 1H, H_b), 7.85 (s, 1H, H_n), 7.75 (d, *J* = 7.7 Hz, 1H, H_d), 7.67 (s, 2H, H_o, H_l), 7.60 (t, *J* = 7.6 Hz, 1H, H_c), 7.45 (s, 1H, H_t), 7.38 (m, 2H, H_r, H_q), 7.31 (d, *J* = 7.0 Hz, 1H, H_s), 7.21 (s, 1H, H_h), 6.99 (s, 1H, H_i), 6.95 (s, 1H, H_g), 5.25 (s, 2H, H_f), 5.22 (s, 2H, H_p), 3.92 (s, 2H, H_u), 3.84 (s 2H, H_j), 3.68 (s, 3H, H_X), 2.87 (t, *J* = 7.2 Hz, 2H, H_F), 2.78 (m, 2H, H_B), 2.64 (m, 4H, H_Z, H_Y), 1.90-1.78 (m, 4H, H_C, H_E), 1.67 (m, 2H, H_D) Assignment of the signals was accomplished by means of 2D NMR (COSY, ROESY); ^{13}C NMR (201 MHz, $CDCl_3$): δ = 191.98, 175.41, 172.23, 159.90, 159.81, 147.77, 142.26, 141.41, 137.78, 137.37, 137.33, 136.91, 136.78, 135.50, 133.28, 131.77, 129.63, 129.47, 129.07, 128.94, 128.42, 128.39, 126.65, 118.56, 117.34, 116.14, 114.04, 113.20, 111.96, 106.25, 106.25, 70.09, 69.62, 51.89, 43.25, 41.26, 38.73, 33.86, 33.81, 33.41, 29.35, 28.50, 24.71; UV (CH_2Cl_2): λ_{max} = 286, 248 nm; ε (CH_2Cl_2, 290 nm) = 17.2 × 10^3 $dm^3mol^{-1}cm^{-1}$;LRMS (ESI): *m*/*z* = 864.1 $[M+Na]^+$.

3-((3-Azido-5-(3-formylbenzyloxy)benzyl)disulfanyl)propanoic acid

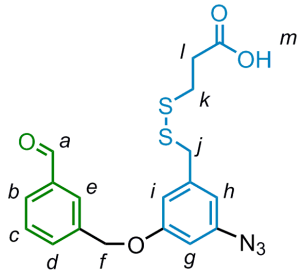

E17

Under N_2, **E9** (287 mg, 0.84 mmol, 1.0 equiv.) and *p*-TsOH (8 mg, 42 µmol, 0.05 equiv.) were dissolved in dry MeOH (10 mL). A solution of trimethyl orthoformate (94 mg, 0.883 mmol, 1.05 equiv.) in MeOH (5 mL) was added dropwise and the solution was stirred at room temperature for 20 min. A solution of NaSMe (59 mg, 0.841 mmol, 1.0 equiv.) in MeOH (5 mL) was added and the mixture was stirred for 20 min at room temperature. A solution of NH_4Cl (90 mg, 1.7 mmol, 2.0 equiv.) and H_2O (30 mL) were added and the mixture was extracted with EtOAc (3 × 30 mL). The combined organic phases were washed with brine, dried ($MgSO_4$) and concentrated under reduced pressure. Flash chromatography (SiO_2, toluene/NEt_3 99:1) gave (3-azide-5-(3-(dimethoxymethyl)benzyloxy)phenyl)methanethiol (174 mg, 60%) as a colourless oil. ^{1}H NMR (400 MHz, $CDCl_3$): δ = 7.52 (s, 1H, H_f), 7.40 (m, 3H, H_c, H_d, H_e), 6.74 (s, 1H, H_j), 6.62 (s, 1H, H_i), 6.51 (s, 1H, H_h), 5.42 (s, 1H, H_b), 5.06 (s, 2H, H_g), 3.68 (d, *J* = 7.7 Hz, 2H, H_k), 3.34 (s, 6H, H_a), 3.68 (t, *J* = 7.7 Hz, 1H, H_l); ^{13}C NMR (100 MHz, $CDCl_3$): δ = 160.05, 144.13, 141.50, 138.61, 136.42, 128.60, 127.58, 126.57, 125.85, 111.38, 111.27, 104.53, 102.88, 70.13, 52.75, 28.83.

At room temperature, a solution of 3-mercaptopropionic acid (535 mg, 5.0 mmol, 10.0 equiv.) in MeOH (10 mL) was treated with a solution of NaOMe (272 mg, 5.0 mmol, 10.0 equiv.) in MeOH (2 mL). After stirring for 5 min, this solution was added to a solution of (3-azide-5-(3-(dimethoxymethyl)benzyloxy)phenyl)methanethiol (174 mg, 0.50 mmol, 1.0 equiv.) in MeOH (8 mL). After addition of KI (84 mg, 0.5 mmol, 1.0 equiv.), a solution of I_2 (767 mg, 3.0 mmol, 6.0 equiv.) in CH_2Cl_2 (10 mL) was added dropwise to the reaction mixture until the yellow-brown colour persisted. Na_2SO_3 was added and the mixture was stirred vigorously until decolourisation was complete. 1N HCl (50 mL) was added and the phases separated. The aqueous phase was extracted with CH_2Cl_2 (2 × 20 mL) and the combined organic phases were dried ($MgSO_4$). After

filtration, TFA (370 µL, 5.0 mmol, 10.0 equiv.) was added and the solution was stirred for 1 h at room temperature. Evaporation of the solvents, followed by flash chromatography (SiO_2, $CHCl_3$/EtOAc 2:1) gave **E17** (171 mg, 84%) as a colourless oil. ^{1}H NMR (400 MHz, $CDCl_3$): δ = 10.04 (s, 1H, H_a), 7.97 (s, 1H, H_e), 7.86 (d, *J* = 7.6 Hz, 1H, H_b), 7.70 (d, *J* = 7.6 Hz, 1H, H_d), 7.58 (t, *J* = 7.6 Hz, 1H, H_c), 6.75 (t, *J* = 1.6 Hz, 1H, H_i), 6.63 (t, *J* = 1.6 Hz, 1H, H_h), 6.55 (t, *J* = 2.1 Hz, 1H, H_g), 5.13 (s, 2H, H_f), 3.82 (s, 2H, H_j), 2.68 (s, 4H, H_k, H_l); ^{13}C NMR (100 MHz, $CDCl_3$): δ = 192.21, 176.17, 159.61, 141.62, 140.57, 137.68, 136.69, 133.30, 129.83, 129.42, 128.23, 112.72, 112.31, 105.00, 69.34, 43.20, 33.51, 32.48; HRMS (ESI): *m/z* = 421.1000 $[M+NH_4]^+$ (calcd. 421.0999 for $C_{18}H_{21}N_4O_4S_2$).

Methyl 3-((3-azido-5-(3-(dimethoxymethyl)benzyloxy)benzyl) disulfanyl) propanoate

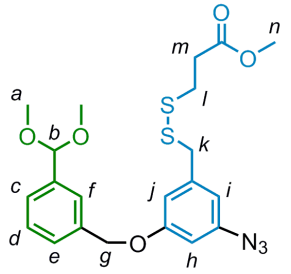

E18

E17 (610 mg, 1.51 mmol, 1.0 equiv.) was dissolved in MeOH (50 mL) and 3 drops of conc. H_2SO_4 were added. The mixture was stirred overnight at room temperature (reaction monitored by TLC, SiO_2, hexane/Et_2O 1:1) after which NEt_3 (1 mL) and H_2O (50 mL) were added. The mixture was extracted with CH_2Cl_2 (3 × 100 mL). The combined organic phases were washed with brine, dried ($MgSO_4$) and concentrated under reduced pressure to give **S25** (485 mg, 70%) as a colourless oil. ^{1}H NMR (400 MHz, $CDCl_3$): δ = 7.52 (s, 1H, H_f), 7.40 (m, 3H, H_c, H_d, H_e), 6.74 (s, 1H, H_j), 6.62 (s, 1H, H_i), 6.55 (t, *J* = 2.1 Hz, 1H, H_h), 5.42 (s, 1H, H_b), 5.06 (s, 2H, H_g), 3.81 (s, 2H, H_k), 3.69 (s, 3H, H_n), 3.34 (s, 6H, H_a), 2.71 (m, 2H, H_l), 2.64 (m, 2H, H_m); ^{13}C NMR (100 MHz, $CDCl_3$): δ = 192.04, 159.92, 141.44, 140.37, 138.60, 136.40, 128.61, 127.59, 126.58, 125.85, 112.42, 112.39, 105.02, 102.86, 70.12, 52.76, 51.90, 43.25, 33.83, 32.89; HRMS (ESI): *m/z* = 481.1577 $[M+NH_4]^+$ (calcd. 481.1574 for $C_{21}H_{29}N_4O_5S_2$).

(*E*)-*S*-3-((3-Ethynyl-5-((2-(3-mercaptohexanoyl)hydrazono)methyl) phenoxy)methyl) benzyl ethanethioate

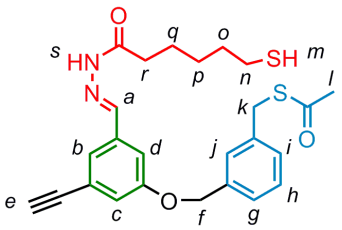

E19

Under N_2, **E14** (313 mg, 0.965 mmol, 1.0 equiv.) was dissolved in MeOH (15 mL) and 4 drops of AcOH were added. A solution of **E3** (172 mg, 1.50 mmol, 1.1 equiv.) in MeOH (5 mL) was added dropwise. The reaction was monitored by TLC (SiO_2, CH_2Cl_2/EtOAc 9:1). After 1 h of stirring at room temperature, the reaction was complete and the product started to precipitate. Stirring was continued for an additional hour after which the mixture was cooled to –10°C and stirred for another 1 h. The precipitate was collected on a glass filter and washed with cold MeOH (5 mL). The product **E19** (390 mg, 86%) was obtained as a slightly yellowish powder. M.p. 91 °C. ^{1}H NMR (400 MHz, $CDCl_3$): δ = 8.84 (s, 1H, H_s), 7.63 (s, 1H, H_a), 7.38 – 7.26 (m, 6H, H_{Ar}), 7.11 (dd, J = 2.3, 1.3 Hz, 1H, H_{Ar}), 5.06 (s, 2H, H_f), 4.14 (s, 2H, H_k), 3.11 (s, 1H, H_e), 2.76 (t, J = 7.5 Hz, 2H, H_r), 2.55 (dt, J = 7.8, 7.3 Hz, 2H, H_n), 2.36 (s, 3H, H_l), 1.74 (dt, J = 7.5, 7.5 Hz, 2H, H_o or H_q), 1.67 (dt, J = 7.5. 7.3 Hz, 2H, H_o or H_q), 1.52 (dt, J = 7.5, 7.5 Hz, 2H, H_p), 1.35 (d, J = 7.8 Hz, 1H, H_m); ^{13}C NMR (100 MHz, $CDCl_3$): δ = 195.03, 175.62, 158.75, 141.73, 138.26, 136.64, 135.29, 129.04, 128.77, 128.00, 126.53, 126.46, 123.92, 123.73, 119.51, 114.01, 82.77, 70.06, 33.78, 33.28, 32.49, 30.37, 28.02, 24.49, 23.97; HRMS (ESI): m/z = 469.1611 $[M+H]^+$ (calcd. 469.1614 for $C_{25}H_{29}N_2O_3S_2$).

(*E*)-23-Ethynyl-2-oxa-10,11-dithia-18,19-diaza-tricyclo[19.3.1.1^{4,8}]hexacosa-1(24),4(26),5,7,19,21(25),22-heptaen-17-one

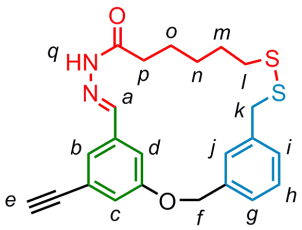

E20

Under N_2, **E19** (434 mg, 0.89 mmol, 1.0 equiv.) was dissolved in MeOH (20 mL) and CH_2Cl_2 (5 mL). A solution of NaOMe (97 mg, 1.79 mmol, 2.0 equiv.) in MeOH (5 mL) was added. After 2 h of stirring at room temperature, CH_2Cl_2 (200 mL) and KI (30 mg, 0.18 mmol, 0.2 equiv.) were added. A solution of I_2 (227 mg, 0.89 mmol, 1.0 equiv.) in CH_2Cl_2 (30 mL) was added dropwise until the brown colour persisted. Na_2SO_3 was added to reduce the excess of I_2 and, when decolourisation was complete, stirring was continued for 15 min. H_2O (250 mL) was added and the phases separated. The H_2O layer was extracted another time with CH_2Cl_2 (100 mL). The combined organic layers were washed with brine (100 mL) and dried ($MgSO_4$). Removal of the solvents under reduced pressure and purification by flash column chromatography (SiO_2, CH_2Cl_2/EtOAc 9:1) yielded pure **E20** (125 mg, 32%) as a colourless solid. M.p. 192 °C. ^{1}H NMR (400 MHz, $CDCl_3$): δ = 9.34 (s, 1H, H_q), 7.65 (s, 1H, H_a), 7.53 (m, 2H, H_{Ar}), 7.31 (d, *J* = 7.5 Hz, 1H, H_{Ar}), 7.27-7.23 (m, 3H, H_{Ar}), 7.17 (m, 1H, H_{Ar}), 7.08 (s, 1H, H_{Ar}), 5.17 (s, 2H, H_f), 3.88 (s, 2H, H_k), 3.11 (s, 1H, H_e), 2.69 (m, 2H, H_l), 2.49 (t, *J* = 7.1 Hz, 2H, H_p), 1.79-1.72 (m, 4H, H_m, H_o), 1.51 (m, 2H, H_n); ^{13}C NMR (100 MHz, $CDCl_3$): δ = 176.11, 158.71, 141.14, 138.31, 136.89, 135.49, 128.92, 128.78, 128.04, 126.09, 125.98, 123.82, 120.67, 112.82, 111.65, 82.60, 69.92, 43.40, 38.36, 33.26, 28.10, 27.99, 24.86; HRMS (ESI): *m*/*z* = 425.1355 $[M+H]^+$ (calcd. 425.1357 for $C_{23}H_{25}O_2N_2S_2$).

E21

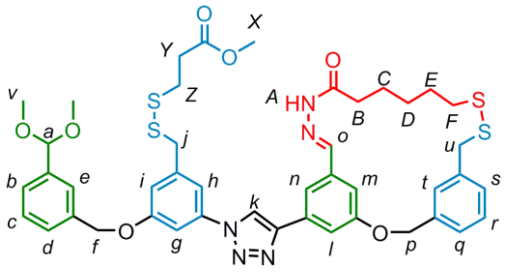

E21

Under N_2, **S25** (48 mg, 103 µmol, 1.0 equiv.) was dissolved in CH_2Cl_2 (5 mL) and a solution of **S27** (53 mg, 124 µmol, 1.2 equiv.) in THF (5 mL) was added. A solution of **E24** (11 mg, 21 µmol, 0.2 equiv.) and $Cu(MeCN)_4PF_6$ (8 mg, 21 µmol, 0.2 equiv.) in MeOH (5 mL) was added to the reaction mixture, which was allowed to stir over night at room temperature. Evaporation of the solvents and flash column chromatography (SiO_2, CH_2Cl_2/EtOAc 8:2 → 7:3) gave **E21** (56 mg, 62%) as a colourless solid. M.p. 105 °C. ^{1}H NMR (400 MHz, $CDCl_3$): δ = 8.79 (s, 1H, H_A), 8.27 (s, 1H, H_k), 7.74 (m, 1H, H_o), 7.62 (s, 1H, H_l), 7.57 (m, 2H, H_t, H_c), 7.55 (s, 1H, H_m), 7.53 (s, 1H, H_n), 7.44 (m, 4H, H_g, H_e, H_b, H_d), 7.35 (s, 1H, H_h), 7.32 (m, 2H, H_r, H_q), 7.24 (d, 1H, H_s), 7.05 (s, 1H, H_i), 5.43 (s, 1H, H_a), 5.28 (s, 2H, H_p), 5.18 (s, 2H, H_f), 3.93 (s, 2H, H_j), 3.91 (s, 2H, H_u), 3.67 (s, 3H, H_X), 3.35 (s, 6H, H_v), 2.80-2.66 (m, 6H, H_Z, H_B, H_Y), 2.52 (t, J = 7.1 Hz, 2H, H_F), 1.79 (m, 4H, H_E, H_C), 1.52 (m, 2H, H_D); Note: Assignment of the signals was accomplished by means of 2D NMR (COSY, ROESY, HMQC, HMBC); ^{13}C NMR (100 MHz, $CDCl_3$): δ = 176.42; 172.09; 159.73; 159.40; 147.39; 142.05; 140.74; 138.65; 138.21; 137.85; 137.12; 136.07; 136.01; 132.08; 128.85; 128.66; 128.62; 128.00; 127.61; 126.69; 125.93; 125.85; 120.06; 118.10; 116.13; 114.40; 113.37; 110.62; 106.30; 102.84; 70.35; 69.89; 52.77; 51.90; 43.35; 42.98; 38.32; 33.83; 33.24; 32.98; 28.10; 27.94; 24.89; UV (CH_2Cl_2): λ_{max} = 252 nm; HRMS (ESI): m/z = 905.2855 $[M+NH_4]^+$ (calcd. 905.2859 for $C_{44}H_{53}N_6O_7S_4$).

***3,4*-1**

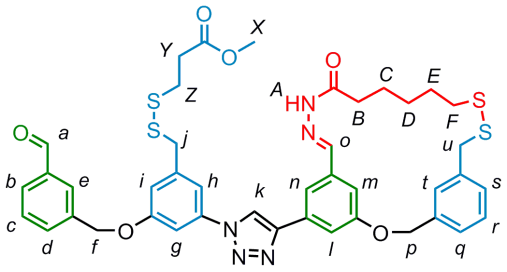

3,4-**1**

E21 (3.0 mg, 3.4 μmol) was dissolved in CH_2Cl_2 (3 mL) and 3 drops of TFA were added. The mixture was stirred overnight at room temperature. Purification by preparative HPLC (see section 1.1 for details) gave *3,4*-**1** (1.9 mg, 66%) as a colourless solid. M.p. 90-95 °C. ^{1}H NMR (500 MHz, $CDCl_3$): δ = 10.07 (s, 1H, H_a), 8.85 (s, 1H, H_A), 8.29 (s, 1H, H_k), 8.02 (s, 1H, H_e), 7.89 (d, *J* = 7.6Hz, 1H, H_b), 7.75 (m, 2H, H_d, H_o), 7.63 (s, 1H, H_l), 7.61 (t, *J* = 7.6 Hz, 1H, H_c), 7.57 (s, 1H, H_t), 7.55 (s, 1H, H_m), 7.53 (s, 1H, H_n), 7.46 (t, *J* = 2.1 Hz, 1H, H_g), 7.36 (s, 1H, H_h), 7.31 (m, 2H, H_r, H_q), 7.25 (d, 1H, H_s), 7.06 (s, 1H, H_i), 5.28 (s, 2H, H_p), 5.26 (s, 2H, H_f), 3.94 (s, 2H, H_j), 3.91 (s, 2H, H_u), 3.67 (s, 3H, H_X), 2.80-2.66 (m, 6H, H_Z, H_B, H_Y), 2.51 (t, *J* = 7.1 Hz, 2H, H_F), 1.78 (m, 4H, H_E, H_C), 1.52 (m, 2H, H_D) Assignment of the signals was accomplished by means of 2D NMR (COSY, ROESY); ^{13}C NMR (100 MHz, $CDCl_3$): δ = 191.96, 175.64, 172.10, 159.46 (2C), 147.46, 141.49, 140.95, 138.23, 137.96, 137.32, 137.12, 136.77, 135.86, 133.26, 132.10, 129.89, 129.48, 128.91, 128.71, 128.19, 128.01, 125.96, 120.02, 118.07, 116.09, 114.65, 113.64, 110.63, 106.33, 69.95, 69.61, 51.95, 43.44, 42.96, 38.38, 33.88, 33.24, 33.05, 28.09, 27.98, 24.80; UV (CH_2Cl_2): λ_{max} = 250 nm; ε (CH_2Cl_2, 290 nm) = 15.1 × 10^3 dm^{3}mol^{-1}cm^{-1}; HRMS (ESI): *m*/*z* = 864.1945 $[M+Na]^+$ (calcd. 864.1988 for $C_{42}H_{43}N_5O_6S_4Na$).

***1,4*-1**

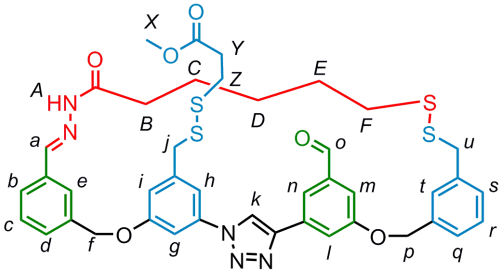

1,4-**1**

3,4-**1** (3.0 mg, 3.4 µmol) was dissolved in CH_2Cl_2 (3 mL) and 3 drops of TFA were added. The mixture was stirred overnight at room temperature. Purification by preparative HPLC (see section 1.1 for details) gave *1,4*-**1** (0.4 mg, 14%) as a colourless solid. ^{1}H NMR (500 MHz, $CDCl_3$): δ = 10.06 (s, 1H, H_o), 8.44 (s, 1H, H_A), 8.21 (s, 1H, H_k), 8.06 (s, 1H, H_n), 7.94 (s, 1H, H_e), 7.70 (s, 1H, H_a), 7.68 (s, 1H, H_l), 7.50 (s, 1H, H_m), 7.45 (m, 6H, H_h, H_t, H_b), 7.34 (m, 4H, H_g, H_q, H_c, H_r), 7.24 (m, 2H, H_s, H_d), 7.06 (m, 2H, H_i), 5.27 (s, 2H, H_f), 5.25 (s, 2H, H_p), 3.93 (s, 2H, H_j), 3.88 (s, 2H, H_u), 3.67 (s, 3H, H_X), 2.77-2.67 (m, 2H, H_B, H_Z, H_Y), 2.31 (t, *J* = 7.3 Hz, 2H, H_F), 1.65 (m, 2H, H_C), 1.55 (m, 2H, H_E), 1.35 (m, 2H, H_D) Assignment of the signals was accomplished by means of 2D NMR (COSY, ROESY); ^{13}C NMR (201 MHz, $CDCl_3$): δ = 191.81, 174.96, 172.11, 159.53, 159.36, 146.94, 141.99, 141.10, 138.49, 138.16, 137.81, 137.12, 136.46, 134.11, 132.41, 129.73, 129.29, 129.11, 128.96, 128.66, 128.48, 126.43, 123.61, 120.70, 118.77, 118.35, 117.02, 114.26, 114.14, 105.88, 70.13, 69.94, 51.94, 43.23, 42.93, 38.29, 33.88, 33.02, 32.54, 28.14, 24.07, 22.69; UV (CH_2Cl_2): λ_{max} = 276 nm; ε (CH_2Cl_2, 290 nm) = 24.7 × 10^3 $dm^3mol^{-1}cm^{-1}$; LRMS (ESI): *m*/*z* = 864.2 $[M+Na]^+$; HRMS (ESI): *m*/*z* = 842.2195 $[M+H]^+$ (calcd. 842.2169 for $C_{42}H_{44}N_5O_6S_4$).

3-(1-(3-(3-Formylbenzyloxy)-5-(hydroxymethyl)phenyl)-1*H*-1,2,3-triazol-4-yl)-5-(3-(hydroxymethyl)benzyloxy)benzaldehyde

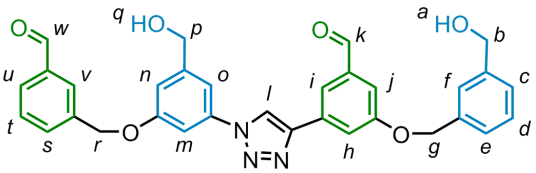

E22

Under N_2, DIPEA (50 µL, 287 µmol, 1.0 equiv.) was added to a solution of **E8** (81 mg, 287 µmol, 1.0 equiv.) and **E13** (84 mg, 315 µmol, 1.1 equiv.) in dry CH_2Cl_2 (10 mL) and dry MeOH (5 mL). A solution of $Cu(MeCN)_4PF_6$ (11 mg, 28.7 µmol, 0.1 equiv.) in dry MeOH (5 mL) was added and the solution was stirred at room temperature for 20 h. After removal of the solvents, purification by flash column chromatography (SiO_2, CH_2Cl_2/MeOH 95:5) yielded **E22** (123 mg, 75%) as a colourless, crystalline solid. ^{1}H NMR (400 MHz, acetone-d_6): δ = 10.10 (s, 1H, H_k or H_w), 10.08 (s, 1H, H_k or H_w), 9.20 (s, 1H, H_l), 8.14 (t, J = 1.4 Hz, 1H, H_{Ar}), 8.10 (s, 1H, H_{Ar}), 7.97 (dd, J = 2.5 Hz, J = 1.5 Hz, 1H, H_{Ar}), 7.93 (d, J = 7.8 Hz, 1H, H_{Ar}), 7.89 (d, J = 7.8 Hz, 1H, H_{Ar}), 7.68 (t, J = 7.6 Hz, 1H, H_{Ar}), 7.60 (m, 1H, H_{Ar}), 7.57 (m, 3H, H_{Ar}), 7.44-7.34 (m, 3H, H_{Ar}), 7.22 (m, 1H, H_{Ar}), 5.39 (s, 2H, H_g or H_r), 5.31 (s, 2H, H_g or H_r), 4.76 (d, J = 5.9 Hz, 2H, H_b or H_p), 4.68 (d, J = 5.8 Hz, 2H, H_b or H_p), 4.54 (t, J = 5.9 Hz, 1H, H_a or H_q), 4.28 (t, J = 5.8 Hz, 1H, H_a or H_q); ^{13}C NMR (100 MHz, acetone-d_6): δ = 193.87, 193.58, 161.85, 161.51, 148.42, 148.36, 144.84, 140.72, 140.18, 139.90, 138.94, 138.60, 135.21, 135.02, 131.24, 131.08, 130.19, 129.96, 128.03 (2 C), 127.70, 121.53, 121.29, 119.71, 115.69, 114.56, 112.20, 106.97, 72.00, 71.13, 65.48, 64.98; HRMS (ESI): m/z = 550.1979 $[M+H]^+$ (calcd. 550.1973 for $C_{32}H_{28}O_6N_3$).

***S*-3-((3-(1-(3-(Acetylthiomethyl)-5-(3-formylbenzyloxy)phenyl)-1*H*-1,2,3-triazol-4-yl)-5-formylphenoxy)methyl)benzyl ethanethioate**

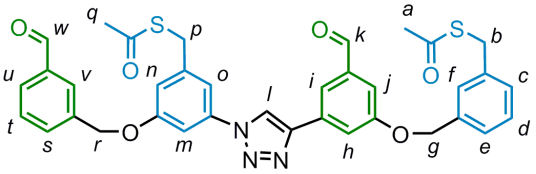

E23

a) Methanesulfonyl chloride (120 mg, 1.05 mmol, 6.0 equiv.) was added dropwise to a solution of **E22** (96 mg, 175 µmol, 1.0 equiv.) and NEt_3 (247 µL, 1.05 mmol, 6.0 equiv.)

in dry CH_2Cl_2 (50 mL). The solution was stirred overnight at room temperature, after which H_2O (30 mL) was added. The phases were separated and the aqueous phase was extracted with CH_2Cl_2 (2 × 20 mL). The combined organic phases were dried ($MgSO_4$) and the solvent removed under reduced pressure to give a mixture of bismesylate and monomesylate/monochloride (according to ^1H NMR and LRMS).

b) The crude mixture was dissolved in dry DMF (15 mL) and a solution of KSAc (63 mg, 552 mmol, 3.15 equiv.) in DMF (5 mL) was added at room temperature. The solution was stirred for 30 min at room temperature after which the bulk of the solvent was removed under reduced pressure. H_2O (10 mL) was added and the mixture was extracted with CH_2Cl_2 (3 × 20 mL). The combined organic phases were dried ($MgSO_4$) and the solvent removed under reduced pressure. Flash column chromatography (SiO_2, CH_2Cl_2/EtOAc 97:3) gave **E23** (62 mg, 54% over two steps) as a light yellow oil. ^1H NMR (400 MHz, $CDCl_3$): δ = 10.03 (s, 1H, H_k or H_w), 10.00 (s, 1H, H_k or H_w), 8.25 (s, 1H, H_l), 7.96 (m, 2H, H_{Ar}), 7.84 (m, 2H, H_{Ar}), 7.70 (d, *J* = 7.9 Hz, 1H, H_{Ar}), 7.56 (t, *J* = 7.6 Hz, 1H, H_{Ar}), 7.43 (s, 1H, H_{Ar}), 7.38 (m, 2H, H_{Ar}), 7.37-7.28 (m, 4H, H_{Ar}), 7.00 (s, 1H, H_{Ar}), 5.19 (s, 2H, H_g or H_r), 5.14 (s, 2H, H_g or H_r), 4.12 (s, 2H, H_b or H_p), 4.12 (s, 2H, H_b or H_p), 2.35 (s, 3H, H_a or H_q), 2.32 (s, 3H, H_a or H_q); ^{13}C NMR (100 MHz, $CDCl_3$): δ = 195.10, 194.74, 192.03, 191.80, 159.75, 159.51, 146.98, 141.57, 138.33, 138.23, 137.93, 137.30, 136.76, 136.58, 133.30, 132.46, 129.75, 129.48, 129.04, 128.76, 128.35, 127.97, 126.51, 120.51, 118.48, 118.34, 115.88, 114.11, 113.23, 106.05, 70.20, 69.57, 33.29, 33.08, 30.40, 30.37.

Methyl 3-((3-((3-formyl-5-(1-(3-(3-formylbenzyloxy)-5-(((3-methoxy-3-oxopropyl)disulfanyl)methyl)phenyl)-1*H*-1,2,3-triazol-4-yl)phenoxy)methyl)benzyl)disulfanyl) propanoate

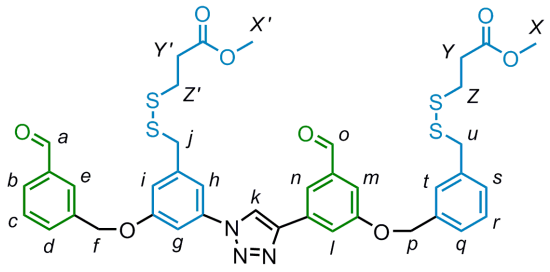

4

Under N_2, **E23** (59 mg, 89 µmol, 1.0 equiv.) was dissolved in a mixture of dry MeOH (5 mL) and dry THF (5 mL). Solid *p*-TsOH (2 mg, 9 µmol, 0.1 equiv.) and a solution of trimethylorthoformate (20 mg, 187 µmol, 2.1 equiv.) in dry MeOH (2 mL) were added

and the solution was stirred at room temperature for 30 min. A solution of NaOMe (19 mg, 357 μmol, 4.0 equiv.) in MeOH (2 mL) was added and the solution was stirred at room temperature for 60 min. Solid KI (7 mg, 45 μmol, 0.5 equiv.) and methyl 3-mercaptopropionate (97 μL, 891 μmol, 10.0 equiv.) were added and I_2 (147 mg, 579 μmol, 6.5 equiv.) was added dropwise until the brown colour persisted. Excess I_2 was reduced by addition of a small amount of solid Na_2SO_3 and stirring for 1 h. H_2O (30 mL) was added and the mixture extracted with CH_2Cl_2 (3 × 30 mL). The combined organic phases were dried ($MgSO_4$) and TFA (84 μL, 10.0 equiv.) was added. After stirring for 1 h at room temperature the solvent was removed under reduced pressure. The crude product was purified by flash column chromatography (SiO_2, CH_2Cl_2/MeCN 98:2 → 85:15) and preparative HPLC (SiO_2, CH_2Cl_2/MeCN 95:5), which gave pure **4** (2 mg, 3% over four steps) as a colourless solid. ^{1}H NMR (500 MHz, $CDCl_3$): δ = 10.07 (s, 1H, H_a), 10.05 (s, 1H, H_o), 8.38 (s, 1H, H_k), 8.01 (m, 2H, H_e, H_n), 7.90 (m, 2H, H_l, H_b), 7.75 (d, J = 7.6 Hz, 1H, H_d), 7.61 (t, J = 7.6 Hz, 1H, H_c), 7.48 (m, 1H, H_m), 7.46 (m, 2H, H_g, H_t), 7.39 (s, 1H, H_h), 7.37 (m, 2H, H_r, H_q), 7.32 (m, 1H, H_s), 7.06 (m, 1H, H_i), 5.25 (s, 2H, H_f), 5.21 (s, 2H, H_p), 3.93 (s, 2H, H_j), 3.92 (s, 2H, H_u), 3.66 (s, 6H, H_X, $H_{X'}$), 2.78 (t, J = 7.3 Hz, 2H, $H_{Z'}$), 2.68 (t, J = 7.3 Hz, 2H, $H_{Y'}$), 2.61 (m, 4H, H_Z, H_Y); ^{13}C NMR (201 MHz, $CDCl_3$): δ = 191.90, 191.69, 172.07, 159.81, 159.53, 147.02, 141.05, 138.42, 137.97, 137.89, 137.37, 136.85, 136.63, 133.24, 132.58, 129.81, 129.49, 129.20, 128.97, 128.42, 128.26, 126.70, 120.54, 118.59, 118.48, 116.24, 114.09, 113.72, 106.38, 70.23, 69.68, 51.92, 51.82, 43.35, 43.03, 33.91, 33.84, 33.14, 32.91; HRMS (ESI): m/z = 818.1672 $[M+H]^+$ (calcd. 818.1693 for $C_{40}H_{40}N_3O_8S_4$).

Tris[(1-benzyl-1*H*-1,2,3-triazol-4-yl)methyl]amine (TBTA)

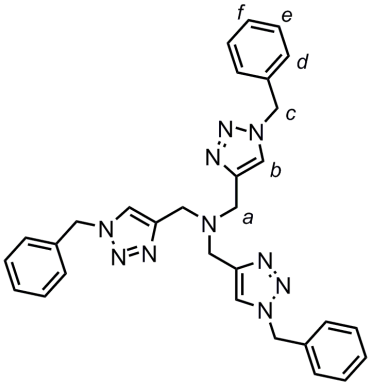

E24

Synthesised according to a modified literature procedure.[39] Benzyl azide (12.3 g, 30.2 mmol, 3.0 equiv.) and trispropargyl amine (4.0 g, 30.2 mmol, 1.0 equiv.) were dissolved in CH_2Cl_2 (150 mL), and H_2O (150 mL) was added. $CuSO_4 \cdot 5H_2O$ (380 mg, 1.5 mmol, 0.05 equiv.) and sodium ascorbate (900 mg, 4.5 mmol, 0.15 equiv.) were added and the reaction mixture was vigorously stirred over night at room temperature. CH_2Cl_2 (200 mL) and H_2O (200 mL) were added and the phases separated. The aqueous phase was extracted with CH_2Cl_2 (2 × 200 mL) and the combined organic phases were washed with brine (200 mL) and dried ($MgSO_4$). Evaporation of the solvent and purification by flash column chromatography (SiO_2, CH_2Cl_2/MeOH 95:5) gave **E24** (15.53 g, 97%) as a colourless, amorphous solid. M.p. 141 °C. ^{1}H NMR (400 MHz, $CDCl_3$): δ = 7.70 (s, 3H, H_b), 7.36 (m, 9H, H_e, H_f), 7.27 (m, 6H, H_d), 5.52 (s, 6H, H_c), 3.72 (s, 6H, H_a); LRMS (ESI): m/z = 531.9 $[M+H]^+$.

Dimethyl 3,3'-disulfanediyldipropanoate

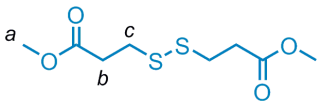

E25

Methyl 3-mercaptopropionate (1.0 mL, 1.1 g, 9.23 mmol, 1.0 equiv.) was dissolved in CH_2Cl_2 (50 mL). KI (0.15 g, 0.9 mmol, 0.1 equiv.) and a solution of I_2 (2.34 g, 9.23 mmol, 1.0 equiv.) in CH_2Cl_2 (50 mL) were added until the brownish colour persisted. Na_2SO_3 was added and the mixture was stirred vigorously until decolourisation was complete. H_2O (100 mL) was added and the phases were separated. The organic layer was dried ($MgSO_4$) and the solvent removed under reduced pressure to give **E25** (1.1 g, quant.) as

a colourless oil. ^{1}H NMR (400 MHz, $CDCl_3$): δ = 3.70 (s, 6H, H_a), 2.92 (t, J = 7.2 Hz, 4H, H_b or H_c), 2.74 (t, J = 7.2 Hz, 4H, H_b or H_c); LRMS (APCI): m/z = 239.3 $[M+H]^+$.

3.6 References

[1] M. Schliwa (ed.), *Molecular Motors*, Wiley-VCH, Weinheim, 2003.

[2] T. R. Kelly, H. De Silva, R. A. Silva, *Nature* **1999**, *401*, 150.

[3] N. Koumura, R. W. J. Zijlstra, R. A. van Delden, N. Harada, B. L. Feringa, *Nature* **1999**, *401*, 152.

[4] D. A. Leigh, J. K. Y. Wong, F. Dehez, F. Zerbetto, *Nature* **2003**, *424*, 174.

[5] P. Thordarson, E. J. A. Bijsterveld, A. E. Rowan, R. J. M. Nolte, *Nature* **2003**, *424*, 915.

[6] R. A. van Delden, M. K. J. ter Wiel, M. M. Pollard, J. Vicario, N. Koumura, B. L. Feringa, *Nature* **2005**, *437*, 1337.

[7] S. P. Fletcher, F. Dumur, M. M. Pollard, B. L. Feringa, *Science* **2005**, *310*, 80.

[8] V. Balzani *et al. Proc. Natl. Acad. Sci. USA* **2006**, *103*, 1178.

[9] T. Muraoka, K. Kinbara, T. Aida, *Nature* **2006**, *440*, 512.

[10] V. Serreli, C.-F. Lee, E. R. Kay, D. A. Leigh, *Nature* **2007**, *445*, 523.

[11] E. R. Kay, D. A. Leigh, F. Zerbetto, *Angew. Chem. Int. Ed.* **2007**, *46*, 72.

[12] W. B. Sherman, N. C. Seeman*, Nano Lett.* **2004**, *4*, 1203.

[13] J.-S. Shin, N. A. Pierce, *J. Am. Chem. Soc.* **2004**, *126*, 10834.

[14] P. Yin, H. Yan, X. G. Daniell, A. J. Turberfield, J. H. Reif, *Angew. Chem. Int. Ed*. **2004**, *43*, 4906.

[15] Y. Tian, Y. He, Y. Chen, P. Yin, C. Mao, *Angew. Chem. Int. Ed*. **2005**, *44*, 4355.

[16] R. Pei, S. K. Taylor, D. Stefanovic, S. Rudchenko, T. E. Mitchell, M. N. Stojanovic, *J. Am. Chem. Soc*. **2006**, *128*, 12693.

[17] P. Yin, H. M. T. Choi, C. R. Calvert, N. A. Pierce, *Nature* **2008**, *451*, 318.

[18] S. J. Green, J. Bath, A. J. Turberfield, *Phys. Rev. Lett.* **2008**, *101*, 238101.

[19] T. Omabegho, R. Sha, N. C. Seeman, *Science* **2009**, *324*, 67.

[20] R. D. Astumian, *Phys. Chem. Chem. Phys*. **2007**, *9*, 5067.

[21] R. D. Astumian, I. Derényi, *Eur. Biophys. J.* **1998**, *27*, 474.

[22] S. J. Rowan, S. J. Cantrill, G. R. L. Cousins, J. K. M. Sanders, J. F. Stoddart, *Angew. Chem. Int. Ed.* **2002**, *41*, 898.

[23] P. T. Corbett, J. Leclaire, L. Vial, K. R. West, J.-L. Wietor, J. K. M. Sanders, S. Otto, *Chem*. *Rev*. **2006**, *106*, 3652.

[24] J.-M. Lehn, *Chem. Soc. Rev*. **2007**, *36*, 151.

[25] V. Goral, M. I. Nelen, A. V. Eliseev, J.-M. Lehn, *Proc. Natl. Acad. Sci. USA* **2001**, *98*, 1347.

[26] A. G. Orrillo, A. M. Escalante, R. L. E. Furlan, *Chem. Commun*. **2008**, 5298.

[27] Z. Rodriguez-Docampo, S. Otto, *Chem. Commun*. **2008**, 5301.

[28] S. Otto, R. L. E. Furlan, J. K. M. Sanders, *J. Am. Chem. Soc*. **2000**, *122*, 12063.

[29] H. Noji, R. Yasuda, M. Yoshida, K. Kinosita, *Nature* **1997**, *386*, 299.

[30] K. Swierczek, A. S. Pandey, J. W. Peters, A. C. Hengge, *J. Med. Chem.* **2003**, *46*, 3703.

[31] N. Iqbal, C.-A. McEwen, E. E. Knaus, *Drug Devel. Res.* **2000**, *51*, 177.

[32] A. M. Becker, R. W. Rickards, R. F. C. Brown, *Tetrahedron* **1983**, *39*, 4189.

[33] W. Rickards, V. Rukachaisirikul, *Aust. J. Chem.* **1987**, *40*, 1011.

[34] K. G. Zbinden, U. Obst-Sander, K. Hiplert, H. Kühne, D. W. Banner, H.-J. Böhm, M. Stahl, J. Ackermann, L. Alig, L. Weber, H. P. Wessel, M. A. Riederer, T. B. Tschopp, T. Lavé, *Bioorg. Med. Chem. Lett.* **2005**, *15*, 5344.

[35] MestReC, version 4.5.6.0.

[36] MOPAC2007, James J. P. Stewart, Stewart Computational Chemistry, Version 8.032L.

[37] Gaussian 03, Revision E.01, Frisch, M. J., Trucks, G. W., Schlegel, H. B., Scuseria, G. E., Robb, M. A., Cheeseman, J. R., Montgomery, Jr., J. A., Vreven, T., Kudin, K. N., Burant, J. C., Millam, J. M., Iyengar, S. S., Tomasi, J., Barone, V., Mennucci, B., Cossi, M., Scalmani, G., Rega, N., Petersson, G. A., Nakatsuji, H., Hada, M., Ehara, M., Toyota, K., Fukuda, R., Hasegawa, J., Ishida, M., Nakajima, T., Honda, Y., Kitao, O., Nakai, H., Klene, M., Li, X., Knox, J. E., Hratchian, H. P., Cross, J. B., Bakken, V., Adamo, C., Jaramillo, J., Gomperts, R., Stratmann, R. E., Yazyev, O., Austin, A. J., Cammi, R., Pomelli, C., Ochterski, J. W., Ayala, P. Y., Morokuma, K., Voth, G. A., Salvador, P., Dannenberg, J. J., Zakrzewski, V. G., Dapprich, S., Daniels, A. D., Strain, M. C., Farkas, O., Malick, D. K., Rabuck, A. D., Raghavachari, K., Foresman, J. B., Ortiz, J. V., Cui, Q., Baboul, A. G., Clifford, S., Cioslowski, J., Stefanov, B. B., Liu, G., Liashenko, A., Piskorz, P., Komaromi, I., Martin, R. L., Fox, D. J., Keith, T., Al-Laham, M. A., Peng, C. Y., Nanayakkara, A., Challacombe, M., Gill, P. M. W., Johnson, B., Chen, W., Wong, M. W., Gonzalez, C. & Pople, J. A. Gaussian, Inc., Wallingford CT, **2004**.

[38] Persistence of Vision Pty. Ltd. (2004). Persistence of Vision (TM) Raytracer. Persistence of Vision Pty. Ltd., Williamstown, Victoria, Australia.

[39] B.-Y. Lee, S. R. Park, H. B. Jeon, K. S. Kim, *Tetrahedron Lett*. **2006**, *47*, 5105.

Chapter IV

Synthetic Small-Molecule Walkers: Investigation of Processivity and the Emergence of Directional Bias

Published as *Design, Synthesis and Operation of Small Molecules That Walk along Tracks*, M. von Delius, E. M. Geertsema, D. A. Leigh, D.-T. D. Tang, *J. Am. Chem. Soc.* **2010**, DOI: 10.1021/ja106486b.

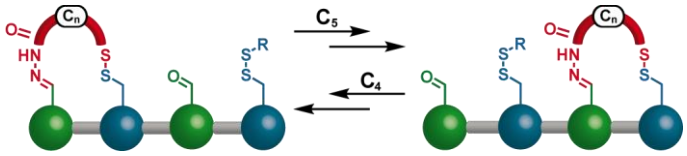

"Science may be described as the art of systematic over-simplification."

(Sir Karl R. Popper, 1991)

Acknowledgements

Dr. Edzard M. Geertsema and Dan-Tam Daniel Tang are gratefully acknowledged for their contribution to the work presented in this Chapter. E. M. G. has performed the multistep syntheses of compounds **E10**, **E14**, and **E39**. D.-T. D. T. has prepared compounds *3,4*-$\mathbf{C_3}$ and *3,4*-$\mathbf{C_4}$ and carried out the investigation of their dynamic properties.

4.1 Synopsis

*In this Chapter the synthesis and system dynamics of a series of small-molecule walker-track conjugates, 3,4-**C_n** (n = 2, 3, 4, 5 and 8), based on dynamic covalent linkages between the 'feet' of the walkers and the 'footholds' of the track is described. Each walker has one acylhydrazide and one sulfur-based foot separated by a spacer chain of 'n' methylene groups, while the track consists of four footholds of alternating complementary functionalities (aldehydes and masked thiols). Upon repeatedly switching between acid and base the walker moiety can be exchanged between the footholds on the track, primarily through a 'passing-leg gait' mechanism, until a steady state, minimum energy, distribution is reached.*

*The introduction of a kinetically-controlled step in the reaction sequence (redox-mediated breaking and reforming of the disulfide linkages) can cause a directional bias in the distribution of the walker on the track. The different length walker molecules exhibit very different walking behaviours: systems n = 2 and 3 cannot actually 'walk' along the track because their stride lengths are too short to bridge the internal footholds. The walkers with longer spacers (n = 4, 5 and 8) do step up and down the track repeatedly, but a directional bias under the acid-redox conditions is only achieved for the **C_4** and **C_5** systems, interestingly in opposite directions (the **C_8** walker has insufficient ring strain with the track). Although they are still rudimentary systems, the **C_4** and **C_5** walker-track conjugates exhibit four of the essential characteristics of linear molecular motor dynamics, namely processive, directional, repetitive and progressive migration of a molecular unit up and down a molecular track.*

4.2 *Introduction*

Many biological processes utilise molecules that convert chemical energy into directed molecular level motion.[1] Despite rapid advances in recent years,[2] the artificial molecular machines prepared to date fall well short of the degree of control over motion exhibited by such biomotors.[3] Rotaxanes have been developed that can do a limited amount of work, bending cantilevers[4] or transporting liquid droplets up a slope against the force of gravity.[5] However, such systems are switches—not motors despite sometimes being called somewhat confusingly 'motor-molecules' by their creators—because they cannot act progressively; that is they cannot be reset to do further work on a system without undoing the physical task they originally performed. Rather they simply switch between two or more states, like stilbene and other molecular switches. Molecules that can genuinely behave as rotary motors have been developed by chemists, working through the sequential application of stimuli[2a,c] or even at a constant photostationary state.[2d-f] However, finding ways to use directional rotary motion to do useful work at the molecular level is not easy. The only clear cut use of rotary molecular motors to do physical work in biology is the bacterial flagella motor.[6] The other celebrated rotary biomotor, F_1F_0-ATPase,[7] only uses the directional 360° rotation of its components to reset the position of catalytic sites in a sequence that ensures that the reverse of the chemical transformation it is performing is not also catalysed. By far the most broadly used molecular motors in biology are linear motors that move down tracks, transporting cargo, progressively exerting force and performing many other tasks.[1]

4.2.1 Molecules that can Walk down Tracks

Some of the most spectacular examples of biological linear molecular motors are the kinesin, myosin and dynein bipedal motor proteins which are directionally-driven along intracellular tracks by adenosine triphosphate (ATP) hydrolysis.[8] The dynamic characteristics of kinesin,[9,10] in particular,[11] are worth highlighting since it exhibits several key features integral to the design of artificial molecular motors: (i) *Processivity*: the ability of the molecular motor to remain attached to its track, i.e. to migrate along the track in a 'hand-over-hand' or 'inchworm' fashion[3] without detaching or exchanging with other molecules in the bulk. Wild-type kinesin exhibits a relatively high level of processivity, falling off its microtubular[12] track only after an average number of roughly 100 steps,[13] which corresponds to a mean run length of ~1 μm.[13]

(ii) *Directionality*: implies that the molecular walker migrates preferentially (or in the ideal case, exclusively) towards one end of the polymeric track. Wild-type kinesin shows near-perfect directionality[9] towards the plus-end of microtubules as long as the chemical potential of ATP is greater than that of ADP and P_i.[14] (iii) *Autonomous operation*: the ability of the molecular motor to perform directional, processive motion as long as a chemical 'fuel' is present, i.e. without external intervention such as the application of a sequence of stimuli. (iv) *Repetitive operation*: the motor's property to repeatedly perform similar mechanical cycles. (v) *Progressive operation*: the ability of the molecular motor to be reset at the end of each mechanical cycle without undoing the physical task that was originally performed. While (i), (ii), (iv) and (v) are strict requirements for making artificial molecular motors, autonomous operation (iii) is not essential and can come at the cost of reduced control of the system (e.g. walker migration cannot be stopped and/or is only possible in one direction).

Until recently,[15] the only synthetic structures that had been shown to exhibit most or all of features (i) to (v) were systems constructed from DNA.[16] Borrowing biological building blocks in this way has some advantages, of course: Commercial DNA synthesis means that once designed the necessary DNA can be ordered from commercial suppliers and the efficiency and selectivity of nature's base-pairing chemistry is appealing. However, all DNA devices published to date suffer from three limitations: (i) they either require stoichiometric, complex fuel (DNA oligomers of precise sequence) while biomotors use the ubiquitous and relatively simple small-molecular fuel ATP and/or irreversibly destroy the track they are walking on[3] (again, not a feature of bipedal motor proteins). (ii) The analytical monitoring of the walking processes is limited by the characteristics of DNA as a biooligomer.[17] (iii) At present the longest 'walk' a DNA device has performed in one direction consists of three strides.[16f] Small-molecule walkers offer important advantages in light of the limitations of DNA devices. Their simpler design allows more detailed spectroscopic insight into the mechanism and processivity of the dynamic processes. Simpler fuels[18] can be applied and polymeric tracks can be synthesised.

In the late nineteen seventies and eighties, Lawton and coworkers developed reagents for the cross-linking of biomolecules, which can be regarded as directionally non-biased molecular walkers.[19] In fact, Lawton's reagents can do a fully reversible bipedal walk along accessible nucleophilic sites on a protein such as ribonuclease.[19a] Although occurring at a constant chemical environment, this migration proceeds in a processive

manner, since the construction of the walker moiety precludes full detachment.[20] Importantly, the migration of Lawton's molecular walker intrinsically leads to the thermodynamic minimum and is thus not directional. More recently Schalley and coworkers have described systems in which crown ether moieties migrate processively along linear or cyclic molecular scaffolds.[21] The described systems lack directionality, however, and are only processive as a result of the applied conditions (extreme molecular 'dilution' in the high vacuum of a FTICR mass spectrometer). In some well-known sigmatropic rearrangement reactions it appears as if one molecular moiety 'walks' along another. However, none of them[22] exhibits the strict motor requirements of processive, directional and repetitive operation.

Here we report on the synthesis and operation of a series of small-molecule walker-track conjugates ($\mathbf{C_n}$). Our studies show that two of the investigated systems ($\mathbf{C_4}$ and $\mathbf{C_5}$) exhibit the four essential characteristics of linear motor protein dynamics, namely processive, directional, repetitive and progressive migration of a walker unit up and down a molecular track.

4.3 Results and Discussion

The design outline for the small molecule walker-track systems is shown in Figure 4.1. The walker unit (shown in red) traverses the track by a 'passing-leg' gait involving two chemically different 'feet' ('*A*' and '*B*') which reversibly bind to different regions of the track. Linear motor proteins and the synthetic DNA walkers use non-covalent interactions for track binding, but the understanding of how to sequentially kinetically lock and release different artificial hydrogen bond (for example) recognition sites in the desired manner is beyond the capabilities of present day synthetic supramolecular chemistry. We instead chose to utilise dynamic covalent chemistry[23] for this purpose, which combines some of the features of supramolecular chemistry (reversibility, dynamics) with those of covalent bond chemistry (bond strength, robustness). To prevent the walker from completely detaching from the track during the walking process, the different feet form covalent bonds that are labile or kinetically locked under mutually exclusive sets of conditions.[24] Under condition I (Figure 4.1a), foot '*A*' can dissociate from the track while the bond between foot 'B' and the track is kinetically locked. Under conditions II or III (Figure 4.1b) the situation is reversed. This unusual property of the system confers processivity on the walking process.

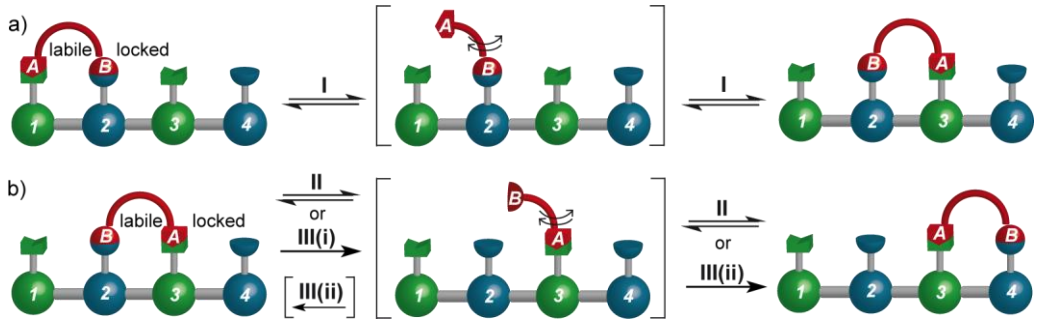

Figure 4.1. *Graphical representation of processive migration of a two-legged 'walker' molecule (red) along a track featuring two different possible binding sites (green and blue) for the two chemically different feet. Two key intermediate states, in which one or other foot is disconnected from the track, are shown in square brackets. For the walking action to be processive, the two feet of the walker (labelled 'A' and 'B') must never be disconnected from the track at the same time. In chemical terms this means that the foot-track bond disconnections (I and either II or III) must occur under mutually exclusive sets of conditions.*

4.3.1 Molecular Design and Synthesis

The construction of walker-track conjugate *1,2*-**C$_5$**, in which the molecular walker is attached to a four-foothold track *via* hydrazone (labile in acid; locked in base) and disulfide (labile in base; locked in acid) linkages is illustrated in Scheme 4.1a.[24b,c] Acylhydrazones were favoured over imines,[25] as they are known to exhibit a good balance between lability when acid is present and robustness in the absence of acid and in the isolated form. Benzylic thiols were employed on part of the track, since they can be introduced under mild conditions at a late stage of the synthesis. One-foothold precursors **1**-**4** were synthesised according to published procedures.[26] Williamson ether synthesis (steps i and vii), mesylation (steps ii and viii) and nucleophilic substitution with potassium thioacetate (steps iii and ix) gave the crucial two-foothold precursors **5** and **6**, from which all other compounds were subsequently prepared. The starting position of the walker at footholds *1* and *2* in the walker-track conjugate was established by synthesizing macrocycle **7** by acid catalyzed condensation (step iv) of aldehyde **5** to the bifunctional walker compound 6-mercaptohexanoic acid hydrazide, subsequent thioacetate methanolysis (step v) and oxidative ring closure (step vi). The free thiol foothold (e.g. foothold *4* in *1,2*-**C$_5$**, Scheme 4.1a) was protected as disulfide (using a 'placeholder' thiol, see Scheme 4.1a), because atmospheric oxygen would gradually cause the free thiol to oxidise and form a dimeric disulfide compound. For this, an unsymmetric disulfide bond (see compound **8** in Scheme 4.1a) had to be established, which was achieved through oxidation of the corresponding thiol in presence of an excess of placeholder thiol (step xii). In a final ligand-assisted[27] copper(I)-catalyzed acetylene azide cycloaddition (CuAAC)[28] macrocycle **7** was

coupled to the building block (**8**) containing footholds *3* and *4* (Scheme 4.1a, step xvi). We chose to use this "click" reaction, because of its compatibility with the present functional groups, as well as the benefit of introducing a rigid triazole linkage into the molecular track. Isomer *3,4*-$\mathbf{C_5}$ (Scheme 4.1b) was prepared unambiguously from two-foothold precursors **5** and **6** following analogous synthetic procedures.[15] We synthesised a small library of walker moieties, which differed solely in the number 'n' of methylene groups in the spacer chain (see experimental section for structures and detailed synthetic procedures).

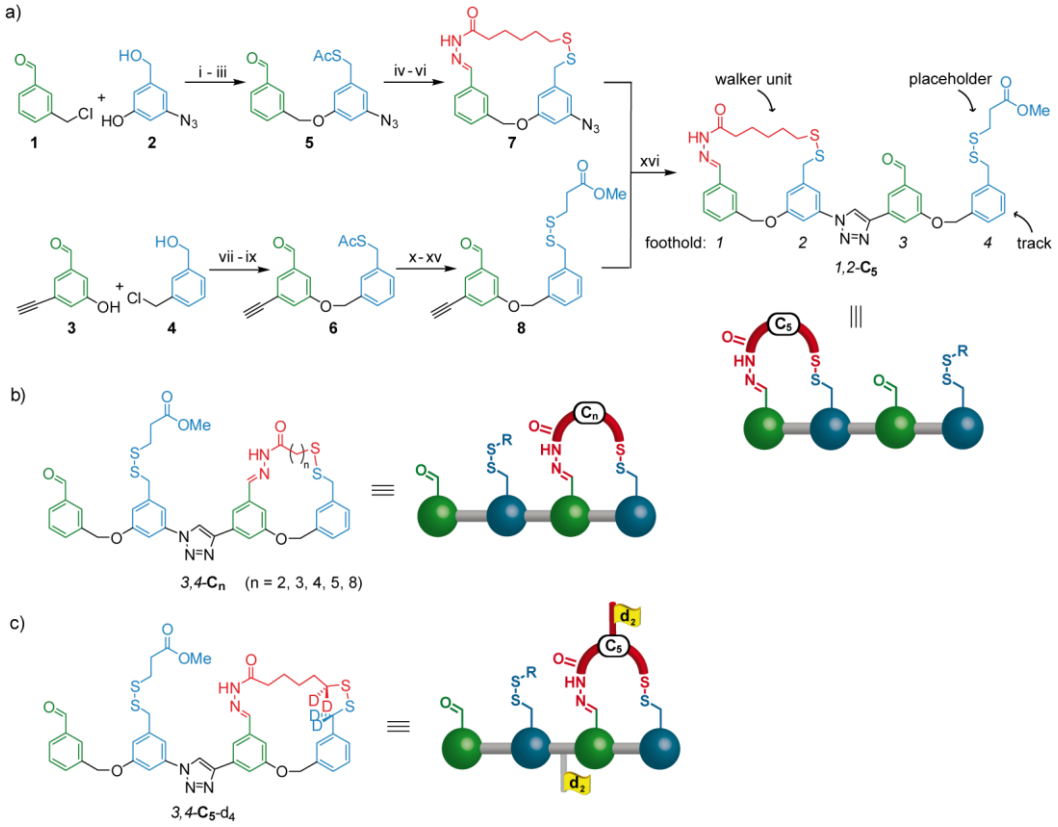

Scheme 4.1. *Synthesis of walker-track conjugate 1,2-$\mathbf{C_5}$ (a), general structure of walker–track conjugates 3,4-$\mathbf{C_n}$ (b) and structure of deuterated analogue 3,4-$\mathbf{C_5}$-d_4 (c). i) NaH, dimethylformamide (DMF), room temperature (RT), 16 h, 88%; ii) methanesulfonyl chloride (MsCl), Et_3N, CH_2Cl_2, 0 °C, 30 min; iii) KSAc, DMF, RT, 3 h, 77% (over two steps); iv) 6-mercaptohexanoic acid hydrazide, AcOH (cat.), MeOH, RT, 2 h, 78%; v) NaOMe, MeOH, RT, 2 h; vi) I_2, KI, CH_2Cl_2, RT, 5 min, 32% (over two steps); vii) NaH, DMF, 0 °C to RT, 16 h, 65%; viii) MsCl, Et_3N, CH_2Cl_2, RT, 16 h; ix) KSAc, DMF, RT, 3 h, 66% (over two steps); x) $HC(OMe)_3$, p-toluenesulfonic acid (p-TsOH), MeOH, RT, 30 min; xi) NaOMe, MeOH, RT, 30 min; xii) 3-mercaptopropionic acid, I_2, KI, CH_2Cl_2, RT, 5 min; xiii) trifluoroacetic acid (TFA), CH_2Cl_2, RT, 30 min, 58% (over four steps); xiv) H_2SO_4 (cat.), MeOH, RT, 16 h; xv) TFA, CH_2Cl_2, RT, 30 min, 40% (over two steps); xvi) $Cu(MeCN)_4PF_6$, tris[(1-benzyl-1H-1,2,3-triazol-4-yl)methyl]amine (TBTA), CH_2Cl_2/tetrahydrofuran (THF)/MeOH, RT, 16 h, 79%.*

The walker moieties were condensed to aldehyde **6** and subsequently converted to walker-track conjugates *3,4*-$\mathbf{C_2}$, *3,4*-$\mathbf{C_3}$, *3,4*-$\mathbf{C_4}$ and *3,4*-$\mathbf{C_8}$ (*3,4*-$\mathbf{C_n}$;[29] see section 4.5.9 for

detailed synthetic procedures and characterisation data). Finally, a fourfold deuterated analogue of *3,4*-**C5** was prepared (*3,4*-**C5**-d_4, Scheme 4.1c) using a similar synthetic route (deuterium labels introduced by reduction with $NaBD_4$).[15]

4.3.2 Directionally Non-Biased Operation (Hydrazone Exchange and Disulfide Exchange under Thermodynamic Control)

We first investigated the migration of the walker moiety along the track under reversible, dynamic covalent, reaction conditions. Dilute solutions of *1,2*-**C5** were submitted to conditions typically used for hydrazone exchange,[30] whereas solutions of *3,4*-**C5** were submitted to conditions for disulfide exchange.[31] In both cases mixtures of the corresponding starting material with constitutional isomer *2,3*-**C5** were obtained (see Scheme 4.1 for structures).[32] Applying the two sets of conditions to a pure sample of *2,3*-**C5**[33] resulted in mixtures of identical composition, confirming that the mixtures were at chemical equilibrium. Systematic optimisation efforts (see section 4.5.3 for details) provided reaction conditions that efficiently and in a practical period of time[34] led to equilibrium between two positional isomers (e.g. *3,4* and *2,3*; see Scheme 4.1 for structures).

For hydrazone exchange[30] (e.g. between *1,2* and *2,3* isomer) we found that adding trifluoroacetic acid (TFA) and a small amount of water to a solution (0.1 mM) of the walker-track conjugate in chloroform ($CHCl_3$) led to reliable and very efficient (essentially quantitative; no detectable amounts of oligomers or other side products) conversion towards the thermodynamic minimum. In the case of reversible disulfide exchange,[31] the optimised conditions involved 0.1 mM concentration in $CHCl_3$, the strong base 1,8-diazabicyclo[5.4.0]undec-7-ene (DBU), the mild reducing agent DL-dithiothreitol (DTT), and dimethyl 3,3'-disulfanediyldipropanoate ($(MeO_2CCH_2CH_2S)_2$), the placeholder disulfide.[35] This optimised procedure reliably gave equilibrium mixtures in yields of ~80%[36] (see sections 4.5.2.1 and 4.5.2.2 for further details).

Submitting *1,2*-**C5** to conditions for disulfide exchange, as well as submitting *3,4*-**C5** to conditions for hydrazone exchange resulted in appearance of constitutional isomer *1,4*-**C5** (albeit in small relative amounts, 9-20%), which we originally suspected to be too strained to be formed in observable quantities using reversible chemical reactions. Scheme 4.2 shows the local equilibria that connect the four positional isomers *1,2*-**Cn**, *2,3*-**Cn**, *3,4*-**Cn** and *1,4*-**Cn** under conditions for hydrazone (I) and disulfide exchange (II), respectively. In addition to the major passing-leg gait mechanism route from *1,2*-**Cn** to *3,4*-**Cn** via *2,3*-**Cn**, the unexpected isomer *1,4*-**Cn** provides a minor 'double step' route

from *1,2*-$\mathbf{C_n}$ to *3,4*-$\mathbf{C_n}$ (Scheme 4.2). It is interesting to note that occasional statistical 'errors' to the major pathway mechanisms also occur with some biological motor proteins.[1,37]

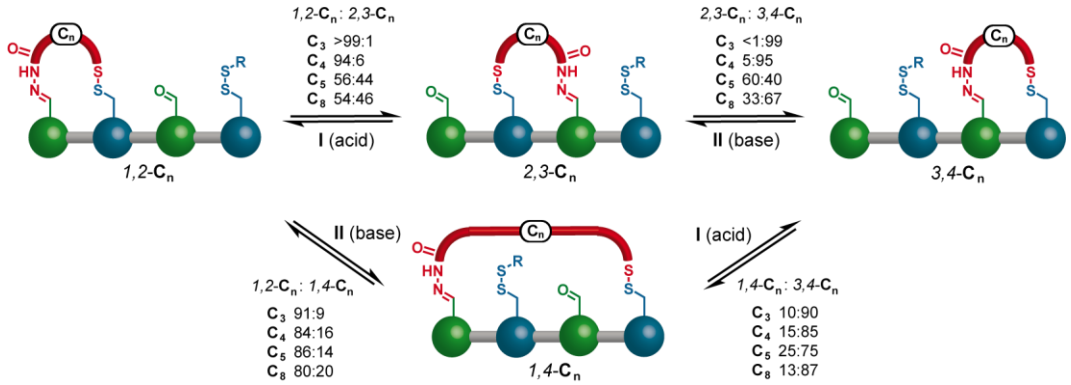

Scheme 4.2. *Local equilibria that connect the four positional isomers 1,2-**Cn**, 2,3-**Cn**, 3,4-**Cn** and 1,4-**Cn** under conditions I and II. Condition I (reversible hydrazone exchange): 0.1 mM, TFA, $CHCl_3$, RT, 6-96 h (allowed to continue until the distribution no longer changed, as monitored by HPLC). Condition II (reversible disulfide exchange): 0.1 mM, DTT (10 equiv.), DBU (40 equiv.), dimethyl 3,3'-disulfanediyldipropanoate (20 equiv.), $CHCl_3$, RT, 12-48 h (allowed to continue until the distribution no longer changed, as monitored by HPLC).*

The next objective of our studies was the quantitative investigation of the walker migration under reversible conditions I and II for all synthesised systems (**C_2**, **C_3**, **C_4**, **C_5**, **C_8**). For each compound series four local equilibria between two monomeric isomers each (*1,2*-**Cn**:*2,3*-**Cn**; *2,3*-**Cn**:*3,4*-**Cn**; *1,2*-**Cn**:*1,4*-**Cn**; *1,4*-**Cn**:*3,4*-**Cn**) had to be investigated. For *3,4*-**C_4**, for example, the optimised conditions for disulfide exchange were applied, the equilibrium ratio between *3,4*-**C_4** and *2,3*-**C_4** was determined by HPLC (see experimental section) and *2,3*-**C_4** was subsequently isolated by means of semi-preparative HPLC. With the pure, isolated sample of *2,3*-**C_4** two experiments were performed: a reverse control experiment leading to equilibrium between *2,3*-**C_4** and *3,4*-**C_4** and the hydrazone exchange experiment resulting in equilibrium between *2,3*-**C_4** and *1,2*-**C_4**. This procedure allowed the unambiguous determination of all equilibrium compositions, even for the systems in which only the *3,4* isomer was synthesised (**C_2**, **C_3**, **C_4**, **C_8**).

Scheme 4.2 summarises the results of the quantitative studies on the local equilibria between the positional isomers (see 4.5.1 for HPLC traces).[38] An interesting observation is the low amount of *2,3* isomer obtained in the **C_3** (<1%) and **C_4** (~5%) systems, which is in contrast to the relatively unvarying amount of *1,4* isomer found in all studied systems (9% to 25%). Another interesting observation is that the equilibria between the 'terminal' isomers *1,2* and *3,4* with the *2,3* isomer are not consistently

either on the side of the terminal isomer or on the side of *2,3* (for **C5** for example: *1,2*-**C5**:*2,3*-**C5** lies on the side of *1,2*-**C5** (56:44), whereas *2,3*-**C5**:*3,4*-**C5** lies on the side of *2,3*-**C5** (60:40)).

Three important conclusions can be drawn from the data presented in Scheme 4.2: (i) the variation in the spacer length has a dramatic effect on the occurrence of isomer *2,3* when in equilibrium with either *1,2* or *3,4*. While *2,3*-**C5** is easily accessible via dynamic covalent exchange, *2,3*-**C4** is only formed in ~5% and *2,3*-**C3** is not detected at all.[39] This can be explained by a sudden increase in ring strain. In the *2,3* isomer the walker moiety forms a macrocycle with an internal triazole linkage, which contains one more atom and is more rigid than the corresponding macrocycle in the *1,2* and *3,4* isomers. (ii) The variation in spacer length has only limited effect on the occurrence of isomer *1,4*. In this compound the track folds along its whole length to form a relatively large macrocycle. Making this large macrocycle smaller or larger by one atom has only limited effect on ring strain and the relative free energy of the compound. (iii) Although the two 'terminal' isomers *1,2* and *3,4* should be subject to the same amount of ring strain, our results indicate that they do not have identical free energy. This must be due to the fact that our system is not an ideal mimick of a polymeric track, where every second foothold would be sterically and electronically identical.[40]

For the **C5** system, where all isomers are accessible in convenient amounts (see Scheme 4.2) and where both the *1,2* and the *3,4* isomer have been independently synthesised (see Scheme 4.1), experiments that sequentially cycled between conditions I and II were conducted. Figure 4.2 (left hand side) shows how, starting from pristine *1,2*-**C5**, switching between conditions I and II over several cycles led to convergence of the isomer distribution to a ratio of *1,2*-**C5**:*2,3*-**C5**:*3,4*-**C5**:*1,4*-**C5** 39:36:19:6 (±2). A very similar distribution of isomers was obtained by starting from pristine *3,4*-**C5** and carrying out the operation sequence over three cycles (Figure 4.2; right hand side). Thus, irrespective of which end of the track the walker starts from, the effect of the passing-leg gait operations is to reach the same steady state distribution of positional isomers of the walker on the track.

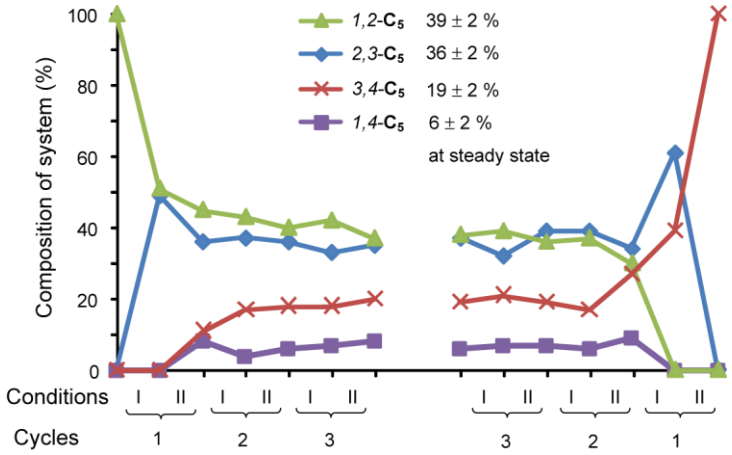

Figure 4.2. *Product distribution during three cycles of non-biased operation starting from pristine 1,2-**C**$_5$ (left hand side) and from pristine 3,4-**C**$_5$ (right hand side). Under each set of conditions (I and II) two different pairs of positional isomers are in equilibrium. Values are based on HPLC integration and are corrected for the absorbance coefficients at 290 nm (see section 4.5.6).*

The behaviour of the system raises the question if the observed steady state distribution is minimizing free energy or, in other words, if it is corresponding to the global thermodynamic minimum. The answer to this question is not trivial, since under one given reaction condition only a subset of all four isomers is in equilibrium. The system can thus only reach the steady state or thermodynamic minimum in a step-wise manner. Furthermore, the relative free energies of the four compounds could theoretically be different under conditions I (acid) and II (base). This would, however, lead to a situation where the system is 'out of equilibrium' upon every change in the conditions.

We have evidence that the steady state shown in Figure 4.2 does indeed correspond to the global thermodynamic minimum of the system and we believe this is due to the applied conditions (I and II) being extremely similar (solvent, concentration and temperature are identical; see experimental section). The particular shape of the graph in Figure 4.2 (both left hand side and right hand side) is the first strong support for this assumption. As soon as the system has reached the steady state, further oscillation of the conditions no longer changes the composition of the mixture (within the experimental error). In a situation where the relative energies are different under the conditions I and II, one would expect a graph that oscillates between two different steady states. This is clearly not the case.

In Figure 4.3 further evidence is presented in favour of the hypothesis that the system does indeed converge to its thermodynamic minimum. Figure 4.3a shows a superimposition of the data acquired during a repetition run and the original

experimental data (as shown in Figure 4.2). Even though the isomer ratios differ slightly during some stages of the two experimental sequences, the final composition is exactly the same in both experiments. This demonstrates the self-correcting properties of the system and provides further support for the hypothesis that the system tends to relax towards the thermodynamic minimum. Figure 4.3b shows a superimposition of the original experimental data (solid lines) with theoretically calculated data (dashed lines) that is based on the extrapolation of the four experimentally determined ratios between the four positional isomers (see Scheme 4.2).

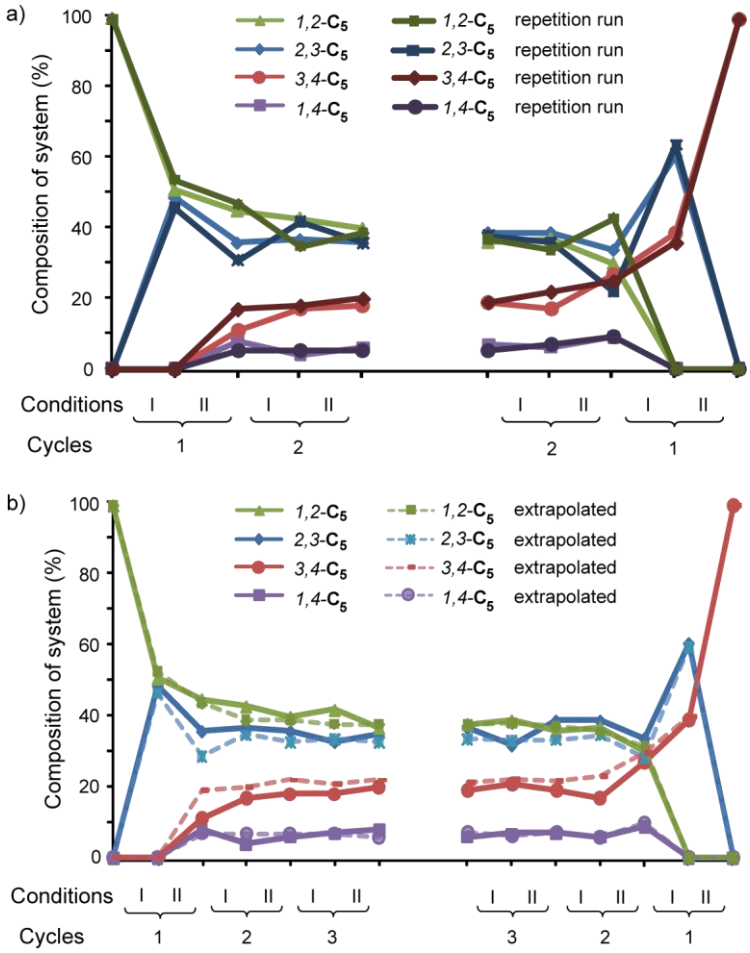

*Figure 4.3. a) Reproducibility of experimental results. Product distribution during two cycles of non-biased operation starting from pristine 1,2-**C5** (left hand side) and from pristine 3,4-**C5** (right hand side). The originally obtained data (lighter shade, identical to Figure 4.2) superimposed with data from a repetition run (darker shade); b) Predictability of experimental results. Product distribution during three cycles of non-biased operation starting from pristine 1,2-**C5** (left hand side) and from pristine 3,4-**C5** (right hand side). Solid lines: first experimental series (identical to Figure 4.2); dashed lines: calculated data, based on extrapolation of the experimental ratios between two individual isomers each (see Scheme 4.2).*

Again, differences occur in the early stages of the experiment,[41] but the final composition of the mixture can accurately be predicted using only the four equilibrium

ratios shown in Scheme 4.2 and a spreadsheet program. This demonstrates that the four initially obtained equilibrium ratios constitute a consistent set of relative energies that is also expressed in the steady state distribution.[42]

Analogous extrapolation calculations were performed for the $\mathbf{C_3}$, $\mathbf{C_4}$ and $\mathbf{C_8}$ systems. The reason for doing this was mainly practical.[43] The resulting steady state compositions are summarised in Table 4.1 (see section 4.5.7 for extrapolation graphs). The minimum energy distributions presented in Table 4.1 are important, since they serve as a zero value for directionally biased walker migration, which must lead away from such a distribution.

Table 4.1. *Steady state isomer distributions. Based on experimentally observed data for* $\boldsymbol{C_5}$ *and on extrapolated data (as indicated by *) for* $\boldsymbol{C_3}$, $\boldsymbol{C_4}$ *and* $\boldsymbol{C_8}$ *(see section 4.5.7 for details on extrapolation).*

	$\mathbf{C_3}^*$	$\mathbf{C_4}^*$	$\mathbf{C_5}$	$\mathbf{C_8}^*$
1,2	52%	41%	39%	26%
2,3	<1%	3%	36%	22%
3,4	43%	48%	19%	45%
1,4	5%	8%	6%	7%
Approx. number of steps to convergence	30*	15*	4	4*

Figure 4.4 shows a plot of relative free energies that can be calculated from the minimum energy distributions presented in Table 4.1 or directly from the isomer ratios presented in Scheme 4.2. These relative energies are only valid under the experimental conditions that we applied and are subject to experimental errors. Nevertheless, the energy diagrams are useful for a qualitative understanding of the observed isomer ratios, as well as for providing a rationale for some of the results obtained under biased operation (see section 4.3.4).

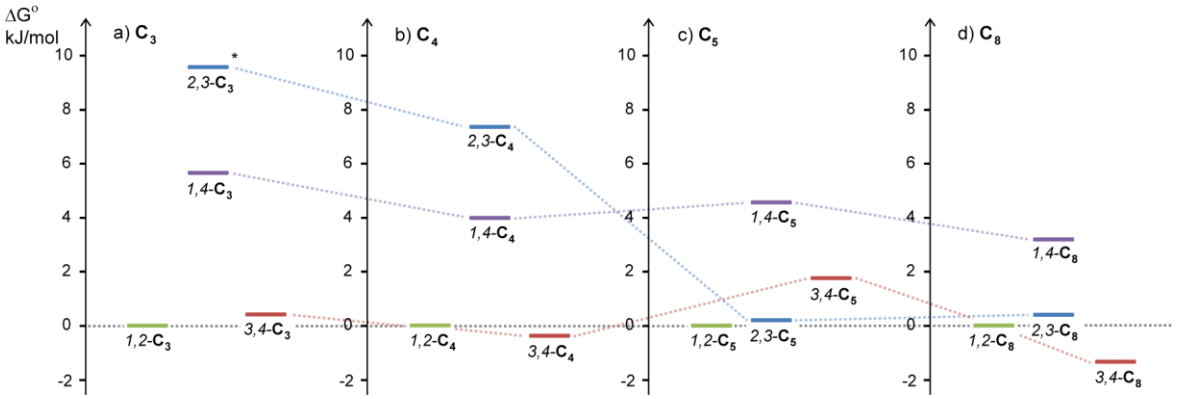

Figure 4.4. *Relative free energies of the four isomers of each compound series as calculated from the experimental equilibrium ratios between two individual isomers (see Scheme 4.2). The energy of the 1,2 isomer was set at 0.0 kJ/mol for each compound series. Dotted lines connect corresponding isomers. These sets of relative energies only apply to the specific reaction conditions (I and II) of the reversible exchange processes ($CHCl_3$, 0.1mM, RT). They should thus be seen as a qualitative aid for the understanding of ring strain effects within the different compound series. a)* ***C3****, *: The relative energy shown for 2,3-****C3*** *does only represent a lower extreme value that we calculated from the estimated detection limit of the analytical method (see caption of Scheme 4.2). b)* ***C4****, c)* ***C5****, d)* ***C8****.*

4.3.3 From Non-Directional to Directional Walker Migration

Starting with the walker at one end of the track (e.g. pristine *3,4*-$\mathbf{C_n}$), cycling between conditions I and II results in some walkers moving from one end of the track to the other (Figure 4.2). However, this is a consequence of the initial distribution of walker-track conjugates being away from the minimum energy distribution and the system, driven by a gain in entropy, relaxing towards it. If we assume that the observed (or extrapolated) steady states correspond to the thermodynamic minimum, then the walking sequence is not intrinsically directional (by this we mean that in the internal region of a polymeric track made of alternating benzaldehyde-benzylic disulfide footholds, the walker would move, over several acid-base oscillations, in each direction with equal probability). This may appear counterintuitive in light of the non-symmetric steady state distributions (the amount of the *1,2* isomer is not equal to the amount of *3,4*) found in systems $\mathbf{C_3}$, $\mathbf{C_4}$, $\mathbf{C_5}$ and $\mathbf{C_8}$ (see Table 4.1). The inequality of the *1,2* and the *3,4* isomers is, however, due to substituent effects, which make the two 'terminal' footholds electronically and sterically different from their internal counterparts.

In order to better understand the prerequisites for directional motion in our concrete system, we will ignore those substituent effects, as well as the formation of folding products, such as the *1,4* isomer and consider a polymeric track based on the molecular design of the current system (see Figure 4.5). There are only two fundamentally different types of macrocycles formed between the walker and the track—one in which

the track ether linkage is internal to the macrocycle (Figure 4.5 'ether-macrocycle') and one in which the track triazole unit is internal to the macrocycle (Figure 4.5 'triazole-macrocycle). Each operation i or ii thermodynamically equilibrates this pair of macrocycles about the pivot (kinetically locked) foot. If the two macrocycles happen to have identical relative thermodynamic stabilities under conditions i and ii, any bias towards one end of the track under condition i will be offset by the opposite directional bias under condition ii ($K_i = K_{ii}$). Net-directionality in the walking can thus only occur, when the forward/backward ratio under condition i is different from the backward/forward ratio under condition ii ($K_i > K_{ii}$ or $K_i < K_{ii}$). If both processes are under thermodynamic control, this can only be the case if the two macrocycles have different relative thermodynamic stabilities under conditions i and ii. We have demonstrated that this is not the case for our optimised conditions I and II. As a result, net-directionality cannot be thus achieved.[44]

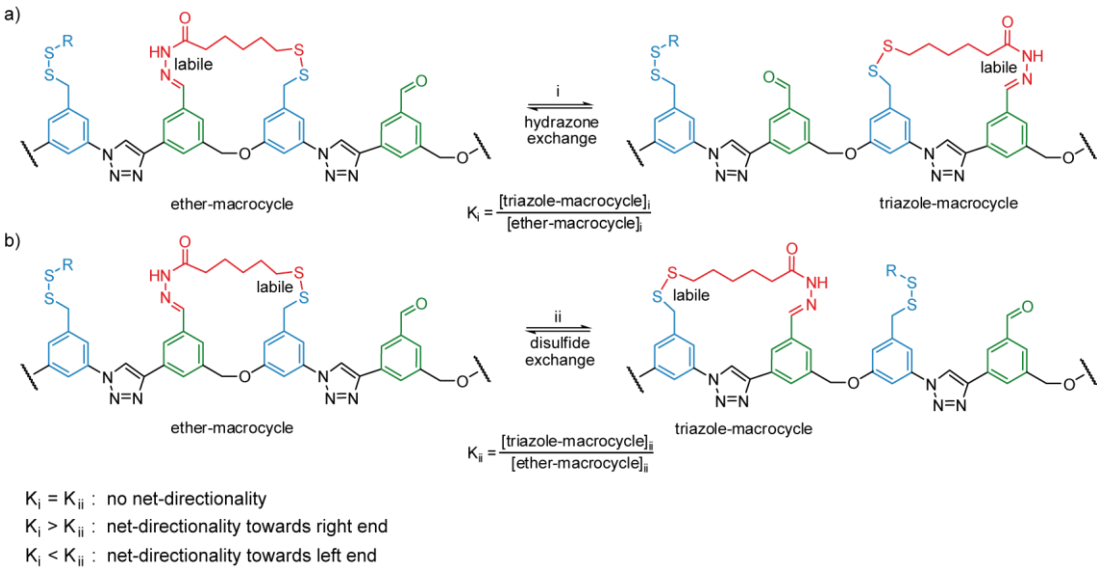

Figure 4.5. *Prerequisites for directional walker migration on a hypothetical polymeric track based on the molecular design of 1,2-**C**$_5$. a) Under conditions i (hydrazone exchange) the walker is pivoted at the disulfide foothold and can form two different kinds of macrocycles: one incorporating the rather flexible ether linker (ether-macrocycle) and one incorporating the more rigid triazole linker (triazole-macrocycle). b) Under conditions ii (disulfide exchange) the walker is pivoted at the hydrazone foothold and the walker can form the same two types of macrocycle with the track.*

One way around this problem is to conduct one of the two exchange processes under kinetic control (see Figure 4.1b). The disulfide linkages in footholds *2* and *4* allow us to operate our walker-track conjugate in a two-stage redox manner, with one of the steps proceeding instantaneously and irreversibly under the reaction conditions. Scheme 4.3 shows how, under conditions III(i) (see section 4.5.2.3), all disulfide bonds in *2,3*-$\mathbf{C_n}$ are

quantitatively reduced, resulting in a ring-opened intermediate (shown in square brackets). Rapid oxidation (conditions III(ii)) regenerates the walker-track disulfide linkages.

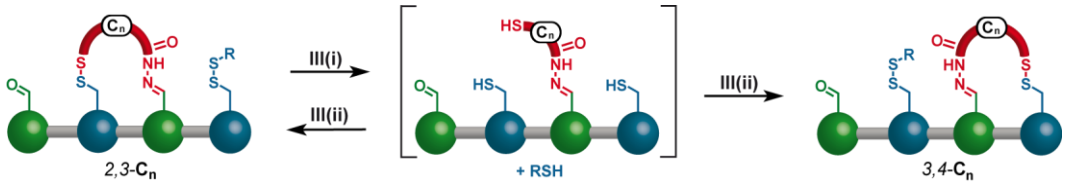

Scheme 4.3. *Kinetically controlled reaction pathway - illustrated for 2,3-**C**$_n$. Condition IIIi (reduction of disulfide bonds): 1.0 mM, DTT (6 equiv.), DBU (3 equiv.), $CDCl_3$, reflux, 2-12 h (progress monitored by ^{1}H NMR). Condition IIIii (irreversible, oxidative disulfide bond regeneration): 0.1 mM, Et_3N (excess), methyl 3-mercaptopropionate (RSH, 8 equiv.), I_2 (ca. 12 equiv.), $CDCl_3$/co-solvent, RT, 5 min.*

Importantly, this oxidation step proceeds efficiently irrespective of solvent addititives, which is why we were able to investigate the effect of a variety of co-solvents ($CHCl_3$ was kept constant in the 1:1 solvent mixtures) on the walker distribution (see Table 4.2).[45]

Table 4.2. *Effect of co-solvent on the observed 2,3-**C**$_n$:3,4-**C**$_n$ isomer ratio after irreversible oxidation of trithiol (compound in brackets, Scheme 4.3). Pure samples of 3,4-**C**$_n$ were submitted to conditions III(i) and III(ii) (see section 4.5.2.3 for details).*

co-solvent	2,3-**C**$_3$: 3,4-**C**$_3$	2,3-**C**$_4$: 3,4-**C**$_4$	2,3-**C**$_5$: 3,4-**C**$_5$
n-hexane	45:55	66:34	65:35
cyclohexane	47:53	65:35	68:32
Et_2O	40:60	61:39	61:39
MeCN	31:69	49:51	54:46
THF	36:64	58:42	56:44
DMF	20:80	55:45	66:34
MeOH	25:75	36:64	32:68
EtOH	35:65	48:52	47:53
i-PrOH	39:61	59:41	54:46
t-BuOH	43:57	62:38	70:30

Table 4.2 shows a large amplitude of ratios produced in presence of the different co-solvents. For example, the oxidation of the **C**$_5$ trithiol can lead to a *2,3*:*3,4* ratio of either 70:30 or 32:68. A second, more important observation is that even highly strained compounds can be accessed using this procedure (see Figure 4.4 for energy levels). It is

remarkable that under thermodynamic control *2,3*-**C$_3$** cannot be synthesised from *3,4*-**C$_3$**, but that using kinetic reaction control a *2,3*:*3,4* ratio of 47:53 can be achieved. These observations promise the possibility of efficient directional bias when replacing the reversible conditions II with the irreversible conditions III (using an appropriate co-solvent). For the selection of the co-solvent it is important to remember that the goal of these experiments is to drive the system away from the thermodynamic minimum composition (see Table 4.1). The most promising entries in this respect are cyclohexane for the **C$_3$** and **C$_4$** systems and methanol for the **C$_5$** system (ratios highlighted in Table 4.2).

4.3.4 Dynamic Behaviour of the Walkers under Biased Operating Conditions (Hydrazone Exchange under Thermodynamic Control; Disulfide Exchange under Kinetic Control)

The effect of introducing the irreversible redox conditions III (co-solvent: MeOH) into the walking sequence of the **C$_5$** system is shown in Table 4.3. In only 1.5 cycles, starting from 100% *1,2*-**C$_5$**, the walker moves down the track to give 43% *3,4*-**C$_5$**, compared to the 19% of *3,4*-**C$_5$** present at the steady state using the two sets of reversible conditions. Extrapolation of these results shows that further pursuing this experiment would not lead to increased bias, since the reversible conditions I would repeatedly bring the composition back towards the thermodynamic minimum. As such, the system clearly possesses the oscillating property that was predicted for an 'out of equilibrium' system. When analyzing the origin of the bias towards the right end of the track, it becomes clear that the *1,4*-**C$_5$** isomer has a significant contribution. For example, after cycle 1 (redox step), an unusually high amount of *1,4*-**C$_5$** (24%) is present, which in the subsequent step is largely converted to *3,4*-**C$_5$**.

Table 4.3. *Isomer distribution during 1.5 cycles of biased operation of **C$_5$** system and comparison to the experimentally observed minimimum energy steady state distribution.*

Cycles	0	0.5	1	1.5	Experimental
Conditions		I[a]	III[a]	I[a]	steady state
1,2-**C$_5$**[b]	100%	52%	28%	24%	39%
2,3-**C$_5$**[b]	-	48%	20%	24%	36%
3,4-**C$_5$**[b]	-	-	28%	**43%**	**19%**
1,4-**C$_5$**[b]	-	-	24%	9%	6%

[a] *Values are based on HPLC integration and are corrected for the absorbance coefficients at 290 nm (see section 4.5.6).* [b] *For details on conditions I and III see section 4.5.2 (co-solvent: MeOH).*

Table 4.4 shows the effect of introducing the irreversible redox conditions III (co-solvent: cyclohexane) into the walking sequence of the **C₄** system. Starting from 100% *3,4*-**C₄**, in two cycles the walker moves down the track to give 62% *1,2*-**C₄**, compared to the 41% present at the steady state using the two sets of reversible conditions. The oscillating property of this system is evident in the first line of Table 4.4, where after only one irreversible step 58% of *1,2*-**C₄** is present, whereas the next reversible step shifts the system considerably towards the steady state, before another irreversible step provides further bias towards *1,2*-**C₄**. In this system the *1,4*-**C₄** isomer does not contribute to the directional bias. In fact, the high amount of *1,4*-**C₄** isomer formed during step 3 (cycle 1.5), counteracts the desired bias towards the left end of the track.

Table 4.4. *Isomer distribution during 2 cycles of biased operation of* ***C₄*** *system and comparison to the extrapolated minimimum energy steady state distribution.*

Cycles	0	0.5	1	1.5	2	Extrapolated
Conditions		III[a]	I[a]	III[a]	I[a]	steady state
1,2-***C₄***[b]	-	-	58%	46%	**62%**	**41%**
2,3-***C₄***[b]	-	63%	4%	25%	5%	3%
3,4-***C₄***[b]	100%	37%	26%	12%	25%	48%
1,4-**C₄**[b]	-	-	12%	17%	8%	8%

[a] *Values are based on HPLC integration and are corrected for the absorbance coefficients at 290 nm (see section 4.5.6).* [b] *For details on conditions I and III see section 4.5.2 (co-solvent: cyclohexane).*

From initial experiments on the biased oxidation of the **C₈** system and extrapolation of the expected isomer distributions after 1.5 to 2 operational cycles, we drew the conclusion that the **C₈** system does not offer any opportunity to achieve significant directional bias. In the **C₂** system the macrocycle that would incorporate the triazole unit would be so strained that isomer *2,3*-**C₂** cannot be accessed, even under kinetic control.

Table 4.5 shows the results that were obtained when introducing the irreversible operation III (co-solvent: cyclohexane) into the walking sequence of the **C₃** system. Starting from 100% *3,4*-**C₃,** two operational cycles gave 53% *1,2*-**C₃**, compared to the 52% present at the steady state. No directional bias has thus been achieved, which is partially due to the lower amount of *2,3*-**C₃** that can be formed (compared to the **C₄** system), but mostly a result of the counteracting right-end bias contributed by the *1,4*-**C₃** isomer.

Table 4.5. *Isomer distribution during 2 cycles of biased operation of* $\boldsymbol{C_3}$ *system and comparison to the extrapolated minimimum energy steady state distribution.*

Cycles	0	0.5	1	1.5	2	Extrapolated
Conditions		III[a]	I[a]	III[a]	I[a]	steady state
1,2-$\boldsymbol{C_3}$[b]	-	-	41%	38%	**53%**	**52%**
2,3-$\boldsymbol{C_3}$[b]	-	44%	~1%	13%	<1%	<1%
3,4-$\boldsymbol{C_3}$[b]	100%	56%	43%	26%	38%	43%
1,4-$\mathbf{C_3}$[b]	-	-	15%	23%	9%	5%

[a] *Values are based on HPLC integration and are corrected for the absorbance coefficients at 290 nm (see section 4.5.6).* [b] *For details on conditions I and III see section 4.5.2 (co-solvent: cyclohexane).*

4.3.5 Discussion of the Observed Directional Bias

The results obtained for the $\mathbf{C_2}$ and $\mathbf{C_3}$ systems indicate that there is a threshold at which ring strain gets too high to allow for optimum bias ($\mathbf{C_3}$), or even for any walker migration via the *2,3* isomer ($\mathbf{C_2}$). However, in case of the $\mathbf{C_3}$ system, it is not only the reduced availability of *2,3*-$\mathbf{C_3}$ under kinetic control (47% compared to 65% for $\mathbf{C_4}$), but also the occurrence of counterbias through the *1,4*-$\mathbf{C_3}$ isomer that reduces the left-end directed bias. The results obtained for the $\mathbf{C_8}$ system suggest that there is also an upper limit of walker length, where ring strain becomes too low and only moderate bias can be achieved by the choice of the right solvent. Interestingly, ring strain has been identified as a key prerequisite for directionality in biological bipeds, such as kinesin[46] and myosin-V.[47]

Table 4.3 clearly shows that for the $\mathbf{C_5}$ system we have achieved significant directional bias away from the energy minimum steady state towards the right end of the track. An interesting question is if this bias would also occur on a polymeric track (see Figure 4.5). In a polymeric system the *1,4*-type isomers would most likely not have a constructive effect. The question can thus be reduced to whether the observed solvent-dependent bias in the $\mathbf{C_5}$ system is a result of end group effects or of the different accessibility of the two fundamental macrocycles under kinetic as opposed to thermodynamic control (see Figure 4.5). Our data does, however, not show consistent trends that would support any of the two possibilities, which is why the answer to this question could only be provided by studies on systems with extended tracks (consisting of six or more footholds).

For the **C4** system the situation is fundamentally different, since the *1,4*-**C4** isomer does not contribute to directional bias. In fact, if the *1,4* isomer was not present, an even more significant bias towards the left end of the track would have been observed. Furthermore, the left-end bias is only to a limited extent dependent on the effect of the co-solvent (Table 4.2). The major mechanism for directional bias is that under kinetic control the highly strained *2,3*-**C4** isomer can be accessed from *3,4*-**C4** in a high ratio (> 50%). This step is 'ratcheting' a large part of the walker-track conjugates to a high-energy state (*2,3*-**C4**, see Figure 4.5), whereas the next TFA-catalyzed reversible step allows relaxation of most high-energy walker-track conjugates towards the lower energy isomer *1,2*-**C4**. This information ratchet mechanism[3,14b] should also be viable in a polymeric system.

4.3.6 Comprehensive Study on the Processivity of the C_5 System

To quantitatively investigate the processivity of the non-biased and biased walking experiments of the **C5** system, we carried out double-labelling crossover experiments (see section 4.5.5 for details). The double-labelled walker-track conjugate *3,4*-**C5**-d_4 was mixed with an unlabelled sample of *3,4*-**C5** in a 1:1 ratio (Scheme 4.4). Such a mixture was subjected in a first experiment to the non-biased walking cycle conditions (Scheme 4.4a) and in a second experiment to the biased walking cycle conditions (Scheme 4.4b). The product distribution during both experiments was analyzed by HPLC-MS (high performance liquid chromatography - mass spectrometry).[48]

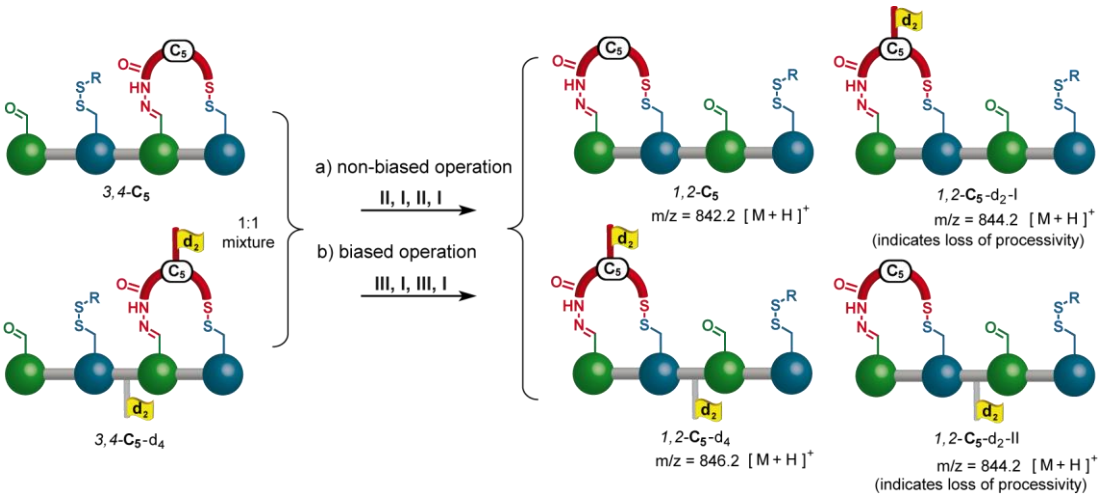

Scheme 4.4. *Crossover study on the processivity of the* ***C5*** *system. For conditions I, II and III, see caption of Scheme 4.3.*

The results of these two experiments are shown in Figure 4.6. The blue bars represent the experimentally obtained isotopic distribution of the sample before operation, while

the green bars represent the theoretical isotopic distribution that would be expected if full statistical scrambling occurred. The red bars show the experimentally obtained isotopic distribution after operation (Figure 4.6a for non-biased operation; Figure 4.6b for biased operation). The displayed experimental distributions (red bars and blue bars) are the average results of a total of ten performed runs for each experiment. This procedure made it possible to assess the reproducibility of the mass spectrometric data and to analyze the data for statistical significance (see section 4.5.5 for further information on the whole study).

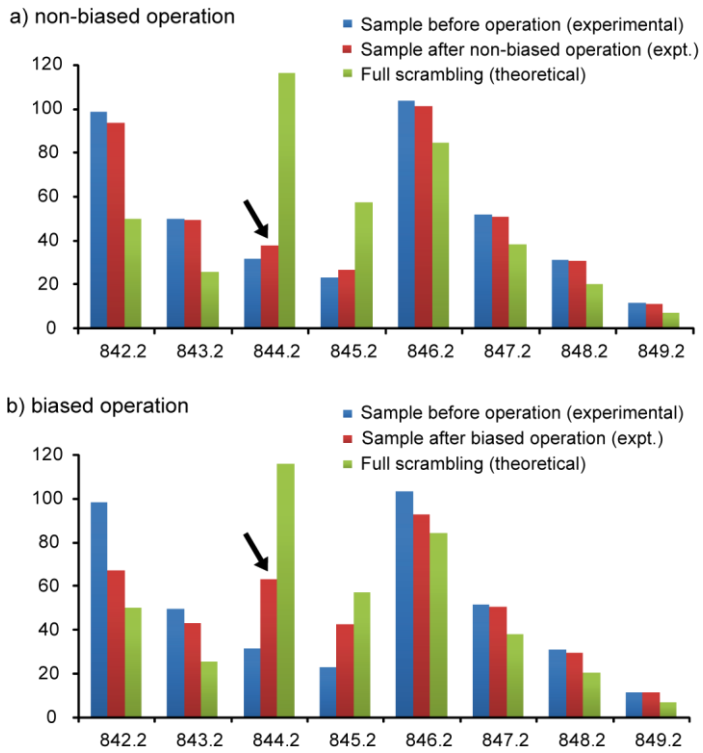

Figure 4.6. *Results of the crossover study on the processivity of the* $\mathbf{C_5}$ *system: a) non-biased operation over two cycles; b) biased operation over two cycles (see Scheme 4). Shown are the (normalised) isotopic distributions of the 1:1 mixture before operation (blue; experimental), after operation (red; experimental) and the distribution that would be expected when full statistical scrambling occurred (green; theoretical).*

The black arrows highlight the m/z value which is indicative of the presence of single-labelled species, which, in turn, are indicators for loss of processivity (see right hand side of Scheme 4.4). The difference between non-biased and biased operation is evident, with the biased operation exhibiting a significantly lower level of processivity after four operational steps. Mathematical analysis of the results (see section 4.5.5) reveals that the non-biased operation leads to a mean step number[49] of 37, whereas the biased operation results in a mean step number of 7. In comparison, wild-type

kinesins typically exhibit a mean step number in the range of 75 to 175 and an average run length of ~1 μm.[13]

The decrease in processivity during non-biased operation (~2% per step) is most likely a result of the formation of oligomers in which a walker moiety acts as a bridge between two tracks and after the following operational step is located on the wrong track (see Scheme 4.6b in section 4.5.5). The higher loss of processivity during biased operation can be explained as a result of the lower chemoselectivity of the two-step redox-mediated disulfide exchange under kinetic control. HPLC analysis of this step showed appearance of oligomers and two monomeric side products that do not occur during the thermodynamically controlled disulfide exchange. These two side products (for the structures see Scheme 4.6c in section4.5.5) necessarily lead to loss of processivity in the subsequent operational step. We can exclude loss of processivity via complete detachment of the walker moiety for two reasons: (i) starting from one pristine isomer, we always only found a mix of two isomers, not all four; i.e. under acidic conditions *1,2*-$\mathbf{C_5}$ only gave *2,3*-$\mathbf{C_5}$ but never *3,4*-$\mathbf{C_5}$ or *1,4*-$\mathbf{C_5}$; likewise, under basic conditions *1,2*-$\mathbf{C_5}$ only gave *1,4*-$\mathbf{C_5}$ but never *2,3*-$\mathbf{C_5}$ or *3,4*-$\mathbf{C_5}$; and (ii) we have never detected[50] a detached walker moiety, bare track or track with two walker moieties.

4.3.7 Relating Molecular Walkers to Systems Chemistry

The molecular walkers presented in this article contribute a new aspect to the emerging field of systems chemistry.[51] In most artificial systems studied to date,[52] every individual molecular component is in equilibrium with all other components. In the walker systems presented here, however, only subsets of the four monomeric isomers (*1,2*-$\mathbf{C_n}$, *2,3*-$\mathbf{C_n}$, *3,4*-$\mathbf{C_n}$ and *1,4*-$\mathbf{C_n}$) are in equilibrium under any given set of conditions. This restriction of the component exchange processes is a fundamental prerequisite for the ability to drive a system away from its thermodynamic minimum.

In Figure 4.7 this is exemplified for a system of three components A, B and C, (corresponding to the walking isomers *1,2*-$\mathbf{C_n}$, *2,3*-$\mathbf{C_n}$ and *3,4*-$\mathbf{C_n}$, while ignoring *1,4*-$\mathbf{C_n}$). It is further assumed that A and C can selectively bind to a host molecule, which decreases their relative free energy (transformation of A to A' and C to C'). If all three components are in equilibrium (Figure 4.7a), the addition of the host will lead to a new distribution, with A' and C' being the major components. This new distribution does, however, correspond to the new thermodynamic minimum of the system, i.e. the

composition is a function of the relative free energies of the three components. Removal of the host molecule consequently leads back to the original distribution, which demonstrates that such a manipulation, even when repeated, cannot result in any out-of-equilibrium state of the system.

The system can be moved away from the thermodynamic minimum, however, if only one of the two exchange processes is possible at any time (Figure 4.7b, indicated by crossed-out reaction arrows and higher kinetic barriers). This restriction results in dynamic exchange only between A and B (while C is an innocent bystander) or between B and C' (while A' is the bystander). Since C' has a lower ground-state energy than A and B, repetitive addition and removal of the host leads to a composition which is far away from the thermodynamic minimum (right hand side of Figure 4.7). Such a concerted manipulation of the thermodynamics and kinetics of a system corresponds to a flashing energy ratchet mechanism.[11,19b] The mutually exclusive nature of hydrazone and thiol/disulfide exchange[24b,c] thus represents an appealing opportunity for the construction of new out-of-equilibrium systems, as well as Brownian ratchets[3,14b] (through manipulation of such systems).

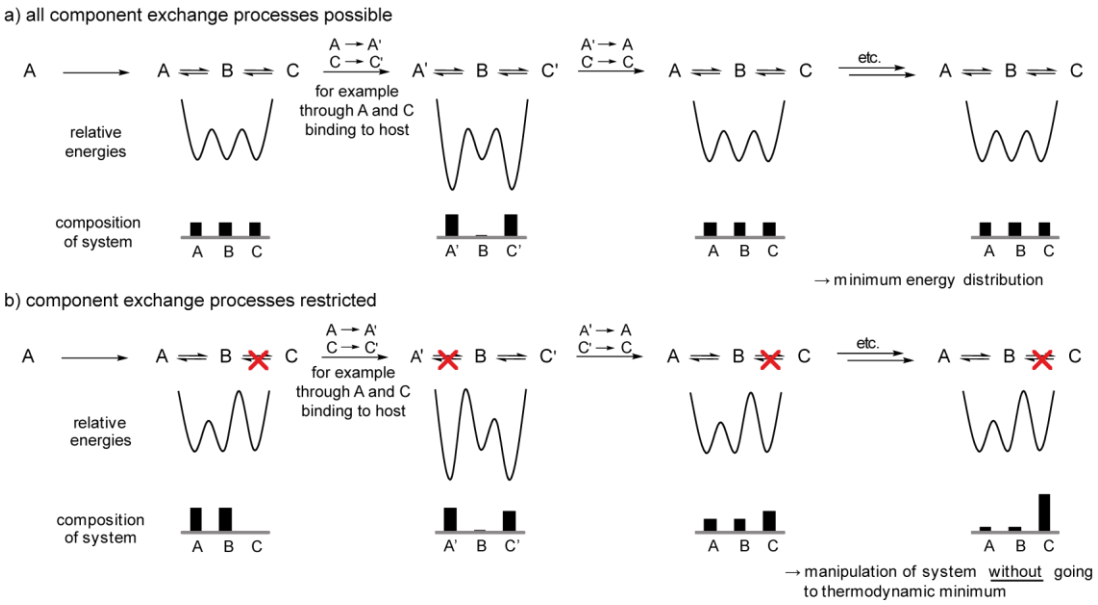

Figure 4.7. *Molecular walkers and systems chemistry: the importance of restricted component exchange processes. a) Chemical system of three components (A, B and C) at equilibrium. Repeated manipulation (through host binding event (A→A', C→C')) does not lead away from thermodynamic minimum. b) Chemical system of three components (A, B and C) with restricted component exchange processes. Repeated manipulation shifts the composition away from thermodynamic minimum.*

4.4 Conclusions

We have described five small-molecule systems in which a molecular walker with chemical 'legs' of varying length moves up and down a four-foothold track primarily through a passing-leg gait mechanism. Repetitive switching of fully-reversible walking operations does not lead to intrinsically directional migration of the walker units, but to a minimum energy distribution of walkers on the tracks. Directionality of the walking sequence can, however, be achieved for two of the five systems studied by replacing one of the reversible reactions with a kinetically-controlled redox operation, the outcome of which can be significantly manipulated by addition of a co-solvent. The length of the spacer unit between the walker feet is crucial for generating ring strain with the track necessary for maximizing directional bias. A crossover isotopic labeling study shows that directionality gained by introducing the kinetically controlled redox step comes at the price of reduced processivity (mean step number 7, compared to 37 under acid-base conditions). Although they are extremely rudimentary systems, the **C$_4$** and **C$_5$** walker-track conjugates exhibit four of the essential characteristics of linear molecular motor dynamics, namely processive, directional, repetitive and progressive migration of a molecular unit up and down a molecular track. Improvements to these first generation designs are required to address problems associated with folding (which generates the "double step" *1,4*-isomer), reaction timescales (currently several hours for each operation), oligomer formation (which results in reduced processivity), chemoselectivity and improved (ratchet) mechanisms for directional bias.

4.5 Experimental Section

4.5.1 General Information

Compounds **E1**,[53] **E8**,[26a] **E11**[26b] **and E12-E15**[26c] were prepared according to literature procedures. The synthesis of compounds **E5**, **E6**, **E17**, **E18**, **E22**, **E27**, **E32**, *1,2*-**C$_5$**, *3,4*-**C$_5$** and *3,4*-**C$_5$**-d$_4$ has been described in Chapter III (see compounds **E2**, **E3**, **E19**, **E20**, **E21**, *3,4*-**C$_5$** there).[15]

Analytical and preparative HPLC was performed on instruments of Gilson Inc., USA and Agilent Technologies (1200 LC system with photodiode array detector). Normal-phase columns (Kromasil-Si, analytical: 250 × 4.6 mm, preparative: 250 × 20 mm) were used with combined isocratic and gradient elution (analytical: 0.8 mL/min, CH_2Cl_2/^{i}PrOH, 3% → 3% → 15% → 15% → 3% ^{i}PrOH; semi-preparative: 5 mL/min, CH_2Cl_2/^{i}PrOH,

4.2% →4.2% → 15% → 15% → 4.2% ^{i}PrOH; preparative: 10 mL/min, CH_2Cl_2/MeOH, 1.0% → 1.0% → 20% → 20% → 1.0% MeOH, UV detection @ 290 nm). LCMS analysis was performed on an Agilent Technologies 1200 LC system with 6130 single quadrupole MS detector (APCI source; column and method as specified above).

4.5.2 General Procedures for Exchange Reactions

4.5.2.1 General Procedure for Acid-Catalysed Hydrazone Exchange (I)

To a 0.1 mM solution of *1,2*-$\mathbf{C_n}$ (typically 1 mg in ca. 10 mL; 1.0 equiv.) in $CHCl_3$ (HPLC grade) were added 5 drops of a solution containing 20% v/v TFA (CF_3CO_2H) and 1% v/v H_2O in $CHCl_3$ (HPLC grade). The mixture was stirred at room temperature and the progress of the equilibration followed by analytical HPLC (see section 4.5.1). When the relative ratios of the isomers were stable (generally 6-96 hours), the mixture was washed with an aqueous solution of $NaHCO_3$. The layers were partitioned and the aqueous layer was extracted with $CHCl_3$. The combined organic layers were dried over $MgSO_4$. The solvents were removed under reduced pressure and the amount and constitution of the mixture determined by weight and, after dissolving in a defined amount of $CHCl_3$, analytical HPLC.

4.5.2.2 General Procedure for Base-Catalysed Disulfide Exchange (II)

To a 0.1 mM solution of *3,4*-$\mathbf{C_n}$ (typically 1 mg in 10 mL; 1.0 equiv.) in $CHCl_3$ (HPLC grade) was added DBU (40 equiv.), DTT (10 equiv.) and dimethyl 3,3'-disulfanediyldipropanoate (20 equiv.) from stock solutions. The mixture was stirred at room temperature and the progress of the equilibration followed by analytical HPLC. When the relative ratios of the isomers were stable (generally 12-48 hours), the excess of DTT was oxidised by dropwise addition of a solution of I_2 in $CHCl_3$ until a slight brown colour persisted. An aqueous solution of NH_4Cl and Na_2SO_3 was added and the mixture was stirred vigorously until decolourisation was complete. The layers were partitioned and the aqueous layer was extracted with $CHCl_3$. The combined organic layers were dried over $MgSO_4$. After work up the product distribution was no longer dynamic (free of DTT and DBU) and the solvent could be removed to allow analysis by weight and analytical HPLC (see section 4.5.1).

4.5.2.3 *General Procedure for Redox-Mediated Disulfide Exchange (III)*

(i) Reduction Step

DTT (6 equiv.) and DBU (3 equiv.) were added from stock solutions to a 1 mM solution of *2,3*-$\mathbf{C_n}$ (1 equiv.) in $CDCl_3$ or $CHCl_3$. The mixture was heated under reflux until ^1H NMR showed that all disulfide bonds had been reduced (2 to 12 hours).

(ii) Oxidation Step

The above solution was diluted to 0.1 mM with a 1:1 mixture of $CHCl_3$ and co-solvent (MeOH for $\mathbf{C_5}$, cyclohexane for $\mathbf{C_3}$ and $\mathbf{C_4}$). Et_3N (5 drops) and methyl 3-mercaptopropionate (8 equiv.) were added. At room temperature, a solution of I_2 in $CHCl_3$ was added to the mixture until the brown colour persisted. An aqueous solution of NH_4Cl and Na_2SO_3 was added and the solution was stirred vigorously until decolourisation was complete. The layers were partitioned and the aqueous layer was extracted with $CHCl_3$. The combined organic layers were dried over $MgSO_4$. For the $\mathbf{C_5}$ system, at this stage a broad-window preparative HPLC was carried out (see reference A for details) to remove excess reagents, waste products, and other impurities (the two-step redox sequence produces more byproducts than the acid or base catalyzed procedures). This purification step was omitted for the processivity study ($\mathbf{C_5}$) and for the operation of the $\mathbf{C_3}$ and $\mathbf{C_4}$ systems.

Note: The molar ratios of DBU and DTT used during the base-catalyzed disulfide exchange experiments (40 and 10 equivalents, respectively) are higher than those used during the reduction step of the redox disulfide exchange experiments (3 and 6 equivalents, respectively) since there is a tenfold difference in concentration at which the experiments were carried out (0.1 mM and 1.0 mM, respectively). The DBU:DTT ratio is also reversed (from 4:1 to 1:2) in the two experiments. The rationale behind these changes reflect the different objectives of the two types of exchange experiments: During the base-catalyzed exchange experiment, DTT is added to increase the rate of disulfide exchange for which thiolates are a necessary intermediate; during the redox operation the excess DTT results in quantitative reduction of the disulfide bonds. The resulting thiols are subsequently rapidly oxidised by iodine to affect a kinetically controlled reaction outcome.

4.5.3 Optimisation and Reproducibility of Exchange Processes

Finding conditions that reliably, efficiently and in a practical period of time lead to equilibrium between two walking isomers (e.g. *3,4* and *2,3*; see section 1 for structures)

was an important achievement in our investigation of the dynamic properties of the walker-track conjugates. In model studies on a related cyclic compound, containing both an internal acylhydrazone and a disulfide bond, we had previously identified conditions that lead to a relatively fast dynamic exchange of hydrazone or disulfide linkages, while the other is strictly inert. There were, however, two challenges that we could not address with model systems: The first was to find optimally dilute conditions for the exchange processes to occur predominantly intramolecularly. For this we varied the concentration and the amounts of all reagents over a vast range. The second one was to make sure that an experimentally found ratio, e.g. between the *1,2* and the *2,3* isomer, truly represented the thermodynamic minimum. The same experiment was therefore independently conducted starting from *1,2* and *2,3*. Only when it was found that the outcome was the same in both cases, we could assume that the true equilibrium was found.

For hydrazone exchange (e.g. between *1,2* and *2,3* isomer) we found that adding trifluoroacetic acid (TFA) to a 0.1 mM solution of the walker-track conjugate in chloroform ($CHCl_3$) led to reliable, extremely efficient (essentially quantitative; no detectable amounts of oligomers or other side products) conversion towards the thermodynamic minimum. Since the $CHCl_3$ we used contained varying amounts of water, which is (catalytically) required in the mechanism for hydrazone exchange, we found that the time until equilibrium is reached can vary from 3 hours to over one week when only TFA is used. Such an enormous fluctuation can be avoided when a stock solution containing 20% TFA and 1% water in $CHCl_3$ is used to initiate the equilibration. For the reversible disulfide exchange we found that optimal conditions involved 0.1 mM concentration in $CHCl_3$, the strong base 1,8-diazabicyclo[5.4.0]undec-7-ene (DBU), the mild reducing agent DL-dithiothreitol (DTT), and dimethyl 3,3'-disulfanediyldipropanoate ($(MeO_2CCH_2CH_2S)_2$), the placeholder disulfide. DTT promotes disulfide exchange by acting as a source of reduced thiol species, which, when deprotonated by the base, can undergo thiol-disulfide exchange. The placeholder disulfide is added to optimise the amount of monomeric products; in its absence higher amounts of oligomers are formed. This optimised procedure reliably leads to the thermodynamic minimum in yields of ~80% (HPLC) within about 12 hours equilibration time (see section 4.5.2 for the precise conditions for hydrazone and disulfide exchange).

4.5.4 HPLC Traces

Figure 4.8 shows the HPLC chromatograms of the mixtures that resulted from biased operation over two cycles starting from pristine *3,4*-**C_3** (Figure 4.8a) and *3,4*-**C_4** (Figure 4.8b). For more detailed information see Figure caption; for information on the chromatographic method see section 4.5.1.

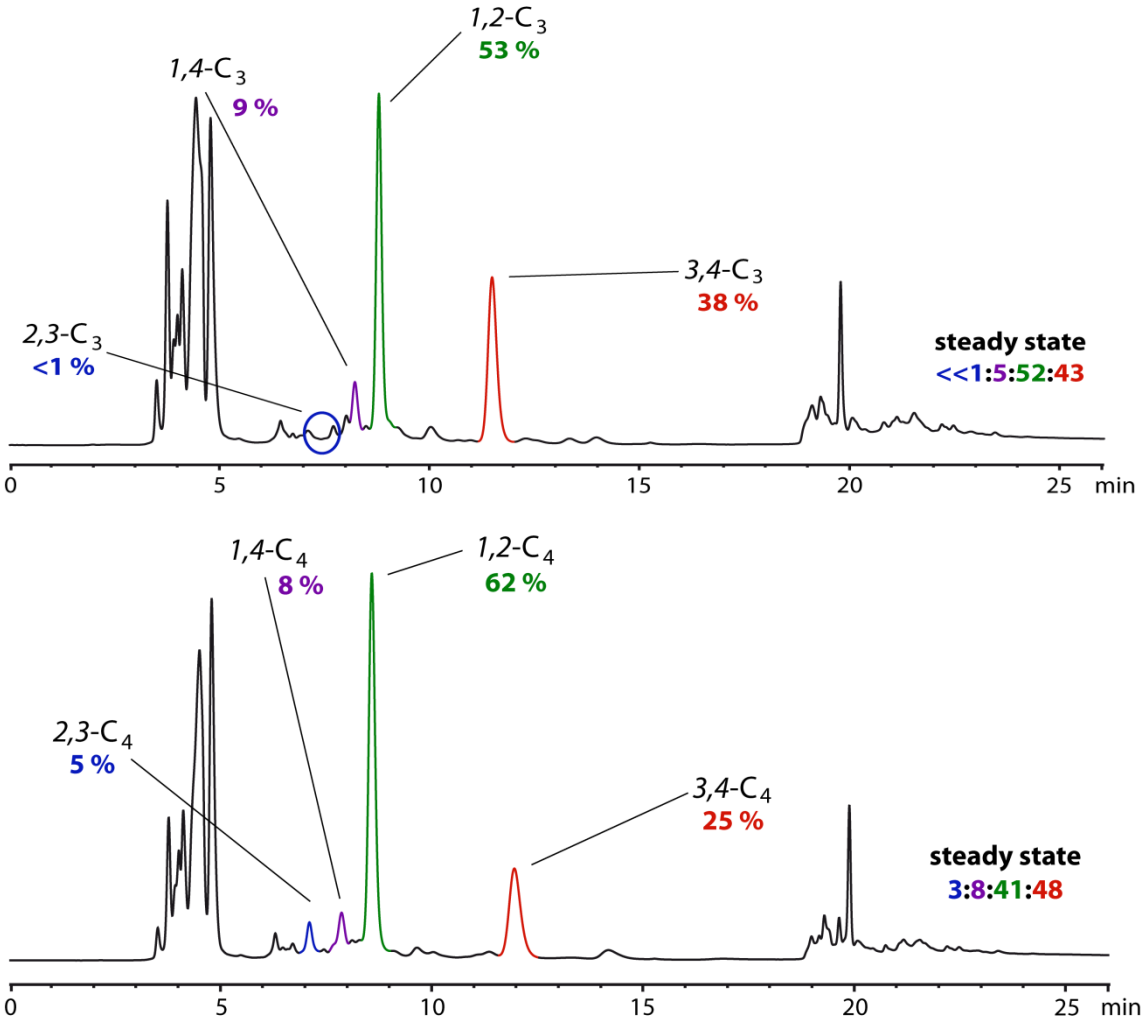

Figure 4.8. *Normal-phase HPLC chromatograms of the mixtures that resulted from two biased operational cycles starting from pristine 3,4-**C_3** (a) and from pristine 3,4-**C_4** (b). Each operational cycle involved two steps: (1) kinetically controlled disulfide exchange (condition III: (i) 1.0 mM, DTT (6 equiv.), DBU (3 equiv.), $CHCl_3$, reflux, 2-12 h; (ii) $MeO_2CCH_2CH_2SH$ (8 equiv.), I_2, Et_3N, $CHCl_3$/cyclohexane 1:1, RT, 5 min); (2) reversible hydrazone exchange (condition I: 0.1 mM, TFA, $CHCl_3$, RT, 6-96 h). The samples were not subjected to any form of purification other than simple aqueous work-up procedures. As a consequence both samples show a significant amount of unpolar impurities that were mostly brought in by solvents and reagents (analysis of UV and MS spectra provided by photo diode array (PDA) and MS detectors). The percentage values shown in the figure are corrected for absorbance coefficients (see section 4.5.6). The calculated steady state compositions (see section 4.5.7) are shown in the boxes for comparison. The identification of the isomers was greatly assisted by their unique UV spectra (PDA detector).*

4.5.5 Processivity Study - Double-labelling crossover experiment under biased and non-biased operation

To determine the approximate loss of processivity during non-biased and biased walking cycles, we conducted two double-labelling crossover studies based on LCMS analysis. The principle behind these studies is shown in Scheme 4.5. A 1:1 mixture of compounds *3,4*-**C$_5$** and *3,4*-**C$_5$**-d$_4$ was subjected to two full cycles of non-biased (conditions II and I) and biased (conditions III and I) exchange experiments. Compound *3,4*-**C$_5$**-d$_4$ differs from *3,4*-**C$_5$** by having a d$_2$-label in both the track and walker moiety. The objective was to measure the amount of d$_2$-labelled species that was formed during two full operation cycles and thus determine the level of processivity of the walking process.

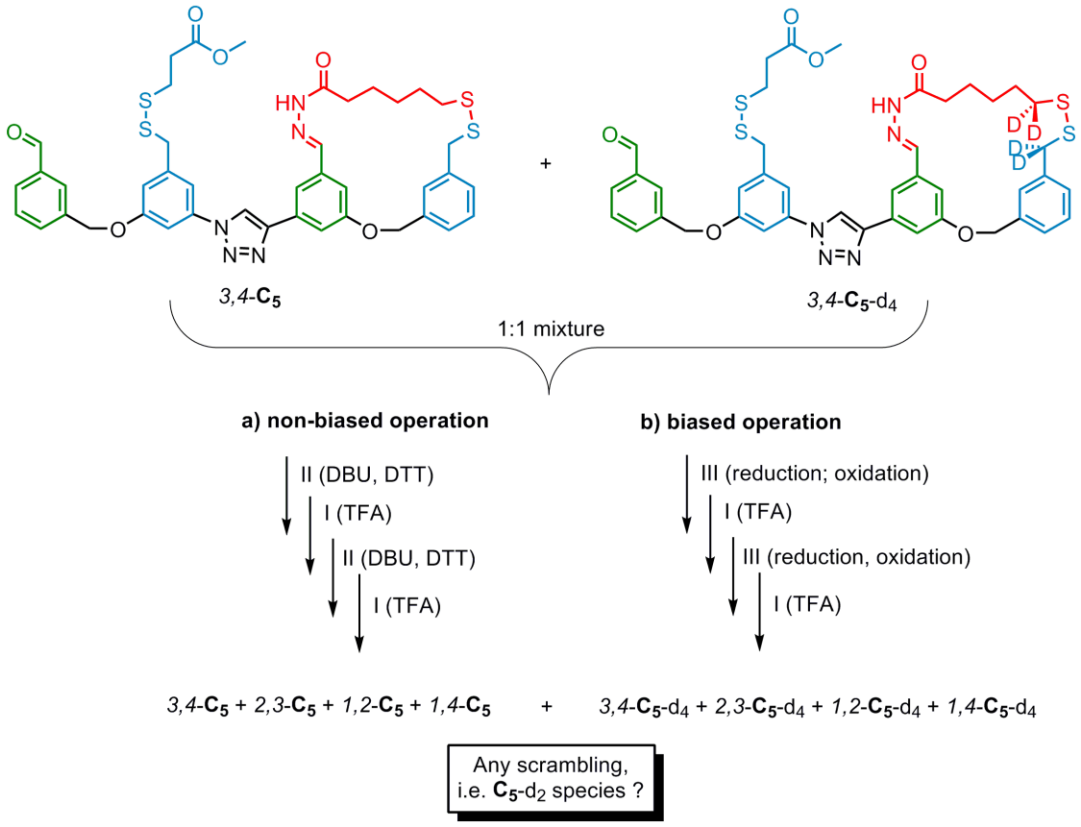

Scheme 4.5. *Concept of the double-labelling crossover experiment. a) non-biased, b) biased operation.*

Such d$_2$-labelled compounds are indicators for loss of processivity (i.e. walker no longer connected to original track), which can theoretically take place in three ways (Scheme 4.6). During the first pathway (a), the walker moiety completely detaches from its corresponding track and subsequently reattaches to a different track. During the second pathway (b), the loss of processivity occurs indirectly via particular types of

oligomers, of which only one example, a d_0-d_4 dimer, is depicted in Scheme 4.6. The third pathway (c) can take place via two monomeric side products that we never detected in measurable quantities during non-biased operation, but that were observed during the kinetically controlled disulfide exchange step of the biased operation.

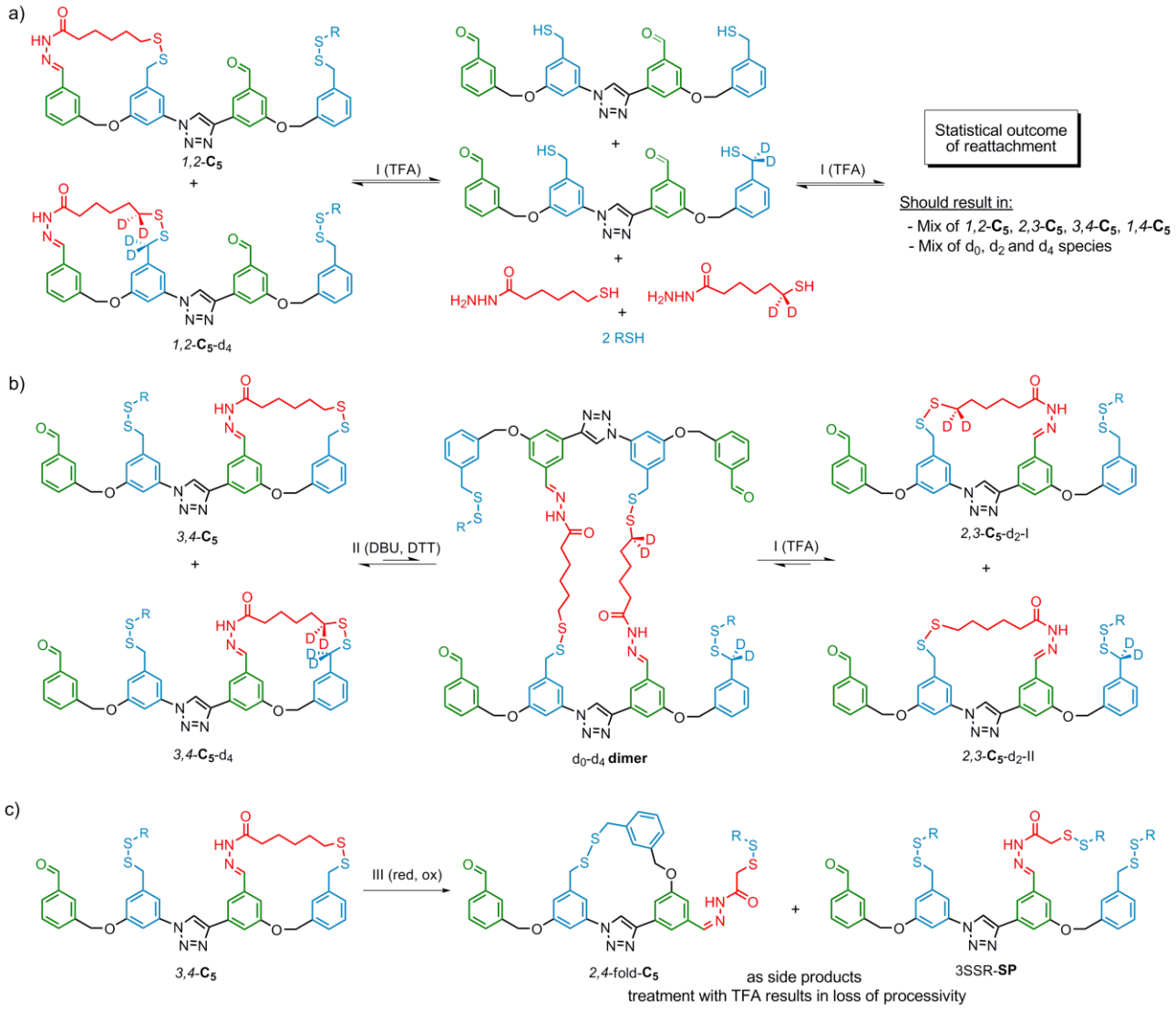

Scheme 4.6. *Three possible pathways (a), (b), and (c) of the double-labelling crossover experiment during which d_2-species are formed and processivity is lost; a) Complete detachment of the walker moiety and statistical reattachment; b) Processivity loss via a d_0-d_4 dimer, leading to formation of d_2-species* 2,3-***C*****5**-*d_2-I, and* 2,3-***C*****5**-*d_2-II; c) Processivity loss via side products* 2,4-*fold*-***C*****5** *(folding of track) and 3SSR-****SP*** *(all three thiol vacancies occupied by placeholder thiol). Since those side products are energetically unfavorable, they were only detected under kinetic control (condition III), but not under thermodynamic control (condition II).*

We are able to rule out pathway (a) for both biased and non-biased operation by means of conventional HPLC and LCMS (starting from one pristine isomer, we only found a mix of two isomers, not all four; i.e. under acidic conditions *1,2*-**C5** only gave *2,3*-**C5** but

never *3,4*-**C$_5$** or *1,4*-**C$_5$**; likewise, under basic conditions *1,2*-**C$_5$** only gave *1,4*-**C$_5$** but never *2,3*-**C$_5$** or *3,4*-**C$_5$**). We can also rule out pathway (c) for the non-biased mode of operation, since we never detected side products *2,4*-fold-**C$_5$** and 3SSR-**SP** (see Scheme 4.6) under reversible disulfide exchange condition II. Thus, the main objective of this experiment was to find out if, and to which extent, processivity is lost during non-biased operation (conditions II and I) via oligomer formation (pathway (b) in Scheme 4.6) and by how much processivity loss is higher during biased operation (conditions III and I), due to side products *2,4*-fold-**C$_5$** and 3SSR-**SP** (pathway (c) in Scheme 4.6).

The results of the mass spectrometric experiments and statistical and mathematical analysis are presented in the following sections. Section 4.5.5.1 shows the isotopic distribution of the 1:1 mixture of *3,4*-**C$_5$** and labelled *3,4*-**C$_5$**-d_4 before any operation (serves as reference). Section 4.5.5.2 shows the isotopic distribution after two cycles of non-biased operation (conditions II and I) and section 4.5.5.3 shows the distribution after two cycles of biased operation (conditions III and I; see Scheme 4.5). In sections 4.5.5.4 and 4.5.5.5 the results are analyzed and discussed.

4.5.5.1 MS Analysis of Reference Mixture of 3,4-C_5 and 3,4-C_5-d_4 (1:1) before Operation

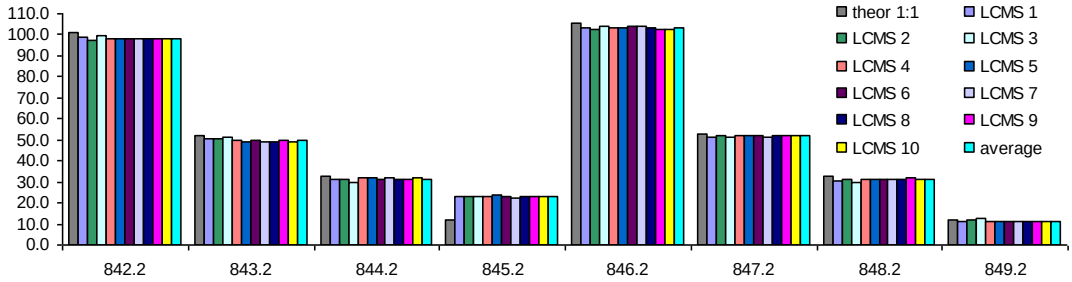

Figure 4.9. *Chart of theoretical, found and average isotopic distributions for the reference mixture of* 3,4- ***C_5*** *and* 3,4- ***C_5***-d_4 *(1:1) before operation. For each of the ten measurements the sum over all 8 abundances (m/z 842.2 to m/z 849.2) was normalised to a value of 400.*

Table 4.6. *Isotopic distributions of reference mixture and statistical analysis. Theor: theoretical isotopic distribution; Mean: average of LCMS 1 to 10; Stddev.: standard deviation. The theoretical isotopic distribution was calculated as a 1:1 sum of the expected individual distributions for the d_0- and the d_4-labelled compounds. As a result of the normalisation, which is necessary for the comparison of the results before and after operation, the sum of columns 2 to 12 is 400.*

m/z	Theor	LCMS 1	LCMS 2	LCMS 3	LCMS 4	LCMS 5	LCMS 6	LCMS 7	LCMS 8	LCMS 9	LCMS 10	Mean	Std.dev.
842.2	101.1	98.6	97.5	99.6	98.3	97.8	98.2	98.4	98.3	98.1	98.4	98.3	0.5
843.2	51.8	50.4	50.3	51.0	49.7	48.7	49.4	49.2	49.4	50.2	49.4	49.8	0.7
844.2	**32.5**	**31.4**	**31.3**	**29.6**	**31.9**	**32.3**	**31.0**	**31.8**	**31.6**	**31.4**	**31.9**	**31.4**	**0.7**
845.2	11.9	23.4	23.4	22.9	22.9	23.7	22.9	22.6	23.1	23.0	22.8	23.1	0.3
846.2	105.3	103.5	102.4	103.7	102.9	103.0	104.3	104.3	103.2	102.5	102.8	103.3	0.7
847.2	53.0	51.1	52.1	51.0	52.1	51.9	51.9	51.2	52.3	52.2	51.9	51.8	0.5
848.2	32.4	30.5	31.3	29.8	31.1	31.3	31.0	31.2	31.1	31.6	31.5	31.0	0.5
849.2	11.9	11.1	11.7	12.3	11.1	11.2	11.2	11.3	11.1	11.0	11.3	11.3	0.4

4.5.5.2 *MS Analysis of Mixture of 3,4-C_5 and 3,4-C_5-d_4 (1:1) after Operation over two Non-Biased Cycles*

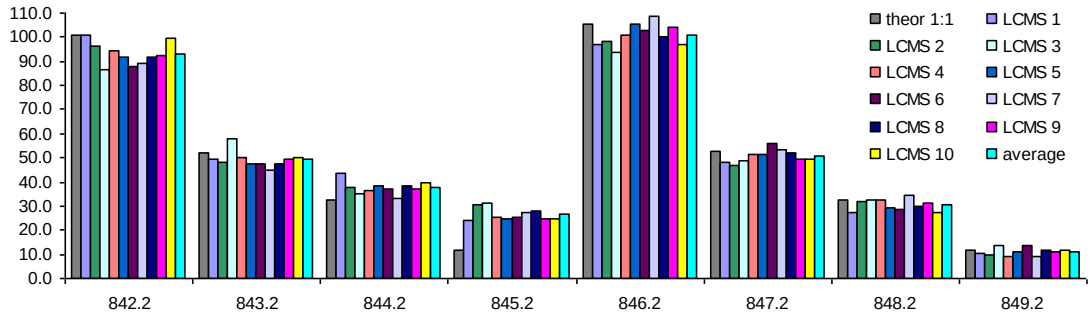

Figure 4.10. *Chart of theoretical, found, and average isotopic distributions of the operated mixture of* 3,4-***C_5*** *and* 3,4-***C_5***-d_4 *(1:1) after non-biased operation (conditions I and II). For each of the ten measurements the sum over all 8 abundances (m/z 842.2 to m/z 849.2) was normalised to a value of 400.*

Table 4.7. *Isotopic distributions for operated mixture (non-biased) and statistical analysis. Theor: theoretical isotopic distribution; Mean: average of LCMS 1 to 10; Stddev.: standard deviation. The theoretical isotopic distribution was calculated as a 1:1 sum of the expected individual distributions for the d_0- and the d_4-labelled compounds (assuming no processivity loss). As a result of the normalisation, which is necessary for the comparison of the results before and after operation, the sum of columns 2 to 12 is 400.*

m/z	Theor	LCMS 1	LCMS 2	LCMS 3	LCMS 4	LCMS 5	LCMS 6	LCMS 7	LCMS 8	LCMS 9	LCMS 10	Mean	Std.dev.
842.2	101.1	101.0	96.5	86.8	94.4	92.1	88.1	89.0	91.6	92.7	99.4	93.2	4.7
843.2	51.8	49.4	48.3	58.1	50.1	47.8	47.4	45.2	47.2	49.6	50.4	49.3	3.5
844.2	32.5	43.4	37.7	35.5	36.2	38.5	37.3	33.4	38.3	37.1	39.6	37.7	2.7
845.2	11.9	24.1	30.4	30.9	25.4	24.7	25.2	27.3	28.3	24.6	24.9	26.6	2.5
846.2	105.3	96.9	98.5	93.6	101.0	105.6	102.9	108.7	100.5	104.1	96.7	100.9	4.6
847.2	53.0	47.9	46.9	48.7	51.6	51.3	56.2	53.1	52.2	49.6	49.7	50.7	2.7
848.2	32.4	27.1	31.7	32.8	32.4	29.3	28.9	34.4	30.1	31.4	27.5	30.6	2.4
849.2	11.9	10.2	9.9	13.6	8.9	10.8	13.8	9.0	11.8	11.1	11.8	11.1	1.7

4.5.5.3 *MS Analysis of Mixture of 3,4-C_5 and 3,4-C_5-d_4 (1:1) after Operation over two Biased Cycles*

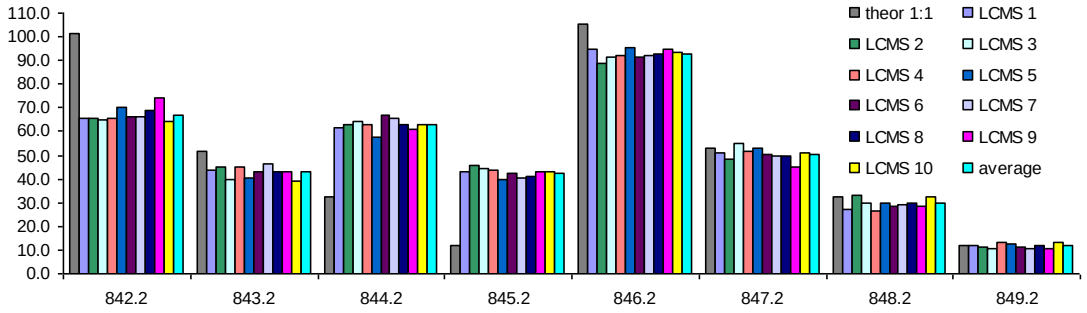

Figure 4.11. *Chart of theoretical, found, and average isotopic distributions of the operated mixture (biased) of* 3,4-***C_5*** *and* 3,4-***C_5***-d_4 *(1:1) after biased operation (conditions I and III). For each of the ten measurements the sum over all 8 abundances (m/z 842.2 to m/z 849.2) was normalised to a value of 400.*

Table 4.8. *Isotopic distributions for operated mixture (biased) and statistical analysis. Theor: theoretical isotopic distribution; Mean: average of LCMS 1 to 10; Stddev.: standard deviation. The theoretical isotopic distribution was calculated as a 1:1 sum of the expected individual distributions for the d_0- and the d_4-labelled compounds (assuming no loss of processivity). As a result of the normalisation, which is necessary for the comparison of the results before and after operation, the sum of columns 2 to 12 is 400.*

m/z	Theor	LCMS 1	LCMS 2	LCMS 3	LCMS 4	LCMS 5	LCMS 6	LCMS 7	LCMS 8	LCMS 9	LCMS 10	Mean	Std.dev.
842.2	101.1	65.7	65.7	64.7	65.6	69.9	65.9	66.2	68.9	74.2	64.3	67.1	3.0
843.2	51.8	44.0	44.9	39.5	44.7	40.7	43.1	46.6	43.4	43.0	39.1	42.9	2.4
844.2	32.5	61.9	63.1	64.1	62.7	57.9	67.2	65.3	62.7	60.8	63.1	62.9	2.5
845.2	11.9	42.7	45.5	44.5	43.6	39.5	42.5	40.7	41.0	43.3	43.3	42.7	1.8
846.2	105.3	95.1	88.7	91.5	91.8	95.7	91.2	92.0	92.7	95.1	93.8	92.7	2.2
847.2	53.0	51.0	48.4	54.8	51.7	53.3	50.5	49.9	49.6	44.9	51.1	50.5	2.7
848.2	32.4	27.4	32.8	29.9	26.7	30.1	28.4	29.1	30.0	28.4	32.5	29.5	2.0
849.2	11.9	12.1	10.9	10.9	13.1	12.9	11.1	10.4	11.9	10.3	12.9	11.6	1.1

4.5.5.4 *Interpretation of the MS Data for Non-Biased Operation*

To assess the degree of processivity loss, we needed to quantitatively compare the average isotopic distributions that were obtained before (section 4.5.5.1, Figure 4.9 and Table 4.6) and after (section 4.5.5.2, Figure 4.10 and Table 4.7) operation. Figure 4.12 shows a direct comparison of the experimentally obtained average distributions before (grey) and after (blue) operation. It was shown in Scheme 4.5 and Scheme 4.6 that loss of processivity would result in formation of d_2-labelled species, which have the highest isotopic abundance at m/z 844.2. When comparing the grey and blue bar at m/z 844.2 it becomes clear that after operation, m/z 844.2 shows a significant increase (by x = 6.3, Figure 4.12). Figure 4.12 furthermore shows the isotopic distribution that would be expected if complete statistical scrambling occurred (yellow bars). It was calculated as a 1:2:1 sum of the isotopic distributions of *3,4*-$\mathbf{C_5}$, *3,4*-$\mathbf{C_5}$-d_2 and *3,4*-$\mathbf{C_5}$-d_4 and was, in the same way as the other two data series, normalised to 400.

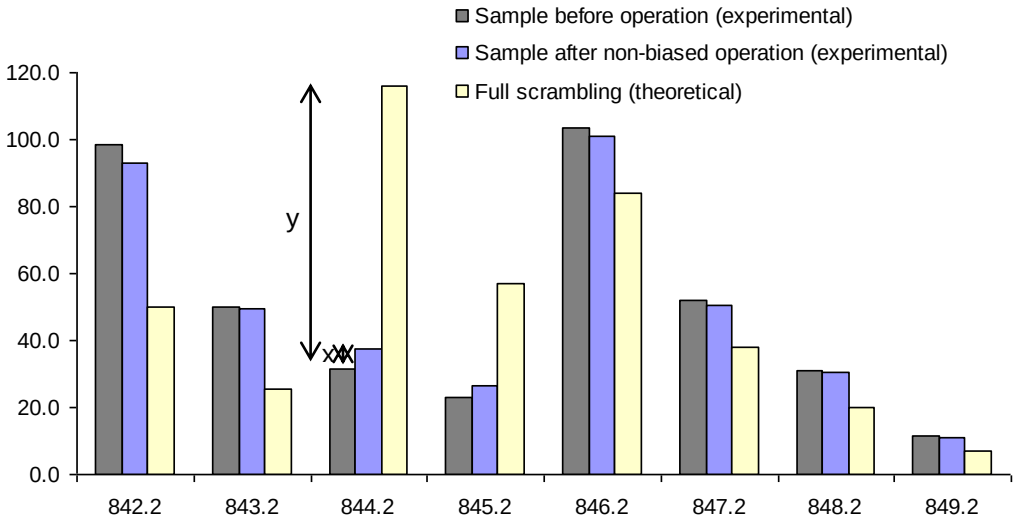

Figure 4.12. *Chart of mean observed isotopic distribution of sample before operation (grey) and sample after non-biased operation (blue), compared to theoretical distribution for full statistical scrambling (yellow). For all three data series the sum over all 8 abundances (m/z 842.2 to m/z 849.2) was normalised to a value of 400.*

We will now consider two extreme cases in order to explain our calculation of the degree of processivity loss. In the first case the blue bar (after operation) would have the exact same height as the grey bar (before) and we would conclude that the loss of processivity is 0%; in all molecules the walker moieties would still be connected to the same track. In the other extreme we would find that the blue bar is equal in height to the yellow bar, from which we would conclude that processivity loss is 100%, full statistical scrambling would have occurred. To assess results that lie in between these

extreme cases we simply have to divide difference value “x” by difference value “y” (shown in Figure 4.12), which gives the fraction of molecules in which the walker moiety is no longer connected to the original track. Table 4.9, which sums up the key conclusions from this study, shows that this value is 7.4%. Since this relative loss of processivity in our experiment has occurred over four steps, division by four gives an average loss of processivity during one operational step of 1.9%.

Table 4.9. *Summary of the key deductions drawn from the experimental data. The first three values can be read from Figure 4.12, Table 4.6 and Table 4.7. The processivity loss of 7.4% was calculated as x/y*100, with x = 37.7-31.4 and y = 116.0-31.4. Note that this procedure is only accurate due to the normalisation of all three isotopic distributions. The processivity loss during one step results from division of 7.4% by 4. The exponential function for processivity decay describes the level of processivity* p *in the system after* n *steps, where* p_0 *is the level of processivity to start with (typically:* p_0*=1). The mean step number is calculated from the exponential function by equation (ii) in Fig. S6 and gives the number of steps after which in 50% of the molecules the walker moiety is no longer connected to the original track.*

m/z	Before operation (expt.)	After operation (expt.)	Full scrambling (theor.)	Processivity loss in % (x/y)	Processivity loss during one step (in %)	Function for processivity decay (p; n = steps)	Mean step number
844.2	31.4	37.7	116.0	7.4	1.9	$p = p_0^{(1-0.019)n} = p_0^{0.981n}$	37

The level of processivity of the system, or in other words the fraction of molecules in which the walker moiety is still connected to its original track, can now be described by an exponential function (equation and graph shown in Figure 4.13). The exponential decay gives a mean step number of 37 at which a molecule loses its processivity, which corresponds to an average run length along a hypothetical infinite track of approximately 26 nm. This average run length was calculated by multiplication of the mean step number with half the length of the repeat unit of our molecular track (1.4 nm). The length of the repeat unit was determined by means of molecular modeling at the B3LYP/cc-pVDZ level of density functional theory (see Chapter III).

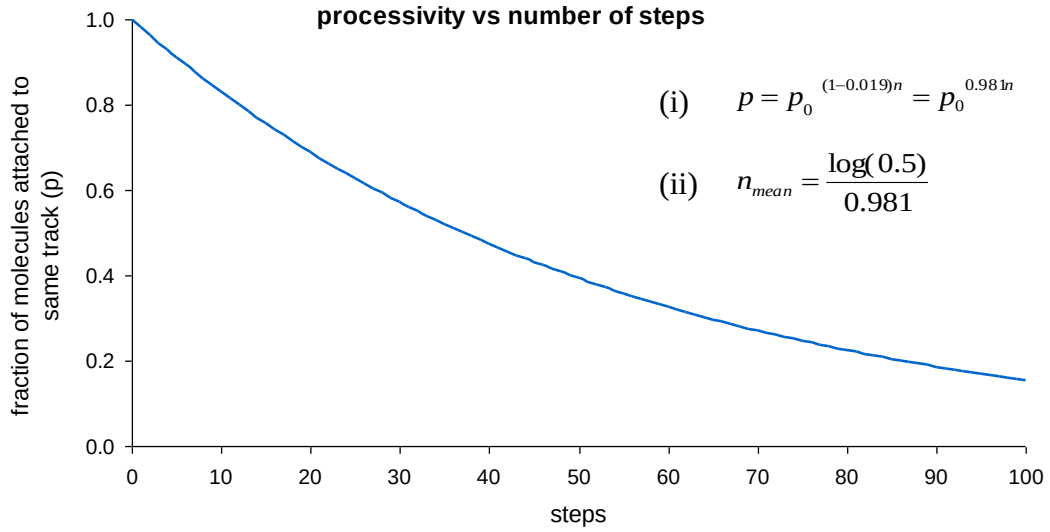

Figure 4.13. *Decay of processivity as described by the exponential function (i). p = fraction of molecules attached to same track; p_0 = initial fraction of molecules connected to original track (in the graph p_0 = 1.0); n = number of steps. Mean step number n_{mean} was calculated according to equation (ii).*

4.5.5.5 Interpretation of the MS Data for Biased Operation

The data obtained after two biased experimental cycles (presented in section 4.5.5.3) was analysed in the same way as outlined above for the non-biased experiment. Table 4.10 and Figure 4.14 show the results.

Table 4.10. *Summary of the key deductions drawn from the experimental data. The first three values can be read from Figure 4.12, Table 4.6 and Table 4.8. The processivity loss in % was calculated as x/y*100, with x = 62.9-31.4 and y = 116.0-31.4. Note that this procedure is only accurate due to the normalisation of all three isotopic distributions. The processivity loss during one step results from division of the previous value by 4. The exponential function for processivity decay describes the level of processivity in the system* p *after* n *steps, where* p_0 *is the level of processivity to start with (typically:* p_0*=1). The mean step number is calculated from the exponential function (in column 7) and gives the number of steps after which in 50% of the molecules the walker moiety is no longer connected to the original track.*

m/z	Before operation (expt.)	After operation (expt.)	Full scrambling (theor.)	Processivity loss in % (x/y)	Processivity loss during one step (in %)	Function for processivity decay (p; n = steps)	Mean step number
844.2	31.4	62.9	116.0	37.2	9.3	$p = p_0^{(1-0.093)n} = p_0^{0.907n}$	7

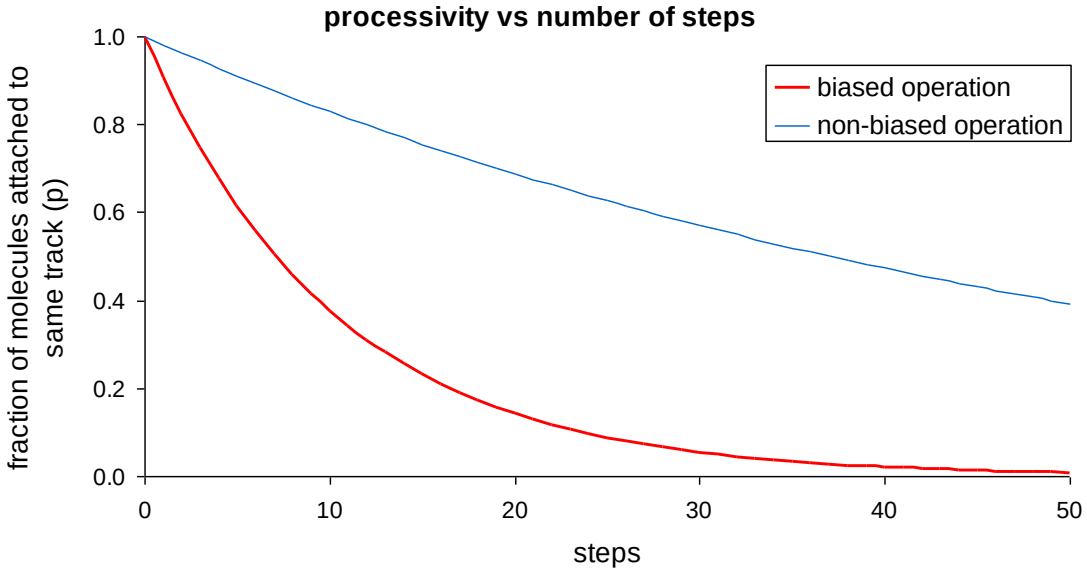

Figure 4.14. *Processivity vs. number of steps during non-biased (blue line) and biased operation (red line).*

From Figure 4.14 it becomes clear that the two modes of operation differ significantly in their degree of processivity. While the mean step number for non-biased operation is 37, the mean step number for biased operation is 7. This means that after 7 steps half of the walker moieties are no longer connected to their original track.

We can explain this rather high loss of processivity during biased operation by the higher amount of side products and oligomers that are occurring when the disulfide exchange reactions are carried out under kinetic, instead of under thermodynamic control. Side products (pathway c in Scheme 4.6) and oligomers (pathway b in Scheme 4.6) can lead to d_2-labelled products in the subsequent TFA catalyzed step. Indeed, we have found that after the first operational step (conditions II or III) no d_2 species were formed under both biased and non-biased conditions. It was only after the second operational step (condition I: TFA) that we detected a small increase of d_2-species in the non-biased experiment and a more pronounced increase in the biased experiment.

4.5.6 Absorbance Coefficients ε

The absorbance coefficients of compounds *1,2*-**C5**, *2,3*-**C5**, *3,4*-**C5**, and *1,4*-**C5** have been determined as previously described.[15] Table 4.11 shows the obtained ε values.

Table 4.11. *Relative and absolute absorbance coefficients ε of positional isomers 1,2-**C5**, 2,3-**C5**, 3,4-**C5**, and 1,4-**C5**. Wavelength: 290 nm; solvent: CH_2Cl_2; estimated error margin: 2-5%.*

Isomer	Relative ε	Absolute ε (10^3 cm^2mol^{-1})
1,2-**C5**	1.08	16300
2,3-**C5**	1.29	19500
3,4-**C5**	1.24	18700
1,4-**C5**	1.00	15100

The set of relative absorbance coefficients (second column in Table 4.11) was used to calculate molar isomer ratios from the integration of HPLC traces (UV detection at 290 nm).

In theory, it would have been possible to apply the same approach to the isomers of the compound series **C2**, **C3**, **C4** and **C8**. In practice, however, this would have been very difficult to achieve and would have led to ε values with a much higher experimental error than 5%. The first reason for this is that for **C2**, **C3**, **C4**, and **C8** only the *3,4* isomer has been synthesised (for **C5** the *1,2* isomer was prepared as well). As a consequence isomers *2,3*, *1,4* and *1,2* would have had to be prepared by "walking" experiments (the *1,2* isomer even in two steps) and subsequent isolation by preparative HPLC. The second reason is that, only a very small quantity of isomers *2,3*-**C3** and *2,3*-**C4** would have been accessible, due to the presence of significant ring strain.

We thus decided to use the set of relative absorbance coefficients that we determined for **C5** (Table 4.11) for **C3**, **C4** and **C8** as well (no ε values were required for the discussion of the results of **C2**), since the UV spectra of the positional isomers appear to be largely independent of the length of the spacer chain in the walker moiety (spectra recorded with diode array detector; spectral comparison of corresponding compounds generally gave >99% similarity[54]). To illustrate this, Figures 4.10 to 4.12 show a superimposition of the UV spectra of *3,4*-**C3**, 3,*4*-**C4** and *3,4*-**C8** each with *3,4*-**C5**.

We are aware that, particularly for the most strained **C3** system, there is a certain difference in the spectra, which will have an impact on the relative ratios given in this

paper. We are taking this into account, however, by giving a rather conservative ± 3% error margin for the isomeric ratios (as compared to ± 2% for $\mathbf{C_5}$). Furthermore we would like to add that, if this approach was seriously flawed, the data for the evolution of the isomeric mixtures would necessarily be inconsistent, which is not the case. Furthermore, the main conclusions that we draw in the main text could as well be drawn from non-ε-corrected HPLC data.

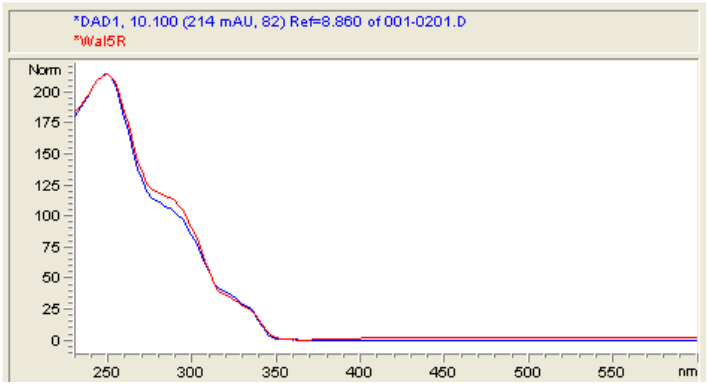

Figure 4.15. *Superimposition of the UV spectra of 3,4-$\mathbf{C_5}$ (red) and 3,4-$\mathbf{C_3}$ (blue).*

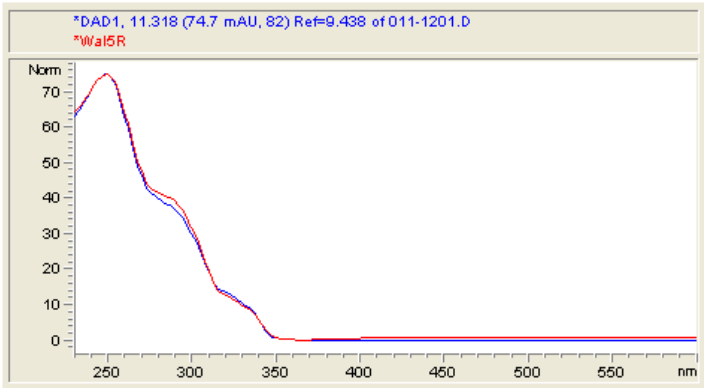

Figure 4.16. *Superimposition of the UV spectra of 3,4-$\mathbf{C_5}$ (red) and 3,4-$\mathbf{C_4}$ (blue).*

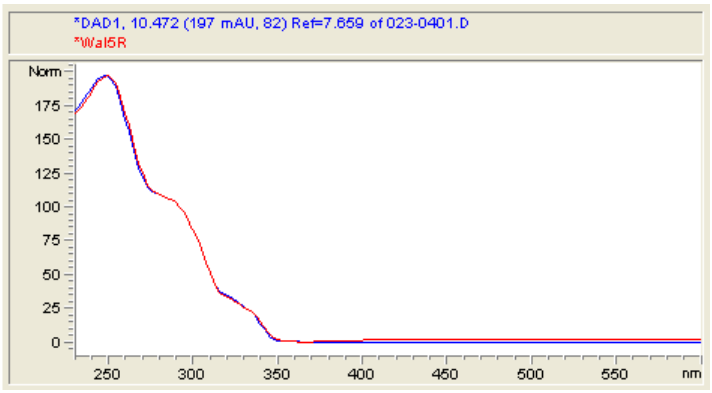

Figure 4.17. *Superimposition of the UV spectra of 3,4-$\mathbf{C_5}$ (red) and 3,4-$\mathbf{C_8}$ (blue).*

4.5.7 Extrapolation of Results for C_3, C_4 and C_8 System

4.5.7.1 C_3 Extrapolation

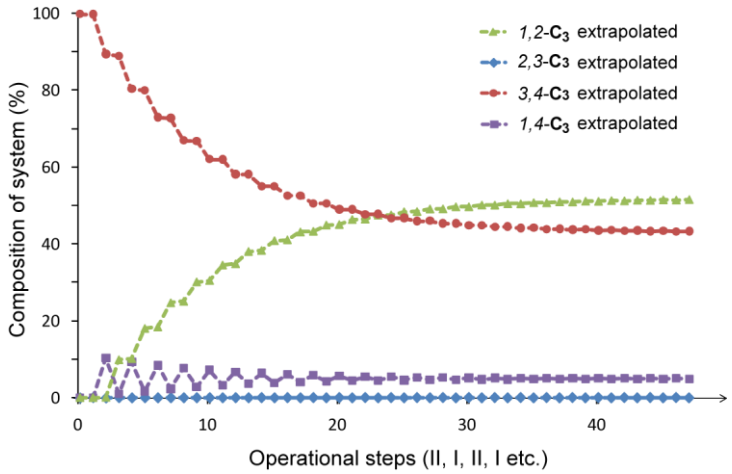

Figure 4.18. *Calculated composition of the* ***C₃*** *system vs. number of steps. Non-biased operation starting from 100%* 3,4-***C₃*** *by oscillation of conditions II and I. Calculation is based on the ratios that were determined by HPLC for the equilibria between two individual isomers. In particular, those equilibrium ratios were:* 3,4-***C₃***/1,4-***C₃*** *= 90:10;* 3,4-***C₃***/2,3-***C₃*** *= ~99:1;* 1,4-***C₃***/1,2-***C₃*** *= 9:91;* 2,3-***C₃***/1,2-***C₃*** *= ~1:99 (results were reproducible within ±2%; estimated error margin due to unconventional ε correction: ±3%).*

Conclusions: the relatively high ground state energy of *2,3*-**C₃** has two consequences: (i) when in equilibrium with another isomer (*1,2*-**C₃** or *3,4*-**C₃**), the HPLC peaks belonging to *2,3*-**C₃** were very close to the (lower) detection limit, implying that for this calculation we had to make the rough assumption that 1% of *2,3*-**C₃** is present. (ii) The convergence towards the thermodynamic minimum requires a large amount of operational steps (approx. 40).

The fact that the four experimentally determined ratios between the positional isomers (see caption Fig. S11) led to convergence of the theoretical data towards a stable steady state, strongly indicates that they form a consistent set that accurately represents the relative energies of the four isomers. If, for example, in one of our extrapolation calculations, we randomly changed one of the four ratios, the graphs did no longer converge, but fluctuate. As a consequence, these calculations serve two purposes: (i) they verify the accuracy of the experimentally obtained ratios, as well as the quality of the ε correction and (ii) they allow calculation of the steady state composition, which, in the case of the **C₃** and **C₄** system, would require 30 and 15 steps, respectively, and which would therefore be too laborious to establish experimentally.

4.5.7.2 C4 Extrapolation

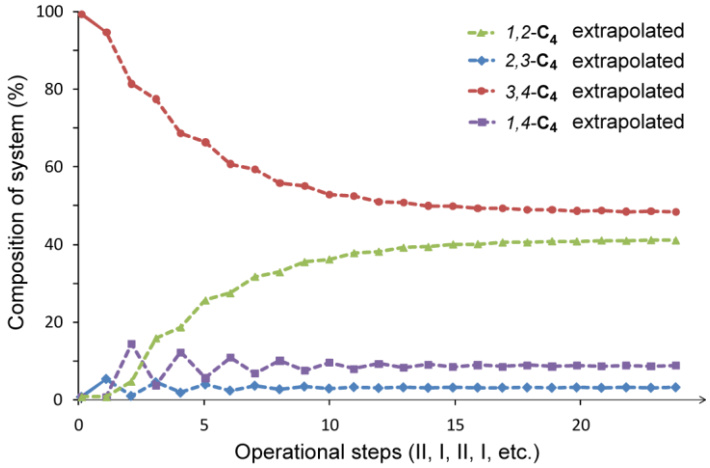

Figure 4.19. *Calculated composition of the* C_4 *system vs. number of steps. Non-biased operation starting from 100%* 3,4-C_4 *by oscillation of conditions II and I. Calculation is based on the ratios that were determined by HPLC for the equilibria between two individual isomers. In particular, those equilibrium ratios were:* 3,4-C_4/1,4-C_4 *= 85:15;* 3,4-C_4/2,3-C_4 *= 95:5;* 1,4-C_4/1,2-C_4 *= 16:84;* 2,3-C_4/1,2-C_4 *= 6:94 (results were reproducible within ±2%; estimated error margin due to unconventional ε correction: ±3%).*

Conclusions: alike the C_3 system, convergence of the C_4 system towards the thermodynamic minimum requires a rather large amount of operational steps (approx. 15). The convergence indicates that the experimental data are reliable (on the same grounds as given for the C_3 system in section 4.5.7.1).

4.5.7.3 C_8 Extrapolation

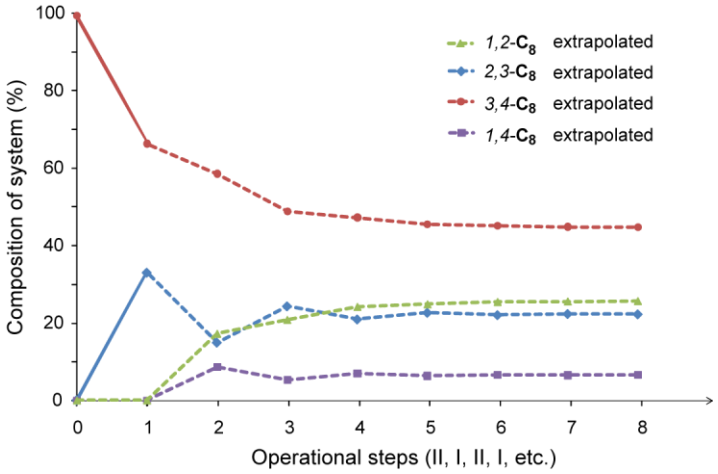

Figure 4.20. *Calculated composition of the* C_8 *system vs. number of steps. Non-biased operation starting from 100%* 3,4-C_8 *by oscillation of conditions II and I. Calculation is based on the ratios that were determined by HPLC for the equilibria between two individual isomers. In particular, those equilibrium ratios were:* 3,4-C_8/1,4-C_8 *= 87:13;* 3,4-C_8/2,3-C_8 *= 67:33;* 1,4-C_8/1,2-C_8 *= 20:80;* 2,3-C_8/1,2-C_8 *= 46:54 (results were reproducible within ±2%; estimated error margin due to unconventional ε correction: ±3%).*

Conclusions: in respect to its convergence towards the thermodynamic minimum, the **C8** system behaves similar to **C5**.

4.5.8 Synthetic Schemes

4.5.8.1 Synthesis of Walker Moieties

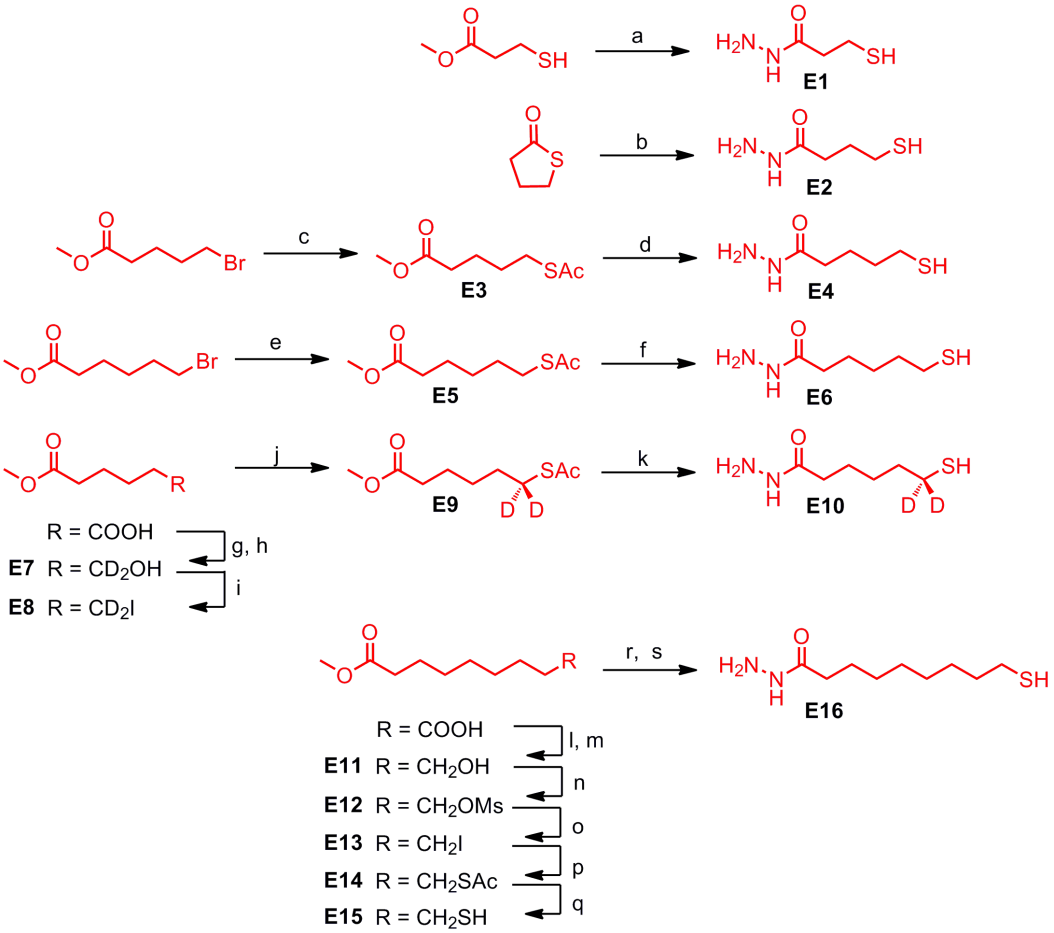

Scheme 4.7. *Reaction conditions: a) $N_2H_4 \cdot H_2O$, MeOH, RT, 16 h, 50%; b) $N_2H_4 \cdot H_2O$, MeOH, RT, 30 min, 74%; c) KSAc, DMF, RT, 15 min, 98%; d) $N_2H_4 \cdot H_2O$, MeOH, reflux, 16 h, 49%; e) KSAc, DMF, RT, 1 h, 85%; f) $N_2H_4 \cdot H_2O$, MeOH, reflux, 16 h, 44%; g) EtOCOCl, NEt_3, THF, RT, 1 h; h) $NaBD_4$, H_2O, RT, 1 h, 68%; i) PPh_3, I_2, imidazole, -10 °C, 12 h, 88%; j) KSAc, DMF, RT, 2 h, 85%; k) $N_2H_4 \cdot H_2O$, MeOH, reflux, 12 h, 76%. l) $ClCO_2Et$, NEt_3, THF, –5°C, 1 h; m) $NaBH_4$, H_2O, 0°C, 1 h, 81% (2 steps); n) NEt_3, CH_2Cl_2, MsCl, 0°C, 1 h, 77%; o) NaI, acetone, RT, 12 h, 85%; p) KSAc, DMF, RT, 1 h, 90%; q) NaOMe, MeOH, RT, 3 h, 79%; r) $N_2H_4 \cdot H_2O$, EtOH, reflux, 16 h; s) DTT, DMF, RT, 16 h, 58% (two-step).*

Note: compounds **E5** and **E6** are included in this overview for completion only - the full synthetic procedures are described in the experimental section of Chapter III (see compounds **E2** and **E3** there).

4.5.8.2 *Synthesis of Non-Deuterated Walker-Track Conjugates 3,4-C_n*

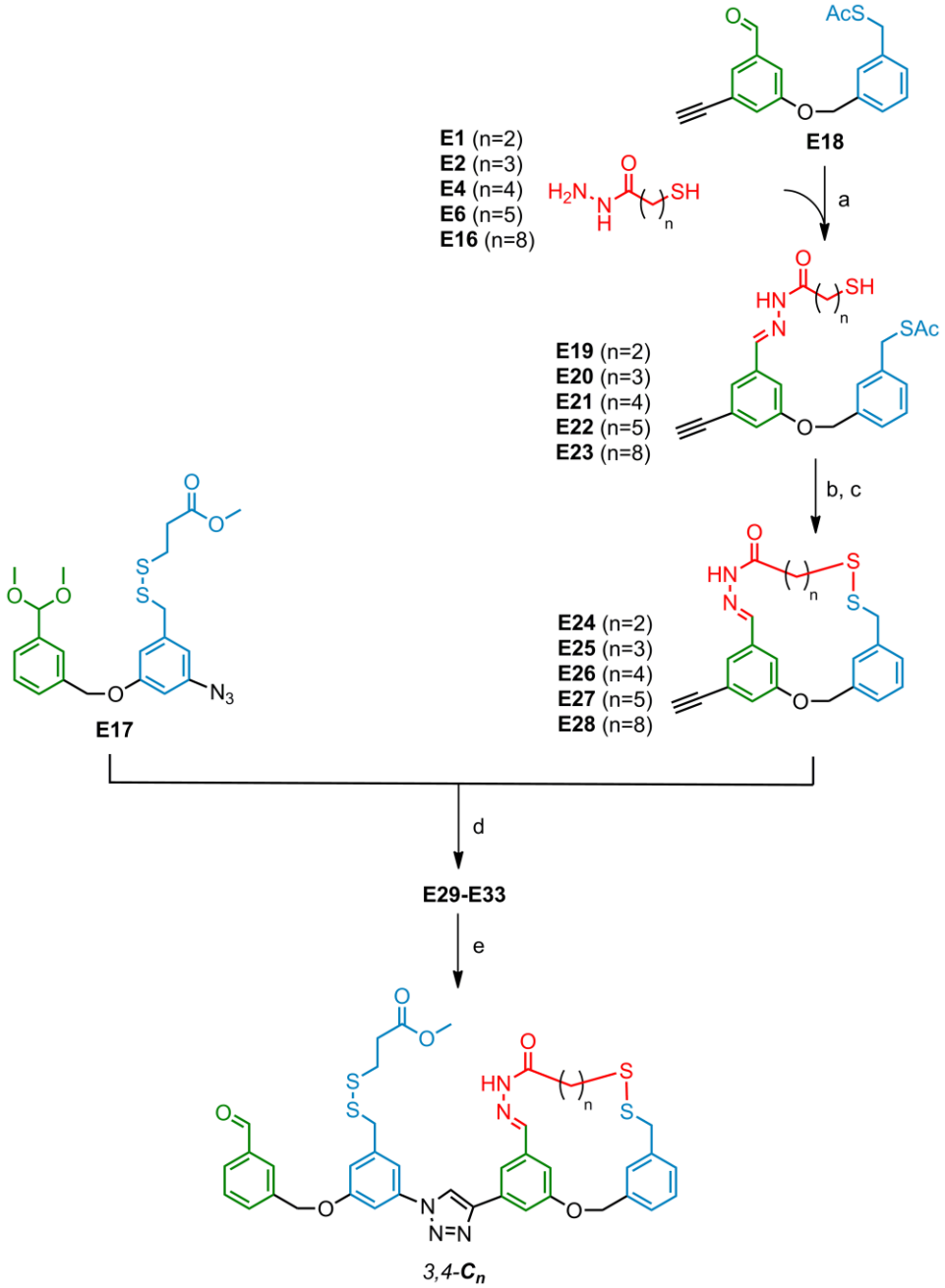

Scheme 4.8. *Reaction conditions: a) AcOH (cat.), MeOH, RT, 2 h, 73–86%; b) NaOMe, MeOH, RT, 2h; c) I_2, KI, CH_2Cl_2, RT, 5 min, 32–59% (two-step); d) $Cu(MeCN)_4PF_6$, tris[(1-benzyl-1*H*-1,2,3-triazol-4-yl)methyl]amine (TBTA), CH_2Cl_2/THF/MeOH, RT, 16 h, 76–97%; e) TFA, CH_2Cl_2, RT, (quant.).*

Note: compounds **E22**, **E27**, **E32** and *3,4*-$\mathbf{C_5}$ are included in this overview for completion only. The full synthetic procedures are described in the experimental section of Chapter III (see compounds **E19, E20, E21** and *3,4*-$\mathbf{C_5}$ there).

4.5.8.3 *Synthesis of Deuterated Walker-Track Conjugate 3,4-1-d_4*

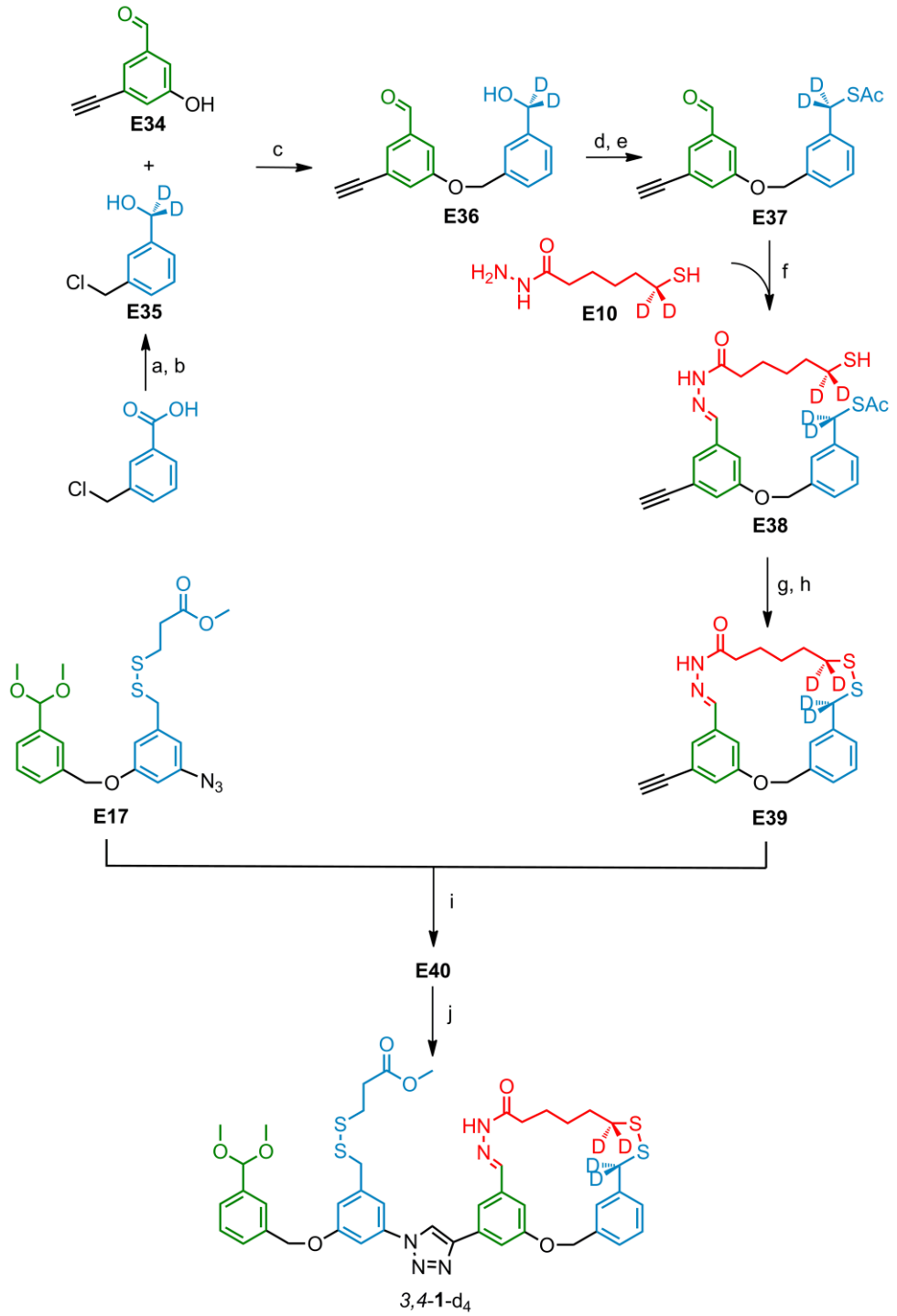

Scheme 4.9. *a) EtOCOCl, NEt_3, THF, 5 °C, 30 min; b) $NaBD_4$, H_2O, RT, 16 h, 85% (two-step); c) NaH, DMF, RT, 48 h, 84%; d) MsCl, NEt_3, CH_2Cl_2, RT, 12 h, 74%; e) KSAc, DMF, RT, 3 h, 77%. f) AcOH (cat.), MeOH, RT → 10 °C, 3 h, 86%; g) NaOMe, MeOH/CH_2Cl_2, RT, 2 h; h) I_2, KI, CH_2Cl_2, RT, 15 min, 35% (two-step); i) $Cu(MeCN)_4PF_6$, TBTA, CH_2Cl_2/THF/MeOH, RT, 16 h, 88%; j) TFA, DCM, RT (quant.).*

4.5.9 Synthesis and Characterisation Data

3-Mercaptopropanehydrazide

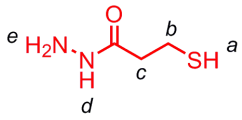

E1

Synthesised according to a modified literature procedure.[53] Under N_2, methyl 3-mercaptopropionate (10 g, 83 mmol, 1.0 equiv.) was added dropwise to a solution of hydrazine monohydrate (10 g, 200 mmol, 2.4 equiv.) in MeOH (30 mL). The reaction mixture was stirred over night at room temperature. Evaporation of the solvent, followed by flash column chromatography (SiO_2, Et_2O/MeOH 8:2) gave **E1** (4.99 g, 50%) as a colourless oil. ^{1}H NMR (400 MHz, $CDCl_3$): δ = 6.81 (bs, 1H, H_d), 3.93 (bs, 2H, H_e), 2.84 (dt, *J* = 8.4 Hz, 6.4 Hz, 2H, H_b), 2.50 (t, *J* = 6.7 Hz, 2H, H_c), 1.61 (t, *J* = 8.4 Hz, 1H, H_a).

4-Mercaptobutanehydrazide

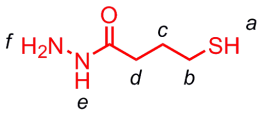

E2

Under N_2, γ-thiobutyrolactone (4.73 g, 46 mmol, 1.0 equiv.) was added dropwise to a solution of hydrazine monohydrate (4.4 g, 68 mmol, 1.5 equiv.) in MeOH (10 mL). The reaction mixture was stirred for 30 min at room temperature. Removal of the solvent under reduced pressure and flash column chromatography (SiO_2, Et_2O/MeOH 5:1) gave **E2** (4.60 g, 74%) as a colourless oil. ^{1}H NMR (400 MHz, $CDCl_3$): δ = 6.90 (bs, 1H, H_e), 3.90 (bs, 2H, H_f), 2.58 (q, *J* = 7.2 Hz, 2H, H_b), 2.30 (t, *J* = 7.3 Hz, 2H, H_d), 1.95 (quint., *J* = 7.2 Hz, 2H, H_c), 1.33 (t, *J* = 8.0 Hz, 1H, H_a); ^{13}C NMR (100 MHz, $CDCl_3$): δ = 173.02, 32.48, 29.22, 24.07; HRMS (ESI$^+$): *m/z* = 135.0588 $[M+H]^+$ (calcd. 135.0587 for $C_4H_{11}ON_2S$).

Methyl 5-(acetylthio)pentanoate

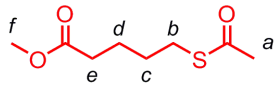

E3

A solution of KSAc (9.02 g, 78.99 mmol, 1.5 equiv.) in DMF (20 mL) was added to a solution of methyl 5-bromopentanoate (9.99 g, 51.20 mmol, 1.0 equiv.) in DMF (30 mL). The reaction was stirred for 15 min at room temperature and the solvent was removed under reduced pressure. The residue was dissolved in Et_2O (50 mL) and saturated NH_4Cl (30 mL) was added. The layers were separated and the aqueous layer was extracted with Et_2O (4 × 30 mL). The combined organic layers were washed with brine and dried over $MgSO_4$. Removal of the solvent under reduced pressure gave **E3** (9.48 g, 98%) as a yellowish oil. ^{1}H NMR (400 MHz, $CDCl_3$): δ = 3.68 (s, 3H, H_f), 2.89 (t, J = 7.1 Hz, 2H, H_b), 2.34 (m, 5H, H_a, H_e), 1.66 (m, 4H, H_c, H_d); ^{13}C NMR (100 MHz, $CDCl_3$): δ = 195.84, 173.73, 162.53, 51.58, 36.49, 33.46, 31.43, 30.64, 28.99, 28.63, 23.96; HRMS (ESI$^+$): m/z = 191.0732 $[M+H]^+$ (calcd. 191.0736 for $C_8H_{15}O_3S$).

5-Mercaptopentanehydrazide

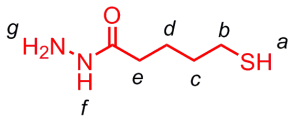

E4

Under N_2, hydrazine monohydrate (8.09 g, 162 mmol, 5 equiv.) was added dropwise to a solution of methyl 5-(acetylthio)pentanoate (4.02 g, 21.13 mmol, 1.0 equiv.) in MeOH (30 mL). The reaction was refluxed over night and the solvent was removed under reduced pressure. Purification by flash column chromatography (SiO_2, Et_2O/MeOH 8:1) gave **E4** (1.51 g, 49%) as a colourless solid. M.p. 43 °C - 45 °C; ^{1}H NMR (400 MHz, $CDCl_3$): δ = 6.80 (bs, 1H, H_f), 3.92 (bs, 2H, H_g), 2.56 (q, J = 7.3 Hz, 2H H_b), 2.19 (t, J = 7.4 Hz, 2H, H_e), 1.72 (m, 4H, H_c, H_d), 1.39 (t, J = 7.8 Hz, 1H, H_a); ^{13}C NMR (100 MHz, $CDCl_3$): δ = 173.39, 33.84, 33.42, 24.23, 24.11; HRMS (ESI$^+$): m/z = 149.0741 $[M+H]^+$ (calcd. 149.0743 for $C_5H_{13}ON_2S$).

Methyl 6-hydroxyhexanoate-d_2

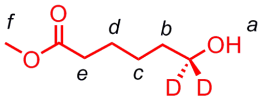

E7

Under N_2, adipic acid monomethyl ester (4.0 g, 24.99 mmol, 1.0 equiv.) and NEt_3 (2.78 g, 3.83 mL, 27.49 mmol, 1.1 equiv.) were dissolved in THF (40 mL). At 0 °C a solution of ethyl chloroformate (2.98 g, 2.63 mL, 27.49 mmol, 1.1 equiv.) in THF (25 mL) was added dropwise. The mixture was stirred for 1 h at room temperature. The mixture was filtrated and the residue washed with THF (25 mL). The combined filtrates were added to a solution of $NaBD_4$ (2.09 mg, 49.98 mmol) in H_2O (50 mL) at 0 °C. After stirring for 1 h at room temperature, the mixture was acidified with 3 M HCl (aq.) to pH 3–4 and extracted with Et_2O (2 × 75 mL). The combined organic layers were washed with 0.5 N NaOH (2 × 50 mL), H_2O (50 mL) and brine (50 mL), dried ($MgSO_4$) and concentrated under reduced pressure to yield a colourless oil. Purification by flash column chromatography (SiO_2, cyclohexane/Et_2O 2:1) gave **E7** (2.52 g, 68%) as a colourless oil. ^{1}H NMR (400 MHz, $CDCl_3$): δ = 3.66 (s, 3H), 2.32 (dd, *J* = 7.5, 7.4 Hz, 2H), 1.69 – 1.62 (m, 2H), 2.32 (dd, *J* = 7.9, 7.2 Hz, 2H), 1.43 – 1.35 (m, 3H); ^{13}C NMR (100 MHz, $CDCl_3$): δ = 174.18, 51.52, 33.97, 32.09, 25.23, 24.63; HRMS (ESI): *m*/*z* = 149.1139 $[M+H]^+$ (calcd. 149.1147 for $C_7H_{13}D_2O_3$).

Methyl 6-iodohexanoate-d_2

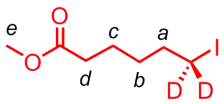

E8

Synthesised according to a modified literature procedure.[26a] Under N_2, PPh_3 (4.81 g, 18.35 mmol, 1.6 equiv.) was dissolved in CH_2Cl_2 (20 mL). At –10 °C I_2 (4.37 g, 17.21 mmol, 1.5 equiv.) was added and the mixture was stirred at -10 °C for 15 min. Imidazole (1.56 g, 22.98 mmol, 2.0 equiv.) was added in CH_2Cl_2 (20 mL) and the mixture was stirred for another 15 min at –10 °C. A solution of methyl 6-hydroxyhexanoate-d_2 (**E7**, 1.70 g, 11.47 mmol, 1.0 equiv.) in CH_2Cl_2 was added dropwise and the mixture was stirred over night during which time it was allowed to warm to room temperature. The solvents were removed under reduced pressure and the mixture was subjected to flash column chromatography (SiO_2, cyclohexane/EtO_2

16:1 → 12:1) to yield **E8** (2.61 g, 88%) as a colourless oil. ^{1}H NMR (400 MHz, $CDCl_3$): δ = 3.67 (s, 3H), 2.32 (dd, *J* = 7.5, 7.4 Hz, 2H), 1.82 (dd, *J* = 7.5, 7.4 Hz, 2H), 1.68 – 1.60 (m, 2H), 1.46 – 1.39 (m, 2H); ^{13}C NMR (100 MHz, $CDCl_3$): δ = 173.89, 51.55, 33.79, 32.84, 30.95, 23.84; HRMS (ESI): *m*/*z* = 276.0430 $[M+NH_4]^+$ (calcd. 276.0430 for $C_7H_{15}D_2INO_2$).

Methyl 6-acetylsulfanylhexanoate-d$_2$

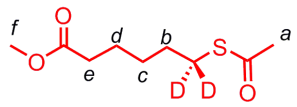

E9

Methyl 6-iodohexanoate-d_2 **E8** (2.60 g, 10.1 mmol, 1.0 equiv.) was dissolved in DMF (15 mL). KSAc (1.44 g, 12.63 mmol, 1.3 equiv.) was added and the mixture was stirred for 2 h at room temperature. The solvent was removed under reduced pressure and the residue dissolved in Et_2O (30 mL) and NH_4Cl (sat., 30 mL). The layers were separated and the aqueous layer was extracted with Et_2O (30 mL). The combined organic layers were washed with 1 M HCl (30 mL), H_2O (30 mL) and brine (30 mL), dried ($MgSO_4$) and concentrated under reduced pressure to yield a residue that was purified by flash column chromatography (SiO_2, hexane/Et_2O 8:1) to give **E9** (1.77 g, 8.58 mmol, 85%) as a brownish oil. ^{1}H NMR (400 MHz, $CDCl_3$): δ = 3.65 (s, 3H), 2.31 (s, 3H), 2.31 (dd, *J* = 7.5, 7.4 Hz, 2H), 1.66 – 1.59 (m, 2H), 1.56 (dd, *J* = 7.9, 7.4 Hz, 2H), 1.42 – 1.34 (m, 2H); ^{13}C NMR (100 MHz, $CDCl_3$): δ = 195.90, 173.98, 51.50, 33.84, 30.65, 28.97, 28.16, 24.41; HRMS (ESI): *m*/*z* = 224.1285 $[M+NH_4]^+$ (calcd. 224.1289 for $C_9H_{18}D_2NO_3S$).

6-Mercaptohexanehydrazide-d$_2$

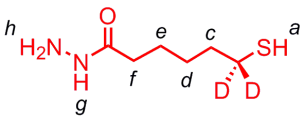

E10

Methyl 6-acetylsulfanylhexanoate-d_2 **E9** (0.80 g, 3.88 mmol, 1.0 equiv.) was dissolved in hydrazine monohydrate (970 mg, 0.95 mL, 19.39 mmol, 5.0 equiv.) and MeOH (25 mL). The mixture was refluxed over night. The solvents were removed under reduced pressure and the residue was purified by flash column chromatography (SiO_2, Et_2O/MeOH 12:1 → 8:1, R_f = 0.45) to yield **E10** (485 mg, 76%) as a colourless powder. ^{1}H NMR (400 MHz, $CDCl_3$): δ = 6.89 (bs, 1H, H_g), 3.90 (bs, 2H, H_h), 2.16 (dd, *J* = 7.6, 7.4 Hz, 2H, H_f), 1.69 – 1.55 (m, 4H, H_c, H_e), 1.45 – 1.37 (m, 2H, H_d), 1.30 (s, 1H); ^{13}C NMR

(100 MHz, $CDCl_3$): δ = 173.64, 34.28, 33.28, 27.78, 24.84; HRMS (ESI): m/z = 165.10306 $[M+H]^+$ (calcd 165.1022 for $C_6H_{13}D_2N_2OS$).

Methyl 9-hydroxynonanoate

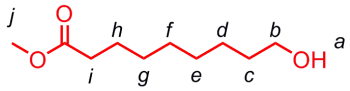

E11

Synthesised according to a literature procedure.[26b] ^1H NMR (400 MHz, $CDCl_3$): δ = 3.66 (s, 3H, H_j), 3.66 - 3.57 (m, 2H, H_b), 2.30 (t, J = 7.5 Hz, 2H, H_i), 1.68 – 1.49 (m, 4H, $H_{c,h}$), 1.41 – 1.25 (m, 9H, $H_{a,d-g}$).

Methyl 9-mesylnonanoate

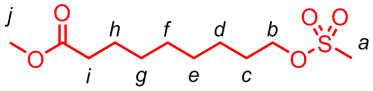

E12

Synthesised according to a literature procedure.[26c] ^1H NMR (400 MHz, $CDCl_3$): δ = 4.22 (t, J = 6.6 Hz, 2H, H_b), 3.67 (s, 3H, H_j), 3.00 (s, 3H, H_a), 2.30 (t, J = 7.5 Hz, 2H, H_i), 1.78 – 1.71 (m, 2H, H_c), 1.65 – 1.59 (m, 2H, H_h), 1.45 – 1.25 (m, 8H, H_{d-g}).

Methyl 9-iodononanoate

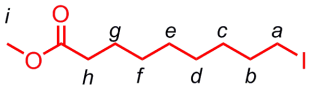

E13

Synthesised according to a literature procedure.[26c] ^1H NMR (400 MHz, $CDCl_3$): δ = 3.67 (s, 3H, H_i), 3.18 (t, J = 7.0 Hz, 2H, H_a), 2.30 (t, J = 7.5 Hz, 2H, H_h), 1.85 – 1.77 (m, 2H, H_b), 1.65 – 1.58 (m, 2H, H_g), 1.43 - 1.25 (m, 8H, H_{c-f}).

Methyl 9-acetylsulfanylnonanoate

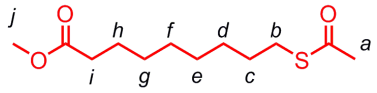

E14

Synthesised according to a literature procedure.[26c] ^{1}H NMR (400 MHz, $CDCl_3$): δ = 3.66 (s, 3H, H_j), 2.85 (t, *J* = 7.3 Hz, 2H, H_b), 2.32 (s, 3H, H_a), 2.30 (t, *J* = 7.5 Hz, 2H, H_i), 1.64 – 1.51 (m, 4H, $H_{c,h}$), 1.38 – 1.23 (m, 8H, $H_{d\text{-}g}$).

Methyl 9-mercaptononanoate

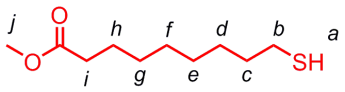

E15

Synthesised according to a literature procedure.[26c] ^{1}H NMR (400 MHz, $CDCl_3$): δ = 3.66 (s, 3H, H_j), 2.51 (dt, *J* = 7.5, 7.2 Hz, 2H, H_b), 2.30 (t, *J* = 7.5 Hz, 2H, H_i), 1.66 – 1.56 (m, 4H, $H_{c,h}$), 1.41 – 1.27 (m, 9H, $H_{a,d\text{-}g}$).

9-Mercaptononanehydrazide

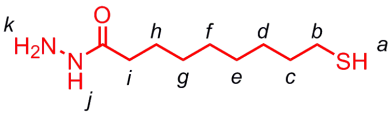

E16

a) **E15** (500 mg, 2.29 mmol) was added dropwise to a solution of hydrazine monohydrate (600 mg, 11.44 mmol) in EtOH (15 mL). This mixture was refluxed over night. Removal of the solvent gave a mixture of product **E16** and the corresponding disulfide, which was used directly for the subsequent reduction step. Characterisation data for the disulfide: M.p. 75 °C. ^{1}H NMR (400 MHz, DMSO-d_6): δ = 8.92 (bs, 1H, H_i), 4.08 (bs, 2H, H_j), 2.45 (t, *J* = 7.1, Hz, 2H, H_a), 1.98 (t, *J* = 7.4 Hz, 2H, H_h), 1.53 – 1.41 (m, 4H, $H_{b,g}$), 1.35 - 1.17 (m, 8H, $H_{c\text{-}f}$).

b) The crude mixture of disulfide and thiol **E16** was dissolved in dry DMF (10 mL) and dithiothreitol (160 mg, 1.03 mmol, 1.1 equiv.) was added. The mixture was stirred at room temperature over night and the bulk of the solvent was removed under reduced pressure. Flash column chromatography (SiO_2, Et_2O/MeOH 9:1) gave **E16** (254 mg, 58% two-step yield) as a colourless solid. M.p. 70 °C. ^{1}H NMR (400 MHz, $CDCl_3$):

δ = 6.65 (bs, 1H, H_j), 3.89 (bs, 2H, H_k), 2.52 (q, *J* = 7.4 Hz, 2H H_b), 2.14 (t, *J* = 7.6 Hz, 2H, H_i), 1.67-1.56 (m, 4H, H_c, H_h), 1.40-1.27 (m, 5H, H_a, H_g, H_f, H_e, H_d); ^{13}C NMR (100 MHz, $CDCl_3$): δ = 173.91, 34.51, 33.92, 29.14, 29.12, 28.83, 28.23, 25.40, 24.59; HRMS (ESI$^+$): *m*/*z* = 205.1372 $[M+H]^+$ (calcd. 205.1369 for $C_9H_{21}ON_2S$).

General synthetic procedure for compounds E19-E23

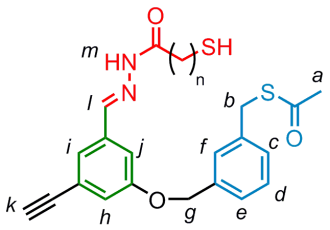

E19 (n=2), **E20** (n=3), **E21** (n=4), **E22** (n=5),[15] **E23** (n=8)

Under N_2, **S14** (900 mg, 2.76 mmol, 1.0 equiv.) was dissolved in dry MeOH (c ≈ 0.1 M). After addition of 3-5 drops of acetic acid, a solution of the walker hydrazide (**E1**/**E2**/**E4**/**E6**/**E16**) (1.1-1.7 equiv.) in dry MeOH (c ≈ 0.5 M) was added dropwise. The reaction was monitored by TLC (SiO_2, *n*-hexane/EtOAc 3:2). After 2 h the reaction was usually complete and the solvent was removed under reduced pressure. Purification by flash column chromatography (SiO_2, *n*-hexane/EtOAc 3:2) gave the pure compounds.

E19 (n=2): (*E*)-*S*-3-((3-ethynyl-5-((2-(3-mercaptopropanoyl)hydrazono)-methyl)phenoxy)methyl)benzyl ethanethioate. **E18** (900 mg, 2.76 mmol, 1.0 equiv.) and **E1** (500 mg, 4.76 mmol, 1.7 equiv.) gave **E19** (954 mg, 81%) as a colourless solid. ^{1}H NMR (400 MHz, $CDCl_3$): δ = 8.92 (s, 1H, H_m), 7.64 (s, 1H, H_l), 7.36–7.26 (m, 6H, H_{Ar}), 7.12 (dd, *J* = 2.4 Hz, 1.3 Hz, 1H, H_{Ar}), 5.06 (s, 2H, H_g), 4.14 (s, 2H, H_b), 3.10 (t, *J* = 6.8 Hz, 2H, H_n), 3.10 (s, 1H, H_k), 2.90 (dt, *J* = 8.3 Hz, 6.8 Hz, 2H, H_o), 2.36 (s, 3H, H_a), 1.74 (t, *J* = 8.3 Hz, 1H, H_p); ^{13}C NMR (100 MHz, $CDCl_3$); δ = 195.09, 173.49, 158.74, 142.42, 138.25, 136.64, 135.12, 129.05, 128.76, 127.97, 126.50, 124.03, 123.76, 119.74, 113.95, 82.71, 77.93, 70.06, 36.90, 33.28, 30.38, 19.35; HRMS (ESI$^+$): *m*/*z* = 427.1145 $[M+H]^+$ (calcd. 427.1145 for $C_{22}H_{23}N_2O_3S_2$).

E20 (n=3): (*E*)-*S*-3-((3-ethynyl-5-((2-(4-mercaptobutanoyl)hydrazono)methyl)-phenoxy)methyl)benzyl ethanethioate. **E18** (164 mg, 0.51 mmol, 1.0 equiv.) and **E2** (75 mg, 0.56 mmol, 1.1 equiv.) gave **E20** (180 mg, 81%) as a yellowish powder. M.p. 110 °C; ^{1}H NMR (400 MHz, $CDCl_3$): *δ* = 8.74 (s, 1 H, H_m), 7.62 (s, 1 H, H_l), 7.37-7.27 (m, 6 H, H_{Ar}), 7.12 (dd, *J* = 2.31 Hz, 1.27 Hz, 1 H, H_{Ar}), 5.06 (s, 2 H, H_g), 4.14 (s, 2 H, H_b), 3.11

(s, 1 H, H_k), 2.89 (t, J = 7.3 Hz, 2 H, H_n), 2.67 (dt, J = 7.4 Hz, 2 H, H_p), 2.36 (s, 3 H, H_a), 2.05 (tt, J = 7.1 Hz, 2 H, H_o), 1.74 (m, 2 H, H_p), 1.39 (t, J = 8.1 Hz, 1 H, H_q); ^{13}C NMR (100 MHz, $CDCl_3$): δ = 195.05, 174.90, 158.75, 141.96, 138.25, 136.65, 135.22, 129.04, 128.75, 127.97, 126.49 (2 C), 124.03, 123.74, 119.70, 113.86, 82.73, 70.05, 33.28, 31.15, 30.37, 28.74, 24.30; HRMS (ESI$^+$): m/z = 441.1300 $[M+H]^+$ (calcd. 441.1301 for $C_{23}H_{25}N_2O_3S_2$).

E21 (n=4): (*E*)-*S*-3-((3-ethynyl-5-((2-(5-mercaptopentanoyl)hydrazono)methyl)-phenoxy)methyl)benzyl ethanethioate. **E18** (140 mg, 0.43 mmol, 1.0 equiv.) and **E4** (70 mg, 0.48 mmol, 1.1 equiv.) gave **E21** (143 mg, 73%) as a yellowish powder. M.p. 109 °C; ^{1}H NMR (400 MHz, $CDCl_3$): δ = 8.80 (s, 1 H, H_m), 7.63 (s, 1 H, H_l), 7.39-7.27 (m, 6 H, H_{Ar}), 7.12 (dd, J = 2.3 Hz, 1.2 Hz, 1 H, H_{Ar}), 5.06 (s, 2 H, H_g), 4.14 (s, 2 H, H_b), 3.11 (s, 1 H, H_k), 2.77 (t, J = 7.3 Hz, 2 H, H_n), 2.60 (dt, J = 7.3 Hz, 2 H, H_q), 2.36 (s, 3 H, H_a), 1.84 (m, 2 H, H_o), 1.74 (m, 2 H, H_p), 1.39 (t, J = 7.9 Hz, 1 H, H_r); ^{13}C NMR (100 MHz, $CDCl_3$): δ = 195.05, 175.51, 158.75, 141.95, 138.25, 136.65, 135.31, 129.04, 128.76, 127.98, 126.51 (2 C), 123.97, 123.72, 119.56, 113.95, 82.76, 70.05, 33.61, 33.28, 32.05, 30.37, 24.39, 23.26; HRMS (ESI$^+$): m/z = 455.1459 $[M+H]^+$ (calcd. 455.1458 for $C_{24}H_{27}N_2O_3S_2$).

E23 (n=8): (*E*)-*S*-3-((3-ethynyl-5-((2-(9-mercaptononanoyl)hydrazono)methyl)-phenoxy)methyl)benzyl ethanethioate. **E18** (256 mg, 0.79 mmol, 1.0 equiv.) and **E16** (243 mg, 1.19 mmol, 1.5 equiv.) gave **E23** (343 mg, 85%) as a colourless, waxy solid. M.p. 93 °C. ^{1}H NMR (400 MHz, $CDCl_3$): δ = 8.78 (s, 1H, H_m), 7.62 (s, 1H, H_l), 7.36 – 7.28 (m, 6H, H_{Ar}), 7.11 (s, J = 2.3 Hz, 1.3 Hz, 1H, H_{Ar}), 5.05 (s, 2H, H_g), 4.16 (s, 2H, H_b), 3.11 (s, 1H, H_k), 2.74 (t, J = 7.6 Hz, 2H, H_n), 2.50 (q, J = 7.4 Hz, 2H, H_u), 2.36 (s, 3H, H_a), 1.72 (quint., J = 7.4 Hz, 2H, H_o), 1.59 (quint., J = 7.2 Hz, 2H, H_t), 1.37 (m, 8H, H_s, H_r, H_q, H_p), 1.31 (t, J = 7.7 Hz, 1H, H_v); ^{13}C NMR (100 MHz, $CDCl_3$): δ = 195.02, 176.11, 158.70, 141.70, 138.22, 136.62, 135.39, 129.01, 128.74, 127.98, 126.50, 126.43, 123.86, 123.66, 119.41, 114.01, 82.78, 70.02, 34.00, 33.25 (2C), 32.60, 30.33, 29.24, 28.90, 28.30, 24.61 (2C); HRMS (ESI$^+$): m/z = 511.2084 $[M+H]^+$ (calcd. 511.2084 for $C_{28}H_{35}N_2O_3S_2$).

General synthetic procedure for compounds E24-S28

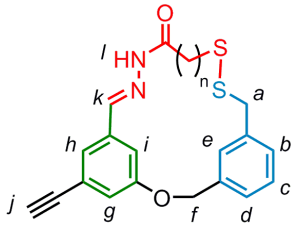

E24 (n=2), **E25** (n=3), **E26** (n=4), **E27** (n=5),[15] **E28** (n=8)

Under N_2, thioacetate (**E19-E23**) (1.0 equiv.) was dissolved in a 1:1 mixture of MeOH and CH_2Cl_2 (c ≈ 0.05 M). A solution of NaOMe (1.5 - 2.0 equiv.) in MeOH (c ≈ 0.5 M) was added. After 2 h of stirring at room temperature, the mixture was diluted with CH_2Cl_2 (c ≈ 0.005 M) and KI (0.2 equiv.) was added. A solution of I_2 (1.0 equiv.) in CH_2Cl_2 (c ≈ 0.1 M) was added dropwise until the brown colour persisted. Na_2SO_3 was added to reduce the excess of I_2 and, when decolourisation was complete, stirring was continued for 15 min. H_2O was added and the phases were separated. The H_2O layer was extracted another time with CH_2Cl_2. The combined organic layers were washed with brine and dried ($MgSO_4$). Removal of the solvents under reduced pressure and purification by flash column chromatography (SiO_2, CH_2Cl_2/EtOAc 9:1) gave the pure compounds.

E24 (n=2): (*E*)-20-Ethynyl-2-oxa-10,11-dithia-15,16-diaza-tricyclo[16.3.1.1^{4,8}]tricosa-1(21),4(23),5,7,16, 18(22),19-heptaen-14-one. **E19** (570 mg, 1.34 mmol, 1.0 equiv.) gave **E24** (300 mg, 59%) as a colourless solid. ^{1}H NMR (400 MHz, DMSO-d_6): δ = 11.66 (s, 1H, H_l), 8.07 (s, 1H, H_k), 7.83 (s, 1H, H_{Ar}), 7.70 (s, 1H, H_{Ar}), 7.55–7.43 (m, 3H, H_{Ar}), 7.32 (d, *J* = 2.4 Hz, 1H, H_{Ar}), 7.30 (s, 1H, H_{Ar}), 5.54 (s, 2H, H_f), 4.48 (s, 1H, H_j), 4.19 (s, 2H, H_a), 3.39 (dd, *J* = 6.8 Hz, 6.5 Hz, 2H, H_m or H_l), 3.24 (dd, *J* = 6.8 Hz, 6.5 Hz, 2H, H_m or H_l); ^{13}C NMR (100 MHz, DMSO-d_6); δ = 172.44, 157.79, 141.06, 137.12, 136.97, 136.01, 129.68, 129.07, 128.28, 126.06, 125.34, 123.25, 122.40, 108.37, 82.40, 79.14, 69.02, 41.04, 31.14, 30.31; HRMS (ESI$^+$): *m/z* = 383.0881 [M+H]$^+$ (calcd. 383.0882 for $C_{20}H_{19}N_2O_2S_2$).

E25 (n=3): (*E*)-21-Ethynyl-2-oxa-10,11-dithia-16,17-diaza-tricyclo[17.3.1.1^{4,8}]-tetracosa-1(23),4,6,8(24),17, 19,21-heptaen-15-one. **E20** (178 mg, 0.40 mmol, 1.0 equiv.) gave **E25** (71 mg, 44%) as a colourless solid. M.p. 210 °C; ^{1}H NMR (400 MHz, $CDCl_3$): δ = 9.40 (s, 1H, H_l), 7.61 (s, 1H, H_k), 7.36-7.28 (m, 4H, H_{Ar}), 7.28-7.25 (m, 1H, H_{Ar}) 7.23 (m, 1H, H_{Ar}), 7.04 (s, 1H, H_{Ar}), 5.30 (s, 2H, H_f), 3.86 (s, 2H, H_a), 3.10 (s, 1H, H_j) 2.69 (t, *J* = 7.4 Hz, 2H, H_o), 2.31 (t, *J* = 7.4 Hz, 2H, H_m), 1.97 (quint., *J* = 7.4 Hz, 2H, H_n); ^{13}C NMR

(100 MHz, $CDCl_3$): δ = 175.07, 159.07, 141.81, 138.51, 137.72, 135.21, 128.94, 128.35, 126.28, 126.23, 124.70, 123.94, 123.70, 108.83, 82.35, 70.43, 43.27, 38.32, 32.03, 25.34; HRMS (EI^+): m/z = 396.0962 $[M]^+$ (calcd. 396.0961 for $C_{21}H_{20}N_2O_2S_2$).

E26 (n=4): (*E*)-22-Ethynyl-2-oxa-10,11-dithia-17,18-diaza-tricyclo[19.3.1.1^{4,8}]-pentacosa-1(24),4,6,8(25),18, 20,22-heptaen-16-one. **E21** (135 mg, 0.30 mmol, 1.0 equiv.) gave **E26** (57 mg, 47%) as a colourless solid. M.p. 210 °C; ^{1}H NMR (400 MHz, $CDCl_3$): δ = 9.54 (s, 1H, H_l), 7.65 (s, 1H, H_k), 7.36 (m, 1H, H_{Ar}), 7.33 (bs, 1H, H_{Ar}), 7.29-7.23 (m, 3H, H_{Ar}), 7.15 (d, 1H, H_{Ar}), 7.07 (bs, 1H, H_{Ar}), 5.33 (s, 2H, H_f), 3.86 (s, 2H, H_a), 3.11 (s, 1H, H_j), 2.56 (m, 2H, H_p), 2.26 (m, 2H, H_m), 1.68 (m, 2H, H_n), 1.59 (m, 2H, H_o); ^{13}C NMR (100 MHz, $CDCl_3$): δ = 175.74, 159.11, 141.83, 138.63, 137.42, 135.30, 128.85 (2C), 128.20, 126.54, 126.44, 124.45, 123.84, 123.41, 108.90, 82.35, 69.85, 44.01, 37.84, 32.47, 29.06, 24.38; HRMS (EI^+): m/z = 410.1116 $[M]^+$ (calcd. 410.1117 for $C_{22}H_{22}N_2O_2S_2$).

E28 (n=8): (*E*)-26-Ethynyl-2-oxa-10,11-dithia-21,22-diaza-tricyclo[22.3.1.1^{4,8}]-nonacosa-1(27),4(29),5,7,22, 24(28),25-heptaen-20-one. **E23** (316 mg, 0.62 mmol, 1.0 equiv.) gave **E28** (95 mg, 32%) as a colourless solid. ^{1}H NMR (400 MHz, $CDCl_3$): δ = 8.64 (s, 1H, H_l), 7.65 (s, 1H, H_k), 7.55 (s, 1H, H_{Ar}), 7.43 (s, 1H, H_{Ar}), 7.39-7.33 (m, 3H, H_{Ar}), 7.17 (m, 1H, H_{Ar}), 7.12 (s, 1H, H_{Ar}), 5.03 (s, 2H, H_f), 3.68 (s, 2H, H_a), 3.11 (s, 1H, H_j), 2.72 (m, 2H, H_m), 2.06 (t, J = 7.1 Hz, 2H, H_t), 1.77 (m, 2H, H_n), 1.40-12.21 (m, 10H, H_s, H_r, H_q, H_p, H_o); ^{13}C NMR (100 MHz, $CDCl_3$): δ = 176.78, 158.86, 141.63, 138.51, 135.89, 135.53, 129.61, 129.56, 128.97, 127.29, 125.99, 123.72, 120.77, 109.92, 82.56, 70.10, 43.01, 38.96, 33.00, 30.29, 29.31, 29.25, 28.71, 28.66, 28.58, 25.32; HRMS (ESI^+): m/z = 467.1821 $[M+H]^+$ (calcd. 467.1821 for $C_{26}H_{31}N_2O_2S_2$).

General synthetic procedure for compounds E29-E33

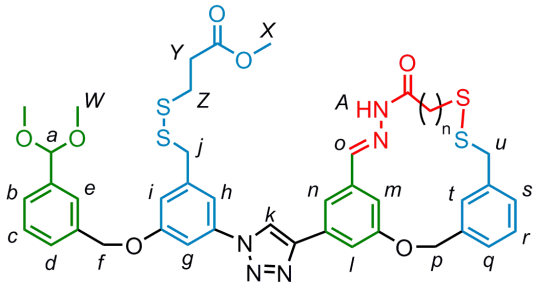

E29 (n=2), **E30** (n=3), **E31** (n=4), **E32** (n=5),[15] **E33** (n=8)

Under N_2, **E17** (1.0 equiv.) was dissolved in DCM (c ≈ 0.02 M) and a solution of the alkyne (**E24**-**E28**) (1.0-1.2 equiv.) in THF (c ≈ 0.02 M) was added. Tris[(1-benzyl-1*H*-1,2,3-triazol-4-yl)methyl]amine (TBTA, 0.1 equiv.) and $Cu(MeCN)_4PF_6$ (0.1 equiv.) were dissolved in MeOH (c ≈ 0.01 M) and the solution was added to the reaction mixture, which was allowed to stir over night at room temperature. Removal of the solvents under reduced pressure followed by flash column chromatography (SiO_2, DCM/EtOAc 85:15 → 7:3) gave the pure compounds.

E29 (n=2): **E17** (37 mg, 80 µmol, 1.0 equiv.) and **E24** (31 mg, 80 µmol, 1.0 equiv.) gave **E29** (61 mg, 90%) as a colourless solid. M.p. 142 °C. ^{1}H NMR (400 MHz, $CDCl_3$): δ = 9.45 (s, 1H, H_A), 8.25 (s, 1H, H_k), 7.74 (s, 1H, H_o), 7.57 (m, 2H, H_e, H_l), 7.52 (s, 1H, H_n), 7.49 (s, 1H, H_t), 7.42 (m, 5H, H_b, H_c, H_d, H_g, H_q), 7.34 (s, 1H, H_h), 7.30 (m, 2H, H_r, H_m), 7.20 (d, *J* = 7.3 Hz, H_s), 7.03 (s, 1H, H_i), 5.43 (s, 1H, H_a), 5.32 (s, 2H, H_p), 5.17 (s, 2H, H_f), 3.92 (s, 2H, H_u or H_j), 3.90 (s, 2H, H_u or H_j), 3.67 (s, 3H, H_X), 3.35 (s, 6H, H_W), 3.17 (t, *J* = 7.4 Hz, 2H, H_B), 2.95 (t, *J* = 7.4 Hz, 2H, H_C), 2.77 (m, 2H, H_Z), 2.67 (m, 2H, H_Y); ^{13}C NMR (100 MHz, $CDCl_3$): δ = 173.26, 172.15, 159.78, 159.01, 147.27, 142.87, 140.77, 138.70, 137.90, 137.63, 137.40, 136.11, 135.32, 132.00, 129.34, 128.68, 128.39, 128.25, 127.66, 126.74, 126.19, 125.91, 120.32, 118.10, 117.62, 116.18, 113.44, 108.48, 106.37, 102.88, 70.41, 70.23, 52.82, 51.96, 43.38, 43.03, 33.88, 33.03, 32.46, 32.12; HRMS (ESI$^+$): *m*/*z* = 800.1705 [M-acetal+H]$^+$ (calcd. 800.1699 for $C_{39}H_{38}N_5O_6S_4$).

E30 (n=3): **E17** (29 mg, 63 µmol, 1.0 equiv.) and **E25** (30 mg, 76 µmol, 1.2 equiv.) gave **E30** (41 mg, 76%) as a colourless solid. M.p. 138 °C; ^{1}H NMR (400 MHz, $CDCl_3$): δ = 9.84 (s, 1H, H_A), 8.28 (s, 1H, H_k), 7.82 (s, 1H, H_o),7.61-7.60 (m, 1H, H_l), 7.57 (bs, 1H, H_b), 7.54 (bs, 1H, H_n), 7.46-7.38 (m, 4H, H_g, H_c, H_d, H_e), 7.37 (bs, 1H, H_t), 7.35 (bs, 1H, H_h), 7.33-7.26 (m, 4H, H_q, H_r, H_s, H_m), 7.03 (bs, 1H, H_i), 5.43 (s, 1H, H_a), 5.34 (s, 2H, H_p), 5.17 (s, 2H, H_f), 3.92 (s, 2H, H_j), 3.86 (s, 2H, H_u), 3.67 (s, 3H, H_X), 3.35 (s, 6H, H_W), 2.77 (t, *J* = 6.7 Hz,

2H, H_Y or H_Z), 2.69 (m, 4H, H_B, H_Y or H_Z), 2.32 (t, J = 7.4 Hz, 2H, H_D), 1.98 (t, J = 7.4 Hz, 2H, H_C); ^{13}C NMR (100 MHz, $CDCl_3$): δ = 175.46, 172.15, 159.77, 159.75, 147.29, 142.86, 140.78, 138.69, 138.49, 138.02, 137.90, 136.13, 135.93, 131.94, 128.89, 128.67, 128.31, 127.67, 126.72, 126.29, 125.91, 124.73, 120.53, 118.16, 117.37, 116.19, 113.43, 108.01, 106.28, 102.89, 70.47, 70.39, 52.82, 51.96, 43.30, 43.02, 38.37, 33.87, 33.02, 32.14, 25.52; HRMS (ESI$^+$): m/z = 877.2539 $[M+NH_4]^+$ (calcd. 877.2540 for $C_{42}H_{49}N_6O_7S_4$).

E31 (n=4): **E17** (28 mg, 61 µmol, 1.0 equiv.) and **E26** (30 mg, 73 µmol, 1.2 equiv.) gave **E31** (43 mg, 80%) as a colourless solid. M.p. 210 °C; ^{1}H NMR (400 MHz, $CDCl_3$): δ = 9.87 (s, 1H, H_A), 8.29 (s, 1H, H_k), 7.84 (s, 1H, H_a), 7.63-7.62 (m, 1 H, H_l), 7.57 (s, 2H, H_b, H_n), 7.45-7.41 (m, 4H, H_g, H_c, H_d, H_e), 7.36-7.33 (m, 3H, H_h, H_m, H_t), 7.28-7.26 (m, 2H, H_r, H_s), 7.26-7.20 (m, 1 H, H_q), 7.04 (bs, 1H, H_i), 5.43 (s,1H, H_o),5.39 (s, 2H, H_p), 5.17 (s, 2H, H_f), 3.92 (s, 2H, H_j), 3.86 (s, 2H, H_u), 3.67 (s, 3H, H_X), 3.35 (s, 6H, H_W), 2.77 (t, J = 6.6 Hz, 2H, H_Y or H_Z), 2.67 (t, J = 6.7 Hz, 2H, H_Y or H_Z), 2.58 (m, 2H, H_B), 2.27 (m, 2H, H_E), 1.70 (t, J = 7.3 Hz, 2H, H_C), 1.59 (t, J = 7.2 Hz, 2H, H_D); ^{13}C NMR (100 MHz, $CDCl_3$): δ = 176.05, 172.14, 159.78 (2C), 147.27, 142.84, 140.79, 138.70, 138.59, 137.90, 137.69, 136.12, 135.96, 132.09, 128.84, 128.67, 128.13, 127.66, 126.73, 126.45, 125.91, 124.50, 120.75, 118.20, 116.90, 116.20, 113.43, 107.96, 106.30, 102.88, 70.40, 69.83, 52.82, 51.96, 44.02, 43.02, 37.86, 33.87, 33.02, 32.55, 29.12, 24.50; HRMS (ESI$^+$): m/z = 891.2696 $[M+NH_4]^+$ (calcd. 891.2697 for $C_{43}H_{51}N_6O_7S_4$).

E33 (n=8): **E17** (48 mg, 103 µmol, 1.0 equiv.) and **E28** (58 mg, 124 µmol, 1.2 equiv.) gave **E33** (91 mg, 97%) as a colourless solid. ^{1}H NMR (400 MHz, $CDCl_3$): δ = 8.99 (s, 1H, H_A), 8.26 (s, 1H, H_k), 7.81 (s, 1H, H_o), 7.62-7.54 (m, 4H, H_c, H_l, H_n, H_t), 7.47-7.32 (m, 9H, H_b, H_d, H_e, H_g, H_h, H_m, H_q, H_r, H_s), 7.04 (bs, 1H, H_i), 5.43 (s, 1H, H_a), 5.17 (s, 2H, H_p), 5.13 (s, 2H, H_f), 3.92 (s, 2H, H_j), 3.87 (s, 2H, H_u), 3.66 (s, 3H, H_X), 3.34 (s, 6H, H_W), 2.80-2.72 (m, 4H, H_B, H_Y or H_Z), 2.67 (t, J = 7.7 Hz ,2H, H_Y or H_Z), 2.07 (t, J = 7.0 Hz, 2H, H_I), 1.85-1.75 (m, 2H, H_C), 1.52-1.34 (m, 6H, H_D, H_G, H_H), 1.34-1.16 (m, 4H, H_E, H_F). ^{13}C NMR (100 MHz, $CDCl_3$): δ = 176.76, 172.09, 159.75, 159.59, 147.38, 142.29, 140.75, 138.67, 138.45, 137.87, 136.12, 136.07, 136.06, 132.02, 129.58, 129.53, 128.96, 128.62, 127.61, 127.29, 126.69, 125.86, 120.08, 118.12, 116.16, 114.60, 113.40, 108.80, 106.32, 102.85, 70.37, 70.14, 52.77, 51.90, 43.01 (2C), 38.97, 33.84, 33.07, 33.00, 29.39, 29.33, 28.77, 28.68, 28.63, 25.37; HRMS (ESI$^+$): m/z = 947.3323 $[M+NH_4]^+$ (calcd. 947.3328 for $C_{47}H_{59}N_6O_7S_4$).

Note: Assignment of the ^{1}H NMR signals was accomplished by means of 2D NMR (COSY, ROESY, HMQC, HMBC).

General synthetic procedure for compounds *3,4*-C_n

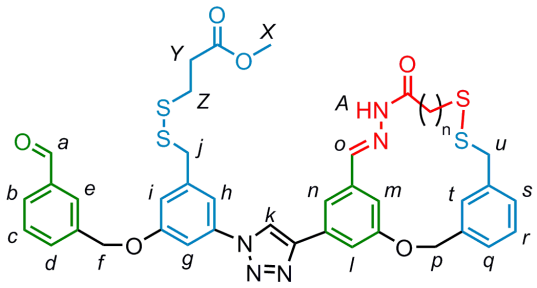

3,4-C_n

The acetal (**E29-E33**) (1.0 equiv.) was dissolved in $CHCl_3$ (c ≈ 0.01 M) and 3 drops of TFA were added. The solution was vigorously stirred for 1 minute before saturated $NaHCO_3$ was added. The layers were separated and the aqueous phase was extracted with $CHCl_3$. The combined organic layers were dried over $MgSO_4$. The pure compounds were obtained as colourless solids in quantitative yield (HPLC). This deprotection procedure was carried out in small batches (1-5 mg of starting material) and the obtained product was used directly for subsequent experiments.

3,4-C_3: ^{1}H NMR (400 MHz, $CDCl_3$): δ = 10.07 (s, 1H, H_a), 9.00 (s, 1H, H_A), 8.29 (s, 1H, H_k), 8.02 (s, 1H, H_e), 7.88 (d, *J* = 7.6 Hz, 1H, H_b), 7.76-7.73 (m, 2H, H_o, H_d), 7.63-7.59 (m, 2H, H_c, H_l), 7.56 (s, 1H, H_n), 7.46 (t, *J* = 2.0 Hz, 1H, H_g), 7.38-7.28 (m, 6H, H_h, H_m, H_q, H_r, H_s, H_t), 7.05 (bs, 1H, H_i), 5.35 (s, 2H, H_p), 5.26 (s, 2H, H_f), 3.94 (s, 2H, H_j), 3.87 (s, 2H, H_u), 3.68 (s, 3H, H_X), 2.78 (t, *J* = 6.7 Hz, 2H, H_Y or H_Z), 2.73 (t, *J* = 7.4 Hz, 2H, H_B), 2.68 (t, *J* = 6.7 Hz, 2H, H_Y or H_Z), 2.35 (t, *J* = 7.4 Hz, 2H, H_D), 2.00 (quint., *J* = 7.4 Hz, 2H, H_C); ^{13}C NMR (100 MHz, $CDCl_3$): δ = 190.99, 174.41, 173.86, 158.72, 158.43, 146.30, 141.29, 139.93, 137.46, 136.94, 136.90, 136.30, 135.74, 134.72, 132.26, 130.89, 128.82, 128.47, 127.91, 127.29, 127.24, 125.29, 123.73, 119.39, 117.07, 116.44, 115.08, 112.62, 107.03, 105.24, 69.43, 68.57, 50.95, 42.25, 41.91, 37.33, 32.84, 32.00, 31.04, 24.33; HRMS (ESI$^+$): *m/z* = 814.1847 $[M+H]^+$ (calcd. 814.1856 for $C_{40}H_{40}N_5O_6S_4$).

3,4-C_4: ^{1}H-NMR (400 MHz, $CDCl_3$): δ = 10.07 (s, 1H, H_a), 8.96 (s, 1H, H_A), 8.30 (s, 1H, H_k), 8.02 (s, 1H, H_e), 7.88 (d, *J* = 7.6 Hz, 1H, H_b), 7.76-7.74 (m, 2H, H_o, H_d), 7.63-7.54 (m, 2H, H_c, H_l), 7.52 (s, 1H, H_n), 7.46 (t, *J* = 2.0 Hz, 1H, H_g), 7.38-7.37 (m, 3H, H_h, H_m, H_t), 7.29-7.26 (m, 2H, H_r, H_q), 7.22-7.20 (m, 1H, H_s), 7.06 (bs, 1H, H_i), 5.40 (s, 2H, H_p), 5.26 (s, 2H, H_f), 3.94 (s, 2H, H_j), 3.87 (s, 2H, H_u), 3.67 (s, 3H, H_X), 2.78 (t, *J* = 6.7 Hz, 2H, H_Y or H_Z), 2.68

(t, J = 6.7 Hz, 2H, H_Y or H_Z), 2.59 (m, 2H, H_B), 2.28 (m, 2H, H_E), 1.70 (quint, J = 7.2 Hz, 2H, H_C), 1.60 (quint, J = 7.3 Hz, 2H, H_D). ^{13}C NMR (100 MHz, $CDCl_3$): δ = 192.01, 175.42, 172.13, 159.82, 159.48, 147.32, 142.27, 140.99, 138.63, 137.98, 137.64, 137.34, 136.78, 135.79, 133.29, 132.08, 129.88, 129.50, 128.86, 128.24, 128.16, 126.43, 124.49, 120.65, 118.14, 117.03, 116.13, 113.66, 108.02, 106.31, 69.85, 69.62, 51.97, 44.04, 42.96, 37.87, 33.88, 33.05, 32.54, 29.09, 24.38; HRMS (ESI$^+$): m/z = 828.2005 $[M+H]^+$ (calcd. 828.2012 for $C_{41}H_{42}N_5O_6S_4$).

3,4-**C_8:** ^{1}H NMR (400 MHz, $CDCl_3$): δ = 10.07 (s, 1H, H_a), 8.90 (s, 1H, H_A), 8.28 (s, 1H, H_k), 8.01 (s, 1H, H_e), 7.88 (d, J = 7. Hz, 1H, H_b), 7.80 (bs, 1H, H_o), 7.74 (d, J = 7.6 Hz, 1H, H_d), 7.62-7.55 (m, 4H, H_c, H_g, H_l, H_n), 7.38-7.37 (m, 6H, H_h, H_m, H_q, H_r, H_s, H_t), 7.05 (bs, 1H, H_i), 5.25 (s, 2H, H_p), 5.13 (s, 2H, H_f), 3.93 (s, 2H, H_j), 3.66 (s, 3H, H_X), 2.79-2.71 (m, 4H, H_B, H_Y or H_Z), 2.67 (t, J = 6.8 Hz, 2H, H_Y or H_Z), 2.07 (t, J = 7.0 Hz, 2H, H_I), 1.85-1.77 (m, 2H, H_C), 1.48-1.36 (m, 6H, H_D, H_G, H_H), 1.35-1.25 (m, 4H, H_E, H_F); ^{13}C NMR (100 MHz, $CDCl_3$): δ = 192.00, 176.22, 172.12, 159.65, 159.47, 147.46, 141.85, 140.98, 138.51, 137.98, 137.33, 136.78, 136.10, 135.97, 133.28, 132.02, 129.88, 129.74, 129.61, 129.50, 129.01, 128.22, 127.31, 120.03, 118.11, 116.12, 114.73, 113.65, 108.87, 106.31, 70.19, 69.61, 51.96, 43.04, 42.96, 39.01, 33.87, 33.05, 29.70, 29.42, 29.34, 28.80, 28.71, 28.66, 25.33; HRMS (ESI$^+$): m/z = 901.2903 $[M+NH_4]^+$ (calcd. 901.2904 for $C_{45}H_{53}N_6O_6S_4$).

3-Chloromethylbenzyl alcohol-d_2

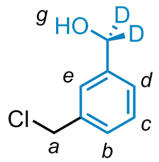

E35

At 5 °C, a solution of ethyl chloroformate (3.19 mL, 32.4 mmol, 1.0 equiv.) in THF (15 mL) was added dropwise to a solution of 3-(chloromethyl)-benzoic acid (5.69 g, 32.4 mmol, 1.0 equiv.) and Et_3N (4.55 mL, 32.4 mmol, 1.0 equiv.) in THF (60 mL). The reaction was allowed to proceed for 30 min at 5 °C and the Et_3NHCl precipitate was filtered off and washed with THF (80 mL). The combined THF phases were added over 30 min to a solution of $NaBD_4$ (3.76 g, 80.9 mmol, 2.5 equiv.) in H_2O (25 mL) at 10 °C. The mixture was stirred over night at room temperature and was acidified with 10% HCl (17 mL). The solution was extracted with Et_2O (3 × 100 mL). The combined organic layers were washed with a solution of 10% NaOH (100 mL) and brine (100 mL), dried

($MgSO_4$), and the solvents removed under reduced pressure to give **E35** (4.35 g, 85%) as a colourless oil. ^{1}H NMR (400 MHz, $CDCl_3$): δ = 7.41-7.31 (m, 4H, H_b, H_c, H_d, H_e), 4.60 (s, 2H, H_a), 1.81 (bs, 1H, H_g); ^{13}C NMR (100 MHz, $CDCl_3$): δ = 128.91, 127.78, 127.06, 126.94, 46.10; HRMS (EI): m/z = 158.0463 $[M]^+$ (calcd. 158.0462 for $C_8H_7D_2ClO$).

3-Ethynyl-5-(3-(hydroxymethyl)benzyloxy)benzaldehyde-d$_2$

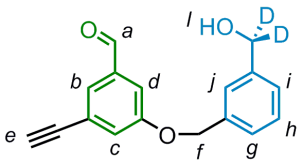

E36

Under N_2, **E34** (1.40 g, 9.58 mmol, 1.0 equiv.) was dissolved in DMF (30 mL). NaH (60% in mineral oil, 372 mg, 9.3 mmol, 0.97 equiv.) was added at 0 °C and the mixture was stirred for 30 min, while the temperature was allowed to rise to room temperature. A solution of **E35** (2.03 g, 12.77 mmol, 1.3 equiv.) in DMF (15 mL) was added dropwise and the mixture was stirred for 48 h at room temperature. The reaction was monitored by TLC (SiO_2, toluene/EtOAc 3:1). 1 M HCl (30 mL) was added and the mixture was extracted with EtOAc (2 × 60 mL). The combined organic layers were washed with 1M HCl (30 mL), H_2O (30 mL) and brine (30 mL), dried ($MgSO_4$) and concentrated under reduced pressure. Purification by flash column chromatography (SiO_2, toluene/EtOAc 10:1 → 4:1) gave **E36** (2.16 g, 84%) as an orange oil. ^{1}H NMR (400 MHz, $CDCl_3$): δ = 9.93 (s, 1H), 7.59 (dd, J = 1.3, 1.3 Hz, 1H), 7.47 – 7.45 (m, 2H), 7.43 – 7.39 (m, 1H), 7.37 – 7.35 (3H), 5.12 (s, 2H), 3.15 (s, 1H), 1.66 (s, broad, 1H); ^{13}C NMR (100 MHz, $CDCl_3$): δ = 191.18, 158.95, 141.32, 137.69, 136.18, 128.91, 127.26, 126.88, 126.73, 126.00, 124.75, 124.24, 114.07, 81.90, 78.73, 70.22; HRMS (ESI): m/z = 286.1403 $[M+NH_4]^+$ (calcd. 286.1407 for $C_{17}H_{16}D_2NO_3$).

***S*-3-((3-Ethynyl-5-formylphenoxy)methyl)benzyl ethanethioate d$_2$**

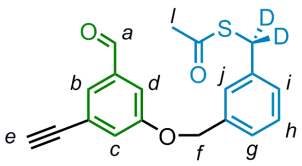

E37

a) At 0 °C, **E36** (2.14 g, 7.98 mmol, 1.0 equiv.) was dissolved in CH_2Cl_2 (20 mL) and Et_3N (5 mL, 35.87 mmol, 4.5 equiv.) was added. After 5 min, MsCl (5 mL, 64.6 mmol,

8.1 equiv.) was added dropwise and the mixture stirred overnight at room temperature. H_2O (50 mL) was added and the layers were partitioned. The aqueous layer was extracted with CH_2Cl_2 (2 × 50 mL). The combined organic phases were washed with brine, dried ($MgSO_4$) and concentrated under reduced pressure. Purification by flash column chromatography (SiO_2, *c*-hexane/CH_2Cl_2 2:1) gave 3-ethynyl-5-(3-(chloromethyl)benzyloxy)benzaldehyde-d_2 (1.70 g, 5.93 mmol, 74%) as a colourless oil. ^{1}H NMR (400 MHz, $CDCl_3$): δ = 9.93 (s), 7.59 (dd, *J* = 1.2 Hz, 1H), 7.48 – 7.45 (m, 2H), 7.40 – 7.37 (m, 3H), 7.35 (dd, *J* = 1.3, 2.4 Hz, 1H), 5.11 (s, 2H), 3.16 (s, 1H); ^{13}C NMR (100 MHz, $CDCl_3$); δ = 191.06, 158.88, 137.86, 137.74, 136.51, 129.12, 128.47, 127.55, 127.44, 127.31, 124.71, 124.29, 114.04, 81.87, 78.77, 69.95.

b) 3-Ethynyl-5-(3-(chloromethyl)benzyloxy)benzaldehyde-d_2 (1.7 g, 6.33 mmol, 1.0 equiv.) was dissolved in dry DMF (50 mL) and a solution of KSAc (1.44 g, 12.61 mmol, 2.0 equiv.) in DMF (20 mL) was added dropwise. The mixture was stirred at room temperature for 3 h and the bulk of DMF was removed under reduced pressure. H_2O (100 mL) was added and the mixture extracted with EtOAc (3 × 50 mL). The combined organic phases were washed with brine, dried ($MgSO_4$) and concentrated under reduced pressure. Flash column chromatography (SiO_2, cyclohexane/EtOAc 8:1) gave **E37** (1.60 g, 4.90 mmol, 77%) as a yellow oil. ^{1}H NMR (400 MHz, $CDCl_3$): δ = 9.93 (s, 1H), 7.59 (d, *J* = 1.2 Hz, 1H), 7.45 (dd, *J* = 2.5, 1.3 Hz, 1H), 7.37 – 7.26 (m, 5H), 5.08 (s, 2H), 3.15 (s, 1H), 2.36 (s, 3H); ^{13}C NMR (100 MHz, $CDCl_3$): δ = 194.98, 191.12, 158.98, 138.19, 137.78, 136.35, 129.04, 128.80, 127.93, 127.19, 126.47, 124.73, 124.27, 114.23, 82.00, 78.87, 70.13, 30.37; HRMS (ESI): *m*/*z* = 344.1285 $[M+NH_4]^+$ (calcd. 344.1289 for $C_{19}H_{18}D_2NO_3S$).

(*E*)-*S*-3-((3-Ethynyl-5-((2-(3-mercaptohexanoyl)hydrazono)methyl) phenoxy)methyl) benzyl ethanethioate-d_4

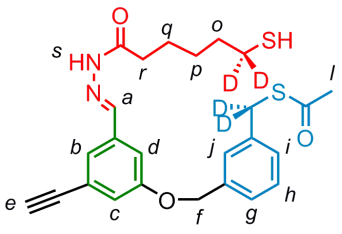

E38

Under N_2, **E37** (326 mg, 1.00 mmol) was dissolved in MeOH (15 mL) and 4 drops of AcOH were added. A solution of **E10** (180 mg, 1.09 mmol, 1.1 equiv.) in MeOH (5 mL)

was added dropwise. The reaction was monitored by TLC (SiO_2, CH_2Cl_2/EtOAc 9:1). After 1 h of stirring at room temperature, the reaction was complete and the product started to precipitate. Stirring was continued for an additional hour after which the mixture was cooled to –10°C and stirred for another 1 h. The precipitate was collected on a glass filter and washed with cold MeOH (5 mL). **E38** (405 mg, 0.86 mmol, 86%) was obtained as a slightly yellowish powder. ^{1}H NMR (400 MHz, $CDCl_3$): δ = 9.42 (s, 1H, H_a), 7.68 (s, 1H, H_s), 7.35 – 7.27 (m, 3H, H_{Ar}), 7.27 – 7.30 (m, 2H, H_{Ar}), 7.29 – 7.26 (m, 2H, H_{Ar}), 7.11 (dd, *J* = 2.3, 1.3 Hz, 1H, H_{Ar}), 5.05 (s, 2H, H_f), 3.11 (s, 1H, H_e), 2.35 (s, 3H, H_l), 1.78 – 1.66 (m, 4H, H_o and H_q), 1.56 – 1.48 (m, H_p), 1.32 (s, broad, 1H, H_m); ^{13}C NMR (100 MHz, $CDCl_3$): δ = 195.09, 176.00, 158.74, 142.04, 138.12, 136.66, 135.41, 129.02, 128.74, 127.98, 126.53, 123.93, 123.71, 119.50, 114.01, 82.80, 77.84, 70.05, 33.51, 32.47, 30.37, 27.97, 24.03; HRMS (ESI): *m/z* = 473.18564 $[M+H]^+$ (calcd. 473.18707 for $C_{25}H_{25}D_4N_2O_3S_2$).

(E)-23-Ethynyl-2-oxa-10,11-dithia-18,19-diaza-tricyclo[19.3.1.1^{4,8}]hexacosa-1(24),4(26),5,7,19,21(25),22-heptaen-17-one d$_4$

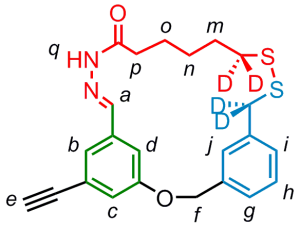

E39

Under N_2, **E38** (410 mg, 0.87 mmol, 1.0 equiv.) was dissolved in MeOH (100 mL) and CH_2Cl_2 (100 mL). A solution of NaOMe (94 mg 1.74 mmol, 2.0 equiv.) in MeOH (10 mL) was added. After 2 h of stirring at room temperature, KI (22 mg, 0.13 mmol, 0.15 equiv.) was added and subsequently a solution of I_2 (221 mg, 0.87 mmol, 1.0 equiv.) in CH_2Cl_2 (30 mL) was added dropwise until the brown colour persisted. Na_2SO_3 was added to reduce excess of I_2 and, when decolourisation was complete, stirring was continued for 15 min. H_2O (250 mL) was added and the phases were separated. The H_2O layer was extracted another time with CH_2Cl_2 (100 mL). The combined organic layers were washed with brine (100 mL) and dried ($MgSO_4$). Removal of the solvents under reduced pressure and purification by flash column chromatography (SiO_2, CH_2Cl_2/EtOAc 9:1) yielded pure **E39** (130 mg, 35%) as a colourless solid. ^{1}H NMR (400 MHz, $CDCl_3$): δ = 9.13 (s, 1H, H_q), 7.64 (s, 1H, H_a), 7.51 –

7.54 (m, 2H, H_{Ar}), 7.31 (d, J = 7.5 Hz, 1H, H_{Ar}), 7.28 – 7.23 (m, 3H, H_{Ar}), 7.17 (dd, 1H, J = 1.2, 1.1 Hz, H_{Ar}), 7.08 (s, 1H, H_{Ar}), 5.17 (s, 2H, H_f), 3.12 (s, 1H, H_e), 2.49 (m, 2H, H_p), 1.82 – 1.70 (m, 4H, H_m, H_o), 1.51 (m, 2H, H_n); ^{13}C NMR (100 MHz, $CDCl_3$): δ = 175.98, 158.69, 141.05, 138.18, 136.87, 135.45, 128.93, 128.77, 128.02, 126.07, 125.99, 123.81, 120.68, 111.62, 82.59, 77.22, 69.90, 33.25, 28.04, 27.75, 24.85; HRMS (ESI): m/z = 429.16298 $[M+H]^+$ (calcd. 429.16085 for $C_{23}H_{21}D_4N_2O_2S_2$).

E40

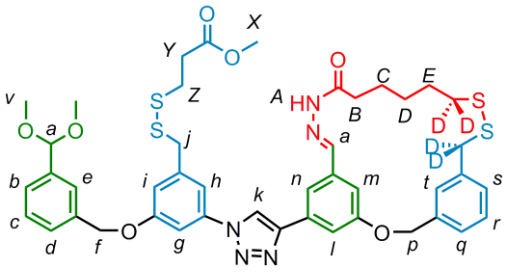

E40

Under N_2, **E17** (113 mg, 244 µmol, 1.2 equiv.) was dissolved in CH_2Cl_2 (10 mL) and a solution of **E39** (87 mg, 203 µmol, 1.0 equiv.) in THF (10 mL) was added. A solution of TBTA (11 mg, 20 µmol, 0.1 equiv.) and $Cu(MeCN)_4PF_6$ (8 mg, 20 µmol, 0.1 equiv.) in MeOH (10 mL) was added to the reaction mixture, which was allowed to stir over night at room temperature. Evaporation of the solvents under reduced pressure and flash column chromatography (SiO_2, CH_2Cl_2/EtOAc 8:2 → 7:3) gave *3,4*-**C$_5$**-d4-dimethylacetal (156 mg, 88%) as a colourless solid. M.p. 105 °C. ^{1}H NMR (400 MHz, $CDCl_3$): δ = 9.16 (s, 1H, H_A), 8.28 (s, 1H, H_k), 7.77 (m, 1H, H_o), 7.63 (s, 1H, H_l), 7.57 (m, 2H, H_t, H_c), 7.55 (s, 1H, H_m), 7.53 (s, 1H, H_n), 7.44 (m, 4H, H_g, H_e, H_b, H_d), 7.35 (s, 1H, H_h), 7.31 (m, 2H, H_r, H_q), 7.25 (d, 1H, H_s), 7.04 (s, 1H, H_i), 5.43 (s, 1H, H_a), 5.27 (s, 2H, H_p), 5.18 (s, 2H, H_f), 3.93 (s, 2H, H_j), 3.67 (s, 3H, H_X), 3.35 (s, 6H, H_v), 2.80-2.66 (m, 6H, H_Z, H_B, H_Y), 1.79-1.73 (m, 4H, H_E, H_C), 1.53 (m, 2H, H_D); assignment of the signals was accomplished by means of 2D NMR (COSY, ROESY, HMQC, HMBC); ^{13}C NMR (100 MHz, $CDCl_3$): δ = 175.92, 172.12, 159.77, 159.43, 147.40, 141.71, 140.76, 138.68, 138.11, 137.88, 137.13, 136.08, 135.90, 132.13, 128.90, 128.68, 128.65, 128.00, 127.64, 126.72, 125.97, 125.88, 120.05, 118.10, 116.15, 114.56, 113.41, 110.59, 106.38, 102.86, 70.39, 69.92, 52.80, 51.93, 43.01, 33.85, 33.24, 32.99, 28.03, 27.74, 24.84; HRMS (ESI): m/z = 909.3097 $[M+NH_4]^+$ (calcd. 909.3104 for $C_{44}H_{49}D_4N_6O_7S_4$).

***3,4*-C$_5$-d$_4$**

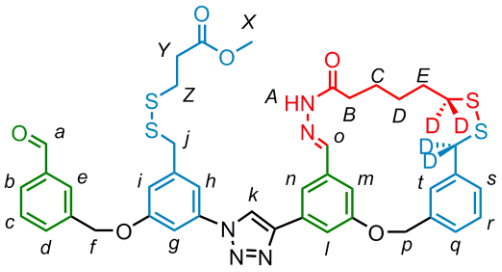

3,4-**C$_5$**-d$_4$

3,4-**C$_5$**-d$_4$-dimethylacetal (5.0 mg) was dissolved in $CHCl_3$ (10 mL) and 3 drops of TFA were added. After 60 seconds, a saturated solution of $NaHCO_3$ was added. After vigorous stirring, the phases were separated and the $CHCl_3$ layer dried ($MgSO_4$). Evaporation of the solvent gave pure *3,4*-**C$_5$**-d$_4$ (4.8 mg, quant.) as a colourless solid. M.p. 90 °C. ^{1}H NMR (400 MHz, $CDCl_3$): δ = 10.30 (s, 1H, H_A), 10.07 (s, 1H, H_a), 8.32 (s, 1H, H_k), 8.02 (s, 1H, H_e), 7.87 (d, *J* = 7.6Hz, 1H, H_b), 7.75 (m, 2H, H_d, H_o), 7.63 (s, 1H, H_l), 7.61 (t, *J* = 7.6 Hz, 1H, H_c), 7.56 (m, 2H, H_t, H_m), 7.52 (s, 1H, H_n), 7.45 (t, *J* = 2.1 Hz, 1H, H_g), 7.36 (s, 1H, H_h), 7.31 (m, 2H, H_r, H_q), 7.25 (d, 1H, H_s), 7.07 (s, 1H, H_i), 5.28 (s, 2H, H_p), 5.26 (s, 2H, H_f), 3.94 (s, 2H, H_j), 3.67 (s, 3H, H_X), 2.77 (m, 4H, H_Z, H_Y), 2.68 (t, *J* = 6.8 Hz, 2H, H_B), 1.83-1.73 (m, 4H, H_E, H_C), 1.54 (m, 2H, H_D) Assignment of the signals was accomplished by means of 2D NMR (COSY, ROESY); ^{13}C NMR (100 MHz, $CDCl_3$): δ = 192.12, 178.42, 172.20, 159.52, 159.47, 147.26, 144.69, 141.04, 138.13, 137.80, 137.28, 137.02, 136.72, 135.36, 133.32, 131.85, 129.94, 129.50, 128.92, 128.72, 128.21, 127.93, 125.95, 120.53, 118.34, 116.31, 115.20, 113.68, 110.99, 106.34, 69.96, 69.60, 51.98, 42.90, 33.87, 33.02, 32.76, 27.85, 27.59, 24.82; HRMS (ESI): *m/z* = 846.2409 $[M+H]^+$ (calcd. 864.2420 for $C_{42}H_{40}D_4N_5O_6S_4$).

4.6 Notes and References

[1] *Molecular Motors* (Ed.: M. Schliwa), Wiley-VCH, Weinheim, **2003**.

[2] a) T. R. Kelly, H. De Silva, R. A. Silva, *Nature* **1999**, *401*, 150; b) N. Koumura, R. W. J. Zijlstra, R. A. van Delden, N. Harada, B. L. Feringa, *Nature* **1999**, *401*, 152; c) D. A. Leigh, J. K. Y. Wong, F. Dehez, F. Zerbetto, *Nature* **2003**, *424*, 174; d) P. Thordarson, E. J. A. Bijsterveld, A. E. Rowan, R. J. M. Nolte, *Nature* **2003**, *424*, 915; e) R. A. van Delden, M. K. J. ter Wiel, M. M. Pollard, J. Vicario, N. Koumura, B. L. Feringa, *Nature* **2005**, *437*, 1337; f) S. P. Fletcher, F. Dumur, M. M. Pollard, B. L. Feringa, *Science* **2005**, *310*, 80; g) V. Balzani, M. Clemente-León, A. Credi, B. Ferrer, M. Venturi, A. H. Flood, J. F. Stoddart, *Proc. Natl. Acad. Sci. U.S.A.* **2006**, *103*, 1178; h) T. Muraoka, K. Kinbara, T. Aida, *Nature* **2006**, *440*, 512; i) V. Serreli, C.-F. Lee, E. R. Kay, D. A. Leigh, *Nature* **2007**, *445*, 523.

[3] E. R. Kay,D. A. Leigh, F. Zerbetto, *Angew. Chem. Int. Ed.* **2007**, *46*, 72.

[4] T. J. Huang, B. Brough, C.-M. Ho, Y. Liu, A. H. Flood, P. A. Bonvallet, H.-R. Tseng, J. F. Stoddart, M. Baller, S. Magonov, *Appl. Phys. Lett.* **2004**, *85*, 5391.

[5] J. Berná, D. A. Leigh, M. Lubomska, S. M. Mendoza, E. M. Pérez, P. Rudolf, G. Teobaldi, F. Zerbetto, *Nature Mater* **2005**, *4*, 704.

[6] a) M. Silverman, M. Simon, *Nature* **1974**, *249*, 73; b) G. Lowe, M. Meister, H. C. Berg, *Nature* **1987**, *325*, 637.

[7] J. E. Walker, *Angew. Chem. Int. Ed.* **1998**, *37*, 2308.

[8] For two short reviews covering linear motors from the kinesin, myosin and dynein families see: a) R. D. Vale, *Cell* **2003**, *112*, 467; (b) M. Schliwa, G. Woehlke, *Nature* **2003**, *422*, 759.

[9] For reviews on kinesin see: a) G. Woehlke, M. Schliwa, *Nature Rev. Mol. Cell Biol.* **2000**, *1*, 50; b) C. L. Asbury, *Curr. Opin. Cell Biol.* **2005**, *17*, 89; c) N. J. Carter, R. A. Cross, *Curr. Opin. Cell Biol.* **2006**, *18*, 61; d) S. M. Block, *Biophys. J.* **2007**, *92*, 2986.

[10] a) S. P. Gilbert, M. R. Webb, M. Brune, K. A. Johnson, *Nature* **1995**, *373*, 671; b) F. J. Kull, P. S. Sablin, R. Lau, R. J. Fletterick, R. D. Vale, *Nature* **1996**, *380*, 550; c) M. J. Schnitzer, S. M. Block, *Nature* **1997**, *388*, 386; d) W. Hua, J. Chung, J. Gelles, *Science* **2002**, *295*, 844; e) N. Naber, T. J. Minehardt, S. Rice, X. Chen, J. Grammer, M. Matuska, R. D. Vale, P. A. Kollman, R. Car, R. G. Yount, R. Cooke, E. Pate, *Science* **2003**, *300*, 798; f) C. L. Asbury, A. N. Fehr, S. M. Block, *Science* **2003**, *302*, 2130; g) A. Yildiz, M. Tomishige, R. D. Vale, P. R. Selvin, *Science* **2004**, *303*, 676; h) N. J. Carter, R. A. Cross, *Nature* **2005**, *435*, 308; i) Q. Shao, Y. Q. Gao, *Proc. Natl. Acad. Sci. U.S.A.* **2006**, *103*, 8072; j) Q. Shao, Y. Q. Gao, *Biochem.* **2007**, *46*, 9098; k) M. C. Alonso, D. R. Drummond, S. Kain, J. Hoeng, L. Amos, R. A. Cross, *Science* **2007**, *316*, 120; l) T. Mori, R. D. Vale, M. Tomishige, *Nature* **2007**, *450*, 750; m) N. R. Guydosh, S. M. Block, *Nature* **2009**, *461*, 125.

[11] Most motors from the myosin family do not operate processively. The processivity of dyneins depends on the cargo load (see reference 1).

[12] a) K. Hirose, J. Löwe, M. Alonso, R. A. Cross, L. A. Amos, *Cell Struct. Funct.* **1999**, *24*, 277; b) F. Kozielski, I. Arnal, R. H. Wade, *Curr. Biol.* **1998**, *8*, 191; c) A. Marx, J. Müller, E.-M. Mandelkow, A. Hoenger, E. Mandelkow, *J. Muscle Res. Cell. Motil.* **2006**, *27*, 125.

[13] a) J. Howard, A. J. Hudspeth, R. D. Vale, *Nature* **1989**, *342*, 154; b) S. M. Block, L. S. B. Goldstein, B. J. Schnapp, *Nature* **1990**, *348*, 348; c) D. D. Hackney, *Nature* **1995**, *377*, 448; d) R. D. Vale, T. Funatsu, D. W. Pierce, L. Romberg, Y. Harada, T. Yanagida, *Nature* **1996**, *380*, 451; e) R. B. Case, D. W. Pierce, N. Hom-Booher, C. L. Hart, R. D. Vale, *Cell* **1997**, *90*, 959; f) L. Romberg, D. W. Pierce, R. D. Vale, *J. Cell Biol.* **1998**, *140*, 1407; g) K. S. Thorn, J. A. Ubersax, R. D. Vale, *J. Cell Biol.* **2000**, *151*, 1093; h) J. Yajima, M. C. Alonso, R. A. Cross, Y. Y. Toyoshima, *Curr. Biol.* **2002**, *12*, 301.

[14] a) R. D. Astumian, *Phys. Chem. Chem. Phys*. **2007**, *9*, 5067; b) R. D. Astumian, I. Derényi, *Eur. Biophys. J.* **1998**, *27*, 474.

[15] M. von Delius, E. M. Geertsema, D. A. Leigh, *Nature Chem.* **2010**, *2*, 96.

[16] a) W. B. Sherman, N. C. Seeman, *Nano Lett.* **2004**, *4*, 1203; b) J.-S. Shin, N. A. Pierce, *J. Am. Chem. Soc.* **2004**, *126*, 10834; c) P. Yin, H. Yan, X. G. Daniell, A. J. Turberfield, J. H. Reif, *Angew. Chem. Int. Ed*. **2004**, *43*, 4906; d) Y. Tian, Y. He, Y. Chen, P. Yin, C. Mao, *Angew. Chem. Int. Ed*. **2005**, *44*, 4355; e) R. Pei, S. K. Taylor, D. Stefanovic, S. Rudchenko, T. E. Mitchell, M. N. Stojanovic, *J. Am. Chem. Soc*. **2006**, *128*, 12693 ; f) P. Yin, H. M. T. Choi, C. R. Calvert, N. A. Pierce, *Nature* **2008**, *451*, 318 ; g) S. J. Green, J. Bath, A. J. Turberfield, *Phys. Rev. Lett.* **2008**, *101*, 238101; h) T. Omabegho, R. Sha, N. C. Seeman, *Science* **2009**, *324*, 67.

[17] In the DNA systems, the degree of processivity is assessed by analytically excluding the presence of the fully detached walker molecule and/or the bare track. Loss of processivity can occur, however, via other intermolecular mechanisms and these are not experimentally addressed in the DNA walker studies.

[18] Instead of a chemical fuel, small-molecule walkers could also be designed to consume other input of energy (e.g. light).

[19] a) S. Mitra, R. G. Lawton, *J. Am. Chem. Soc*. **1979**, *101*, 3097; b) S. J. Brocchini, M. Eberle, R. G. Lawton, *J. Am. Chem. Soc.* **1988**, *110*, 5211.

[20] Loss of processivity could, however, occur through intermolecular bridges. The presence of such bridges has been reported (reference 19a). Lawton and coworkers have not conducted studies on the processivity of their systems.

[21] a) H. D. F. Winkler, D. P. Weimann, A. Springer, C. A. Schalley, *Angew. Chem. Int. Ed.* **2009**, *48*, 7246; b) D. P. Weimann, H. D. F. Winkler, J. A. Falenski, B. Koksch, C. A. Schalley, *Nature Chem.* **2009**, *1*, 573.

[22] In many sigmatropic rearrangement reactions in fact only bonds, rather than atomic moieties migrate (e.g. Payne rearrangement). In others, such as the Cope rearrangement, migration of atoms does indeed proceed processively (i.e. intramolecularly) and under some circumstances directionally. The migration process is, however, neither repetitive nor progressive (for example some variants of the Cope rearrangement). The migration of ketones, such as acetone, along oligo-ol scaffolds would be an example where for a non-directional and non-processive process (the track-bound walker moieties (acetals) would also be in equilibrium with the detached walker (ketone)). For information on the mentioned rearrangement reactions see: *Strategic applications of named reactions*, L. Kürti, B. Czakó, Elsevier, Oxford, **2005** and references cited therein.

[23] a) S. J. Rowan, S. J. Cantrill, G. R. L. Cousins, J. K. M. Sanders, J. F. Stoddart, *Angew. Chem. Int. Ed.* **2002**, *41*, 898; b) P. T. Corbett, J. Leclaire, L. Vial, K. R. West, J.-L. Wietor, J. K. M. Sanders, S. Otto, *Chem. Rev*. **2006**, *106*, 3652; c) J.-M. Lehn, *Chem. Soc. Rev*. **2007**, *36*, 151.

[24] a) V. Goral, M. I. Nelen, A. V. Eliseev, J.-M. Lehn, *Proc. Natl. Acad. Sci. U.S.A.* **2001**, *98*, 1347; b) A. G. Orrillo, A. M. Escalante, R. L. E. Furlan, *Chem. Commun*. **2008**, 5298; c) Z. Rodriguez-Docampo, S. Otto, *Chem. Commun*. **2008**, 5301.

[25] For one example where the unstable imines were reduced to the stable secondary amines see: M. Hochgurtel, H. Kroth, D. Piecha, M. W. Hofmann, K. C. Nicolaou, S. Krause, O. Schaaf, G. Sonnenmoser, A. V. Eliseev, *Proc. Natl. Acad. Sci. U.S.A.* **2002**, *99*, 3382.

[26] a) M. D. Costioli, D. Berdat, R. Freitag, X. André, A. H. E. Müller, *Macromol.* **2005**, *38*, 3630; b) D. Lin, J. Zhang, L. M. Sayre, *J. Org. Chem*. **2007**, *72*, 9471; c) L. Klein, C. M. Yeung, P. Kurath, J. C. Mao, P. B. Fernandes, P. A. Lartey, A. G. Pernet, *J. Med. Chem.* **1989**, *32*, 151.

[27] a) T. R. Chan, R. Hilgraf, K. B. Sharpless, V. V. Fokin, *Org. Lett*. **2004**, *17*, 2853; b) V. V. Fokin, P. Wu, *Aldrichimica Acta* **2007**, *40*, 7; c) B.-Y. Lee, S. R. Park, H. B. Jeon, K. S. Kim, *Tetrahedron Lett*. **2006**, *47*, 5105.

[28] (a) C. W. Tornøe, C. Christensen, M. J. Meldal, *J. Org. Chem.* **2002**, *67*, 3057; b) V. V. Rostovtsev, L. G. Green, V. V. Fokin, K. B. Sharpless, *Angew. Chem. Int. Ed.* **2002**, *41*, 2596.

[29] The abbreviation $\mathbf{C_n}$ is used for the whole series of compounds (n corresponds to the number of methylene units in the spacer chain of the walker moiety).

[30] Selected references for hydrazone exchange in organic solvent: a) G. R. L. Cousins, S. A. Poulsen, J. K. M. Sanders, *Chem. Commun.* **1999**, 1575; b) T. S. Lam, A. Belenguer, S. L. Roberts, C. Naumann, T. Jarrosson, S. Otto, J. K. M. Sanders, *Science* **2005**, *308*, 667; c) R. L. E. Furlan, G. R. L. Cousins, J. K. M. Sanders, *Chem. Commun.* **2000**, 1761; d) G. R. L. Cousins, R. L. E. Furlan, Y.-F. Ng, J. E. Redman, J. K. M. Sanders, *Angew. Chem. Int. Ed.* **2001**, *40*, 423; e) R. L. E. Furlan, Y.-F. Ng, S. Otto, J. K. M. Sanders, *J. Am. Chem. Soc.* **2001**, *123*, 8876; f) R. L. E. Furlan, Y.-F. Ng, G. R. L. Cousins, J. E. Redman, J. K. M. Sanders, *Tetrahedron* **2002**, *58*, 771; g) S. Choudhary, J. R. Morrow, *Angew. Chem. Int. Ed.* **2002**, *41*, 4096.

[31] Selected references for disulfide exchange in organic solvent: a) H. Hioki, W. C. Still, *J. Org. Chem.* **1998**, *63*, 904; b) A. L. Kieran, A. D. Bond, A. M. Belenguer, J. K. M. Sanders, *Chem. Commun.* **2003**, 2674; c) A. T. ten Cate, P. Y. W. Dankers, R. P. Sijbesma, E. W. Meijer, *J. Org. Chem.* **2005**, *70*, 5799 ; d) A. L. Kieran, S. I. Pascu, T. Jarrosson, J. K. M. Sanders, *Chem. Commun*. **2005**, 1276 ; e) A. L. Kieran, S. I. Pascu, T. Jarrosson, M. J. Gunter, J. K. M. Sanders, *Chem. Commun*. **2005**, 1842; f) B. Danieli, A. Giardini, G. Lesma, D. Passarella, B. Peretto, A. Sacchetti, A. Silvani, G. Pratesi, F. Zunino, *J Org. Chem.* **2006**, *71*, 2848.

[32] The structural identity of *2,3*-$\mathbf{C_5}$ was confirmed by two-dimensional ^{1}H NMR spectroscopy (ROESY, COSY). Further characterisation involved high-resolution mass spectrometry, HPLC and LCMS.

[33] Isomer *2,3*-$\mathbf{C_5}$ was isolated by means of preparative HPLC (see section 4.5.1).

[34] Disulfide exchange in organic solvent can require long periods of time (until equilibrium is reached). See references 31c and 31f where 20 to 120 days appear to be necessary.

[35] The placeholder disulfide was added to minimise the amount of oligomeric species.

[36] The term yield is employed here to describe the fraction of monomeric constitutional isomers in the mixture.

[37] H. Noji, R. Yasuda, M. Yoshida, K. Kinosita, *Nature* **1997**, *386*, 299.

[38] The equilibria for the $\mathbf{C_2}$ system were not studied in the same detail, because it became apparent at an early stage of our studies that the $\mathbf{C_2}$ walker is too short for useful operation.

[39] The HPLC detection limit was estimated to be ~1%.

[40] In fact it is this property of the system that allows HPLC separation of all four isomers.

[41] Those differences can be explained by insufficient equilibration time (i.e. thermodynamic equilibrium was not reached at the moment when the reaction was quenched).

[42] Interestingly, we are able to simulate the speculative 'out of equilibrium' situation by randomly changing one or more of the four equilibrium ratios in that serve as input variables in the spreadsheet program. Thereafter the ratios do not form a consistent set and, as a result, the graph does not converge towards a constant composition and instead oscillates indefinitely between two states.

[43] The high amount of ring strain present in the *2,3* and *1,4* isomers of the $\mathbf{C_3}$ and $\mathbf{C_4}$ system would make a very lengthy experimental procedure necessary (~30 steps until convergence to steady state for $\mathbf{C_3}$ and ~15 steps for $\mathbf{C_4}$).

[44] We have attempted to achieve net-directional walker migration by changing the solvent for one of the reversible processes. We have found, however, that such changes either make only little difference in the observed isomer ratios or don't allow the dynamic exchange to occur at all.

[45] Other oxidants (e.g. Br_2 and $K_3[Fe(CN)_6]$) were investigated but none were superior to I_2 in terms of reaction bias and/or chemoselectivity.

[46] a) C. Hyeon, J. N. Onuchic, *Proc. Natl. Acad. Sci. U.S.A.* **2007**, *104*, 2175; b) A. Yildiz, M. Tomishige, A. Gennerich, R. D. Vale, *Cell* **2008** *134*, 1030; c) J. C. Cochran, F. J. Kull, *Cell* **2008**, *134*, 918.

[47] a) C. Veigel, S. Schmitz, F. Wang, J. R. Sellers, *Nature Cell Biol.* **2005**, *7*, 861; b) K. M. Trybus, *Nature Cell Biol.* **2005**, *7*, 854.

[48] The product mixtures were <u>not</u> purified by HPLC. All oligomers and other side-products were retained in the sample.

[49] The mean step number describes the number of operational steps after which half of the molecules have lost processivity.

[50] No peaks with the corresponding m/z values were observed by HPLC-MS.

[51] J. R. Nitschke, *Nature* **2009**, *462*, 736.

[52] R. F. Ludlow, S. Otto, *Chem. Soc. Rev.* **2008**, *37*, 101.

[53] S. El Fangour, A. Guy, V. Despres, J.-P. Vidal, J.-C. Rossi, T. Durand, *J. Org. Chem*. **2004**, *69*, 2498.

[54] ChemStation for LC 3D systems 3D, Rev. B.04.01 [481], Agilent Technologies Inc..

Chapter V

A Light-Driven Small-Molecule Walker which can be Transported along a Track in either Direction

Published as *Light-Driven Transport of a Molecular Walker in Either Direction along a Molecular Track*, M. J. Barrell, A. G. Campaña, M. von Delius, E. M. Geertsema, D. A. Leigh, *Angew. Chem. Int. Ed.* **2010**, DOI: 10.1002/anie.201004779.

Highlighted in: *Walking Molecule Follows the Light*, S. Everts, *Chem. & Eng. News* **2010**, *88*, 44.

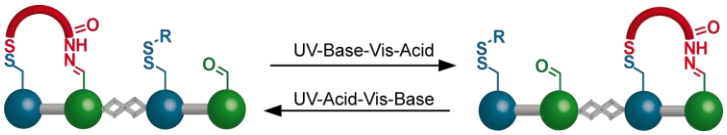

"Mehr Licht!"

(*More light!* Last words of Johann Wolfgang von Goethe)

Acknowledgments

The following people are very gratefully acknowledged for their contribution to this Chapter: Michael J. Barrell conducted model studies and attempted the synthesis of walker-track conjugate *E-1,2*-**1** *via* alternative synthetic routes (not described in this thesis). Dr. Edzard M. Geertsema and Dr. Araceli G. Campaña contributed to the scale-up of the syntheses of *E-1,2*-**1** and *E-3,4*-**1**. A. G. C. also contributed to the investigation of the dynamic properties of *E-1,2*-**1** and *E-3,4*-**1**.

5.1 Synopsis

In this Chapter a small-molecule walker-track conjugate is described in which the walker unit is able to walk in either direction of a four-foothold molecular track, depending on the sequence of the application of four external stimuli: acid, base, UV light and visible light.

Key for achieving directional bias through a Brownian energy ratchet mechanism was the isomerisation of the stilbene moiety at the centre of the molecular track. Significant ring strain could be induced in the positional (constitutional) isomer where the walker unit bridges the E-stilbene linkage. E→Z isomerisation thus enabled the walker unit to 'step' from one end of the track onto the central stilbene gap, while subsequent Z→E isomerisation resulted in a majority of the walker units to be transported away from the stilbene gap towards the other end of the track.

5.2 Introduction

Nature uses bipedal molecular walkers, such as kinesin, myosin or dynein for a variety of essential cellular processes.[1] Although the mechanisms through which these fascinating linear molecular motors operate are increasingly well understood,[2] there are still relatively few synthetic mimicks which exhibit the most important characteristics of the biological walkers: repetitive, processive and directional walker transport along a track. To date, several walker systems based on DNA have been described and the dynamic behaviour of such devices has reached a remarkable level of complexity.[3] Recently, our group has reported the first small-molecule example of a molecular walking device in which directionally biased walker migration in one direction of the track was achieved through an information type of Brownian ratchet mechanism.[4]

Herein, we report the synthesis and operation of a small-molecule walker-track conjugate (**1**, see Scheme 5.1) in which the walker unit is able to walk in either direction of a four-foothold molecular track, depending on the sequence of the application of four external stimuli: acid or base for mutually exclusive 'foot' dissociation; UV light or visible light for the generation of directional bias (see (i)-(iv) in Figure 5.1a). The molecular design of the system is closely related to a walker-track conjugate previously described by our group,[4] with the crucial structural difference of a stilbene moiety in the centre of the molecular track (Scheme 5.1). The key to achieving directionality in the walker migration lies in the photoisomerisation of the stilbene moiety (Scheme 5.2), through which significant ring strain can be induced in the positional (constitutional) isomer where the walker unit bridges the stilbene linkage (see Figure 5.1a or Scheme 5.2b).[5] $E \rightarrow Z$ isomerisation thus enables the walker unit to 'step' from one end of the track onto the stilbene gap, while subsequent $Z \rightarrow E$ isomerisation results in a majority of the walker units to be transported away from the stilbene gap towards the other end of the track (Figure 5.1a). Such a manipulation of the thermodynamic minima (here by strain induction through stilbene isomerisation) and kinetic barriers (here by addition of either base or acid) experienced by a Brownian particle (Figure 5.1b) corresponds to an energy type of Brownian ratchet mechanism.[6]

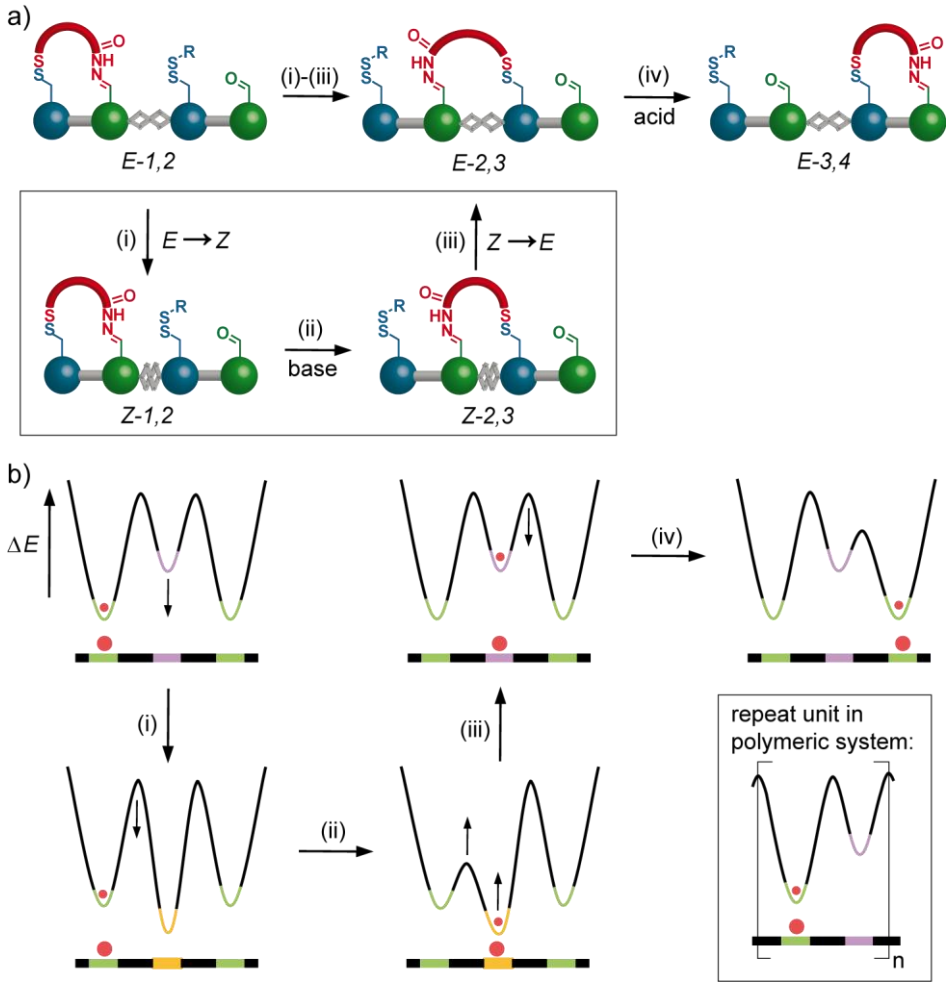

Figure 5.1. *a) Operation principle of the reported light-driven walker-track conjugate; b) schematic energy profile experienced by the transported particle (i.e. walker unit); profiles correspond to the processes shown in Figure 5.1a and illustrate the underlying energy ratchet mechanism[6] (repeat unit of a hypothetical polymeric system shown in brackets). External stimuli: (i): UV light (E→Z); (ii): base (disulfide exchange); (iii): visible light (Z→E); (iv): acid (hydrazone exchange).*

5.3 Results and Discussion

5.3.1 Synthesis

Molecular walker-track conjugate *E-1,2*-**1**[7] was synthesised as shown in Scheme 5.1 (see section 5.5.8 for full experimental procedures and characterisation data). The initial position of the walker unit at footholds *1* and *2* was established by the synthesis of macrocycle **7** from simple aromatic starting materials (**2** and **3**) and the bipedal walker unit **6**. Compound **8**, which contains thiol foothold *3* (masked as disulfide with 'placeholder' thiol) and aldehyde foothold *4*, was prepared from precursors **4** and **5**. The synthesis was completed by a Ru-catalysed, statistical cross-metathesis reaction,[8] which, after thorough optimisation of the reaction parameters,[9] gave *E-1,2*-**1** in

satisfying yield. Walker-track conjugate *E-3,4*-**1**, in which the walker unit is located on the other end of the molecular track, was unambiguously prepared through an analogous synthetic route (see section 5.5.8).

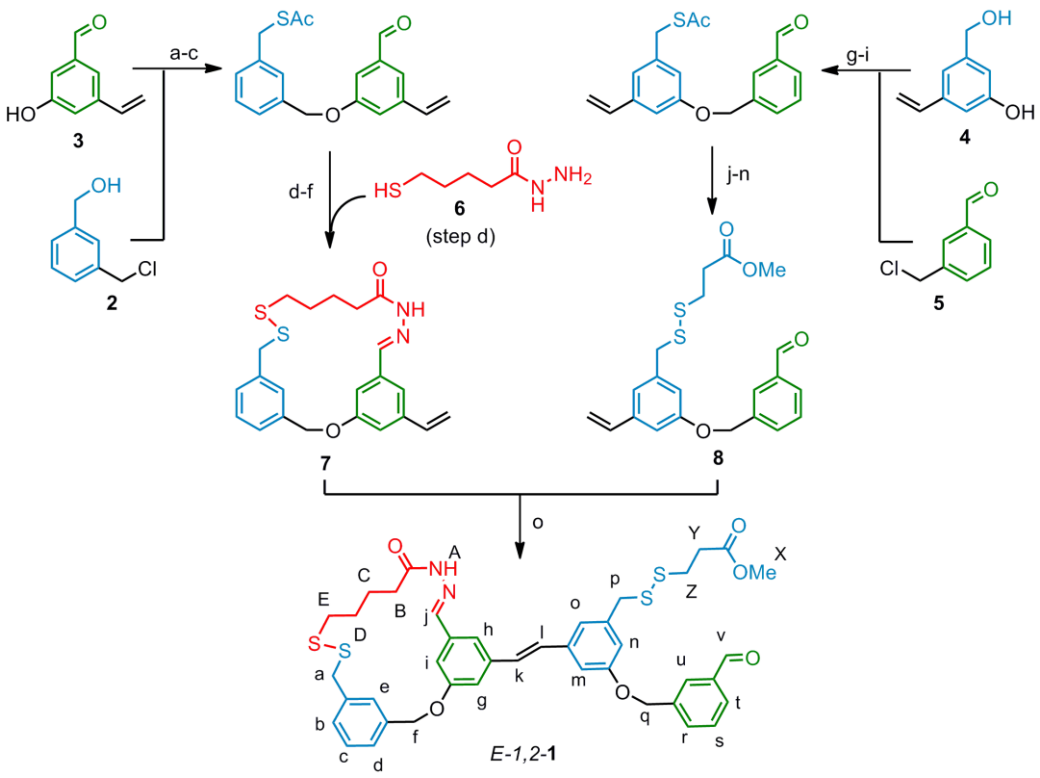

Scheme 5.1. *Synthesis of molecular walker-track conjugate E-1,2-**1**. a) NaH, DMF, RT, 16 h; b) MsCl, NEt_3, CH_2Cl_2, 0 °C → RT, 1.5 h; c) KSAc, DMF, RT, 3 h, 59% (three steps); d) AcOH (cat.), MeOH, RT, 2 h, 83%; e) NaOMe, MeOH, RT, 2 h; f) I_2, KI, CH_2Cl_2, RT, 5 min, 48% (two steps); g) NaH, DMF, RT, 16 h; h) MsCl, NEt_3, CH_2Cl_2, 0 °C → RT, 2 h; i) KSAc, DMF, RT, 3 h, 35% (three steps); j) $HC(OMe)_3$,* p-*TsOH, MeOH, RT, 1 h; k) NaOMe, MeOH, RT, 3 h; l) 3-mercaptopropionic acid, I_2, KI, CH_2Cl_2, RT, 5 min; m) HCl (1M), CH_2Cl_2, RT, 15 min, 69% (four steps); n) AcCl, MeOH, 0 °C → RT, 5 h, 76%; o) Ω_A-SIMes-CF_3™ catalyst,[9] CH_2Cl_2, μw (300 W), 100 °C, 3 h, 23%.*

5.3.2 Stilbene *Z*-*E* Isomerisation

An investigation of the photochemical behaviour of walker-track conjugates *E-1,2*-**1** and *E-3,4*-**1** in deuterated dichloromethane (CD_2Cl_2) revealed the possibility to carry out direct (i.e. unsensitized) *E*→*Z* stilbene photoisomerisation,[10] using light of 365 nm wavelength (Scheme 5.2a). The observed, excellent photostationary states (~9:1 *Z*/*E* starting from *E-1,2*-**1** or *E-3,4*-**1**) are a result of the higher molar absorptivities of the *E* isomers in comparison to the corresponding *Z* isomers.[11] The reverse process, *Z*→*E* stilbene isomerisation, proceeded efficiently in CD_2Cl_2 (with >9:1 *E*/*Z* steady state ratios for *1,2*-**1** and *3,4*-**1**), using elemental iodine and visible light of 500 nm wavelength (see sections 5.5.2 and 5.5.3 for experimental details and ^{1}H NMR spectra).[12]

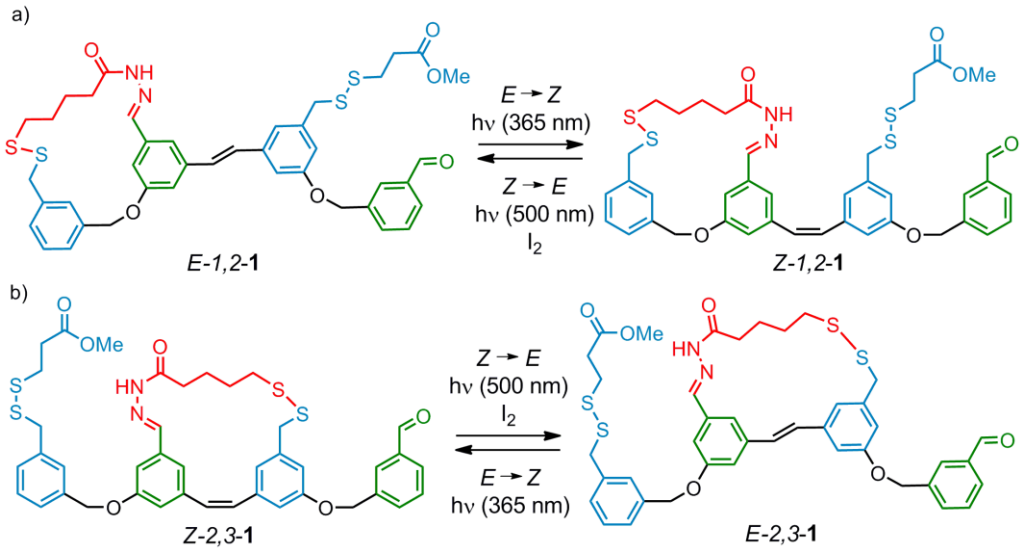

Scheme 5.2. *Reversible stilbene Z-E-isomerisation and implications on ring strain: a) Z-E isomerisation of 1,2-**1** (no effect on ring strain); b)* Z-E *isomerisation of 2,3-**1** (significant ring strain present in E-2,3-**1**). Conditions: E→Z: 0.1 to 10 mM, hν (365 nm; bandwidth: 10 nm), CD_2Cl_2, RT, 5 min to 1h; Z→E: 0.1 mM[13], I_2 (ca. 10 equiv.), hν (500 nm; bandwidth: 10 nm), CD_2Cl_2, RT, 4 to 8 h.*

The structural implications of stilbene *Z-E* isomerisation on *E/Z* isomer pairs *E/Z-1,2*-**1** and *E/Z-2,3*-**1** are illustrated in Scheme 5.2. While the interconversion between *E-1,2*-**1** and *Z-1,2*-**1** (Scheme 5.2a) has no impact on ring strain in both isomers, the *E-2,3*-**1** isomer (Scheme 5.2b) is significantly more strained than the corresponding *Z* isomer.[14] The resulting ring-strain induced difference in free energy between *Z-2,3*-**1** and *E-2,3*-**1**, which is not present between *Z-1,2*-**1** and *E-1,2*-**1** for example, is the molecular basis of the energy ratchet-type, directionally biased walker transport presented herein (see Figure 5.1).

5.3.3 Preliminary Experiments and ^{1}H NMR Spectra

In a series of preliminary experiments we were able to confirm that the strained *E-2,3*-**1** isomer can be prepared from *Z-2,3*-**1** as shown in Scheme 5.2b and that, in a subsequent dynamic covalent[15] exchange reaction, the walker unit is efficiently transported to either the *1,2* or the *3,4* position of the track (depending on the use of either base or acid). To demonstrate this, we first prepared a mixture of *Z-1,2*-**1** and *Z-2,3*-**1** *via* base induced disulfide exchange and subsequently isolated pure *Z-2,3*-**1** from the mixture. Applying the conditions for *Z→E* isomerisation (see Scheme 5.2) to pristine *Z-2,3*-**1** reproducibly led to a 75:25 (*E/Z*) steady state mixture, which in two separate experiments was submitted to conditions for disulfide (base) or hydrazone exchange (acid). In both experiments approximately 80% of the walker units were

transported to either the *1,2* (base) or *3,4* (acid) position of the track. This confirmed the presence of significant ring strain in *E-2,3*-**1**, as well as the high efficiency of the applied exchange processes (see section 5.5.4 for experimental details and ^{1}H NMR spectra).

During the investigation of the system over several operational steps, ^{1}H NMR spectroscopy enabled us to determine the product distributions, even in complex mixtures containing all eight monomeric isomers (*Z*/*E*-*1,2*-**1**, *Z*/*E*-*2,3*-**1**, *Z*/*E*-*3,4*-**1**, *Z*/*E*-*1,4*-**1**[16]). The partial ^{1}H NMR spectra of the six isomers, which are involved in the major 'passing-leg'[6a] gait (see Figure 5.1a), are shown in Figure 5.2. Significant differences in chemical shift, indicative for the position of the walker unit on the track, occur for the protons of the methylene groups in the four-carbon spacer unit (shown in red, H_B to H_E). Protons H_k and H_l serve as distinctive markers for the configuration of the stilbene double bond ($\delta < 7$ ppm for *Z* and $\delta > 7$ ppm for *E* isomers). The protons of the free aldehyde group around 10.0 ppm (H_v or H_j) and the methylene-disulfide protons around 3.8 ppm (H_a and H_p) are the most useful probes for the analysis of complex mixtures, since they experience distinctive differences in chemical shift as a function of both the walker position and the stilbene configuration.

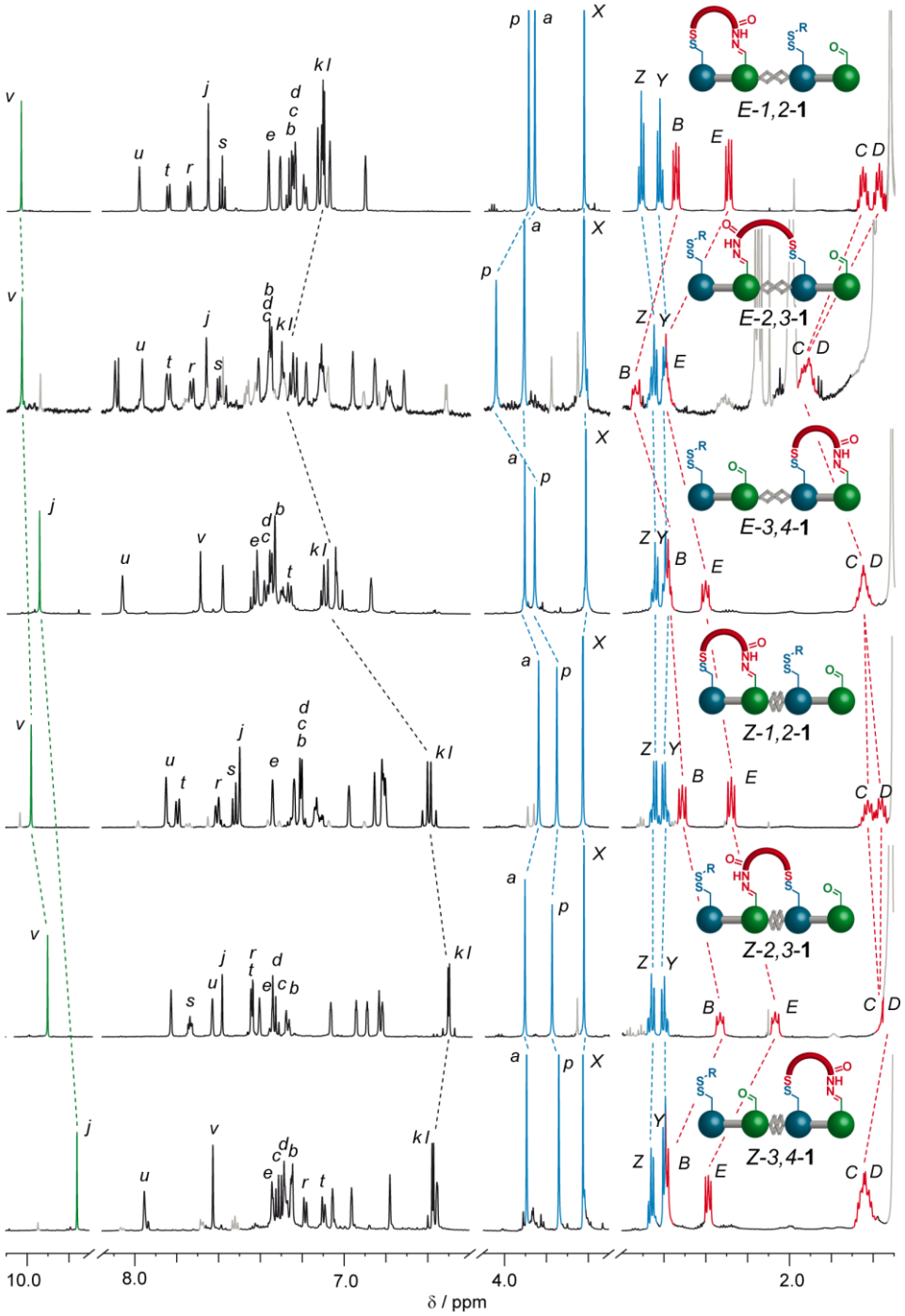

Figure 5.2. *Partial ^{1}H NMR spectra (500 MHz, CD_2Cl_2, 298 K) of the six isomers involved in the 'passing-leg'[6a] gait. Dotted lines connect signals that differ significantly in chemical shift as a result of the position of the red walker unit or the configuration of the stilbenoid double bond. Signals corresponding to residual walking isomers (e.g. 'E-2,3-**1**' spectrum contains 25% of Z-2,3-**1**), solvent and other impurities are shown in grey. Selected assignments are given for the aromatic protons (see Scheme 5.1 for proton labelling).*

5.3.4 Directionally Biased Walker Transport

The operation of the system over one cycle, i.e. the sequential application of all four described external stimuli (i to iv), is illustrated in Scheme 5.3. Starting from pristine *E-1,2*-**1**, photochemical stilbene *E*→*Z* isomerisation (i) gives a photostationary mixture containing 90% of the desired *Z-1,2*-**1** isomer. Under basic conditions (ii) the hydrazone linkage between the walker unit (shown in red) and the track is kinetically stable,[17] while the disulfide foot can dissociate from the track and rebind at footholds *1* or *3*. This leads to an equilibrium that, presumably due to entropic reasons,[18] lies on the side of positional isomer *Z-2,3*-**1**. Light-induced stilbene *Z*→*E* isomerisation (iii) results in 75% conversion of *Z-2,3*-**1** into the strained *E-2,3*-**1** isomer. In the following acid-catalyzed step (iv), the hydrazone foot is able to dissociate from the track and rebind at either foothold *2* or *4*, while the disulfide foot acts as a fixed pivot.[17] This results in the large majority (>95%) of walker units being transported away from the *E*-stilbene gap (*2,3* position), towards the energetically favourable *3,4* position (see Figure 5.1b for a schematic energy diagram which corresponds to the discussed processes).

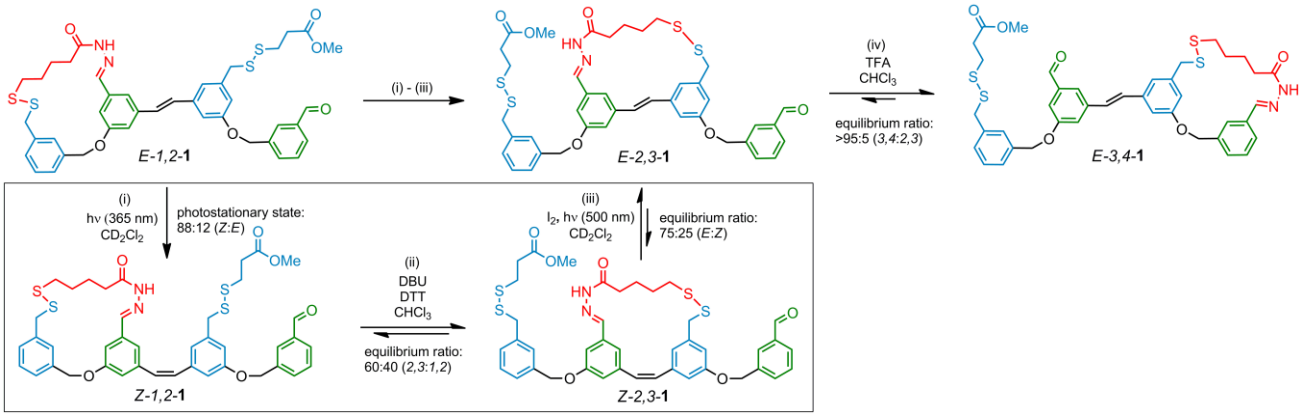

Scheme 5.3. *Directionally biased walker migration over one cycle of operation, starting from E-1,2-**1**. For reasons of clarity, only the major isomer is shown after each stilbene isomerisation or dynamic covalent exchange process (see graphs in Figure 5.3 for data representing the entire system). Isomer ratios are based on ^{1}H NMR integration (see Supporting Information). Conditions: (i) 0.1 to 10 mM, hν (365 nm; bandwidth: 10 nm), CD_2Cl_2, RT, 5 min to 1h; (ii) 0.1 mM, DTT (10 equiv.), DBU (40 equiv.), $(MeO_2CCH_2CH_2S)_2$ (20 equiv.), $CHCl_3$, RT, 12-24 h; (iii) 0.1 mM[13], I_2 (ca. 10 equiv.), hν (500 nm; bandwidth: 10 nm), CD_2Cl_2, RT, 4 to 8 h.; (iv) 0.1 mM, TFA (excess), $CHCl_3$, RT, 6 to 96 h.*

A more accurate description of the dynamic behaviour of the system is provided by graphs, such as the ones presented in Figure 5.3, where the combined amount of each *E*/*Z* isomer pair (*1,2*-**1**, *2,3*-**1**, *3,4*-**1** and *1,4*-**1**) is plotted against the applied sequence of stimuli. The graph in Figure 5.3a, for example, shows the composition of the system during the application of the stimuli sequence shown in Scheme 5.3. More specifically,

the graph presents the expected behaviour of the system (solid dots and lines), which is calculated from the individual, experimentally observed equilibrium or steady state ratios (see Scheme 5.3 for example), along with the experimentally observed results (hollow dots, see Figure 5.3 legend). The data presented in Figure 5.3a indicates that, starting from pristine *E-1,2*-**1**, one cycle of the 'i-ii-iii-iv' stimuli sequence led to a mixture with *3,4*-**1** as the major component (48%), which deviates only slightly from the theoretically expected amount (54%).[19] When a similar experiment is conducted with the stilbene isomerisation stimuli in reversed order (iii-ii-i-iv, Figure 5.3b), only a marginal amount of *3,4*-**1** (4%, expected: 3%) is found after one cycle of operation. This observation confirms that the large amount of *3,4*-**1** formed in the original experiment (Figure 5.3a) is indeed a result of an energy ratchet mechanism (see Figure 5.1b).

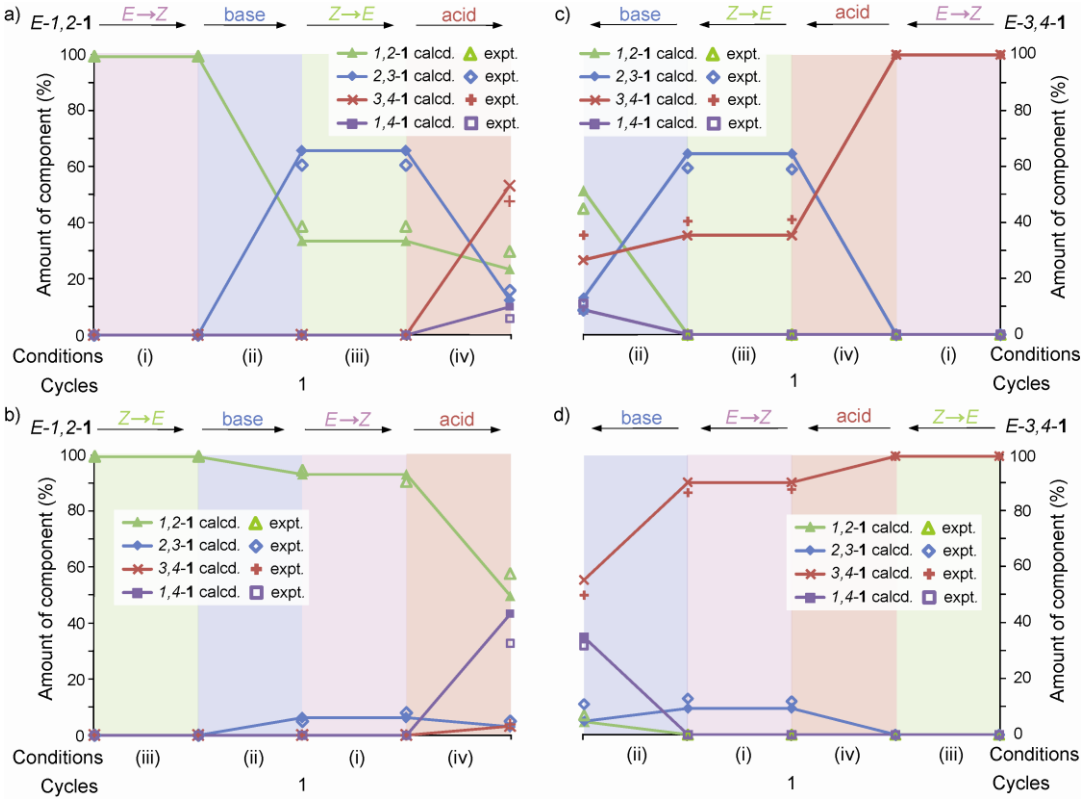

Figure 5.3. *Dynamic behaviour of the system under variation of starting material and stimuli sequence. a-d) Calculated (calcd.; see note below) and experimental (expt.) product distribution[19] during one cycle of operation: a) starting material E-1,2-***1***, stimuli sequence 'i-ii-iii-iv'; b) starting material E-1,2-***1***, stimuli sequence 'iii-ii-i-iv'; c) starting material E-3,4-***1***, stimuli sequence 'i-iv-iii-ii' (from right to left); d) starting material E-3,4-***1***, stimuli sequence 'iii-iv-i-ii' (from right to left); Note: Calculated data is based on simple mathematical extrapolation of empirical data, such as the observed steady state ratios between all Z/E isomer pairs under conditions (i) and (iii) and the observed equilibrium ratios between individual positional isomers under conditions (ii) and (iv) (see section 5.5.4). Experimental data is based on ^{1}H NMR integration; estimated error margin: ±3% (see section 5.5.5). See Scheme 5.3 for conditions 'i' to 'iv'.*

A very similar behaviour was observed when pristine *E-3,4*-**1** was employed as starting material (Figure 5.3c,d). Application of the stimuli sequence, which is expected to provide directional bias towards the left end of the track (i-iv-iii-ii), led to 48% of *1,2*-**1** (expected: 51%; Figure 5.3c), while application of the reverse stimuli sequence (iii-iv-i-ii) gives only 7% of *1,2*-**1** (expected: 5%, Figure 5.3d). A comparison of Figure 5.3a (directionally biased operation) with the graphs shown in Figure 5.4a and Figure 5.4b (behaviour of the system in the absence of stilbene isomerisation) highlights the dramatic influence of the energy ratchet mechanism on the number of necessary operational cycles (7 cycles necessary in Figure 5.4a), as well as on the eventual product distribution (*Z-2,3*-**1**[18] as major product in Figure 5.4b). In an ideal Brownian ratchet system, a second cycle of operation should shift the composition even further away from a statistical distribution. The occurrence of folding products,[16] such as *1,4*-**1**, does, however, in the present system lead to a situation where further operation does not lead to significant improvement of the product distribution.

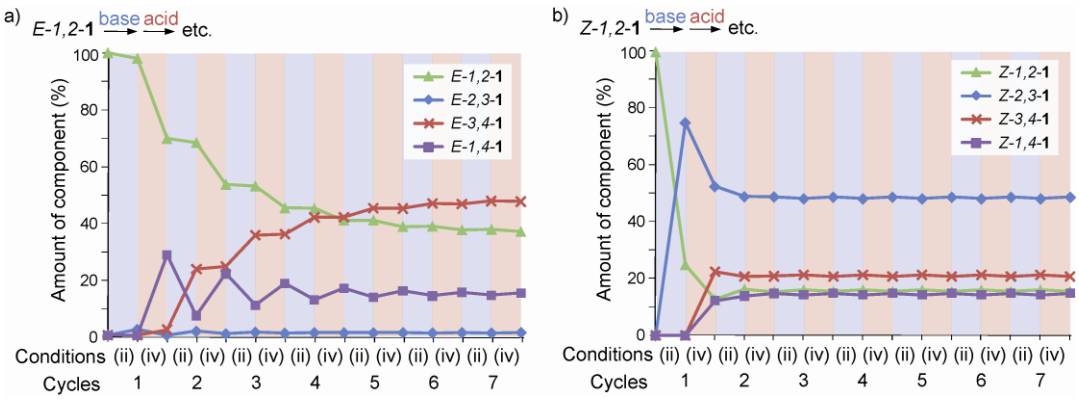

Figure 5.4. *Dynamic behaviour of the system in the absence of stilbene isomerisation; calculated (see note below) product distribution during 15 base-acid cycles, starting from a) pristine E-1,2-**1**; b) pristine Z-1,2-**1**. Note: Calculated data is based on simple mathematical extrapolation of empirical data, such as the observed steady state ratios between all Z/E isomer pairs under conditions (i) and (iii) and the observed equilibrium ratios between individual positional isomers under conditions (ii) and (iv) (see section 5.5.4). Experimental data is based on ^{1}H NMR integration; estimated error margin: ±3% (see section 5.5.5). See Scheme 5.3 for conditions 'ii' and 'iv'.*

5.3.5 Processivity during Light-Driven Walker Migration

Processivity, i.e. the ability of the walker unit to remain attached to its original track during the applied conditions, is (besides directional bias) a key consideration for the design and operation of synthetic molecular walkers.[4] In a double-labelling crossover experiment previously described by our group,[4] an average step number[20] of 37 was obtained for the loss of processivity during disulfide and hydrazone exchange. Since the

conditions for dynamic covalent bond exchange are identical in the present study and since we have not observed any indications for walker dissociation during the photochemical experiments, we would estimate the average step number to be in the range of 30 to 40, which compares to ~100 steps observed for the biological biped kinesin.[21]

5.4 Conclusions

In conclusion, we have demonstrated the operation of the first light-driven, linear molecular motor system. Significant directional bias, stemming from a Brownian energy ratchet mechanism, has been obtained for the transport of the walker unit in both directions of the molecular track. While both the photochemical stilbene isomerisation and the acid- and base-induced reversible foot migration processes proceed with remarkable efficiency, it is evident that a major weakness of the present system originates in the flexibility of its track and the resulting folding products, which reduce the observed directional bias and prevent operation over more than one operational cycle. A system with a polymeric track based on the present design would furthermore use the supplied light energy very inefficiently, switching all of the manifold double bonds in the track from *Z* to *E*, whereas only one double bond would actually 'ratchet' the walker unit energetically uphill. Future work will thus be aimed at systems with rigid molecular tracks and conformationally switchable walker units.

5.5 Experimental Section

5.5.1 General Information

The synthesis of compounds **2**, **5** and **6** was described in Chapter III and IV. The Ω_A-SIMes-CF_3™ catalyst[9,22] used for the final cross-metathesis reactions was purchased from Omega CAT SYSTEM, France. Analytical and preparative HPLC was performed on instruments of Agilent Technologies (1200 LC system with photodiode array detector) and Gilson. Normal-phase columns (Kromasil-Si, analytical: 250 × 4.6 mm, semi-preparative: 250 × 10 mm, preparative: 250 × 20 mm) were used with combined isocratic and gradient elution (analytical: 0.8 mL/min, CH_2Cl_2/^{i}PrOH, 3% → 3% → 15% → 15% → 3% ^{i}PrOH; semi-preparative: 5 mL/min, CH_2Cl_2/^{i}PrOH, 3.5% → 3.5% → 15% → 15% → 3.5% ^{i}PrOH; preparative: 10 mL/min, CH_2Cl_2/MeOH, 1.0% → 1.0% → 20% → 20% → 1.0% MeOH, UV detection @ 290 nm). For photochemical irradiation a LOT Oriel 150 W mercury lamp was used. Several Bandpass Interference Filters were

purchased from Edmund Optics and used as specified in section 5.5.2 for the different isomerisation experiments: 500 nm filter (500±2 nm Center Wave Length (CWL), 10±2 nm Full Width Half Maximum (FWHM)); 365 nm filter (365±2 nm CWL, 10±2 nm FWHM).

5.5.2 General Procedures for *E*-*Z* Isomerisation and Dynamic Covalent Exchange

5.5.2.1 Photochemical, direct E→Z Isomerisation

A sample containing the *E*-isomer or mixture of *E*-isomers (not more than 1 mg (1.2 μmol) in total) was dissolved in CD_2Cl_2 (500 μL) and transferred into a regular NMR tube (fitted with a small magnetic stirring bar). The stirred sample solution was irradiated with light of 365 nm (see section 5.5.1 for filter specification) until the photochemical steady state was reached (typically after 5 to 60 min; monitored by ^1H NMR).

5.5.2.2 Light-Induced, Iodine-Catalysed Z→E Isomerisation

A sample containing the *Z*-isomer or mixture of *Z*-isomers (not more than 1 mg (1.2 μmol) in total) was dissolved in CD_2Cl_2 (500 μL) and transferred into a regular NMR tube (fitted with a small magnetic stirring bar). I_2 (0.1 mg) was added from a stock solution (CD_2Cl_2). The stirred sample solution was irradiated with light of 500 nm (see 5.5.1 for filter specification) until the steady state composition was reached (typically after 4 to 8 h; monitored by ^1H NMR).

5.5.2.3 Base-Induced Disulfide Exchange (ii)

Disulfide exchange was carried out under exclusion of light (flasks/vials covered with black aluminium foil). To a 0.1 mM solution of walker-track conjugate (typically ~1 mg (1.2 μmol) in 10 mL; 1.0 equiv.) in $CHCl_3$ (HPLC grade) was added DBU (40 equiv.), DTT (10 equiv.) and dimethyl 3,3'-disulfanediyldipropanoate (20 equiv.) from stock solutions ($CHCl_3$). The mixture was stirred at room temperature and the progress of the equilibration followed by analytical HPLC. When the relative ratios of the isomers were stable (generally 12-48 hours), the excess of DTT was oxidised by dropwise addition of a solution of I_2 in $CHCl_3$ until a slight brown colour persisted. An aqueous solution of NH_4Cl and Na_2SO_3 was added immediately and the mixture was stirred vigorously until decolourisation was complete. The layers were separated and the aqueous layer was extracted with $CHCl_3$. The combined organic layers were dried over $MgSO_4$. After work

up the product distribution was no longer dynamic (free of DTT and DBU) and the solvent could be removed to allow analysis by analytical HPLC and ^{1}H NMR spectroscopy.

5.5.2.4 *Acid-Catalysed Hydrazone Exchange*

Hydrazone exchange was carried out under exclusion of light (flasks/vials covered with black aluminium foil). To a 0.1 mM solution of walker-track conjugate (typically ~1 mg (1.2 μmol) in 10 mL; 1.0 equiv.) in $CHCl_3$ (HPLC grade) were added 5 drops of a solution containing 20% v/v TFA (CF_3CO_2H) and 1% v/v H_2O in $CHCl_3$ (HPLC grade). The mixture was stirred at room temperature and the progress of the equilibration followed by analytical HPLC. When the relative ratios of the isomers were stable (generally 6-96 h), the mixture was washed with an aqueous solution of $NaHCO_3$. The layers were separated and the aqueous layer was extracted with $CHCl_3$. The combined organic layers were dried over $MgSO_4$. The solvents were removed under reduced pressure and the constitution of the mixture determined by analytical HPLC and ^{1}H NMR spectroscopy.

5.5.3 Stilbene Isomerisation and Dynamic Covalent Exchange Reactions – Establishing the ^{1}H NMR Shifts of all Isomeric Species

^{1}H NMR evidence for the fundamental stilbene *Z*-*E* isomerisation and dynamic covalent exchange processes between individual isomers is presented. Shown is the diagnostic aldehyde region (δ = 10.1 to 9.7 ppm). The data is presented in a way that allows the unambiguous deduction of the NMR shift of the aldehyde proton for all isomeric species (summarised in Table 5.1 on page 220).

a) *E-1,2*-**1**

E-1,2-**1** was synthesised unambiguously (see Scheme 5.4) and its identity confirmed by means of 1D (^{1}H, ^{13}C) and 2D (COSY, ROESY, HSQC, HMBC) NMR spectroscopy, as well as High-Resolution Mass Spectrometry (HRMS) and Liquid Chromatography Mass Spectrometry (LCMS). The aldehyde proton in *E-1,2*-**1** exhibits a chemical shift of 10.032 ppm (500 MHz, CD_2Cl_2, RT).

b) *Z-1,2*-**1**

Direct *E*→*Z* photoisomerisation of pristine *E-1,2*-**1** gave *Z-1,2*-**1** (photostationary state ~ 88:12 (*Z*/*E*)).

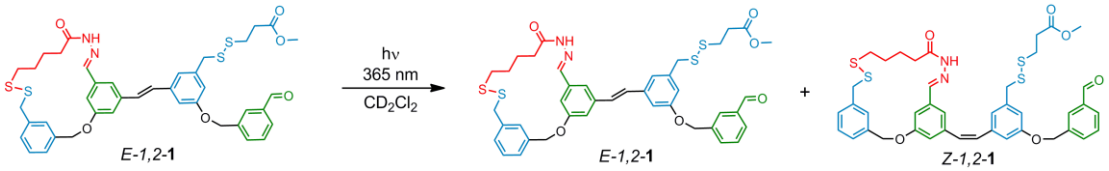

E-1,2-**1** ⟶ *Z-1,2*-**1** (500 MHz, CD_2Cl_2, RT)

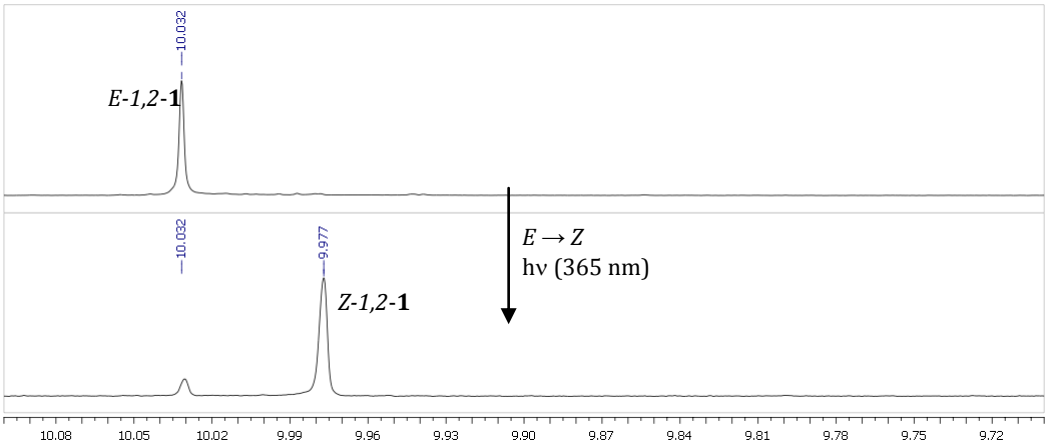

The reverse *Z*⟶*E* photoisomerisation (iodine-mediated) starting from a *E/Z-1,2*-**1** mixture led back to *E-1,2*-**1** (steady state ~ 95:5 (*E*/*Z*)).

Z-1,2-**1** ⟶ *E-1,2*-**1** (500 MHz, CD_2Cl_2, RT)

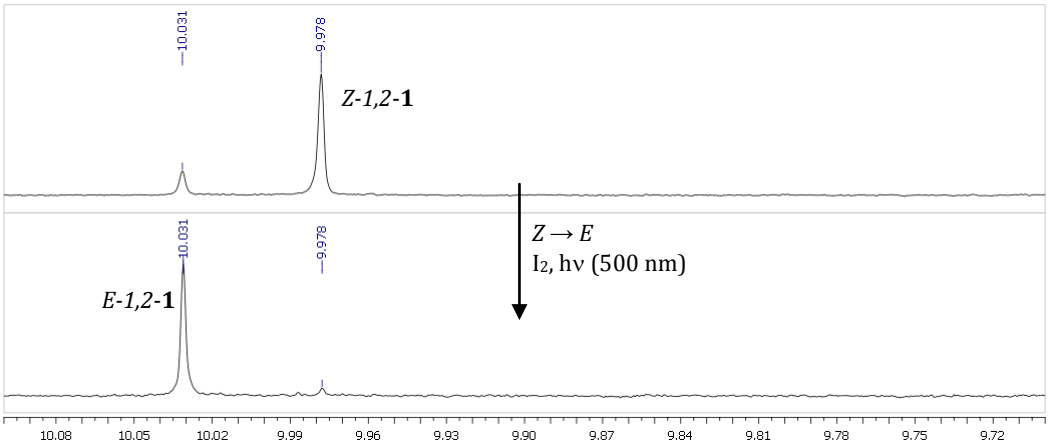

c) *E-3,4*-**1**

E-3,4-**1** was unambiguously synthesised (see Scheme S1) and its identity confirmed by means of 1D (^1H, ^{13}C) and 2D (COSY, ROESY, HSQC, HMBC) NMR spectroscopy, as well as HRMS and LCMS. The aldehyde proton in *E-3,4*-**1** exhibits a chemical shift of 9.944 ppm (500 MHz, CD_2Cl_2, RT).

d) *Z-3,4*-**1**

Direct *E*⟶*Z* photoisomerisation of pristine *E-3,4*-**1** gave *Z-3,4*-**1** (photostationary state ~ 92:8 (*Z*/*E*)).

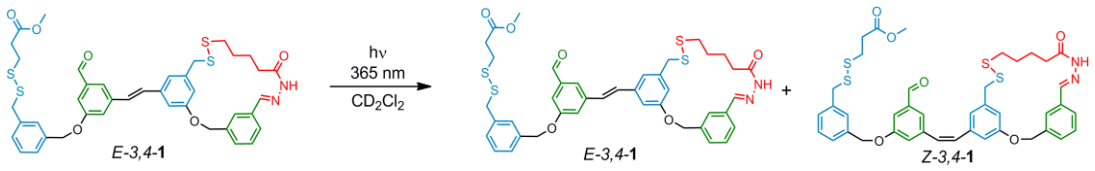

E-3,4-**1** → *Z-3,4*-**1** (500 MHz, CD_2Cl_2, RT)

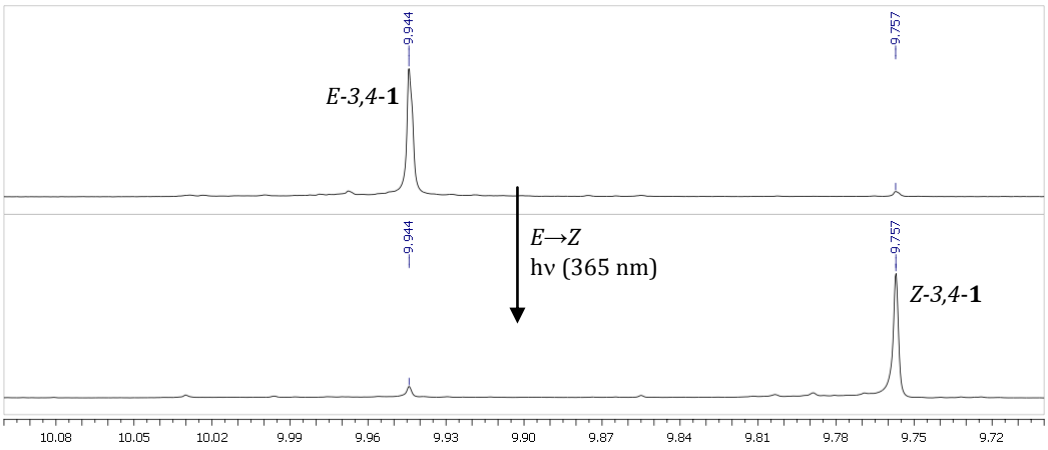

The reverse *Z*⟶*E* photoisomerisation (iodine-mediated) starting from a *E/Z-3,4*-**1** mixture led back to *E-3,4*-**1** (photostationary state ~ 89:11 (*E*/*Z*)).

Z-3,4-**1** → *E-3,4*-**1** (500 MHz, CD_2Cl_2, RT)

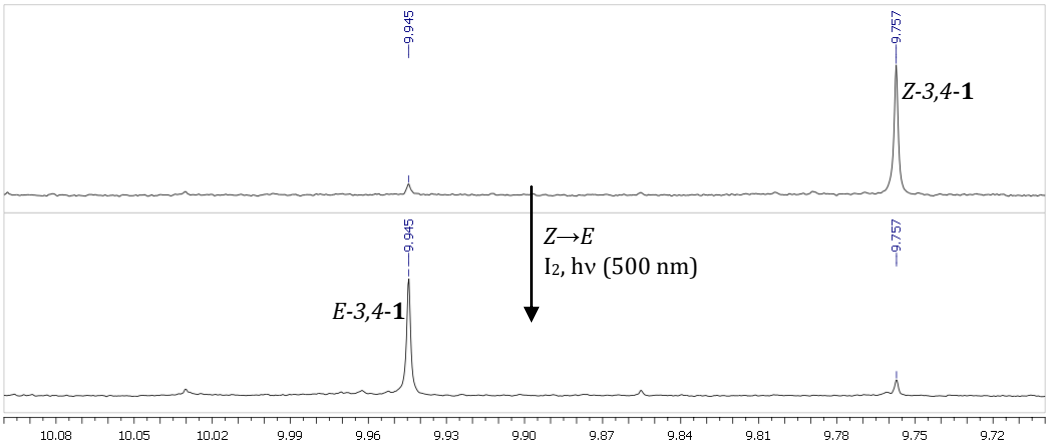

e) *Z-2,3*-**1** and *Z-1,3*-**1**-I

Reversible disulfide exchange starting from a *Z/E-1,2*-**1** mixture can theoretically give four new monomeric species: *Z-2,3*-**1**, *E-2,3*-**1**, *Z-1,3*-**1**-I and *E-1,3*-**1**-I. In the corresponding experiment starting from pure *E-1,2*-**1**, isomer *E-2,3*-**1** occurred only as trace (relatively strained) and isomer *E-1,3*-**1**-I was not detected at all (extremely strained).

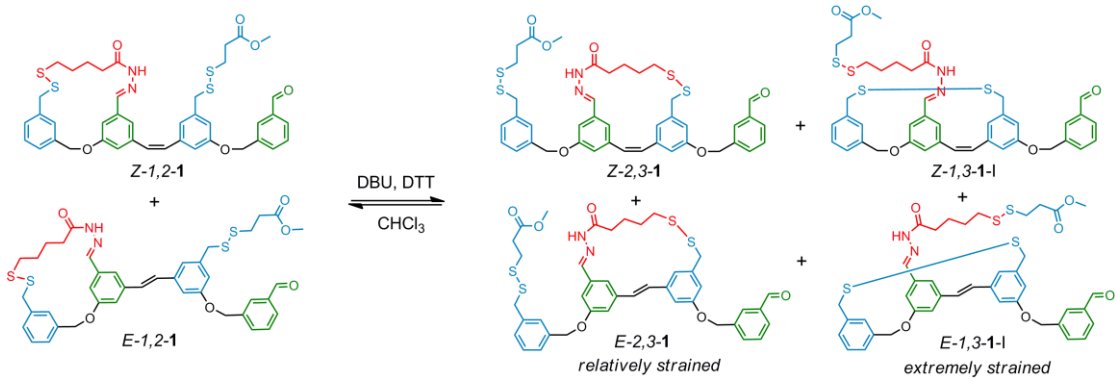

Z-2,3-**1** was isolated from such a mixture (semipreparative HPLC) and its identity confirmed by means of 1D (^{1}H, ^{13}C) and 2D (COSY, ROESY, HSQC, HMBC) NMR spectroscopy, as well as HRMS and LCMS (m/z = 787.2 $[M+H]^+$). As expected, *Z-2,3*-**1** was in equilibrium with *Z-3,4*-**1** upon acid-catalysed hydrazone exchange and gave *E-2,3*-**1** upon I_2-mediated photoisomerisation (see below).

We were not able to isolate *Z-1,3*-**1**-I from the mixtures by HPLC. Treatment of any mixture containing *Z-1,3*-**1**-I with acid (TFA) did, however, lead to appearance of a peak at 9.764 ppm, which can only belong to the other possible *1,3*-track-folded isomer *Z-1,3*-**1**-II (see subsection h). LCMS confirmed that *Z-1,3*-**1**-I is a monomeric isomer (m/z = 787.2 $[M+H]^+$).

Z-1,2-**1** + *E-1,2*-**1** ⟶ *Z-1,2*-**1** + *E-1,2*-**1** + *Z-2,3*-**1** + *Z-1,3*-**1**-I + *E-2,3*-**1** (500 MHz, CD_2Cl_2, RT)

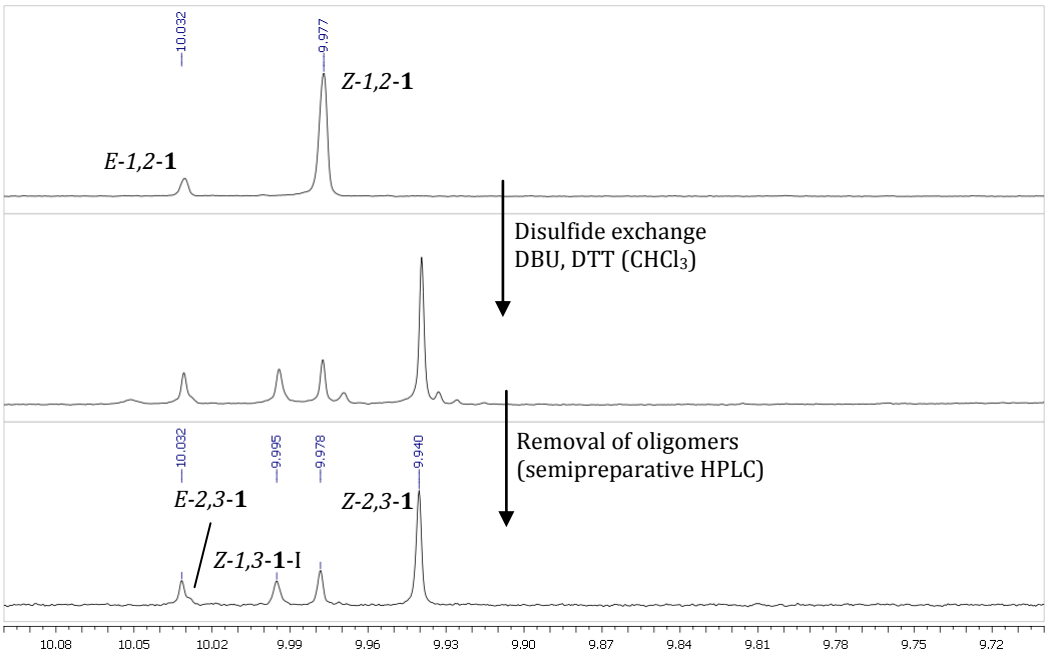

f) *E-2,3*-**1**

Z⟶*E* photoisomerisation (iodine-mediated) starting from pristine *Z-2,3*-**1** gave *E-2,3*-**1** (photostationary state ~ 75:25 (*E*/*Z*)).

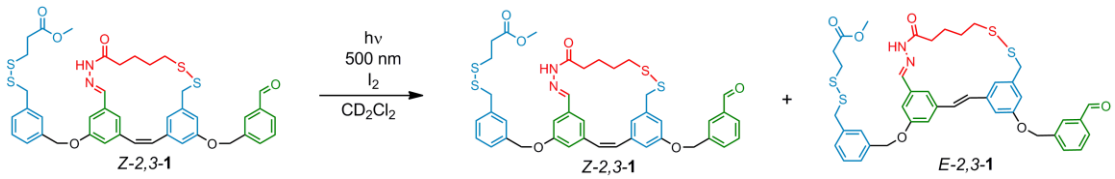

Z-2,3-**1** → *E-2,3*-**1** (500 MHz, CD_2Cl_2, RT)

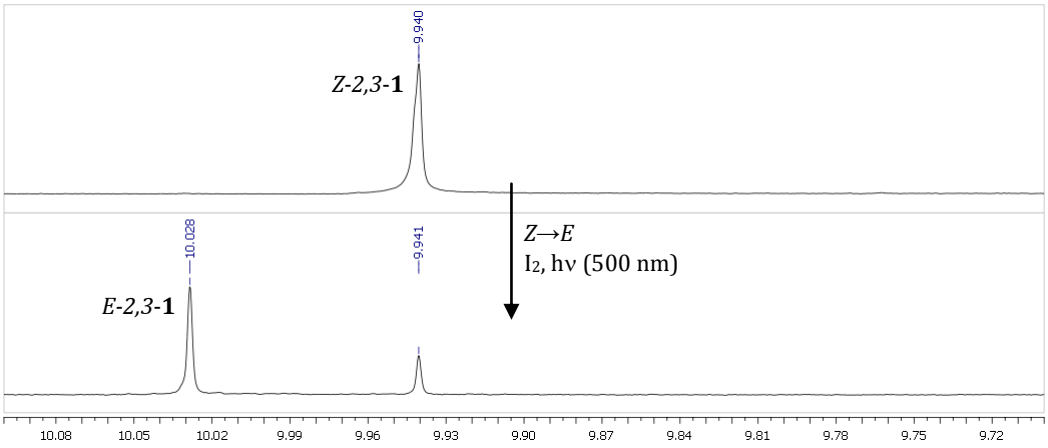

The reverse direct *E*⟶*Z* photoisomerisation of a *E/Z-2,3*-**1** mixture led back to *Z-2,3*-**1** (photostationary state ~ 68:32 (*Z*/*E*)). Comment on photostationary state: Direct photoisomerisation relies on the different molar absorptivities of the *E* and *Z* isomer at a given wavelength (here: 365 nm). For *Z-2,3*-**1** and *E-2,3*-**1** this difference is less significant as for *E*- and *Z-1,2*-**1**, for example.

E-2,3-**1** → *Z-2,3*-**1** (500 MHz, CD_2Cl_2, RT)

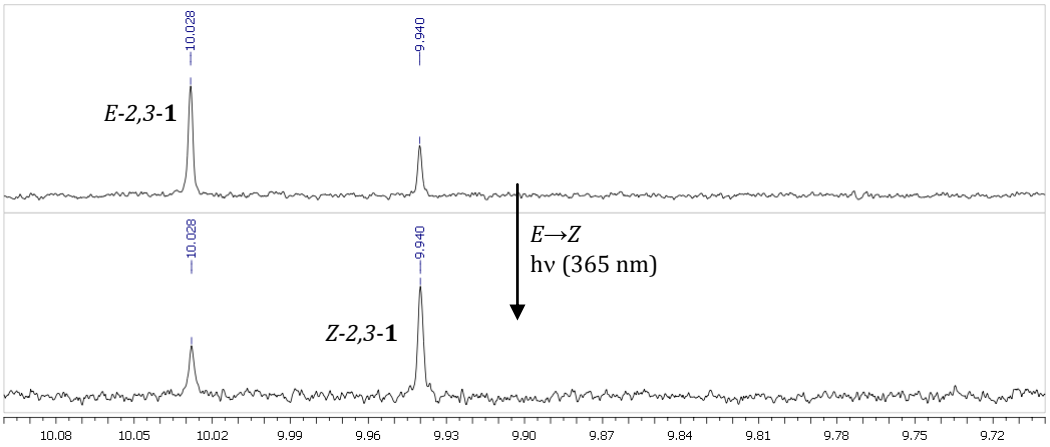

g) *E-1,4*-**1** and *Z-1,4*-**1**

Reversible hydrazone exchange starting from a *Z/E-1,2*-**1** mixture can only give positional isomers *Z-1,4*-**1** and *E-1,4*-**1**.

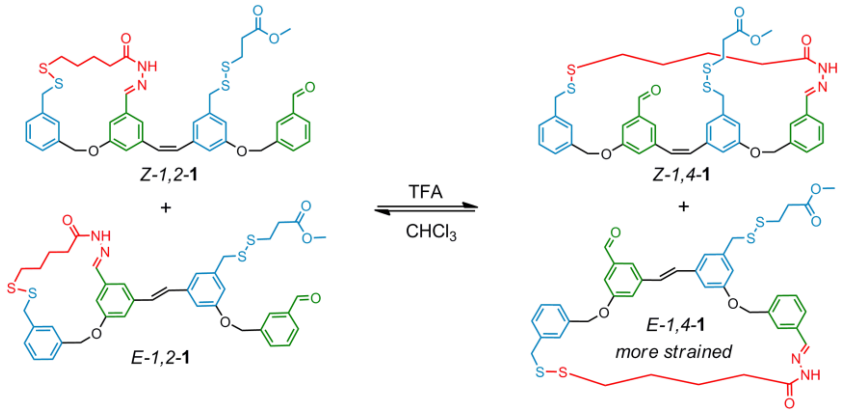

E-1,2-**1** + *Z-1,2*-**1** ⟶ *E-1,2*-**1** + *Z-1,2*-**1** + *Z-1,4*-**1** + *E-1,4*-**1** (400 MHz, CD_2Cl_2, RT)

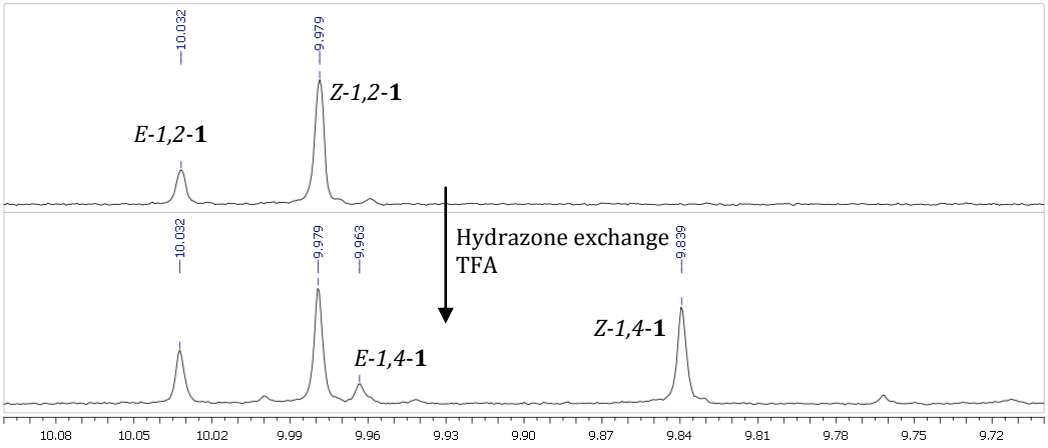

h) *Z-1,3*-**1**-II

Dynamic covalent disulfide exchange starting from a *Z/E-3,4*-**1** mixture gives positional isomers *Z-1,4*-**1**, *E-1,4*-**1** and undesired isomeric side product *Z-1,3*-**1**-II. Treatment of the sample with acid gives *Z-1,3*-**1**-I. No evidence was found for *E-1,3*-**1**-II (small peaks correspond to oligomeric species).

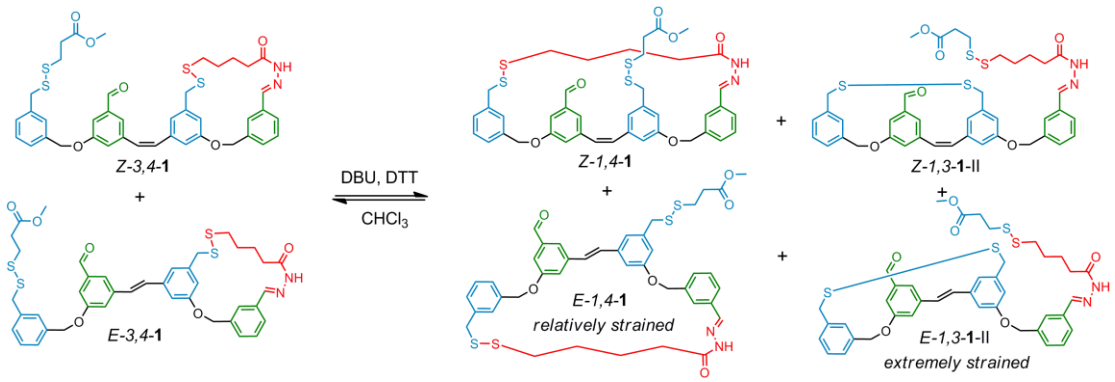

Z-3,4-**1** + *E-3,4*-**1** ⟶ *Z-3,4*-**1** + *E-3,4*-**1** + *Z-1,4*-**1** + *E-1,4*-**1** + *Z-1,3*-**1**-II (400 MHz, CD_2Cl_2, RT)

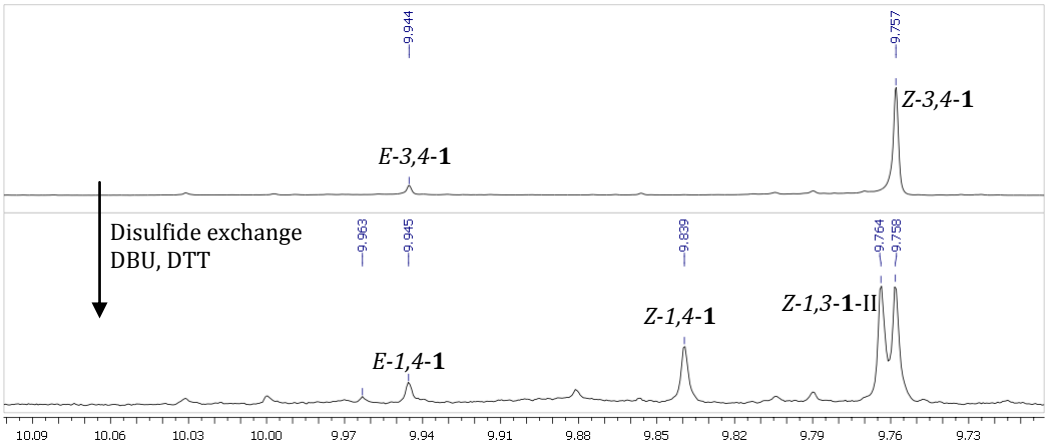

i) Summary

The NMR shifts of the aldehyde proton in the different isomers are given in Table 5.1. The structures of the corresponding compounds are presented in Figure 5.5.

Table 5.1. *^{1}H NMR shifts of the aldehyde proton (H_j or H_v) in all positional isomers and undesired isomeric side products Z-1,3-**1**-I and Z-1,3-**1**-II. Referenced to residual solvent ($CDHCl_2$, δ = 5.300 ppm).*

Entry	Isomer	Chemical Shift δ/ppm	Proton
1	*E-1,2*-**1**	10.031	H_v
2	*Z-1,2*-**1**	9.977	H_v
3	*E-2,3*-**1**	10.028	H_v
4	*Z-2,3*-**1**	9.940	H_v
5	*E-3,4*-**1**	9.944	H_j
6	*Z-3,4*-**1**	9.759	H_j
7	*E-1,4*-**1**	9.840	H_j
8	*Z-1,4*-**1**	9.759	H_j
9	*Z-1,3*-**1**-I	9.994	H_v
10	*Z-1,3*-**1**-II	9.764	H_j

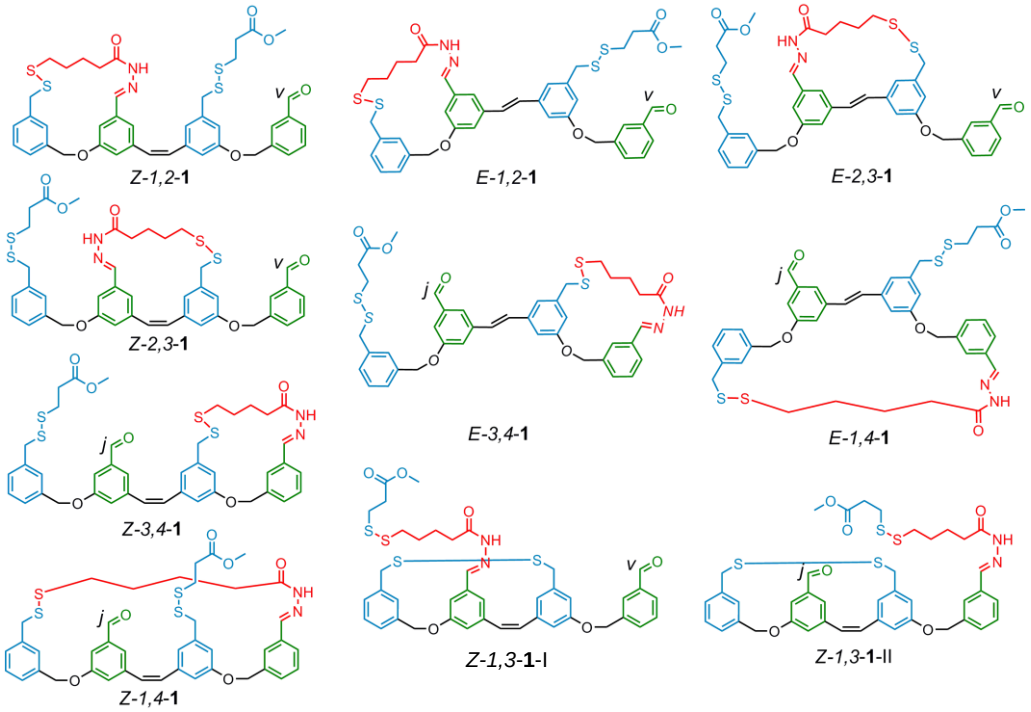

Figure 5.5. *Structures of the eight walking isomers and Z-1,3-**1**-I and Z-1,3-**1**-II.*

5.5.4 Preliminary Experiments Starting from Pristine *Z*-2,3-1

5.5.4.1 Directional bias towards E-3,4-1 when starting from pristine Z-2,3-1

500 MHz, CD_2Cl_2, RT

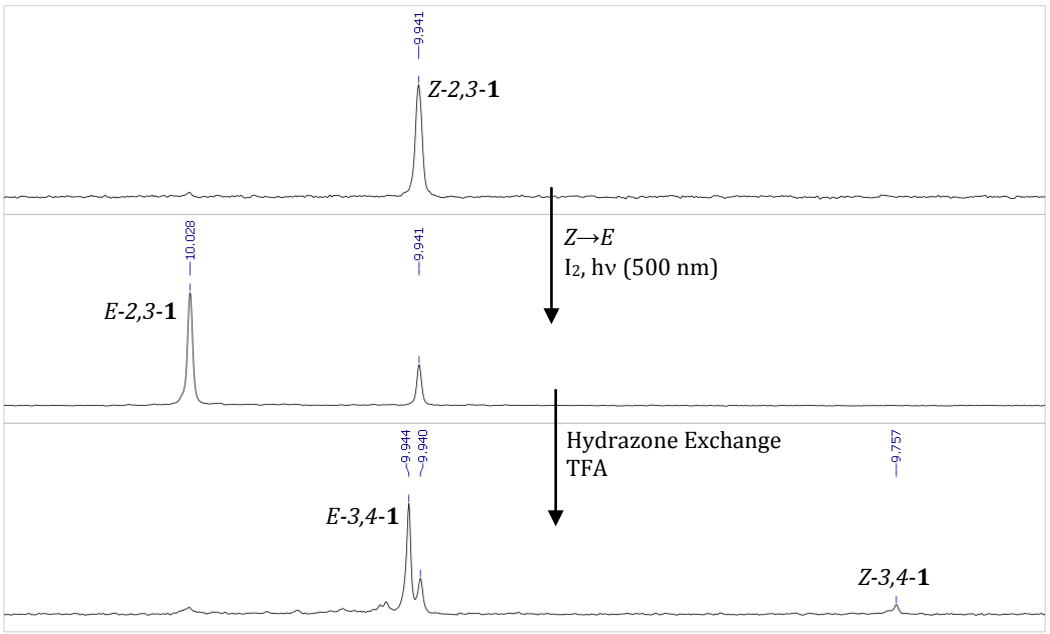

Figure 5.6. *Partial ^{1}H NMR stacked plot (10.1 to 9.7 ppm, 500MHz, CD_2Cl_2, RT) showing all spectra obtained during directionally biased transport of the walker unit from footholds 2,3 towards footholds 3,4. For experimental details see section 5.5.2.*

Table 5.2. *Composition of the system (in %) during the experiment. Values obtained by ^{1}H NMR integration. Estimated error margin: ±3%. Overlapping peaks integrated by means of Gaussian linefitting (MestreNova 6.0[23]).*

	Z-2,3-**1**	*E*-2,3-**1**	*E*-3,4-**1**	*Z*-3,4-**1**
Start	100%			
Z→*E*	25%	75%		
Hydrazone exchange	20%		74%	6%

5.5.4.2 *Directional bias towards E-1,2-1 when starting from pristine Z-2,3-1*

500 MHz, CD_2Cl_2, RT

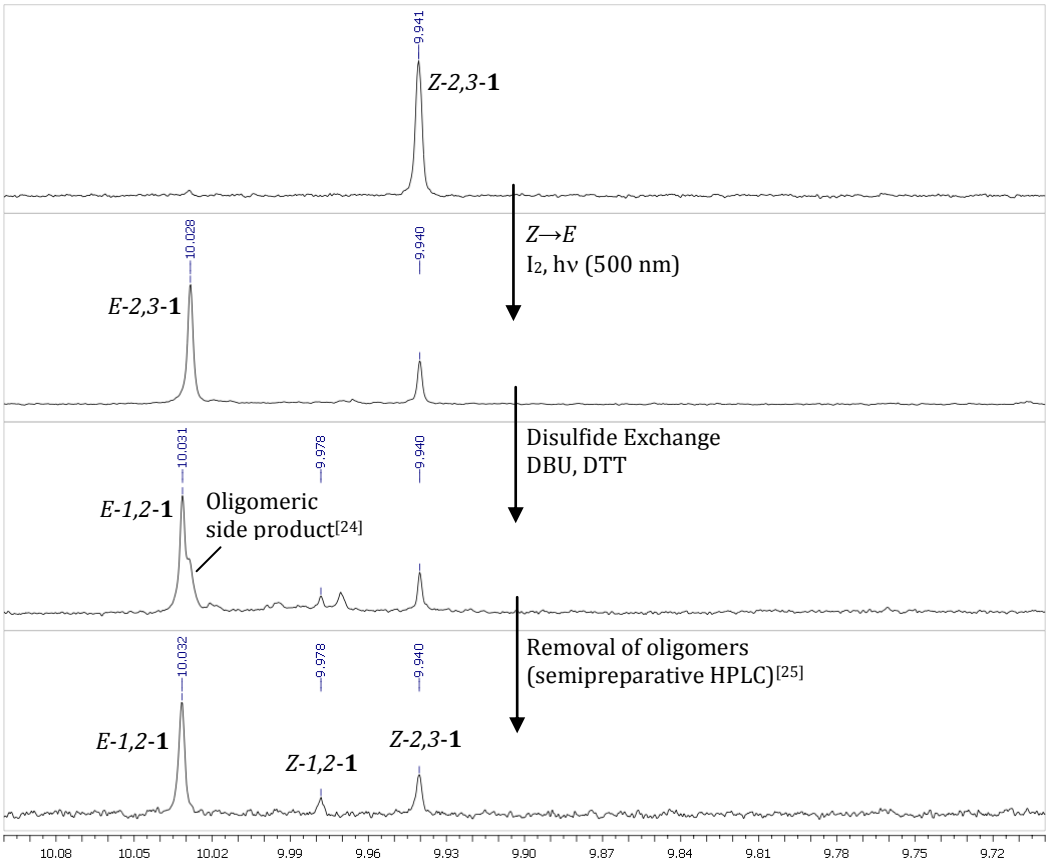

Figure 5.7. *Partial ^{1}H NMR stacked plot (10.1 to 9.7 ppm, 500MHz, CD_2Cl_2, RT) showing all spectra obtained during directionally biased transport of the walker unit from footholds 2,3 towards footholds 1,2. For experimental details see section 5.5.2.* [24,25]

Table 5.3. *Composition of the system (in %) during the experiment. Values obtained by ^{1}H NMR integration. Estimated error margin: ±3%. Overlapping peaks integrated by means of Gaussian linefitting (MestreNova 6.0*[23]*).*

	Z-2,3-**1**	*E-2,3*-**1**	*E-1,2*-**1**	*Z-1,2*-**1**
Start	100%			
Z→E	25%	75%		
Hydrazone exchange	20%		70%	10%
Purification	23%		69%	8%

5.5.5 Operation over one Full Cycle Starting from *E*-1,2-1 or *E*-3,4-1

5.5.5.1 Directionally biased operation starting from pristine E-1,2-1 (Figure 5.3a)

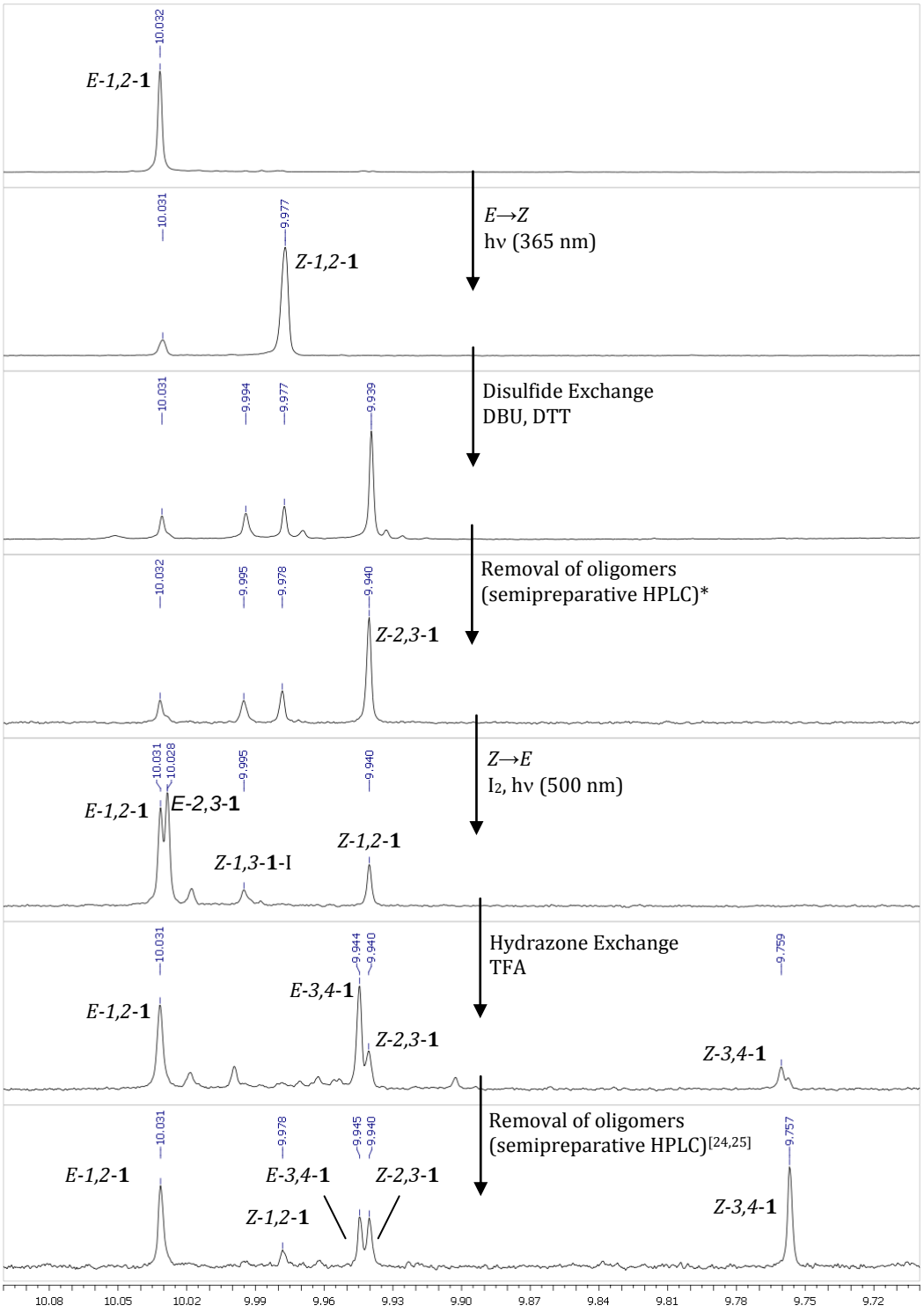

Figure 5.8. *Partial ^{1}H NMR stacked plot (10.1 to 9.7 ppm, 500 MHz, CD_2Cl_2, RT) showing all spectra obtained during directionally biased transport of the walker unit from footholds 1,2 towards footholds 3,4 (corresponds to Figure 5.3a in main text). For experimental details see section 5.5.2.[24,25]*

Table 5.4. *Composition of the system (in %) at different stages of the experiment. Values obtained by ^{1}H NMR integration. Estimated error margin: ±3%. Overlapping peaks integrated by means of Gaussian linefitting (MestreNova 6.0[23]).*

	E-1,2-**1**	*Z-1,2*-**1**	*E-2,3*-**1**	*Z-2,3*-**1**	*E-3,4*-**1**	*Z-3,4*-**1**	*E-1,4*-**1**	*Z-1,4*-**1**
Start	100%							
E→*Z*	12%	88%						
Disulfide exchange	14%	21%	~2%	63%				
purified	14%	20%	~2%	64%				
Z→*E*	39%		44%	17%				
Hydrazone exchange	36%	4%		10%	37%	8%	5%	
purified	30%	4%		16%	14%	32%	2%	1%

Table 5.5. *Reproduction of previous experiment. Composition of the system (in %) at different stages of the experiment. Values obtained by ^{1}H NMR integration. Estimated error margin: ±3%. Overlapping peaks integrated by means of Gaussian linefitting (MestreNova 6.0[23]).*

	E-1,2-**1**	*Z-1,2*-**1**	*E-2,3*-**1**	*Z-2,3*-**1**	*E-3,4*-**1**	*Z-3,4*-**1**	*E-1,4*-**1**	*Z-1,4*-**1**
Start	100%							
E→*Z*	19%	81%						
Disulfide exchange	17%	25%		58%				
purified	15%	24%	2%	59%				
Z→*E*	39%		41%	20%				
Hydrazone exchange	20%	10%		14%	9%	36%	5%	6%
purified	12%	18%		16%	6%	42%		6%

5.5.5.2 *Directionally counter-biased operation starting from E-1,2-1 (Figure 5.3b)*

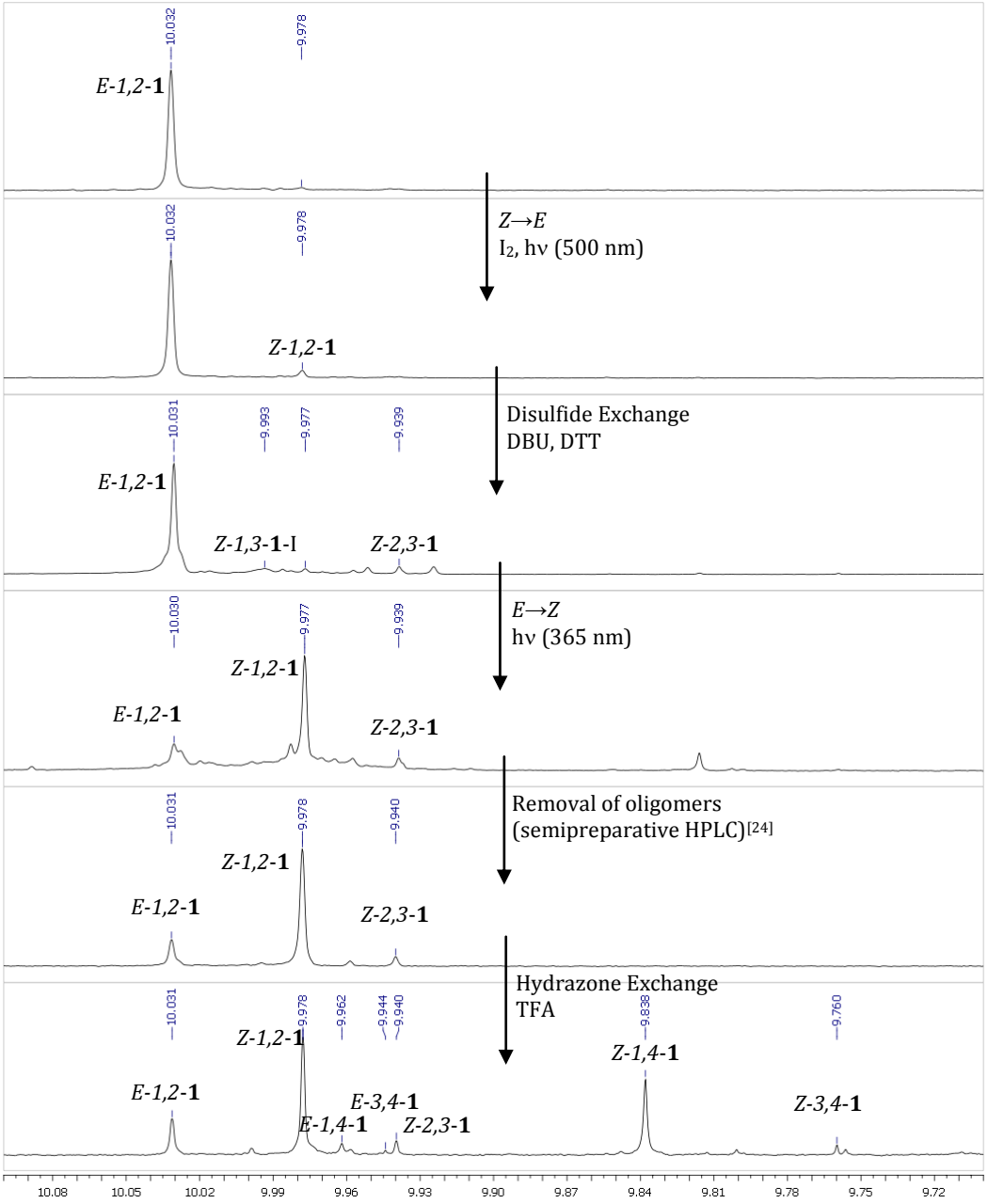

Figure 5.9. *Partial ^{1}H NMR stacked plot (10.1 to 9.7 ppm, 500 MHz, CD_2Cl_2, RT) showing all spectra obtained during directionally counter-biased transport of the walker unit from footholds 1,2 towards footholds 3,4 (corresponds to Figure 5.3b in main text). For experimental details see section 5.5.2.*[24]

Table 5.6. *Composition of the system (in %) at different stages of the experiment. Values obtained by ^{1}H NMR integration. Estimated error margin: ±3%. Overlapping peaks integrated by means of Gaussian linefitting (MestreNova 6.0[23]).*

	E-1,2-**1**	*Z-1,2*-**1**	*E-2,3*-**1**	*Z-2,3*-**1**	*E-3,4*-**1**	*Z-3,4*-**1**	*E-1,4*-**1**	*Z-1,4*-**1**
Start	100%							
Z→*E*	94%	6%						
Disulfide exchange	92%	3%		5%				
E→*Z*	20%	72%		8%				
purified	16%	77%	~2%	5%				
Hydrazone exchange	15%	43%		5%	2%	2%	4%	29%

Table 5.7. *Reproduction of previous experiment. Composition of the system (in %) at different stages of the experiment. Values obtained by ^{1}H NMR integration. Estimated error margin: ±3%. Overlapping peaks integrated by means of Gaussian linefitting (MestreNova 6.0[23]).*

	E-1,2-**1**	*Z-1,2*-**1**	*E-2,3*-**1**	*Z-2,3*-**1**	*E-3,4*-**1**	*Z-3,4*-**1**	*E-1,4*-**1**	*Z-1,4*-**1**
Start	100%							
Z→*E*	94%							
Disulfide exchange	90%	5%		5%				
E→*Z*	28%	64%		8%				
purified	18%	76%		6%				
Hydrazone exchange	14%	44%		5%	2%	3%	4%	28%

5.5.5.3 *Directionally biased operation starting from pristine E-3,4-1 (Figure 5.3c)*

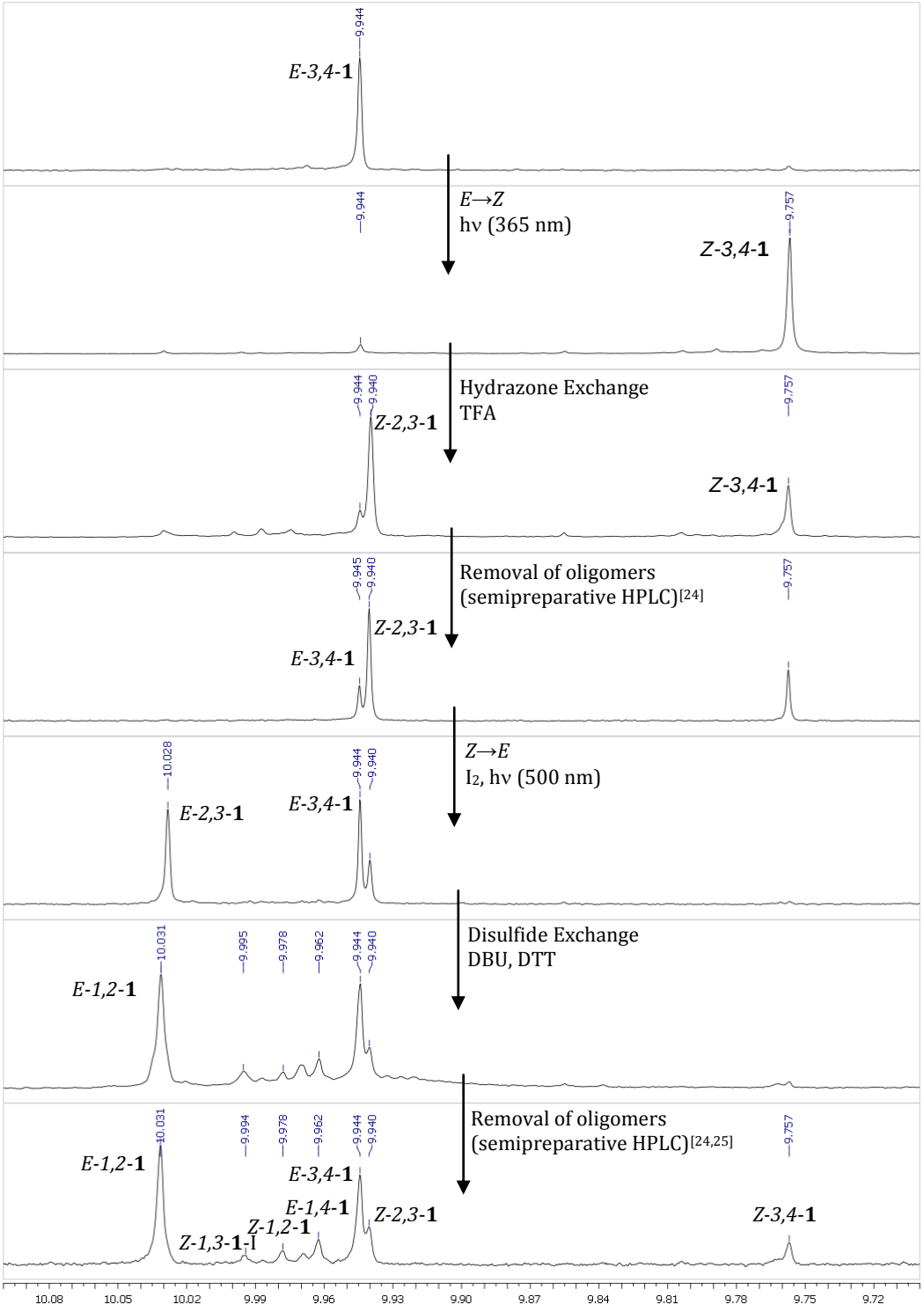

Figure 5.10. *Partial ^{1}H NMR stacked plot (10.1 to 9.7 ppm, 500 MHz, CD_2Cl_2, RT) showing all spectra obtained during directionally biased transport of the walker unit from footholds 3,4 towards footholds 1,2 (corresponds to Figure 5.3c in main text). For experimental details see section 5.5.2.*[24,25]

Table 5.8. *Composition of the system (in %) at different stages of the experiment. Values obtained by ^{1}H NMR integration. Estimated error margin: ±3%. Overlapping peaks integrated by means of Gaussian linefitting (MestreNova 6.0[23]).*

	E-1,2-**1**	*Z-1,2*-**1**	*E-2,3*-**1**	*Z-2,3*-**1**	*E-3,4*-**1**	*Z-3,4*-**1**	*E-1,4*-**1**	*Z-1,4*-**1**
Start					100%			
E→*Z*					9%	91%		
Hydrazone exchange				59%	12%	29%		
Purification				60%	15%	25%		
Z→*E*			43%	16%	39%	2%		
Disulfide exchange	39%	6%		9%	34%	~1%	10%	1%
Purification	43%	5%		7%	30%	6%	8%	

5.5.5.4 *Directionally counter-biased operation starting from E-3,4-1 (Figure 5.3d)*

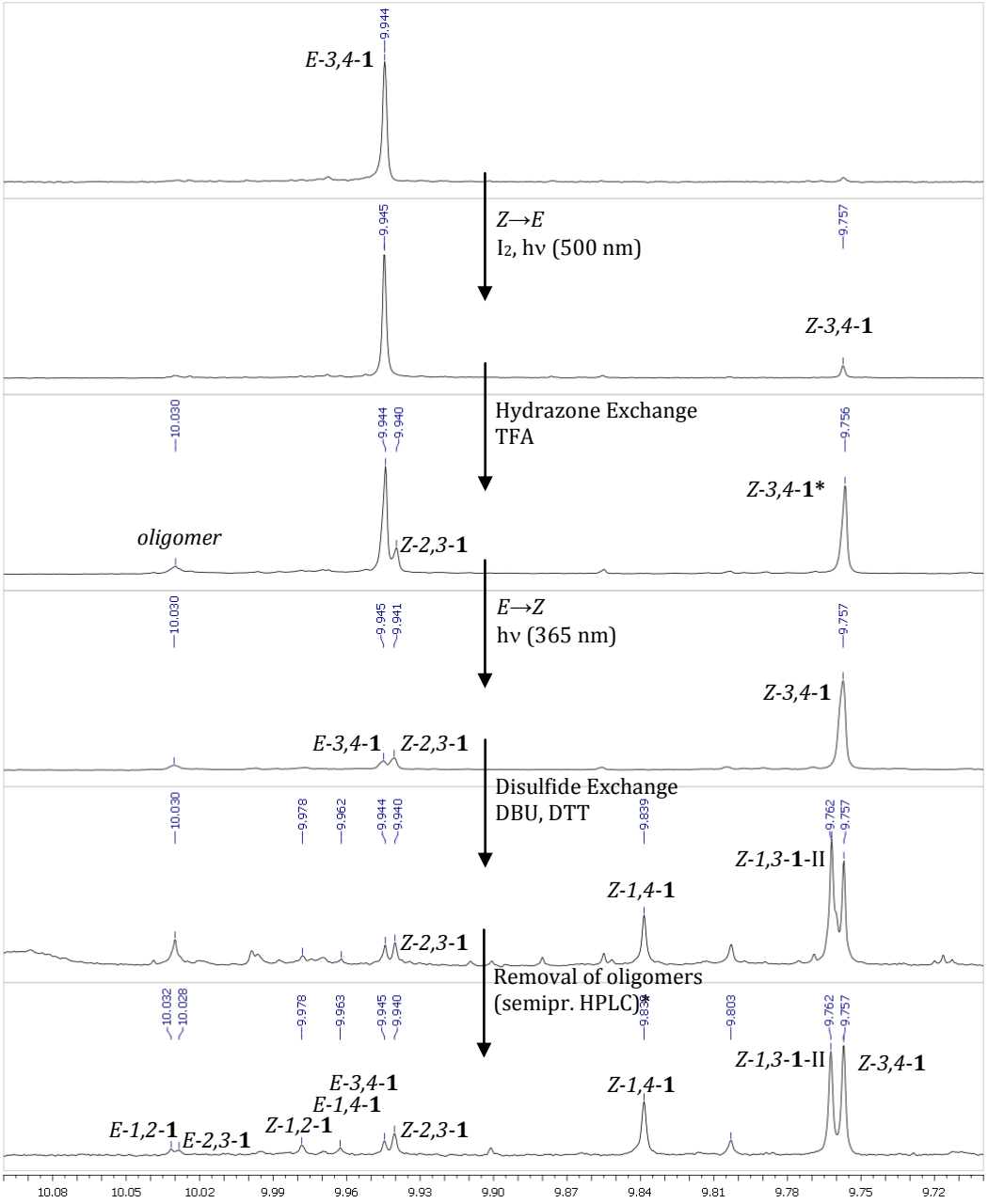

Figure 5.11. *Partial ^{1}H NMR stacked plot (10.1 to 9.7 ppm, 500 MHz, CD_2Cl_2, RT) showing all spectra obtained during directionally counter-biased transport of the walker unit from footholds 3,4 towards footholds 1,2 (corresponds to Figure 5.3c in main text). For experimental details see section 5.5.2.[24] *: Z/E ratio changed after workup as a result of the sample being exposed to sunlight.*

Table 5.9. *Composition of the system (in %) at different stages of the experiment. Values obtained by ^{1}H NMR integration. Estimated error margin: ±3%. Overlapping peaks integrated by means of Gaussian linefitting (MestreNova 6.0[4]).*

	E-1,2-**1**	*Z*-1,2-**1**	*E*-2,3-**1**	*Z*-2,3-**1**	*E*-3,4-**1**	*Z*-3,4-**1**	*E*-1,4-**1**	*Z*-1,4-**1**
Start					100%			
Z→*E*					91%	9%		
Hydrazone exchange			4%	8%	49%*	39%*		
E→*Z*			2%	11%	7%	80%		
Disulfide exchange	10%	4%		9%	10%	40%	2%	25%
Purification	2%	5%	~1%	10%	5%	45%	5%	27%

*: Z/E ratio changed after workup as a result of the sample being exposed to sunlight.

5.5.6 Isomer Ratios Employed for Extrapolation Calculations

Table 5.10. *Fundamental isomer ratios obtained by ^{1}H NMR integration from individual experiments such as the ones presented in section 5.5.3. Estimated error margin: ±3%. Based on these ratios, the behaviour of the system can be predicted with good accuracy. The calculated data presented in Figure 5.3 and Figure 5.4 is based on such a 'spreadsheet' extrapolation.*

Dynamic covalent exchange	Equilibrium ratio
E-1,2-**1**/*E-2,3*-**1**	~98:2
E-1,2-**1**/*E-1,4*-**1**	71:29
E-3,4-**1**/*E-2,3*-**1**	~98:2
E-3,4-**1**/*E-1,4*-**1**	77:23
Z-1,2-**1**/*Z-2,3*-**1**	25:75
Z-1,2-**1**/*Z-1,4*-**1**	51:49
Z-3,4-**1**/*Z-2,3*-**1**	30:70
Z-3,4-**1**/*Z-1,4*-**1**	60:40
Stilbene *E*→*Z* isomerisation	Steady state ratio
Z-1,2-**1**/*E-1,2*-**1**	88:12
Z-2,3-**1**/*E-2,3*-**1**	68:32
Z-3,4-**1**/*E-3,4*-**1**	92:8
Z-1,4-**1**/*E-1,4*-**1**	~90:10
Stilbene *Z*→*E* isomerisation	Steady state ratio
E-1,2-**1**/*Z-1,2*-**1**	94:6
E-2,3-**1**/*Z-2,3*-**1**	75:25
E-3,4-**1**/*Z-3,4*-**1**	89:11
E-1,4-**1**/*Z-1,4*-**1**	~90:10

5.5.7 Synthesis Overview

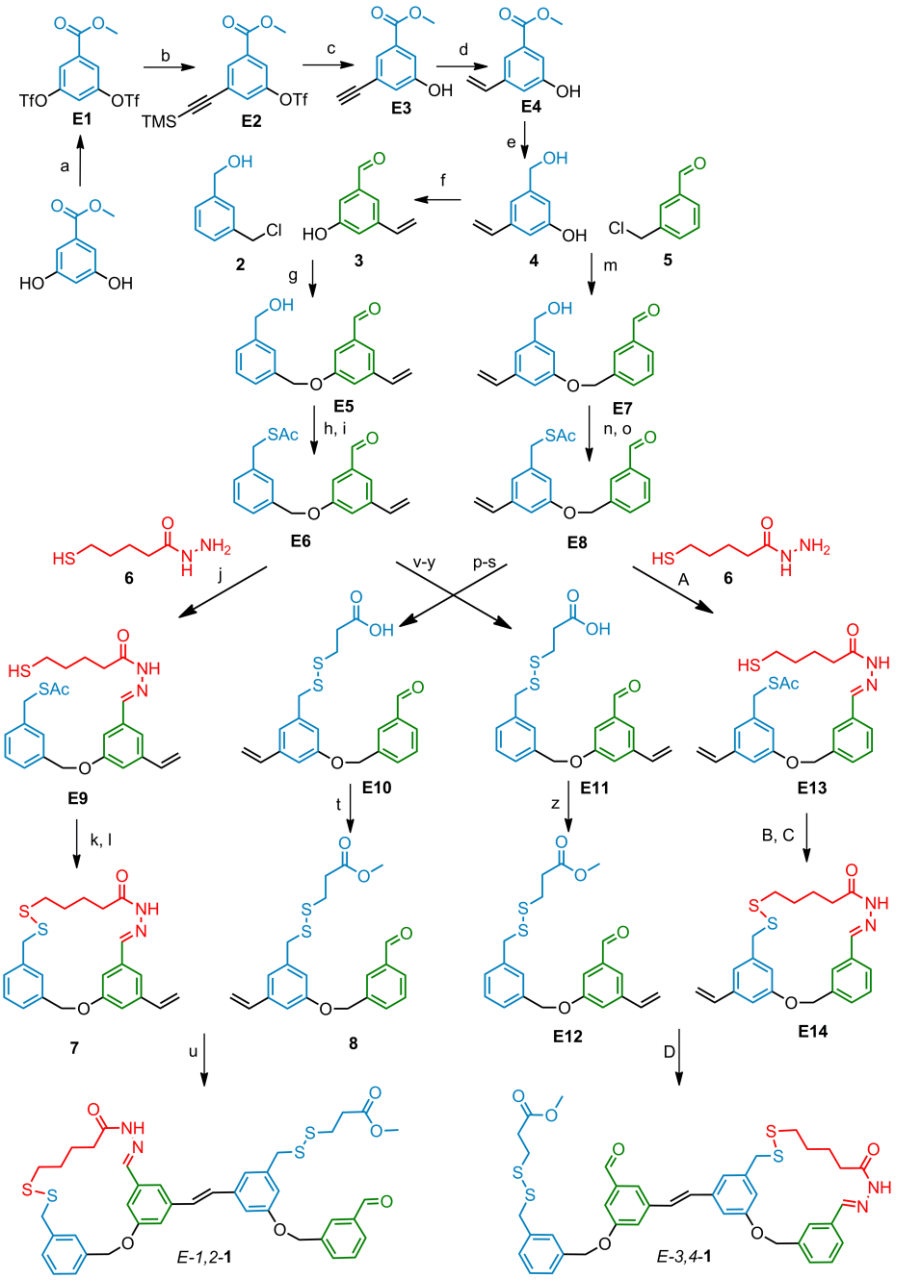

Scheme 5.4. *Reaction conditions: a) Tf_2O, NEt_3, CH_2Cl_2, 0 °C → RT, 16 h, 96%; b) TMS-acetylene, $Pd(PPh_3)_2$, CuI, NEt_3 THF, RT, 16 h, 79%; c) KF, DMSO, r.t, 16 h, 96%; d) Lindlar cat., H_2, CH_2Cl_2/n-hexane/EtOH, RT, 2 h; e) $LiAlH_4$, THF, 0 °C → RT, 81% (two steps); f) MnO_2, Acetone, RT, 16 h, 90%; g) NaH, DMF, RT, 16 h; h) MsCl, NEt_3, CH_2Cl_2, 0 °C → RT, 1.5 h; i) KSAc, DMF, RT, 3 h, 59% (three steps); j) AcOH (cat.), MeOH, RT, 2 h, 83%; k) NaOMe, MeOH, RT, 2 h; l) I_2, KI, CH_2Cl_2, RT, 5 min, 48% (two steps); m) NaH, DMF, RT, 16 h; n) MsCl, NEt_3, CH_2Cl_2, 0 °C → RT, 2 h; o) KSAc, DMF, RT, 3 h, 35% (three steps); p) $HC(OMe)_3$,* p*-TsOH, MeOH, RT, 1 h; (q) NaOMe, MeOH, RT, 3 h; (r) 3-mercaptopropionic acid, I_2, KI, CH_2Cl_2, RT, 5 min; s) HCl 1M, CH_2Cl_2, RT, 15 min, 69% (four steps); t) AcCl, MeOH, 0 °C → RT, 5 h, 76%; u) Ω_A-SIMes-CF_3 catalyst, μw, 100 °C, 3 h, 23%; v) $HC(OMe)_3$, p-TsOH, MeOH, RT, 1 h; w) NaOMe, MeOH, RT, 3 h; x) 3-mercaptopropionic acid, I_2, KI, CH_2Cl_2, RT, 5 min; y) HCl 1M, CH_2Cl_2, RT, 15 min, 59% (four steps); z) AcCl, MeOH, 0 °C → RT, 5 h, 50%; A) AcOH (cat.), MeOH, RT, 2 h, 92%; B) NaOMe, MeOH, RT, 2 h; C) I_2, KI, CH_2Cl_2, RT, 5 min, 35% (two steps); D) Ω_A-SIMes-CF_3 catalyst, μw, 100 °C, 3 h, 25%.*

5.5.8 Synthetic Procedures and Characterisation Data

Compounds **2**, **5** and **6** (**C$_4$** walker moiety) were synthesised as described in Chapters III and IV.

Methyl 3,5-bis(trifluoromethylsulfonyloxy)benzoate

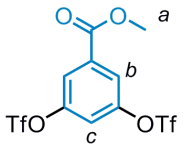

E1

Under N_2, a solution of trifluoromethanesulfonic anhydride (40.0 mL, 235 mmol, 2.05 equiv.) in CH_2Cl_2 (50 mL) was added dropwise to an ice cold solution of methyl 3,5-dihydroxybenzoate (19.9 g, 115 mmol, 1.0 equiv.) and NEt_3 (40 ml, 287 mmol, 2.5 equiv.) in CH_2Cl_2 (200 mL). The reaction mixture was stirred at room temperature over night, H_2O (200 mL) was added and the aqueous phase was extracted with CH_2Cl_2 (3 × 100 mL). The combined organic phases were washed with 1 M HCl (100 mL) and brine (100 mL) before drying over $MgSO_4$. Removal of the solvent under reduced pressure and flash column chromatography (SiO_2, petrol ether/CH_2Cl_2 1:1) gave **E1** (47.8 g, 96%) as a colourless solid. M.p. 56 – 58 °C; ^{1}H NMR (400 MHz, $CDCl_3$): δ = 8.00 (d, *J* = 2.3 Hz, 2 H, H_b), 7.44 (d, *J* = 2.3 Hz, 1 H, H_c), 4.00 (s, 3 H, H_a); ^{13}C NMR (100 MHz, $CDCl_3$): δ = 149.4, 134.3, 122.6, 120.2, 119.2, 117.0, 53.3; HRMS (ESI): *m*/*z* = 430.9330 $[M-H]^-$ (calcd. 430.9336 for $C_{10}H_5F_6O_8S_2$).

Methyl 3-(trifluoromethylsulfonyloxy)-5-((trimethylsilyl)ethynyl)benzoate

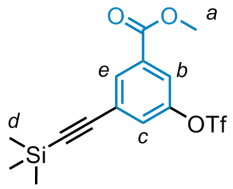

E2

Under N_2, a solution of trimethylsilylacetylene (15.9 mL, 112.6 mmol, 1.02 equiv.) in THF (10 mL) was added dropwise via a syringe pump (4 mL/h) to a solution of **E1** (47.74 g, 110.4 mmol, 1.0 equiv.), CuI (1.99 g, 11.0 mmol, 0.1 equiv.) and $Pd(PPh_3)_2Cl_2$ (3.88 g, 5.5 mmol, 0.05 equiv.) in THF (250 mL) and NEt_3 (50 ml). The reaction was stirred at room temperature over night, the solvents were removed under reduced

pressure and the residue was dissolved in CH_2Cl_2 (100 ml). Saturated NH_4Cl (4 x 50 ml) was added and the mixture was extracted with CH_2Cl_2 (4 x 50 ml). The combined organic phases were dried over $MgSO_4$ and the solvent was removed under reduced pressure. Purification by flash column chromatography (SiO_2, petrol ether/EtOAc 98:2) gave **E2** as a yellow oil (33.13 g, 79%). ^{1}H NMR (400 MHz, $CDCl_3$): δ = 8.13 (m, 1 H, H_b), 7.85 (m, 1 H, H_e), 7.52 (m, 1 H, H_c), 3.95 (s, 3 H, H_a), 0.26 (s, 9 H, H_d); ^{13}C NMR (100 MHz, $CDCl_3$): δ = 164.5, 149.0, 132.9, 132.9, 128.5, 126.1, 122.2, 120.2, 117.0, 101.4, 98.6, 52.8, -0.3; HRMS (ESI$^+$): m/z = 398.0702 $[M+NH_4]^+$ (calcd. 398.0700 for $C_{14}H_{19}F_3O_5NSSi$).

Methyl 5-ethynyl-3-hydroxybenzoate

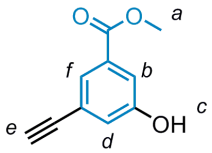

E3

A solution of KF (15.2 g, 261.3 mmol, 3.0 equiv.) in H_2O (20 mL) was added dropwise to a solution of **E2** (33.1 g, 87.1 mmol, 1.0 equiv.) in DMSO (200 mL). The mixture was stirred at room temperature over night, 1 M HCl (100 mL) and H_2O (200 mL) was added and the mixture was extracted with Et_2O (4 × 200 mL). The combined organic phases were washed with saturated $NaHCO_3$ (200 mL), H_2O (200 mL) and brine (200 mL) and were dried over $MgSO_4$. Removal of the solvent under reduced pressure and purification by flash column chromatography (SiO_2, petrol ether/EtOAc 7:3) gave **E3** as a colourless oil that crystallised after several days (14.7 g, 96%). M. p. 88-90 °C. ^{1}H NMR (400 MHz, $CDCl_3$): δ = 7.74 (m, 1 H, H_{Ar}), 7.54 (m, 1 H, H_{Ar}), 7.16 (m, 1 H, H_{Ar}), 5.51 (s, 1 H, H_c), 3.92 (s, 3 H, H_a), 3.10 (s, 1H, H_e); ^{13}C NMR (100 MHz, $CDCl_3$): δ = 166.3, 155.6, 131.6, 125.8, 123.7, 123.3, 117.1, 82.3, 78.1, 52.5; HRMS (ESI$^+$): m/z = 194.0810 $[M+NH_4]^+$ (calcd. 194.0812 for $C_{10}H_{12}NO_3$).

Methyl 3-hydroxy-5-vinylbenzoate

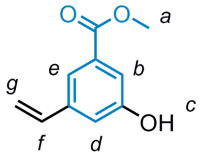

E4

To a solution of **E3** (7.10 g, 40.3 mmol, 1.0 equiv.) in CH_2Cl_2 (150 mL), *n*-hexane (150 mL) and EtOH (150 mL) was added quinoline (4.86 mL, 40.3 mmol, 1.0 equiv.) and Lindlar catalyst (1.72 g, 0.81 mmol, 0.02 equiv. in respect to Pd(0)). After stirring the solution for 15 min, the flask was fitted with a rubber septum and the gas volume was repeatedly evacuated and flushed with H_2. The mixture was stirred for 2 h at room temperature under an H_2 atmosphere (^{1}H NMR monitoring every 15 min). N_2 was bubbled through the flask and the mixture was filtered over a celite plug (washing with EtOH). Removal of the solvents under reduced pressure gave a mixture of **E4** and quinoline that was used for the next step without further purification. ^{1}H NMR (400 MHz, acetone-d_6): δ = 7.57-7.56 (m, 1H, H_e), 7.40-7.39 (m, 1H, H_b), 7.19-7.18 (m, 1H, H_d), 6.75 (dd, J = 17.6, 10.9 Hz, 1H, H_f), 5.83 (d, J = 17.6 Hz, 1H, H_g), 5.30 (d, J = 11.0 Hz, 1H, H_g), 3.86 (s, 3H, H_a); LRMS (EI): m/z = 178.1 $[M]^+$.

3-(Hydroxymethyl)-5-vinylphenol

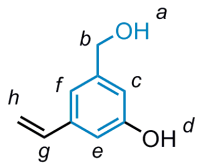

4

Under N_2, a solution of **E4** (14.8 g, 83 mmol, 1.0 equiv.) in THF (150 mL) was added dropwise to an ice-cooled suspension of $LiAlH_4$ (12.6 g, 332 mmol, 4.0 equiv.) in THF (500 mL). After slow warming to room temperature the solution was stirred over night. The mixture was carefully quenched with a H_2O/THF (2:1) mixture and dilute H_2SO_4 was added until most of the precipitate had dissolved. H_2O (300 mL) was added and the mixture was extracted with Et_2O (3 × 200 mL). The combined organic phases were washed with saturated $NaHCO_3$ (200 mL), brine (200 mL) and dried over $MgSO_4$. Removal of the solvents under reduced pressure and purification by flash column

chromatography (SiO_2, CH_2Cl_2/MeOH 98:2 → 95:5) gave **4** as a yellowish oil (10.07 g, 81% two step yield). ^{1}H NMR (400 MHz, acetone-d_6): δ = 8.41 (bs, 1 H, H_d), 6.93 (s, 1 H, H_{Ar}), 6.81 (m, 2 H, H_{Ar}), 6.66 (dd, *J* = 17.6 Hz, 10.9 Hz, 1 H, H_g), 5.73 (d, *J* = 17.6 Hz, 1 H, H_h), 5.19 (d, *J* = 10.9 Hz, 1 H, H_h), 5.55 (d, *J* = 5.5 Hz, 2 H, H_b), 4.37 (t, *J* = 5.5 Hz, 1 H, H_a); ^{13}C NMR (150 MHz, acetone-d_6): δ = 159.46, 146.10, 140.63, 138.98, 117.71, 115.01, 114.81, 113.11, 65.46; HRMS (ESI$^+$): m/z = 168.1017 $[M+NH_4]^+$ (calcd. 168.1019 for $C_9H_{14}O_2N_1$).

3-Hydroxy-5-vinylbenzaldehyde

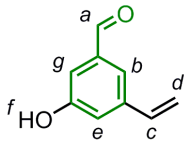

3

4 (223 mg, 1.49 mmol, 1.0 equiv.) was dissolved in acetone (30 mL). Active manganese dioxide (388 mg, 4.47 mmol, 3.0 equiv.) was added and the suspension was allowed to stir for 3 h. A second portion of active manganese dioxide (258 mg, 2.98 mmol, 2.0 equiv.) was added and the reaction mixture was stirred at room temperature over night. The reaction mixture was filtered, dried over $MgSO_4$ and the solvent was removed under reduced pressure. Purification by flash column chromatography (SiO_2, DCM/MeOH 98:2) gave **3** as a colourless solid (199 mg, 90%). M.p. 48-50 °C. ^{1}H NMR (400 MHz, $CDCl_3$): δ = 9.94 (s, 1 H, H_a), 7.48 (s, 1 H, H_{Ar}), 7.27 (m, 1 H, H_{Ar}), 7.18 (m, 1 H, H_{Ar}), 6.70 (dd, *J* = 17.6 Hz, 10.9 Hz, 1 H, H_c), 6.22 (bs, 3 H, H_f), 5.82 (d, *J* = 17.6 Hz, 1 H, H_d), 5.37 (d, *J* = 10.9 Hz, 1 H, H_d); ^{13}C NMR (201 MHz, $CDCl_3$): δ = 192.71, 156.53, 140.08, 137.75, 135.11, 121.18, 119.18, 115.92, 114.04; HRMS (ESI$^+$): m/z = 148.0516 $[M+H]^+$ (calcd. 148.0519 for $C_9H_8O_2$).

3-(3-(Hydroxymethyl)benzyloxy)-5-vinylbenzaldehyde

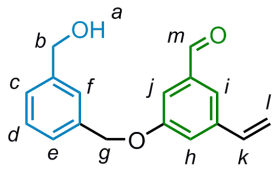

E5

Under N_2, **3** (2.69 g, 18.14 mmol, 1.0 equiv.) was dissolved in dry DMF (40 mL). At 0 °C, NaH (60% in mineral oil, 457 mg, 19.04 mmol, 1.05 equiv.) was added and the solution was allowed to stir for 1 h, while warming to room temperature. At 0 °C, a solution of **2** (2.84 g, 18.14 mmol, 1.00 equiv.) in dry DMF (15 mL) was added dropwise and the mixture was allowed to stir over night at room temperature. Polymerisation inhibitor 4-tert-butylcatechol (0.3 mg, 0.02 mmol, 0.1%) was added and the solvent was removed under reduced pressure in the dark. The crude product was used directly for the next step (a small aliquot was worked up (NH_4Cl, Et_2O) to obtain the characterisation data). ^{1}H NMR (400 MHz, $CDCl_3$): δ = 9.97 (s, 1H, H_m), 7.53 (s, 1H, H_{Ar}), 7.48 (s, 1H, H_{Ar}), 7.41-7.32 (m, 4H, H_{Ar}), 7.29 (t, *J* = 2.0 Hz, 1H, H_{Ar}), 6.73 (dd, *J* = 17.6 Hz, 10.9 Hz, 1H, H_k), 5.84 (d, *J* = 17.6 Hz, 1H, H_l), 5.37 (d, *J* = 10.9 Hz, 1H, H_l), 5.14 (s, 2H, H_g), 4.74 (s, 2H, H_b); ^{13}C NMR (100 MHz, $CDCl_3$): δ = 192.07, 159.43, 141.37, 139.89, 137.89, 136.57, 135.37, 128.94, 126.83, 126.80, 126.05, 121.70, 119.62, 116.07, 112.30, 70.15, 65.13; HRMS (ESI$^+$): *m*/*z* = 286.1438 $[M+NH_4]^+$ (calcd. 286.1439 for $C_{17}H_{20}NO_3$).

S-3-((3-Formyl-5-vinylphenoxy)methyl)benzyl ethanethioate

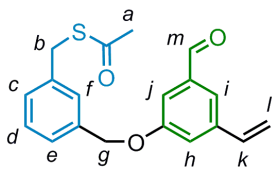

E6

a) At 0 °C, the crude **E5** (18.14 mmol, 1.0 equiv.) was dissolved in CH_2Cl_2 (100 mL) and NEt_3 (10.08 mL, 72.5 mmol, 4.0 equiv.) was added. After 5 min a solution of MsCl (4.15 g, 36.3 mmol, 2.0 equiv.) in CH_2Cl_2 (20 mL) was added dropwise and the mixture was stirred for 1.5 h at room temperature. The reaction was monitored by TLC (SiO_2, *n*-hexane/EtOAc 1:1). H_2O (100 mL) was added and the layers were separated. The aqueous layer was extracted with CH_2Cl_2 (3 × 50 mL) and the combined organic phases

were washed with brine and dried ($MgSO_4$). Removal of the solvent under reduced pressure gave the crude mesylate as a yellowish oil.

b) The crude mesylate (18.14 mmol, 1.0 equiv.) was dissolved in dry DMF (50 mL) and a solution of KSAc (3.11 g, 27.21 mmol, 1.5 equiv.) in DMF (10 mL) was added dropwise. The mixture was stirred for 3 h at room temperature and the bulk of DMF was removed under reduced pressure. H_2O (30 mL) was added and the mixture extracted with CH_2Cl_2 (3 × 30 mL). The combined organic phases were washed with brine, dried ($MgSO_4$) and concentrated under reduced pressure. Flash column chromatography (SiO_2, *n*-hexane/EtOAc 9:1) gave **E6** (3.52 g, 10.77 mmol, 59% three step yield) as a colourless oil. ^{1}H NMR (400 MHz, $CDCl_3$): δ = 9.97 (s, 1H, H_m), 7.53 (s, 1H, H_{Ar}), 7.39-7.35 (m, 2H, H_{Ar}), 7.34-7.32 (m, 2H, H_{Ar}), 7.29-7.27 (m, 2H, H_{Ar}), 6.73 (dd, *J* = 17.6 Hz, 10.9 Hz, 1H, H_k), 5.84 (d, *J* = 17.6 Hz, 1H, H_l), 5.37 (d, *J* = 10.9 Hz, 1H, H_l), 5.10 (s, 2H, H_g), 4.14 (s, 2H, H_b), 2.36 (s, 3H, H_a); ^{13}C NMR (150 MHz, $CDCl_3$); δ = 195.02, 192.00, 159.40, 139.87, 138.18, 137.90, 136.64, 135.38, 128.99, 128.70, 127.94, 126.47, 121.58, 119.55, 116.04, 112.48, 70.03, 33.23, 30.32; HRMS (ESI$^+$): *m*/*z* = 327.1054 $[M+H]^+$ (calcd. 327.1049 for $C_{19}H_{19}O_3S$).

3-((3-(Hydroxymethyl)-5-vinylphenoxy)methyl)benzaldehyde

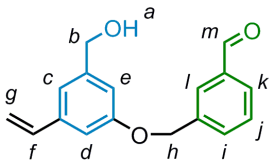

E7

Under N_2, **4** (3.00 g, 19.98 mmol, 1.0 equiv.) was dissolved in dry DMF (30 mL). At 0 °C, NaH (60% in mineral oil, 839 mg, 20.98 mmol, 1.05 equiv.) was added and the solution was allowed to stir for 3 h, while warming to room temperature. At 0 °C, a solution of **5** (3.24 g, 20.98 mmol, 1.05 equiv.) in dry DMF (15 mL) was added dropwise and the mixture was allowed to stir over night at room temperature. The reaction was monitored by TLC (SiO_2, *n*-hexane/EtOAc 1:1). Polymerisation inhibitor 4-tert-butylcatechol (3 mg, 0.02 mmol, 0.1%) was added and the solvent was removed under reduced pressure in the dark. The crude was used directly, since several attempts to isolate this compound in pure and dry form led to polymerisation. ^{1}H NMR (400 MHz, $CDCl_3$): δ = 10.03 (s, 1H, H_m), 7.96 (s, 1H, H_l), 7.85 (d, *J* = 7.6 Hz, 1H, H_k), 7.71 (d, *J* = 7.7 Hz, 1H, H_i), 7.58-7.55 (m, 1H, H_j), 7.03 (s, 1H, H_c), 6.95 (s, 1H, H_e), 6.92 (s, 1H, H_d), 6.67

(dd, J = 17.6 Hz, 10.9 Hz, H_f), 5.75 (d, J = 17.6 Hz, 1H, H_g), 5.27 (d, J = 10.9 Hz, 1H, H_g), 5.15 (s, 2H, H_h), 4.67 (s, 2H, H_b); ^{13}C NMR (150 MHz, $CDCl_3$): δ = 192.17, 158.84, 142.82, 139.26, 138.12, 136.57, 136.37, 133.19, 129.32, 129.25, 128.27, 117.76, 114.59, 112.41, 111.70, 69.07, 64.87.

S-3-(3-Formylbenzyloxy)-5-vinylbenzyl ethanethioate

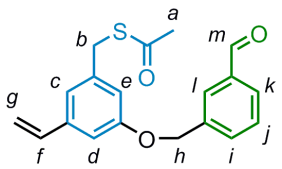

E8

a) At 0 °C, the crude **E7** (20.0 mmol, 1.0 equiv.) was dissolved in CH_2Cl_2 (100 mL) and NEt_3 (11.2 mL, 80.0 mmol, 4.0 equiv.) was added. After 5 min a solution of MsCl (4.58 g, 40.0 mmol, 2.0 equiv.) in CH_2Cl_2 (25 mL) was added dropwise and the mixture was stirred for 2 h at room temperature. The reaction was monitored by TLC (SiO_2, *n*-hexane/EtOAc 1:1). H_2O (100 mL) was added and the layers were separated. The aqueous layer was extracted with CH_2Cl_2 (2 × 75 mL) and the combined organic phases were washed with brine and dried ($MgSO_4$). Removal of the solvent under reduced pressure gave the crude mesylate as a colourless oil.

b) **The crude mesylate** (19.98 mmol, 1.0 equiv.) was dissolved in dry DMF (50 mL) and a solution of KSAc (3.42 g, 29.97 mmol, 1.5 equiv.) in DMF (15 mL) was added dropwise. The mixture was stirred over night at room temperature and the reaction was monitored by TLC (SiO_2, *n*-hexane/EtOAc 4/1). The bulk of DMF was removed under reduced pressure. H_2O (30 mL) was added and the mixture extracted wit CH_2Cl_2 (3 × 50 mL). The combined organic phases were washed with brine, dried ($MgSO_4$) and the solvent was removed under reduced pressure. Flash column chromatography (SiO_2, cyclohexane/EtOAc 85/15) gave **S8** (2.30 g, 7.05 mmol, 35% three step yield) as a colourless oil. ^{1}H NMR (400 MHz, $CDCl_3$): δ = 10.05 (s, 1H, H_m), 7.96 (s, 1H, H_l), 7.85 (d, J = 7.6 Hz, 1H, H_i or H_k), 7.71 (d, J = 7.6 Hz, 1H, H_i or H_k), 7.57 (t, J = 7.6 Hz, 1H, H_j), 6.95 (s, 1H, H_c or H_d or H_e), 6.91 (m, 1H, H_c or H_d or H_e), 6.83 (m, 1H, H_c or H_d or H_e), 6.64 (dd, J = 17.6 Hz, 10.9 Hz, 1H, H_f), 5.73 (d, J = 17.6 Hz, 1H, H_g), 5.26 (d, J = 10.9 Hz, 1H, H_g), 5.13 (s, 2H, H_h), 4.08 (s, 2H, H_b), 2.35 (s, 3H, H_a); ^{13}C NMR (150 MHz, $CDCl_3$); δ = 194.96, 192.08, 158.81, 139.43, 139.41, 138.08, 136.67, 136.25, 133.24, 129.29 (2C), 128.45,

119.96, 114.76, 114.57, 111.42, 69.15, 33.30, 30.29; HRMS (ESI+): m/z = 327.1046 $[M+H]^+$ (calcd. 327.1049 for $C_{19}H_{19}O_3S$).

(E)-S-3-((3-((2-(5-Mercaptopentanoyl)hydrazono)methyl)-5-vinylphenoxy)methyl)benzyl ethanethioate

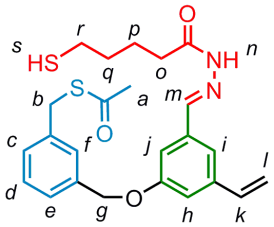

E9

Under N_2, **S6** (858 mg, 2.63 mmol, 1.0 equiv.) was dissolved in dry MeOH (20 mL). Three drops of acetic acid were added after which a solution of **6** (428 mg, 2.89 mmol, 1.1 equiv.) in dry MeOH (5 mL) was added dropwise. The reaction was monitored by TLC (SiO_2, CH_2Cl_2/EtOAc 9:1). After 2 h the solvent was removed under reduced pressure and the residue was purified by flash column chromatography (SiO_2, CH_2Cl_2/EtOAc 9:1) which gave **S9** (998 mg, 83%) as a colourless oil. ^{1}H NMR (600 MHz, $CDCl_3$): δ = 10.12 (s, 1H, H_n), 7.79 (s, 1H, H_m), 7.38 (s, 1H, H_{Ar}), 7.34-7.26 (m, 5H, H_{Ar}), 7.22 (m, 1H, H_{Ar}), 7.06 (m, 1H, H_{Ar}), 6.59 (dd, J = 17.6 Hz, 10.9 Hz, 1H, H_k), 5.78 (d, J = 17.6 Hz, 1H, H_l), 5.31 (d, J = 10.9 Hz, 1H, H_l), 5.07 (s, 2H, H_g), 4.14 (s, 2 H, H_b), 2.79 (t, J = 7.4 Hz, 2H, H_o), 2.60 (q, J = 7.6 Hz, H_r), 2.35 (s, 3H, H_a), 1.86-1.75 (m, 4H, H_p, H_q), 1.39 (t, J = 7.6 Hz, H_r); ^{13}C NMR (150 MHz, $CDCl_3$): δ = 194.98, 176.06, 159.20, 143.44, 139.45, 138.10, 137.01, 136.03, 135.30, 128.94, 128.58, 127.94, 126.47, 118.75, 115.13, 114.38, 111.81, 69.93, 33.58, 33.26, 32.00, 30.29, 24.31, 23.37; HRMS (ESI+): submitted m/z = 457.1622 $[M+H]^+$ (calcd. 457.1614 for $C_{24}H_{29}N_2O_3S_2$).

(E)-22-Vinyl-2-oxa-10,11-dithia-17,18-diaza-tricyclo[18.3.1.1^{4,8}]pentacosa-1(23),4,6,8(25),18,20(24),21-heptaen-16-one

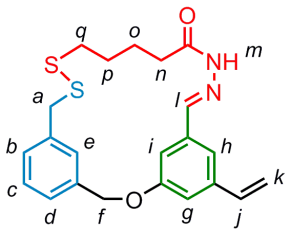

7

Under N_2, **E9** (52 mg, 114 µmol, 1.0 equiv.) was dissolved in MeOH (5 mL) and CH_2Cl_2 (2 mL). A solution of NaOMe (12.3 mg, 228 µmol, 2.0 equiv.) in MeOH (2 mL) was added. After 1.5 h of stirring at room temperature, CH_2Cl_2 (50 mL) and KI (3.8 mg, 23 µmol, 0.2 equiv.) were added. A solution of I_2 (29 mg, 114 µmol, 1.0 equiv.) in CH_2Cl_2 (30 mL) was added dropwise until the brown colour persisted. Na_2SO_3 was added to reduce the excess of I_2 and, when decolourisation was complete, stirring was continued for 15 min. H_2O (20 mL) was added and the phases were separated. The H_2O layer was extracted another time with CH_2Cl_2 (20 mL). The organic layers were combined, dried ($MgSO_4$) and the solvent was removed under reduced pressure. Purification by flash column chromatography (SiO_2, CH_2Cl_2/EtOAc 9:1) yielded pure **7** (22 mg, 48%) as a colourless solid. M.p. 134-135 °C. ^{1}H NMR (600 MHz, $CDCl_3$): δ = 9.18 (s, 1H, H_m), 7.77 (s, 1H, H_l), 7.45 (s, 1H, H_{Ar}), 7.37 (m, 3H, H_{Ar}), 7.29 (d, *J* = 6.7 Hz, 1H, H_{Ar}), 7.12 (s, 1H, H_{Ar}), 6.80 (dd, *J* = 17.5 Hz, 10.9 Hz, 1H, H_j), 5.90 (d, *J* = 17.5 Hz, 1H, H_k), 5.46 (s, 2H, H_f), 5.45 (d, *J* = 10.9 Hz, 1H, H_k), 3.97 (s, 2H, H_a), 2.68 (t, *J* = 7.8 Hz, 2H, H_n), 2.36 (t, *J* = 7.8 Hz, 2H, H_q), 1.79 (quin, *J* = 7.8 Hz, 2H, H_o), 1.69 (quin, *J* = 7.8 Hz, 2H, H_p); ^{13}C NMR (150 MHz, $CDCl_3$): δ = 175.56, 159.62, 142.67, 139.62, 138.62, 137.80, 135.69, 135.16, 128.79, 128.08, 126.32, 124.43, 121.22, 117.68, 115.34, 107.29, 69.77, 44.05, 37.89, 32.52, 29.09, 24.40; HRMS (ESI$^+$): *m*/*z* = 413.1360 [M+H]$^+$ (calcd. 413.1352 for $C_{24}H_{25}N_2O_2S_2$).

3-((3-(3-Formylbenzyloxy)-5-vinylbenzyl)disulfanyl)propanoic acid

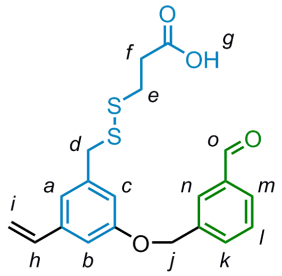

E10

Under N_2, **E8** (800 mg, 2.45 mmol, 1.0 equiv.), trimethyl orthoformate (274 mg, 2.58 mol, 1.05 equiv.) and *p*-TsOH·H_2O (10 mg, 53 µmol, 0.02 equiv.) were dissolved/suspended in MeOH (15 mL). The mixture was stirred at room temperature for 1 h. A solution of NaOMe (265 mg, 4.91 mmol, 2.0 equiv.) in MeOH (15 mL) was added and the mixture was stirred for 3 h at room temperature. KI (102 mg, 0.61 mol, 0.25 equiv.) and a solution containing 3-mercaptopropionic acid (2.60 g, 24.5 mmol, 10.0 equiv.) and NaOMe (1.32 g, 24.5 mmol, 10.0 equiv.) in MeOH (15 mL) was added. The resulting mixture was titrated with a solution of I_2 (3.81 g, 15.0 mmol) in DCM (50 mL) until the brown colour persisted. Na_2SO_3 was added and the mixture was stirred until decolourisation was complete. 1M HCl (75 mL) and CH_2Cl_2 (75 mL) were added and after stirring the mixture for 1 hour the two layers were separated. The aqueous layer was extracted with CH_2Cl_2 (3 × 50 mL). The combined CH_2Cl_2 layers were dried over $MgSO_4$. The solvents were removed under reduced pressure and the resulting residue was purified by flash column chromatography (SiO_2, CH_2Cl_2/MeOH 95:5) to yield 1.20 g of a ~3:5 (mol ratio) mixture of **E10** (657 mg, 69%) and dipropionic acid disulfide mono methyl ester as a colourless oil. No further purification was undertaken at this step. ^{1}H NMR (600 MHz, $CDCl_3$): δ = 10.05 (s, 1H, H_o), 7.99 (s, 1H, H_n), 7.85 (d, *J* = 7.6 Hz, 1H, H_m or H_k), 7.72 (d, *J* = 7.6 Hz, 1H, H_m or H_k), 7.57 (t, *J* = 7.6 Hz, 1H, H_l), 6.99 (s, 1H, H_a or H_b or H_c), 6.95 (s, 1H, H_a or H_b or H_c), 6.87 (s, 1H, H_a or H_b or H_c), 6.66 (dd, *J* = 17.6 Hz, 10.9 Hz, 1H, H_h), 5.75 (d, *J* = 17.6 Hz, 1H, H_i), 5.28 (d, *J* = 10.9 Hz,1H, H_i), 5.16 (s, 2H, H_j), 3.86 (s, 2H, H_d), 2.92 (t, *J* = 7.2 Hz, 2H, H_e), 2.80 (t, *J* = 7.2 Hz, 2H, H_f); ^{13}C NMR (150 MHz, $CDCl_3$): δ = 192.22, 176.76, 158.81, 139.41, 139.04, 138.14, 136.68, 136.25, 133.29, 129.56, 129.33, 128.32, 120.45, 115.00, 114.84, 111.76, 69.21, 43.49, 33.56, 32.43; HRMS (ESI$^+$): *m/z* = 406.1139 $[M+NH_4]^+$ (calcd. 406.1141 for $C_{20}H_{24}NO_4S_2$).

Methyl 3-((3-(3-formylbenzyloxy)-5-vinylbenzyl)disulfanyl)propanoate

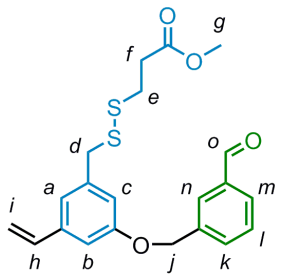

8

Acetyl chloride (353 mg, 0.32 mL, 4.50 mmol, 1.1 equiv.) was added to an ice cold solution of 1.20 g (4.09 mmol) of a ~3:5 (mol ratio) mixture of **E10** and dipropionic acid disulfide mono methyl ester in MeOH (40 mL). The solution was allowed to slowly warm to room temperature and stirred for further 5 h. The reaction was monitored by TLC (SiO_2, *n*-hexane/EtOAc 4:1). The solvent was removed under reduced pressure. Purification by flash column chromatography (SiO_2, petrol ether/EtOAc 9/1) gave **8** as a colourless oil (520 mg, 76%). ^{1}H NMR (600 MHz, $CDCl_3$): δ = 10.05 (s, 1H, H_o), 7.89 (s, 1H, H_n), 7.85 (d, J = 7.6 Hz, 1H, H_m or H_k), 7.72 (d, J = 7.6 Hz, 1H, H_m or H_k), 7.58 (t, J = 7.6 Hz, 1H, H_l), 7.00 (s, 1H, H_a or H_b or H_c), 6.95 (s, 1H, H_a or H_b or H_c), 6.87 (s, 1H, H_a or H_b or H_c), 6.66 (dd, J = 17.6 Hz, 10.8 Hz, 1H, H_h), 5.75 (d, J = 17.6 Hz, 1H, H_i), 5.28 (d, J = 10.9 Hz, 1H, H_i), 5.16 (s, 2H, H_j), 3.86 (s, 2H, H_d), 3.67 (s, 3H, H_g), 2.70 (t, J = 7.0 Hz, 2H, H_e), 2.63 (t, J = 7.0 Hz, 2H, H_f); ^{13}C NMR (150 MHz, $CDCl_3$): δ = 192.05, 172.12, 158.79, 139.39, 139.03, 138.13, 136.72, 136.28, 133.24, 129.40, 129.33, 128.38, 120.46, 114.96, 114.80, 111.76, 69.22, 51.82, 43.50, 33.83, 32.89; HRMS (ESI$^+$): m/z = 403.1025 $[M+H]^+$ (calcd. 403.1032 for $C_{21}H_{23}O_4S_2$).

3-{3-(3-Formyl-benzyloxy)-5-[(E)-2-((E)-16-oxo-2-oxa-10,11-dithia-17,18-diaza-tricyclo[18.3.1.1^{4,8}]pentacosa-1(23),4,6,8(25),18,20(24),21-heptaen-22-yl)-vinyl]-benzyldisulfanyl}-propionic acid methyl ester

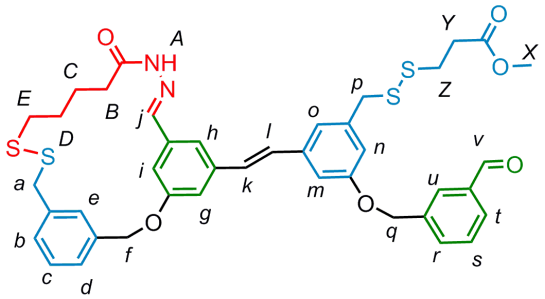

E-1,2-**1**

Under N_2, **7** (49.5 mg, 0.12 mmol, 1.0 equiv.), **8** (48.2 mg, 0.12 mmol, 1.0 equiv.) and Ω_A-SIMes™ catalyst[2,3] (8.8 mg, 0.012 mmol, 0.1 equiv.) were dissolved in CH_2Cl_2 (5 mL). The mixture was subjected to microwave irradiation for 3 hours (300 W, 100 °C) and the solvent was removed under reduced pressure. Purification by flash column chromatography (SiO_2, hexane/AcOEt 9:1 → 1:1) gave *E-1,2*-**1** (>95:5 *E/Z*) as a colourless solid (22 mg, 23%). ^{1}H NMR (600 MHz, $CDCl_3$): δ = 10.07 (s, 1H, H_v), 8.44 (s, 1H, H_A), 8.01 (s, 1H, H_u), 7.87 (d, *J* = 7.6 Hz, 1H, H_t), 7.74 (d, *J* = 7.6 Hz, 1H, H_r), 7.64 (s, 1H, H_j), 7.60 (t, *J* = 7.6 Hz, 1H, H_s), 7.35 (s, 1H, H_e). 7.28 (s, 1H, H_g), 7.27-7.25 (m, 4H, H_b, H_c, H_d, H_i), 7.12 (s, 1H, H_o), 7.09-7.06 (m, 4H, H_k, H_l, H_m, H_h), 6.90 (s, 1H, H_n), 5.37 (s, 2H, H_f), 5.20 (s, 2H, H_q), 3.90 (s, 2H, H_p), 3.87 (s, 2H, H_a), 3.67 (s, 3H, H_X), 2.73 (t, *J* = 7.3 Hz, 2H, H_Z), 2.65 (t, *J* = 7.3 Hz, 2H, H_Y), 2.57 (t, *J* = 7.9 Hz, 2H, H_B), 2.27 (t, *J* = 7.9 Hz, 2H, H_E), 1.69 (quint., *J* = 7.9 Hz, 2H, H_C), 1.59 (quint., *J* = 7.9 Hz, 2H, H_D); Assignment of the signals was accomplished by means of 2D NMR (COSY, ROESY, HSQC); ^{13}C NMR (125 MHz, $CDCl_3$): δ = 191.97, 174.73, 171.96, 159.70, 159.00, 141.90, 139.57, 139.16, 138.64, 138.25, 137.90, 136.85, 135.63, 133.22, 129.90, 129.74, 129.37, 129.33, 128.72, 128.17, 128.15, 128.09, 126.70, 124.54, 121.31, 120.75, 117.54, 115.25, 112.00, 107.50, 69.78, 69.30, 51.67, 43.96, 43.33, 37.97, 33.77, 33.02, 29.78, 29.69, 24.33; HRMS (ESI$^+$): *m/z* = 787.1984 $[M+H]^+$ (calcd. 787.1998 for $C_{20}H_{22}NO_4S_2$).

3-[3-(3-Formyl-5-vinyl-phenoxymethyl)-benzyldisulfanyl]-propionic acid

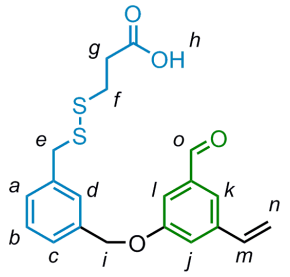

E11

Under N_2, **E6** (700 mg, 2.14 mmol, 1.0 equiv.), trimethyl orthoformate (239 mg, 2.25 mmol, 1.05 equiv.) and *p*-TsOH·H_2O (20 mg, 0.11 mmol, 0.05 equiv.) were dissolved/suspended in MeOH (35 mL). The mixture was stirred at room temperature for 1 h. A solution of NaOMe (232 mg, 4.29 mmol, 2.0 equiv.) in MeOH (14 mL) was added and the mixture was stirred for 1 h at room temperature. KI (178 mg, 1.07 mmol, 0.5 equiv.) and a solution containing 3-mercaptopropionic acid (2.2 g, 1.84 mL, 21.4 mmol, 10.0 equiv.) and NaOMe (1.2 g, 21.4 mmol, 10.0 equiv.) in MeOH (14 mL) were added. The resulting mixture was titrated with a solution of I_2 (3.2 g, 12.8 mmol, 6.0 equiv.) in DCM (50 mL) until the brown colour persisted. Na_2SO_3 was added and the mixture was stirred until decolourisation was complete. 1M HCl (50 mL) and CH_2Cl_2 (50 mL) were added and after stirring the mixture for 10 min the two layers were separated. The aqueous layer was extracted with CH_2Cl_2 (3 × 20 mL). The combined CH_2Cl_2 layers were dried over $MgSO_4$. The solvents were removed under reduced pressure and the resulting residue was purified by flash column chromatography (SiO_2, CH_2Cl_2/MeOH 95:5) to yield **E11** (491 mg, 59%) as a colourless oil. A minor impurity was observed, however, no further purification was undertaken at this step. ^{1}H NMR (400 MHz, $CDCl_3$): δ = 9.95 (s, 1H, H_o), 7.52 (s, 1H, H_j or H_k or H_l), 7.41 (s, 1H, H_j or H_k or H_l), 7.36-7.34 (m, 3H, H_{Ar}) 7.31-7.28 (m, 2H, H_{Ar}) 6.72 (dd, *J* = 17.6 Hz, 10.9 Hz, 1H, H_m), 5.83 (d, *J* = 17.6 Hz, 1H, H_n), 5.37 (d, *J* = 10.9 Hz, 1H, H_n), 5.12 (s, 2H, H_e), 3.80 (s, 2H, H_i), 2.64-2.57 (m, 4H, H_f, H_g); ^{13}C NMR (100 MHz, $CDCl_3$): δ = 192.12, 177.28, 159.44, 139.95, 137.92, 137.83, 136.73, 135.39, 129.18, 128.99, 128.53, 126.74, 121.99, 119.67, 116.14, 112.47, 69.90, 43.25, 33.62, 32.34; HRMS (ESI$^+$): *m*/*z* = 406.1143 $[M+NH_4]^+$ (calcd. 406.1141 for $C_{20}H_{24}NO_4S_2$).

3-[3-(3-Formyl-5-vinyl-phenoxymethyl)-benzyldisulfanyl]-propionic acid methyl ester

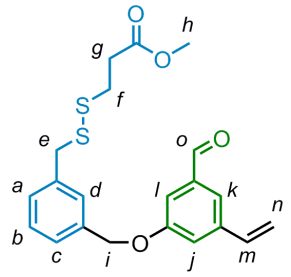

E12

Acetyl chloride (78 mg, 71 µL, 100 µmol, 1.0 equiv.) was added to an ice cold solution of **E11** (389 mg, 100 µmol, 1.0 equiv.) in MeOH (15 mL). The solution was allowed to slowly warm to room temperature and stirred for 5 h. The solvent was removed under reduced pressure. Purification by flash column chromatography (SiO_2, petrol ether/EtOAc 4:1) gave **S12** as a colourless oil (201 mg, 50%). ^{1}H NMR (400 MHz, $CDCl_3$): δ = 9.97 (s, 1H, H_o), 7.52 (s, 1H, H_j or H_k or H_l), 7.41 (s, 1H, H_j or H_k or H_l), 7.36-7.34 (m, 3H, H_{Ar}) 7.31-7.28 (m, 2H, H_{Ar}) 6.73 (dd, J = 17.6 Hz, 10.9 Hz, 1H, H_m), 5.84 (d, J = 17.6 Hz, 1H, H_n), 5.37 (d, J = 10.9 Hz,1H, H_n), 5.13 (s, 2H, H_i), 3.91 (s, 2H, H_e), 3.67 (s, 3H, H_h), 2.64-2.60 (m, 4H, H_f, H_g); ^{13}C NMR (100 MHz, $CDCl_3$): δ = 191.99, 172.12, 159.41, 139.91, 137.92, 137.79, 136.66, 135.37, 129.15, 128.92, 128.37, 126.65, 121.63, 119.57, 116.07, 112.46, 70.01, 51.82, 43.23, 33.75, 32.75; HRMS (ESI$^+$): m/z = 403.1030 $[M+H]^+$ (calcd. 403.1032 for $C_{21}H_{23}O_4S_2$).

(E)-S-3-(3-((2-(5-Mercaptopentanoyl)hydrazono)methyl)-benzyloxy)-5-vinyl-benzyl ethanethioate

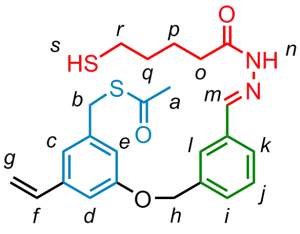

E13

Under N_2, **E8** (750 mg, 2.30 mmol, 1.0 equiv.) and 5-mercapto pentanoic acid hydrazide (409 mg, 2.76 mmol, 1.2 equiv) were dissolved in dry MeOH (20 mL). Three drops of

acetic acid were added and the mixture was stirred at room temperature. The reaction was monitored by TLC (SiO_2, *n*-hexane/EtOAc 10:1). After 1 h a white precipitate was observed. After another hour TLC revealed the reaction was complete and the mixture was stirred at −15°C for 1 h. The product was collected and dried on a filter to yield **S13** (963 mg, 2.11 mmol, 92%) as a colourless waxy solid. ^{1}H NMR (400 MHz, $CDCl_3$): δ = 8.90 (bs, 1H, H_n), 7.74 (s, 1H, H_l or H_m), 7.72 (s, 1H, H_l or H_m), 7.62 (d, *J* = 5.9 Hz, 1H, H_i or H_k), 7.47 (d, *J* = 5.9 Hz, 1H, H_i or H_k), 7.44 (dd, *J* = 5.9 Hz, 5.9 Hz, 1H, H_j), 6.95 (s, 1H, H_c or H_d or H_e), 6.92 (s, 1H, H_c or H_d or H_e), 6.84 (s, 1H, H_c or H_d or H_e), 6.65 (dd, *J* = 17.6 Hz, 10.9 Hz, 1H, H_f), 5.73 (d, *J* = 17.6 Hz, 1H, H_g), 5.26 (d, *J* = 10.9 Hz, 1H, H_g), 5.08 (s, 2H, H_h), 4.09 (s, 2H, H_b), 2.79 (dd, *J* = 7.6 Hz, 7.1 Hz, 2H, H_o), 2.59 (dt, *J* = 7.9 Hz, 7.1 Hz, 2H, H_r), 2.35 (s, 3H, H_a), 1.89 – 1.81 (m, 2H, H_p or H_q), 1.78 – 1.71 (m, 2H, H_p or H_q), 1.39 (t, *J* = 7.9 Hz, 1H, H_s); ^{13}C NMR (100 MHz, $CDCl_3$): δ = 195.08, 175.63, 158.94, 143.02, 139.36, 139.32, 137.48, 136.26, 134.04, 129.20, 129.07, 126.74, 126.07, 119.80, 114.73, 114.52, 111.34, 69.54, 33.60, 33.31, 32.06, 30.35, 24.36, 23.31; HRMS (ESI$^+$): *m*/*z* = 457.1610 $[M+H]^+$ (calcd. 457.1614 for $C_{24}H_{29}N_2O_3S_2$).

(E)-22-Vinyl-2-oxa-17,18-dithia-10,11-diaza-tricyclo[18.3.1.1^{4,8}]pentacosa-1(24),4,6,8(25),9,20,22-heptaen-12-one

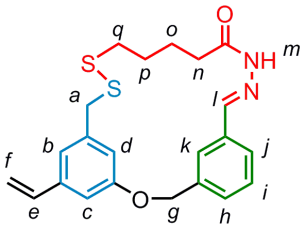

E14

Under N_2, **E13** (950 mg, 2.08 mmol, 1.0 equiv.) was dissolved in MeOH (50 mL) and CH_2Cl_2 (10 mL). A solution of NaOMe (225 mg, 4.16 mol, 2.0 equiv.) in MeOH (10 mL) was added. After 5 h of stirring at room temperature, CH_2Cl_2 (150 mL) and KI (69 mg, 0.42 mmol, 0.2 equiv.) were added. A solution of I_2 (528 mg, 2.08 mmol, 1.0 equiv.) in CH_2Cl_2 (20 mL) was added dropwise until the brown colour persisted. Na_2SO_3 was added to reduce the excess of I_2 and, when decolourisation was complete, stirring was continued for 15 min. H_2O (100 mL) was added and the phases were separated. The H_2O layer was extracted with CH_2Cl_2 (3 × 100 mL). The organic layers were combined, dried ($MgSO_4$) and the solvent was removed under reduced pressure. The residue was recrystallised from chloroform to yield pure **E14** (300 mg, 0.73 mmol, 35%) as a

colourless solid. M.p. 134-135 °C. ^{1}H NMR (400 MHz, $CDCl_3$): δ = 8.77 (bs, 1H, H_m), 8.05 (s, 1H, H_k or H_l), 7.70 (s, 1H, H_k or H_l), 7.42 (dd, *J* = 7.6, 7.6 Hz, 1H, H_i), 7.34 (d, *J* = 7.6 Hz, 1H, H_h or H_j), 7.25 (d, *J* = 7.6 Hz, 1H, H_h or H_j), 7.01 (s, 1H, H_b or H_c or H_d), 6.96 (s, 1H, H_b or H_c or H_d), 6.75 (s, 1H, H_b or H_c or H_d), 6.59 (dd, *J* = 17.6 Hz, 10.9 Hz, 1H, H_e), 5.64 (d, *J* = 17.6 Hz, 1H, H_f), 5.08 (s, 2H, H_g), 5.20 (d, *J* = 10.9 Hz, 1H, H_f), 3.83 (s, 2H, H_a), 2.64 (dd, *J* = 9.2, 6.7 Hz, 2H, H_n), 2.37 (dd, *J* = 9.6, 8.2 Hz, 2H, H_q), 1.75 – 1.60 (m, 4H, H_p and H_o); ^{13}C NMR (100 MHz, DMSO-d_6): δ = 174.46, 158.51, 141.99, 139.54, 138.60, 138.43, 136.28, 134.46, 128.95, 128.67, 127.69, 120.89, 119.67, 116.71, 114.84, 110.37, 68.66, 42.57, 37.03, 32.08, 28.90, 24.24; HRMS (ESI$^+$): *m/z* = 435.1170 $[M+Na]^+$ (calcd. 435.1171 for $C_{22}H_{24}N_2O_2S_2Na$).

3-(3-{3-Formyl-5-[(E)-2-((E)-12-oxo-2-oxa-17,18-dithia-10,11-diaza-tricyclo[18.3.1.14,8]pentacosa-1(23),4,6,8(25),9,20(24),21-heptaen-22-yl)-vinyl]-phenoxymethyl}-benzyldisulfanyl)-propionic acid methyl ester

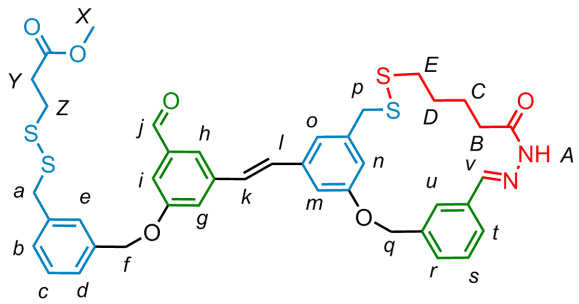

E-3,4-**1**

Under N_2, **E12** (29.3 mg, 0.07 mmol, 1.2 equiv.), **E14** (25 mg, 0.06 mmol, 1.0 equiv.) and Ω_A-SIMes-CF_3™ catalyst[2,3] (4.4 mg, 6.06 µmol, 0.1 equiv.) were dissolved in CH_2Cl_2 (5 mL). The mixture was subjected to microwave irradiation for 3 hours (300 W, 100 °C) and the solvent was removed under reduced pressure. Purification by flash column chromatography (SiO_2, hexane/EtOAc 9:1 → 1:1) gave *E-3,4*-**1** (>95:5 *E/Z*) as a colourless solid (12 mg, 25%) (20% starting material **E14** recovered). ^{1}H NMR (500 MHz, CD_2Cl_2): δ = 9.94 (s, 1H, H_j), 8.56 (s, 1H, H_A), 8.06 (s, 1H, H_u), 7.69 (s, 1H, H_v), 7.58 (s, 1H, H_h), 7.45-7.25 (m, 9H, H_s, H_e, H_r, H_g, H_i, H_d, H_c, H_b, H_t), 7.11-7.01 (m, 4H, H_o, H_k, H_l, H_n), 6.88 (s, 1H, H_m), 5.29 (s, 2H, H_q), 5.14 (s, 2H, H_f), 3.91 (s, 2H, H_a), 3.86 (s, 2H, H_p), 3.62 (s, 3H, H_X), 2.65 (m, 2H, H_Z), 2.60 (m, 4H, H_Y, H_B), 2.40 (t, *J* = 7.7 Hz, 2H, H_E), 1.65 (m, 4H, H_C, H_D); Assignment of the signals was accomplished by means of 2D NMR (COSY, ROESY, HSQC, HMBC); ^{13}C NMR (125 MHz, CD_2Cl_2): δ = 191.78, 175.19, 171.96,

159.60, 159.36, 142.15, 140.33, 139.51, 138.65, 138.31, 138.24, 138.00, 136.89, 134.43, 130.21, 129.11, 128.96 (2C), 128.84, 128.81, 128.44, 127.52, 126.65, 121.67, 121.31, 120.33, 119.31, 117.31, 112.83, 111.02, 70.11, 69.85. 51.65, 44.17, 43.15, 38.09, 33.71, 32.93 (2C), 29.70, 24.82; HRMS (ESI$^+$): m/z = 787.1992 $[M+H]^+$ (calcd. 787.1998 for $C_{20}H_{22}NO_4S_2$).

3-{3-[(2Z,18E)-6-(3-Formyl-benzyloxy)-16-oxo-10,11-dithia-17,18-diaza-tricyclo[18.3.1.1^{4,8}]pentacosa-1(24),2,4(25),5,7,18,20,22-octaen-22-yloxymethyl]-benzyldisulfanyl}-propionic acid methyl ester

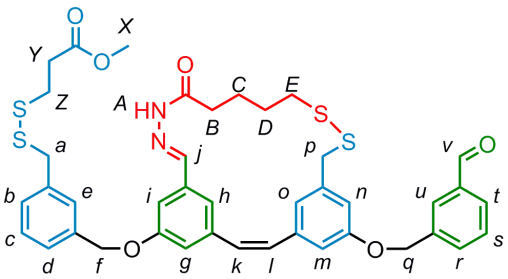

Z-2,3-**1**

E-1,2-**1** was subjected to photochemical *E*→*Z* isomerisation (see section 1.2). The photostationary *E*/*Z-1,2*-**1** mixture was subjected to conditions for disulfide exchange (see general conditions). *Z-2,3*-**1** was isolated from the resulting mixture, by means of semipreparative HPLC (see section 1.1). ^{1}H NMR (500 MHz, CD_2Cl_2): δ = 9.94 (s, 1H, H_v), 8.43 (s, 1H, H_A), 7.85 (s, 1H, H_h), 7.76 (m, 1H, H_s), 7.65 (s, 1H, H_u), 7.61 (s, 1H, H_j), 7.46 (m, 2H, H_r, H_t), 7.43 (s, 1H, H_e), 7.36-7.28 (m, 3H, H_d, H_c, H_b), 7.08 (s, 1H, H_m) , 6.96 (s, 1H, H_n), 6.91 (s, 1H, H_g), 6.85 (s, 1H, H_o), 6.83 (s, 1H, H_i), 6.55-6.48 (m, 2H, H_k, H_l), 5.11 (s, 2H, H_f), 5.12 (s, 2H, H_q), 3.91 (s, 2H, H_a), 3.78 (s, 2H, H_p), 3.62 (s, 3H, H_X), 2.66 (m, 2H, H_Z), 2.60 (m, 2H, H_Y), 2.33 (m, 2H, H_B), 2.27 (m, 2H, H_E), 1.50 (m, 4H, H_C, H_D); Assignment of the signals was accomplished by means of 2D NMR (COSY, ROESY, HSQC); ^{13}C NMR (125 MHz, CD_2Cl_2): δ = 192.53, 175.21, 172.59, 160.03, 158.76, 142.54, 141.45, 139.51, 138.87, 138.52, 137.91, 137.73, 137.29, 135.22, 133.42, 130.82, 129.94, 129.81, 129.60, 129.39, 129.00, 128.23, 127.18, 125.54, 117.66, 116.94, 116.14, 115.98, 112.64, 70.52, 69.79, 64.72, 52.25, 44.62, 43.67, 37.35, 34.30, 33.52, 32.66, 29.67, 25.71, 25.06; HRMS (ESI$^+$): m/z = 787.1997 $[M+H]^+$ (calcd. 787.1998 for $C_{20}H_{22}NO_4S_2$).

5.6 Notes and References

[1] a) Molecular Motors (Ed.: M. Schliwa), Wiley-VCH, Weinheim, 2003; b) R. D. Vale, *Cell* **2003**, *112*, 467; c) M. Schliwa, G. Woehlke, *Nature* **2003**, *422*, 759.

[2] For selected, concise reviews on motor proteins from the kinesin (a,b), myosin (c,d) and dynein (e,f) families see: a) S. M. Block, *Biophys. J.* **2007**, *92*, 2986; b) N. Hirokawa, Y. Noda, Y. Tanaka, S. Niwa, *Nature Rev. Mol. Cell Biol.* **2009**, *10*, 682; c) J. R. Sellers, C. Veigel, *Curr. Opin. Cell Biol.* **2006**, *18*, 68; d) H. L. Sweeney, A. Houdusse, *Annu. Rev. Biophys.* **2010**, *39*, 539; e) M. P. Koonce, M. Samsó, *Trends Cell Biol.* **2004**, *14*, 612; f) K. Oiwa, H. Sakakibara, *Curr. Opin. Cell Biol.* **2005**, *17*, 98.

[3] a) W. B. Sherman, N. C. Seeman, *Nano Lett.* **2004**, *4*, 1203; b) J.-S. Shin, N. A. Pierce, *J. Am. Chem. Soc.* **2004**, *126*, 10834; c) P. Yin, H. Yan, X. G. Daniell, A. J. Turberfield, J. H. Reif, *Angew. Chem. Int. Ed*. **2004**, *43*, 4906; d) Y. Tian, Y. He, Y. Chen, P. Yin, C. Mao, *Angew. Chem. Int. Ed*. **2005**, *44*, 4355; e) P. Yin, H. M. T. Choi, C. R. Calvert, N. A. Pierce, *Nature* **2008**, *451*, 318; f) S. J. Green, J. Bath, A. J. Turberfield, *Phys. Rev. Lett.* **2008**, *101*, 238101; g) T. Omabegho, R. Sha, N. C. Seeman, *Science* **2009**, *324*, 67; h) H. Gu, J. Chao, S.-J. Xiao, N. C. Seeman, *Nature* **2010**, *465*, 202; i) K. Lund, A. J. Manzo, N. Dabby, N. Michelotti, A. Johnson-Buck, J. Nangreave, S. Taylor, R. Pei, M. N. Stojanovic, N. G. Walter, E. Winfree, H. Yan, *Nature* **2010**, *465*, 206.

[4] M. von Delius, E. M. Geertsema, D. A. Leigh, *Nature Chem.* **2010**, *2*, 96.

[5] For two elegant mechanistic studies based on ring strain in macrocycles containing a 'stiff stilbene' linkage see: a) Q. Z. Yang, Z. Huang, T. J. Kucharski, D. Khvostichenko, J. Chen, R. Boulatov, *Nature Nanotech.* **2009**, *4*, 302; b) T. J. Kucharski, Z. Huang, Q. Z. Yang, Y. C. Tian, N. C. Rubin, C. D. Concepcion, R. Boulatov, *Angew. Chem. Int. Ed.* **2009**, *48*, 7040. For a dynamic covalent library consisting of macrocycles with internal acyl hydrazone and (photoswitchable) azobenzene linkages see: c) L. A. Ingerman, M. L. Waters, *J. Org. Chem.* **2009**, *74*, 111.

[6] a) E. R. Kay, F. Zerbetto, D. A. Leigh, *Angew. Chem. Int. Ed.* **2007**, *46*, 72; b) R. D. Astumian, *Phys. Chem. Chem. Phys*. **2007**, *9*, 5067; c) R. D. Astumian, I. Derényi, *Eur. Biophys. J.* **1998**, *27*, 474.

[7] *E* denominates the configuration of the stilbene double bond; *1,2* specifies the position of the walker unit on the four-foothold track.

[8] a) A. K. Chatterjee, T.-L. Choi, D. P. Sanders, R. H. Grubbs, *J. Am. Chem. Soc.* **2003**, *125*, 11360; b) S. P. Nolan, H. Clavier, *Chem. Soc. Rev.* **2010**, *39*, 3305.

[9] The best results were obtained with commercially available catalyst Ω_A-SIMes-CF_3™, described as compound **2h** in: D. Rix, F. Caijo, I. Laurent, F. Boeda, H. Clavier, S. P. Nolan, M. Mauduit, *J. Org. Chem.* **2008**, *73*, 4225.

[10] For an excellent review on the photochemistry of stilbene derivatives see: a) H. Meier, *Angew. Chem.* **1992**, *104*, 1425; for sensitized *Z-E* photoisomerisation of stilbenes, see: b) G. S. Hammond, J. Saltiel, A. A. Lamola, N. J. Turro, J. S. Bradshaw, D. O. Cowan, R. C. Counsell, V. Vogt, C. J. Dalton, *J. Am. Chem. Soc.* **1964**, *86*, 3197.

[11] The photostationary equilibrium ratio for direct *Z-E* isomerization can be calculated as a function of the quantum yields (ϕ) and molar absorptivities (ε) of the *E* and *Z* species (at a given wavelength): $[Z]/[E] = (\phi_{E\rightarrow Z}\,\varepsilon_E) / (\phi_{Z\rightarrow E}\,\varepsilon_Z)$, with the quantum yield ratio usually approximating 1 (see reference 10a).

[12] The mechanism for iodine-mediated stilbene *Z*→*E* isomerisation involves the reversible addition of I· radicals (here generated by irradiation with visible light) to the double bond. See for example: S. Yamashita, *Bull. Chem. Soc. Jpn.* **1961**, *34*, 972.

[13] Iodine-mediated stilbene *Z*→*E* isomerisation had to be conducted at low concentration (0.1mM) to avoid decomposition.

[14] The length of the methylene spacer in the walker unit is crucial in order to generate ring strain in *E-2,3*-**1**, but not *Z-2,3*-**1**. We based our choice of a four carbon spacer on model studies conducted on a simpler system (see: M. J. Barrell, PhD thesis, University of Edinburgh, **2010**) and on molecular modelling (semi-empiric, PM3).

[15] a) S. J. Rowan, S. J. Cantrill, G. R. L. Cousins, J. K. M. Sanders, J. F. Stoddart, *Angew. Chem. Int. Ed.* **2002**, *41*, 898; b) P. T. Corbett, J. Leclaire, L. Vial, K. R. West, J.-L. Wietor, J. K. M. *Sanders*, S. Otto, *Chem*. *Rev*. **2006**, *106*, 3652; c) J.-M. Lehn, *Chem. Soc. Rev*. **2007**, *36*, 151.

[16] The *1,4*-**1** isomers, which result from folding of the track (see Supporting Information for structures), add an additional double-step gait to the major passing-leg gait. Other side products resulting from track folding were observed during disulfide exchange experiments (see Supporting Information).

[17] For studies on the dynamic chemistry of hydrazone-disulfide systems under mutually exclusive (acid-base) conditions see: a) M. von Delius, E. M. Geertsema, D. A. Leigh, A. M. Z. Slawin, *Org. Biomol. Chem*. **2010**, DOI: 10.1039/C0OB00214C; b) A. G. Orrillo, A. M. Escalante, R. L. E. Furlan, *Chem. Commun*. **2008**, 5298; c) Z. Rodriguez-Docampo, S. Otto, *Chem. Commun*. **2008**, 5301.

[18] In contrast to the flexible ether linkages between footholds *1* and *2* as well as *3* and *4*, the rigid *Z*-stilbene linker 'preorganises' footholds *2* and *3* for the attachment of the walker unit.

[19] Possible reasons for the observed discrepancies between experimental and calculated data include: insufficient equilibration time for dynamic covalent exchange processes, non-ideal photochemical steady state ratios in mixtures and inaccuracies in ^{1}H NMR integration.

[20] The average step number is defined as the number of steps after which 50% of the walker units are no longer attached to their original track (*via* walker dissociation or an intermolecular mechanism).

[21] See R. B. Case, D. W. Pierce, N. Hom-Booher, C. L. Hart, R. D. Vale, *Cell* **1997**, *90*, 959 and references cited therein.

[22] Systematic name: (1,3-Bis(2,4,6-trimethylphenyl)imidazolidin-2-ylidene)(2-isopropoxy-5-(2,2,2-trifluoroacetamido)benzylidene)ruthenium(II) Dichloride

Structure:

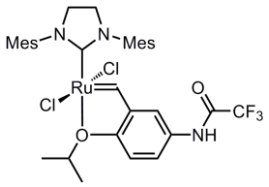

[23] MestReNova v6.0.3-5604 by Mestrelab Research S.L.

[24] Dynamic covalent exchange generally gave 5 to 20% oligomeric side products, which for analytical purposes were removed from the mixtures (by broad-window semipreparative HPLC).

[25] Purification by semipreparative HPLC did in some cases result in $E \rightarrow Z$ isomerisation, presumably due to the brief, but intense exposure to UV light in the photodiode array (PDA) detector.

Outlook

The walker-track systems presented in Chapters III, IV and V represent a significant advance in the development of synthetic, linear molecular motors. The most important characteristics of bipedal motor proteins, namely processive, directional, repetitive and progressive walker transport along a track, have been demonstrated in three of the prepared systems. The dynamic foot-labilisation processes proceed with remarkable efficiency, particularly when conducted in dilute solution under thermodynamic control and the degree of processivity under such conditions is comparable to that of the biological biped kinesin.

The primary weakness of the presented systems stems from the flexibility of the molecular tracks. The resulting folding of the track has in most studied cases significantly reduced the observed directional bias. Moreover, some of the occurring byproducts have been shown to reduce processivity and extended molecular tracks based on the present design would in all likelihood lead to serious analytical complications. As a result, the next 'step' that synthetic molecular walkers need to take, is the development of rigid molecular tracks that prevent, or at least minimize, the tendency of the walker unit to make large strides (e.g. in a '*1,4'* isomer).

Several projects are currently being pursued in the Leigh group that address this weakness. In one example the target structure is related to the system presented in Chapter V, with the difference that the molecular track is completely rigid. The track is also designed such that the distance between footholds *1* and *2* is different from the distance between footholds *2* and *3* and a switchable stilbenoid double bond is part of the walker unit. In a second project, the rigid track plays a more active role, enabling directional walker transport by the reversible coordination of a metal ion in the space between walker unit and track. A third project aims at autonomous (yet non-directional) walker transport along a rigid track. The potential coupling of an electrochemically stimulated pH-oscillating system to one of the previously synthesised walker-track systems is currently being investigated in collaboration.

In the more remote future, walker systems could walk along extended tracks (which could be deposited on surfaces and might feature junctions) and carry and release molecular cargo. A "molecular football player" could also be realised based on the findings presented in this thesis.

Appendix

Published papers

"Synthesis and solid state structure of a hydrazone-disulfide macrocycle and its dynamic covalent ring-opening under acidic and basic conditions" M. von Delius, E. M. Geertsema, D. A. Leigh, A. M. Z. Slawin, *Org. Biomol. Chem.* **2010**, *8*, 4617.

"A synthetic small molecule that can walk down a track" M. von Delius, E. M. Geertsema, D. A. Leigh, *Nature Chem.* **2010**, *2*, 96.

"*Design, Synthesis, and Operation of Small Molecules That Walk along Tracks*" M. von Delius, E. M. Geertsema, D. A. Leigh, D.-T. D. Tang, *J. Am. Chem. Soc.* **2010**, DOI: 10.1021/ja106486b.

"*Light-Driven Transport of a Molecular Walker in Either Direction along a Molecular Track*" M. J. Barrell, A. G. Campana, M. von Delius, E. M. Geertsema, D. A. Leigh, *Angew. Chem. Int. Ed.* **2010**, DOI: 10.1002/anie.201004779.

Synthesis and solid state structure of a hydrazone-disulfide macrocycle and its dynamic covalent ring-opening under acidic and basic conditions†

Max von Delius,[a] Edzard M. Geertsema,[a] David A. Leigh*[a] and Alexandra M. Z. Slawin[b]

Received 4th June 2010, Accepted 8th July 2010
DOI: 10.1039/c0ob00214c

The synthesis and characterisation, including solid state structure, of a macrocycle containing both a hydrazone and a disulfide linkage is described. Selective ring-opening of the macrocycle under thermodynamic control could be achieved at either the disulfide or the hydrazone linkage by applying mutually exclusive sets of reaction conditions.

Introduction

The chemistry of covalent bonds that are dynamic under particular conditions has attracted considerable interest over the past decade.[1] When the components of a dynamic chemical system are interconnected by several types of reversible exchange reactions—rather than just one—complex behaviour of the molecular network can emerge, a phenomenon that lies at the core of systems chemistry.[2] To date several such multi-level constitutionally dynamic[3] systems have been described.[4] In these systems the various exchange processes can relate to each other in one of two ways: (i) orthogonal,[4a] where the exchange reactions do not interfere with each other; and (ii) communicating,[4b] where the products of the exchange reactions cross over and influence the outcome of the other. Adding a further level of control by having the reactions no longer occur concurrently could prove useful for ratcheting the distribution away from the thermodynamic minimum,[5] a feature useful for—amongst other things—the development of new molecular motor systems.[6] To achieve this the conditions under which the different exchange reactions occur need to be mutually exclusive. In a double-level[7] system this requires that under one set of conditions only one of the two bond types is dynamic and the other is kinetically locked, and that under a second set of conditions the relative rates of bond forming/breaking are reversed.

In recent independent studies, the groups of Furlan[8a] and Otto[8b] described simple (acyclic) substrates containing a disulfide and hydrazone moiety that undergo reversible exchange reactions under different sets of reaction conditions. We were interested in the implications of applying reactions that occur under mutually exclusive conditions to a cyclic substrate featuring such linkages .[8] Aside from establishing a viable synthetic route to such systems, our aim was to investigate the dynamic covalent ring-opening of such a macrocycle in a situation where fully reversible intra- and intermolecular exchange processes compete. Here we report on the synthesis (Scheme 1) and dynamic chemistry (Fig. 1, Fig. 2 and Scheme 2) of macrocycle $\mathbf{1}_1$,[9] which contains both a hydrazone and a disulfide unit within the bonds that make up the ring. We demonstrate selective ring-opening of $\mathbf{1}_1$ at either the disulfide or the hydrazone moiety by reversible covalent bond formation under two sets of mutually exclusive reaction conditions (acidic and basic).

We probe the dynamic chemistry of $\mathbf{1}_1$ through three types of experiments, each carried out under thermodynamic control: First, we treated $\mathbf{1}_1$ with acid or base conditions to demonstrate that under either set of conditions reversible covalent bond formation gives rise to a mixture of cyclic oligomers of type $\mathbf{1}_n$[9] (Fig. 1). Second, $\mathbf{1}_1$ was treated with an acyclic disulfide or hydrazone scavenger, in the presence of acid or base, to demonstrate that the disulfide bonds exchange only under basic conditions and the hydrazone bonds exchange only under acidic conditions (Scheme 2 and Fig. 2). Finally, $\mathbf{1}_1$ was subjected to basic or acidic conditions in the presence of both a disulfide *and* a hydrazone scavenger (Fig. 3) to demonstrate that each dynamic exchange reaction is not affected by the presence of the other building blocks (which are inactive under the other's set of reaction conditions).

Results and discussion

Synthesis of macrocycle $\mathbf{1}_1$

Macrocycle $\mathbf{1}_1$ was prepared according to the route shown in Scheme 1. Bis-aromatic scaffold **3** was obtained from benzylic chloride **2** and 3-hydroxybenzaldehyde *via* Williamson ether synthesis (step a). Alcohol **3** was converted into bromide **4**, followed by nucleophilic substitution with potassium thioacetate. Condensation of hydrazide **6** with aldehyde **5** yielded hydrazone **7** (step d). The synthesis was completed by sodium methoxide mediated deprotection of the thioacetate group and oxidative ring-closure using iodine, which provided macrocycle $\mathbf{1}_1$ in 56% yield.[10]

Solid state structure of macrocycle $\mathbf{1}_1$

Single crystals of $\mathbf{1}_1$ suitable for X-ray crystallography were obtained by slow cooling of a hot saturated solution of $\mathbf{1}_1$ in ethanol. The solid state structure revealed several interesting features of macrocycle $\mathbf{1}_1$ (Scheme 1): the two aromatic rings are almost orthogonal (torsion angle 94°) and the hydrazone double bond is in the *E* configuration (also shown by ^{1}H NMR studies in $CDCl_3$) and planar (conjugated) with the adjacent aromatic

[a]*School of Chemistry, University of Edinburgh, The King's Buildings, West Mains Road, Edinburgh, UK EH9 3JJ. E-mail: David.Leigh@ed.ac.uk; Fax: +44 131 650 6453; Tel: +44 131 650 4721*
[b]*School of Chemistry, University of St. Andrews, Purdie Building, St. Andrews, Fife, UK KY16 9ST*

† Electronic supplementary information (ESI) available: ^{1}H NMR spectra of all synthesised compounds. CCDC reference number 783640. For ESI and crystallographic data in CIF or other electronic format see DOI: 10.1039/c0ob00214c

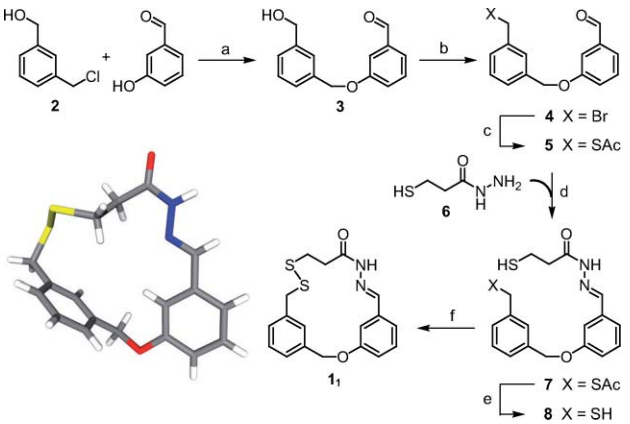

Scheme 1 Synthesis and X-ray crystal structure of macrocycle $\mathbf{1}_1$. Reaction conditions: (a) NaH, DMF, RT, 3 h, 83%; (b) $SOBr_2$, benzene, RT, 36 h, 73%; (c) KSAc, DMF, RT, 12 h, 95%; (d) AcOH (cat.), MeOH, RT, 3 h, 88%; (e) NaOMe, MeOH, RT, 2 h, 78%; (f) I_2, MeOH–CH_2Cl_2, 0 °C, 30 min, 56%. Bottom left: Solid state structure of $\mathbf{1}_1$ determined by single crystal X-ray diffraction. C: grey, H: white, O: red, N: blue, S: yellow. Selected bond lengths [Å] and angles [°]: S–S 2.0335(11); N–N 1.376(3); C–S–S–C 100.92(13).

ring. The C–S–S–C torsion angle (101°) deviates by 11° from the 90° angle typically found[11] for such functional groups and the two adjacent methylene groups between the disulfide and the hydrazone moiety are closer to an eclipsed than to a staggered conformation (dihedral angle 137°). These observations suggest that the presence of the three rigid elements (two aromatic rings and the acyl hydrazone) in the macrocycle result in a significant amount of ring strain in $\mathbf{1}_1$.

Dynamic Chemistry I: Oligomerisation of macrocycle $\mathbf{1}_1$ in the absence of scavengers

To investigate different aspects of the dynamic chemistry of macrocycle $\mathbf{1}_1$, we carried out three types of experiments that involved macrocycle ring-opening under thermodynamic control. In the first experimental series we subjected $\mathbf{1}_1$ to different chemical reagents (trifluoroacetic acid-d_1 (TFA-d_1), triethylamine (Et_3N), diazabicyclo-[5,4,0]undec-7-ene (DBU), DL-dithiothreitol (DTT)),[8,12] solvents ($CDCl_3$, DMSO-d_6) and reaction temperatures (RT, 55 °C), in order to find effective conditions for cyclooligomerisation *via* reversible disulfide and hydrazone exchange (see Fig. 1a). Deuterated solvents were employed to enable the progress of reactions to be followed by ^{1}H NMR spectroscopy.

Acid-mediated oligomerisation proved efficient at room temperature in $CDCl_3$ (one day equilibration time) using five equivalents of TFA-d_1 and millimolar initial concentrations of substrate ($\mathbf{1}_1$). Base-induced oligomerisation was most efficient (two days equilibration time at room temperature) in $CDCl_3$ employing the strong base DBU (1.0 equiv.) and DTT (0.1 equiv.) as a catalytic reducing agent (Fig. 1a). Hydrazone exchange did not occur using DMSO-d_6 and disulfide exchange was extremely slow (equilibration time more than 7 days at 55 °C) when the weaker base triethylamine was employed. Under the two most efficient sets of acidic and basic conditions (TFA-d_1 in $CDCl_3$ and DBU/DTT in $CDCl_3$), small, but detectable amounts (see ESI for a typical ^{1}H NMR spectrum†) of dimeric ($\mathbf{1}_2$), trimeric ($\mathbf{1}_3$) and tetrameric ($\mathbf{1}_4$) macrocyclic analogues[13] of $\mathbf{1}_1$ were found in the equilibrium

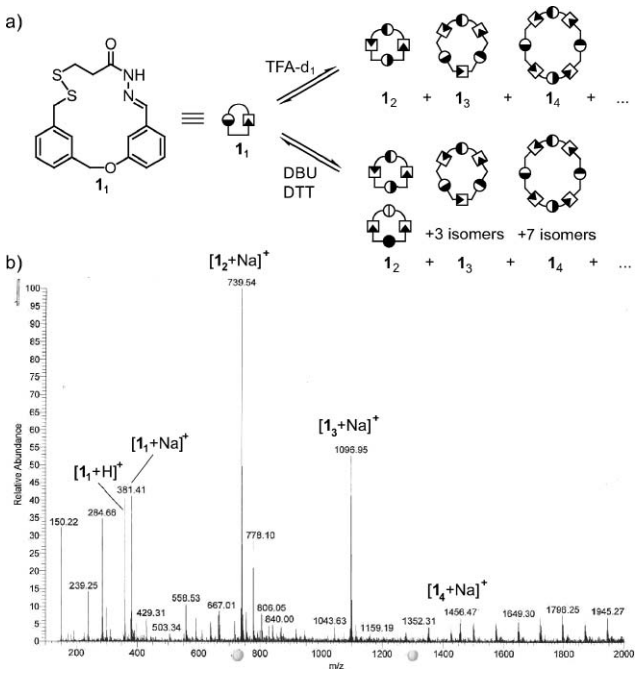

Fig. 1 (a) Two sets of reaction conditions for the efficient conversion of macrocycle $\mathbf{1}_1$ into a distribution of cyclic oligomers $\mathbf{1}_n$ by dynamic covalent bond formation:[13] (acidic) $\mathbf{1}_1$ (7.0 µmol, 1 equiv.), 0.5 mL $CDCl_3$, TFA-d_1 (35 µmol, 5 equiv.) 1 day, RT; (basic) $\mathbf{1}_1$ (7.0 µmol, 1 equiv.), 0.5 mL $CDCl_3$, DBU (7 µmol, 1 equiv.) and DTT (0.7 µmol, 0.1 equiv.), 2 days, RT. (b) ESI$^+$ mass spectrum of an equilibrium mixture containing $\mathbf{1}_1$ and higher oligomers $\mathbf{1}_n$ after treatment of $\mathbf{1}_1$ in $CDCl_3$ under acidic conditions: $\mathbf{1}_1$ (7.0 µmol, 1 equiv.), 0.5 mL $CDCl_3$, TFA-d_1 (35 µmol, 5 equiv.) 1 day, RT. Note: The mass spectrum gives a disproportionate bias to higher oligomeric macrocycles, which appear to bind to Na^+ more effectively than $\mathbf{1}_1$. See ESI† for the corresponding ^{1}H NMR spectrum which shows that, in fact, <5% oligomers higher than $n = 1$ are present in the reaction mixture.

mixtures after an equilibration time of 1–2 days at RT (after which time the composition of the reaction mixtures no longer changed) as confirmed by electrospray ionisation-mass spectrometry (ESI-MS) (Fig. 1b). (Note: the two mixtures resulting from acidic or basic conditions should not be identical—experimental evidence for this was provided by slight differences in the ^{1}H NMR spectra—because disulfide exchange can result in a higher number of constitutional isomers for each group of cyclic oligomers $\mathbf{1}_n$ with $n > 1$; see Fig. 1a.[13])

Dynamic Chemistry II: Ring-opening of macrocycle $\mathbf{1}_1$ in the presence of a single disulfide or hydrazone scavenger

A second series of experiments was conducted with the objective of confirming which functional group was dynamic under which set of conditions, opening macrocycle $\mathbf{1}_1$ at either the disulfide or at the hydrazone linkage in the presence of acyclic 'scavenger' molecules (Scheme 2).

For disulfide exchange the symmetric benzylic disulfide **9** was used as the scavenger (Scheme 2a) and for hydrazone exchange the scavenger employed was acyl hydrazone **10** (Scheme 2b). First, the optimised basic conditions determined from the dynamic experiments in the absence of scavengers (initial concentration of $\mathbf{1}_1$ 12 mM, $CDCl_3$, 1.0 equiv. DBU and 0.1 equiv. DTT, RT,

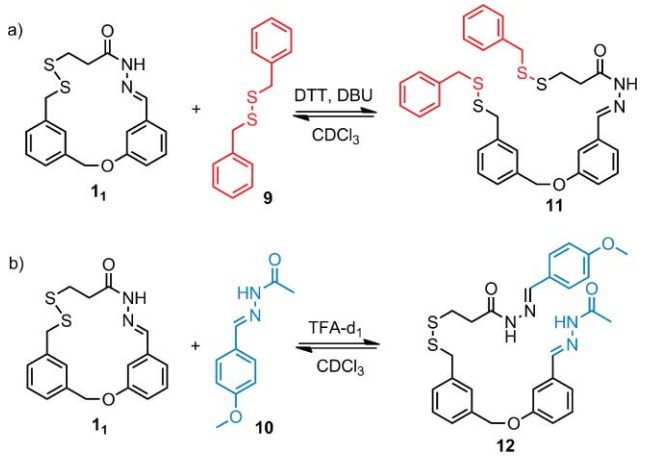

Scheme 2 Dynamic covalent ring-opening of macrocycle $\mathbf{1}_1$ in the presence of an acyclic disulfide or hydrazone scavenger. (a) Disulfide exchange of macrocycle $\mathbf{1}_1$ (59 μmol, 1 equiv.) with disulfide scavenger **9** (0.29 mmol, 5 equiv.) under basic conditions (DBU, 59 μmol, 1 equiv.; DTT, 5.9 μmol, 0.1 equiv.) in $CDCl_3$ (5 mL, initial concentration of $\mathbf{1}_1$ 12 mM) after 24–48 h at RT led to an equilibrium mixture of $\mathbf{1}_1$, **9** and ring-opened product **11** (molar ratios: $\mathbf{1}_1$:**9**:**11** 13 : 82 : 5). (b) Acid-mediated (TFA-d_1, 0.29 mmol, 5 equiv.) hydrazone exchange of macrocycle $\mathbf{1}_1$ (59 μmol, 1 equiv.) with hydrazone scavenger **10** (0.29 mmol, 5 equiv.) in $CDCl_3$ (5 mL, initial concentration of $\mathbf{1}_1$ 12 mM) after 6–12 h at RT led to an equilibrium mixture of $\mathbf{1}_1$, **10** and ring-opened product **12** (molar ratios $\mathbf{1}_1$:**10**:**12** 13 : 82 : 5). Note: Small amounts of oligomers (<5% as indicated by ^{1}H NMR) were also present in the equilibrium mixtures.

1–2 days) were applied to a mixture of $\mathbf{1}_1$ and an excess (5 equiv.) of **9** (Scheme 2a), resulting in formation of **11** in 28% isolated yield (along with $\mathbf{1}_1$ and small amounts of higher cyclic and open-chain oligomers). In a separate experiment $\mathbf{1}_1$ was subjected to the optimised acidic conditions (initial concentration of $\mathbf{1}_1$ 12 mM, $CDCl_3$, 5 equiv. of TFA-d_1, RT, 6–12 h) in the presence of an excess (5 equiv.) of hydrazone scavenger **10** (Scheme 2b), which gave **12** in 26% isolated yield (along with small amounts of oligomeric species).

When only one equivalent of scavenger was used, **11** and **12** were each formed as roughly 5% of the product mixture (as determined by ^{1}H NMR) under the basic and acidic conditions, respectively (see Fig. 2a). To prove that these mixtures were indeed at thermodynamic minimum, pristine ring-opened products **11** and **12** in the absence of scavenger were subjected to basic (**11**) or acidic (**12**) conditions in two 'reverse-equilibration' experiments (Fig. 2).

Fig. 2b shows the conversion of **11** back into $\mathbf{1}_1$ as monitored by ^{1}H NMR spectroscopy. Starting from pure **11**, a 95% conversion into macrocycle $\mathbf{1}_1$ was observed over 24 h under the standard basic conditions (Fig. 2a). Similarly **12** was converted back into $\mathbf{1}_1$ in approximately 95% yield under acidic conditions. These results confirmed that under the basic and acidic reaction conditions an ~95 : 5 molar ratio of macrocycle to ring-opened product corresponds to the thermodynamic minimum of the system (at a substrate concentration of 12 mM in $CDCl_3$ at RT). The ^{1}H NMR spectrum displayed at the front of Fig. 2b also shows minor peaks indicative of higher cyclic oligomers, $\mathbf{1}_n$ ($n > 1$). The total amount of these oligomers did not exceed ~5% of the mixture.

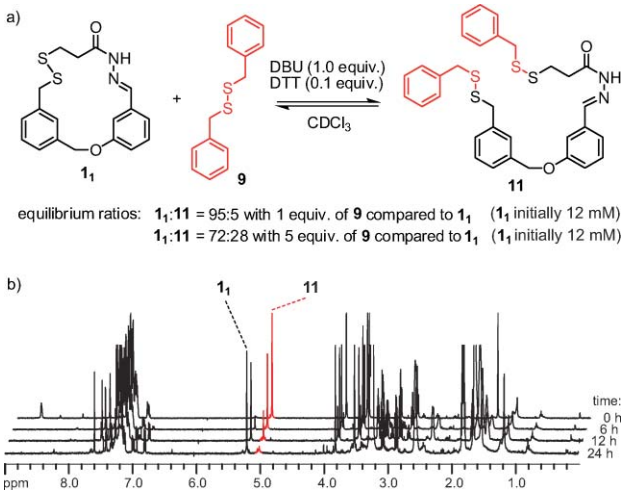

Fig. 2 (a) Composition of equilibrium between $\mathbf{1}_1$, **9** (1 or 5 equiv.) and **11**. Reaction conditions: Initial concentration of $\mathbf{1}_1$ or **11**: 12 mM, DBU (1 equiv.), DTT (0.1 equiv.), RT, 24–48 h. (b) ^{1}H NMR monitoring of reverse-equilibration experiment (initial concentration of **11** 12 mM). Pristine ring-opened product **11** (rear spectrum) was converted back into a mixture containing predominantly macrocycle $\mathbf{1}_1$ ($\mathbf{1}_1$:**11** ~95 : 5) (front spectrum). The signals for the methylene groups in the ether linkages (in the region δ = 5.0–5.15 ppm), which differ significantly in chemical shift in $\mathbf{1}_1$ and **11**, are highlighted.

Dynamic Chemistry III: Competition experiments with macrocycle $\mathbf{1}_1$ in the presence of both disulfide and hydrazone scavengers 9 and 10

Fig. 3a shows a third series of experiments on the dynamic ring-opening of macrocycle $\mathbf{1}_1$. In a competition experiment, a mixture of macrocycle $\mathbf{1}_1$ and both scavenger compounds **9** (5 equiv.) and **10** (5 equiv.) was subjected to the optimised conditions for either, (i), disulfide or, (ii), hydrazone exchange (see experimental section for reaction conditions). HPLC analysis (Fig. 3b) of the resulting mixtures revealed that under basic conditions only ring-opened compound **11** (resulting from disulfide exchange) was obtained (yellow peak in trace (i)), whereas **12** (which would arise from hydrazone exchange) was not observed. Under acidic conditions the opposite result occurred, hydrazone-exchanged ring-opened product **12** (purple peak in trace (ii)) was formed without any of **11**. As in the previous experiments, ^{1}H NMR indicated the presence of a small amount (<5%) of oligomers formed as byproducts under the reaction conditions. These results confirm that conditions (i) and (ii) are, indeed, mutually exclusive with respect to the dynamic covalent exchange processes that they induce. Basic conditions, (i), promote disulfide exchange and preclude hydrazone exchange and *vice versa*: acidic conditions, (ii), induce hydrazone exchange and preclude disulfide exchange. Equally importantly, neither set of conditions are affected by the presence of the scavenger that does not undergo dynamic exchange under those conditions.

The macrocyclic hydrazone-disulfide system is subject to different entropic considerations to the previously studied acyclic systems.[8] This is apparent in the remarkable dependence of the equilibrium composition on concentration. For example, we were only able to obtain HPLC trace (ii) shown in Fig. 3b when hydrazone exchange was quenched in the concentrated reaction mixture (12 mM in $CDCl_3$) by addition of Et_3N prior to dilution

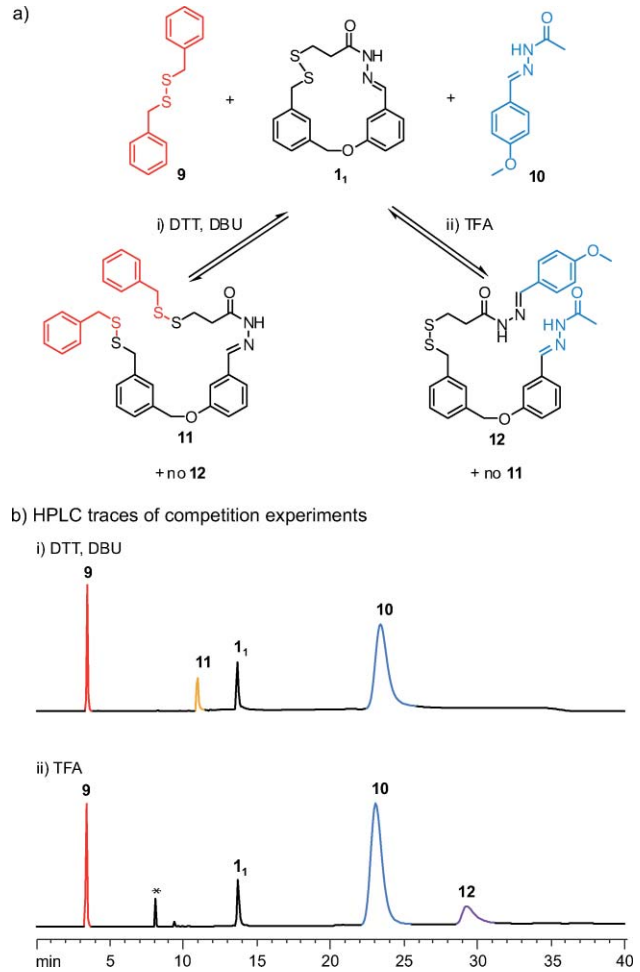

Fig. 3 Competition experiments in the presence of both scavengers **9** and **10** which demonstrated the mutually exclusive nature of conditions (i) and (ii) for disulfide and hydrazone exchange. (a) A mixture of macrocycle $\mathbf{1_1}$ (1 equiv.), disulfide scavenger **9** (5 equiv.) and hydrazone scavenger **10** (5 equiv.) was subjected to two sets of conditions in independent experiments: (i) basic conditions; DTT (0.1 equiv.), DBU (1.0 equiv.) in $CDCl_3$ (5 mL); (ii) acidic conditions; TFA (5 equiv.) in $CDCl_3$ (5 mL), 6 h. Initial concentration of $\mathbf{1_1}$ 12 M in both experiments (see experimental section for further details). (b) HPLC traces showing the outcome of the two competition experiments. (i) Equilibrium composition after treatment of a mixture of $\mathbf{1_1}$, **9** and **10** with DBU and DTT (see experimental section for details). (ii) Equilibrium composition after treatment with TFA (mixture was quenched with Et_3N prior to dilution for HPLC analysis). * Hydrolysis product of **10**, *p*-methoxybenzaldehyde. Note: The chromatographic method (see experimental section) does not account for the small amount of oligomers present, which are significantly more polar.

for HPLC analysis (after dilution: ~0.5 mM in $CHCl_3/CDCl_3$). When the diluted, unquenched solution (still containing 5 equiv. TFA) was not immediately injected for analysis, the still-dynamic system quickly responded to the dilution by a dramatic change in composition so that product **12** was no longer detected (see Fig. 4a). Fig. 4 provides a direct comparison of the HPLC traces corresponding to the unquenched (Fig. 4a) and quenched (Fig. 4b) samples.

These observations are explained by the fact that formation of **12** by reaction of macrocycle $\mathbf{1_1}$ with scavenger **10** is a bimolecular

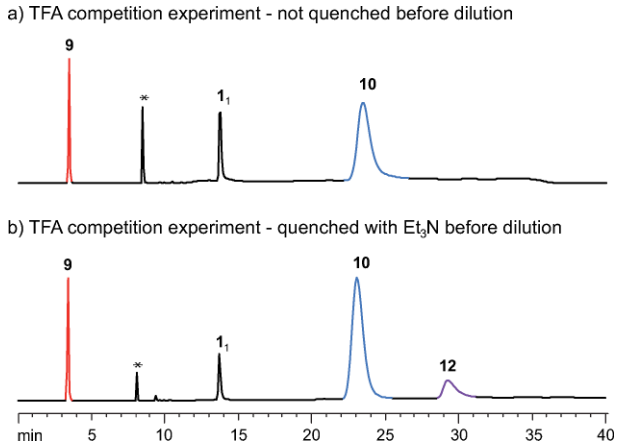

Fig. 4 Two HPLC traces obtained from one TFA-promoted hydrazone exchange competition experiment (see Fig. 3a and conditions (ii) specified in the caption of Fig. 3). (a) Sample prepared by dilution (~20-fold) and left standing for an hour prior to HPLC analysis. Since this sample was still dynamic after dilution, virtually all of **12** that had been present had been converted back to $\mathbf{1_1}$ and **10**. (b) Sample treated with excess Et_3N before dilution and left standing for an hour prior to HPLC analysis. Since addition of the base neutralised the acid, hydrazone exchange was switched off. Therefore this HPLC trace reflects the composition of the mixture before dilution. Note: The chromatographic method (see experimental section) does not account for the small amount of oligomers present, which are significantly more polar.

process and is therefore slower at lower concentrations. The reverse process of **12** into $\mathbf{1_1}$ and **10** is unimolecular and therefore occurs independent of concentration. This may also explain why, despite the solid state structure of macrocycle $\mathbf{1_1}$ showing evidence of ring strain, equilibration in the presence of scavengers under the conditions investigated (the second and third series of dynamic experiments) only gave minor amounts of the ring-opened products. The dynamic chemistry of the hydrazone-disulfide macrocyclic system is thus governed by a delicate balance of enthalpic and entropic effects. This offers the opportunity to manipulate relatively strained monomeric macrocycles under thermodynamic control without obtaining significant amounts of less strained ring-opened or oligomeric side products. These features were recently exploited to provide a mechanism by which a small molecule can "walk" processively down a molecular track.[5]

Conclusions

We have developed methodology for the synthesis of a novel macrocycle that contains both a disulfide and a hydrazone moiety and studied its dynamic chemistry. The solid state structure suggests that a certain amount of strain is caused by having several rigid elements within the framework of a 17-membered macrocycle. Sets of reaction conditions were established whereby the disulfide and hydrazone moieties can selectively undergo dynamic covalent exchange reactions in a mutually exclusive manner. Applications based on these systems are currently on-going in our laboratory.

Experimental

Materials and methods

Unless otherwise stated, all reagents were purchased from commercial sources and used without further purification. Dry CH_2Cl_2, $CHCl_3$ and THF were obtained by passing the solvent through an activated alumina column on a PureSolv™ solvent purification system (InnovativeTechnologies, Inc., MA). $CDCl_3$, DMSO-d_6, DMF, MeOH and benzene were purchased from Sigma-Aldrich. Compounds **2**,[14] **6**[15] and **10**[16] were prepared according to modified literature procedures. Compound **9** and 3-hydroxybenzaldehyde were purchased from Sigma Aldrich. Flash column chromatography was carried out using Kieselgel C60 (Merck, Germany) as the stationary phase. Analytical TLC was performed on precoated silica gel plates (0.25 mm thick, 60F254, Merck, Germany) and observed under UV light. All ^{1}H and ^{13}C NMR spectra were recorded on a Bruker AV 400 instrument, at a constant temperature of 298 K. Chemical shifts are reported in parts per million and referenced to residual solvent. Coupling constants (J) are reported in Hertz (Hz). Standard abbreviations indicating multiplicity were used as follows: m = multiplet, quint. = quintet, q = quartet, t = triplet, d = doublet, s = singlet, b = broad. Assignment of the ^{1}H NMR signals was accomplished by two-dimensional NMR spectroscopy (COSY, NOESY, HSQC, HMBC). See ESI for the labelling of the protons.† All melting points were determined using a Sanyo Gallenkamp apparatus and are uncorrected. ESI mass spectrometry was carried out by the mass spectrometry services at the University of Edinburgh and by the EPSRC National Centre at the University of Wales, Swansea. Analytical and preparative HPLC was performed on instruments of Gilson Inc., USA. For all shown chromatograms, a normal-phase column (Kromasil-Si, 250 × 4.6 mm) was used with gradient elution (1 mL min^{-1}, CH_2Cl_2–MeCN, 0 → 62.5% MeCN, UV detection @ 260 nm).

Procedures for competition experiments

(i) Dibenzyl disulfide **9** (72 mg, 0.29 mmol, 5.0 equiv.), benzoic acid [1-phenyl-meth-(*E*)-ylidene]-hydrazide **10** (56 mg, 0.29 mmol, 5.0 equiv.), DBU (8.8 mg, 58.6 µmol, 1.0 equiv.), DTT (1 mg, 6.5 µmol, 0.1 equiv.) and macrocycle $\mathbf{1_1}$ (21 mg, 58.6 µmol, 1.0 equiv.) were dissolved in $CDCl_3$ (5 mL, initial concentration of $\mathbf{1_1}$ 12 mM) and the mixture was stirred at room temperature until analytical HPLC indicated that the equilibrium composition was reached (24–48 h).

(ii) Dibenzyl disulfide **9** (72 mg, 0.29 mmol, 5.0 equiv.), benzoic acid [1-phenyl-meth-(*E*)-ylidene]-hydrazide **10** (56 mg, 0.29 mmol, 5.0 equiv.), TFA (33 mg, 22 µL, 0.29 mmol, 5.0 equiv.) and macrocycle $\mathbf{1_1}$ (21 mg, 58.6 µmol, 1.0 equiv.) were dissolved in $CDCl_3$ (5 mL, initial concentration of $\mathbf{1_1}$ 12 mM) and the mixture was stirred at room temperature until analytical HPLC indicated that the equilibrium composition was reached (6–12 h).

Syntheses

3-Chloromethylbenzyl alcohol (2). Synthesized according to a modified literature procedure.[14] At 5 °C, a solution of ethyl chloroformate (1.69 mL, 17.2 mmol, 1.0 equiv.) in THF (7 mL) was added dropwise to a solution of 3-(chloromethyl)-benzoic acid (3.02 g, 17.2 mmol, 1.0 equiv.) and Et_3N (2.39 mL, 17.2 mmol, 1.0 equiv.) in THF (30 mL). The reaction was allowed to proceed at 5 °C for 30 min before the Et_3NHCl precipitate was filtered off and washed with THF (40 mL). The combined THF phases were added over 30 min to a solution of $NaBH_4$ (1.66 g, 43 mmol, 2.5 equiv.) in H_2O (14 mL) at 10 °C. The mixture was stirred over night at room temperature and then acidified with 10% HCl (17 mL). The solution was extracted with Et_2O (3 × 50 mL), washed with a solution of 10% NaOH (50 mL) and brine (50 mL), dried ($MgSO_4$), and concentrated under reduced pressure. Flash column chromatography (SiO_2, hexane–EtOAc 8 : 2) of the residue gave **2** (2.50 g, 85%) as a colourless oil. ^{1}H NMR (400 MHz, $CDCl_3$): δ = 7.34 (m, 4H, H_b, H_c, H_d, H_e), 4.68 (s, 2H, H_f), 4.60 (s, 2H, H_a), 2.32 (bs, 1H, H_g); LRMS (EI): m/z = 156.1 [M]$^+$.

3-(3-(Hydroxymethyl)benzyloxy)benzaldehyde (3). Under N_2, 3-hydroxybenzaldehyde (3.87 g, 31.69 mmol, 1.0 equiv.) was dissolved in DMF (25 mL) and cooled to 0 °C. NaH (60% in mineral oil, 1.27 g, 31.75 mmol, 1.0 equiv.) was added and the mixture was stirred until all NaH was dissolved (temperature allowed to raise to room temperature). A solution of **2** (3.31 g, 21.14 mmol, 0.67 equiv.) in DMF (25 mL) was added dropwise. The reaction was stirred for 48 h at room temperature and monitored by TLC (silica gel, toluene–EtOAc 3 : 1). After TLC showed that no starting material remained, 1 M HCl (50 mL) was added and the mixture was extracted with EtOAc (3 × 50 mL). The combined organic layers were washed with 1 M HCl (50 mL) H_2O (50 mL) and brine (50 mL), and dried over $MgSO_4$. Concentration under reduced pressure yielded a residue, which was purified by flash column chromatography (SiO_2, toluene–EtOAc 15 : 2) to give **3** (4.27 g, 83%) as a colourless oil. ^{1}H NMR (400 MHz, $CDCl_3$): δ = 9.97 (s, 1H, H_a), 7.50–7.45 (m, 4H, H_{Ar}), 7.42–7.34 (m, 3H, H_{Ar}), 7.27–7.24 (m, 1H, H_{Ar}), 5.13 (s, 2H, H_f), 4.73 (s, 2H, H_k), 1.79 (bs, 1H, H_l); ^{13}C NMR (100 MHz, $CDCl_3$): δ = 192.13 (d), 159.27 (s), 141.46 (s), 137.81 (s), 136.65 (s), 130.15 (d), 128.91 (d), 127.60 (d), 127.60 (d), 126.03 (d), 123.79 (d), 122.20 (d), 113.21 (d), 70.12 (t), 65.07 (t); HRMS (ESI): m/z = 260.1279 [M+NH$_4$]$^+$ (calcd. 260.1281 for $C_{15}H_{18}NO_3$).

3-(3-(Bromomethyl)benzyloxy)benzaldehyde (4). Under N_2, **3** (2.10 g, 8.67 mmol, 1.0 equiv.) was dissolved in benzene (25 mL). A solution of $SOBr_2$ (3.75 g, 1.40 mL, 18.05 mmol, 2.1 equiv.) in benzene (20 mL) was added dropwise at 0 °C. The reaction was monitored by TLC (SiO_2, toluene–EtOAc 3 : 1). Stirring was continued for 48 h at room temperature until TLC indicated that no starting materials remained. H_2O (25 mL) was added and the mixture was extracted with EtOAc (2 × 25 mL). The combined organic layers were washed with H_2O (50 mL), dried with brine (50 mL) and over $MgSO_4$ and concentrated under reduced pressure to yield a brownish oil. The residue was purified by flash column chromatography (SiO_2, cyclohexane/CH_2Cl_2–EtOAc 15 : 1 : 1) to yield **4** (1.92 g, 73%) as a colourless oil. ^{1}H NMR (400 MHz, $CDCl_3$): δ = 9.98 (s, 1H, H_a), 7.51–7.45 (m, 4H, H_{Ar}), 7.39–7.37 (m, 3H, H_{Ar}), 7.27–7.24 (m, 1H, H_{Ar}), 5.12 (s, 2H, H_f), 4.52 (s, 2H, H_k); ^{13}C NMR (100 MHz, $CDCl_3$): δ = 192.00 (d), 159.18 (s), 138.29 (s), 137.86 (s), 137.04 (s), 130.18 (d), 129.18 (d), 128.86 (d), 128.05 (d), 127.50 (d), 123.86 (d), 122.16 (d), 113.20 (d), 69.81 (t), 33.15 (t); HRMS (ESI): m/z = 322.0433 [M+NH$_4$]$^+$ (calcd. 322.0437 for $C_{15}H_{17}NO_2Br$).

Thioacetic acid *S*-[3-(3-formyl-phenoxymethyl)-benzyl] ester (5). **4** (1.81 g, 5.93 mmol, 1.0 equiv.) was dissolved in DMF (20 mL) and a solution of KSAc (1.36 g, 11.91 mmol, 2.0 equiv.) in DMF (20 mL) was added dropwise. The mixture was stirred over night at room temperature. The reaction was quenched by addition of a saturated aqueous solution of NH_4Cl (20 mL). The mixture was extracted with EtOAc (3 × 30 mL) and the combined organic layers were washed with 1 M HCl (20 mL), H_2O (20 mL), and brine (20 mL) and dried ($MgSO_4$). Concentration under reduced pressure yielded **5** (1.70 g, 95%) as a brownish oil that did not require further purification. ^{1}H NMR (400 MHz, $CDCl_3$): δ = 9.98 (s, 1H, H_a), 7.50–7.44 (m, 3H, H_{Ar}), 7.37 (s, 1H, H_{Ar}), 7.34–7.31 (m, 2H, H_{Ar}), 7.29–7.24 (m, 2H, H_{Ar}), 5.09 (s, 2H, H_f), 4.14 (s, 2H, H_k), 2.36 (s, 3H, H_l); ^{13}C NMR (100 MHz, $CDCl_3$): δ = 195.02 (s), 192.09 (d), 159.22 (s), 138.22 (s), 137.81 (s), 136.75 (s), 130.16 (d), 129.01 (d), 128.70 (d), 127.97 (d), 126.50 (d), 123.73 (d), 122.15 (d), 113.27 (d), 69.95 (t), 33.27 (t), 30.36 (q); HRMS (ESI): m/z = 318.1157 $[M+NH_4]^+$ (calcd. 318.1158 for $C_{17}H_{20}NO_3S$).

3-Mercaptopropanehydrazide (6). Synthesized according to a modified literature procedure.[15] Methyl 3-mercaptopropionate (10 g, 83 mmol, 1.0 equiv.) was added dropwise to a solution of hydrazine monohydrate (10 g, 200 mmol, 2.4 equiv.) in MeOH (30 mL). The reaction mixture was stirred over night at room temperature. Evaporation of the solvent, followed by flash column chromatography (SiO_2, Et_2O–MeOH 8 : 2) gave **6** (4.99 g, 50%) as a colourless oil. ^{1}H NMR (400 MHz, $CDCl_3$): δ = 6.81 (bs, 1H, H_d), 3.93 (bs, 2H, H_c), 2.84 (dt, J = 8.4 Hz, 6.4 Hz, 2H, H_b), 2.50 (t, J = 6.7 Hz, 2H, H_c), 1.61 (t, J = 8.4 Hz, 1H, H_a).

Thioacetic acid *S*-(3-{3-[(3-mercapto-propionyl)-hydrazono-methyl]-phenoxymethyl}-benzyl) ester (7). **5** (1.33 g, 4.38 mmol, 1.0 equiv.) was dissolved in MeOH (25 mL) and 5 drops of acetic acid were added. A solution of **6** (673 mg, 5.60 mmol, 1.3 equiv.) in MeOH (15 mL) was added dropwise after which the mixture was stirred for 3 h at room temperature. The reaction was monitored by TLC (SiO_2, cyclohexane/EtOAc 5 : 2). The solvent was removed *in vacuo* and the residue was purified by flash column chromatography (SiO_2, cyclohexane/EtOAc 5 : 2 → 3 : 2) to yield a mixture of thioester **7** and dithiol **8** in a ratio of 85 : 15 (1.52 g, 88%). *E*/Z ratio of the hydrazone was approximately 9 : 1. Major *E*-isomer: ^{1}H NMR (400 MHz, $CDCl_3$): δ = 9.13 (s, 1H, H_p), 7.72 (s, 1H, H_a), 7.34 (s, 1H, H_{Ar}), 7.34–7.27 (m, 5H, H_{Ar}), 7.21 (d, J = 7.6 Hz, 1H, H_{Ar}), 7.02 (ddd, J = 8.2, 2.7, 0.8 Hz, 1H, H_{Ar}), 5.07 (s, 2H, H_f), 4.14 (s, 2H, H_k), 3.12 (t, J = 6.9 Hz, 2H, H_o), 2.91 (dt, J = 8.3, 6.9 Hz, 2H, H_n), 2.36 (s, 3H, H_l), 1.74 (t, J = 8.3 Hz, 1H, H_m); some characteristic signals of the minor *Z*-isomer; 8.70 (s, 1H, H_p), 8.12 (s, 1H, H_a), 5.06 (s, 2H, H_f), 2.64 (t, J = 6.6 Hz, 2H, H_o); ^{13}C NMR (100 MHz, $CDCl_3$): δ = 195.04 (s), 173.83 (s), 159.02 (s), 143.85 (d), 138.14 (s), 137.10 (s), 135.04 (s), 129.88 (d), 128.99 (d), 128.61 (d), 127.95 (d), 126.50 (d), 120.58 (d), 117.01 (d), 112.66 (d), 69.96 (t), 36.95 (t), 33.32 (t), 30.35 (q), 19.47 (t); HRMS (ESI): m/z = 403.1144 $[M+H]^+$ (calcd. 403.1145 for $C_{20}H_{23}N_2O_3S_2$).

3-Mercapto-propionic acid [1-[3-(3-mercaptomethyl-benzyloxy)-phenyl]-meth-(*E*)-ylidene]-hydrazide (8). Under N_2, a mixture of starting material **7** and the product **8** (85 : 15, 1.50 g, 3.80 mmol, 1.0 equiv.) was dissolved in MeOH (25 mL). A solution of NaOMe (246 mg, 4.55 mmol, 1.2 equiv.) in MeOH (15 mL) was added. After 2 h NH_4Cl, (satd., 20 mL) was added and the mixture was stirred for another 15 min. The mixture was extracted with EtOAc (3 × 25 mL) and the combined organic layers were washed with H_2O (2 × 50 mL) and brine (25 mL) and dried ($MgSO_4$). The solvent was removed under reduced pressure to yield a 15 : 1 mixture of **8** and $\mathbf{1_1}$ (1.07 g, 78%) as a thick transparent oil. The dithiol **8** was found in an *E*/*Z* ratio of about 9 : 1. Major *E*-isomer. ^{1}H NMR (400 MHz, $CDCl_3$): δ = 9.23 (s, 1H, H_n), 7.72 (s, 1H, H_a), 7.43 (s, 1H, H_{Ar}), 7.38–7.30 (m, 5H, H_{Ar}), 7.22 (d, J = 7.7 Hz, 1H, H_{Ar}), 7.02 (ddd, J = 8.2, 2.6, 0.8 Hz, 1H, H_{Ar}), 5.10 (s, 2H, H_f), 3.77 (d, J = 7.6 Hz, 2H, H_k), 3.12 (t, J = 6.9 Hz, 2H, H_o), 2.91 (dt, J = 8.2, 6.9 Hz, 2H, H_n), 1.79 (t, J = 7.6 Hz, 1H, H_l), 1.74 (t, J = 8.2 Hz, 1H_m); characteristic signals of the minor *Z*-isomer: 8.71 (s, 1H, H_n), 8.12 (s, 1H, H_a), 5.08 (s, 2H, H_f), 2.64 (t, J = 6.5 Hz, 2H, H_m); ^{13}C NMR (100 MHz, $CDCl_3$): δ = 174.10 (s), 159.01 (s), 144.08 (d), 141.61 (s), 137.14 (s), 135.10 (s), 129.90 (d), 129.04 (d), 127.86 (d), 127.20 (d), 126.27 (d), 120.64 (d), 116.99 (d), 112.60 (d), 69.94 (t), 36.94 (t), 28.89 (t), 19.52 (t); HRMS (ESI): m/z = 378.1300 $[M+NH_4]^+$ (calcd. 378.1304 for $C_{18}H_{24}N_3O_2S_2$).

2-Oxa-10,11-dithia-15,16-diazatricyclo[16.3.1.1^{4,8}] tricosa-1(22),4,6,8(23),16,18,20-heptaen-14-one ($\mathbf{1_1}$). Under N_2, a mixture of dithiol **8** and disulfide $\mathbf{1_1}$ (15 : 1, 360 mg, 1.00 mmol, 1.0 equiv.) was dissolved in MeOH (100 mL) and CH_2Cl_2 (100 mL). A solution of KI (51 mg, 0.303 mmol, 0.3 equiv.) in MeOH (~5 mL) was added and subsequently, at 0 °C, a solution of I_2 (267 mg, 1.05 mmol, 1.05 equiv.) in MeOH (~ 25 mL) was added dropwise until the brown colour persisted. Na_2SO_3 was added and, when decolourisation was complete, stirring was continued for 15 min. H_2O (100 mL) and CH_2Cl_2 (100 mL) were added and the H_2O layer was extracted another time with CH_2Cl_2 (100 mL). The combined organic layers were washed with H_2O (100 mL) and with brine (100 mL) and dried ($MgSO_4$). Removal of the solvents under reduced pressure and purification by flash column chromatography (SiO_2, $CHCl_3$–EtOAc 3 : 1) yielded pure $\mathbf{1_1}$ (200 mg, 56%) as a colourless solid. M.p. 188 °C. ^{1}H NMR (400 MHz, $CDCl_3$): δ = 9.48 (s, 1H, H_n), 7.66 (s, 1H, H_a), 7.48 (s, 1H, H_j), 7.39 (dd, J = 2.6, 1.5 Hz, 1H, H_e), 7.30–7.28 (m, 3H, H_c, H_g, H_h), 7.19 (ddd, J = 6.7, 1.5, 0.9 Hz, 1H, H_i), 7.06 (ddd, J = 8.4, 2.6, 0.9 Hz, 1H, H_d), 6.89 (d, J = 7.4 Hz, 1H, H_b), 5.28 (s, 2H, H_f), 3.89 (s, 2H, H_k), 3.14 (dd, J = 7.7, 7.1 Hz, 2H, H_m), 2.92 (dd, J = 7.7, 7.1 Hz, 2H, H_l); ^{13}C NMR (100 MHz, DMSO-d_6): δ = 172.37 (s), 157.95 (s), 142.07 (d), 137.35 (s), 137.05 (s), 135.36 (s), 129.91 (d), 129.68 (d), 129.00 (d), 128.19 (d), 126.10 (d), 122.24 (d), 119.69 (d), 107.31 (d), 68.81 (t), 41.08 (t), 31.14 (t), 30.37 (t); ε (260 nm, CH_2Cl_2) = 7872.5 dm^3 mol^{-1} cm^{-1}; HRMS (ESI): m/z = 359.0882 $[M+H]^+$ (calcd. 359.0882 for $C_{18}H_{19}N_2O_2S_2$).

Benzoic acid [1-phenyl-meth-(*E*)-ylidene]-hydrazide (10). Synthesized according to a modified literature procedure.[16] A mixture of *p*-anisaldehyde (2.0 g, 14.7 mmol, 1.0 equiv.) and acethydrazide (1.21 g, 14.7 mmol, 1.0 equiv.) in EtOH (100 mL) was stirred at room temperature for 3 h. Filtration of the precipitate and recrystallisation from EtOH gave **10** (1.84 g, 65%) as a colourless, crystalline solid. ^{1}H NMR (400 MHz, $CDCl_3$): δ = 9.58 (bs, 1H, H_e), 7.75 (sb, 1H, H_d), 7.61 (d, J = 8.8 Hz, 2H, H_c), 6.92 (d, J = 8.8 Hz, 2H, H_b), 3.85 (s, 3H, H_a), 2.37 (s, 3H, H_f); ε (260 nm, CH_2Cl_2) = 6353.5 dm^3 mol^{-1} cm^{-1}.

3-Benzyldisulfanyl-propionic acid [1-[3-(3-benzyl disulfanyl-methyl-benzyloxy)-phenyl]-meth-(*E*)-ylidene]-hydrazide (11).

Dibenzyl disulfide **9** (72 mg, 0.29 mmol, 5.0 equiv.), DBU (45 mg, 0.30 mmol, 5.1 equiv.), DTT (1 mg, 6.48 μmol, 0.1 equiv.) and macrocycle $\mathbf{1_1}$ (21 mg, 58.6 μmol, 1.0 equiv.) were dissolved in $CDCl_3$ (5 mL, initial concentration of $\mathbf{1_1}$ 12 mM) and the mixture was stirred for 48 h. The reaction mixture was directly subjected to flash column chromatography (SiO_2, $CHCl_3$–EtOAc 5 : 1) to yield **11** (10 mg, 28%) as an oil. Signals for the minor *Z*-isomer were also observed (<10%). Major *E*-isomer: ^{1}H NMR (400 MHz, $CDCl_3$): δ = 9.13 (s, 1H, H_g), 7.66 (s, 1H, H_h), 7.36–7.16 (m, 17H, $H_{a–c}$, H_i, H_j, H_l, $H_{n–q}$, $H_{t–v}$), 7.03 (ddd, J = 8.2, 1.9, 0.7 Hz, 1H, H_k), 5.09 (s, 2H, H_m), 3.93 (s, 2H, H_r), 3.59 (s, 2H, H_s or H_d), 3.57 (s, 2H, H_s or H_d), 3.08 (t, J = 7.3 Hz, 2H, H_f), 2.82 (t, J = 7.3 Hz, 2H, H_e); characteristic signals of minor *Z*-isomer: 8.48 (s, 1H, H_g), 8.05 (s, 1H, H_h), 3.92 (s, 2H, H_r), 2.72 (t, J = 7.0 Hz, 2H, H_e), 2.50 (t, J = 7.0 Hz, 2H, H_f);^{13}C NMR (100 MHz, $CDCl_3$): δ = 173.48 (s), 158.99 (s), 143.39 (d), 137.88 (s), 137.31 (s), 137.22 (s), 136.98 (s), 134.95 (s), 129.91 (d), 129.43 (d), 129.32 (d), 129.19 (d), 128.80 (d), 128.57 (d), 128.51 (d), 128.48 (d), 127.50 (d), 127.47 (d), 126.56 (d), 120.58 (d), 117.81 (d), 112.55 (d), 69.87 (t), 43.57 (t), 43.28 (t), 43.03 (t), 32.98 (t), 32.79 (t); ε (260 nm, CH_2Cl_2) = 9677.9 dm^3 mol^{-1} cm^{-1}; HRMS (ESI): m/z = 626.11647 $[M+Na–H]^+$ (calcd. 626.11606 for $C_{32}H_{31}N_2O_2S_4Na$).

3-{3-[3-(Acetyl-hydrazonomethyl)-phenoxymethyl]-benzyl disulfanyl}-propionic acid [1-(4-methoxy-phenyl)-meth-(*E*)-ylidene]-hydrazide (12). Hydrazide **10** (67 mg, 0.35 mmol, 5.0 equiv.) and macrocycle $\mathbf{1_1}$ (25 mg, 69.7 μmol, 1.0 equiv.) were dissolved/suspended in $CDCl_3$ (6 mL, initial concentration of $\mathbf{1_1}$ 12 mM). TFA-d_1 (40 mg, 26 μL, 0.35 mmol, 5.0 equiv.) was added and the mixture was stirred for 12 h. The reaction was monitored by ^{1}H NMR. During the reaction, the mixture slowly turned transparent yellowish. The reaction mixture was directly subjected to flash column chromatography (SiO_2, $CHCl_3$–EtOAc 1 : 1 → 1 : 3) to give **12** (10 mg, 26%) as an oil. Signals for the minor *Z*-isomers were also observed (<10%). Major *E*-isomer: ^{1}H NMR (400 MHz, $CDCl_3$): δ = 10.39 (s, 1H, H_e or H_s), 10.13 (s, 1H, H_e or H_s), 7.77 (s, 1H, H_d or H_r), 7.75 (s, 1H, H_d or H_r), 7.60 (d, J = 8.8 Hz, 2H, H_c), 7.41 (s, 1H, H_l), 7.32–7.26 (m, 5H, H_i, H_j, H_k, H_o, H_q), 7.12 (d, J = 1.7 Hz, 1H, H_p), 6.98 (ddd, J = 6.7, 2.7, 2.4 Hz, 1H, H_n), 6.90 (d, J = 8.8 Hz, 2H, H_b), 5.10 (s, 2H, H_m), 3.93 (s, 2H, H_h), 3.83 (s, 3H, H_a), 3.10 (dd, J = 7.1, 6.9 Hz, 2H, H_f), 2.89 (dd, J = 7.1, 6.9 Hz, 2H, H_g), 2.35 (s, 3H, H_t); ^{13}C NMR (100 MHz, $CDCl_3$): δ = 174.26 (s), 174.02 (s), 161.27 (s), 158.80 (s), 144.22 (d), 144.15 (d), 137.93 (s), 137.18 (s), 135.19 (s), 129.81 (d), 129.03 (d), 128.97 (d), 128.75 (d), 128.21 (d), 126.42 (s), 126.37 (d), 119.37 (d), 117.46 (d), 114.22 (d), 113.39 (d), 69.85 (t), 55.38 (q), 43.22 (t), 34.30 (t), 33.06 (t), 20.32 (q); ε (260 nm, CH_2Cl_2) = 14079.0 dm^3 mol^{-1} cm^{-1}; HRMS (ESI): m/z = 551.1777 $[M+H]^+$ (calcd. 551.1781 for $C_{28}H_{31}N_4O_4S_2$).

Crystallographic data

$\mathbf{1_1}$. Empirical formula $C_{18}H_{18}N_2O_2S_2$, Formula weight 358.46, Temperature 93(2) K, Wavelength 0.71073 Å, Crystal system Monoclinic, Space group $P2_1/n$, Unit cell dimensions a = 6.886(2) Å α = 90°, b = 9.252(3) Å, β = 96.481(5)°, c = 26.755(8) Å, γ = 90°, Volume 1693.5(10) Å3 Z 4, Density (calculated) 1.406 Mg/m3, Absorption coefficient 0.327 mm^{-1}, F(000) 752, Crystal size 0.0800 × 0.0800 × 0.0800 mm3,Theta range for data collection 2.33 to 25.33°, Index ranges −8 < h < 8, −11 < k < 11, −32 < l < 29, Reflections collected 14385, Independent reflections 2984 [R(int) = 0.0813], Completeness to theta = 25.00° 96.6%, Absorption correction multiscan, max. and min. transmission 1.0000 and 0.9163, Refinement method full-matrix least-squares on F2, Data/restraints/parameters 2984/1/223, Goodness-of-fit on F2 0.949, Final R indices [$I > 2\sigma(I)$] R_1 = 0.0517, wR_2 = 0.1273, R indices (all data) R_1 = 0.0553, wR_2 = 0.1344, Extinction coefficient 0.050(9), Largest diff. peak and hole 0.311 and −0.283 e.Å^{-3}.

Acknowledgements

We thank the EPSRC National Mass Spectrometry Service Centre (Swansea, UK) for high resolution mass spectrometry. This research was funded through the European Research Council Advanced Grant *WalkingMols* and the EPSRC. D.A.L. is an EPSRC Senior Research Fellow and holds a Royal Society-Wolfson Research Merit Award.

Notes and references

1 (*a*) S. J. Rowan, S. J. Cantrill, G. R. L. Cousins, J. K. M. Sanders and J. F. Stoddart, *Angew. Chem., Int. Ed.*, 2002, **41**, 898; (*b*) J.-M. Lehn, *Chem. Soc. Rev.*, 2007, **36**, 151; (*c*) J.-M. Lehn and A. V. Eliseev, *Science*, 2001, **291**, 2331; (*d*) J.-M. Lehn, *Chem.–Eur. J.*, 1999, **5**, 2455; (*e*) P. T. Corbett, J. Leclaire, L. Vial, K. R. West, J.-L. Wietor, J. K. M. Sanders and S. Otto, *Chem. Rev.*, 2006, **106**, 3652.

2 (*a*) R. F. Ludlow and S. Otto, *Chem. Soc. Rev.*, 2008, **37**, 101; (*b*) J. R. Nitschke, *Nature*, 2009, **462**, 736.

3 We use the term 'constitutionally dynamic' here to include both reversible metal coordination and dynamic covalent processes (see reference 1b).

4 (*a*) V. Goral, M. I. Nelen, A. V. Eliseev and J.-M. Lehn, *Proc. Natl. Acad. Sci. U. S. A.*, 2001, **98**, 1347; (*b*) J. Leclaire, L. Vial, S. Otto and J. K. M. Sanders, *Chem. Commun.*, 2005, 1959; (*c*) D. Schultz and J. R. Nitschke, *Angew. Chem., Int. Ed.*, 2006, **45**, 2453; (*d*) R. J. Sarma, S. Otto and J. R. Nitschke, *Chem.–Eur. J.*, 2007, **13**, 9542; (*e*) N. Christinat, R. Scopelliti and K. Severin, *Angew. Chem., Int. Ed.*, 2008, **47**, 1848; (*f*) M. Hutin, G. Bernardinelli and J. R. Nitschke, *Chem.–Eur. J.*, 2008, **14**, 4585; (*g*) R. J. Sarma and J. R. Nitschke, *Angew. Chem., Int. Ed.*, 2008, **47**, 377; (*h*) V. E. Campbell, X. de Hatten, N. Delsuc, B. Kauffmann, I. Huc and J. R. Nitschke, *Chem.–Eur. J.*, 2009, **15**, 6138; (*i*) P. Mal and J. R. Nitschke, *Chem. Commun.*, 2010, **46**, 2417.

5 M. von Delius, E. M. Geertsema and D. A. Leigh, *Nat. Chem.*, 2010, **2**, 96.

6 E. R. Kay, D. A. Leigh and F. Zerbetto, *Angew. Chem., Int. Ed.*, 2007, **46**, 72.

7 The term double-level (dynamic covalent) system denotes a system whose building blocks are interconnected by two different types of exchange processes (see, for example, references 4a,4b, 8a and 8b).

8 (*a*) A. G. Orrillo, A. M. Escalante and R. L. E. Furlan, *Chem. Commun.*, 2008, 5298; (*b*) Z. Rodriguez-Docampo and S. Otto, *Chem. Commun.*, 2008, 5301.

9 $\mathbf{1_1}$ is the smallest cyclic oligomer of type $\mathbf{1_n}$, where **1** denotes the repeat structure and the subscript **n** denotes the numbers of repeat units in the molecule.

10 An alternative strategy to introduce the disulfide linkage prior to ring-closure by hydrazone condensation failed, as various methodologies for the synthesis of unsymmetric disulfide bonds [(*a*) R. Hunter, M. Caira and N. Stellenboom, *J. Org. Chem.*, 2006, **71**, 8268; (*b*) S. Antoniow and D. Witt, *Synthesis*, 363; (*c*) J. Kowalczyk, P. Barski, D. Witt and B. A. Grzybowski, *Langmuir*, 2007, **23**, 2318] proved low yielding or unsuccessful in our hands.

11 T. J. Kucharski, Z. Huang, Q.-Z. Yang, Y. Tian, N. C. Rubin, C. D. Concepcion and R. Boulatov, *Angew. Chem., Int. Ed.*, 2009, **48**, 7040.

12 (*a*) G. R. L. Cousins, S.-A. Poulsen and J. K. M. Sanders, *Chem. Commun.*, 1999, 1575; (*b*) A. T. ten Cate, P. Y. W. Dankers, R. P. Sijbesma and E. W. Meijer, *J. Org. Chem.*, 2005, **70**, 5799; (*c*) A. L. Kieran, A. D. Bond, A. M. Belenguer and J. K. M. Sanders, *Chem. Commun.*, 2003, 2674.
13 Cyclooligomerisation of $\mathbf{1}_1$ *via* disulfide exchange is possible either in a head-to-head (two benzylic disuflide fragments), tail-to-tail (two thioethyl hydrazone fragments) or head-to-tail (one of each) fashion, while hydrazone exchange alone can only give rise to head-to-tail oligomers.
14 N. Iqbal, C.-A. McEwen and E. E. Knaus, *Drug Dev. Res.*, 2000, **51**, 177.
15 M. D. Costioli, D. Berdat, R. Freitag, X. André and A. H. E. Müller, *Macromolecules*, 2005, **38**, 3630.
16 J. R. Dimmock, S. C. Vashishtha and J. P. Stables, *Eur. J. Med. Chem.*, 2000, **35**, 241.

FEBRUARY 2010 VOL 2 NO 2
www.nature.com/naturechemistry

nature chemistry

These molecules are made for walking

QUANTUM COMPUTING
Calculating chemistry

FULLERENE CHEMISTRY
Reactions under the microscope

CARBOHYDRATE SYNTHESIS
Enzymes hit the sweet spot

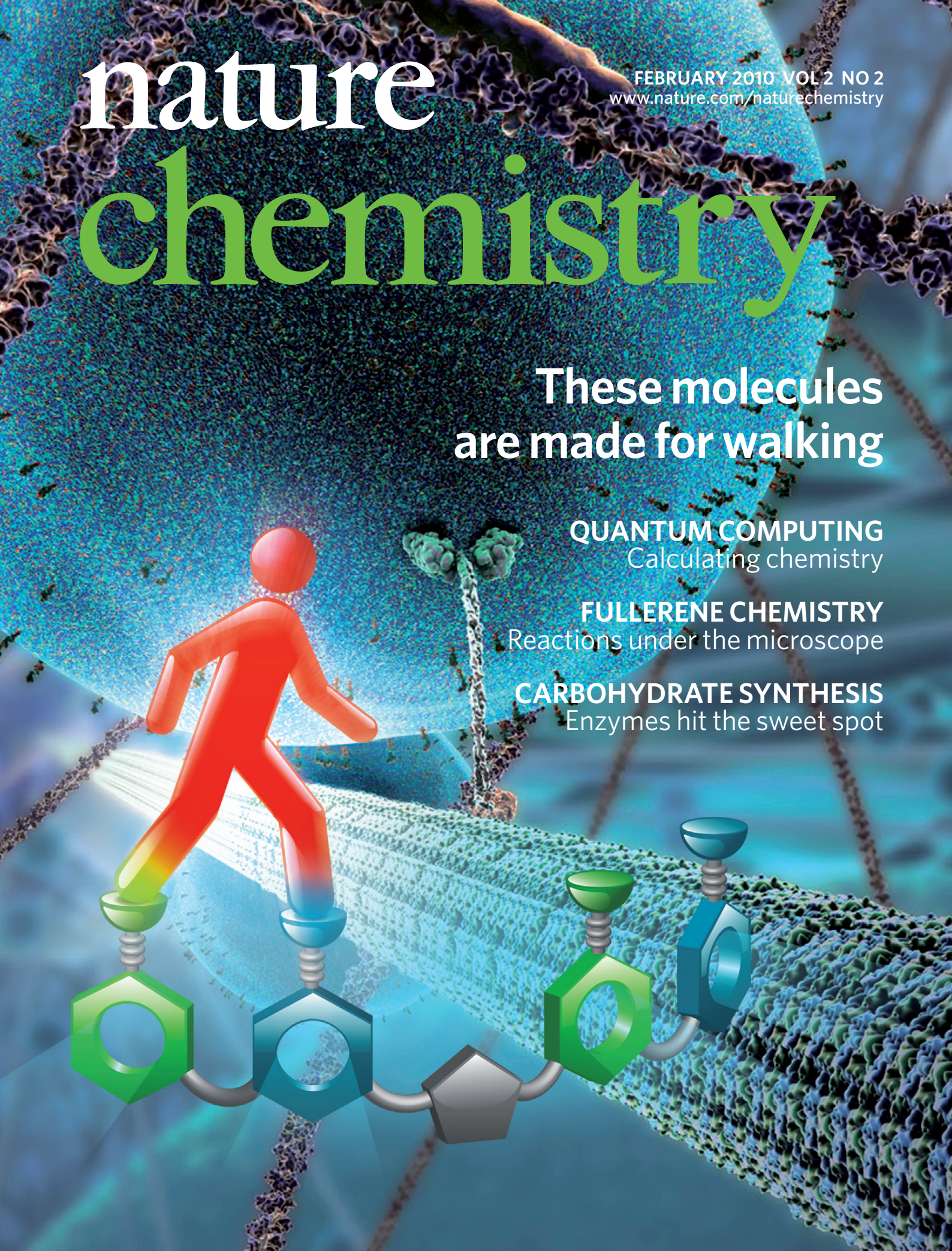

ARTICLES
PUBLISHED ONLINE: 20 DECEMBER 2009 | DOI: 10.1038/NCHEM.481
nature chemistry

A synthetic small molecule that can walk down a track

Max von Delius, Edzard M. Geertsema and David A. Leigh*

Although chemists have made small-molecule rotary motors, to date there have been no reports of small-molecule linear motors. Here we describe the synthesis and operation of a 21-atom two-legged molecular unit that is able to walk up and down a four-foothold molecular track. High processivity is conferred by designing the track-binding interactions of the two feet to be labile under different sets of conditions such that each foot can act as a temporarily fixed pivot for the other. The walker randomly and processively takes zero or one step along the track using a 'passing-leg' gait each time the environment is switched between acid and base. Replacing the basic step with a redox-mediated, disulfide-exchange reaction directionally transports the bipedal molecules away from the minimum-energy distribution by a Brownian ratchet mechanism. The ultimate goal of such studies is to produce artificial, linear molecular motors that move directionally along polymeric tracks to transport cargoes and perform tasks in a manner reminiscent of biological motor proteins.

Molecular motors are used throughout biology to drive chemical systems away from equilibrium, and thereby enable tasks to be performed, cargoes to be transported directionally and work to be done[1]. Spectacular examples include the kinesin, myosin and dynein bipedal motor proteins, which are directionally driven along microtubule or actin filament tracks by adenosine triphosphate hydrolysis[1]. Despite fundamental advances in recent years[2–10], most of the artificial molecular machines prepared so far fall well short of the degree of control over motion exhibited by such biomolecules[11]. To date the only synthetic structures that can, even in principle, take repetitive, processive (that is, without detaching or exchanging with other molecules in the bulk) steps along a molecular track are systems constructed from DNA[12–19].

Here we report the synthesis and operation of a synthetic small molecule that is able to walk repetitively up and down a four-foothold molecular track in response to a changing chemical environment. High processivity is conferred by designing the track-binding interactions of the two feet to be labile under different sets of conditions (acidic and basic). Under acidic conditions the disulfide bond between one foot of the walker and the track is locked kinetically, and the hydrazone unit that joins the other foot to the track is labile, which allows that foot to sample two different (forward and backward) footholds through hydrazone exchange. Under basic conditions the relative kinetic stabilities of the foot–track interactions are reversed, so the disulfide foot samples the forward and backward binding sites on the track, and the hydrazone foot is locked in place. The walker molecule thus randomly and processively takes zero or one step along the track using a passing-leg gait each time the environment is switched between acidic and basic. For an ensemble of walker–track conjugates a steady-state, minimum-energy distribution of walkers on the four-foothold tracks is reached after several acid–base oscillations, irrespective of which end of the track the walkers start from. Alternating between acidic conditions and a kinetically controlled redox reaction causes the two-legged molecule to walk down the track with inherent directionality through an information-ratchet[10,11,20,21] type of Brownian ratchet mechanism.

Results

Design of a dynamically processive, small-molecule walker–track system. Motors and machines at the molecular level operate by (and must be designed according to) chemical laws and statistical mechanisms, not the Newtonian laws for momentum and inertia that dictate the mechanisms of mechanical machines in the macroscopic world[11,20]. The design outline for the small-molecule walker–track system intended to mimic some of the basic characteristics of linear motor protein dynamics, namely progressive, processive and repetitive motion of a walker unit up and down a molecular track without fully detaching or exchanging with others in the bulk, is shown in Fig. 1. The walker unit (shown in red) traverses the track by a passing-leg gait that involves two chemically different 'feet' ('A' and 'B'), which reversibly bind to different regions of the track. Linear motor proteins and the synthetic DNA walkers use non-covalent interactions for track binding, but our understanding of how to lock and release sequentially and kinetically different artificial hydrogen-bond recognition sites (for example) in the desired manner is beyond the capabilities of present-day synthetic supramolecular chemistry.

We instead chose to use dynamic covalent chemistry[22–24] for this purpose, which combines some of the features of supramolecular chemistry (reversibility, dynamics) with those of covalent bond chemistry (bond strength, robustness). To prevent the walker from completely detaching from the track during the walking process, the different feet form covalent bonds that are labile or kinetically locked under different sets of conditions[25–27]. Under condition I (Fig. 1a), foot A can dissociate from the track and then rebind, either to its original foothold or to another one within reach, and foot B remains in position on the track. Under condition II (Fig. 1b) the situation is reversed and foot B can detach from the track and rebind, with the bond between foot A and the track locked kinetically. Switching repeatedly between conditions I and II should cause the walker to move randomly up and down the track, taking zero or one step each time the conditions change. If the reactions employed are fully reversible then, without the consumption of any additional fuel, the oscillation in conditions eventually leads to a steady-state, energy-minimum distribution of the walker on the track. Interestingly, although this distribution is arrived at through a process analogous to that of attaining a thermodynamic equilibrium (it is the average of a statistical sampling of exchanging chemical entities), each walker–track positional (constitutional) isomer is actually only ever in chemical equilibrium with a limited number of the other isomers. For

School of Chemistry, University of Edinburgh, The King's Buildings, West Mains Road, Edinburgh EH9 3JJ, UK. *e-mail: david.leigh@ed.ac.uk

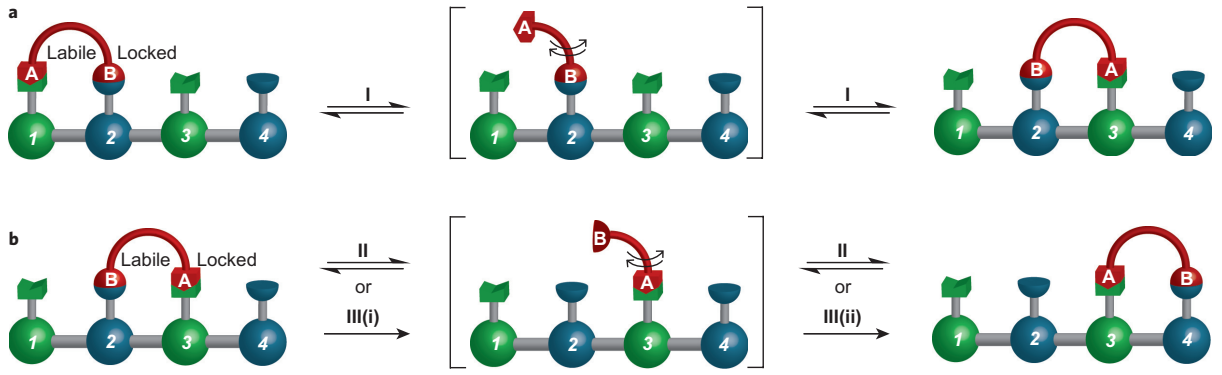

Figure 1 | Binding requirements for the processive migration of a two-legged walker molecule (red) along a track that features two possible binding sites (green and blue) for each foot. For the walking action to be processive, the two feet of the walker (A and B) must not be disconnected from the track at the same time (in the two key intermediate states, shown in square brackets, one or other foot is disconnected from the track). A way to achieve this is to design the foot–track bond-forming and -breaking events to occur under different sets of conditions (I and either II or III) for each foot. If conditions are used in which the chemical reaction that generates one of the two steps proceeds with a different forward–backward ratio to the other step (pathway I + III), directional processive transport of the walker along the track occurs.

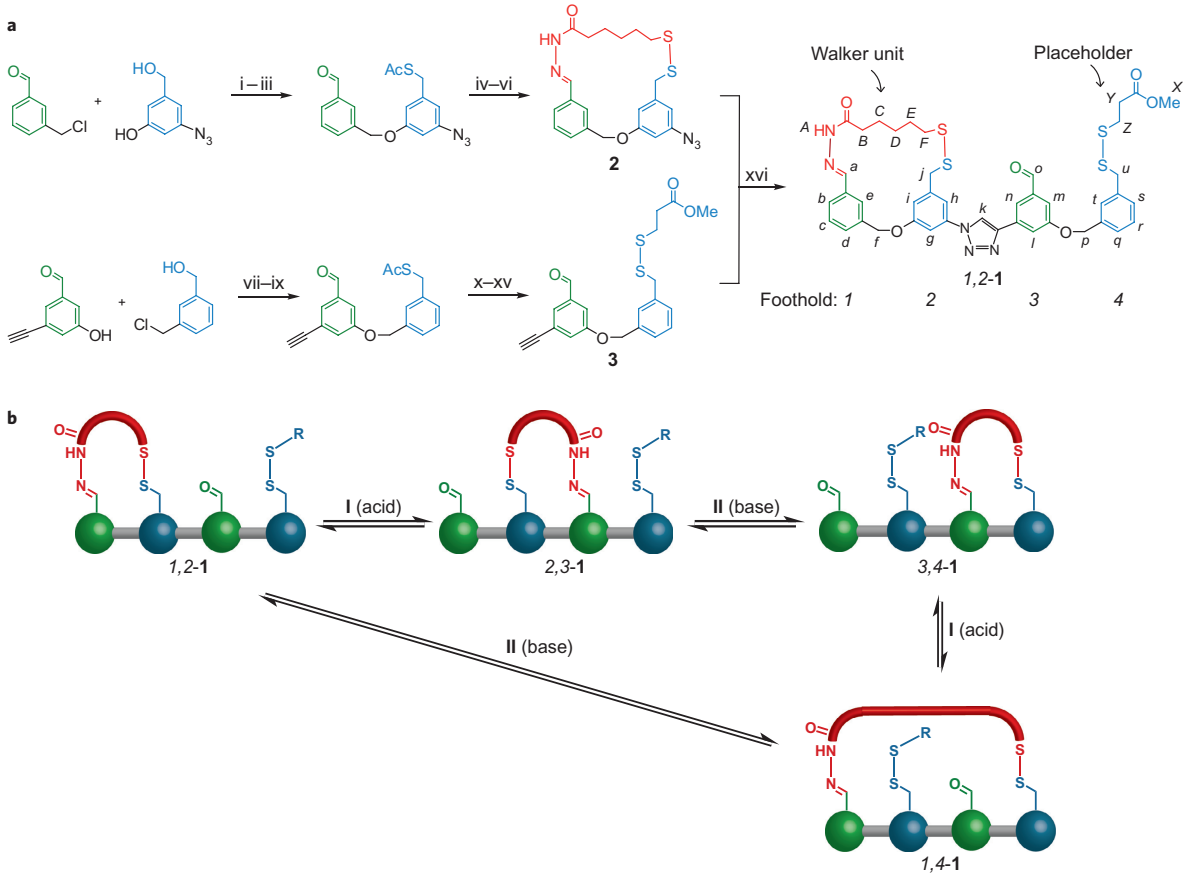

Figure 2 | Synthesis and operation of molecular walker–track conjugate *1,2*-1 under different sets of conditions (acid–base) for reversible covalent bonding of each foot with footholds on the track. a, Synthesis of *1,2*-**1**: i, NaH, dimethylformamide (DMF), room temperature (RT), 16 h, 88%; ii, methanesulfonyl chloride (MsCl), Et_3N, CH_2Cl_2, 0 °C, 30 min; iii, potassium thioacetate (KSAc), DMF, RT, 3 h, 77% (over two steps); iv, 6-mercaptohexanoic acid hydrazide, AcOH, MeOH, RT, 2 h, 78%; v, NaOMe, MeOH, RT, 2 h; vi, I_2, KI, CH_2Cl_2, RT, 5 min, 32% (over two steps); vii, NaH, DMF, 0 °C to RT, 16 h, 65%; viii, MsCl, Et_3N, CH_2Cl_2, RT, 16 h; ix, KSAc, DMF, RT, 3 h, 66% (over two steps); x, $HC(OMe)_3$, *p*-toluenesulfonic acid, MeOH, RT, 30 min; xi, NaOMe, MeOH, RT, 30 min; xii, 3-mercaptopropionic acid, I_2, KI, CH_2Cl_2, RT, 5 min; xiii, TFA, CH_2Cl_2, RT, 30 min, 58% (over four steps); xiv, H_2SO_4, MeOH, RT, 16 h; xv, TFA, CH_2Cl_2, RT, 30 min, 40% (over two steps); xvi, $Cu(MeCN)_4PF_6$, tris((1-benzyl-1H-1,2,3-triazol-4-yl)methyl)amine, CH_2Cl_2–tetrahydrofuran–MeOH, RT, 16 h, 79%. **b**, Local equilibria that connect the four positional isomers *1,2*-**1**, *2,3*-**1**, *3,4*-**1** and *1,4*-**1** under various conditions. The upper pathway represents the major passing-leg mechanism from *1,2*-**1** to *3,4*-**1** (through *2,3*-**1**), and the lower pathway (through *1,4*-**1**) is a minor double-step mechanism. Oscillation between acid (condition I) and base (condition II) leads to a steady-state distribution of 39:36:19:6 (±2) for *1,2*-**1**:*2,3*-**1**:*3,4*-**1**:*1,4*-**1** (see Fig. 4).

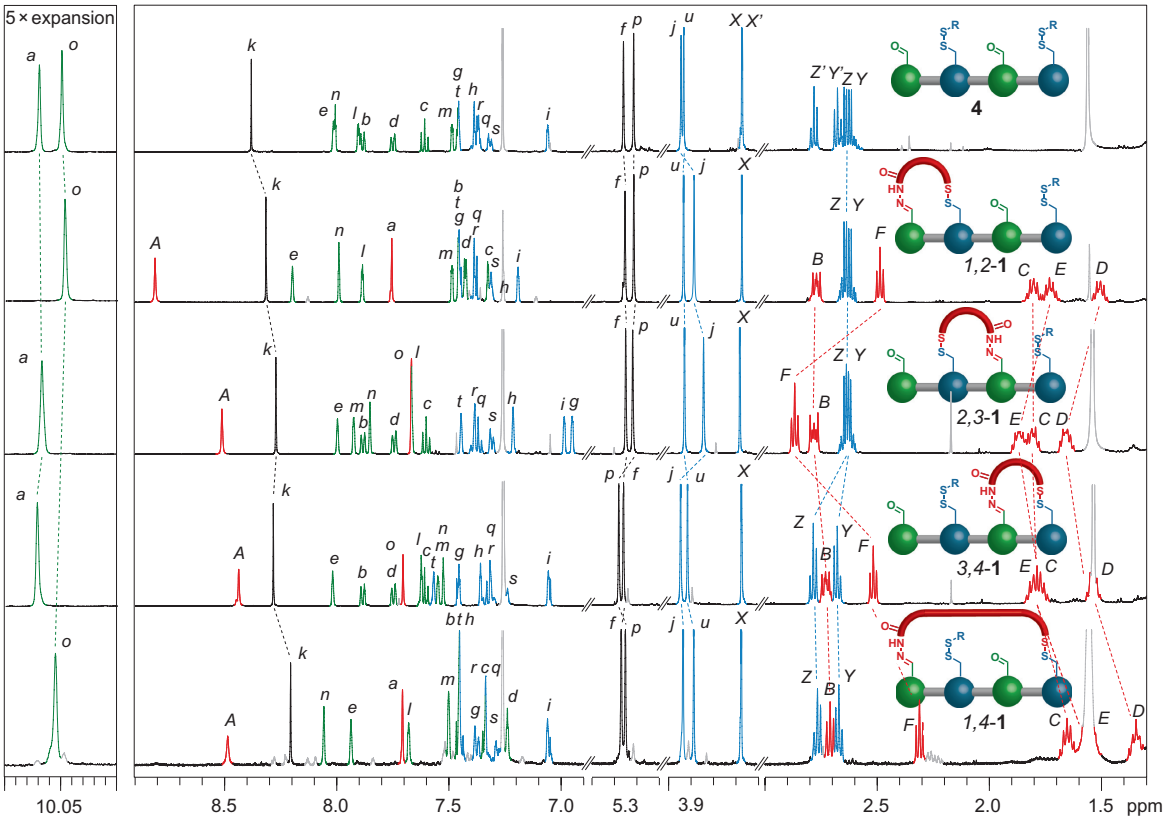

Figure 3 | Partial ^{1}H NMR (500 MHz, $CDCl_3$, 298 K) spectra of molecular track 4 and the four walker–track positional isomers *1,2*-1, *2,3*-1, *3,4*-1 and *1,4*-1. Dotted lines connect signals that differ significantly in chemical shift as a result of the position of the red walker unit. For example, the expanded aldehyde region (framed) shows distinctive shifts for the two chemically different protons labelled *o* and *a* (see chemical structures in Fig. 2 for the labelling system).

example, there is no single set of conditions whereby the *1,2*-isomer (Fig. 1a) is able to exchange with the *3,4*-isomer (Fig. 1b). Their interconversion only occurs through the *2,3*-isomer, which under condition I is in equilibrium with the *1,2*-isomer and under condition II is in equilibrium with the *3,4*-isomer. This unusual property of the system confers processivity on the walking process.

Synthesis, characterization and directionally unbiased walking. A walker–track conjugate, *1,2*-**1**, in which the molecular walker is attached to a four-foothold track by hydrazone (labile in acid, locked in base) and disulfide (labile in base, locked in acid) linkages[26,27], was constructed as shown in Fig. 2 (see Supplementary Information for the full experimental procedures and compound characterization). The four-foothold track contains two potential sites of attachment for the hydrazide foot (position *1* and the aldehyde at position *3*, shown in green) and two potential sites of attachment for the sulfur foot (position *2* and the benzylic mercaptan at position *4* (shown in blue), masked with a 'placeholder' aliphatic unit as a disulfide in *1,2*-**1**).

The starting position of the walker at footholds *1* and *2* in the walker–track conjugate was established by synthesizing macrocycle **2** and coupling this to the building block **3** that contained footholds *3* and *4* (Fig. 2a, step xvi). We also prepared isomer *3,4*-**1** unambiguously through synthesis (see Supplementary Information) and isolated and characterized isomers *2,3*-**1** and *1,4*-**1** from reactions that could not produce unknown positional isomers. The partial ^{1}H NMR spectra of the four walker–track positional isomers *1,2*-**1**, *2,3*-**1**, *3,4*-**1** and *1,4*-**1** confirmed their structures and, together with that of the parent track **4**, are shown in Fig. 3. Although the structural similarity between the compounds is immediately evident from the spectra, differences in chemical shift occur for the protons of the methylene groups in the five-carbon spacer unit (shown in red, H_B and H_F), which reflect the difference in the shape and environment of the macrocycle formed between the walker and track in each isomer. A useful probe for the position of the walker is shown in the expanded aldehyde region at a chemical shift around 10.05 parts per million (ppm) (Fig. 3). In the four walker–track positional isomers the aldehyde proton (H_o in *1,2*-**1** and *1,4*-**1**; H_a in *2,3*-**1** and *3,4*-**1**) is diagnostic of the aldehyde foothold that is free. Similarly, the methylene protons (H_Z and H_Y) serve as distinctive markers for the position of the placeholder disulfide.

The dynamic behaviour of the walker–track conjugate system on cycling between acid and base is shown in Fig. 4. When a dilute solution of *1,2*-**1** in chloroform ($CHCl_3$) was treated with a catalytic amount of trifluoroacetic acid (TFA), intramolecular hydrazone exchange gave rise to a mixture of *1,2*-**1** and its positional isomer *2,3*-**1** in a 51:49 ratio (Fig. 4b, cycle 1, condition I). Treatment of this mixture with a strong base, *1,8*-diazabicyclo[5.4.0]undec-7-ene (DBU), D,L-dithiothreitol (DTT) (which promotes disulfide exchange by acting as a source of a nucleophilic thiolate anion[28]) and dimethyl 3,3′-disulfanediyldipropanoate ($(MeO_2CCH_2CH_2S)_2$), the placeholder disulfide, generated a mixture of all four positional isomers, *1,2*-**1**, *2,3*-**1**, *3,4*-**1** and *1,4*-**1**, in a 45:36:11:8 ratio, as determined by high-performance liquid chromatography (HPLC) (Fig. 4b, cycle 1, condition II; see Supplementary Information for details). Switching between conditions I and II over several cycles (Fig. 4a,i) led to convergence of the distribution of the positional isomers to a ratio for *1,2*-**1**:*2,3*-**1**:*3,4*-**1**:*1,4*-**1** of 39:36:19:6 (±2) (Fig. 4b). A very similar distribution of isomers was obtained by starting from pristine *3,4*-**1** and carrying out the operation sequence over two or three cycles (Figs 4a,ii and 4b). Thus, irrespective of which end of the track the walker starts

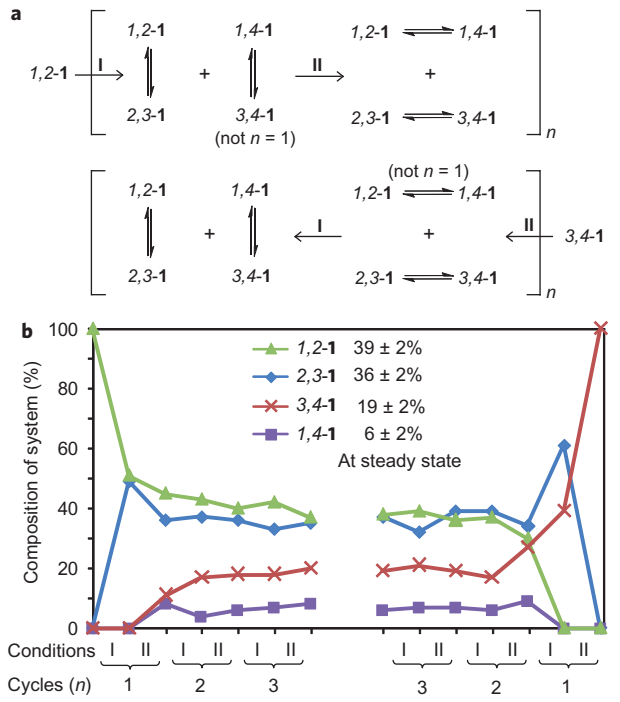

Figure 4 | Dynamic behaviour of molecular walker–track conjugates *1,2*-1 and *3,4*-1, each under cycling of the conditions (acid–base) for reversible covalent bonding of each foot with pairs of footholds on the track. a, Experimental sequence that, over a number of operational cycles (*n*), leads to a steady-state, minimum-energy distribution of the walker on the track. Condition I (reversible hydrazone exchange): 0.1 mM, TFA, $CHCl_3$, RT, 6–96 h (allowed to continue until the distribution no longer changed, as monitored by HPLC). Condition II (reversible disulfide exchange): 0.1 mM, DTT (10 equiv.), DBU (40 equiv.), $(MeO_2CCH_2CH_2S)_2$ (20 equiv.), $CHCl_3$, RT, 12–48 h (allowed to continue until the distribution no longer changed, as monitored by HPLC). **b**, Product distribution. Under each set of conditions (I and II) two different pairs of positional isomers are in equilibrium. Values are based on HPLC integration and are corrected for the absorbance coefficients at 290 nm (see Supplementary Information).

from, the effect of the passing-leg gait operations is to reach the same (global minimum energy) distribution of positional isomers of the walker on the track.

In addition to the major passing-leg gait mechanism for the route from *1,2*-**1** to *3,4*-**1**, the somewhat unexpected presence of *1,4*-**1** in the product distributions (albeit in small amounts, 4–10%) (we originally suspected it might be too strained to be present in observable quantities using reversible chemical reactions) provides a minor 'double-step' route from *1,2*-**1** to *3,4*-**1** (Fig. 2b). It is interesting that occasional statistical 'errors' to the major pathway mechanisms also occur with some biological motor proteins[1,29].

Processivity studies of directionally unbiased walking. To determine the processivity of the walking experiments shown in Fig. 4, we carried out double-labelling cross-over experiments (see Supplementary Information for details). Deuterium labels were introduced into both the walker moiety (d_2 unit at position *F*, Fig. 2) and the track part (d_2 unit at position *u*, Fig. 2) of the molecule in *3,4*-**1** (the labelling experiments were performed on *3,4*-**1** rather than *1,2*-**1** solely for synthetic convenience). The doubly labelled walker–track conjugate was mixed with an unlabelled sample of *3,4*-**1** in a 1:1 ratio. This mixture was subjected to the walking-cycle conditions shown in Fig. 4 and the product distribution analysed by HPLC-MS. The small amount (typically less than 1%) of singly labelled products obtained (a labelled walker on an unlabelled track or an unlabelled walker on a labelled track) can occur only by the swapping of a walker between tracks, and so by comparing the amount of doubly labelled and unlabelled products with that of the singly labelled products the processivity of the walking process could be determined quantitatively. The results (see Supplementary Information) show that the small-molecule walker is highly processive under the operating conditions, with a mean step number of 37 before losing its processivity, which corresponds to an average run length of ~26 nm on a hypothetical infinite track. In comparison, wild-type kinesins typically exhibit a mean step number in the range 75–175 (refs 30,31) and an average run length of ~1 μm (refs 30,31) (the stride lengths of wild-type kinesins are ~10 times longer than that of the 21-atom walker reported here).

Directionally biased walking. Starting with the walker at one end of the track (that is, pristine *1,2*-**1** or *3,4*-**1**) and cycling between conditions I and II results in some walkers moving from one end of the track to the other (Fig. 4). However, this is a consequence of the initial distribution of walker–track conjugates not being at the minimum-energy distribution and the system relaxing towards it, so the walking sequence outlined in Fig. 4a is not intrinsically directional. (By this we mean that in the internal region of a polymeric track made of alternating benzaldehyde and benzylic disulfide footholds, the walker would move, over several acid–base oscillations, in each direction with equal probability.) The lack of intrinsic directionality in the movement of the walker may appear counterintuitive given the stimuli-induced changes in its position reported in Fig. 4b, but (ignoring substituents and the minor *1,4*-isomer) only two fundamentally different types of macrocycles are formed between the walker and the track—one in which the track ether linkage is internal to the macrocycle (present in *1,2*-**1** and *3,4*-**1**) and one in which the track triazole unit is internal to the macrocycle (*2,3*-**1**). Each operation I or II thermodynamically equilibrates this pair of macrocycles about the pivot (kinetically locked) foot and, unless the macrocycles happen to have different relative thermodynamic stabilities in acid and base, the ratio produced should not depend on which foot, disulfide or hydrazone, is fixed to the track. The difference in the amount of *1,2*-**1** and *3,4*-**1** present in the minimum-energy distribution is, therefore, largely a consequence of the different substitution patterns on the macrocycles in these compounds. In the internal region of a polymeric track made of alternating benzaldehyde and benzylic disulfide footholds no net directionality of walking would occur using a pair of operations that give the same ratio (for example, both give the thermodynamic ratio) of the two different macrocycles.

To create a system in which the walker can be transported with a directional bias, even in the middle of a polymeric track, and therefore be able to transport cargo or generate a progressively increasing force, it is necessary to replace one of the walking operations with a step that proceeds with a different forward–backward ratio to the other step. This was achieved for the four-foothold track by replacing the base-promoted disulfide exchange reaction with a two-stage redox process (Fig. 5a,b) in which the ring-opened intermediate (shown in square brackets) is generated in the absence of the placeholder disulfide (1 mM walker–track conjugate, DBU (3 equiv.), DTT (6 equiv.), $CHCl_3$, reflux), and then reoxidized rapidly with iodine (0.1 mM walker–track conjugate, I_2 (12 equiv.), $MeO_2CCH_2CH_2SH$ (8 equiv.), Et_3N, $CHCl_3$/MeOH 1:1) to regenerate the walker–track disulfide linkages. As the reoxidation occurs virtually instantaneously and is irreversible under the reaction conditions, reattachment of the sulfur foot to the track occurs under kinetic control and gives a product ratio different to that achieved by the reversible disulfide-exchange reaction. The effect of introducing this operation into the walking sequence is shown in Fig. 5c. In just 1.5 cycles starting from 100%, *1,2*-**1** (the walker) moves down the track to give 43% *3,4*-**1**, compared to the 19% of

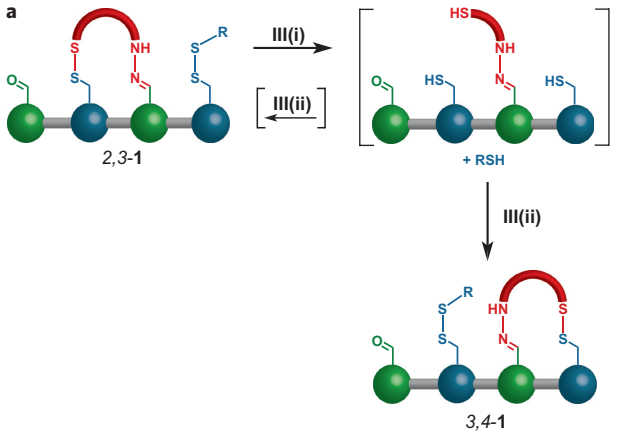

c

Cycles	0	0.5	1	1.5	Steady state from Fig. 4b, *n* = 3
Conditions		I	III	I	
1,2-**1**	100	52	28	24	39
2,3-**1**	0	48	20	24	36
3,4-**1**	0	0	28	**43**	**19**
1,4-**1**	0	0	24	9	6

Figure 5 | Processive directionally biased walk from *1,2*-1 under cycling of conditions (acid–redox) for covalent bonding of each foot with pairs of footholds on the track. a, Redox-mediated reaction sequence illustrated for *2,3*-**1**. III(i): reductive ring-opening quantitatively generates the trithiol. III(ii): rapid oxidation recyclizes to give the disulfides. The redox sequence is carried out under kinetic control and gives a different product ratio to the base-promoted, reversible disulfide exchange shown in Figs 2 and 4. This bias in the product distribution leads to an inherently directional transport of the walker away from the minimum-energy distribution. **b**, Reaction sequence. Condition I (reversible hydrazone exchange): 0.1 mM, TFA, $CHCl_3$. Condition III (kinetically controlled disulfide exchange): III(i) 1.0 mM, DTT (6 equiv.), DBU (3 equiv.), $CHCl_3$, reflux, 2–12 h (allowed to continue until the reduction of all disulfide bonds was complete, as monitored by ^{1}H NMR spectroscopy); III(ii) $MeO_2CCH_2CH_2SH$ (8 equiv.), I_2, Et_3N, $CHCl_3$/MeOH 1:1, RT, 5 min. **c**, Evolution of the mixture of positional isomers over three acid–redox operations compared to the acid–base sequence. The right-hand column shows the composition of the mixture at its steady state using the acid–base conditions (see Fig. 4b). The remarkable difference in the amount of *3,4*-**1** after only one biased step is highlighted in bold. Percentages are based on HPLC integration and are corrected for the absorbance coefficients at 290 nm (see Supplementary Information). RSH = $MeO_2CCH_2CH_2SH$.

3,4-**1** present at the steady state using the two sets of reversible conditions. As long as the product ratio obtained from condition III is different to that obtained from condition II on a polymeric (or cyclic) track, then directionally biased walking occurs at any point (although the bias on a polymer may not be as great as that for the four-foothold track, the disulfide foothold of which is unsubstituted at the end of the track). The biased walking mechanism reported in Fig. 5 relies on the increased rate of accessibility of a foothold given the particular position of the walker on the track (that is, which is the pivot foot). As such it corresponds to an information ratchet[10,11,20,21] type of Brownian ratchet mechanism.

Conclusions

We describe here a system in which a 21-atom molecular walker moves up and down a four-foothold track primarily through a passing-leg gait mechanism, each step induced by an acid–base oscillation. The feet–track interactions feature covalent bonds that are dynamic under mutually exclusive sets of conditions and ensure a level of processivity (mean step number 37) that is 20–50% that of wild-type kinesins. Replacing one of the reactions with a kinetically controlled redox operation biases the directionality of one of the steps. This is sufficient to transport the walker directionally away from its minimum-energy distribution on the four-foothold track. The two passing-leg gait steps taken by the walker to go from one end of the four-foothold track to the other are the full repeat cycle necessary for the molecule to walk down a hypothetical polymeric track made of alternating benzaldehyde and benzylic disulfide footholds. Such extended tracks, and walkers that can carry cargoes along them, are currently under construction in our laboratory.

Methods

General procedure for acid-catalysed hydrazone exchange (condition I). To a 0.1 mM solution of *1,2*-**1** (typically 1 mg in ca. 10 ml; 1.0 equiv.) in $CHCl_3$ (HPLC grade) were added five drops of a solution that contained 20% vol/vol TFA and 1% vol/vol H_2O in $CHCl_3$ (HPLC grade). The mixture was stirred at room temperature and the progress of equilibration followed by analytical HPLC (see Supplementary Information). When the relative ratios of the isomers were stable (6–96 hours), the mixture was washed with an aqueous solution of $NaHCO_3$. The layers were partitioned and the aqueous layer extracted with $CHCl_3$. The combined organic layers were dried over $MgSO_4$. The solvents were removed under reduced pressure and the amount and constitution of the mixture determined by weight and, after dissolving in a defined amount of $CHCl_3$, analytical HPLC.

General procedure for base-catalysed disulfide exchange (condition II). To a 0.1 mM solution of *3,4*-**1** (typically 1 mg in 10 ml; 1.0 equiv.) in $CHCl_3$ (HPLC grade) was added DBU (40 equiv.), DTT (10 equiv.) and $(MeO_2CCH_2CH_2S)_2$ (20 equiv.) from stock solutions. The mixture was stirred at room temperature and the progress of the equilibration followed by analytical HPLC. When the relative ratios of the isomers were stable (12–48 hours), the excess of DTT was oxidized by dropwise addition of a solution of iodine in $CHCl_3$ until a slightly brown colour persisted. An aqueous solution of NH_4Cl and Na_2SO_3 was added and the mixture stirred vigorously until decolourization was complete. The layers were partitioned and the aqueous layer extracted with $CHCl_3$. The combined organic layers were dried over $MgSO_4$. After work up the product distribution was no longer dynamic (free of DTT and DBU) and the solvent could be removed to allow analysis by weight and analytical HPLC (see Supplementary Information).

General procedure for redox-mediated disulfide exchange (condition III). (i) Reduction step. DTT (6 equiv.) and DBU (3 equiv.) were added from stock solutions to a 1 mM solution of *2,3*-**1** (1 equiv.) in $CDCl_3$ or $CHCl_3$. The mixture was heated under reflux until ^{1}H NMR spectroscopy showed that all disulfide bonds had been reduced (2–12 hours). (ii) Oxidation step. The solution from step (i) was diluted to 0.1 mM with a 1:1 mixture of $CHCl_3$ and MeOH (both HPLC grade). Et_3N (five drops) and methyl 3-mercaptopropionate (8 equiv.) were added. At room temperature, a solution of iodine in $CHCl_3$ was added to the mixture until the brown colour persisted. An aqueous solution of NH_4Cl and Na_2SO_3 was added and the solution stirred vigorously until decolourization was complete. The layers were partitioned and the aqueous layer extracted with $CHCl_3$. The combined organic layers were dried over $MgSO_4$. At this stage a broad-window preparative HPLC was carried out (retaining the products in a window of 5–12 minutes retention time, see Supplementary Information) to remove excess reagents, waste products and other impurities (the two-step redox sequence produces more by-products than the acid- or base-catalysed procedures). The samples were analysed by HPLC before and after to confirm that the walker–track isomer ratios remained unchanged by this procedure.

Note on molar ratios. The molar ratios of DBU and DTT used during the base-catalysed disulfide exchange experiments (40 and 10 equiv., respectively) are higher than those used during the reduction step of the redox disulfide-exchange experiments (3 and 6 equiv., respectively) because there is a tenfold difference in concentration at which the experiments were carried out (0.1 mM and 1.0 mM, respectively). The DBU:DTT ratio is also reversed (from 4:1 to 1:2) in the two experiments. The rationale behind these changes reflects the different objectives of the two types of exchange experiments: During the base-catalysed exchange experiment, DTT is added to increase the rate of disulfide exchange for which thiolates are a necessary intermediate; during the redox operation the excess DTT results in quantitative reduction of the disulfide bonds. The resulting thiols were

subsequently oxidized rapidly by iodine to effect a kinetically controlled reaction outcome.

Received 9 October 2009; accepted 11 November 2009; published online 20 December 2009

References

1. Schliwa, M. (ed.) *Molecular Motors* (Wiley-VCH, 2003).
2. Kelly, T. R., De Silva, H. & Silva, R. A. Unidirectional rotary motion in a molecular system. *Nature* **401,** 150–152 (1999).
3. Koumura, N., Zijlstra, R. W. J., van Delden, R. A., Harada, N. & Feringa, B. L. Light-driven monodirectional molecular rotor. *Nature* **401,** 152–155 (1999).
4. Leigh, D. A., Wong, J. K. Y., Dehez, F. & Zerbetto, F. Unidirectional rotation in a mechanically interlocked molecular rotor. *Nature* **424,** 174–179 (2003).
5. Thordarson, P., Bijsterveld, E. J. A., Rowan, A. E. & Nolte, R. J. M. Epoxidation of polybutadiene by a topologically linked catalyst. *Nature* **424,** 915–918 (2003).
6. van Delden, R. A. *et al.* Unidirectional molecular motor on a gold surface. *Nature* **437,** 1337–1340 (2005).
7. Fletcher, S. P., Dumur, F., Pollard, M. M. & Feringa, B. L. A reversible, unidirectional molecular rotary motor driven by chemical energy. *Science* **310,** 80–82 (2005).
8. Balzani, V. *et al.* Autonomous artificial nanomotor powered by sunlight. *Proc. Natl Acad. Sci. USA* **103,** 1178–1183 (2006).
9. Muraoka, T., Kinbara, K. & Aida, T. Mechanical twisting of a guest by a photoresponsive host. *Nature* **440,** 512–515 (2006).
10. Serreli, V., Lee, C.-F., Kay, E. R. & Leigh, D. A. A molecular information ratchet. *Nature* **445,** 523–527 (2007).
11. Kay, E. R., Leigh, D. A. & Zerbetto, F. Synthetic molecular motors and mechanical machines. *Angew. Chem. Int. Ed.* **46,** 72–191 (2007).
12. Sherman, W. B. & Seeman, N. C. A precisely controlled DNA biped walking device. *Nano Lett.* **4,** 1203–1207 (2004).
13. Shin, J.-S. & Pierce, N. A. A synthetic DNA walker for molecular transport. *J. Am. Chem. Soc.* **126,** 10834–10835 (2004).
14. Yin, P., Yan, H., Daniell, X. G., Turberfield, A. J. & Reif, J. H. A unidirectional DNA walker that moves autonomously along a track. *Angew. Chem. Int. Ed.* **43,** 4906–4911 (2004).
15. Tian, Y., He, Y., Chen, Y., Yin, P. & Mao, C. A DNAzyme that walks processively and autonomously along a one-dimensional track. *Angew. Chem. Int. Ed.* **44,** 4355–4358 (2005).
16. Pei, R. *et al.* Behavior of polycatalytic assemblies in a substrate-displaying matrix. *J. Am. Chem. Soc.* **128,** 12693–12699 (2006).
17. Yin, P., Choi, H. M. T., Calvert, C. R. & Pierce, N. A. Programming biomolecular self-assembly pathways. *Nature* **451,** 318–322 (2008).
18. Green, S. J., Bath, J. & Turberfield, A. J. Coordinated chemomechanical cycles: a mechanism for autonomous molecular motion. *Phys. Rev. Lett.* **101,** 238101 (2008).
19. Omabegho, T., Sha, R. & Seeman, N. C. A bipedal DNA Brownian motor with coordinated legs. *Science* **324,** 67–71 (2009).
20. Astumian, R. D. Design principles for Brownian molecular machines: how to swim in molasses and walk in a hurricane. *Phys. Chem. Chem. Phys.* **9,** 5067–5083 (2007).
21. Astumian, R. D. & Derényi, I. Fluctuation driven transport and models of molecular motors and pumps. *Eur. Biophys. J.* **27,** 474–489 (1998).
22. Rowan, S. J., Cantrill, S. J., Cousins, G. R. L., Sanders, J. K. M. & Stoddart, J. F. Dynamic covalent chemistry. *Angew. Chem. Int. Ed.* **41,** 898–952 (2002).
23. Corbett, P. T. *et al.* Dynamic combinatorial chemistry. *Chem. Rev.* **106,** 3652–3711 (2006).
24. Lehn, J.-M. From supramolecular chemistry towards constitutional dynamic chemistry and adaptive chemistry. *Chem. Soc. Rev.* **36,** 151–160 (2007).
25. Goral, V., Nelen, M. I., Eliseev, A. V. & Lehn, J.-M. Double-level 'orthogonal' dynamic combinatorial libraries on transition metal template. *Proc. Natl Acad. Sci. USA* **98,** 1347–1352 (2001).
26. Orrillo, A. G., Escalante, A. M. & Furlan, R. L. E. Covalent double level dynamic combinatorial libraries: selectively addressable exchange processes. *Chem. Commun.* 5298–5300 (2008).
27. Rodriguez-Docampo, Z. & Otto, S. Orthogonal or simultaneous use of disulfide and hydrazone exchange in dynamic covalent chemistry in aqueous solution. *Chem. Commun.* 5301–5303 (2008).
28. Otto, S., Furlan, R. L. E. & Sanders, J. K. M. Dynamic combinatorial libraries of macrocyclic disulfides in water. *J. Am. Chem. Soc.* **122,** 12063–12064 (2000).
29. Noji, H., Yasuda, R., Yoshida, M. & Kinosita, K. Direct observation of the rotation of F_1-ATPase. *Nature* **386,** 299–302 (1997).
30. Vale, R. D. *et al.* Direct observation of single kinesin molecules moving along microtubules. *Nature* **380,** 451–453 (1996).
31. Case, R. B., Pierce, D. W., Hom-Booher, N., Hart, C. L. & Vale, R. D. The directional preference of kinesin motors is specified by an element outside of the motor catalytic domain. *Cell* **90,** 959–966 (1997).

Acknowledgements

We thank the Engineering and Physical Sciences Research Council (EPSRC) National Mass Spectrometry Service Centre (Swansea, UK) for high-resolution mass spectrometry and Juraj Bella for assistance with high-field NMR spectroscopy. This research was funded through the European Research Council Advanced Grant *WalkingMols*. D.A.L. is an EPSRC Senior Research Fellow and holds a Royal Society–Wolfson Research Merit Award.

Author contributions

M.v.D. and E.M.G. carried out the experimental work. All the authors contributed to the design of the experiments, the analysis of the data and the writing of the paper.

Additional information

The authors declare no competing financial interests. Supplementary information and chemical compound information accompany this paper at www.nature.com/naturechemistry. Reprints and permission information is available online at http://npg.nature.com/reprintsandpermissions/. Correspondence and requests for materials should be addressed to D.A.L.

J|A|C|S
ARTICLES

Design, Synthesis, and Operation of Small Molecules That Walk along Tracks

Max von Delius, Edzard M. Geertsema, David A. Leigh,* and Dan-Tam D. Tang

School of Chemistry, University of Edinburgh, The King's Buildings, West Mains Road, Edinburgh EH9 3JJ, United Kingdom

Received July 22, 2010; E-mail: david.leigh@ed.ac.uk

Abstract: The synthesis and system dynamics of a series of small-molecule walker-track conjugates, 3,4-$\mathbf{C}_n$ (n = 2, 3, 4, 5, and 8), based on dynamic covalent linkages between the "feet" of the walkers and the "footholds" of the track, is described. Each walker has one acyl hydrazide and one sulfur-based foot separated by a spacer chain of "n" methylene groups, while the track consists of four footholds of alternating complementary functionalities (aldehydes and masked thiols). Upon repeatedly switching between acid and base, the walker moiety can be exchanged between the footholds on the track, primarily through a "passing-leg gait" mechanism, until a steady state, minimum energy, distribution is reached. The introduction of a kinetically controlled step in the reaction sequence (redox-mediated breaking and reforming of the disulfide linkages) can cause a directional bias in the distribution of the walker on the track. The different length walker molecules exhibit very different walking behaviors: Systems n = 2 and 3 cannot actually "walk" along the track because their stride lengths are too short to bridge the internal footholds. The walkers with longer spacers (n = 4, 5, and 8) do step up and down the track repeatedly, but a directional bias under the acid−redox conditions is only achieved for the $\mathbf{C_4}$ and $\mathbf{C_5}$ systems, interestingly in opposite directions (the $\mathbf{C_8}$ walker has insufficient ring strain with the track). Although they are extremely rudimentary systems, the $\mathbf{C_4}$ and $\mathbf{C_5}$ walker−track conjugates exhibit four of the essential characteristics of linear molecular motor dynamics: processive, directional, repetitive, and progressive migration of a molecular unit up and down a molecular track.

Introduction

Although many biological processes utilize molecules that convert chemical energy into directed molecular level motion,[1] most of the artificial molecular machines prepared to date only do so to a very limited degree.[2,3] For example, rotaxanes have been developed that can change the relative positions of their components to collectively cause the transport of liquid droplets up a slope against the force of gravity[4] or to bend cantilevers.[5] However, such systems cannot act progressively; that is, they cannot be reset to do further mechanical work on a system without undoing the task they originally performed, and so are best considered molecular switches, not motors.[2] Synthetic molecules that behave as rotary motors have been developed, working either through the sequential application of stimuli[3a,c,e,g] or at a constant photostationary state.[3b,f,i,k,n] Linear molecular motors are widely used to carry out mechanical work in biology, moving down tracks, transporting cargo, progressively exerting force, and performing many other tasks.[1] There are currently no synthetic small-molecule systems that can carry out such functions, and so we have embarked on a program to pursue these goals, starting with the design and construction of artificial molecules that can be transported progressively and directionally, without detaching, along a molecular track. Here, we report on the synthesis and behavior under operating conditions of a series of small-molecule walker−track conjugates, 3,4-$\mathbf{C}_n$ (n = 2, 3, 4, 5, and 8), based on dynamic covalent linkages between the "feet" of the walkers and the "footholds" of the track. The

(1) *Molecular Motors*; Schliwa, M., Ed.; Wiley-VCH: Weinheim, Germany, 2003.
(2) Kay, E. R.; Leigh, D. A.; Zerbetto, F. *Angew. Chem., Int. Ed.* **2007**, *46*, 72–191.
(3) (a) Kelly, T. R.; De Silva, H.; Silva, R. A. *Nature* **1999**, *401*, 150–152. (b) Koumura, N.; Zijlstra, R. W. J.; van Delden, R. A.; Harada, N.; Feringa, B. L. *Nature* **1999**, *401*, 152–155. (c) Leigh, D. A.; Wong, J. K. Y.; Dehez, F.; Zerbetto, F. *Nature* **2003**, *424*, 174–179. (d) Thordarson, P.; Bijsterveld, E. J. A.; Rowan, A. E.; Nolte, R. J. M. *Nature* **2003**, *424*, 915–918. (e) Hernandez, J. V.; Kay, E. R.; Leigh, D. A. *Science* **2004**, *306*, 1532–1537. (f) van Delden, R. A.; ter Wiel, M. K. J.; Pollard, M. M.; Vicario, J.; Koumura, N.; Feringa, B. L. *Nature* **2005**, *437*, 1337–1340. (g) Fletcher, S. P.; Dumur, F.; Pollard, M. M.; Feringa, B. L. *Science* **2005**, *310*, 80–82. (h) Balzani, V.; Clemente-León, M.; Credi, A.; Ferrer, B.; Venturi, M.; Flood, A. H.; Stoddart, J. F. *Proc. Natl. Acad. Sci. U.S.A.* **2006**, *103*, 1178–1183. (i) Eelkema, R.; Pollard, M. M.; Vicario, J.; Katsonis, N.; Serrano Ramon, B.; Bastiaansen, C. W. M.; Broer, D. J.; Feringa, B. L. *Nature* **2006**, *440*, 163. (j) Muraoka, T.; Kinbara, K.; Aida, T. *Nature* **2006**, *440*, 512–515. (k) Pijper, D.; Feringa, B. L. *Angew. Chem., Int. Ed.* **2007**, *46*, 3693–3696. (l) Serreli, V.; Lee, C.-F.; Kay, E. R.; Leigh, D. A. *Nature* **2007**, *445*, 523–527. (m) Alvarez-Pérez, M.; Goldup, S. M.; Leigh, D. A.; Slawin, A. M. Z. *J. Am. Chem. Soc.* **2008**, *130*, 1836–1838. (n) Klok, M.; Boyle, N.; Pryce, M. T.; Meetsma, A.; Browne, W. R.; Feringa, B. L. *J. Am. Chem. Soc.* **2008**, *130*, 10484–10485. (o) Panman, M. R.; Bodis, P.; Shaw, D. J.; Bakker, B. H.; Newton, A. C.; Kay, E. R.; Brouwer, A. M.; Buma, W. J.; Leigh, D. A.; Woutersen, S. *Science* **2010**, *328*, 1255–1258.
(4) Berná, J.; Leigh, D. A.; Lubomska, M.; Mendoza, S. M.; Pérez, E. M.; Rudolf, P.; Teobaldi, G.; Zerbetto, F. *Nat. Mater.* **2005**, *4*, 704–710.
(5) Huang, T. J.; Brough, B.; Ho, C.-M.; Liu, Y.; Flood, A. H.; Bonvallet, P. A.; Tseng, H.-R.; Stoddart, J. F.; Baller, M.; Magonov, S. *Appl. Phys. Lett.* **2004**, *85*, 5391–5393.

synthesis and some of the properties of the C_5 system were recently reported in a preliminary communication.[6]

Molecules That Walk along Tracks. Spectacular examples of biological linear molecular motors include the kinesin, myosin, and dynein bipedal motor proteins, which are directionally driven along intracellular tracks by adenosine triphosphate (ATP) hydrolysis.[7] The main features[8,9] of biological linear molecular motor dynamics are processivity, directionality, and repetitive, progressive, and autonomous operation.

(i) Processivity is the ability of the molecular motor to remain attached to its track while it is directionally transported, that is, without detaching or exchanging with other molecules in the bulk.[10] Most wild-type kinesins exhibit a relatively high level of processivity, falling off their microtubular[11] tracks after an average of ~100 steps.[12]

(ii) Directionality is the tendency of a molecular walker to migrate preferentially toward a particular end of a polymeric track. Most kinesins show near-perfect directionality,[8] moving toward the plus-end of microtubules as long as the chemical potential of ATP is greater than that of adenosine diphosphate (ADP) and inorganic phosphate (P_i).[13] However, some kinesins, such as KIF1A,[14] only migrate with modest net directionality; that is, they take almost as many steps in the backward direction as they do in the forward direction. This type of dynamics has been described as "biased Brownian movement" or "diffusion with a drift".[15]

(iii) Repetitive operation is the motor's ability to repeatedly perform similar mechanical cycles. Kinesin takes one 8 nm step, putting one foot in front of the other, and each time an ATP molecule is hydrolyzed by the protein.[8]

(iv) Progressive operation is the ability of the molecular motor to be reset at the end of each mechanical cycle without undoing the physical task that was originally performed. The two feet of kinesin are identical, and yet it selectively moves first one foot and then the other in a passing-leg gait to transport itself continuously in the same direction along the track.[8]

(v) Autonomous operation is the ability of the molecular motor to undergo directional, processive motion as long as a chemical "fuel" is present, that is, without further external intervention (such as the application of a sequence of stimuli).

Features i−iv are key requirements for most types of molecular motor.[10] Autonomous operation, (v), can be an additional desirable trait but could also result in reduced control over a system; for example, it may not be possible to control the speed or distance traveled by a walker, nor to stop it unless and until the "fuel" runs out or the system is "clocked". Autonomous operation also implies that walker transport is only possible in one direction with a given fuel, a feature of biological motors but not necessarily a constraint that synthetic systems must adhere to. Our initial aim was to learn how to construct and operate synthetic small molecules that possess some of these key features of linear molecular motor dynamics. Until recently,[6] the only synthetic molecular structures that had been shown to exhibit most of these features were systems constructed from DNA.[16] Small-molecule walkers that do not utilize building blocks taken from biology are more fundamental systems that could offer advantages in terms of size, function, and modes of operation.

(6) (a) von Delius, M.; Geertsema, E. M.; Leigh, D. A. *Nat. Chem.* **2010**, *2*, 96–101. (b) Otto, S. *Nat. Chem.* **2010**, *2*, 75–76.

(7) For excellent concise reviews of the kinesin, myosin, and dynein linear motor families, see: (a) Vale, R. D. *Cell* **2003**, *112*, 467–480. (b) Schliwa, M.; Woehlke, G. *Nature* **2003**, *422*, 759–765.

(8) For reviews on kinesin, see: (a) Woehlke, G.; Schliwa, M. *Nat. Rev. Mol. Cell Biol.* **2000**, *1*, 50–58. (b) Asbury, C. L. *Curr. Opin. Cell Biol.* **2005**, *17*, 89–97. (c) Carter, N. J.; Cross, R. A. *Curr. Opin. Cell Biol.* **2006**, *18*, 61–67. (d) Block, S. M. *Biophys. J.* **2007**, *92*, 2986–2995.

(9) (a) Gilbert, S. P.; Webb, M. R.; Brune, M.; Johnson, K. A. *Nature* **1995**, *373*, 671–676. (b) Kull, F. J.; Sablin, P. S.; Lau, R.; Fletterick, R. J.; Vale, R. D. *Nature* **1996**, *380*, 550–555. (c) Schnitzer, M. J.; Block, S. M. *Nature* **1997**, *388*, 386–390. (d) Hua, W.; Chung, J.; Gelles, J. *Science* **2002**, *295*, 844–848. (e) Naber, N.; Minehardt, T. J.; Rice, S.; Chen, X.; Grammer, J.; Matuska, M.; Vale, R. D.; Kollman, P. A.; Car, R.; Yount, R. G.; Cooke, R.; Pate, E. *Science* **2003**, *300*, 798–801. (f) Asbury, C. L.; Fehr, A. N.; Block, S. M. *Science* **2003**, *302*, 2130–2134. (g) Yildiz, A.; Tomishige, M.; Vale, R. D.; Selvin, P. R. *Science* **2004**, *303*, 676–678. (h) Carter, N. J.; Cross, R. A. *Nature* **2005**, *435*, 308–312. (i) Shao, Q.; Gao, Y. Q. *Proc. Natl. Acad. Sci. U.S.A.* **2006**, *103*, 8072–8077. (j) Shao, Q.; Gao, Y. Q. *Biochemistry* **2007**, *46*, 9098–9106. (k) Alonso, M. C.; Drummond, D. R.; Kain, S.; Hoeng, J.; Amos, L.; Cross, R. A. *Science* **2007**, *316*, 120–123. (l) Mori, T.; Vale, R. D.; Tomishige, M. *Nature* **2007**, *450*, 750–754. (m) Guydosh, N. R.; Block, S. M. *Nature* **2009**, *461*, 125–128.

(10) Most motors from the myosin family do not operate processively. The processivity of dyneins depends on the concentration of ATP (see ref 7b).

(11) (a) Hirose, K.; Löwe, J.; Alonso, M.; Cross, R. A.; Amos, L. A. *Cell Struct. Funct.* **1999**, *24*, 277–284. (b) Kozielski, F.; Arnal, I.; Wade, R. H. *Curr. Biol.* **1998**, *8*, 191–198. (c) Marx, A.; Müller, J.; Mandelkow, E.-M.; Hoenger, A.; Mandelkow, E. *J. Muscle Res. Cell Motil.* **2006**, *27*, 125–137.

(12) (a) Howard, J.; Hudspeth, A. J.; Vale, R. D. *Nature* **1989**, *342*, 154–158. (b) Block, S. M.; Goldstein, L. S. B.; Schnapp, B. J. *Nature* **1990**, *348*, 348–352. (c) Hackney, D. D. *Nature* **1995**, *377*, 448–450. (d) Vale, R. D.; Funatsu, T.; Pierce, D. W.; Romberg, L.; Harada, Y.; Yanagida, T. *Nature* **1996**, *380*, 451–453. (e) Case, R. B.; Pierce, D. W.; Hom-Booher, N.; Hart, C. L.; Vale, R. D. *Cell* **1997**, *90*, 959–966. (f) Romberg, L.; Pierce, D. W.; Vale, R. D. *J. Cell Biol.* **1998**, *140*, 1407–1416. (g) Thorn, K. S.; Ubersax, J. A.; Vale, R. D. *J. Cell Biol.* **2000**, *151*, 1093–1100. (h) Yajima, J.; Alonso, M. C.; Cross, R. A.; Toyoshima, Y. Y. *Curr. Biol.* **2002**, *12*, 301–306.

(13) (a) Astumian, R. D. *Phys. Chem. Chem. Phys.* **2007**, *9*, 5067–5083. (b) Astumian, R. D.; Derényi, I. *Eur. Biophys. J.* **1998**, *27*, 474–489. (c) Astumian, R. D. *Biophys. J.* **2010**, *98*, 2401–2409.

(14) Hirokawa, N.; Nitta, R.; Okada, Y. *Nat. Rev. Mol. Cell Biol.* **2009**, *10*, 877–884.

(15) Okada, Y.; Hirokawa, N. *Science* **1999**, *283*, 1152–1157.

(16) (a) Sherman, W. B.; Seeman, N. C. *Nano Lett.* **2004**, *4*, 1203–1207. (b) Shin, J.-S.; Pierce, N. A. *J. Am. Chem. Soc.* **2004**, *126*, 10834–10835. (c) Yin, P.; Yan, H.; Daniell, X. G.; Turberfield, A. J.; Reif, J. H. *Angew. Chem., Int. Ed.* **2004**, *43*, 4906–4911. (d) Tian, Y.; He, Y.; Chen, Y.; Yin, P.; Mao, C. *Angew. Chem., Int. Ed.* **2005**, *44*, 4355–4358. (e) Pei, R.; Taylor, S. K.; Stefanovic, D.; Rudchenko, S.; Mitchell, T. E.; Stojanovic, M. N. *J. Am. Chem. Soc.* **2006**, *128*, 12693–1269. (f) Yin, P.; Choi, H. M. T.; Calvert, C. R.; Pierce, N. A. *Nature* **2008**, *451*, 318–322. (g) Green, S. J.; Bath, J.; Turberfield, A. J. *Phys. Rev. Lett.* **2008**, *101*, 238101. (h) Omabegho, T.; Sha, R.; Seeman, N. C. *Science* **2009**, *324*, 67–71. (i) Gu, H.; Chao, J.; Xiao, S.-J.; Seeman, N. C. *Nature* **2010**, *465*, 202–205. (j) Lund, K.; Manzo, A. J.; Dabby, N.; Michelotti, N.; Johnson-Buck, A.; Nangreave, J.; Taylor, S.; Pei, R.; Stojanovic, M. N.; Walter, N. G.; Winfree, E.; Yan, H. *Nature* **2010**, *465*, 206–210.

(17) In some cases (e.g., the Payne rearrangement), only bonds, rather than molecular fragments, migrate. In others, such as the Cope rearrangement, the migration of atoms proceeds processively (i.e., intramolecularly). However, such migrations are generally neither repetitive, nor progressive (the 1,4-Cope rearrangement of an allyl ether can occur twice in a row if the 2-position is blocked: Ryan, J. P.; O'Connor, P. R. *J. Am. Chem. Soc.* **1952**, *74*, 5866−5869). Metal complexes often migrate around ring systems and along other molecular frameworks, for example: Strawser, D.; Karton, A.; Zenkina, O. V.; Iron, M. A.; Shimon, L. J. W.; Martin, J. M. L.; van der Boom, M. E. *J. Am. Chem. Soc.* **2005**, *127*, 9322–9323, but not directionally in a sense that can be repetitively propagated. In other reactions, for example, the exchange of acetals between the hydroxyl groups of carbohydrates, the migration of the molecular fragments is an intrinsically nondirectional and non-processive process (intramolecular exchange competes with exchange with the bulk). For details of these, and other examples of rearrangements, see: Kürti, L.; Czakó, B. *Strategic Applications of Named Reactions*; Elsevier: Oxford, UK, 2005; and references cited therein.

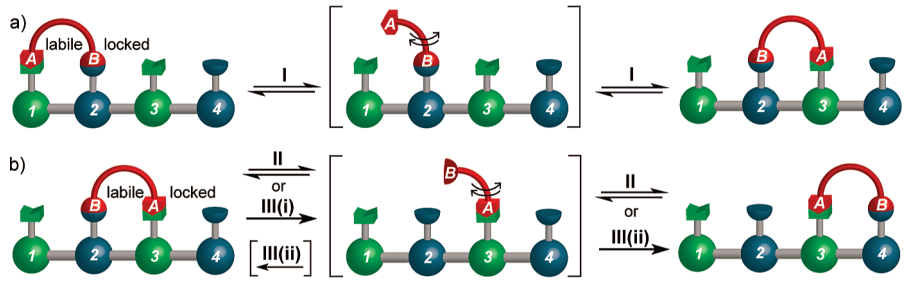

Figure 1. Graphical representation of processive migration of a two-legged "walker" molecule (red) along a track featuring two different possible binding sites (green and blue) for the two chemically different feet. Two key intermediate states, in which one or the other foot is disconnected from the track, are shown in square brackets. For the walking action to be processive, the two feet of the walker (labeled "A" and "B") must never be disconnected from the track at the same time. In chemical terms, the way that this is achieved in this system is that the foot−track bond disconnections (I and either II or III) are designed to occur under mutually exclusive sets of conditions.

Design of a Synthetic Small-Molecule Walker. Although there are many chemical reactions that feature the migration of molecular fragments, few appear well-suited for developing into a processive, directional, and repetitive motor mechanism.[17] There are, however, some reports of small molecular units that move processively (i.e., without detaching) along molecular frameworks. Lawton and co-workers have described a series of reagents for the cross-linking of biomolecules under thermodynamic control.[18] These molecules are transferred between accessible nucleophilic (amine and thiol) sites on proteins such as ribonuclease.[16a] The transport proceeds intramolecularly (i.e., processively) due to the clever construction of the cross-linking moiety: only one or two, never zero, of the nucleophilic footholds are attached to the cross-linking molecule at any one time as it is passed from one nucleophilic site to another intramolecularly toward the thermodynamic minimum.[19] During polymer synthesis, catalytic metal species have been shown to migrate intramolecularly for considerable distances along polymer chains growing by Kumada catalyst-transfer polycondensation[20] and during ethylene polymerization.[21] Finally, Schalley and co-workers have described systems in which crown ethers apparently migrate processively along linear or cyclic molecular scaffolds under the extreme dilution conditions present in the high vacuum of a FTICR mass spectrometer.[22]

Our approach to a bipedal small molecule that can walk down a molecular track is outlined in Figure 1. The walker unit (shown in red) is intended to traverse the track by a "passing-leg" gait involving two chemically different "feet" ("A" and "B") that reversibly bind to different regions of the track. Linear motor proteins and the synthetic DNA walkers use noncovalent interactions for track binding, but the understanding of how to sequentially kinetically lock and release different artificial hydrogen bond (for example) recognition sites in the desired manner is beyond the capabilities of present day synthetic supramolecular chemistry. We instead chose to utilize dynamic covalent chemistry[23] for this purpose, which combines some of the features of supramolecular chemistry (reversibility, dynamics) with those of covalent bond chemistry (bond strength, robustness). To prevent the walker from completely detaching from the track during the walking process, the different feet form covalent bonds that are labile or kinetically locked under mutually exclusive sets of conditions.[24] Under condition I (Figure 1a), foot "A" can dissociate from the track, while the bond between foot "B" and the track is kinetically locked. Under conditions II or III (Figure 1b), the situation is reversed. This unusual property of the system confers processivity on the walking process.

Results and Discussion

Synthesis. The construction of walker−track conjugate 1,2-$\mathbf{C_5}$, in which the molecular walker is attached to a four-foothold track via hydrazone (labile in acid; locked in base) and disulfide (labile in base; locked in acid) linkages,[24b−d] is shown in Scheme 1.[6] Acyl hydrazones were chosen for the acid-labile linkage rather than imines as they are generally more kinetically inert under neutral or basic conditions and when isolated.[25] Benzylic thiols were utilized on the track, because they can be introduced under mild conditions at a late stage of the synthesis.

Building blocks **1**−**4** were synthesized according to published procedures.[26] Williamson ether synthesis (steps i and vii), mesylation (steps ii and viii), and nucleophilic substitution with potassium thioacetate (steps iii and ix) generated the key two-

(18) (a) Mitra, S.; Lawton, R. G. *J. Am. Chem. Soc.* **1979**, *101*, 3097–3110. (b) Liberatore, F. A.; Comeau, R. D.; McKearin, J. M.; Pearson, D. A.; Belonga, B. Q.; Brocchini, S. J.; Kath, J.; Phillips, T.; Oswell, K.; Lawton, R. G. *Bioconjugate Chem.* **1990**, *1*, 36–50. (c) del Rosario, R. B.; Brocchini, S. J.; Lawton, R. G.; Wahl, R. L.; Smith, R. *Bioconjugate Chem.* **1990**, *1*, 50–58. (d) del Rosario, R. B.; Baron, L. A.; Lawton, R. G.; Wahl, R. L. *Nucl. Med. Biol.* **1992**, *19*, 417–421.

(19) Loss of processivity in these systems may occur through intermolecular bridges, the presence of which has been reported (ref 18a). Lawton and coworkers did not (and had no cause to) conduct studies on the processivity of their systems.

(20) Tkachov, R.; Senkovskyy, V.; Komber, H.; Sommer, J.-U.; Kiriy, A. *J. Am. Chem. Soc.* **2010**, *132*, 7803–7810.

(21) (a) Johnson, L. K.; Killian, C. M.; Brookhart, M. *J. Am. Chem. Soc.* **1995**, *117*, 6414–6415. (b) Möhring, M.; Fink, G. *Angew. Chem., Int. Ed. Engl.* **1985**, *24*, 1001–1002.

(22) (a) Winkler, H. D. F.; Weimann, D. P.; Springer, A.; Schalley, C. A. *Angew. Chem., Int. Ed.* **2009**, *48*, 7246–7250. (b) Weimann, D. P.; Winkler, H. D. F.; Falenski, J. A.; Koksch, B.; Schalley, C. A. *Nat. Chem.* **2009**, *1*, 573–577.

(23) (a) Rowan, S. J.; Cantrill, S. J.; Cousins, G. R. L.; Sanders, J. K. M.; Stoddart, J. F. *Angew. Chem., Int. Ed.* **2002**, *41*, 898–952. (b) Corbett, P. T.; Leclaire, J.; Vial, L.; West, K. R.; Wietor, J.-L.; Sanders, J. K. M.; Otto, S. *Chem. Rev.* **2006**, *106*, 3652–3711. (c) Lehn, J.-M. *Chem. Soc. Rev.* **2007**, *36*, 151–160.

(24) (a) Goral, V.; Nelen, M. I.; Eliseev, A. V.; Lehn, J.-M. *Proc. Natl. Acad. Sci. U.S.A.* **2001**, *98*, 1347–1352. (b) Orrillo, A. G.; Escalante, A. M.; Furlan, R. L. E. *Chem. Commun.* **2008**, 5298–5300. (c) Rodriguez-Docampo, Z.; Otto, S. *Chem. Commun.* **2008**, 5301–5303. (d) von Delius, M.; Geertsema, E. M.; Leigh, D. A.; Slawin, A. M. Z. *Org. Biomol. Chem.* **2010**, *8*, 4617−4624.

(25) For an example where unstable imines are reduced to stable secondary amines, see: Hochgurtel, M.; Kroth, H.; Piecha, D.; Hofmann, M. W.; Nicolaou, K. C.; Krause, S.; Schaaf, O.; Sonnenmoser, G.; Eliseev, A. V. *Proc. Natl. Acad. Sci. U.S.A.* **2002**, *99*, 3382–3387.

(26) (a) Costioli, M. D.; Berdat, D.; Freitag, R.; André, X.; Müller, A. H. E. *Macromolecules* **2005**, *38*, 3630–3637. (b) Lin, D.; Zhang, J.; Sayre, L. M. *J. Org. Chem.* **2007**, *72*, 9471–9480. (c) Klein, L. L.; Yeung, C. M.; Kurath, P.; Mao, J. C.; Fernandes, P. B.; Lartey, P. A.; Pernet, A. G. *J. Med. Chem.* **1989**, *32*, 151–160.

Scheme 1. (a) Synthesis of Walker−Track Conjugate 1,2-$\mathbf{C_5}$,[a] (b) General Structure of Walker−Track Conjugates 3,4-$\mathbf{C_n}$, and (c) 3,4-$\mathbf{C_5}$-d_4, a Walker−Track System Deuterium-Labeled on Both the Walker and the Track Units

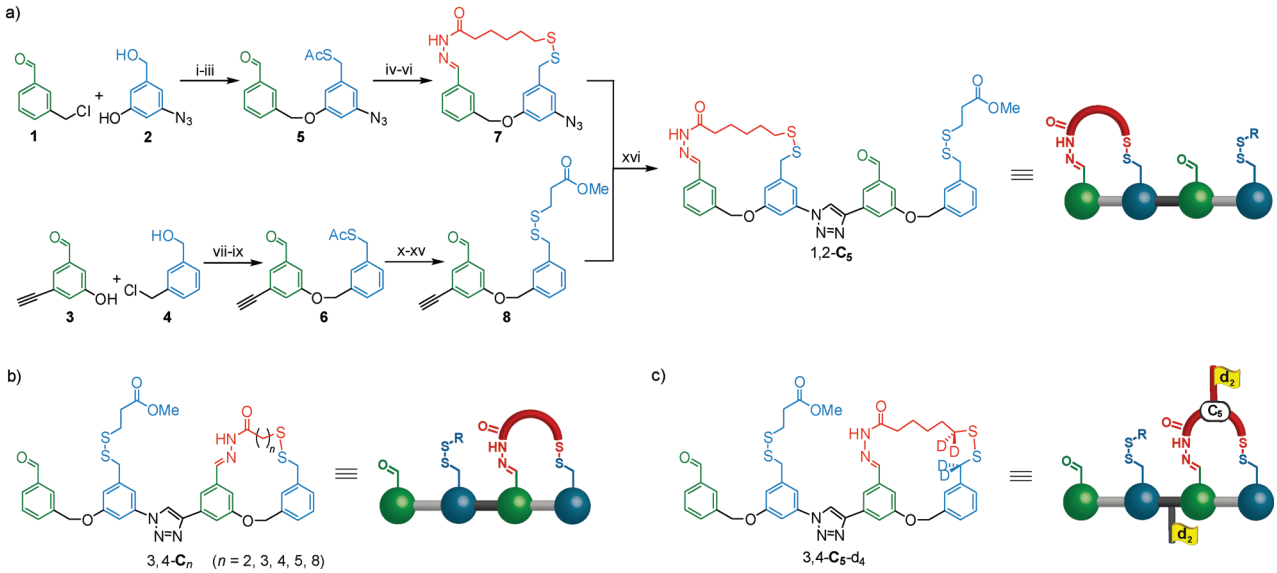

[a] (i) NaH, dimethylformamide (DMF), room temperature, 16 h, 88%; (ii) methanesulfonyl chloride (MsCl), Et_3N, CH_2Cl_2, 0 °C, 30 min; (iii) KSAc, DMF, room temperature, 3 h, 77% (over two steps); (iv) 6-mercaptohexanoic acid hydrazide, AcOH (cat.), MeOH, room temperature, 2 h, 78%; (v) NaOMe, MeOH, room temperature, 2 h; (vi) I_2, KI, CH_2Cl_2, room temperature, 5 min, 32% (over two steps); (vii) NaH, DMF, 0 °C to room temperature, 16 h, 65%; (viii) MsCl, Et_3N, CH_2Cl_2, room temperature, 16 h; (ix) KSAc, DMF, room temperature, 3 h, 66% (over two steps); (x) $HC(OMe)_3$, *p*-toluenesulfonic acid (*p*-TsOH), MeOH, room temperature, 30 min; (xi) NaOMe, MeOH, room temperature, 30 min; (xii) 3-mercaptopropionic acid, I_2, KI, CH_2Cl_2, room temperature, 5 min; (xiii) trifluoroacetic acid (TFA), CH_2Cl_2, room temperature, 30 min, 58% (over four steps); (xiv) H_2SO_4 (cat.), MeOH, room temperature, 16 h; (xv) TFA, CH_2Cl_2, room temperature, 30 min, 40% (over two steps); (xvi) $Cu(MeCN)_4PF_6$, tris[(1-benzyl-1*H*-1,2,3-triazol-4-yl)methyl]amine (TBTA), CH_2Cl_2/tetrahydrofuran (THF)/MeOH, room temperature, 16 h, 79%.

foothold precursors **5** and **6**. The starting position of the walker at footholds 1 and 2 in the walker−track conjugate was established by synthesizing macrocycle **7** by acid-catalyzed condensation (step iv) of aldehyde **5** to the bifunctional walker compound 6-mercaptohexanoic acid hydrazide, subsequent thioacetate methanolysis (step v), and oxidative ring closure (step vi). The sulfur foothold of the track (e.g., foothold 4 in 1,2-$\mathbf{C_5}$) was protected as a disulfide (using a "placeholder" thiol; see Scheme 1a), to prevent atmospheric oxygen oxidizing the free thiol to a dimeric disulfide. To achieve this, an unsymmetric disulfide bond (see compound **8** in Scheme 1a) had to be constructed, which was achieved through oxidation of the track thiol in the presence of an excess of the placeholder thiol (step xii). Finally, a ligand-assisted copper(I)-catalyzed alkyne−azide cycloaddition (CuAAC)[27] was used to couple macrocycle **7** to the building block (**8**) containing footholds 3 and 4 (Scheme 1a, step xvi). The CuAAC reaction has excellent functional group compatibility and introduces a rigid triazole linkage into the molecular track, which reduces the tendency for track folding.

Positional isomer 3,4-$\mathbf{C_5}$ (Scheme 1b), in which the walker unit is located at the other end of the track, was prepared unambiguously from **5** and **6** following analogous synthetic procedures,[6] together with a series of walker moieties differing in the number (2, 3, 4, and 8) of methylene groups between the functional group "feet". The various walker units were condensed with aldehyde **6** and subsequently converted to walker−track conjugates 3,4-$\mathbf{C_2}$, 3,4-$\mathbf{C_3}$, 3,4-$\mathbf{C_4}$, and 3,4-$\mathbf{C_8}$[28] (see the Supporting Information for synthetic procedures and characterization data). Finally, an analogue of 3,4-$\mathbf{C_5}$ was prepared that was deuterium-labeled on both the walker unit and the track (3,4-$\mathbf{C_5}$-d_4, Scheme 1c) to investigate the processivity of the walking dynamics (vide infra).

Hydrazone Exchange and Disulfide Exchange under Thermodynamic Control (Walking with No Directional Bias). We initially investigated the change of position of the various walker units on the track under conditions for reversible (dynamic) covalent bond exchange (Scheme 2). Dilute solutions of 1,2-$\mathbf{C_5}$ were subjected to acidic conditions typically used[29] for hydrazone exchange (Scheme 2, conditions I), whereas solutions of 3,4-$\mathbf{C_5}$ were subjected to basic conditions typically used[30] for

(27) (a) Chan, T. R.; Hilgraf, R.; Sharpless, K. B.; Fokin, V. V. *Org. Lett.* **2004**, *17*, 2853–2855. (b) Fokin, V. V.; Wu, P. *Aldrichimica Acta* **2007**, *40*, 7–17. (c) Lee, B.-Y.; Park, S. R.; Jeon, H. B.; Kim, K. S. *Tetrahedron Lett.* **2006**, *47*, 5105–5109.

(28) We use the abbreviation $\mathbf{C_n}$ to indicate the whole series of walker−track conjugates (*n* corresponds to the number of methylene units in the spacer chain of the walker moiety).

(29) For examples of hydrazone exchange in organic solvents, see: (a) Cousins, G. R. L.; Poulsen, S. A.; Sanders, J. K. M. *Chem. Commun.* **1999**, 1575–1576. (b) Furlan, R. L. E.; Cousins, G. R. L.; Sanders, J. K. M. *Chem. Commun.* **2000**, 1761–1762. (c) Cousins, G. R. L.; Furlan, R. L. E.; Ng, Y.-F.; Redman, J. E.; Sanders, J. K. M. *Angew. Chem., Int. Ed.* **2001**, *40*, 423–426. (d) Furlan, R. L. E.; Ng, Y.-F.; Otto, S.; Sanders, J. K. M. *J. Am. Chem. Soc.* **2001**, *123*, 8876–8877. (e) Furlan, R. L. E.; Ng, Y.-F.; Cousins, G. R. L.; Redman, J. E.; Sanders, J. K. M. *Tetrahedron* **2002**, *58*, 771–778. (f) Choudhary, S.; Morrow, J. R. *Angew. Chem., Int. Ed.* **2002**, *41*, 4096–4098. (g) Lam, T. S.; Belenguer, A.; Roberts, S. L.; Naumann, C.; Jarrosson, T.; Otto, S.; Sanders, J. K. M. *Science* **2005**, *308*, 667–669.

(30) For examples of disulfide exchange in organic solvents, see: (a) Hioki, H.; Still, W. C. *J. Org. Chem.* **1998**, *63*, 904–905. (b) Kieran, A. L.; Bond, A. D.; Belenguer, A. M.; Sanders, J. K. M. *Chem. Commun.* **2003**, 2674–2675. (c) ten Cate, A. T.; Dankers, P. Y. W.; Sijbesma, R. P.; Meijer, E. W. *J. Org. Chem.* **2005**, *70*, 5799. (d) Kieran, A. L.; Pascu, S. I.; Jarrosson, T.; Sanders, J. K. M. *Chem. Commun.* **2005**, 1276–1278. (e) Kieran, A. L.; Pascu, S. I.; Jarrosson, T.; Gunter, M. J.; Sanders, J. K. M. *Chem. Commun.* **2005**, 1842–1844. (f) Danieli, B.;

Scheme 2. Reversible Reactions That Connect Various Pairs of the Four Positional Isomers 1,2-$\mathbf{C}_n$, 2,3-$\mathbf{C}_n$, 3,4-$\mathbf{C}_n$, and 1,4-$\mathbf{C}_n$ under Conditions I or II[a]

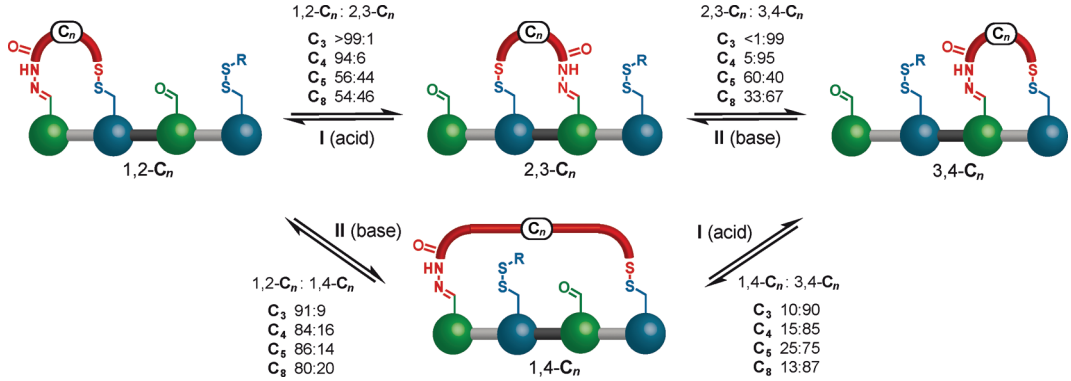

[a] Condition I (reversible hydrazone exchange): 0.1 mM, TFA, $CHCl_3$, room temperature, 6−96 h (monitored by HPLC until the distribution no longer changed). Condition II (reversible disulfide exchange): 0.1 mM, DTT (10 equiv), DBU (40 equiv), dimethyl 3,3′-disulfanediyldipropanoate (20 equiv), $CHCl_3$, room temperature, 12−48 h (monitored by HPLC until the distribution no longer changed).

disulfide exchange (Scheme 2, conditions II). In both cases, mixtures of the starting material together with positional (constitutional) isomer 2,3-$\mathbf{C_5}$ were obtained (Scheme 2).[31] Applying either set of conditions to a pristine sample of 2,3-$\mathbf{C_5}$[32] resulted in mixtures of identical composition, confirming that the dynamic exchange reactions were at chemical equilibrium.

Systematic optimization of the reaction parameters (see the Supporting Information for details) provided a set of conditions that led to equilibrium between each set of positional isomers in each walker system within a reasonable time period.[33] For hydrazone exchange[29] (e.g., exchange between the 1,2 and 2,3 isomers), adding trifluoroacetic acid (TFA) and a small amount of water (5% v/v with respect to TFA) to a solution (0.1 mM) of the walker−track conjugate in chloroform ($CHCl_3$) led to reliable and efficient conversion (no detectable amounts of oligomers or other side products) to a steady-state distribution of isomers. In the case of reversible disulfide exchange,[30] the optimized conditions utilized the same concentration (0.1 mM) of the walker−track conjugate in $CHCl_3$, a strong base (1,8-diazabicyclo[5.4.0]undec-7-ene (DBU)), a mild reducing agent (DL-dithiothreitol (DTT)), and dimethyl 3,3′-disulfanediyldipropanoate ($(MeO_2CCH_2CH_2S)_2$) as the placeholder disulfide.[34] To our surprise, subjecting 1,2-$\mathbf{C_5}$ to conditions for disulfide exchange (or 3,4-$\mathbf{C_5}$ to conditions for hydrazone exchange) also resulted in the formation of positional isomer 1,4-$\mathbf{C_5}$ (albeit in small relative amounts, 9−20%). We originally suspected this isomer would be too strained to be formed in appreciable quantities using reversible chemical reactions.

Scheme 2 shows the reversible reactions that connect various pairs of the four positional isomers 1,2-$\mathbf{C}_n$, 2,3-$\mathbf{C}_n$, 3,4-$\mathbf{C}_n$, and 1,4-$\mathbf{C}_n$ under conditions for hydrazone (I) and disulfide (II) exchange. In addition to the major passing-leg gait mechanism from 1,2-$\mathbf{C}_n$ to 3,4-$\mathbf{C}_n$ via 2,3-$\mathbf{C}_n$, 1,4-$\mathbf{C}_n$ provides a minor "double step" route from 1,2-$\mathbf{C}_n$ to 3,4-$\mathbf{C}_n$ (Scheme 2). It is interesting to note that occasional statistical "errors" to the major pathway mechanisms also occur with the working action of some biological motor proteins.[1,35]

We next quantified the position of equilibrium for every step of the walker migration under reversible conditions I and II for each set of walker−track conjugates ($\mathbf{C_2}$, $\mathbf{C_3}$, $\mathbf{C_4}$, $\mathbf{C_5}$, $\mathbf{C_8}$). In each case, the four sets of reactions that connect two pairs of positional isomers (1,2-$\mathbf{C}_n$:2,3-$\mathbf{C}_n$; 2,3-$\mathbf{C}_n$:3,4-$\mathbf{C}_n$; 1,2-$\mathbf{C}_n$:1,4-$\mathbf{C}_n$; 1,4-$\mathbf{C}_n$:3,4-$\mathbf{C}_n$) were investigated. For 3,4-$\mathbf{C_4}$, for example, the optimized conditions for disulfide exchange were applied, the equilibrium ratio between 3,4-$\mathbf{C_4}$ and 2,3-$\mathbf{C_4}$ was determined by HPLC (see the Supporting Information), and 2,3-$\mathbf{C_4}$ was subsequently isolated by semipreparative HPLC. With the pure sample of 2,3-$\mathbf{C_4}$ obtained from that experiment, two further experiments were performed: a reverse control reaction to equilibrate 2,3-$\mathbf{C_4}$ and 3,4-$\mathbf{C_4}$ and the hydrazone exchange reaction that results in equilibrium between 2,3-$\mathbf{C_4}$ and 1,2-$\mathbf{C_4}$. This procedure allowed the unambiguous determination of the equilibrium composition of every positional isomer pair, including the systems in which only the 3,4-isomer was initially prepared according to Scheme 1 ($\mathbf{C_2}$, $\mathbf{C_3}$, $\mathbf{C_4}$, and $\mathbf{C_8}$).

Scheme 2 summarizes the results of the quantitative studies on the steady-state composition of the reversible reaction between the various positional isomers (see the Supporting Information for examples of HPLC traces).[36] Three significant conclusions can be drawn from these results:

(i) The spacer length for the different walkers has a dramatic effect on the amount of 2,3-isomer that can be formed under the dynamic covalent bond exchange reactions. While 2,3-$\mathbf{C_5}$ is readily formed (44% from 1,2-$\mathbf{C_5}$ under acidic conditions and 60% from 3,4-$\mathbf{C_5}$ under basic conditions), 2,3-$\mathbf{C_4}$ is only formed in 5−6% yield, and 2,3-$\mathbf{C_3}$ is not detected at all.[37] This can be explained by a significant increase in ring strain with the smaller walkers. The net result is that the short "stride length" of these walkers limits their ability to walk down the molecular track. In effect, taking a step to the middle footholds becomes a rare event, and it requires many acid−base oscillations for a

Giardini, A.; Lesma, G.; Passarella, D.; Peretto, B.; Sacchetti, A.; Silvani, A.; Pratesi, G.; Zunino, F. *J. Org. Chem.* **2006**, *71*, 2848–2853.

(31) The structure of 2,3-$\mathbf{C_5}$ was confirmed by two-dimensional ^{1}H NMR spectroscopy (ROESY, COSY).[6] Further characterization involved high-resolution mass spectrometry, HPLC, and LCMS (see the Supporting Information).

(32) 2,3-$\mathbf{C_5}$ was isolated by preparative HPLC.[6]

(33) Disulfide exchange in organic solvents can require long periods of time to reach equilibrium. See refs 30c and 30f, where 20−120 days appear to be necessary.

(34) The placeholder disulfide is necessary to prevent oligomerization through disulfide bridges.

(35) Noji, H.; Yasuda, R.; Yoshida, M.; Kinosita, K. *Nature* **1997**, *386*, 299–302.

(36) The equilibria for the $\mathbf{C_2}$ system were not studied in detail as initial studies showed that the walker unit is too short to bridge the internal footholds to any significant degree.

(37) The HPLC detection limit is <1%.

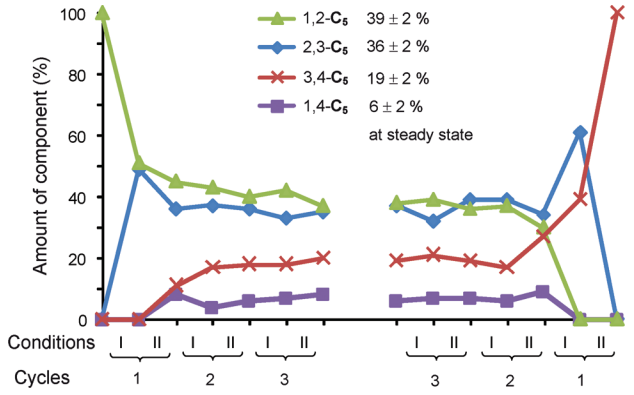

Figure 2. Product distribution during three cycles of directionally nonbiased, acid−base operation starting from pristine 1,2-$\mathbf{C_5}$ (left-hand side) and from pristine 3,4-$\mathbf{C_5}$ (right-hand side). Under each set of conditions (I and II), two different pairs of positional isomers are in equilibrium (see Scheme 2). Values are based on HPLC integration and are corrected for the absorbance coefficients at 290 nm (see the Supporting Information).

significant amount of these walkers to traverse the central footholds and thus move from one end of the track to the other.

(ii) The variation in spacer length of the walker unit has a marginal effect on the amount of 1,4-isomer formed (9−25%). In this positional isomer, the track forms a relatively large macrocycle with the walker. Making this large macrocycle smaller or larger by one atom has a negligible effect on ring strain and the relative free energy of the compound.

(iii) The equilibria between each "terminal" isomer (1,2 and 3,4) and the "internal" 2,3 isomer do not consistently favor or disfavor the formation of the internal macrocycle (for example, with the $\mathbf{C_5}$ walker the 1,2-isomer is preferred over the 2,3-isomer, 1,2-$\mathbf{C_5}$:2,3-$\mathbf{C_5}$ (56:44), whereas the internal macrocycle is more thermodynamically stable than the 3,4-terminal isomer, 2,3-$\mathbf{C_5}$:3,4-$\mathbf{C_5}$ (60:40)).

For the $\mathbf{C_5}$ system, where all isomers were accessible in appreciable amounts (see Scheme 2), and where both the 1,2 and the 3,4 isomers were independently synthesized (Scheme 1), experiments that sequentially cycled between conditions I and II were conducted. Figure 2 (left-hand-side) shows how, starting from pristine 1,2-$\mathbf{C_5}$, switching between conditions I and II over several cycles leads to convergence of the positional isomer distribution to a ratio of 1,2-$\mathbf{C_5}$:2,3-$\mathbf{C_5}$:3,4-$\mathbf{C_5}$:1,4-$\mathbf{C_5}$ 39:36:19:6 (±2). A very similar distribution of positional isomers was obtained starting from pristine 3,4-$\mathbf{C_5}$ and carrying out the operation sequence over three cycles (Figure 2; right-hand side). Thus, irrespective of which end of the track the walker starts from, the effect of the "walking" operations is to reach the same steady-state positional distribution of the walker units on the track.

The behavior of the system raises the question if the observed steady-state distribution is minimizing free energy (in other words, if it corresponds to the lowest energy distribution for the walkers on the tracks). The answer to this question is not trivial, because under any one particular set of reaction conditions each of the four isomers can only exchange with the one positional isomer that it is "paired" with. The system can thus only move toward the thermodynamic minimum in a stepwise manner by switching back and forth between the different sets of conditions several times. Furthermore, in principle at least, the minimum energy distribution could be different under different sets of conditions (i.e., conditions I and II).

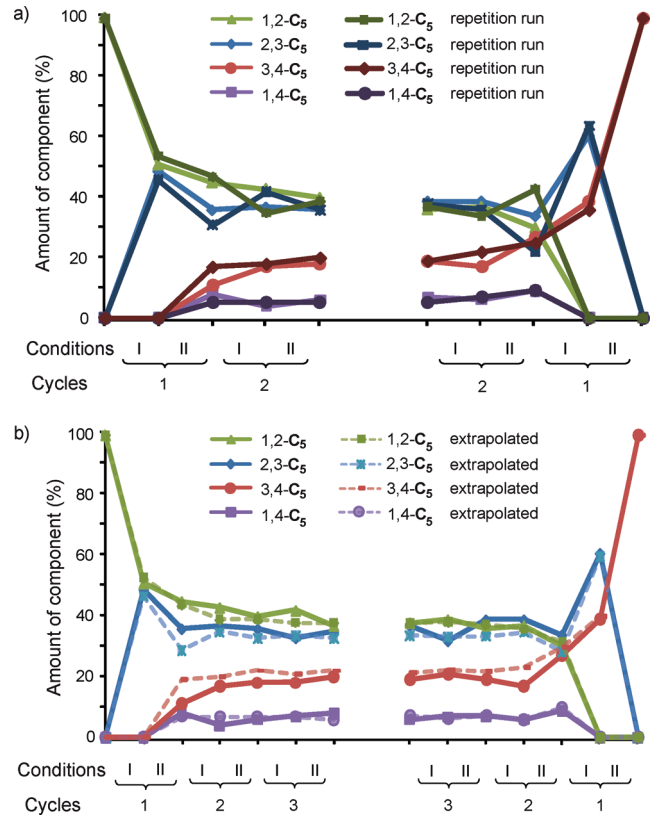

Figure 3. (a) Demonstration of the reproducibility of the experimental results from the operation of the $\mathbf{C_5}$ walker−track system and its "self-correcting" behavior. Product distribution during two cycles of directionally nonbiased, acid−base operation starting from pristine 1,2-$\mathbf{C_5}$ (left-hand side) and from pristine 3,4-$\mathbf{C_5}$ (right-hand side). The originally obtained data (lighter shade, identical to Figure 2) superimposed with data from a repetition run (darker shade). (b) Predictability of system evolution based on the equilibrium ratio of each pair of positional isomers. Product distribution during three cycles of directionally nonbiased, acid−base operation starting from pristine 1,2-$\mathbf{C_5}$ (left-hand side) and from pristine 3,4-$\mathbf{C_5}$ (right-hand side). Solid lines, first experimental series (identical to Figure 2); dashed lines, calculated data, based on extrapolation of the experimental ratios between each pair of positional isomers (see Scheme 2).

There is, however, compelling evidence that the steady-state distribution shown in Figure 2 does indeed correspond to the minimum energy of the system under both acidic and basic conditions:

(i) Once the system has reached the steady state (Figure 2), further oscillation of the conditions no longer changes (within experimental error) the composition of the mixture. In a situation where the relative energies of the positional isomers are different under conditions I and II, one would expect a graph that oscillates between two different steady states. This is not the case in Figure 2.

(ii) During the walking operations, the system moves to correct errors caused by imperfect experiments. Figure 3a shows a superimposition of the data from the original experimental data (from Figure 2) with data acquired during a repetition of the experimental sequence. Even though the isomer ratios differ slightly during some stages of the two experimental sequences (through normal variations and errors in the execution of the experiments; some reactions might not have gone to completion, sometimes the analysis might have errors, etc.), the final composition of positional isomers is the same in both experiments. The self-correcting nature of the system is an indication that the composition of the mixture always moves toward the minimum energy distribution.

Table 1. Steady-State Positional Isomer Distributions, Based on Experimentally Determined Multiple Cycles for C_5 and on Data Extrapolated from the Equilibrium between Each Pair of Positional Isomers for C_3, C_4, and C_8[a]

	C_3	C_4	C_5	C_8
1,2	52%	41%	39%	26%
2,3	<1%	3%	36%	22%
3,4	43%	48%	19%	45%
1,4	5%	8%	6%	7%
approx. number of cycles to converge	15	8	2	2

[a] See section 6 of the Supporting Information for graphs showing the evolution of the system (similar to the type of graphs used in Figures 2 and 3).

(iii) Figure 3b shows a superimposition of the original experimental data (solid lines) with theoretically calculated data (dashed lines) based on the extrapolation of the four experimentally determined equilibrium ratios between the individual pairs of positional isomers (see Scheme 2). Again, differences occur in the early cycles,[38] but the final composition of the mixture can be accurately predicted using only the four pairs of equilibrium ratios shown in Scheme 2. This demonstrates that the four equilibrium ratios between the pairs of positional isomers constitute a consistent set of relative energies that corresponds to the steady-state distribution.[39]

Having established that the composition of the system is determined only by the equilibrium between the four pairs of positional isomers and the number of cycles performed, analogous extrapolation calculations were performed for the C_3, C_4, and C_8 systems.[40] The resulting steady-state compositions are shown in Table 1 (see the Supporting Information for the extrapolation graphs). The minimum energy distributions of the walker units on the track are significant because they correspond to the distribution that a directionally biased walker must be transported away from.

Figure 4 shows a plot of the relative free energies of the positional isomers generated from the experimentally determined positional isomer ratios shown in Scheme 2. These relative energies only refer to the particular experimental conditions used in Scheme 2, but, nevertheless, provide a qualitative basis for understanding the observed isomer ratios and a rationale for the behavior of the different length walker units under operating conditions that could bias the directionality of walker migration (vide infra).

From Nondirectional Walker Migration to Directional Walker Transport (Hydrazone Exchange under Thermodynamic Control; Disulfide Exchange under Kinetic Control). Starting with the walker unit at one end of the track (e.g., pristine 3,4-C_n), cycling between conditions I and II results in some walkers moving from one end of the track to the other (Figure 2). However, this is a consequence of the initial distribution of walker−track conjugates being away from the minimum energy distribution and the system, driven by a gain in entropy, relaxing toward it. Because the steady states correspond to this minimum energy distribution, the walking sequence is not intrinsically directional (by this we mean that in the internal region of a polymeric track made of alternating benzaldehyde−benzylic disulfide footholds, the walker would move, over several acid−base oscillations, in each direction with equal probability). This may appear counterintuitive in light of the nonsymmetric steady-state distributions (the amount of the 1,2 isomer is not equal to the amount of 3,4) found in systems C_3, C_4, C_5, and C_8 (Table 1). The inequality of the 1,2 and the 3,4 isomers is, however, due to substituent effects, which make the two "terminal" footholds electronically and sterically different from their internal counterparts.

To understand the requirements for directional motion, we can consider a polymeric track based on the current track (Figure 5). Here, there are only two fundamentally different types of macrocycles formed between the walker and the track, one in which the track ether linkage is internal to the macrocycle (shown as "ether-macrocycle" in Figure 5) and one in which the track triazole unit is internal to the macrocycle (shown as "triazole-macrocycle" in Figure 5). Each operation i or ii thermodynamically equilibrates this pair of macrocycles about the pivot (kinetically locked) foot. If the two macrocycles have identical relative thermodynamic stabilities under conditions i and ii, any bias toward one end of the track under condition i will be offset by the opposite directional bias under condition ii ($K_i = K_{ii}$). Net-directionality in the walking can thus only occur when the forward/backward ratio under condition i is different from the backward/forward ratio under condition ii

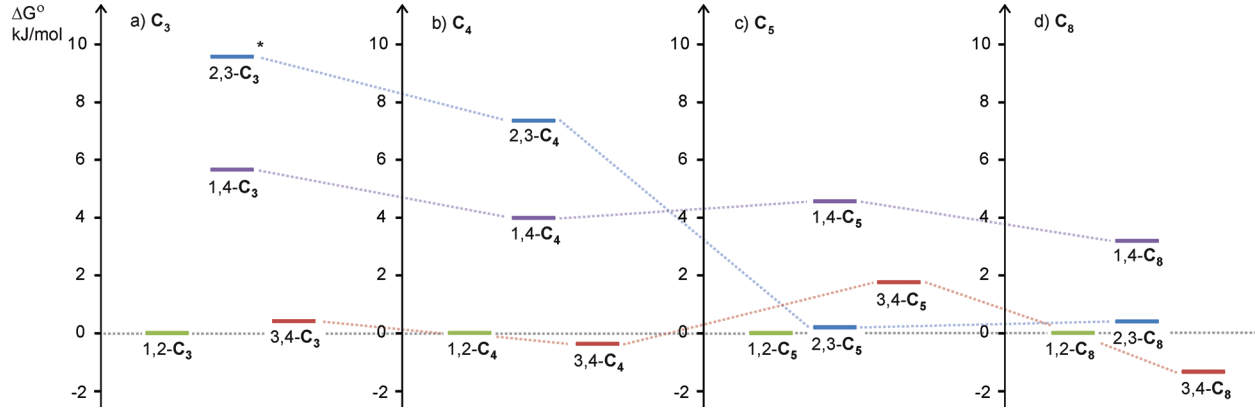

Figure 4. Relative free energies of the four positional isomers of each walker−track conjugate C_n (n = 3, 4, 5, 8) determined by the experimental equilibrium ratios between each pair of positional isomers (Scheme 2). The relative energies only apply to the specific reaction conditions (I and II) of the reversible exchange processes ($CHCl_3$, 0.1 mM, room temperature) and should only be considered a qualitative aid for the understanding of ring strain effects within the different compound series. The energies are assumed to be similar in acidic and basic conditions because the product distributions converge to a steady state in Figures 2 and 3 (and section 6 in the Supporting Information) rather than oscillate (which would be the behavior expected if the relative energies change in acid and base). The energy of the 1,2 isomer was set at 0.0 kJ mol^{-1} for each compound series. Dotted lines connect isomers at the same track position. (a) C_3, (b) C_4, (c) C_5, (d) C_8. *The relative free energy shown for 2,3-C_3 is a lower limit value, based on the detection limit of the analytical method (see Scheme 2 caption).

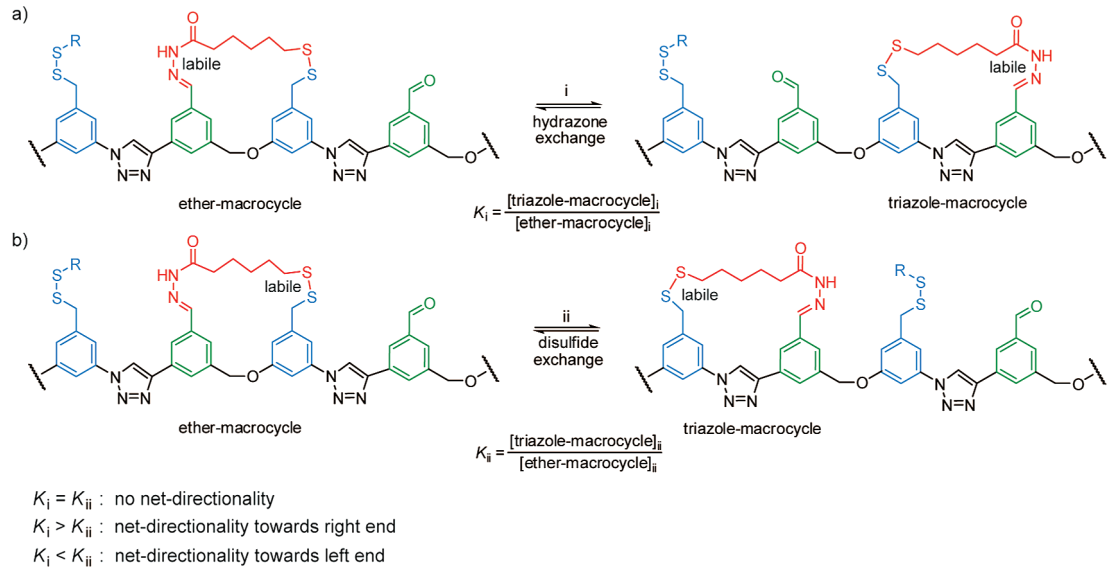

Figure 5. Requirements for directional walker migration along a hypothetical polymeric track based on the $\mathbf{C_5}$ walker−track system. (a) Under conditions i (hydrazone exchange), the walker can pivot at the disulfide foothold and form two different kinds of macrocycles, one incorporating the flexible ether linker (ether-macrocycle) and one incorporating the more rigid triazole linker (triazole-macrocycle). (b) Under conditions ii (disulfide exchange), the walker can pivot about the hydrazone foothold, and the walker can form the same two types of macrocycle with the track. For net-directionality of walker transport, K_i and K_{ii} must have different values.

Scheme 3. Kinetically Controlled Redox Operation for Disulfide Exchange, Illustrated for 2,3-$\mathbf{C}_n$[a]

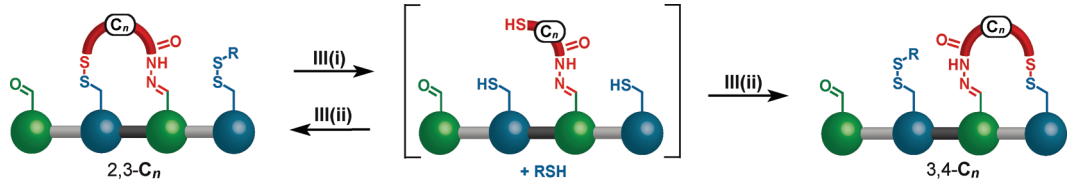

[a] Condition III (i) (reduction of disulfide bonds): 1.0 mM, DTT (6 equiv), DBU (3 equiv), $CDCl_3$, reflux, 2−12 h (progress monitored by ^1H NMR). Condition III (ii) (irreversible, oxidative disulfide bond regeneration): 0.1 mM, Et_3N (excess), methyl 3-mercaptopropionate (RSH, 8 equiv), I_2 (ca. 12 equiv), $CDCl_3$/cosolvent, room temperature, 5 min.

($K_i > K_{ii}$ or $K_i < K_{ii}$). If both processes are under thermodynamic control, this will only be the case if the two macrocycles happen to have different relative thermodynamic stabilities under conditions i and ii. We have demonstrated that this is not the case for our walker−track systems using our standard acidic and basic conditions. As a result, net-directional transport cannot be achieved with such systems using only reversible reactions that proceed under thermodynamic control.[41]

One way to overcome this issue is to carry out one of the two exchange processes under kinetic control (Scheme 3). In such a situation, the ratio of positional isomers formed depends on their relative rates of formation, which can differ from their relative thermodynamic stabilities. Under conditions III(i) (1 mM, DTT (6 equiv), DBU (3 equiv), $CDCl_3$, reflux, 2−12 h), the disulfide bonds in 2,3-$\mathbf{C}_n$ can be quantitatively reduced, resulting in a ring-opened intermediate (shown in square brackets in Scheme 3). Rapid oxidation (conditions III(ii), 0.1 mM, Et_3N (excess), $MeO_2CCH_2CH_2SH$ (8 equiv), I_2 (ca.12 equiv), $CDCl_3$/cosolvent, room temperature, 5 min) subsequently regenerates the walker−track disulfide linkages under kinetic control with a different positional isomer ratio to the reversible (thermodynamically controlled) reaction.

The oxidation step for the various walker−track trithiols proceeded efficiently in a variety of solvent systems, and, remarkably, the use of a cosolvent ($CHCl_3$ was kept constant in the 1:1 solvent mixtures) could have a very significant effect on the positional isomer ratio that resulted (Table 2).[42] For example, the oxidation of the $\mathbf{C_5}$ trithiol leads to a 2,3:3,4 ratio of 70:30 in $CHCl_3$:*t*-BuOH (1:1) but a 32:68 ratio; that is, the terminal macrocycle is preferred, in $CHCl_3$:MeOH (1:1). Even highly strained positional isomers (Figure 4) can be accessed using this procedure: although isomer 2,3-$\mathbf{C_3}$ is not detectable in the reaction mixture when 3,4-$\mathbf{C_3}$ is subjected to basic conditions under thermodynamic control (Table 1), the redox reaction under kinetic reaction control using cyclohexane as

(38) These differences are probably a result of insufficient equilibration times (i.e., equilibrium was not reached when the reaction was quenched).

(39) We were also able to simulate "out-of-equilibrium" situations by randomly changing one or more of the four equilibrium ratios that serve as input variables in the spreadsheet program. Thereafter, the ratios do not form a consistent set, and, as a result, the graph does not converge toward a constant composition and instead oscillates indefinitely between two states.

(40) The significant ring strain present in the 2,3 and 1,4 isomers of the $\mathbf{C_3}$ and $\mathbf{C_4}$ systems would make a very lengthy experimental procedure necessary until convergence to the steady states (~15 cycles for $\mathbf{C_3}$ and ~8 cycles for $\mathbf{C_4}$, Table 1).

(41) Directional walking can be achieved solely using reactions that are carried out under thermodynamic control by coupling the stepping processes to energy consumption. For example, in some of the artificial DNA walker systems (refs 16g−i), the "walking" events are reversible, and directionality is achieved by ratchet mechanisms that couple the "walking" equilibria to the consumption of a chemical "fuel".

(42) Other oxidants (e.g., Br_2 and $K_3[Fe(CN)_6]$) were investigated but did not prove superior to I_2 in terms of positional isomer ratios or chemoselectivity.

Table 2. Effect of Cosolvent (1:1 with $CHCl_3$) on the Observed 2,3-$\mathbf{C}_n$:3,4-$\mathbf{C}_n$ Isomer Ratio after Irreversible Oxidation of Trithiol (Compound in Brackets, Scheme 3)[a]

cosolvent	2,3-$\mathbf{C_3}$:3,4-$\mathbf{C_3}$	2,3-$\mathbf{C_4}$:3,4-$\mathbf{C_4}$	2,3-$\mathbf{C_5}$:3,4-$\mathbf{C_5}$
n-hexane	45:55	66:34	65:35
cyclohexane	**47:53**	**65:35**	68:32
Et_2O	40:60	61:39	61:39
MeCN	31:69	49:51	54:46
THF	36:64	58:42	56:44
DMF	20:80	55:45	66:34
MeOH	25:75	36:64	**32:68**
EtOH	35:65	48:52	47:53
i-PrOH	39:61	59:41	54:46
t-BuOH	43:57	62:38	70:30

[a] Pure samples of 3,4-$\mathbf{C}_n$ were submitted to conditions III(i) and III(ii) (see Experimental Section for details). Values are based on HPLC integration and are corrected for the absorbance coefficients at 290 nm (see the Supporting Information).

Table 3. Positional Isomer Distribution during 1.5 Cycles of Biased Operation of $\mathbf{C_5}$ System and Comparison to the Experimentally Observed Minimum Energy Steady-State Distribution a

cycles/conditions	0	0.5/I	1/III	1.5/I	steady-state from conditions I and II (*Table 1*)
1,2-$\mathbf{C_5}$	100%	52%	28%	24%	39%
2,3-$\mathbf{C_5}$	0%	48%	20%	24%	36%
3,4-$\mathbf{C_5}$	0%	0%	28%	**43%**	**19%**
1,4-$\mathbf{C_5}$	0%	0%	24%	9%	6%

[a] See Experimental Section for details on conditions I and III (cosolvent: MeOH). Values are based on HPLC integration and are corrected for the molar absorptivities at 290 nm (see the Supporting Information).

cosolvent affords a 2,3:3,4 ratio of 47:53! Such observations indicated the possibility of obtaining significant directional bias in walker migration by using the irreversible conditions III with an appropriate cosolvent. For the selection of the cosolvent, it is important to consider that the goal of these experiments is to drive the system away from the minimum energy distribution of walkers on the tracks (Table 1). The most promising entries in this respect are cyclohexane for the $\mathbf{C_3}$ and $\mathbf{C_4}$ systems and methanol for the $\mathbf{C_5}$ system (ratios highlighted in Table 2).

Directional Bias of the $\mathbf{C_5}$ System. The effect of introducing the redox conditions III (cosolvent: MeOH) into the walking sequence of the $\mathbf{C_5}$ system is shown in Table 3. In only 1.5 cycles, starting from 100% 1,2-$\mathbf{C_5}$, the walker moves along the track to give 43% 3,4-$\mathbf{C_5}$, as compared to the 19% of 3,4-$\mathbf{C_5}$ present at the steady state using the two sets of reversible conditions (Figure 2 and Table 1). However, further cycles would not increase this directional bias, because each time the reversible conditions I were applied the composition of the mixture would move back toward the minimum energy distribution. When analyzing the origin of the bias toward the right end of the track, it becomes clear that the 1,4-$\mathbf{C_5}$ isomer makes a significant contribution. For example, after cycle 1 (redox step), an unusually high amount of 1,4-$\mathbf{C_5}$ (24%) is present, which in the subsequent step is largely converted to 3,4-$\mathbf{C_5}$.

Directional Bias of the $\mathbf{C_4}$ System. Table 4 shows the effect of introducing the redox conditions III (cosolvent: cyclohexane) into the walking sequence of the $\mathbf{C_4}$ system. Starting from 100% 3,4-$\mathbf{C_4}$, in two cycles the walker moves along the track to give 62% 1,2-$\mathbf{C_4}$, as compared to the 41% present at the steady state using the two sets of reversible conditions (Table 1). It is remarkable to note that using the same reaction sequence (and same track) the $\mathbf{C_5}$ and $\mathbf{C_4}$walkers are transported with biases

Table 4. Positional Isomer Distribution during Two Cycles of Acid−Redox Operation of the $\mathbf{C_4}$ System and Comparison to the Extrapolated Minimum Energy Steady-State Distribution[a]

cycles/conditions	0	0.5/III	1/I	1.5/III	2/I	steady state[b] from conditions I and II
1,2-$\mathbf{C_4}$	0%	0%	58%	46%	**62%**	**41%**
2,3-$\mathbf{C_4}$	0%	63%	4%	25%	5%	3%
3,4-$\mathbf{C_4}$	100%	37%	26%	12%	25%	48%
1,4-$\mathbf{C_4}$	0%	0%	12%	17%	8%	8%

[a] See Experimental Section for details on conditions I and III (cosolvent: cyclohexane). Values are based on HPLC integration and are corrected for the molar absorptivities at 290 nm (see the Supporting Information). [b] Extrapolated from the experimentally determined equilibrium ratio of each pair of positional isomers (Table 1).

Table 5. Positional Isomer Distribution during Two Cycles of Acid−Redox Operation of the $\mathbf{C_3}$ System and Comparison to the Extrapolated Minimum Energy Steady-State Distribution[a]

cycles/conditions	0	0.5/III	1/I	1.5/III	2/I	steady state[b] from conditions I and II
1,2-$\mathbf{C_3}$	0%	0%	41%	38%	**53%**	**52%**
2,3-$\mathbf{C_3}$	0%	44%	~1%	13%	<1%	<1%
3,4-$\mathbf{C_3}$	100%	56%	43%	26%	38%	43%
1,4-$\mathbf{C_3}$	0%	0%	15%	23%	9%	5%

[a] See Experimental Section for details on conditions I and III (cosolvent: cyclohexane). Values are based on HPLC integration and are corrected for the molar absorptivities at 290 nm (see the Supporting Information). [b] Extrapolated from the experimentally determined equilibrium ratio of each pair of positional isomers (Table 1).

to the opposite ends of the track! The oscillating behavior of the composition of the $\mathbf{C_4}$ system under these operating conditions is evident: for example, the amount of 1,2-$\mathbf{C_4}$ present goes from 0%→58%→46%→62%. In this system, the 1,4-$\mathbf{C_4}$ isomer does not contribute to the directional bias. In fact, the high amount of 1,4-$\mathbf{C_4}$ isomer formed during step 3 (cycle 1.5) counteracts the bias toward the left end of the track.

Directional Bias of the $\mathbf{C_2}$, $\mathbf{C_3}$, and $\mathbf{C_8}$ Systems. The relative energies of the various positional isomers in the $\mathbf{C_8}$ system (see Figure 4) suggest that the acid−base and acid−redox operation should give rather similar steady-state values (neither 2,3-$\mathbf{C_8}$ nor 1,4-$\mathbf{C_8}$ are strained enough to give significant directionality by the mechanisms seen for $\mathbf{C_4}$ or $\mathbf{C_5}$, respectively). In the $\mathbf{C_2}$ system, the macrocycle that would incorporate the triazole unit would be so strained that isomer 2,3-$\mathbf{C_2}$ cannot be accessed, even under kinetic control.

Table 5 shows the results obtained when introducing the redox operation III (cosolvent: cyclohexane) into the walking sequence of the $\mathbf{C_3}$ system. Starting from 100% 3,4-$\mathbf{C_3}$, two operational cycles gave 53% 1,2-$\mathbf{C_3}$, a value similar to the 52% present at the steady state for acid−base operations. The lack of directional bias with this walker length is partially due to the lower amount of 2,3-$\mathbf{C_3}$ that can be formed (as compared to the $\mathbf{C_4}$ system), but is mostly a result of the right-end bias contributed by the 1,4-$\mathbf{C_3}$ isomer counterbalancing the left-end bias promoted by the 2,3-$\mathbf{C_3}$ isomer.

The results obtained for the $\mathbf{C_2}$ and $\mathbf{C_3}$ systems indicate that there is a threshold at which ring strain gets too high to allow for the optimum degree of directional bias ($\mathbf{C_3}$), or even for any walker migration to occur via the 2,3 isomer ($\mathbf{C_2}$). However, in case of the $\mathbf{C_3}$ system, it is not only the reduced availability of the 2,3-$\mathbf{C_3}$ isomer under kinetic control (47% formed from 3,4-$\mathbf{C_3}$ as compared to 65% for the 2,3-isomer using the $\mathbf{C_4}$ walker; Table 2) that reduces bias toward the left-end of the

Scheme 4. Crossover Study on the Processivity of the $\mathbf{C_5}$ System[a]

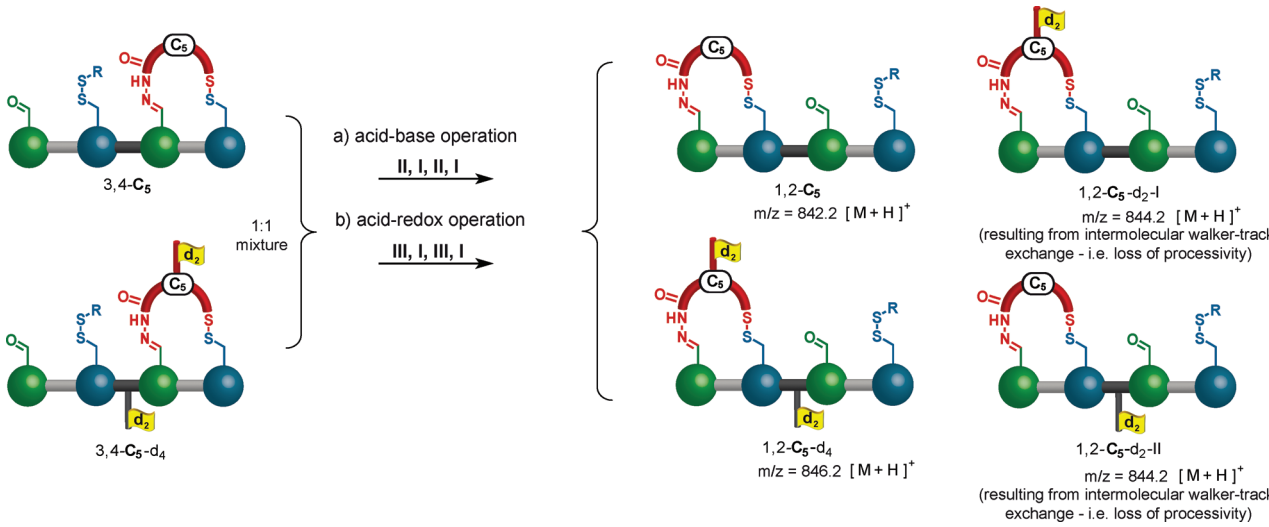

[a] Condition I (reversible hydrazone exchange): 0.1 mM, TFA, $CHCl_3$, room temperature, 6−96 h (monitored by HPLC until the distribution no longer changed). Condition II (reversible disulfide exchange): 0.1 mM, DTT (10 equiv), DBU (40 equiv), dimethyl 3,3′-disulfanediyldipropanoate (20 equiv), $CHCl_3$, room temperature, 12−48 h (monitored by HPLC until the distribution no longer changed). Condition III (i) (reduction of disulfide bonds): 1.0 mM, DTT (6 equiv), DBU (3 equiv), $CDCl_3$, reflux, 2−12 h (progress monitored by ^{1}H NMR). Condition III (ii) (irreversible, oxidative disulfide bond regeneration): 0.1 mM, Et_3N (excess), methyl 3-mercaptopropionate (RSH, 8 equiv), I_2 (ca. 12 equiv), $CDCl_3$/MeOH, room temperature, 5 min.

track, but also the fact that the 1,4-$\mathbf{C_3}$ isomer favors transport in the opposite direction. The small energy differences between the various positional isomers of the $\mathbf{C_8}$ system (Figure 4) suggest that there is also an upper limit to the walker length after which ring strain becomes too low to bias directionality effectively. Interestingly, ring strain has been identified as a key feature thought to generate the directional bias in kinesin[43] and myosin-V.[44]

Determining the Processivity of Walking in the $\mathbf{C_5}$ Walker−Track System. The processivity of the acid−base and acid−redox walking experiments of the $\mathbf{C_5}$ system was determined by double-labeling crossover experiments (see the Supporting Information for details). The double-labeled walker−track conjugate 3,4-$\mathbf{C_5}$-d_4 (Scheme 1c) was mixed with an unlabeled sample of 3,4-$\mathbf{C_5}$ in a 1:1 ratio (Scheme 4). This mixture was subjected to either the acid−base walking cycle conditions (Scheme 4a) or the acid−redox walking cycle conditions (Scheme 4b). The product distribution of both experiments was analyzed by HPLC−MS (high performance liquid chromatography−mass spectrometry).[45]

The results of these two experiments are shown in Figure 6. The blue bars represent the experimentally obtained isotopic distribution of the sample before operation, while the green bars represent the theoretical isotopic distribution that would be expected if full statistical scrambling (intermolecular exchange of the walker molecules with the tracks) had occurred. The red bars show the experimentally obtained isotopic distribution after operation (Figure 6a for two acid−base cycles; Figure 6b for two acid−redox cycles).

The arrows indicate the *m*/*z* value of single-labeled species, which are indicators of a loss of processivity during the migration of the walker along the track (Scheme 4). The difference between the nondirectionally biased (acid−base) and directionally biased (acid−redox) operations is evident, with the former exhibiting a significantly higher level of processivity after four operational steps. Mathematical analysis (see the Supporting Information) gives a mean step number[46] of 37 for acid−base operation, whereas using acid−redox cycles the

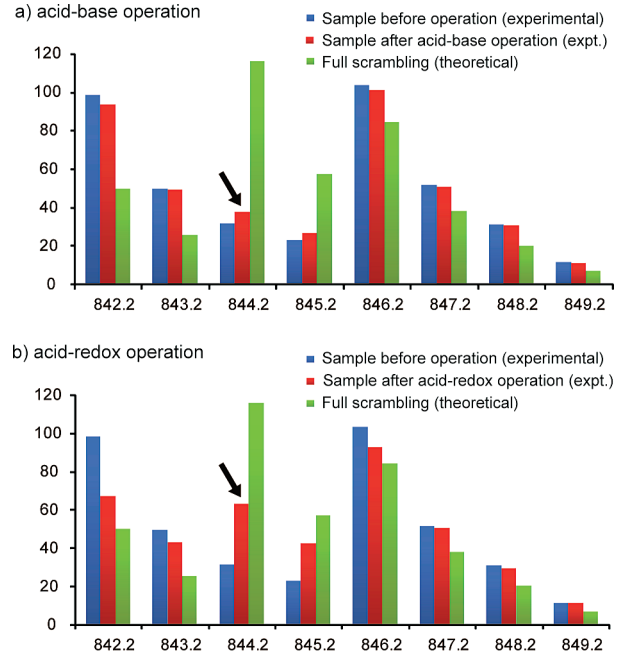

Figure 6. Results of the crossover study on the processivity of the $\mathbf{C_5}$ system: (a) acid−base operation over two cycles; (b) acid−redox operation over two cycles (see Scheme 4). Shown are the (normalized) isotopic distributions of the 1:1 mixture before operation (blue; experimental), after operation (red; experimental), and the distribution that would be expected when full statistical scrambling occurred (green; theoretical). The distribution (red bars and blue bars) of experimental data points is the average of 10 runs for each experiment. This procedure demonstrated the reproducibility of the mass spectrometry data and enabled the isotope scrambling to be analyzed for statistical significance (see the Supporting Information).

(43) (a) Hyeon, C.; Onuchic, J. N. *Proc. Natl. Acad. Sci. U.S.A.* **2007**, *104*, 2175–2180. (b) Yildiz, A.; Tomishige, M.; Gennerich, A.; Vale, R. D. *Cell* **2008**, *134*, 1030–1041. (c) Cochran, J. C.; Kull, F. J. *Cell* **2008**, *134*, 918–919.

(44) (a) Veigel, C.; Schmitz, S.; Wang, F.; Sellers, J. R. *Nat. Cell Biol.* **2005**, *7*, 861–869. (b) Trybus, K. M. *Nat. Cell Biol.* **2005**, *7*, 854–856.

(45) The product mixtures were not purified by HPLC. All oligomers and other side-products were retained in the sample.

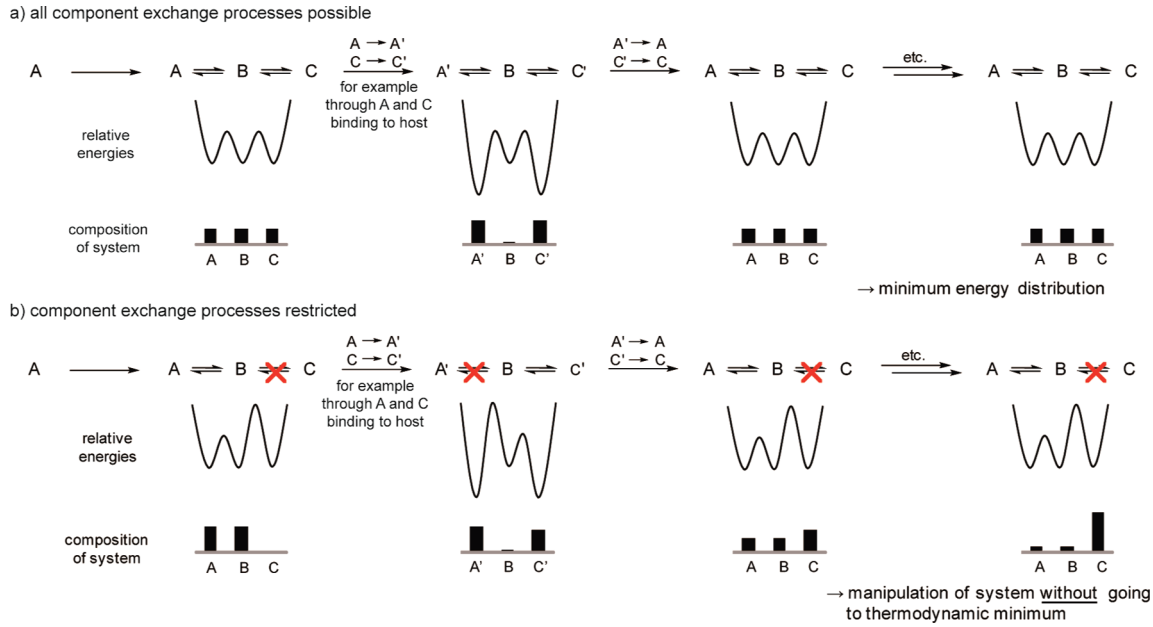

Figure 7. Ratchet mechanisms and systems chemistry: the potential utility of restricted component exchange processes. (a) Chemical system of three components (A, B, and C) at equilibrium. Repeated manipulation (through host binding event (A→A′, C→C′)) does not lead away from thermodynamic minimum. (b) Chemical system of three components (A, B, and C) with restricted component exchange processes (an energy ratchet mechanism). Repeated manipulation shifts the composition away from thermodynamic minimum.

walker takes an average of seven steps before detaching. In comparison, wild-type kinesins have a mean step number of 75−175 with an average run length of ∼1 μm.[12]

The loss of processivity during the reactions under thermodynamic control (acid and base catalyzed cycles) is most likely a result of the formation of oligomers in which a walker moiety bridges two tracks and, after the following operational step (which breaks one of the walker−track bonds), is no longer located on its original track (see the Supporting Information, Scheme S4b). Loss of processivity via complete detachment of the walker moiety can be excluded for two reasons: (i) Starting from one pristine isomer, only mixtures of two isomers, never all four, are ever observed (Scheme 2; see, for example, the first half-cycle in Figure 2); and (ii) under any of the operating conditions, we never detected[47] a detached walker moiety, bare track, or track with two walker moieties.

The higher loss of processivity during the kinetically controlled step probably results from the formation of intramolecular disulfide bonds between the sulfur groups on the track, the sulfur group of the walker forming a disulfide with the placeholder group, which causes the walker to detach from the track during the subsequent acidic step. Indeed, HPLC analysis of the redox step showed the appearance of oligomers and two monomeric side products that do not occur during the thermodynamically controlled disulfide exchange (see the Supporting Information, Scheme S4c).

Relating Molecular Walkers to Systems Chemistry. Motors and machines at the molecular level operate by chemical laws and statistical mechanisms, not the Newtonian laws for momentum and inertia that determine the mechanisms of mechanical machines in the macroscopic world.[2,13a] The manipulation of the statistical distribution of the molecular walkers presented in this Article can be seen as a new facet of synthetic systems chemistry.[48] In most of the mixtures studied to date from the point of view of systems chemistry,[49] each molecular component is in equilibrium with all the other components. In the walker systems presented here, however, only subsets of the four positional isomers (1,2-$\mathbf{C}_n$, 2,3-$\mathbf{C}_n$, 3,4-$\mathbf{C}_n$, and 1,4-$\mathbf{C}_n$) can exchange with each other under any given set of conditions. This restriction of the component exchange processes is a fundamental property that can be exploited in a mechanism (a ratchet mechanism[2]) to drive the system away from the thermodynamic minimum energy distribution of the components.

Such behavior is illustrated in Figure 7 for a system of three components A, B, and C in which both the relative depths of the energy minima can be varied (e.g., A and C can bind to a host molecule, decreasing their relative free energy (A→A′ and C→C′ in Figure 7) and, in Figure 7b only, the relative heights of the energy maxima can be varied (e.g., if A exchanges only with B under conditions in which B does not exchange with C).

If all three components are in equilibrium (Figure 7a), the addition of the host leads to a new distribution (with A′ and C′ being the major components) corresponding to the new thermodynamic minimum of the system; that is, the composition of the system is a function of the relative free energies of the three components. Removal of the host molecule leads back to the original distribution. Such a manipulation, even when repeated, cannot result in an out-of-equilibrium state of the system.

(46) The mean step number describes the number of operational steps after which one-half of the molecules have lost processivity (i.e., have detached or exchanged with others in the bulk).
(47) No peaks with these *m/z* values were detected by HPLC−MS.

(48) (a) Ludlow, R. F.; Otto, S. *Chem. Soc. Rev.* **2008**, *37*, 101–108. (b) Nitschke, J. R. *Nature* **2009**, *462*, 736–738.
(49) For examples, see: (a) Grote, Z.; Scopelliti, R.; Severin, K. *Angew. Chem., Int. Ed.* **2003**, *42*, 3821–3825. (b) Buryak, A.; Severin, K. *Angew. Chem., Int. Ed.* **2005**, *44*, 7935–7938. (c) Chung, M.-K.; Hebling, C.; Jorgenson, J.; Severin, K.; Lee, S. J.; Gagné, M. R. *J. Am. Chem. Soc.* **2008**, *130*, 11819–11827. (d) Ludlow, R. F.; Otto, S. *J. Am. Chem. Soc.* **2008**, *130*, 12218–12219. (e) Sarma, R. J.; Nitschke, J. R. *Angew. Chem., Int. Ed.* **2008**, *47*, 377–380. (f) Ludlow, R. F.; Otto, S. *J. Am. Chem. Soc.* **2010**, *132*, 5984–5986. (g) Mal, P.; Nitschke, J. R. *Chem. Commun.* **2010**, *46*, 2417–2419. (h) Campbell, V. E.; de Hatten, X.; Delsuc, N.; Kauffmann, B.; Huc, I.; Nitschke, J. R. *Nat. Chem.* **2010**, *2*, 684.

If only one of the two exchange processes is possible under any one set of conditions, however, the composition of the system can be moved away from the thermodynamic minimum (Figure 7b). Repetitive addition and removal of the host, while switching between the pairs of components that are able to exchange, leads to a composition that is far away from the thermodynamic minimum (right-hand side of Figure 7b). Such a concerted manipulation of the thermodynamics and kinetics of a system corresponds to a flashing energy ratchet mechanism.[2,3e,13a] The mutually exclusive conditions available for hydrazone and thiol/disulfide exchange[24b−d] represent an appealing opportunity for the manipulation of out-of-equilibrium chemical systems, as well as ratcheted machine mechanisms,[2,13a] through such concepts.

Conclusions

We have described five small-molecule systems in which a molecular walker with chemical "legs" of varying length moves up and down a four-foothold track primarily through a passing-leg gait mechanism. Repetitive switching of fully reversible walking operations does not lead to intrinsically directional migration of the walker units, but to a minimum energy distribution of walkers on the tracks. Directionality of the walking sequence can, however, be achieved for two of the five systems studied by replacing one of the reversible reactions with a kinetically controlled redox operation, the outcome of which can be significantly manipulated by addition of a cosolvent. The length of the spacer unit between the walker feet is crucial for generating ring strain with the track necessary for maximizing directional bias. A crossover isotopic labeling study shows that directionality gained by introducing the kinetically controlled redox step comes at the price of reduced processivity (mean step number 7, as compared to 37 under acid−base conditions). Although they are extremely rudimentary systems, the $\mathbf{C_4}$ and $\mathbf{C_5}$ walker−track conjugates exhibit four of the essential characteristics of linear molecular motor dynamics: processive, directional, repetitive, and progressive migration of a molecular unit up and down a molecular track. Improvements to these first generation designs are required to address problems associated with folding (which generates the "double step" 1,4-isomer), reaction time scales (currently several hours for each operation), oligomer formation (which results in reduced processivity), chemoselectivity, and improved (ratchet) mechanisms[50] for directional bias. Such systems, as well as extended tracks and walkers that can capture and release cargoes, are currently under investigation in our laboratory.

Experimental Section

General Procedure for Acid-Catalyzed Hydrazone Exchange (I). To a 0.1 mM solution of 1,2-$\mathbf{C}_n$ (typically 1 mg in ca. 10 mL; 1.0 equiv) in $CHCl_3$ (HPLC grade) was added 5 drops of a solution of 20% v/v TFA (CF_3CO_2H) and 1% v/v H_2O in $CHCl_3$ (HPLC grade). The mixture was stirred at room temperature, and the progress of the equilibration was followed by analytical HPLC (see the Supporting Information). When the relative ratios of the isomers were stable (generally 6−96 h), the mixture was washed with an aqueous solution of $NaHCO_3$. The layers were partitioned, and the aqueous layer was extracted with $CHCl_3$. The combined organic layers were dried over $MgSO_4$. The solvents were removed under reduced pressure, and the amount and constitution of the mixture were determined by weight and, after dissolving in a defined amount of $CHCl_3$, analytical HPLC.

General Procedure for Base-Catalyzed Disulfide Exchange (II). To a 0.1 mM solution of 3,4-$\mathbf{C}_n$ (typically 1 mg in 10 mL; 1.0 equiv) in $CHCl_3$ (HPLC grade) were added DBU (40 equiv), DTT (10 equiv), and dimethyl 3,3′-disulfanediyldipropanoate (20 equiv) from stock solutions. The mixture was stirred at room temperature, and the progress of the equilibration was followed by analytical HPLC. When the relative ratios of the isomers were stable (generally 12−48 h), the excess of DTT was oxidized by dropwise addition of a solution of I_2 in $CHCl_3$ until a slight brown color persisted. An aqueous solution of NH_4Cl and Na_2SO_3 was added, and the mixture was stirred vigorously until decolorization was complete. The layers were partitioned, and the aqueous layer was extracted with $CHCl_3$. The combined organic layers were dried over $MgSO_4$. After workup, the product distribution (free of DTT and DBU) was no longer dynamic, and the solvent could be removed to allow analysis by weight and analytical HPLC (see the Supporting Information).

General Procedure for Redox-Mediated Disulfide Exchange (III). (i) Reduction step: DTT (6 equiv) and DBU (3 equiv) were added from stock solutions to a 1 mM solution of 2,3-$\mathbf{C}_n$ (1 equiv) in $CDCl_3$ or $CHCl_3$. The mixture was heated under reflux until ^1H NMR showed that all disulfide bonds had been reduced (2−12 h).

(ii) Oxidation step: The above solution was diluted to 0.1 mM with a 1:1 mixture of $CHCl_3$ and cosolvent (MeOH for $\mathbf{C_5}$, cyclohexane for $\mathbf{C_3}$ and $\mathbf{C_4}$). Et_3N (5 drops) and methyl 3-mercaptopropionate (8 equiv) were added. At room temperature, a solution of I_2 in $CHCl_3$ was added to the mixture until the brown color persisted. An aqueous solution of NH_4Cl and Na_2SO_3 was added, and the solution was stirred vigorously until decolorization was complete. The layers were partitioned, and the aqueous layer was extracted with $CHCl_3$. The combined organic layers were dried over $MgSO_4$. For the $\mathbf{C_5}$ system, at this stage a broad-window preparative HPLC was carried out (see reference A for details) to remove excess reagents, waste products, and other impurities (the two-step redox sequence produces more byproducts than the acid or base catalyzed procedures). This purification step was omitted for the processivity study ($\mathbf{C_5}$) and for the operation of the $\mathbf{C_3}$ and $\mathbf{C_4}$ systems.

Note: The molar ratios of DBU and DTT used during the base-catalyzed disulfide exchange experiments (40 and 10 equiv, respectively) are higher than those used during the reduction step of the redox disulfide exchange experiments (3 and 6 equiv, respectively) because there is a 10-fold difference in concentration at which the experiments were carried out (0.1 and 1.0 mM, respectively). The DBU:DTT ratio is also reversed (from 4:1 to 1:2) in the two experiments. The rationale behind these changes reflects the different objectives of the two types of exchange experiments: During the base-catalyzed exchange experiment, DTT is added to increase the rate of disulfide exchange for which thiolates are a necessary intermediate; during the redox operation, the excess DTT results in quantitative reduction of the disulfide bonds. The resulting thiols are subsequently rapidly oxidized by iodine to affect a kinetically controlled reaction outcome.

Acknowledgment. We thank the EPSRC National Mass Spectrometry Service Centre (Swansea, UK) for high resolution mass spectrometry. This research was funded through the European Research Council Advanced Grant WalkingMols. D.A.L. is an EPSRC Senior Research Fellow and holds a Royal Society-Wolfson Research Merit Award.

Supporting Information Available: Full experimental procedures for the synthesis of compounds 3,4-$\mathbf{C_2}$, 3,4-$\mathbf{C_3}$, 3,4-$\mathbf{C_4}$, and 3,4-$\mathbf{C_8}$, HPLC traces for $\mathbf{C_3}$ and $\mathbf{C_4}$, detailed information on the processivity study, and extrapolation graphs. This material is available free of charge via the Internet at http://pubs.acs.org.

JA106486B

(50) For a small molecule that can walk in either direction along a track through a light-driven energy ratchet mechanism, see: Barrell, M. J.; Campaña, A. G.; von Delius, M.; Geertsema, E. M.; Leigh, D. A. *Angew. Chem., Int. Ed.* **2010**, *49*. DOI: 10.1002/anie.201004779.

Molecular Devices

DOI: 10.1002/anie.201004779

Light-Driven Transport of a Molecular Walker in Either Direction along a Molecular Track **

*Michael J. Barrell, Araceli G. Campaña, Max von Delius, Edzard M. Geertsema, and David A. Leigh**

Nature uses bipedal motor proteins that "walk" down intracellular tracks to perform essential tasks in a variety of key biological processes.[1] Although the molecular mechanisms through which these fascinating linear motors operate are beginning to be understood,[2] there are still few synthetic mimics that exhibit the most important characteristics of natural motors, namely repetitive, progressive, processive, and directional walker transport along a molecular track. Several walker–track systems based on DNA have been described,[3] and recently our research group reported a small-molecule system,[4] in which the migration of a walker unit along a four-foothold track could be biased in one direction through an information ratchet type of Brownian ratchet mechanism.[5,6]

Herein we report the design, synthesis, and operation of a small-molecule walker–track conjugate, in which the walker can be transported in either direction along a four-foothold molecular track (roughly 1.5 times more likely to take a step in one direction than the other), depending on the sequence of four applied stimuli: acid or base for mutually exclusive "foot" dissociation and UV light or visible light (plus iodine) to induce or release ring strain between the walker and the track.[7] The design (Figure 1) is closely related to the previously reported small-molecule walker–track system, which features a walker with one hydrazone foot (labile in acid; locked in base) and one disulfide foot (labile in base; locked in acid).[4] The crucial difference is that a stilbene unit has been added between the internal aldehyde and the disulfide footholds of the track (Scheme 1). The key to achieving directionality lies in the isomerization of the stilbene moiety, through which significant ring strain can be induced in the positional (constitutional) isomer in which the walker unit bridges the stilbene linkage (Figure 1 and Scheme 2b).[8] $E \rightarrow Z$ isomerization provides a driving force for the walker to "step" onto the central stilbene unit, while subsequent $Z \rightarrow E$ isomerization results in a majority of the walkers being transported away from the stilbene group in a direction determined by which foot–track interaction is labilized next. Such a manipulation of the thermodynamic minima (here by strain induction through stilbene isomerization) and kinetic barriers (here by addition of either base or acid) experienced by a substrate corresponds to an energy ratchet type of Brownian ratchet mechanism (Figure 1b).[6,9,10]

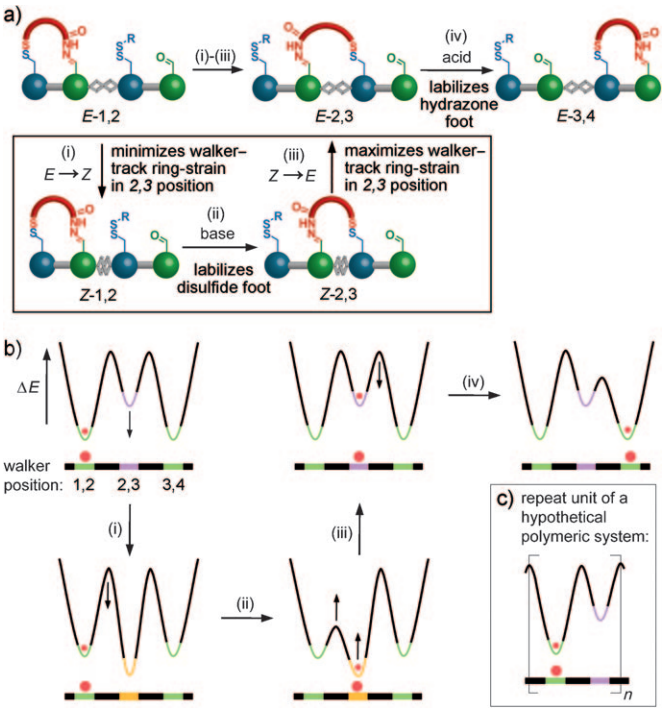

Figure 1. a) Operating mechanism of a light-driven walker–track system based on selectively labile "feet" and adjustable ring strain between the walker (red) and the track in one positional isomer. The reaction sequence shown results in transport of the walker from left to right; switching steps (ii) and (iv) would cause the walker to be transported from right to left. b) Potential energy profile experienced by the walker unit (an energy ratchet mechanism[6,10]). c) Repeat unit of a hypothetical polymeric system along which the walker could be transported in either direction depending on the order of the stimuli applied. Stimuli: (i) UV light, (ii) base, (iii) visible light and iodine, (iv) acid.[11]

Molecular walker–track conjugate *E*-1,2-**1**[12] was synthesized according to Scheme 1 (see the Supporting Information for experimental procedures and characterization data). The

[*] Dr. M. J. Barrell, Dr. A. G. Campaña, M. von Delius, Dr. E. M. Geertsema, Prof. D. A. Leigh
School of Chemistry, University of Edinburgh
The King's Buildings, West Mains Road, Edinburgh EH9 3JJ (UK)
Fax: (+44) 131-650-6453
E-mail: david.leigh@ed.ac.uk
Homepage: http://www.catenane.net

[**] We thank the EPSRC National Mass Spectrometry Service Centre (Swansea, UK) for high-resolution mass spectrometry. This research was funded through the European Research Council Advanced Grant WalkingMols. A.G.C. thanks the Fundación Ramón Areces for a postdoctoral fellowship. D.A.L. is an EPSRC Senior Research Fellow and holds a Royal Society Wolfson Research Merit Award.

Supporting information for this article is available on the WWW under http://dx.doi.org/10.1002/anie.201004779.

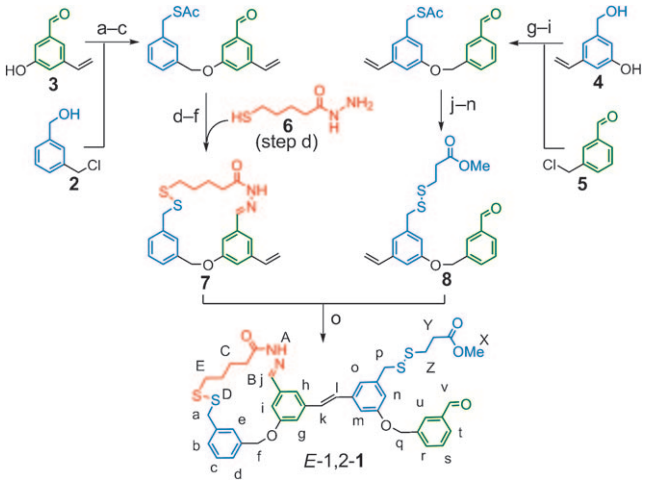

Scheme 1. Synthesis of molecular walker–track conjugate *E*-1,2-**1**. a) NaH, DMF, RT, 16 h; b) methanesulfonyl chloride (MsCl), NEt_3, CH_2Cl_2, 0 °C→RT, 1.5 h; c) potassium thioacetate (KSAc), DMF, RT, 3 h, 59% (three steps); d) AcOH (cat.), MeOH, RT, 2 h, 83%; e) NaOMe, MeOH, RT, 2 h; f) I_2, KI, CH_2Cl_2, RT, 5 min, 48% (two steps); g) NaH, DMF, RT, 16 h; h) MsCl, NEt_3, CH_2Cl_2, 0 °C→RT, 2 h; i) KSAc, DMF, RT, 3 h, 35% (three steps); j) $HC(OMe)_3$, *p*-toluenesulfonic acid (*p*-TsOH), MeOH, RT, 1 h; k) NaOMe, MeOH, RT, 3 h; l) 3-mercaptopropionic acid, I_2, KI, CH_2Cl_2, RT, 5 min; m) HCl (1 M), CH_2Cl_2, RT, 15 min, 69% (four steps); n) AcCl, MeOH, 0 °C→RT, 5 h, 76%; o) Ω_A-SIMes-CF_3 catalyst,[15] CH_2Cl_2, microwave (300 W), 100 °C, 3 h, 23%. See the Supporting Information for details.

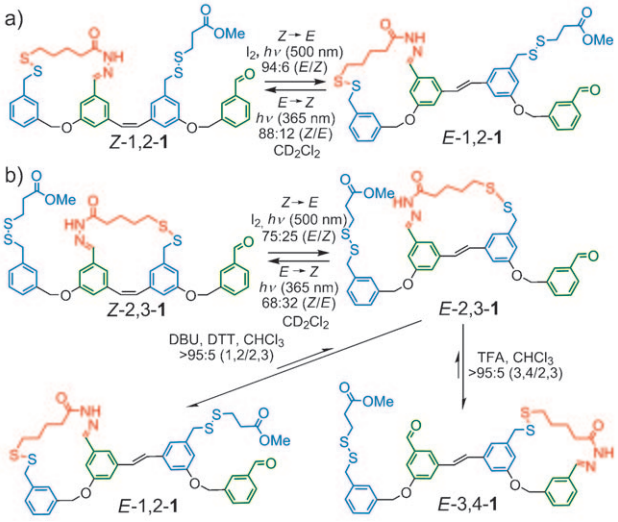

Scheme 2. *Z*→*E* and *E*→*Z* stilbene isomerization of individual positional isomers of **1** and ring opening of *E*-2,3-**1** in either direction under dynamic covalent conditions (acid or base) to release ring strain between the walker and track. Conditions: *E*→*Z*: 0.1–10 mM, *hν* (365 nm; bandwidth: 10 nm), CD_2Cl_2, RT, 5 min; *Z*→*E*: 0.1 mM,[20] I_2 (ca. 10 equiv), *hν* (500 nm; bandwidth: 10 nm[20]), CD_2Cl_2, RT, 4–8 h. Dynamic disulfide exchange (basic conditions): 0.1 mM, D,L-dithiothreitol (DTT, 10 equiv), 1,8-diazabicyclo[5.4.0]undec-7-ene (DBU, 40 equiv), $(MeO_2CCH_2CH_2S)_2$ (20 equiv), $CHCl_3$, RT, 24 h. Dynamic hydrazone exchange (acidic conditions): 0.1 mM, excess CF_3CO_2H (TFA), $CHCl_3$, RT, 48 h.

initial position of the walker unit at footholds 1 and 2 of the track was established by the synthesis of macrocycle **7**, starting from the simple aromatic building blocks **2** and **3** and the bipedal walker unit **6**. Compound **8**, which contains thiol foothold 3 (masked as a disulfide with methyl 3-mercaptopropionate, a "placeholder" thiol[13]) and aldehyde foothold 4, was prepared from precursors **4** and **5**. The synthesis was completed by a ruthenium-catalyzed cross-metathesis reaction,[14] which afforded *E*-1,2-**1** in 23% yield.[15,16] The positional isomer where the walker unit is located on the other end of the molecular track, *E*-3,4-**1**, was prepared unambiguously through an analogous synthetic route (see the Supporting Information).

An investigation of the photochemistry of *E*-1,2-**1** and *E*-3,4-**1**, the positional isomers in which the walker unit is not located over the track stilbene unit, showed that it was possible to efficiently carry out direct (i.e., unsensitized) *E*→*Z* stilbene photoisomerization[17] at 365 nm in CD_2Cl_2 (Scheme 2a). The excellent diastereomeric ratios at the photostationary states (ca. 9:1 *Z*/*E*) are a result of the high molar absorptivities of the *E* isomers compared to the corresponding *Z* isomers.[18] The reverse process, that is, *Z*→*E* stilbene isomerization, also proceeded well in CD_2Cl_2 (>9:1 *E*/*Z*) by using iodine and narrow-bandwidth green light (500 nm; 10 nm bandwidth).[19,20]

We next confirmed that the strained[21] *E*-2,3-**1** isomer could be formed from *Z*-2,3-**1** and that, in a subsequent dynamic covalent[22] exchange reaction, the walker unit could be efficiently transported to either the 1,2 or the 3,4 position of the track, depending on the use of either base or acid (Scheme 2b). Irradiation of pristine *Z*-2,3-**1** (obtained from *Z*-1,2-**1** by base-induced disulfide exchange) at 365 nm generated a 75:25 (*E*/*Z*) photostationary state, which was subjected to conditions for disulfide (base) or hydrazone exchange (acid) in separate experiments. Under basic conditions, approximately 80% of the walker units from this *E*/*Z* mixture were transported to the 1,2-positional isomer (>95% of *E*-2,3-**1** converted into the 1,2 isomer; 25% of residual *Z*-2,3-**1**); under acidic conditions approximately 80% of the 3,4-positional isomer was formed (>95% of *E*-2,3-**1** converted into the 3,4 isomer; 30% of residual *Z*-2,3-**1**).

Having established that the key principles of the energy ratchet mechanism would operate by using individual positional isomers, we needed to establish a procedure for analyzing the mixture of isomers expected to be generated during the full sequence of operations of a statistical molecular-motor mechanism. Pleasingly, the composition of the walker–track system could be accurately determined after each step by 500 MHz ^{1}H NMR spectroscopy, even for complex mixtures that contain all eight isomers (*Z*/*E*-1,2-**1**, *Z*/*E*-2,3-**1**, *Z*/*E*-3,4-**1**, *Z*/*E*-1,4-**1**[11]). The partial ^{1}H NMR spectra of the six isomers involved in the major "passing-leg gait"[10a] mechanism (Figure 1a) are shown in Figure 2. Differences in chemical-shift values that are indicative of the position of the walker unit on the track arise for the protons of the four methylene groups in the walker unit (shown in red, H_B–H_E). Protons H_k and H_l serve as distinctive markers for the configuration of the stilbene olefinic bond

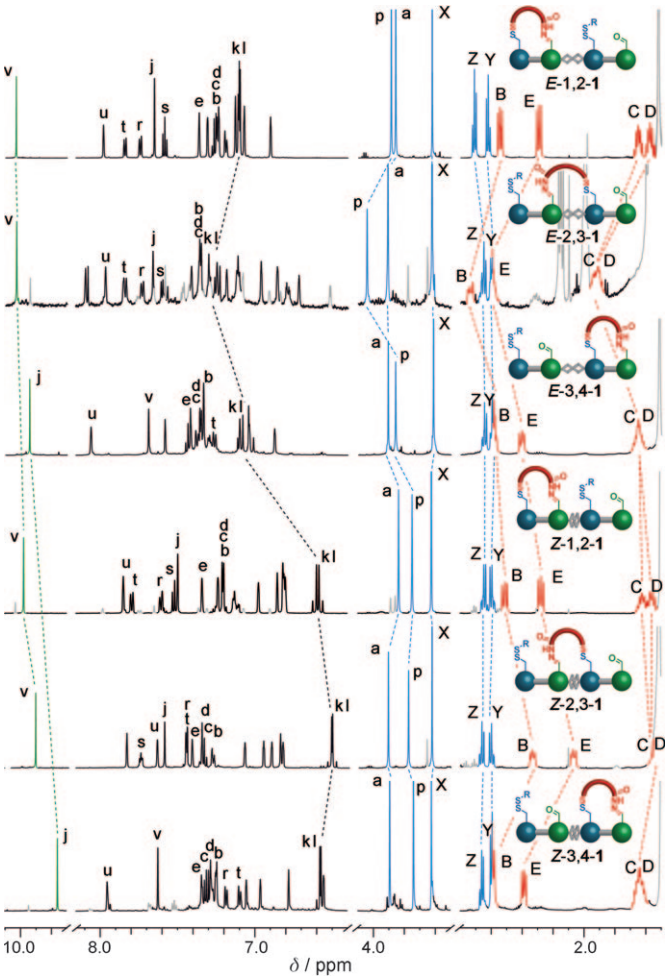

Figure 2. Partial ^{1}H NMR spectra (500 MHz, CD_2Cl_2, 298 K) of the six isomers of **1** involved in the passing-leg gait mechanism[10a] (Figure 1a and Scheme 3). The dashed lines connect some of the key signals that are indicative of the position of the walker unit or the configuration of the track olefin. The signals corresponding to minor isomers (e.g. the "*E*-2,3-**1**" spectrum contains 25% of *Z*-2,3-**1**), solvent, and other impurities are shown in gray. The lettering corresponds to the proton labeling shown in Scheme 1.

($\delta < 7$ ppm for *Z* and $\delta > 7$ ppm for *E* isomers). The signal at around $\delta = 10.0$ ppm (green, H_v or H_j), which corresponds to the free aldehyde group, and the signal at around $\delta = 3.8$ ppm (blue, H_a and H_p), which corresponds to the methylene disulfide protons, are also particularly useful probes because their chemical shifts vary with both the walker position and the stilbene configuration (see the Supporting Information for full ^{1}H NMR spectra of individual positional and configurational isomers).

Directionally biased transport of the walker from left to right through the sequential application of the four external stimuli in the order i–ii–iii–iv is shown in Scheme 3. Starting from pristine *E*-1,2-**1**, photochemical $E \rightarrow Z$ isomerization (i) gives a photostationary state that consists of 88% of the *Z*-1,2-**1** isomer. Subjecting this mixture to the basic conditions (ii), in which the hydrazone linkage between the walker unit and the track is kinetically stable,[23] allows the disulfide foot to dissociate from the track and rebind at footholds 1 or 3. This process leads to an equilibrium in which the positional isomer *Z*-2,3-**1** is favored. Light-induced $Z \rightarrow E$ isomerization (iii) of the stilbene in this mixture results in 75% conversion of *Z*-2,3-**1** into the strained *E*-2,3-**1** isomer. In the following acid-catalyzed step (iv), the hydrazone foot is able to dissociate from the track and rebind at either foothold 2 or 4, while the disulfide foot acts as a fixed pivot.[23] This process results in a large majority (>95%) of walker units being transported away from the *E*-stilbene unit (2,3 position) towards the now energetically favorable 3,4 position (see Figure 1b for the schematic energy diagram that corresponds to these processes). Note that all the energy required to fuel directional transport in Scheme 3 is supplied through the $E \rightarrow Z$ photoisomerization reaction (i), which creates configurational strain in the track. The other three reactions (ii–iv), which are all under thermodynamic control, each dissipate some of that energy (even reaction (iii), which uses the energy to induce conformational strain between the walker and the track in the 2,3 position) in a way designed to achieve the desired directional migration of the walker.

The behavior of the walker–track system **1** under these operating conditions (Figure 3a), and when the stimuli are applied in a different order (iii–ii–i–iv; Figure 3b) or starting from a different positional isomer (*E*-3,4-**1**; Figure 3c,d), are shown in Figure 3. The amount of each *E*/*Z* isomer pair (1,2-**1**, 2,3-**1**, 3,4-**1**, and 1,4-**1**[11]) is shown after each step of the applied sequence of stimuli. The graphs show both the behavior of the system (solid symbols and lines) extrapolated from the experimentally determined equilibrium and steady-state ratios between each pair of exchanging isomers (Scheme 2a for example), and the experimentally determined composition during full-system operation (hollow symbols).[24]

Figure 3a shows the change in composition of the system during the reaction sequence intended to transport the walker from left to right, (i.e., that shown in Scheme 3), starting from *E*-1,2-**1**. After the full cycle of reactions, which corresponds to up to two steps being taken by the walker, 48% of the walker units are on the right-hand side of the track (3,4-**1**), 30% of the walker units are on the left-hand side (1,2-**1**), and the remainder are in the middle (16% 2,3-**1**) or have taken a "double step" from left to right (6% 1,4-**1**). In other words, 50% more walkers have taken two steps to the right under the operating sequence than have taken one step to the right and one step back (or remained on the left-hand side throughout).

Figure 3b shows the results of a change in the sequence of reactions; following the $E \rightarrow Z$ ring-strain-inducing reaction, the hydrazone foot–track interaction is labilized (under acidic conditions) rather than that of the disulfide. This reaction sequence (iii–ii–i–iv) should bias transport of the walker from right to left (see caption to Figure 1) and indeed, only 4% of 3,4-**1** is present in the mixture after these reactions are applied to 1,2-**1** (interestingly, a significant amount (33%) of the 1,4 "double step" isomer is formed through folding of the track[11]).

Figure 3c shows that the walker unit can be effectively transported from right to left by this sequence. Starting from *E*-3,4-**1**, 48% of the walkers are found on the left-hand side of

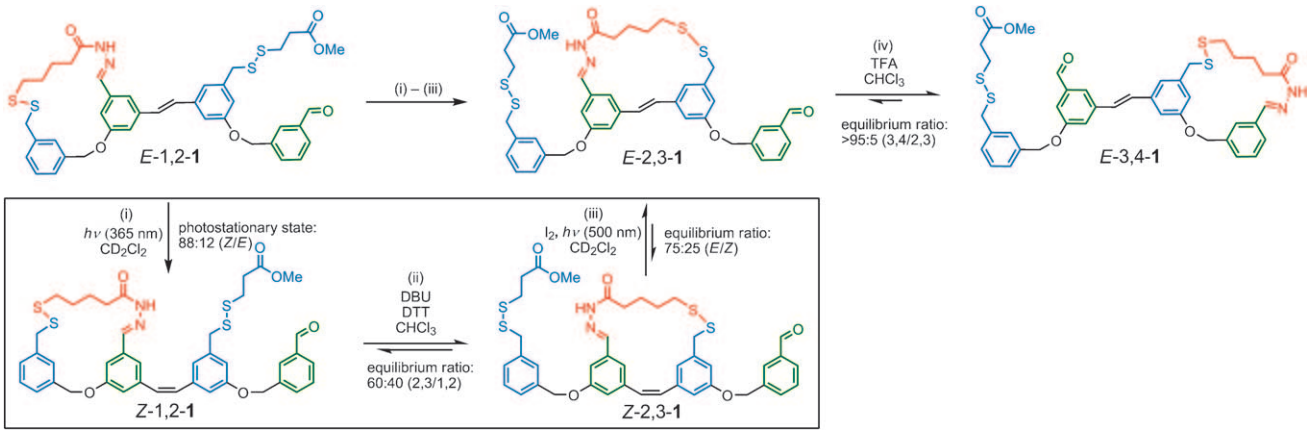

Scheme 3. Directionally biased (left to right) walker migration over one full cycle of operation starting from *E*-1,2-**1**, following the layout used in Figure 1. For clarity, only the major isomer is shown after each reaction (see Figure 3a for the composition of the entire system at each stage). Isomer ratios were obtained from the integration of the ^{1}H NMR spectra (see the Supporting Information). Conditions: (i) 0.1–10 mM, *hν* (365 nm; bandwidth: 10 nm), CD_2Cl_2, RT, 5 min (0.1 mM) to 1 h (10 mM); (ii) 0.1 mM, DTT (10 equiv), DBU (40 equiv), $(MeO_2CCH_2CH_2S)_2$ (20 equiv), $CHCl_3$, RT, 24 h; (iii) 0.1 mM,[20] I_2 (ca. 10 equiv), *hν* (500 nm; bandwidth: 10 nm[20]), CD_2Cl_2, RT, 6 h; (iv) 0.1 mM, TFA (excess), $CHCl_3$, RT, 48 h.

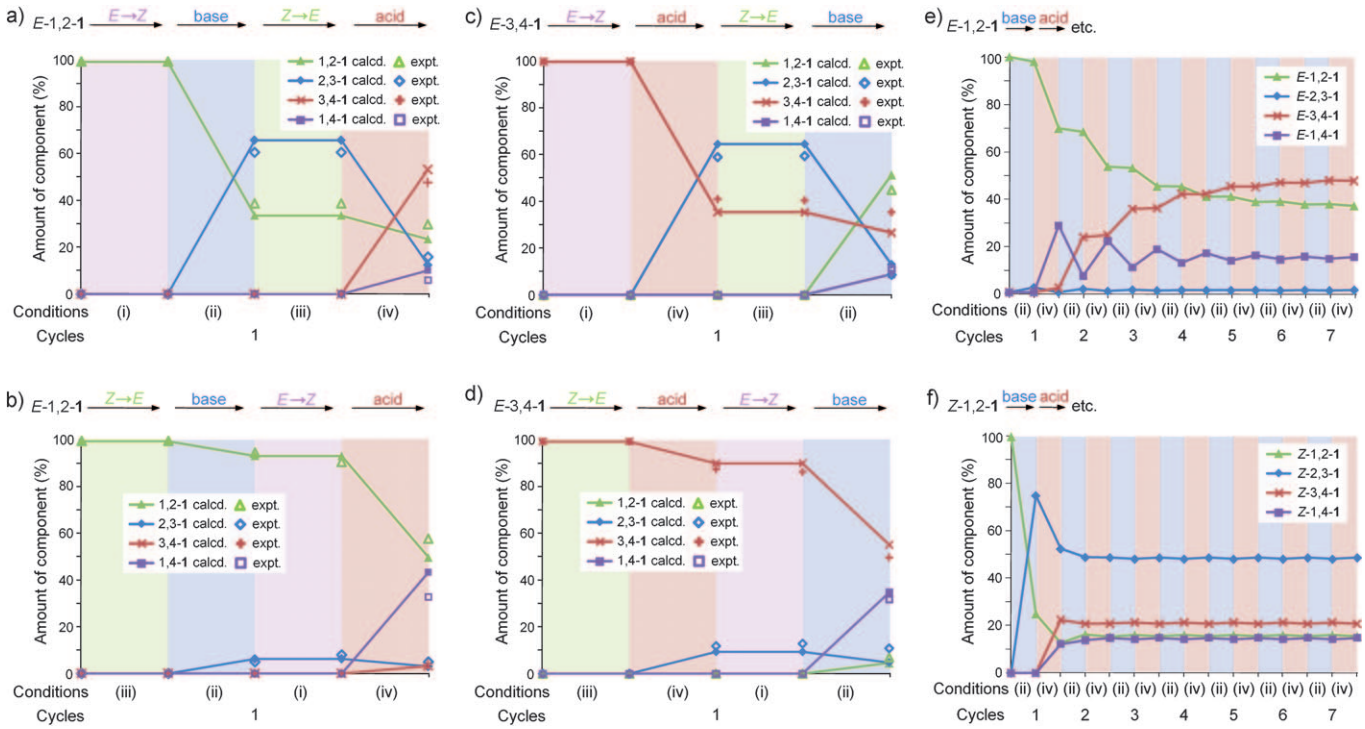

Figure 3. Dynamic behavior of walker–track system **1**, varying the starting position of the walker and the stimuli sequence (denoted through colored bands; purple: *E*→*Z* isomerization at 365 nm; blue: base-catalyzed disulfide exchange; green: *Z*→*E* isomerization at 500 nm (I_2 catalyst); red: acid-catalyzed hydrazone exchange). Experimental (expt.) and calculated (calcd.) product distribution[24] over one full cycle of operation: a) starting compound *E*-1,2-**1**, stimuli sequence i–ii–iii–iv; b) starting compound *E*-1,2-**1**, stimuli sequence iii–ii–i–iv (a mismatch as this sequence tends to transport the walker from right to left); c) starting compound *E*-3,4-**1**, stimuli sequence i–iv–iii–ii; d) starting compound *E*-3,4-**1**, stimuli sequence iii–iv–i–ii (a mismatch as this sequence tends to transport the walker from left to right). Calculated product distribution over seven base/acid cycles (no stilbene isomerization), starting from e) pristine *E*-1,2-**1** and f) pristine *Z*-1,2-**1**. The calculated data are based on simple mathematical extrapolation of the observed steady-state ratios between each *Z*/*E* isomer pair under conditions (i) and (iii) and the observed equilibrium ratios between individual positional isomers under conditions (ii) and (iv) (see Section 5 in the Supporting Information). Experimental data are based on the integrals of the ^{1}H NMR spectra of mixtures obtained after each step of the reaction sequence, margin of error ±3% (see Section 4 in the Supporting Information). A small amount of oligomers (ca. 5%) was also obtained during each experiment. Conditions: (i) 0.1–10 mM, *hν* (365 nm; bandwidth: 10 nm), CD_2Cl_2, RT, 5 min–1 h; (ii) 0.1 mM, DTT (10 equiv), DBU (40 equiv), $(MeO_2CCH_2CH_2S)_2$ (20 equiv), $CHCl_3$, RT, 12–48 h; (iii) 0.1 mM,[20] I_2 (ca. 10 equiv), *hν* (500 nm; bandwidth: 10 nm[20]), CD_2Cl_2, RT, 4–8 h; (iv) 0.1 mM, TFA (excess), $CHCl_3$, RT, 6–96 h.

the track after the full reaction sequence and only 36% remain on the right-hand side.

Figure 3d shows the effect of applying the right-to-left directionally biased reaction sequence starting with the isomer for which the walker is already on the left.

These results collectively illustrate the characteristics typical of energy ratchet mechanisms.[6,10a] Irrespective of the initial walker position on the track (e.g., starting from 1,2-**1** (Figure 3a), 3,4-**1** (Figure 3d), or any combination of walker positions) after the sequence i–ii–iii–iv (or iii–iv–i–ii) the majority of walkers are found on the right-hand side (3,4-**1**). Conversely, irrespective of the initial walker position on the track (Figure 3b and c), after the sequence iii–ii–i–iv (or i–iv–iii–ii) the majority of walkers are on the left-hand side (1,2-**1**). The position of the walker does not influence the sequence of reactions applied, nor their basic effect on the track,[25] and statistical "errors" (e.g., the walker does not take a step every time a foot–track interaction is labilized) are an intrinsic feature of the mechanism.

Figures 3e and 3f (*E*-stilbene track and *Z*-stilbene track, respectively) show the behavior of the system when no stilbene isomerization reactions are carried out. Repeatedly switching between treatment with acid and base (labilizing first one foot–track interaction and then the other) allows the distribution of the walkers on the track to approach the minimum-energy distribution.[4] In the case of the *E*-stilbene track (Figure 3e), the gap between footholds 2 and 3 is too wide for the walkers to bridge easily (note the very small amounts of the 2,3 isomer formed) and it would take seven full operational cycles to approach the steady state of the system, which features roughly equal amounts of walkers at each end of the track. With the *Z*-stilbene track (Figure 3f), the 2,3 position is, of course, very accessible to the walker units and so the steady-state is reached after only two cycles. However, the 2,3 position is actually energetically more favored than the ends of the tracks, so the majority of walkers remain in the center (49% *Z*-2,3-**1**). The differences in behavior and walker distribution produced by switching between acid and base alone (Figure 3e,f) and when additional stilbene isomerization is carried out (e.g., Figure 3a,c) show the dramatic effect that the energy ratchet mechanism has on walker transport.

The operations of walker–track conjugate **1** shown in Scheme 3 and Figure 3a,c correspond to a light-driven linear molecular motor system.[26] Significant directional bias, which stems from an energy ratchet mechanism, can transport the walker unit in either direction along the molecular track; the control over the sense of direction is a feature not found in biological linear motor proteins. While both the photochemical stilbene isomerization and the acid- and base-induced reversible foot-migration processes proceed with good efficiencies, a weakness of the present system lies in the flexibility of the track and the resulting folding products, which reduce the net directionality of transport and prevent improvement of the bias over multiple cycles. Furthermore, a hypothetical polymeric track based on the current design would utilize the light energy used to power directional transport very inefficiently by switching the configuration of many of the double bonds in the track each time, whereas only one double bond would actually "ratchet" the walker unit energetically uphill. Work aimed at overcoming these deficiencies is currently underway.

Received: August 2, 2010
Revised: September 3, 2010
Published online: ■■ ■■, 2010

Keywords: Brownian ratchets · dynamic covalent chemistry · molecular devices · molecular motors · photochemistry

[1] a) *Molecular Motors* (Ed.: M. Schliwa), Wiley-VCH, Weinheim, **2003**; b) R. D. Vale, *Cell* **2003**, *112*, 467–480; c) M. Schliwa, G. Woehlke, *Nature* **2003**, *422*, 759–765.

[2] For concise reviews on motor proteins, see: kinesin family: a) S. M. Block, *Biophys. J.* **2007**, *92*, 2986–2995; b) N. Hirokawa, Y. Noda, Y. Tanaka, S. Niwa, *Nat. Rev. Mol. Cell Biol.* **2009**, *10*, 682–696; myosin family: c) J. R. Sellers, C. Veigel, *Curr. Opin. Cell Biol.* **2006**, *18*, 68–73; d) H. L. Sweeney, A. Houdusse, *Annu. Rev. Biophys.* **2010**, *39*, 539–557; dynein family: e) M. P. Koonce, M. Samsó, *Trends Cell Biol.* **2004**, *14*, 612–619; f) K. Oiwa, H. Sakakibara, *Curr. Opin. Cell Biol.* **2005**, *17*, 98–103.

[3] a) W. B. Sherman, N. C. Seeman, *Nano Lett.* **2004**, *4*, 1203–1207; b) J.-S. Shin, N. A. Pierce, *J. Am. Chem. Soc.* **2004**, *126*, 10834–10835; c) P. Yin, H. Yan, X. G. Daniell, A. J. Turberfield, J. H. Reif, *Angew. Chem.* **2004**, *116*, 5014–5019; *Angew. Chem. Int. Ed.* **2004**, *43*, 4906–4911; d) Y. Tian, Y. He, Y. Chen, P. Yin, C. Mao, *Angew. Chem.* **2005**, *117*, 4429–4432; *Angew. Chem. Int. Ed.* **2005**, *44*, 4355–4358; e) P. Yin, H. M. T. Choi, C. R. Calvert, N. A. Pierce, *Nature* **2008**, *451*, 318–322; f) S. J. Green, J. Bath, A. J. Turberfield, *Phys. Rev. Lett.* **2008**, *101*, 238101; g) T. Omabegho, R. Sha, N. C. Seeman, *Science* **2009**, *324*, 67–71; h) H. Gu, J. Chao, S.-J. Xiao, N. C. Seeman, *Nature* **2010**, *465*, 202–205; i) K. Lund, A. J. Manzo, N. Dabby, N. Michelotti, A. Johnson-Buck, J. Nangreave, S. Taylor, R. Pei, M. N. Stojanovic, N. G. Walter, E. Winfree, H. Yan, *Nature* **2010**, *465*, 206–210.

[4] a) M. von Delius, E. M. Geertsema, D. A. Leigh, *Nat. Chem.* **2010**, *2*, 96–101; b) S. Otto, *Nat. Chem.* **2010**, *2*, 75–76.

[5] a) V. Serreli, C.-F. Lee, E. R. Kay, D. A. Leigh, *Nature* **2007**, *445*, 523–527; b) M. Alvarez-Pérez, S. M. Goldup, D. A. Leigh, A. M. Z. Slawin, *J. Am. Chem. Soc.* **2008**, *130*, 1836–1838.

[6] We use the term "ratcheting" in a manner that is consistent with its use in biology and nonequilibrium statistical physics: namely, it is the capturing of a positional displacement of a substrate through the imposition of a kinetic energy barrier that prevents the displacement being reversed when the thermodynamic driving force is removed; see M. N. Chatterjee, E. R. Kay, D. A. Leigh, *J. Am. Chem. Soc.* **2006**, *128*, 4058–4073. An information ratchet is a Brownian ratchet mechanism in which the position of the particle on a potential energy surface causes the potential energy surface to change (at an energetic cost), thus leading to directional transport of the particle. In an energy ratchet mechanism the potential energy surface is periodically or stochastically varied irrespective of the position of the particle in order to cause directional transport (for example, the relative depths of two pairs of minima and the relative heights of the maxima that connect them could be repeatedly switched, as in Figure 1b). See ref. [10a].

[7] For examples of light-driven synthetic molecular machines, see: a) S. Shinkai, T. Nakaji, T. Ogawa, K. Shigematsu, O. Manabe, *J. Am. Chem. Soc.* **1981**, *103*, 111–115; b) H. Murakami, A. Kawabuchi, K. Kotoo, M. Kunitake, N. Nakashima, *J. Am. Chem. Soc.* **1997**, *119*, 7605–7606; c) N. Koumura, R. W. J. Zijlstra, R. A. van Delden, N. Harada, B. L. Feringa, *Nature* **1999**, *401*, 152–155; d) T. Hugel, N. B. Holland, A. Cattani, L.

Moroder, M. Seitz, H. E. Gaub, *Science* **2002**, *296*, 1103 – 1106; e) T. Muraoka, K. Kinbara, Y. Kobayashi, T. Aida, *J. Am. Chem. Soc.* **2003**, *125*, 5612 – 5613; f) E. M. Pérez, D. T. F. Dryden, D. A. Leigh, G. Teobaldi, F. Zerbetto, *J. Am. Chem. Soc.* **2004**, *126*, 12210 – 12211; g) Q.-C. Wang, D.-H. Qu, J. Ren, K. Chen, H. Tian, *Angew. Chem.* **2004**, *116*, 2715 – 2719; *Angew. Chem. Int. Ed.* **2004**, *43*, 2661 – 2665; h) J. Berná, D. A. Leigh, M. Lubomska, S. M. Mendoza, E. M. Pérez, P. Rudolf, G. Teobaldi, F. Zerbetto, *Nat. Mater.* **2005**, *4*, 704 – 710; i) R. Eelkema, M. M. Pollard, J. Vicario, N. Katsonis, B. S. Ramon, C. W. M. Bastiaansen, D. J. Broer, B. L. Feringa, *Nature* **2006**, *440*, 163; j) V. Balzani, M. Clemente-León, A. Credi, B. Ferrer, M. Venturi, A. H. Flood, J. F. Stoddart, *Proc. Natl. Acad. Sci. USA* **2006**, *103*, 1178 – 1183; k) T. Muraoka, K. Kinbara, T. Aida, *Nature* **2006**, *440*, 512 – 515; l) M. Yamada, M. Kondo, J.-i. Mamiya, Y. Yu, M. Kinoshita, C. J. Barrett, T. Ikeda, *Angew. Chem.* **2008**, *120*, 5064 – 5066; *Angew. Chem. Int. Ed.* **2008**, *47*, 4986 – 4988; m) M. Klok, N. Boyle, M. T. Pryce, A. Meetsma, W. R. Browne, B. L. Feringa, *J. Am. Chem. Soc.* **2008**, *130*, 10484 – 10485; n) M. R. Panman, P. Bodis, D. J. Shaw, B. H. Bakker, A. C. Newton, E. R. Kay, A. M. Brouwer, W. J. Buma, D. A. Leigh, S. Woutersen, *Science* **2010**, *328*, 1255 – 1258.

[8] For elegant mechanistic studies based on ring strain in macrocycles that contain a "stiff stilbene" linkage, see: a) Q. Z. Yang, Z. Huang, T. J. Kucharski, D. Khvostichenko, J. Chen, R. Boulatov, *Nat. Nanotechnol.* **2009**, *4*, 302 – 306; b) T. J. Kucharski, Z. Huang, Q. Z. Yang, Y. C. Tian, N. C. Rubin, C. D. Concepcion, R. Boulatov, *Angew. Chem.* **2009**, *121*, 7174 – 7177; *Angew. Chem. Int. Ed.* **2009**, *48*, 7040 – 7043. For a dynamic covalent library that consists of macrocycles with internal acyl hydrazone and (photoswitchable) azobenzene linkages, see: c) L. A. Ingerman, M. L. Waters, *J. Org. Chem.* **2009**, *74*, 111 – 117.

[9] a) D. A. Leigh, J. K. Y. Wong, F. Dehez, F. Zerbetto, *Nature* **2003**, *424*, 174 – 179; b) J. V. Hernandez, E. R. Kay, D. A. Leigh, *Science* **2004**, *306*, 1532 – 1537; c) S. P. Fletcher, F. Dumur, M. M. Pollard, B. L. Feringa, *Science* **2005**, *310*, 80 – 82.

[10] a) E. R. Kay, F. Zerbetto, D. A. Leigh, *Angew. Chem.* **2007**, *119*, 72 – 196; *Angew. Chem. Int. Ed.* **2007**, *46*, 72 – 191; b) R. D. Astumian, *Phys. Chem. Chem. Phys.* **2007**, *9*, 5067 – 5083; c) R. D. Astumian, I. Derényi, *Eur. Biophys. J.* **1998**, *27*, 474 – 489; d) P. Hänggi, F. Marchesoni, *Rev. Mod. Phys.* **2009**, *81*, 387 – 442; e) R. D. Astumian, *Biophys. J.* **2010**, *98*, 2401 – 2409.

[11] The 1,4 isomers of **1**, which result from folding of the track (see the Supporting Information for structures), add an additional double-step mechanism to the major passing-leg gait mechanism (see ref. [4]). This pathway has the opposite bias to the main mechanism and so actually reduces the net directionality of the walker transport.

[12] *E* or *Z* denotes the configuration of the stilbene double bond in the track; the numerical prefixes (e.g., 1,2) specify the position of the walker unit on the four-foothold track.

[13] The sulfur foothold of the track was protected as a disulfide with a "placeholder" thiol in order to prevent oxidation of the free thiol to a dimeric disulfide by atmospheric oxygen.

[14] a) A. K. Chatterjee, T.-L. Choi, D. P. Sanders, R. H. Grubbs, *J. Am. Chem. Soc.* **2003**, *125*, 11360 – 11370; b) S. P. Nolan, H. Clavier, *Chem. Soc. Rev.* **2010**, *39*, 3305 – 3316.

[15] Screening gave best results with the commercially available catalyst Ω_A-SIMes-CF_3, compound **2h** in: D. Rix, F. Caijo, I. Laurent, F. Boeda, H. Clavier, S. P. Nolan, M. Mauduit, *J. Org. Chem.* **2008**, *73*, 4225 – 4228.

[16] The styrene (Type II) olefins in **7** and **8** have similar reactivities and so the maximum yield of *E*-1,2-**1** expected from their statistical cross-metathesis is 50% (see ref. [14a]). This synthetic disconnection was chosen to prevent scrambling of the sensitive (different) disulfide and aldehyde/hydrazone functionalities in the final molecule.

[17] For an excellent review on the photochemistry of stilbene derivatives, see: H. Meier, *Angew. Chem.* **1992**, *104*, 1425 – 1446; *Angew. Chem. Int. Ed. Engl.* **1992**, *31*, 1399 – 1420.

[18] The photostationary equilibrium ratio for direct $Z \rightarrow E$ isomerization can be calculated as a function of the quantum yields (Φ) and molar absorptivities (ε) of the *E* and *Z* species (at a given wavelength): $[Z]/[E] = (\Phi_{E\rightarrow Z}\varepsilon_E)/(\Phi_{Z\rightarrow E}\varepsilon_Z)$, the quantum yield ratio is usually approximately 1 (see ref. [17]).

[19] The mechanism for iodine-mediated stilbene $Z \rightarrow E$ isomerization involves the reversible addition of I$^{\bullet}$ radicals (here photogenerated with green light) to the double bond. See, for example: S. Yamashita, *Bull. Chem. Soc. Jpn.* **1961**, *34*, 972 – 976.

[20] The iodine-mediated stilbene $Z \rightarrow E$ isomerization reactions were conducted at relatively low concentrations (0.1 mM) of the walker–track conjugate and with a narrow (10 nm) bandwidth of green light (500 nm) to avoid side-reactions of the disulfide groups.

[21] The length of the methylene spacer in the walker unit is crucial in order to generate ring strain in *E*-2,3-**1**, but not in *Z*-2,3-**1**. The choice of a four-carbon atom spacer was based on model studies and molecular modeling (semi-empirical, PM3).

[22] a) S. J. Rowan, S. J. Cantrill, G. R. L. Cousins, J. K. M. Sanders, J. F. Stoddart, *Angew. Chem.* **2002**, *114*, 938 – 993; *Angew. Chem. Int. Ed.* **2002**, *41*, 898 – 952; b) P. T. Corbett, J. Leclaire, L. Vial, K. R. West, J.-L. Wietor, J. K. M. Sanders, S. Otto, *Chem. Rev.* **2006**, *106*, 3652 – 3711; c) J.-M. Lehn, *Chem. Soc. Rev.* **2007**, *36*, 151 – 160.

[23] For studies on the dynamic chemistry of hydrazone–disulfide systems under mutually exclusive (acid–base) conditions, see: a) A. G. Orrillo, A. M. Escalante, R. L. E. Furlan, *Chem. Commun.* **2008**, 5298 – 5300; b) Z. Rodriguez-Docampo, S. Otto, *Chem. Commun.* **2008**, 5301 – 5303; c) M. von Delius, E. M. Geertsema, D. A. Leigh, A. M. Z. Slawin, *Org. Biomol. Chem.* **2010**, *8*, 4617 – 4624.

[24] Possible reasons for the minor differences between the data extrapolated from the individual isomer experiments and the experimental results from operation on the full system include insufficient equilibration time for dynamic covalent exchange processes, nonideal photochemical steady-state ratios in mixtures, and inaccuracies in ^{1}H NMR integration.

[25] The presence of the walker at the 2,3-position lowers the *E*/*Z* ratio at the photostationary state of the $Z \rightarrow E$ reaction (Scheme 2b), thus reducing the net directionality of the transport mechanism.

[26] In a double-labeling crossover experiment on the previously reported small-molecule walker–track system (see ref. [4]), an average step number (the number of steps after which 50% of the walkers are no longer attached to their original track) of 37 was obtained for the loss of processivity during disulfide and hydrazone exchange. The conditions for dynamic covalent bond exchange are the same in the present study, and walker dissociation is not observed during the photochemical experiments. Therefore, the average step number during the operation of **1** should be similar. The average step number for wild-type kinesin is approximately 100 (R. B. Case, D. W. Pierce, N. Hom-Booher, C. L. Hart, R. D. Vale, *Cell* **1997**, *90*, 959 – 966).

Communications

Molecular Devices

M. J. Barrell, A. G. Campaña, M. von Delius, E. M. Geertsema, D. A. Leigh* _____ ■■■■–■■■■

Light-Driven Transport of a Molecular Walker in Either Direction along a Molecular Track

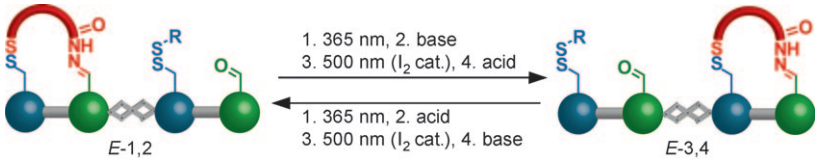

Walk this way! A walker unit is able to walk in either direction along a four-foothold molecular track, depending on the sequence of application of four external stimuli: acid, base, UV light, and visible light in the presence of iodine (see picture). The isomerization of the stilbene moiety in the molecular track is key for the achievement of directional transport through a Brownian ratchet mechanism.